Chair of Geology and Economic Geology

Doctoral Thesis

# Development of an Analytical Proof of Origin Method for Natural Graphite Deposits

Valentina Elisa Dietrich, MSc

July 2024

**MONTANUNIVERSITÄT LEOBEN**
www.unileoben.ac.at

## AFFIDAVIT

I declare on oath that I wrote this thesis independently, did not use any sources and aids other than those specified, have fully and truthfully reported the use of generative methods and models of artificial intelligence, and did not otherwise use any other unauthorized aids.

I declare that I have read, understood and complied with the "Good Scientific Practice" of the Montanuniversität Leoben.

Furthermore, I declare that the electronic and printed versions of the submitted thesis are identical in form and content.

Date 27.05.2024

Valentina Dietrich

Signature Author
Valentina Elisa Dietrich

## Acknowledgements

I would like to express my heartfelt gratitude to everyone who has supported me throughout this journey. Each of you knows who you are.

Firstly, I am truly grateful to my supervisor, Frank Melcher, for his irreplaceable guidance and support. His expertise has been instrumental in shaping this work.

I also wish to extend my appreciation to my colleagues at Montanuniversität Leoben and GTK in Espoo, as well as the entire CERA and MaDiTraCe project network. Your collaboration and insights have enriched my research in countless ways.

To my friends and mentors, thank you for your unwavering support and wisdom. Your encouragement has been a constant source of motivation.

I am profoundly thankful to my family for their unconditional love and belief in me. Your support has been my foundation throughout this journey.

Finally, to my husband, your patience, understanding and endless support have been my anchor.

Thank you all for being part of this challenging journey.

# Abstract

Graphite is considered as a critical raw material due to its essential role in various industrial applications, particularly in the steel, refractories and energy storage sectors. The latter, encompassing the production of lithium-ion batteries, is especially significant, as these batteries are essential to electric vehicles and numerous electronic devices. The escalating demand for lithium-ion batteries has consequently increased the demand for graphite and the interest in the provenance of this raw material. This thesis, as part of a larger initiative, focused on the traceability of graphite as an important battery raw material, aiming to enhance the transparency, reliability and sustainability of complex supply chains.

The study introduces an innovative multi-parameter analytical approach to differentiate graphite concentrate samples from various global locations, including major graphite producing countries. Stable carbon isotopes serve as a primary parameter for distinguishing between carbon sources. Flake and amorphous graphite, originating from organic materials, contrast with hydrothermal graphite. Through this methodology, three distinct sample groups were identified: Ukraine, Sri Lanka and the rest of the world. The Raman spectrum, characterizing the microstructural state of graphite, provides information about the peak metamorphic temperatures during graphite formation and also allows a differentiation between different graphite types. However, the microstructure can be altered by mineral processing activities such as crushing and grinding, impacting the natural structure of the material. This technique enables the distinction of amorphous graphite from flake and hydrothermal graphite types.

Trace element analysis potentially differentiates the origin of graphite on the most detailed, the deposit level. The geographic provenance of individual deposits can be traced through characteristic trace elements (including V, Mo, Cr, Co, Cu, Ga, As, Rb, Sr, Ba and REE patterns). Developing methods for solution-based analysis (such as ICP-MS) was necessary due to the inherent challenges in fully dissolving graphite, given the robust carbon layers. Laser Ablation-ICP-MS offers a less time- and cost-intensive method, though it also required significant method development for sample preparation and calibration. The ablation of very fine-grained compressed materials and the lack of reference and calibration materials presented notable challenges. A significant proportion of trace elements in graphite concentrates are associated with impurities and accompanying mineralogical components. These impurities can be identified and delineated through the application of advanced statistical methods and data processing techniques.

Analytical proof of origin (APO) methods are considered incorruptible, as they directly relate to the chemical composition of the raw material, offering significant potential for verification and control purposes. Unlike methods such as documents, tracers, QR codes and barcodes, which can be manipulated or falsified, APO methods provide a robust means of authentication. The developed APO methodology serves to facilitate the implementation of supply chain laws and battery regulations within the graphite industry.

# Zusammenfassung

Graphit gilt aufgrund seiner bedeutenden Rolle in verschiedenen industriellen Anwendungen, wie der Stahl- und Feuerfestindustrie, als wichtiger und auch kritischer mineralischer Rohstoff. Die aktuell signifikanteste Anwendung dieses Rohstoffs liegt aber in der Batterieerzeugung. Graphit ist eine entscheidende Komponente in Lithium-Ionen-Batterien, die weit verbreitet in Elektrofahrzeugen und anderen elektronischen Geräten eingesetzt werden. Die Nachfrage nach Lithium-Ionen-Batterien steigt rapide an, somit auch die Nachfrage nach Graphit und damit auch das Interesse an der Herkunft dieses Rohstoffs. Eingebettet in ein Projekt zur Rückverfolgbarkeit von Batterierohstoffen zielt diese Arbeit darauf ab, die Transparenz und Zuverlässigkeit komplexer Lieferketten für Graphit zu stärken.

Die Studie entwickelt einen analytischen multiparametrischen Ansatz, um Graphitproben aus verschiedenen globalen Lagerstätten, einschließlich Länder, die wesentlich zur Graphit- Weltproduktion beitragen, zu unterscheiden. Stabile Kohlenstoffisotope dienen als primärer Parameter zur Unterscheidung zwischen den unterschiedlichen Kohlenstoffquellen und Graphittypen. Flocken- und amorpher Graphit, der aus organischen Materialien stammt, kontrastiert mit hydrothermalem Graphit. Drei Probenkategorien, die voneinander unterschieden werden können, wurden identifiziert: Ukraine, Sri Lanka und RoW (Rest der Welt). Das Raman-Spektrum von Graphit ist charakteristisch für seinen mikrostrukturellen Zustand und dient als Grundlage für die Berechnung der Metamorphose Temperaturen während der Graphitbildung Die Struktur von Graphit wird jedoch auch durch Verarbeitung (Brechen, Mahlen) verändert und repräsentiert nicht nur die natürliche Struktur des Materials. Mit Raman Spektroskopie kann amorpher Graphit von den anderen Graphittypen (Flockengraphit und hydrothermaler Graphit) unterschieden werden.

Die Spurenelementanalyse kann potenziell die Herkunft des Graphitkonzentrates auf der detailliertesten Ebene, der Lagerstätte, unterscheiden. Der geografische Ursprung einzelner Lagerstätten kann durch charakteristische Spurenelemente (einschließlich V, Mo, Cr, Co, Cu, Ga, As, Rb, Sr, Ba und REE-Muster) analysiert durch induktiv gekoppelte Plasma-Massenspektroskopie (ICP-MS) zurückverfolgt werden. Die Entwicklung von Methoden für lösungsbasierte Analysen war aufgrund der Herausforderungen bei der vollständigen Auflösung von Graphit, bedingt durch die robusten Kohlenstoffschichten, notwendig. Laser Ablation-ICP-MS bietet eine weniger zeit- und kostenintensive Methode, erforderte jedoch ebenfalls eine signifikante Methodenentwicklung für die Probenvorbereitung und Kalibrierung. Die Ablation von sehr feinkörnigen komprimierten Materialien und das Fehlen von Referenz- und Kalibrierungsmaterialien stellten erhebliche Herausforderungen dar. Ein erheblicher Anteil der Spurenelemente in Graphitkonzentraten ist mit Verunreinigungen und begleitenden mineralogischen Komponenten verbunden. Diese Verunreinigungen können durch die Anwendung fortschrittlicher statistischer Methoden und Datenverarbeitungstechniken identifiziert und abgegrenzt werden.

Analytische Herkunftsnachweismethoden (APO) gelten als manipulationssicher, da sie sich direkt auf die chemische Zusammensetzung des Rohmaterials beziehen und ein erhebliches Potenzial für Verifikations- und Kontrollzwecke bieten. Im Gegensatz zu Methoden wie Dokumenten, künstlich hinzugefügte Materialien oder Tracer, QR-Codes und Barcodes, die manipuliert oder gefälscht werden können, bieten APO-Methoden eine robuste Möglichkeit zur Authentifizierung von mineralischen Rohstoffen. Die entwickelte APO-Methodik dient zur Unterstützung der Implementierung von Lieferkettengesetzen und Batterieregulatorien in der Graphitindustrie.

# List of Abbreviations

**Abbreviations**

| | |
|---|---|
| AFP | Analytical Fingerprinting |
| Ag | Silver |
| Al | Aluminium |
| APO | Analytical Proof of Origin |
| As | Arsenic |
| Au | Gold |
| B | Boron |
| Ba | Barium |
| BAM | Bundesanstalt für Materialforschung |
| Be | Beryllium |
| Bi | Bismuth |
| C | Carbon |
| Ca | Calcium |
| Cd | Cadmium |
| Ce | Cer |
| CERA | Certification of Raw Materials |
| Co | Cobalt |
| Cr | Chromium |
| CRM(s) | Critical Raw Material(s) |
| Cu | Copper |
| DNA | Deoxyribonucleic acid |
| DRC | Democratic Republic Congo |
| Dy | Dysprosium |
| EIT-RM | European Institute of Innovation & Technology – Raw Materials |
| EMPA | Electron Micro Probe Analyzer |
| Er | Erbium |
| ETAAS | Electro Thermal Atomic Absorption |
| EU | European Union |
| Eu | Europium |
| FAAS | Flame Atomic Absorption Spectroscopy |
| Fe | Iron |
| FI-CVG-AAS | flow-injection chemical vapor-generation atomic absorption spectrometric |
| FTIR | Fourier-Transform Infrared Spectroscopy |
| Ga | Gallium |
| Gas-MS | Gas-mass Spectrometry |
| Gd | Gadolinium |
| Ge | Germanium |
| GTK | Finnish Geological Survey |
| H | Hydrogen |
| He | Helium |
| Hg | Mercury |
| HHI | Herfindahl-Hirschman Index |
| hhXRF | Handheld X-ray Fluorescence |
| Ho | Holmium |
| ICP-MC-MS | Inductively-Coupled Plasma Multi Collector Mass Spectrometry |

| | |
|---|---|
| ICP-MS | Inductively-Coupled Plasma Mass Spectrometry |
| ICP-OES | Inductively-Coupled Plasma Optical Emission Spectrometry |
| INAA | Instrumental Neutron Activation Analysis |
| ISMC | Iberian Sustainable Mining Cluster |
| ISO | International Organization for Standardization |
| km | Kilometer |
| KSD | Kolmogorov–Smirnov Test |
| La | Lanthanum |
| LA-ICP-MS | Laser Ablation Inductively-Coupled Plasma Mass Spectrometry |
| LA-MC-ICP-MS | Laser Ablation Multi Collector Inductively-Coupled Plasma Mass Spectrometry |
| LA-QQQ-ICP-MS | Laser Ablation Triple Quadrupole Inductively-Coupled Plasma Mass |
| LDA | Linear Discriminant Analysis |
| Li | Lithium |
| LIBS | Laser-Induced Breakdown Spectroscopy |
| LOD | Limit of Detection |
| LOD | Limit of Detection |
| LOQ | Limit of Quantification |
| LRM | Linear Regression Model |
| Lu | Lutetium |
| Ma | Million Years |
| MaDiTraCe | Material and Digital Traceability of Critical Raw Materials |
| MC-ICP-MS | Multicollector Inductively-Coupled Plasma Mass Spectrometry |
| Mg | Magnesium |
| MIC | Microwave Induced Combustion |
| MLA | Mineralogy |
| Mn | Manganese |
| Mo | Molybdenum |
| MW | Microwave |
| n | Number |
| na | Not Attributable |
| Na | Sodium |
| Nd | Neodymium |
| Nda | No Data Available |
| Ni | Nickel |
| O | Oxygen |
| OECD | Organisation for Economic Co-operation and Development |
| P | Phosphorous |
| Pb | Lead |
| PCA | Principal Component Analysis |
| Pr | Praseodymium |
| Rb | Rubidium |
| REE | Rare Earth Element |
| RFID | Radio-Frequency Identification |
| RJC | Responsible Jewellery Council |
| S | Sulfur |
| Sb | Antimony |
| Sc | Scandium |

| | |
|---|---|
| Se | Selenium |
| SEM | Scanning Electron Microscope |
| Si | Silicon |
| Sm | Samarium |
| Sn | Tin |
| Sr | Strontium |
| T | Temperature |
| Tb | Terbium |
| Te | Tellurium |
| TGA | Thermogravimetric Analysis |
| TGC | Total Graphitic Carbon |
| Th | Thorium |
| Ti | Titanium |
| TIMS | Thermal Ionization Mass Spectrometry |
| Tl | Tellurium |
| Tm | Thulium |
| U | Uranium |
| UN | United Nations |
| US | United States |
| USP | Unique Selling Point |
| V | Vanadium |
| VOC | Volatile Organic Compound |
| VPDB | Vienna Bee-Dee Pelemnite |
| W | Tungsten |
| WGC | World Gold Council |
| WMD | World Mining Data |
| WP | Work Package |
| wt% | Weight Percent |
| XRF | X-ray Fluorescence |
| Y | Ytterbium |
| Yb | Ytterbium |
| Zn | Zinc |
| Zr | Zirconium |

# List of Figures

# List of Tables

# Table of Content

# 1. Introduction

This introduction provides background information on the involvement in projects related to the traceability of mineral raw materials, the choice of graphite as the research material for the PhD thesis and the subsequent continuation of the research through the current MaDiTraCe project. It also emphasizes the importance and potential impact of traceability in the raw materials industry and sets the stage for the subsequent chapters, where I will provide details of the research and present the findings.

The thesis can be traced back to the project CERA4in1 (Certification of Raw Materials) project, which received funding from the EIT Raw Materials program. The Chair of Geology and Economic Geology assumed responsibility for work package 2, which involved the evaluation and development of proof of origin methods for mineral raw materials. Although the project commenced in early 2017, my involvement began towards the end of 2019 when I joined as a project staff member at the Chair of Geology and Economic Geology. At the beginning of 2022, thanks to a grant from the BMF (Bundesministerium für Finanzen), obtained through the RIC (Resources Innovation Center) at Montanuniversität Leoben, I was able to resume the development of methods for analytical proof of origin.

My personal motivation stems from my profound interest in the possibility of traceability for raw materials based on attributes directly related to the raw material itself, such as trace elements or isotope ratios. I strongly believe that this research topic will gain significant relevance in the coming years, as European and international legislation is rapidly emerging, necessitating compliance from companies that often lack solutions. Even industry giants are establishing departments for sustainable raw material procurement, employing geologists and sociologists together to tackle these issues. Thus, it becomes imperative for research to support industry and pave the way forward, as scientists should serve as thought leaders.

Returning to the research topic, the traceability of raw materials, particularly graphite, remains largely unexplored. In the first stage of the development of a proof of origin for graphite, the focus is on distinguishing between different economically significant graphite deposits distributed worldwide. The scope is global. Only once the deposit and the correlating traded product, namely the graphite concentrate, is identified, one can proceed to trace the processed raw materials along the whole supply chain.

This thesis primarily addresses the initial stages of the supply chain, specifically mining and the resulting processed product, known as concentrate. The raw ore corresponding to each concentrate was not available for every economically relevant graphite mine. Hence, the analysis primarily involves concentrates, which undergo basic processing steps such as grinding, milling and flotation to separate the ore from the surrounding rock. In this initial step, no chemical treatment of the ore takes place, making graphite an interesting material for analytical proof of origin, as there are minimal chemical reactions involved in the first steps.

Several parameters were utilized to differentiate between various graphite deposits, including carbon isotope ratios, trace elements, grain sizes and crystallinity. These parameters were determined through a preliminary study, conducted in 2021.

In this thesis, a comprehensive examination of the issues related to the certification of raw materials has been worked on, focusing not only on the broader context of raw material supply chains and the issues related to it, but also delving into the specific case of fingerprinting graphite. By addressing the challenges faced, developing and describing analytical methods, processing and documenting the outcomes of the research, this thesis aims to contribute to the understanding and development of proof of origin methods for mineral raw materials and provides an outlook and recommendations for advancing research on tracing graphite origins.

# 2. Literature Review on Existing Proof of Origin Methods and (Raw) Materials

Methods for traceability for non-mineral (raw) materials, such as food and other organic substances are presented, as well as other applications of traceability. Research on fingerprinting has gained importance, especially in the last two decades and in the last years many initiatives and research projects had been initiated. A lot of further publications, especially on critical raw materials and raw materials needed for the Green Transformation, can be expected in the coming years. The chapter highlights the evolving landscape of research, new initiatives and the increasing focus on critical raw materials and materials required for the Green Transformation. Most of the literature review on mineral commodities had been done for a deliverable for the CERA project and has now been supplemented with recent work on mineral commodities. The list and descriptions from the CERA report were published in 2021 in the article "Analytical Proof of Origin for Raw Materials" (Melcher et al. 2021). It should be noted that the list of selected non-mineral raw materials is not exhaustive and shows only prominent examples and serves as an inspiration for the current work.

## 2.1. Exploring the Origins of this Research Topic: Archaeometry - A Multidisciplinary Branch of Science

### 2.1.1. Definition

Before going into more detail about analytical proof of origin methods, the origin of analytical provenance must first be clarified. It lies in another research discipline, namely archaeometry. Archaeometry encompasses the development and also the use of scientific methods to solve cultural-historical questions. This includes the interdisciplinary participation of the biological sciences, chemistry, earth sciences and physics from the natural science side and the archaeological disciplines, art history, historic preservation, and restoration from the cultural history side (GNAA – ARCHAEOMETRIE e.V 2024). In addition to important methods for age determination, such as the $^{14}C$ or radiometric age determination, there are a number of other applications of the methods for the proof of origin on finds from earlier times. Common finds represent coins, e.g. gold, silver or copper, as well as ceramics or glasses, tools or swords.

### 2.1.2 Examples

The origin of gold found on plaques for swords from the Early Bronze Age in Saxony-Anhalt was compared to naturally occurring gold from Cornwall. Trace element analysis was carried out using LA-ICP-MS (Co, Ni, Pd, Ag, Sn and Sb) and showed similar signatures to the naturally occurring gold from the Cornon river gold deposit. This important finding would thus prove the close cultural relationship between the British Isles and Germany in the early Bronze Age and a development of trade (Ehser et al. 2011).

Trace element and Pb isotopic analyses in Celtic Gold Coins were carried out to explore whether there is a connection between gold deposits and Celtic gold coins. Important findings from this are that any

alloying addition to a gold coin makes it impossible to assign the sample to a gold source, since silver, copper, lead and antimony are the main alloying components, but on the other hand they are the main impurities/trace elements of a gold source. Only non-alloyed artifacts can thus be used to assign them to their origin. Furthermore, the overlap of geochemical signatures in placer deposits complicates the the research question (Bendall et al. 2009).

Another prominent example from the connection of geoscientific and cultural-historical research is the origin of the Venus of Willendorf, a small prehistoric figurine, discovered near Willendorf, a town in lower Austria, that remained a mystery since its discovery more than 100 years ago. Chronologically, the Venus Oolite could be assigned to the Mesozoic, based on the sampling of many other Oolite Limestone occurrences in Europe within a radius of 2500 km from the site of discovery. The grain size distribution of the natural occurring rocks is compared to an existing database (analysis of oolite from up to 2500 km distance from site of discovery) to proof the origin, which resulted to be the region around Lake Garda in Italy (Weber et al. 2022).

Pre-historic and cultural interactions during the Neolithic in Germany were analyzed by determining the provenance of amphibolitic raw material used for axes by elemental and Sr, Pb isotopic methods. This combination of geochemical and isotopic data provided a valuable tool for identifying the provenance of stone material used as various tools. Reference samples from Fichtelgebirge in Germany and Jistebsko in the Czech Republic were collected and analyzed before, to compare unknown samples to (Christensen et al. 2006).

The research that emerged from this multidisciplinary branch of science was also transferred to the modern era and one was first faced with questions about the provenance of gemstones (jewelry). The determination of identity, origin (natural or synthetic), geological or geographical origin also describes the value of the gemstone.

## 2.2. Literature Review on Mineral Raw Materials

### 2.2.1. Excerpt of Literature Examples

Gemstones are considered one of the first obviously valuable raw materials of human mankind and are therefore briefly described:

Emerald samples from 62 occurrences and 19 different countries were differentiated by using O isotope ratios, which serves as an important parameter to distinguish different deposits. The samples from Russia, Brazil, Madagascar and Zambia however overlap by just using O isotope ratios as a single parameter (Giuliani et al. 1998).

O isotope analyses using laser-fluorination techniques were carried out and combined with gemological parameters, such as color, clarity, cut and others to allow the discrimination between ruby and sapphire from different deposits worldwide (Giuliani et al. 2005).

LA-ICP-MS analyses on tourmalines from three different countries (Nigeria, Mozambique and Brasil) were performed to differentiate their origin by using bivariate and ternary diagrams of Ga, Pb, Cu, Mn, Be, Mg, Zn, Pb and interelement ratios (Abduriyim et al. 2006).

Other raw materials and the analytical methods used are described in detail in (Melcher et al. 2021). Table 1 serves as an overview for existing proof of origin methods for mineral raw materials.

*Table 1:Analytical proof of origin methods used for mineral raw material provenance analysis elaborated until 2019*

| Raw material | Method & Parameters | Regional focus | References |
|---|---|---|---|
| **3T (Ta, Sn, W) concentrates** | AFP: combination of MLA (mineralogy) and ICP-MS (mineral chemistry) | Central Africa | (Melcher, 2008) ; (Martyna et al. 2018) ; (Gäbler et al. 2011) ; (Gäbler et al. 2013) ; (Gäbler et al. 2017)) |
| **3T (Ta, Sn, W) concentrates** | LIBS (Mineral chemistry) | | (Harmon et al. 2011) ; (Hark et al. 2012) |
| **Gold** | LA-ICP-MS (Mineral chemistry) | South Africa, South America | (Dixon 2014) ; (Dixon and Schouwstra 2017) ; (Roberts et al. 2016) (Dixon and Merkle 2019) |
| **Gold** | LA-ICP-MS (Mineral chemistry) | W Australia, South Africa | (Watling et al. 1994) |
| **Gold** | LA-ICP-MS (Mineral chemistry) | Central Europe | (Schmiderer 2008) |
| **Diamonds, chromite, garnet** | LA-ICP-MS (Mineral chemistry) | worldwide | (Watling et al. 1995) |
| **Diamonds** | LA-ICP-MS (Mineral chemistry) | | (Dalpé et al. 2010) |
| **Diamonds** | Morphology, FTIR, LA-ICP-MS | African countries | (Coney et al. 2012) |
| **Platinum ores and intermediate products** | Complex Procedure for Identification of the Nature and the Source of Origin of Precious Metals Containing Products of Mining and Metallurgical Operations | Russia, South Africa | (Perelygin et al. 2008) |
| **Heterogenite** | Raman spectroscopy; chemistry, U-Pb dating | Katanga, DR Congo | (Burlet et al. 2011) ; (Decree et al. 2014) ; (Decrée et al. 2015) |
| **Massive sulphide deposits** | Microtexture, EMPA | Urals versus Spain | (Machault 2012; Machault et al. 2014) |
| **Uranium ore concentrates, yellow cake** | ICP-MS (ore chemistry), TIMS (Pb isotopes) | Australia | (Švedkauskaitė-LeGore et al. 2008) |
| **Uranium ore concentrates** | ICP-MS, XRF, TIMS, SIMS | Australia | (Keegan et al. 2008) |
| **Yellow cake** | LIBS | worldwide | (Sirven et al. 2009) |
| **Phosphate fertilizers** | ICP-MS, MC-ICP-MS, TIMS | worldwide | (Sattouf et al. 2008) |
| **Emerald** | $^{18}O/^{16}O$ isotopes | worldwide | (Giuliani et al. 1998; Giuliani et al. 2005) |
| **Marble** | C-O isotopes, trace elements, fluid composition | Mediterranean area | (Attanasio et al. 2013) ; (Attanasio et al. 2015) ; (Prochaska & Grillo 2010; Prochaska 2013) |
| **Vermiculite** | Chemical composition by INAA, XRF | USA versus foreign materials | (Wright & Palmer 2008) |
| **Gemstone (tourmaline)** | Trace elements (LA-ICP-MS) | Brazil, Nigeria, Mozambique | (Abduriyim et al. 2006) |

### 2.2.2. Recently Published Work on Analytical Proof of Origin Methods

The effectiveness of laser-induced breakdown spectroscopy (LIBS) as a portable tool for quantifying the silver content in natural gold was examined. The study involved the analysis of commercial gold alloys, natural gold and unidentified samples, which were successfully matched to their respective origins by referencing a comprehensive database (Pochon et al. 2020).

A three-step approach was developed to identify illicit gold from French Guiana a conflict-affected area with widespread illegal mining. In the first step they revealed Hg amalgamation with either optical microscopy or handheld methods such as LIBS. The Ag content of a gold grain population referenced against KSD statistics provides information about the origin. Also, minor and trace elements assessed by LA-ICP-MS together with the use of a multivariate statistics were used as a robust tool to differentiate between different deposits in almost 70 % of the investigated cases. The remaining 30 % of the samples cannot be differentiated due to their geological similarity to other populations (Pochon et al. 2021).

Diamonds can be certified by distinguishing between two specific types of spectral features, namely elemental emission peaks and emission clusters of C-N and C-C molecules analyzed by laser-induced breakdown spectroscopy and emission peaks. The origin signal is directly contained in the carbon structure. C-N molecule emission peaks are associated with the N concentration of the diamond. The molecular C-C intensities fluctuate based on the bond strength between carbon atoms and the presence of elemental impurities (McManus et al. 2020).

The use of Li isotopy as a fingerprint for Li in raw ores and intermediates was also investigated. Although Li isotopy seems to change during beneficiation, it remains a reliable tool for determining origin and paves the way for a new method to ensure the certification of lithium in lithium-ion batteries. Although the Li isotope primarily only allows the distinction of the deposit type, namely brines and spodumene, certain deposits or geographic origins can still be distinguished from each other (e.g. South America and Australia) (Desaulty et al. 2022).

## 2.3. Traceability Methods for Non-Mineral Raw Materials Such as Food, Organic Substances and Beyond

### 2.3.1. Examples

Not only mineral raw materials, but also other products of our daily life are subjected to the analytical proof of origin.

Numerous research investigations have focused on the analysis of pumpkin seed oil. A notable study aimed to differentiate and categorize the geographical origins of pumpkin seeds sourced from Austria, China, and Russia. Their approach involved the measurement of stable isotope ratios, namely hydrogen, carbon, and nitrogen, as well as the evaluation of trace elements, particularly rare earth elements (REE). By employing a combination of two or more parameters, this methodology enables a differentiation among specific localities and, crucially, distinguishes between domestically produced and foreign-sourced materials (Bandoniene et al. 2013).

Another investigation was conducted on the incorporation of rare earth elements (REE) into tomato plants. Dissolved forms of REE were added to the substrate of tomato plants and the uptake of REE by the plants and their subsequent incorporation into the fruit (tomato) was analyzed. Remarkably, even when administered in very small quantities and for a short duration (rather than the entire growing season), the REE exhibited significant labeling effects on the tomatoes (Bandoniene et al. 2018).

REE patterns, specifically terbium and thulium, had been examined in eggs and chicken products, such as meat and bones. To achieve this, laying hens were provided with a controlled diet containing low

levels of REE. The researchers successfully achieved REE labeling in all sample types through the use of spiked chicken feed, demonstrating the effectiveness of this approach. The REE analysis was performed using both conventional techniques and laser ablation inductively coupled plasma mass spectrometry (LA-ICP-MS) (Bandoniene et al. 2018).

The provenance of flower bulbs was assessed through the correlation of isotope fingerprints and chemical fingerprints. Specifically, the study focused on the analysis of $^{12}C/^{13}C$, $^{14}N/^{15}N$, and $^{16}O/^{18}O$ isotopes to differentiate between materials originating from Europe and China. The investigation successfully achieved this separation, highlighting the efficacy of isotope fingerprinting in determining the geographic origin of flower bulbs. Additionally, the study also employed volatile organic compound (VOC) patterns to further distinguish between different groups. Notably, the VOC patterns allowed for the classification of three distinct groups: flower bulb materials from The Netherlands, other European Union (EU) countries, and China. This comprehensive analysis of both isotope and chemical fingerprints proved instrumental in discerning the origin of flower bulbs with enhanced precision (van Ruth and Visser 2015).

Published proposals for proof of origin methods do not always contain analytical methods only. Often, artificially added tracers or even managerial instruments, such as documents are also used as proof of origin.

Technical, managerial and environmental key issues were defined that need to be considered in the food supply chain and propose a set of technical instruments for traceability. Their research proposes a range of technical tools for traceability. Various technologies, including alphanumeric codes, barcodes, radio frequency identification tags (RFID), and Wireless Sensor Networks, were analyzed. However, it was determined that none of these methods offers comparable efficacy to analytical fingerprinting, which enables the examination of the authentic DNA of the product. In this study, artificial tracers are utilized as "fingerprints" to facilitate accurate traceability within the food supply chain (Aung and Chang 2014).

Isotope analysis was proposed as a parameter for food traceability, while pointing out that advancing technology also brings enormous benefits for food traceability, including increased efficiency and effectiveness. Wireless monitoring devices such as RFID (radio-frequency identification) have improved enormously, but none of these methods is capable of meeting all the requirements of the heterogeneous food supply chain. New advancements such as DNA barcoding can fill some of the gaps, but are prohibitively expensive for many agents of the food chain (Badia-Melis et al. 2015).

An analysis of the impact of traceability concepts on contemporary supply chain management was conducted. The study primarily focuses on two key aspects: firstly, exploring the influence of traceability concepts on supply chain management practices, and secondly, discussing future trends and perspectives in this field. The authors emphasized that the increasing consumer demand for food products with specific attributes, such as ethical sourcing, organic production, and reduced carbon footprint, necessitates the implementation of robust and efficient traceability systems. To achieve this, they suggest integrating traceability techniques with complementary tools like Hazard Analysis and Critical Control Point (HACCP) and production planning. This integration would enhance the effectiveness and reliability of traceability systems, thereby meeting the evolving demands of the modern food supply chain (Dabbene et al. 2014).

# 3. The Analytical Proof of Origin

## 3.1. Traceability: Definitions and Perspectives

Given that the term **traceability** will be frequently referred to in this study, it becomes imperative to provide a clear and precise definition for this term (Table 2). In essence, traceability is intrinsically linked to the availability of information. However, it is crucial that this information is generated at the outset of the value chain, whether it is related to mineral resources, food products, or any other goods. The information is subsequently traced throughout the supply chain, ultimately reaching the end of the chain, ideally visible to the consumer in the final product. Thus, access to information becomes vital in achieving traceability, facilitating informed decision-making processes, which are highly valued. There is an increase in the need to know more about the where and how (raw) materials of our daily lives were mined but also as a result of intervention by regulators, such as the European Union, who are now mandating more transparency in supply chains than ever.

Another term associated with traceability is **provenance**. Provenance and traceability are not the same. Transparency and trust are not simply interchangeable. Trace and track are not the same. Provenance describes a single point of origin, while traceability is the ability to trace back. Arguably, the associated **transparency** refers to the familiar chronological proof of ownership, also known as chain of custody. All of these devices of transparency of a supply chain refer to shared information to various stakeholders in the supply chain.

### 3.1.1. Delimitation of This Study with Respect to the Above-Mentioned Terms

In this graphite provenance study, samples were assigned only to their origin. The verification or determination where the samples came from was made by analyzing the sample (concentrate) itself. This does not provide any information about traceability. Describing the proof of origin as traceability is fundamentally misleading and confusing for stakeholders looking for solutions to specific supply chain needs and problems. Nevertheless, knowing the origin also lays the foundation for traceability purposes.

What is the purpose of this study? Track? Trace? Verify? It is a verification of the origin of the sample (intermediate product/concentrate). No tracking and tracing were conducted in this study. But still, it is an important feature to limit the risk for consumers, but also for any retailer and also supplier. Ensuring transparency, traceability and resilience within our supply chains, necessitates the establishment of a comprehensive infrastructure.

### 3.1.2. Definitions and Literature

*Table 2: Different definitions for traceability, listed from oldest to most recent*

| Author and Year | Definiton |
|---|---|
| **(Moe 1998)** | Traceability is the ability to track a product batch and its history through the whole, or part, of a production chain from harvest through transport, storage, processing, distribution, and sales. |
| **(Lamming et al. 2001)** | Transparency is translucent with limited exchange, transparent with full and free exchange; two-way exchange of information and knowledge between customer and supplier. Certain level of transparency is needed for achieving traceability. |

| | |
|---|---|
| **(Jansen-Vullers et al. 2003)** | Traceability can be viewed in a passive and in an active sense based on its use. In the passive sense, traceability provides the visibility to where items are at all times and their disposition. But in an active sense, the on-line tracking information is additionally used to optimize and control processes in and between the different links of the supply chain in addition to keeping historical records by means of recorded identification. |
| **(Skilton & Robinson 2009)** | Supply chain transparency, defined on a network level as a state or mode of being, is the extent to which information about sources, processes, and relationships is readily accessible to counterparties in an exchange and to outside observers. |
| **(Olsen & Borit 2013)** | The ability to access, through recorded identifications, all information related to the object under consideration throughout its life cycle They pointed out the difference between having traceability and verifying the claims in a traceability system by analytical tools and methods. This includes systematically recording properties and some of these can be verified by analytical tools and methods. |
| **(van Ruth and Visser 2015)** | Authenticity of origin by analytical tools |
| **(Souali et al. 2017)** | Traceability is the ability to maintain a detailed history of all activities and changes that a particular object may experience throughout its life cycle, taking into account the various relationships that may occur. This particular object can be a material, a product, a model, or even a class in a software development platform. |

## 3.2. Does Provenance Matter? Exploring Consumers Perspectives, Regulatory Frameworks and Governmental Impact

Consumers simply lack access to information regarding the mineral raw materials contained in products they purchase, limiting their ability to make informed decisions. There is a growing demand for visibility into the movement of material throughout the entire supply chain. From the mine to the processing plant, factory, customer and beyond, there is an interest for traceability at every stage. The information generated at the very beginning of the supply chain, namely provenance must be verified, traced throughout the supply chain and shared with relevant stakeholders, which also includes customers in the end. At least since the collapse of many supply chains as a result of the Covid-crisis and the Russian war against Ukraine, the interdependence of the world economy has reached the awareness of the broad public society. Both of these miserable events shifted the focus to supply chain resilience. The systems had shown to be fragile and not resilient at all. This realization has raised concerns about consumer trust, social license and the freedom to operate. The scarcity of essential raw materials due to supply bottlenecks during these events highlighted interest in the origin of consumer goods and the provenance of raw materials in general. Furthermore, global production has undergone significant changes, with various industries being distributed across different countries within global production networks. This necessitates the establishment of global rules for companies, which will be addressed by future supply

chain laws. Governments and regulators are already acting as society' s interest in responsible raw material extraction grows and legislative pressure increases (Dietrich and Melcher 2022).

The EU Conflict Minerals Regulation, based on the OECD Due Diligence Guideline (OECD 2016), applies globally and imposes supply chain obligations on importers of tin, tantalum, tungsten and gold sourced from conflict-affected and high-risk areas. The US Dodd-Frank Act, since 2010, requires disclosure and reporting from US listed companies using specific raw materials from the Democratic Republic of Congo (DRC) and neighboring countries (Dodd-Frank Wall Street Reform and Consumer Protection Act). The European Supply Chain Act, effective from 2023, mandates EU companies to address human rights violations and environmental damage in their supply chains, regardless of the raw material involved (ibid.; COM: Proposal for a Directive Of The European Parliament And Of Proposal for a Directive of the European Parliament and of the Council on Corporate Sustainability Due Diligence and amending Directive EU (2019/1937) ing Directive (EU) 2019/1937 2021). The UK Modern Slavery Act, implemented in 2015, aims to eradicate modern-day slavery in business operations and global supply chains (Modern Slavery Act 2015). In December 2020 the EU Commission proposed the EU Battery Regulation, which will replace the Battery Directive from 2006 and includes battery categories such as transport batteries, industrial batteries with a capacity above 2kWh and electric vehicle batteries (The European Parliament and the council of the European Union, battery regulation).

These legal obligations are crucial for prompting company action. More raw materials, especially critical ones, and conflict regions are expected to be included in these regulations. Certification systems and initiatives have emerged in the past 20 years to address these challenges, although they often focus on specific raw materials or segments of the value chain. Harmonization among these systems is urgently needed (Dietrich and Melcher 2022).

## 3.3. Geo-based Analytical Proof of Origin: Mechanisms, Functionality and Opportunities

The geo-based Analytical Proof of Origin describes analytical/geochemical methods and mathematical and statistical procedures and evaluation methods to proof the origin of (mineral) raw materials. Analytical provenance is also used to verify the origin of raw materials and is a forensic tool that can be used when the origin of a raw material needs to be verified or even when there is doubt about the origin. The result of these analytical methods is a fingerprint, which is ideally not corruptible throughout the entire supply chain and refers to the chemical/mineralogical composition of the raw material itself. Mineral raw materials in general are extracted from a wide variety of deposit types. Each deposit type is to be found in a special geological setting, with special geological properties and features, therefore they inherit unique natural characteristics to the location, deposit or mine from where the raw materials originate.

### 3.3.1. How? The Approach to Analytical Fingerprinting and Providing the Scientific Evidence

From reviewing literature of existing APO methods for specific raw materials (Melcher et al. 2021) a general work flow emerges that is characterized by analytical procedures and data processing and can be applied in modified forms for different raw materials. However, each raw material has to be treated separately. There is no standardized work flow and recipe for raw materials and the methods to be applied have to be re-evaluated for each raw material. If the availability of samples is given, a distinction must be made between raw ores, rocks, minerals and concentrates. According to this, the further steps of sample preparation may be as follows: crushing, grinding, sizing, preparation of thin sections or polished blocks, dissolution, pellet pressing and others if necessary. Then the analytical workflow must be discussed. This can happen in a separate preliminary study to identify the properties of the material or already emerges from the experience of the processors. The next step is the data evaluation, containing

data reduction and pre-processing, before applying various statistical methods. Different types of data can be generated. The results from analytical work must also be reproducible and a sufficient amount of data must be available, in order to be able to continue working with it and to be able to perform (multivariate) statistics. Following this statistical data evaluation and analysis a reference database containing geochemical and mineralogical properties of known deposits must be established in order to be able to compare future samples with unknown origin to this database. This database needs to be updated and enlarged regularly. APO works only with comparing unknown (daughter/reference) samples to a database (also daughter samples). The reason for the comparison between daughter samples along the same level and not in relation to mother-daughter is the fact that a mother sample would represent all parameters of a deposit. Only some aspects of a deposit can be captured through the daughter sample, never the entire deposit. Reference samples and sample to be identified contain the same level of information. The output is information about the origin and weather is could be identified (referred to a sample in the database) or not.

Figure 1 presents a concept for establishing the geo-based proof of origin through a multi-step approach. The workflow starts with the sample collection, followed by the sample preparation and the application of analytical methods. All of the obtained data is then subjected to data processing, data reduction and various statistical methods, finally leading to a robust database, which serves as the foundation for the determination of the proof of origin. Only samples that refer to the database, can be identified, otherwise they are attributed to an unknown origin.

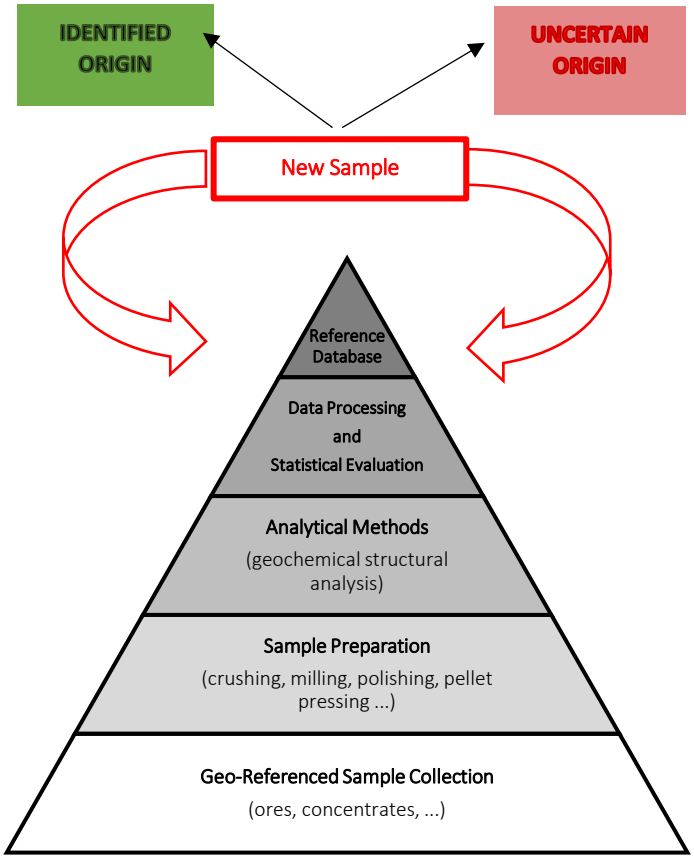


*Figure 1: Concept of a geo-based proof of origin*

### 3.3.2. Advantages and Opportunities

The application of APO methods in the mineral resources sector will bring a number of advantages. It is a powerful tool to ensure quality, safety and authenticity.

- Creates trust and enhanced raw material authentication
- Contaminant detection: Detection of undesirable by-products or elements
- Increased consumer awareness and informed-decision making for consumers: Consumers can choose products based on their budget or preferences, supporting local or sustainable companies and avoid regions with potential concerns on e.g. environmental or ethical issues, which fosters a more conscious marketplace in general
- Increased supply chain transparency and resilience: By verifying the product origin it becomes possible to establish a clear chain of custody from the mine (source) to the consumer and serves as a quality assurance
- Marketing Opportunity and USP (Unique Selling Point): The quality and distinctiveness associated with a special geographic origin can be a very powerful selling point
- Regulatory compliance: Meeting the needs from political/governmental measures
- Process optimization and quality control: manufacturing processes can be optimized by identifying critical parameters that affect the quality of the (intermediate) product
- Strong market interest and security for producers: APO helps to preserve the economic value of regionally specific raw materials/products, it allows producers to help to defend their reputation
- Sustainability aspects along the supply chain can be considered (knowing where the product comes from, can also estimate how much $CO_2$ it has emitted and under which conditions it has been mined and/or produced)

### 3.3.3. Limitations, Challenges and Pitfalls

**Technical Challenges:**

- Time-consuming procedure, if complex laboratory methods have to be applied: Sample preparation for analysis (e.g. solution analysis) is usually time-consuming, complex and expensive
- Equipment, expertise (trained personnel) and resources can be very expensive especially in underdeveloped regions or for small-scale producers
- Lack of Harmonization: Certified lab techniques and devices, reference databases and standardized lab protocols need to be widely available for a widespread acceptance
- Inconsistencies across different countries and labs: Establishment of certified laboratory facilities (analytical devices and staff); modern and well-equipped technical laboratory facilities must be available

**Obstacles:**

- Host frameworks need to be developed (harmonization and standardization)
- In early stages, with limited awareness, the benefits might be minimal (cost/use ratio); persuasion needs to be done (regulatory impact from governments might help)
- Most traceability solutions until now are based on digitalization, such as blockchain technologies
- A database needs to be built for each raw material, i.e. samples can only be identified by correlation to a reference sample.

**Limitations and Pitfalls:**

- The APO has only been developed for a few mineral raw materials (Table 1). There may also be no natural way of tracing for some raw materials due to various aspects, such as chemical processing in an early stage of the supply chain.
- Altered signatures: post-production treatments and mineral processing can modify or mask the original geochemical signature of a mineral raw material
- Blending of materials: Mixed signatures can hardly be traced back to one certain place of origin
- Overlapping signatures and natural variations: Multiple factors such as weathering, diagenetic processes and host environment influence geochemical signatures of raw materials. These factors are highly variable within a given region or deposit and might cause overlapping signatures.
- Garbage in-garbage out problematics: If poor or even wrong information enters the system, misleading information will come out (e.g. when sample material is not geo-referenced)
- Criminal activity might cause false information
- Access to sample material: Sample material from certain regions may not be accessible
- Equipment and expertise not available at all

To conclude it, a probability might be provided indicating the likelihood that the unknown sample matches a known sample from the database. The higher the number of producers/mine in the database, the higher the probability that an unknown origin of samples can be identified with a high degree of certainty.

## 3.4. Artificial Tracers: Exploring Innovative Methods for Ensuring Supply Chain Transparency

This study focuses on chemical/mineralogical compositions of mineral raw materials. It does not encompass methods such as labeling (e.g., barcodes, QR codes or RFID), documentary traceability (blockchain), or the use of artificial tracers. Artificial tracers are materials intentionally introduced into a product to enable its traceability. While these alternative methods do exist and possess their own merits, they are susceptible to potential falsification and do not directly relate to the composition of the raw material itself. Based on the chemical/physical properties of the material there are a variety of taggants available, such as chemical or physical taggants. Barcodes and QR codes, RFID tracers or even added REE are incorporated into materials. The use of a combination of blockchain and physical tracking technologies to enable traceability within raw materials supply chains was applied to bridge gaps by increasing transparency in supply chains by combining two different traceability methods (Bacchetta et al. 2021).

## 3.5. The Application of APO in Research Projects: CERA4in1 and MaDiTraCe

It must be stated, that APO plays a minor role in most certification systems and is not a standard application, but in some cases (with increased demand) it has already become a routine application (especially gold, gemstone and diamonds). The problem with certification schemes for mineral commodities is as follows: There are already a number of certification schemes existing, all of which either target only specific commodities, or are applicable to only part of the value chain. Examples of commodity-specific certification schemes, already on the market are the Bettercoal Code ( (BetterCoal), applicable to coal materials, or Fair Stone (Fair Stone 2018) and Xertifix (XertifiX 2024) for natural stones and the Aluminum Stewardship Initiative for the aluminum industry (Aluminium Stewardship Initiative 2022). Furthermore, the well-known Kimberley Process for diamonds (The Kimberley Process (KP) | KimberleyProcess 2024) and the RJC (Responsible Jewellery Council 2024) for diamonds and other gemstones. There are also a number of certification systems for gold, such as Fairmined (Alliance

for Responsible Mining) or the WGC (World Gold Council). So far, there is no single certification system that covers all mineral raw materials and all areas of the supply/value chain. Due to the above facts such as the non-harmonization among certification systems, there have been EU-wide efforts to develop and also establish certification systems for raw materials for several years. APO is expected to play a role in both of the projects mentioned below and provide important and trustworthy commodity-specific information. One of these projects was the CERA4in1 project (2017 - 2021). This project aimed to establish 4 sub-standards within one certification system. The four sub standards cover each area of the supply chain from exploration to the final product, as a label, visible to the consumer. These sub standards refer to different areas in the supply chain, which do not have the same requirements for certification, but should nevertheless be included in one system. Thus, each participant in the supply chain should receive an individual solution tailored to the area of the supply chain. CERA4in1 aimed to be the first certification system for raw materials that captures and considers its complexity, making it the first system adapted to all mineral raw materials and to each area of the supply chain.

The 4 sub standards can be described as followed:

- The CERA 4in1 Readiness Standard (CRS) governs the objectives for evaluating a deposit in terms of social and environmental issues during the exploration process.
- The CERA 4in1 Performance Standard (CPS) applies to a production facility or group of production facilities and covers mining, processing and refining.
- The CERA 4in1 Chain of Custody Standard (CCS) refers to the product and establishes criteria to ensure full traceability of responsibly sourced raw materials and traded goods.
- The CERA 4in1 Final Product Standard (CFS) certifies a final product made from raw materials that have been sustainably sourced and traded.

The overall system is supposed to lead to a certification of the entire trade chain of primary and secondary raw materials. The follow-up project is MaDiTraCe (Material and digital Traceability and Certification) (https://lgi.earth, LGI Sustainable Innovation - Maditrace 2024). Here, the CERA 4 in1 approach will further be pursued. The main objective of MaDiTraCe is to expand and integrate the portfolio of technological solutions to improve the reliability of critical raw material tracking (CRM) and the transparency of complex supply chains. The project aims to develop and test independent digital and geo-based approaches to CRM traceability and integrate them into a general certification system throughout the mineral supply chain from mine to manufactured and recycled products. The project aims to increase the technical readiness level of experimental or largely untested methods in both digital and materials sciences. Special attention will be given to the complexity of mineral supply chains with points of material aggregation and transformation (processing, refining etc.) including circular economy (recycling). This methodology will allow downstream industries to demonstrate the reliability of their sustainability claims while complying with current regulations (in particular the EU Battery Regulation and the German Supply Chain Act) and anticipating the implementation of future regulations (EU Corporate Due Diligence Directive). MaDiTraCe's fundament is a strong stakeholder process, with upstream and downstream industrial players from mining to manufacturing industry and large networks involved via the consortia (EIT-RM) and clusters (ISMC – Iberian Sustainable Mining Cluster) participating in the project. Continuous interaction with this industrial and policy-oriented stakeholder community on the traceability technology and the certification schemes developed in the project will ensure to stay in line with industrial needs and expectations with respect to regulatory compliance.

## 3.6. Conceptualization and Analytical Approaches for the Proof of Origin of Graphite

One critical aspect in the determination of the significance of graphite lies in understanding its geographical origin, which can significantly impact its properties and suitability for various applications.

The ability to trace the provenance of graphite has become crucial in today's globalized market, where sourcing sustainable and ethically-mined materials is eminent. The concept for the proof of origin of graphite should be as robust and as consistent as possible. This approach to the Analytical Proof of Origin is the first ever for an industrial mineral. On the one hand, graphite is a raw material that undergoes only basic processing, i.e. in the first processing steps the raw ore is crushed and ground and then floated, on the other hand it is a very challenging material to work with due to its special properties (e.g. it is very brittle and prone to fracturing). This processing results in graphite concentrates with different concentrations, but mostly >94 % carbon. These concentrates are then passed on, which is the first point where the material is traded in the supply chain and leaves its place of origin. The basic processing happens mostly in or near the mine, as it is not economically viable to transport large quantities of raw ore, along with the surrounding rock. The proof of origin refers mainly to these traded concentrates.

The three-step approach described in this thesis is a powerful tool to proof the geographical origin of graphite. This approach focuses on the analysis of carbon isotope ratios, trace elements and crystallographic parameters found within the graphite sample material. Elements can be qualitatively classified into **major** (>0.4 wt %), **minor** (0.1–0.4 wt %), and **trace** elements (<0.1 wt %) (Lee 2019). Each deposit individually assembles trace elements based on geological processes and thus represents an individual tool to assign respective elements to specific geographic regions. The third factor to be considered are the crystallographic properties of the graphite assessed by Raman spectroscopy. (Rantitsch et al. 2016a) showed the differentiation of semi graphite and graphite by Raman spectroscopic investigations. It is a three-step approach whose individual parameters together result in a holistic approach for fingerprinting graphite and is therefore more robust than a one-step approach with the analysis of only one parameter. Each of these steps contributes insights to the material's history and geological formation, enabling to make informed decisions regarding the origin and authenticity of the graphite. An outlook on how to proceed in the future will be given in the last chapter of this thesis. In summary, as with many examples in the field of proof of origin methods, multi element analytics is the most significant tool for distinguishing the geographic origin of graphite concentrates.

Figure 2 illustrates the three-step workflow for the analytical proof of origin of graphite.

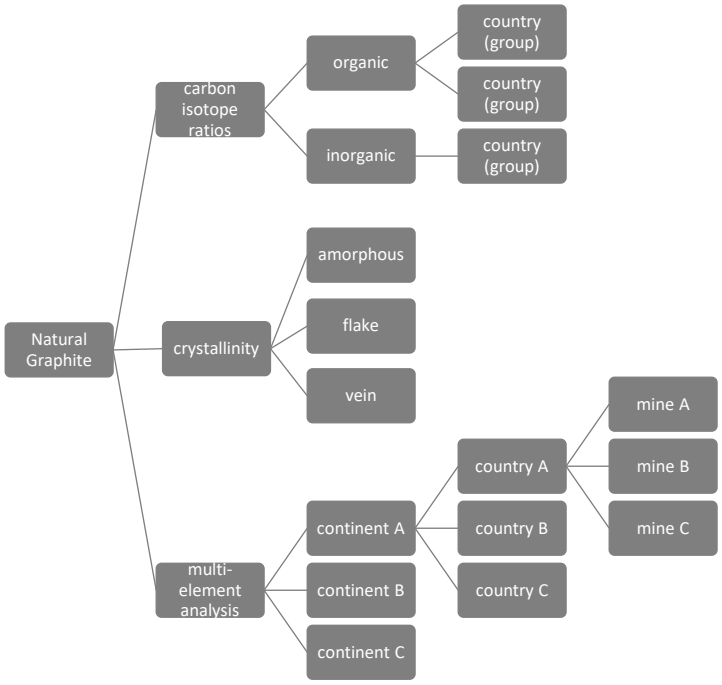


*Figure 2: Workflow Analytical Proof of Origin for Graphite*

# 4. Graphite

## 4.1. Introduction

Graphite, a raw material especially important for the transition to a low-$CO_2$ economy is used far beyond the well-known use in pencils. There is a large number of applications. The raw material is indispensable in lithium-ion batteries, which are built into laptops, smartphones and electric cars, graphite is the leading material for construction of bipolar plates which are then used in fuels cells, as well as the use in the steelmaking industry. For the production of graphene, graphite is used as electrical and thermal conductor. The rapidly growing market for Li-ion batteries has been driving the demand for graphite, thus increasing interest in the origin of this raw material. There is more graphite used in Li-ion batteries than any other raw material; the estimated demand for lithium for batteries only for e-mobility in 2030 is 32000 t, whereas the demand for graphite is 340000 t by 2030, which is more than 10 times more graphite needed than lithium in a low demand scenario. Another 99000 t of graphite (and 10000 t of Li) are needed in a low demand scenario by 2030 for batteries for renewables, such as solar and wind energy, as well as others for Europe only (Carrara et al. 2023). The use and importance of graphite in Li-ion batteries is often neglected (Tsuji 2022). More than half of the material used in Li-ion batteries is graphite. It can be replaced by synthetic graphite, which however is significantly more expensive and has a higher carbon footprint. Therefore, natural graphite will remain essential. Synthetic graphite is very costly to produce as the precursor material needs to be treated to very high temperatures >2500 °C for several days. The synthetic graphite is manufactured from calcined petroleum coke, coal tar pitch, anthracite or recycled synthetic graphite (Thrane and Kalvig 2019).

The estimated demand for graphite in the EU in 2030 for a low demand scenario is 342448 t/y and 595405 t/y by 2050 for strategic technologies and sectors only. The forecasted demand for graphite in 2030 worldwide is 1239286 t/y (world production 2022 1.7 t/y) and by 2050 9464128 t/y only for strategic technologies and sectors (Carrara et al. 2023). The growing demand for graphite, driven by the widespread application of rechargeable Lithium-ion Batteries (LIBs) into consumer goods and the electrification of mobility, has triggered a keen interest in its provenance.

## 4.2. World Production

In 2022 around 1,7 Mio tons of natural graphite were extracted worldwide (Reichl & Schatz 2024). Figure 3 showcases the dynamics of the global graphite production over a span of the past 38 years. Fluctuations and trends can be observed throughout the specified period. Technological advancements, economic developments and environmental factors have shaped the graphite sectors evolution.

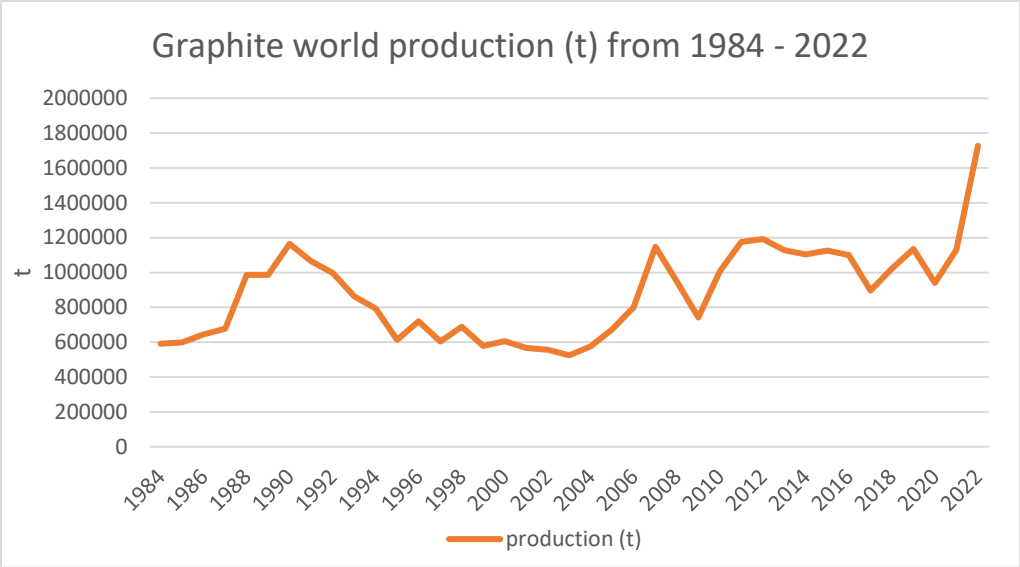


*Figure 3: Evolution of graphite world production from 1984 to 2022 (WMD)*

The graphite world production reaching its high in 2022 with a decrease in demand in 2009, 2017 and 2020 was due to less demand in the refractories industry. USGS reported a marked decrease from 2002 in the consumption of graphite electrodes, owing to the development of more efficient iron and steel production techniques during the late 1980s. The use of natural graphite in lubrication applications is also decreasing because of changes in requirements for lubricants and in processing technologies (Kalyoncu 2002; Olson 2009; Robinson et al. 2017; Olson 2020; Olson 2022).

### 4.2.1. Major Producer Countries

The supply of graphite is dominated by China with 67 % of the world graphite production in 2022, followed by Mozambique (9.61 %), Madagascar (6.76 %) and India (4.77 %). Other graphite producing countries (as seen in Table 3) have a share of 1 % or less of the world production, except Brazil ranking fourth accounting to 4.59 % of the world production. Mozambique as the second largest producing country has gained enormously in importance since 2018 thanks to the world's largest graphite mine, Balama. The four main producing countries (China, Mozambique, Madagascar and India are responsible for 88 % of the global graphite production (Reichl & Schatz 2024).

An overview of the major graphite producing countries is presented in Table 3, along with their respective tonnages and the global production share (Figure 4). The data has been collected for the most recent period available from WMD 2024 (Reichl & Schatz 2024).

*Table 3: Major graphite producing countries and corresponding tonnages (WMD 2024 and USGS 2021 and 2022)*

| Country | Tonnage 2021 USGS 2021 | Tonnage 2022 USGS 2022 | Diff USGS 2021-2022 in t | Diff USGS 2021-2022 in % | Tonnage 2022 WMD 2024 | USGS 2022 Global production share in % | WMD 2024 Global production share in % |
|---|---|---|---|---|---|---|---|
| **Austria** | 500 | 500 | 0 | 0 | 100 | 0.04% | 0.01% |
| **Brazil** | 82000 | 87000 | 5000 | 6 | 79372 | 6.62% | 4.59% |
| **Canada** | 12000 | 15000 | 3000 | 20 | 13000 | 1.14% | 0.75% |
| **China** | 820000 | 850000 | 30000 | 4 | 1161000 | 64.64% | 67.21% |
| **Germany** | 250 | 250 | 0 | 0 | 185 | 0.02% | 0.01% |
| **India** | 7000 | 8300 | 1300 | 16 | 82439 | 0.63% | 4.77% |
| **Korea, North** | 8100 | 8100 | 0 | 0 | 20000 | 0.62% | 1.16% |
| **Korea, Republic** | 10500 | 17000 | 6500 | 38 | 23798 | 1.29% | 1.38% |
| **Madagascar** | 70000 | 110000 | 40000 | 36 | 116700 | 8.37% | 6.76% |
| **Mexico** | 2100 | 1900 | -200 | -11 | 3420 | 0.14% | 0.20% |
| **Mozambique** | 72000 | 170000 | 98000 | 58 | 165932 | 12.93% | 9.61% |
| **Norway** | 6290 | 10000 | 3710 | 37 | 10380 | 0.76% | 0.60% |
| **Russia** | 15000 | 15000 | 0 | 0 | 18800 | 1.14% | 1.09% |
| **Sri Lanka** | 3000 | 3000 | 0 | 0 | 3299 | 0.23% | 0.19% |
| **Tanzania** | | 8000 | 8000 | 100 | x | 0.61% | |
| **Turkey** | 2700 | 2900 | 200 | 7 | 27715 | 0.22% | 1.60% |
| **Ukraine** | 10000 | 3000 | -7000 | -233 | 846 | 0.23% | 0.05% |
| **Vietnam** | 5000 | 5000 | 0 | 0 | 500 | 0.38% | 0.03% |
| **Total** | **1126440 t** | **1314950 t** | **188510 t** | **14%** | **1727486 t** | **100%** | **100%** |

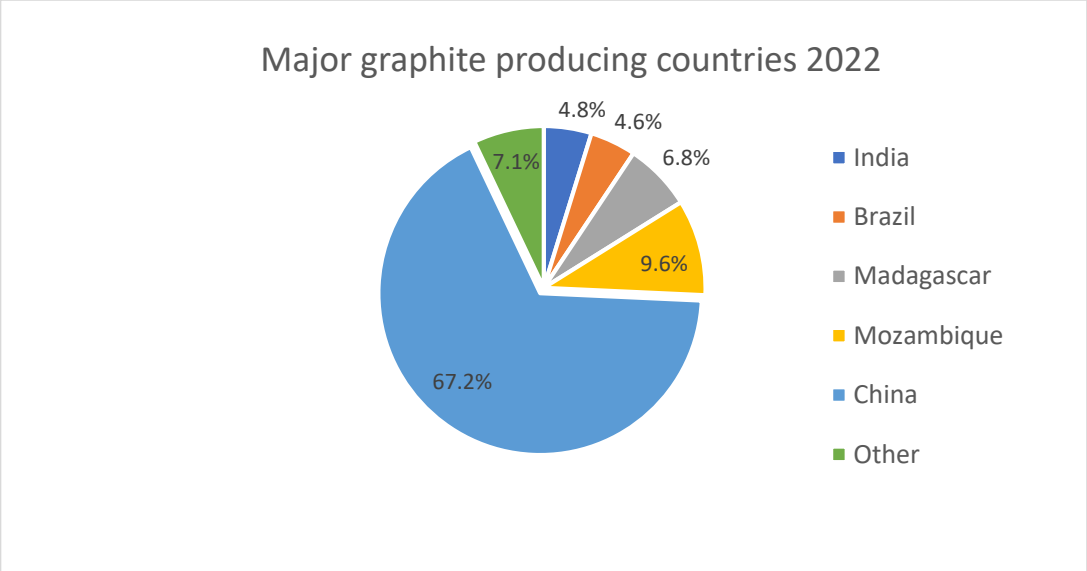


*Figure 4: Major graphite production countries in 2022 (WMD, 2024)*

### 4.2.2. Dependence on China and Diversification of Graphite Resources

China continues to maintain its position as the epicenter of the graphite industry as the largest producer, consumer and exporter of graphite on the global scale (Zhou and Damm 2020).

Wang et al. in 2018 in their simulation analysis of the spread of a supply crisis based on the global natural graphite network proposed that in order to minimize the risks of dependence on China, new technologies need to be developed to optimize the utilization of graphite resources and reduce consumption. This is not an easy task. It is advised to adopt another proposal, which advocates diversifying graphite resources instead of solely depending on China. For the market outside China, but

especially in Europe, there is a strong need to not only focus on the cost effectiveness but also on enhancing environmental sustainability and technical capability to reach supply security.

One of the noteworthy graphite mining projects outside China, is the Munglinup Graphite Project in Western Australia, which was being developed by Mineral Commodities Limited (MRC). They also operate the Skaland mine in Norway. The Munglinup project involves several open pits and flotation plants to process graphite ores. It is located in a zone of graphitic schists within a sequence of hornblende and hornblende-garnet gneisses. The latest mineral resources from 2020 prepared following the 2012 JORC Code are estimated to be at 7,99 Mio t and 12,2 % total graphitic carbon content (TGC), using a 5 % cut off and 4,24 Mio t ore reserves at 12.6 % TGC (Mineral Commodities Ltd 2022).

### 4.2.3. European Natural Mine Production

On a global scale, European graphite production remains constrained, comprising only 0.67 % of the World Production in 2022 (Reichl & Schatz 2024).

Ukraine is the largest producer of natural graphite in Europe. The entire production from Ukraine is coming from a single flake graphite mine operated by Zavalivskiy graphite (Zhou and Damm 2020). Meanwhile Norway is the second largest producer in Europe and the eighth largest producer worldwide, excluding Chinese companies. In 2018, approx. 12.000 t of flake graphite were produced annually with an estimated mine life of 30 years in the Skaland graphite mine. This mine shows an average carbon content of 25 %, making it the world's highest-grade graphite mine in operation (Mineral Commodities Ltd 2022b). Due to the war in Ukraine the production amount of graphite dropped from 17000 t in 2021 to 846 t in 2022, which accounts to only 0.05 % of the world production in 2022 (Reichl & Schatz 2023, 2024).

Other graphite producing countries in Europe are Germany and Austria with one operating mine only in each country. Scandinavia tries to meet the demand for graphite using European resources and is establishing new mining operations (Table 4, Figure 5). A prominent example is the Vittanghi graphite mine in Northern Sweden, which is based on the Nunasvaare graphite deposit and had been assessed by the SGU as a mineral deposit of national interest. In Sweden areas of particularly valuable mineral substances may be declared national interests (SGU, Mineral deposits of national interest 2024) and are therefore protected.

Additionally, the Woxna mine in Sweden is kept in production-ready mode, but is currently not operating (Barrera 2021).

In Finland, Beowulf Mining operates the Aitolampi flake graphite deposit, which is still under exploration and currently undergoing a pre-feasibilty study. Beneficiation tests had also been performed (personal communication Rasmus Blomqvist). Graphite bearing rocks in this deposit are strongly foliated black schist and disseminated graphite flakes within banded gneiss (Al-Ani et al. 2020).

*Table 4: European (Scandinavian) graphite exploration projects and their published reserves and resources, map see Fig. 5*

| Project name | Country | Company | Reserves (mt) | Resources (mt) | References |
|---|---|---|---|---|---|
| Jalkunen | Sweden | Talga Group Ltd. | na | 4.7 | (Zhou and Damm 2020; Barrera 2021) |
| Vittangi | Sweden | Talga Group Ltd | 0.45 | 3.9 | |
| Woxna | Sweden | Leading Edge Materials Corp. | na | 0.6 | |
| Raitajärvi | Sweden | Talga Group Ltd | na | 0.3 | |
| Aitolampi | Finland | Beowulf Mining | na | 26.7 | (Beowulf Mining plc 2024) |
| Skaland | Norway | Mineral Commodities Ltd | 1.78 | 22 | (Olson 2021) |
| Haapamäki | Finland | Beowulf Mining | na | 1.3 | (Zhou and Damm 2020) |

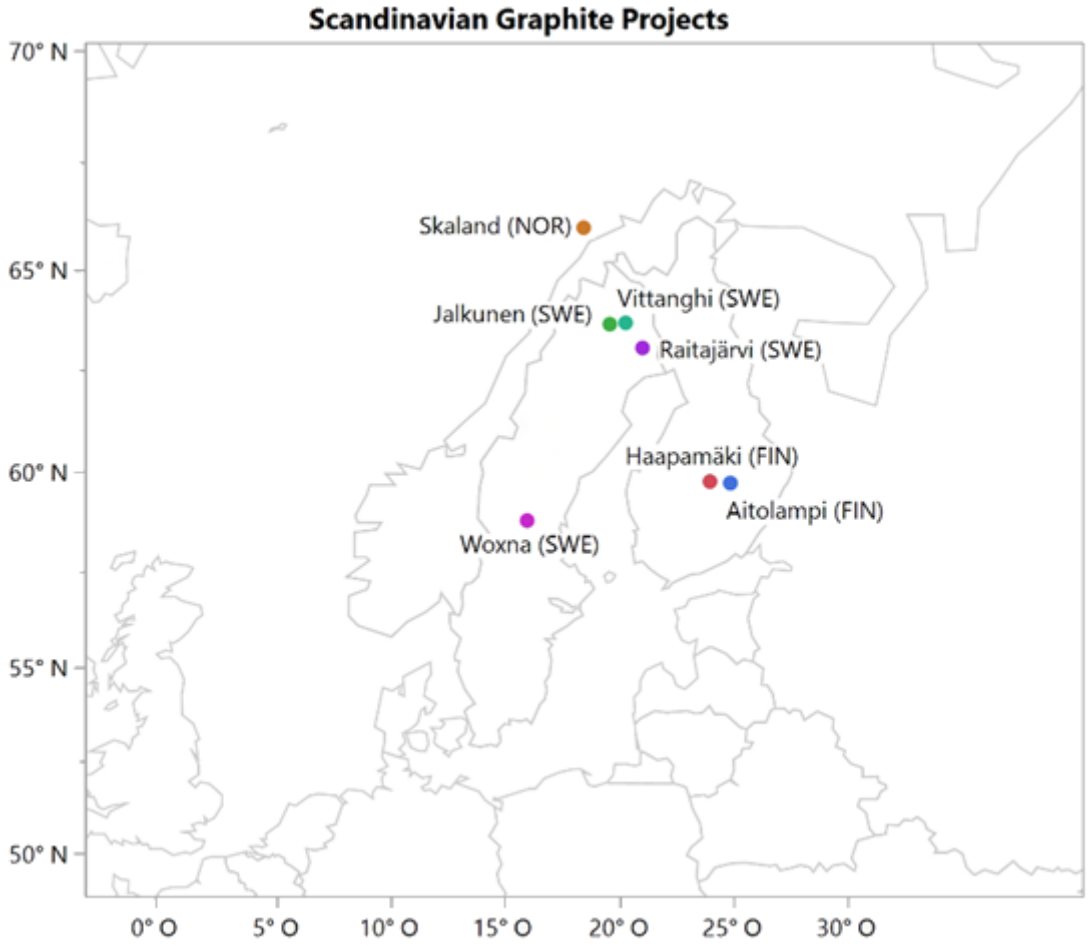


*Figure 5: Map of graphite projects in Scandinavia*

Graphite beneficiation, which requires a number of hazardous chemicals and acids such as HF, is currently concentrated almost exclusively in China. Other ways of processing and the construction of plants in Europe is in preparation (production and processing facilities are currently planned and tested at the Woxna mine site and at the Vittanghi graphite mine site in Northern Sweden) (Barrera 2021).

Weber et al. (2023) analyzed the likelihood of supply bottlenecks for the graphite market and compared the world mine production of graphite in terms of political stability of the producer countries. The study revealed that 98 % of the global graphite production originates from developing countries, while western industrial nations contribute only 1,8 % to graphite production. Madagascar and Mozambique are classified as developing nations. The largest graphite deposits with the highest carbon contents are located in Africa. Among them the Balama mine (Syrah Resources), which started its production in 2018, as well as projects like Nicanda Hill (Triton) in Mozambique and Anjamanga (PRGGlobal) in Madagascar (Weber 2023a). Additionally, Asia and North America are home to significant graphite deposits. However, European deposits exhibit notably lower resources.

### 4.2.4. Supply, Demand and Natural Graphite Reserves and Resources

In terms of quantity, graphite is the major component of modern Li-ion batteries and demand will increase dramatically in the coming years. The risks can be located primarily in the high concentration of supply and the market power of China. China controls almost the entire value chain of this important industrial mineral. The amount of graphite required by 2050 is 4 times higher than the current production from 1984 to 2020, partly due to the already mentioned and forecast demand from e.g. electromobility and other green technologies. The green transition will be significantly mineral intensive.

Global graphite reserves are spread across various regions, totaling an estimated 300 million tons in recoverable reserves by 2019. Worldwide, the recoverable graphite resources exceeded 800 million tons in 2020 (Olson 2020). China possessed substantial reserves and resources, reaching 537 million tons in 2018 (Zhou and Damm 2020). In contrast, European producers had a combined 11 million tons in reserves and resources, with reported reserves of 1.05 million tons, making up less than 1 % of the global total. Notably, Norway contributed half of Europe's reserves, reporting 560,000 tons for the Traelen graphite deposit in 2015 (Gautneb 2015).

Reserves beyond China and Europe amounted to 227 million tons, comprising a substantial 76 % of the global reserves (Olson 2020; Zhou and Damm 2020). Among these, Turkey boasts the world's largest graphite reserves, totaling 90 million t, representing 30 % of the global reserves. However, a significant portion of these reserves is composed of the amorphous type of graphite, not suitable for most applications in the EV sector. Brazilian reserves are estimated at 72 million t, earning them the third-largest position worldwide and accounting for approximately 24 % of the global reserves (Olson 2020).

In recent years, East Africa has emerged as a primary hub for graphite exploration, resulting in a notable surge in the reserve and resource levels of flake graphite, particularly in Mozambique, Tanzania, and Madagascar. As of 2019, the region's combined reserves amounted to 44.6 million tons, comprising a significant 15 % of the global reserves (Zhou and Damm 2020; Taylor 2024).

### 4.2.5. Herfindahl-Hirschman Index (HHI)

The HHI is a widely used and accepted measure of market concentration and thus illustrates the market competition. The closer a market is to a monopoly position, the less competition. 100 % market share of a company/country would correspond to an HHI of 10 000. If, on the other hand, there is a diverse market, the HHI would be 0, indicating perfect distribution (Brezina et al. 2016).

Some ranges are:

- HHI below 1500: a competitive marketplace
- HHI between 1500 and 2500: a moderately concentrated marketplace
- HHI of 2500 or greater: a highly concentrated marketplace

The high HHI of graphite (4707) (Reichl & Schatz 2024) therefore indicates a highly concentrated market place and the risk of bottle necks.

### 4.2.6. Graphite as a Critical Raw Material (CRM)

The classification of a raw material as critical refers to the importance for the EU economy, growth and jobs and the supply risks we are exposed to, due to the dependence on certain supplier countries. This classification has been launched as the first action of the European Raw Materials Initiative (RMI) in 2008. Therefore, the European Commission has established a list of critical raw materials, which is updated regularly. The very first list was published in 2011 with 14 raw materials. In 2014 the list of CRMs was updated to 20 CRMs and in 2017 the list already consisted of 27 CRMs. The most recent additions to the list include arsenic, feldspar, helium, manganese, copper and nickel. The latter are considered as strategic raw materials rather than critical raw materials. Indium and Natural rubber were removed from the list. Graphite was a CRM from the beginning in 2011 and was quoted as Natural Graphite from 2014 (Grohol et al. 2023).

### 4.2.7. The Graphite Supply Chain

The graphite supply chain is complex and characterized by many intermediate processing steps. However, one advantage in the processing of graphite is the basic processing at the beginning of the

value chain, where the raw ore is only crushed and ground and the ore is separated by flotation. This graphite concentrate is then traded worldwide. Graphite raw ore is not traded due to the large amount of material and the corresponding transport cost. In some graphite producing regions graphite is processed in one processing plant, however originating from different mines. This is the case for some samples present in this study. Which samples are affected by mixing materials from mines in a close proximity to each other will be explained in detail in later chapters. The following flow chart (Figure 6) shows the graphite processing value chain from exploration and mining through various processing steps up to the final use of the raw material in products.

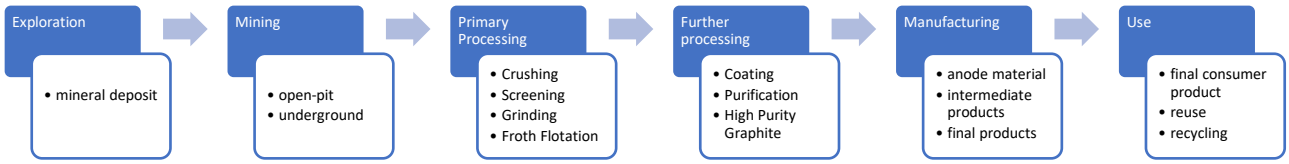


*Figure 6: Simplified graphite processing flow chart (modified after Mitchell, 2022)*

### 4.2.8. Major Producer Companies Worldwide

The following companies (Table 5) represent the most important graphite producers worldwide.

*Table 5: List of the largest graphite mines worldwide including yearly capacity (DERA 2022)*

| Company name | Country | Capacity (t/y) |
|---|---|---|
| **Syrah Resources** | Mozambique | 350.000 |
| **Luobei County Yunshan Graphite** | Mozambique | 100.000 |
| **Aoyu Graphite Group** | Mozambique | 100.000 |
| **Jixi Changyuan Mining** | China | 100.000 |
| **Jixi Pucheng Graphite** | China | 100.000 |
| **Qingdao Haida Graphite** | China | 100.000 |
| **Qingdao Jinhui Graphite** | China | 100.000 |

## 4.3. Understanding Graphite

### 4.3.1. Material Properties

Graphite is one of two stable crystalline forms of pure carbon. Carbon is a crucial element in the Earth's biosphere and, after oxygen, has the highest mass fraction in all living organisms. In the biosphere, carbon is always found in connection with other chemical elements (O, H, S). In nature, however, carbon also occurs in a completely pure form, namely as the two minerals diamond and graphite. By far the more common of these is graphite. On the Mohs hardness scale, graphite is assigned a value of 1-2 and is therefore among the softest minerals. Diamond, in contrast is the hardest of all. The density of graphite is 2.26 g/cm$^3$. Due to its high melting point of 3.700 ° C, graphite is very heat-resistant and very resistant to acids and alkalis. In addition, graphite also has good thermal and electrical conductivity and reduces the kinetic energy of the neutrons released during nuclear fission ( (Regelous & Holzförster unknown year). The average carbon content present in the Earth’s crust is approximately 0.08 wt % (Clarke and Washington 1924).

### 4.3.2. Carbon Origin and Graphite Formation

Graphite formation is primarily a result of graphitization e.g. the continuous transformation of organic matter, known as coalification. This process commences from peat, progressing through bituminous coals and anthracite, ultimately ending in the formation of graphite. Consequently, graphite and semi-graphite indicate a moderate to high metamorphic grade. In contrast, natural coke originates from localized elevated heat flow associated with an intrusive body, leading to its presence across a spectrum of coalification stages. Similarly, natural char occurs in various coalification stages as it is produced by the influence of heat from fire on coal or gelified organic matter in peat. These transformations demonstrate the spectrum of geological processes that shape the formation of these carbonaceous materials (Kwiecińska 2004).

The formation of graphite always requires organic or inorganic carbon, as well as high temperatures and pressures. Graphite is formed over the course of millions of years either from biological or hydrothermal sources (Luque et al. 1998; Beyssac and Rumble 2014) from substances initially deposited on the earth's surface on land or in water such as plants or algae (biological formation). The contained carbon (approx. 50 % of the plant or digested sludge) is enriched up to 90 % in the anthracite coal. Up to this point the enrichment process can run under relatively low pressure and temperature conditions.

For the final formation of graphite however, higher temperatures and pressures (up to granulite facies of metamorphism) are necessary to convert amorphous carbon to crystalline carbon.

These processes can be achieved as long as no oxygen enters the system, since at increased temperatures the carbon reacts with oxygen and escapes as gaseous carbon monoxide and carbon dioxide. Graphite therefore occurs preferentially in formerly deeply buried metamorphic rocks, e.g. within the core of orogens (Bonijoly et al. 1982).

Economically significant natural graphite deposits are typically the result of two main processes (Simandl and Kenan 1997):

1. The maturation and metamorphism of organic material
2. The precipitation of graphite from C-O-H fluids, which can occur due to changes in temperature and pressure conditions, fluid buffering, or the mixing of C-O-H fluids with varying compositions and likely different origins

### 4.3.3. Deposit Types

Within natural graphite, further distinction is made between microcrystalline (amorphous) and macrocrystalline graphite (Table 6, Figure 7). Within the macrocrystalline graphite category, there is a further differentiation between flake graphite and hydrothermal (vein) graphite (Luque et al. 2014). Flake graphite consists of platelets/flakes and occurs in metamorphic rocks such as marble, gneiss or schist. Amorphous graphite is a very fine-grained (semi)-graphite found in coal seams, shales and schist. Vein graphite can occur needle like or massive in igneous rocks or granulite facies rocks.

*Table 6: Natural occurring types of graphite (modified after Keeling 2017; Scherba et al. 2018)*

| Graphite deposit type | main host rocks | (genesis Kwiecinska, 2014) | Origin | Product grade |
|---|---|---|---|---|
| Amorphous (microcrystalline) | quartzites, phyllites, schists | Syngenetic, metamorphic | Contact and/or regional thermal metamorphosis of coal seams | 75 -85 % C |
| Flake (macrocrystalline) | gneiss, marble, quartzite, amphibolite | Syngenetic, metamorphic | Graphitization of organic precursors through regional metamorphosis | 85 – 98 % C |
| Vein (macrocrystalline) | granulite, granite | Epigenetic, hydrothermal | Precipitation from carbon bearing fluids | 90 – 99 % C |

### 4.3.3.1. Amorphous Graphite

The term "amorphous" graphite can be misleading, as even amorphous graphite possesses a crystalline structure. It is often referred to as "semi-graphite" to describe the transitional phase during coalification to graphitization in organic-rich sediments (B. Kwiecińska 2004). Amorphous graphite is the most common form of graphite. Microcrystalline graphite deposits typically form through sub-greenschist to greenschist contact metamorphism or regional metamorphism of coal seams (Taylor 2006). These deposits primarily comprise small graphite particles intermixed with impurities. They often manifest as stratiform or lens-shaped formations, with beds that may exhibit deformation, folding, and faulting. Variations in bed thickness, characterized by pinching and swelling, are common. Such deposits may encompass multiple beds, each a few meters thick and extending for hundreds of meters along their strike. The graphite content in these ores ranges from 30% to 95%, frequently exceeding 80 % (Simandl et al. 2015). Typical host rocks are quartzites, phyllites, schists and metagreywackes with a schistose or massive texture of the graphite ore (Simandl and Kenan 1997).

### 4.3.3.2. Flake Graphite

Flake graphite is the most economically significant type of graphite due to its application in LIB and other battery types. Flake size and crystallinity depend on the temperature during metamorphism. Disseminated graphite flakes are found in various rock types, including marble, paragneiss, iron formation, quartzite, pegmatite, syenite (Simandl et al. 2015), and exceptionally rare cases of serpentinized ultramafic rocks (Crespo et al. 2006). The most common hosts for economically significant crystalline flake deposits are paragneiss and marble grading at 2-3 % graphite or lower.

The highest graphite grades in paragneiss-hosted deposits are typically found near paragneiss-marble contacts. Marbles in granulite-facies terrains typically contain less than 0.5 % crystalline flake graphite, although concentrations of 1 to 3 % crystalline graphite are common. Graphite is uniformly distributed

throughout the host rock, and the size of graphite flakes correlates with calcite or dolomite (Simandl et al. 2015).

#### 4.3.3.3. Vein Graphite

Vein graphite deposits, also described as hydrothermal graphite deposits are found in both granulite-facies metamorphic and igneous rocks are not confined to specific rock types. These deposits are structurally controlled, typically intersecting host rocks, often forming due to hydraulic fracturing. In granulite rocks, graphite veins are typically composed of graphite alone, while in igneous rocks, they can be associated with various hydrous minerals or magmatic sulfides, depending on whether they formed from aqueous fluids or carbon-rich melts. The specific mineral associations are influenced by the deposition mechanisms. Regardless of their geological context, vein graphite exhibits large crystal sizes, commonly referred to as lump graphite in commercial terms and possesses a high degree of crystallinity. Furthermore, vein graphite typically contains a higher carbon content compared to graphite in syngenetic deposits within metamorphic rocks. The carbon source differs between granulite-hosted and igneous-hosted deposits. In granulites, carbon originates from sub-lithospheric sources or, in certain areas, results from decarbonation reactions in carbonate-bearing lithologies. In igneous rocks, graphite primarily derives from the assimilation of rocks containing organic matter. Due to the limited solubility of carbon in silicate magmas, immiscibility leads to the formation of carbon-rich magmas or fluids. Carbon is transported as $CO_2$ and/or $CH_4$ in supercritical aqueous fluids, depending on the oxygen fugacity ($fO_2$), both in granulite and igneous rocks through fracture systems. The principal mechanism driving graphite deposition in granulite-facies rocks involves cooling and the consumption of water through reactions with surrounding rocks. In igneous-hosted deposits, the primary factors leading to graphite deposition are the cooling of the melt or fluid and the consumption of water from these fluids. Water consumption in igneous rocks is typically linked to hydration reactions of host rocks, resulting in the formation of hydrous minerals within graphite-bearing veins (Luque et al. 1998; Luque et al. 2014)

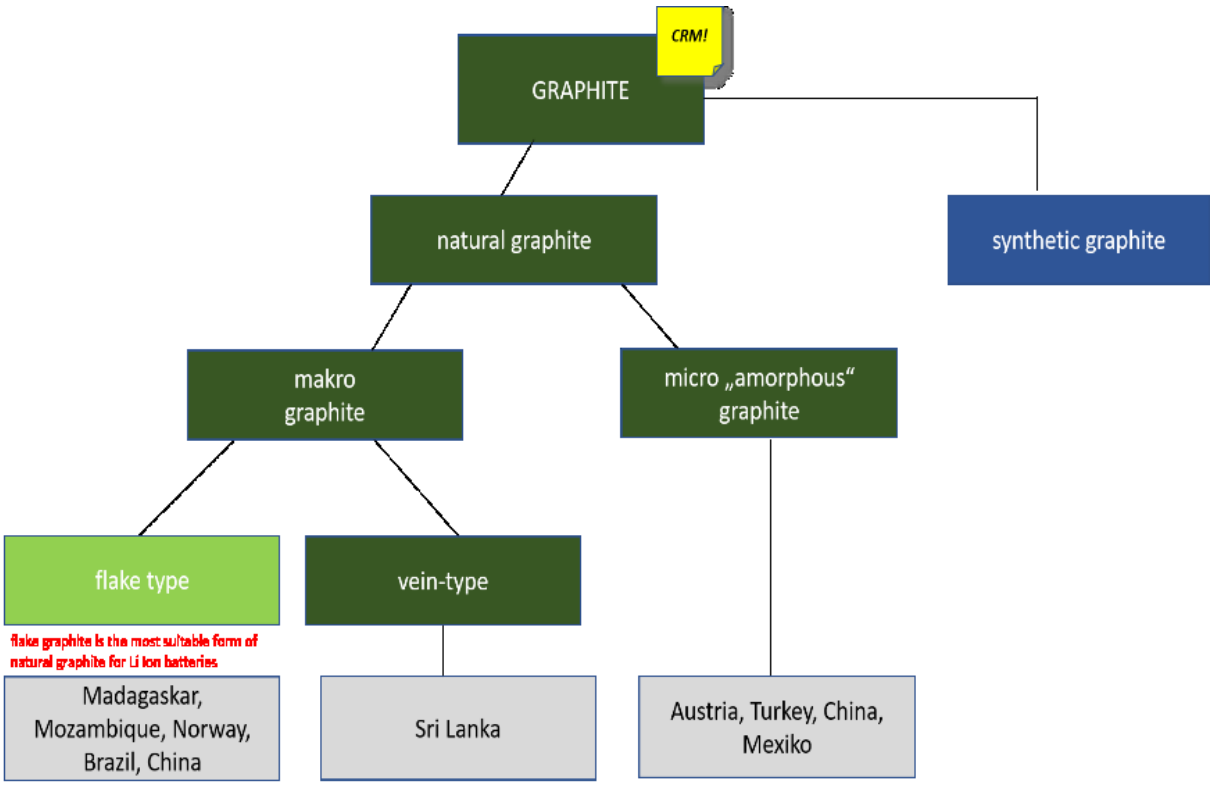


*Figure 7: Classification of graphite deposit types*

## 4.4. Sample Material

### 4.4.1. Explanation and Clarification

The sample collection consists of commercially available graphite concentrates covering the major graphite-producing countries worldwide (Fig. 8).

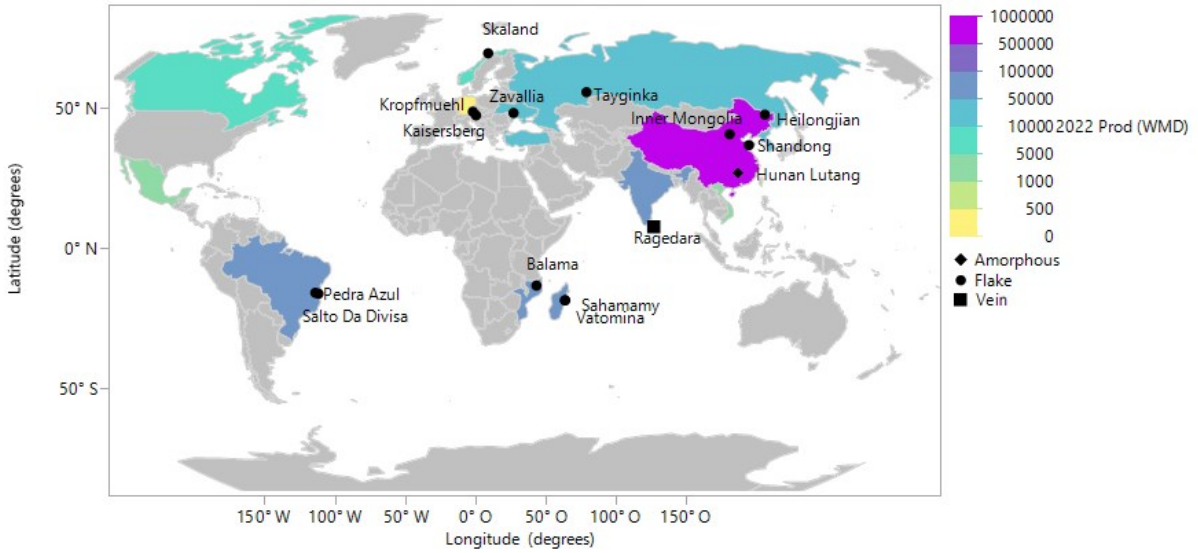


*Figure 8: World map of graphite sample material and production (2022) in t*

These concentrates hold global significance due to their widespread trade. Raw, unprocessed ore from some deposits could be obtained: Kaisersberg (Austria), Passau (Germany), Zavallia (Ukraine), Skaland (Norway) and Balama (Mozambique) and was included in this study. Raw ore is not transported globally due to the large quantities involved and it is processed locally before being traded worldwide in the form of graphite concentrate.

Samples from China are more related to provinces than to specific mines, as the situation in China is highly opaque. A province may have multiple processing plants and various mines, including artisanal mining, or even one processing plant for one province and multiple mines. A more detailed subdivision is not possible for the occurrences in China used in this study. The level of geographic origin for samples from China is therefore one level above the others, referring to the region/province rather than the specific mine site (except Hunan Lutang, which refers to the province Hunan and the mine Lutang). Graphite deposits in China are mainly distributed to Heilongjiang, Inner Mongolia, Sichuan, Shanxi, and Shandong (Sun, 2018). In this study, three out of the five major regions are covered (Inner Mongolia, Heilongjiang, Shandong). Precise production quantities for each province could not be obtained. Samples from Madagascar, specifically Vatomina and Sahamamy Sahasoa, represent mixed concentrates from these two mines. Both mines are in close proximity and processed in a single processing plant, making further differentiation impossible. The province is called Brickaville and includes the two mines named above. The same applies to Brazil. The material from the mines Pedra Azul, Itaperica, and Salto da Divisa is processed and mixed in a single processing plant. The available concentrate samples cannot be traced back to each individual mine, therefore the province Minas Gerais is stated in the further course of the work.

Samples from all other origins directly refer to the mine site along with the associated processing plant in the same location. Commercially available samples were acquired yearly from 2020 to 2023, if available. Some samples represent earlier years (2019 and earlier), due to a collection available at the

university collection. The following list presents localities with the number of available individual samples from the same mine/province (Table 7).

It is still necessary to extend the analysis to encompass additional graphite intermediates, particularly those subjected to more advanced processing. This extension aims to define the degree to which specific identifying features, the unique signatures or fingerprints, can be traced, particularly across multiple stages within the graphite supply chain. The sample collection and analytical efforts were primarily focused on graphite concentrates sourced from various mining operations. This allows to distinguish between various deposit origins and the corresponding graphite concentrates extracted from them. This distinction serves as a starting point for the establishment of a traceability framework aimed at tracking graphite throughout supply chain for graphite.

*Table 7: Summary of the available sample material (nda – no data available)*

| Country | *Mine/province* | *Company* | *Deposit type* | *Resources in t (Weber, 2023)* | *Number of samples (conc)* | *Number of samples (raw ore)* |
|---|---|---|---|---|---|---|
| ***Austria*** | *Kaisersberg* | *Kaisersberg Grafit* | *Amorphous* | *nda* | *2* | *3* |
| ***Brazil*** | *Pedra Azul, Itaperica, Salta da Divisa (Minas Gerais)* | *Nacional de Grafit (NDG)* | *Flake* | *8.045.700 (Itaperica only)* | *5* | *-* |
| ***China*** | *Hunan Lutang* | *na* | *Amorphous* | *27.590.000* | *1* | *-* |
| ***China*** | *Heilongijan* | *na* | *Flake* | *na* | *1* | *-* |
| ***China*** | *Shandong* | *na* | *Flake* | *na* | *2* | *-* |
| ***China*** | *Inner Mongolia* | *na* | *Flake* | *na* | *1* | *-* |
| ***Germany*** | *Kropfmühl* | *AMG Graphite* | *Flake* | *na* | *1* | *1* |
| ***Madagascar*** | *Sahamamy-Sahasoa, Vatomina (Brickaville)* | *Tirupati Graphite* | *Flake* | *7.100.000, 18.400.000* | *3* | *-* |
| ***Mozambique*** | *Balama* | *Syrah Resources* | *Flake* | *1.423.000.000* | *6* | *1* |
| ***Norway*** | *Skaland* | *MRC, Skaland Graphite* | *Flake* | *2.484.000* | *3* | *1* |
| ***Russia*** | *Taiginka* | *JSC Uralgraphite* | *Flake* | *11.000.000* | *3* | *-* |
| ***Sri Lanka*** | *Ragedara* | *Elcora* | *Vein/lump* | *na* | *2* | *-* |
| ***Ukraine*** | *Zavallia* | *Volt, Zavaljevsky Grafit* | *Flake* | *22.913.000* | *2* | *3* |

## 4.4.2. Description of Deposits and Samples

### 4.4.2.1. Kaisersberg, Austria, Europe

Kaisersberg is the only active graphite mine in Austria, operated by Grafitbergbau Kaisersberg Ges.m.b.H. in St. Stefan ob Leoben. The amount of extracted graphite is not reported (Heike 2023). The extracted material is referred to as semi-graphite (Rantitsch et al. 2016a) and is mined underground. The annual extraction quantities are approximately 100 tons (personal communication, Twrdy, G.). This graphite deposit represents one among several stratabound graphite deposits situated within the Eastern

Greywacke Zone, however currently being the only one in operation. These deposits are found within the Upper Carboniferous strata of the Veitsch nappe (Scharfe 1981).

The Veitsch nappe is the lowermost tectonic unit within the Austro-Alpine Greywacke Zone, and it overlies a suite of medium-grade metamorphic rocks and Permo-Mesozoic cover sequences (Ratschbacher 1984, Nievoll 1984, Neubauer & Vozàrovà 1989, Ebner 1991, Neubauer 1994). The graphite deposits are situated within a carbonate-clastic sequence, referred to as the Sunk Formation. This formation is characterized by a coarsening-upward sequence with cyclic sedimentation patterns (Ratschbacher 1984 and 1985). These sequences, with thicknesses ranging from 50 to 150 meters, consist of graphitic schists, meta-argillites, and metaconglomerates. They are interpreted as sediments that originated in deltaic to coastal plain environments. Plant fossils found within this formation provide evidence of its Westphalian A age (Raith & Vali 1998), Rantitsch et al. 2016).

#### 4.4.2.2. Pedra Azul, Itapecerica, Salto da Divisa, Minas Gerais, Brasil, South America

The company Nacional de Grafit operates three mines with processing facilities on-site in Brazil. These mines, namely Pedra Azul, Itapecerica, and Salto da Divisa, collectively produce 70.000 tons of graphite per year (Nacional de Grafite 2024). They are situated within the state of Minas Gerais. Samples from Brazil are concentrate blends. The company operates three mines in close geographical proximity to each other, all associated with the same graphite deposit. In this context, it is not feasible to precisely attribute each sample to its respective mine. However, due to processing practices, it can be reasonably assumed that the samples consist of homogeneous mixtures of the concentrates.

The mines are situated within the southern São Francisco Craton, specifically within the Itapecerica Supracrustal Sequence. The southern portion of the São Francisco Craton encompasses a diverse geological landscape, featuring Meso- to Neoarchaean granite-greenstone terrains, Paleoproterozoic clastic-chemical metasedimentary rocks from the Minas Supergroup, and Neoproterozoic pelitic-carbonate sedimentary rocks of the Bambuí Group (Teixeira et al. 2017). The underlying basement comprises the Campo Belo, Divinópolis, Bonfim and Belo Horizonte metamorphic complexes. This sequence also includes the banded iron formations found in the Quadrilátero Ferrífero (Machado et al. 1996; Moreira et al. 2016).

The Itaperica schist, formed in the Paleoproterozoic is primarily composed of fine to medium-grained graphite, along with the presence of quartz and sillimanite. Graphite is the dominant constituent, establishing the foliation. Quartz, on the other hand, plays a secondary but significant role and exhibits elongated crystal shapes reminiscent of ribbons, which align with the foliation pattern. Sillimanite is also present in the schist, its proportions varying, and it may display either a fibrous or prismatic habit (Miranda et al. 2019).

#### 4.4.2.3. Inner Mongolia, Heilongjian, Hunan Lutang, Hubei, Shandong, China, Asia

Graphite is sourced from 170 mining areas across 25 provinces in China. The predicted graphite resources are estimated at about 1.63 billion tons. The major graphite resources in the Heilongjiang province amount a billion tons representing 60 % of China´s graphite resources. For the Chinese samples only the provinces are known, neither the precise location of the extraction, nor the exact mine is known.

There are two main types of graphite mineralization in China – the regional metamorphic-type, associated with Neoarchean and Paleoproterozoic rocks and the Mesozoic contact metamorphic-type. Among these, flake graphite formed during regional metamorphism of carbonaceous rocks are the most prominent in China. Typically, these deposits are situated in high-grade orogenic zones positioned at the peripheries of tectonic blocks or terranes. Examples are located in the Jiamusi and Alashan blocks, as well as along the boundaries of the Northern China and Yangtze cratons, where the highest levels of

metamorphic grade are observed. Regions with potential for this variety of graphite encompass Heilongjiang, Inner Mongolia, Shandong, Jilin, and Sichuan provinces, with Heilongjiang Province standing out as a location of very high potential for regional metamorphic-type graphite found within metasedimentary rocks (Cui et al. 2017).

Hunan Lutang is a typical contact metamorphic graphite deposit, which was deposited is part of marine and continental environments in the Hunan Province in the east of the country. It formed in the Late Permian Longtan Formation. The rock was altered during the Mesozoic Qitianling Granite intrusion, creating different types of rock near and far from the intrusion – calc-silicate rock near it and marble further away. Graphite is found in areas with structural openings and within altered coal-bearing layers, with varying widths from 0.1 to 11 meters. The graphite consists of small and well-shaped flakes, about 0.3 micrometers wide, and contains between 70 % and 86 % carbon content (An et al. 2016; Cui et al. 2017). Hydrothermal graphite is very rarely found in China and is primarily located in hornfels formations in the western part of the country

#### 4.4.2.4. Kropfmühl, Germany, Europe

Graphit Kropfmühl GmbH (GK), located in Kropfmühl, near Passau in Germany processes graphite raw materials to manufacture customized graphite products and concentrates for specific uses from various sources. They also engaged in labor-intensive underground mining, which restarted in 2012 after a seven-year pause. Furthermore, the company secures its raw material supply through deposits located in various regions of Africa and Asia. Access to the primary graphite deposit is achieved through the Erhard shaft, which facilitates excavation activities extending down to the 10th level of the mine. The Kropfmühl graphite deposit is situated in the Moldanubic geological domain, within the Bohemian Massif. This deposit is characterized by a metamorphosed rock series. These predominantly encompass dark garnet (plagioclase) biotite gneisses, interspersed with light quartzitic gneisses, quartzitic intercalations, amphibolites, and calc-silicate marbles (Krüger et al. 2017).

Of particular importance are the Moldanubic graphites, which exhibit a macrocrystalline morphology, with crystal dimensions surpassing 100 micrometers. The genesis of these graphites is attributed to the regional metamorphic overprinting of sedimentary rocks. An organogenic origin, emphasizing the significance of biophilic trace elements such as molybdenum, vanadium, nickel and boron within the graphite-bearing rock formations had been postulated (Weber 1987).

#### 4.4.2.5. Vatomina und Sahamamy Sahasoa, Brickaville, Madagaskar, Africa

Madagascar has consistently demonstrated its capacity to contribute significantly to the global graphite market due to its ability to supply high quality and large flake graphite from several graphite deposits in Madagascar, with currently five active graphite mining operations (Weber 2023b). The sample material from Madagascar is an aggregate from the Vatomina and Sahamamy Sahasoa mines, both operated by the company Tirupati Graphite. The two mines are located very close to each other in the north east of the country. Graphite deposits in Madagascar are found within the Precambrian metasedimentary basement, comprising schist, gneiss, granitic and basic igneous rocks, forming a wide north-south-oriented belt in the eastern part of the country. These regions are rich in graphite and closely linked to the Manampotsy group. The graphite ore occurs as both, disseminated and layered forms, mainly within gneissic and migmatitic rocks, that have undergone significant decomposition, resulting in clay-rich substrates. The distribution of graphite content within the layers varies, and the primary orientation of these major veins runs in a north-south direction, with widths reaching up to approximately 100 meters (Heritiana et al. 2019).

### 4.4.2.6. Balama, Cabo Delgado Province Mozambique, Africa

Mozambique, a significant supplier of graphite, currently has two active mining operations extracting graphite, along with several additional deposits that are not currently exploited. The material for this study is sourced from the Balama mine, which is located within the Southern Cabo Delgado province in the district of Namuno, northern Mozambique and is regarded as being the world's largest high-grade graphite deposit. The mine is operated by Syrah Resources and the production was commenced in January 2019 after starting various pre-construction activities late 2014 and completing the feasibility study of this project in 2015 (Mining Technology 2021). The rapid execution of the approval process and the commencement of mining activities just four years after the feasibility study demonstrates the enormous demand for this raw material.

Proven and probable reserves are estimated to be 114.5 Mt at an average TGC grade of 16.6 %, containing 18.9 Mt of flake graphite. Resources are estimated to be 1,036 Mt within a life of mine of 50 years. The mining is performed in a simple, low strip open-pit mine. The product is 94 to 98 % fixed carbon graphite concentrate and 80 % fine flake (100 mesh) graphite (Syrah Resources 2024).

The Balama Graphite Mine is situated in the Cabo Delgado province of northern Mozambique. It is located within the Mozambique Belt, a geological region known for its various mineral resources. The Metamorphic Mozambique Belt (NMMB) formed during the Neoproterozoic and Cambrian periods due to the closure of the Mozambique Ocean. It consists of four major rock types: ophiolites, island arc magmatic rocks, metamorphic rocks with raw materials including gemstones and graphite deposits, one of them being the Balama mine and late intrusive formations like granitoids and anorthositic gabbros. This region is renowned for its gemstone deposits and is often referred to as the 'Gemstone belt of East Africa' or the 'Pan-African Gems and Graphite Belt (Feneyrol 2013).

### 4.4.2.7. Skaland - Traelen, Norway, Europe

For nearly a century, Norway has been a leading European producer of flake graphite with three operating graphite mines. Four graphite provinces can be found in Norway, starting in the north, these provinces are: the island of Senja (Skaland/Traelen mine), the Vesteralen islands, the Holandsfjorden area and the Bamble area in southern Norway. Only the Skaland/Traelen mine will be described here. Paleoproterozoic graphite deposits with a notable concentration of high-grade ore, characterized by a high total carbon content, are located on the Fennoscandian Shield, specifically, within Norway, Sweden, Finland and Russian Karelia (Parnell et al. 2021).

Being a stable and reliable supplier of high-quality flake graphite since the 1900's and being the biggest crystalline graphite producer in Europe and the fourth largest producer globally outside of China, Norway accounts for around 2 % of the global annual natural flake graphite production with a production volume of 10380 t/year in 2022 (Reichl & Schatz 2024). The Traelen mine together with the Skaland processing plant has been owned by Skaland Graphite and was acquired by the Australia based company Mineral Commodities (MRC) in October 2019, where the mine permit has been extended for another 10 years until 2029 (NS Energy 2024). Senja Island is situated in the southern region of the West Troms Basement Complex (WTBC). The WTBC consists of tonalitic and granitoid gneisses intruded by a mafic dyke swarm. The basement gneisses are overlain by a variety of supracrustal units, including metapsammites, conglomerates, metavolcanites, dolomitic carbonates, banded-iron formations, and graphite schists. During the Svecofennian orogeny around 1.8 to 1.75 billion years ago, both the basement gneisses and supracrustal rocks underwent deformation. Within this complex, the peak metamorphism levels vary, ranging from lower grades in the northern part to amphibolite to granulite facies in the southern region, particularly on Senja Island (Gautneb et al. 2020).

The deposit consists of two main lithological units: The stratigraphically lower unit is a banded gneiss with alternating biotite-rich and granitic bands (“Traelen Gneiss”) and the upper unit an amphibolitc gneiss. These hornblende gneisses contain graphite horizons, metamorphic greywacke and calcareous rocks (Mineral Commodities Ltd 2022c).

#### 4.4.2.8. Tayginka, Chelyabinsk region, Russia, Asia

With three existing and two operating graphite mines, Russia contributes with 18800 t/year (1.09 %) to the global graphite production. Samples for this study originate from the the Tayginka graphite deposit that is situated in the Chelyabinsk region (Siberia). Graphite mining dates back to 1942 (Uralgraphite - natural graphite producer and supplier 2024)

The Middle Urals represent a significant bend in the Urals mountain range and are the most compressed part of the late Palaeozoic collision zone. This region is mainly composed of metamorphic rocks and cut by large fault lines. The Main Uralian Fault zone (MUF) is a major fault running north-south. It separates the Sysert Complex in the east from the Ufaley Complex in the west. The Sysert Complex is part of the East Uralian Zone where the graphite mineralization can be found (Echtler et al. 1997).

#### 4.4.2.9. Ragedara, Sri Lanka, Asia

There are several active mining operations extracting graphite in Sri Lanka. The mined graphite in Sri Lanka is consistently of the inorganic lump graphite type. In addition to the Ragedara mine, from which the sample material originates, the Bogala Mine, the Queens Mine, and the Karasnagala Mine are currently extracting lump graphite. The occurrence of vein graphite deposits in Sri Lanka is concentrated in the Wanni Complex in the Central Highlands underlain by supracrustal rocks (Dissanayake et al. 1988). The Wanni Complex is a Precambrian high-grade metamorphic terrain and consists of 770 - 1100Ma granitoids, metagabbro, charnockite, gneisses and migmatites (Touret et al. 2019).

The Ragedara Graphite Mine operated by Ragedara Mines Ceylon Private Ltd., held the distinction of being the world's largest graphite producer until the end of World War II. This deposit, located in the southeast of Sri Lanka is renowned for its exceptionally pure graphite content, ranging from 97 % to 99 %. The veins in this deposit typically measure 30 to 50 cm in width, with some extending up to 2 meters and an average vein length of about 25 meters. Veins are tabular or lenticular in shape. The largest one observed at Ragedara was close to 2 meters wide. The massive crystalline graphite shows uniformity throughout the veins and is composed of massive to millimeter size closely packed black graphite (Filion 2012).

There are several explanations for the formation of vein graphite in Sri Lanka (Hewathilake et al. 2018):

- Carbon-rich fluids resulting from decarbonation reactions in calcareous environments could be a source for the vein graphite formation (Hapuarachchi 1997)
- An organic origin for the carbon source, with subsequent deformation and magmatic activities mobilizing carbonaceous material (Dissanayake, 1981 and 1986).
- The role of $CO_2$-rich fluids in promoting vein graphite formation through hydraulic fracturing and crack-seal processes under low oxygen conditions (Katz, 1987).
- Hydrothermal activity in fracture zones of metasedimentary rocks as a contributor to vein graphite formation through decarbonation processes (Silva, 1987).

#### 4.4.2.10. Zavallia, Ukraine, Europe

The Zavalja mine is the only active graphite mining operation in Ukraine. Despite Russia's war with Ukraine, production at the mine continues, production amount however dropped significantly (- 95 %) (Reichl & Schatz 2024). The mining operation is managed by Volt, an Australian mining company that owns 70 % of the company, with the remaining 30 % held by Ukrainian authorities. The mine and its processing facilities have been in operation since 1934. Flotation, concentration, and purification of the graphite material are carried out directly at the mine site. In the future, purity levels of up to 99.95 % are targeted through on-site processing (Zavalievsky Graphite Operation – Volt Resources Limited 2024).

Graphite deposits in Ukraine are primarily situated within the Ukrainian Shield. Extending from the northwest to the southeast of the country, the Ukrainian Shield comprises folded Precambrian basement and overlaying Phanerozoic sedimentary cover, reaching a cumulative thickness of up to 120 meters (Mykhailov 2020). The concentration of graphite deposits is notable within four distinct ore districts: Pobuzhzhia (Zavallivske in Kirovograd Oblast), Kryvyj Rig (Petrivske and Balakhivske in Kirovograd Oblast), Volyn (Burtynske in Khmelnytskyi Oblast), and Near Azov (Troitske in Zaporizhzhia Oblast and Mariupolske in Donetsk Oblast). Presently active mining operations are limited to the Zavallivske/Zavaljevsky deposit.

The Zavaljevsky deposit is confined within the biotite-graphite gneisses of the Hashchevato-Zavallya Archean suite. This deposit encompasses approximately 40 tabular ore bodies, varying in length from 200 to 1200 meters and thickness from 3.5 to 80 meters. Mineralogically, the ore-bearing gneisses exhibit variations, including biotite, amphibole-biotite, biotite-chlorite, chlorite-sericite, chlorite-talc, and chlorite varieties. Graphite within these ores is characterized by a relatively irregular distribution in the form of large flakes (2–4 mm), with graphite content ranging from 6% to 14%, averaging to 6.5%. The mining operation is mined through open-pit methods and processing occurs on site. This processing facility operates at an annual rated capacity of 800 thousand tons of graphite ore or 35 thousand t of graphite concentrate. During the early 1990s, production rates exceeded 40 thousand tonnes but subsequently experienced a sharp decline. Presently, the annual production stands between 4 to 8 thousand tons. The rated capacities of both the open pit and the processing plant allow for increased production of graphite concentrate to meet the demand for raw materials (Mykhailov et al. 2023).

# 5. Methodology - Developed Methodology for Tracing the Origin of Natural Graphite

## 5.1. Selected Parameters for the Analytical Proof of Origin (APO)

The approach to proof the origin of natural graphite includes multiple parameters, some of which have been already used to analyze graphite or carbon rich materials before, such as $\delta^{13}C$ or lattice ordering. Specific parameters, such as the chemical composition (e.g. trace elements) have a proven track record in determining the origin of certain raw materials, yet they have not been employed to graphite so far. The highlighted parameters and methods were addressed in the context of this work (Table 8).

*Table 8: Potential methods and parameters for the analytical determination of the origin of natural graphite – bold letters indicate that the method/parameter had been considered in this study*

| Parameter | Method | | Conclusion |
|---|---|---|---|
| | **Bulk** | **In-situ** | |
| Chemical composition | XRF | LIBS, **LA-QQQ-ICP-MS** | Carbon source |
| $\delta^{13}C$ | **gas-MS** | **LA-MC-ICP-MS** | Depositional environment and genesis |
| $\delta^{34}S$ | -- | LA-MC-ICP-MS | Depositional environment and genesis, sulphur source |
| Lattice ordering | XRD | **Raman** | Temperature conditions |
| Grain morphology | -- | **SEM**, EMPA, **digital light microscopy** | Ore genesis |
| Mineral paragenesis | XRD | **SEM**, EMPA, **digital light microscopy** | Metamorphic history |

### 5.1.1. Structure and Crystallinity

Graphite exhibits a Raman spectrum with several characteristic bands. The most significant Raman band is the G-band (graphitic band) located at around 1580 $cm^{-1}$. Another important band is the D-band (disorder-induced band D1 and D2), typically appearing at around 1350 $cm^{-1}$. In highly crystalline graphite, the D-band is relatively weak compared to the G-band, reflecting the ordered and well-structured nature of the material. The intensity ratio of the D-band to the G-band $I_D/I_G$ is often used as a parameter to assess the degree of disorder and defects in graphite. High-quality, crystalline graphite typically has a low $I_D/I_G$ ratio, while more disordered or lower-quality graphite will exhibit a higher ratio (Ferrari & Robertson 2000).

The Raman spectra of graphite originating from both the amphibolite and granulite facies are defined by the presence of a well-defined G band and the minimal presence or complete absence of the D2 band (Rantitsch et al. 2014). Microcrystalline (amorphous) graphite undergoes a transformation into flake graphite at the transition from the amphibolite to granulite facies. This transition encompasses a metamorphic temperature range of 500 °C to 700 °C, along with a pressure range exhibiting significant variability between 4 and 11 kbar (Rantitsch et al. 2014).

The impact of material preprocessing on Raman spectra was assessed and it was found that differences in Raman parameters between mechanically processed and handpicked/original samples were minor. The processing method of graphite has a limited impact on Raman properties (Rantitsch et al. 2014). Polishing introduces significant, unpredictable changes in the intensity of both D bands relative to the G band. This effect obscures the evaluation of the intrinsic structural order, making this parameter unsuitable for polished carbon materials. The width of the G band appears to remain consistent after polishing (Maslova et al. 2012).

The following factors can influence the structure of graphite:

1.Temperature and Pressure (Graphitization Process): The graphite crystal structure is sensitive to temperature conditions. Changes in these parameters can lead to alterations in the crystal lattice and interlayer spacing of graphite. Graphitization leads to the conversion of structurally disordered carbonaceous material found in anthracite to a more ordered structural state. Semi-graphite serves as an intermediate phase bridging the gap between (meta-) anthracite and graphite (Kwiecińska and Petersen 2004)

2. Time and Geological Processes: The geological history of a graphite deposit plays a significant role in determining its structure and crystallinity. The extent and duration of geological processes, such as metamorphism or regional tectonic events, influence the level of crystallinity and the size of graphite flakes/crystallites. Raman spectroscopy is able to track peak metamorphic conditions of carbon rich materials during regional metamorphism. It had been employed to explore tectono-thermal processes of materials that contain a significant amount of carbon (Lahfid et al. 2010).

### 5.1.2. Chemical Composition

The chemical composition can provide valuable information about the geological origin of graphite as different deposits may have distinct chemical signatures and trace element profiles. The chemical composition can also serve as an indicator for the quality and purity of the graphite, which is an important factor for industrial applications. Understanding the chemical composition of different graphite materials is essential for selecting the right type of graphite for a particular application. Assessing the chemical composition is also essential to ensure compliance with safety and environmental regulations.

Limited research has been conducted on the geochemical characterization of graphite. A comprehensive study on this topic was conducted by Janda and Schroll in 1960, which served as a valuable reference for this work. Using an emission spectrographic method, the elements Ag, As, B, Ba, Be, Bi, Cd, Co, Cr, Cu, Ga, Ge, Hg, Mn, Mo, Ni, Pb, Sb, Sn, Sr, Ti, Tl, V, W, Zn, and Zr were determined in more than 100 graphite samples and graphitic rock samples. In general, the content of trace elements decreases with increasing crystallinity and carbon content. This trend also applies to biophilic elements such as Ge, V, and B. In amorphous (microcrystalline) graphite, traces of Ge, Be and Cr suggest an origin from coals (humitic), while the presence of Mo, Co and Ni, along with high V contents, point to an origin from bituminous rocks and sapropelites (Janda and Schroll 1960). High B contents are likely associated with graphite formed from paralic coal seams. A conclusion about the source rock of vein graphite is considerably more challenging. All examined graphite samples in the study from Schroll and Janda from 1960 exhibit trace element contents of typical biophilic elements such as V, B, Ni, Co and Mo, which can be taken as evidence that these rocks should be classified as organogenic sediments. In the analyzed Ceylon samples, B and V were absent, which corresponds to the non-organic origin of the carbon in these graphites. During graphitization, all elements bound to the organic matter migrate into associated minerals, resulting in a dependence on the degree of crystallinity and ash content. Therefore, a genetic correlation is mostly possible in microcrystalline and anthracitic graphite. The questions concerning the behavior of trace elements during metamorphism of such rocks, however, require further comprehensive investigations (Janda and Schroll, 1960 ; Schroll 1976).

To summarize, the chemical composition of graphite, especially the presence of trace elements, is influenced by various geological processes:

1. Metamorphism: Metamorphic processes, such as regional and contact metamorphism significantly impact on the trace element composition of graphite. During metamorphism, the precursor materials undergo recrystallization and mineral reactions, which can introduce or remove trace elements from the graphite and the other way round.

2. Host Rock Composition: The trace element composition of the host rock can influence the trace elements found in the graphite. The interaction between these rocks and the carbon source can lead to the incorporation of trace elements into graphite.

3. Fluid Infiltration: The movement of fluids through the geological environment can introduce or leach out trace elements from the graphite.

4. Mining and Processing: The mining and processing of graphite ore can introduce trace elements through contamination during extraction and beneficiation processes into the concentrate, but also leach out certain elements through chemical processing.

5. Geological History: The overall geological history of a graphite deposit, including its formation, geological events, and subsequent alterations can leave a fingerprint on the trace element composition of the graphite.

### 5.1.3. Carbon Isotope Ratios

Carbon isotopes in graphite are crucial to identify the origin of carbon. They provide information about the source material and the geological processes that led to the formation of graphite. The interpretation of the source of carbon in graphite relies on the distinct isotopic ranges characterizing the primary carbon origins, including organic matter, carbonates, and the Earth mantle. The average $\delta^{13}C$ value for organic matter typically is around -25 ‰, whereas marine carbonates spanning from the Cambrian to the Cenozoic exhibit higher $\delta^{13}C$ values, ranging from -2 ‰ to 0 ‰. In contrast, the isotopic signatures of diamonds and mid-oceanic ridge basalts (MORB) suggest that mantle-derived carbon is notably heavier, with $\delta^{13}C$ approximately -7 ‰, compared to biogenic carbon (Figure 9). Considering these variables, graphite of biogenic origin that has undergone extensive high-temperature metamorphism and isotopic exchange with a carbonate phase would exhibit an isotopic signature significantly heavier than its original source. Graphite of biogenic origin that has been surrounded by graphite precipitated from a $CO_2$-rich fluid resulting from decarbonation reactions or mantle-derived $CO_2$ would also display a bulk isotopic ratio heavier than the typically lower $\delta^{13}C$ value associated with biogenic graphite (Luque et al. 2014).

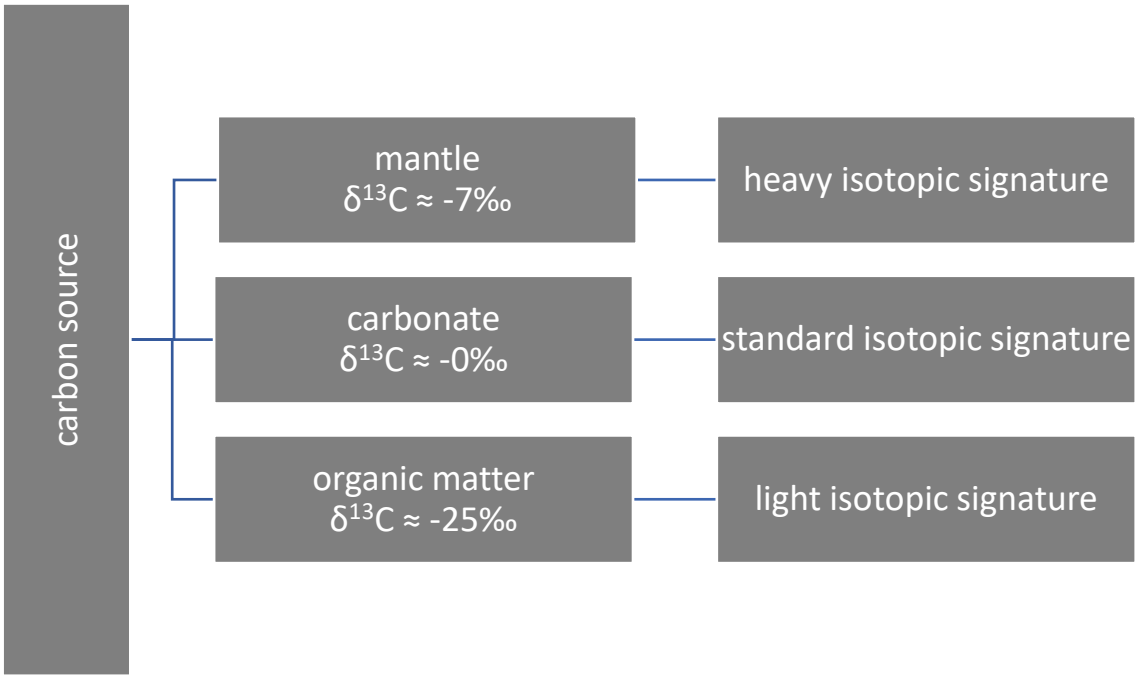


*Figure 9: Relation between carbon source and carbon isotope composition (mod. From Luque et al. 2014)*

The isotopic difference between disseminated and vein graphite shows that they likely come from different sources. As the carbon in vein graphite is not of biogenic origin, it could have two other sources to account for, the heavy isotopic signature: (a) $CO_2$ originating from the mantle and (b) $CO_2$ arising from decarbonation reactions within carbonate-bearing lithologies (Luque et al. 2014).

A straightforward relationship between the carbon isotopic signature of graphite and its source is challenging. It is often altered due to fractionation effects, influenced by factors such as temperature and the presence of other mineral phases, including carbonates. Identifying the origin of carbon in fluid-deposited graphite is even more difficult, given the potential for the mixing of diverse carbon reservoirs before or during graphite precipitation from the fluid, as well as the fractionation of carbon between the different species in the fluid and graphite during the fluid evolution (Luque et al. 2014).

Terrestrial carbon originating from the earth's mantle (diamonds), as well as carbonatites and certain natural carbonates, generally exhibit values similar to meteorites. The significant fractionation of the two isotopes ($^{12}C$ and $^{13}C$) makes it challenging to determine the original composition of carbon in the Earth's crust. This fractionation results from two processes:

1. The establishment of a chemical equilibrium between $CO_2$ - $[HCO_3]^{-1}$ or $[CO_3]^{-2}$, wherein the heavier $^{13}C$ isotope is incorporated into dissolved bicarbonate and precipitated carbonate, while the lighter $^{12}C$ is enriched in atmospheric $CO_2$. Carbonate formed inorganically from seawater typically has a $\delta^{13}C$ value approximately 10 per mil higher than atmospheric $CO_2$.
2. A kinetic effect in the assimilation process of plants, particularly terrestrial plants, which concentrates the lighter $^{12}C$ in the biosphere. Carbon of biogenic origin tends to have a $\delta^{13}C$ value roughly 20‰ lower than atmospheric carbon dioxide. The distinct $CO_2$ regimes on land and in water result in a differentiated isotope distribution in both areas, with terrestrial plants having a higher $^{12}C$ content than marine plants.

In the case of highly metamorphosed graphite occurrences in marble-bearing metamorphic rocks, the carbon isotopic composition alone does not distinguish whether the graphite was formed from organic matter (as observed in Kropfmühl Passau). The difference between the $\delta^{13}C$ values of the graphite (-20 to -26 ‰) and the marble (-2 to -22 ‰) is not particularly distinctive (Schroll 1976).

The carbon isotopic composition of graphite falls into two groups: $\delta^{13}C$ -4 ‰ to -11 ‰ and -19 ‰ to -34 ‰. Graphite derived from coal (e.g., Kaisersberg, 24,4 ‰) fall into the second group. Magmatic graphites fall in the range of -2 ‰ to -12 ‰, while metamorphic graphite exhibits a wide range, varying from -1 ‰ to -45 ‰ (Schroll 1976).

## 5.2. Sample Treatment and Sample Preparation Procedure

### 5.2.1. Sample Material

The available sample material included flake, amorphous and vein type of graphite. Flake and amorphous graphite were available as concentrates and vein graphite as lumps/chunks.

The flake dimensions within the concentrates are influenced partly by the processing methods employed and by the inherent flake size of the graphite ore and its genesis. The flakes and corresponding dimensions are presented in chapter 6.1. Optical Properties. Figure 10 illustrates a flake (left image) and amorphous (right image) graphite concentrate for a visual reference.

*Figure 10: Flake (left) and amorphous (right) graphite concentrate*

The graphite ore from Sri Lanka exists in the form of lumps and chunks (Figure 11), as they are extracted and then crushed. Graphite concentrate from Sri Lanka is not available for the current study; however, high-purity chunky graphite was investigated.

*Figure 11: Vein graphite from Sri Lanka, Ragedara mine*

### 5.2.2. Sample Preparation

Each graphite sample was subsequently homogenized and then split, with approximately one-third of it being used as the working sample, while the remaining two-thirds were retained as back-up samples for future analysis and archival purposes. The ultimate goal was to obtain samples or concentrates from different years at the respective mining sites, as this reflects various extraction areas within the mine, thus allowing to test the natural heterogeneity within a deposit. This sampling approach also takes into consideration different mined sectors within the deposit.

The samples have been prepared for further analyses, which will be discussed in more detail in the following subchapter. The subsequent analyses required tailored sample preparation for each applied method.

### 5.2.3. Powder Pressed Pellets

The majority of samples in this study existed in concentrate or powdered forms, therefore it was necessary to transform them into solid states for specific analyses, notably LA-ICP-MS. This transformation was achieved through a pressing process. Initially, adhesives/binders such as high-purity laboratory wax were employed for this purpose. However, through later, more targeted mechanical press applications, the need for adhesives was not necessary any more. This strategic refinement ensured the avoidance of further dilution or contamination of the already highly pure concentrates by laboratory wax. Two laboratory presses, conventionally employed for fabricating powder pellets for XRF were available. One possessed a press diameter of 11 mm and the other a 31mm press diameter (Figure 12).

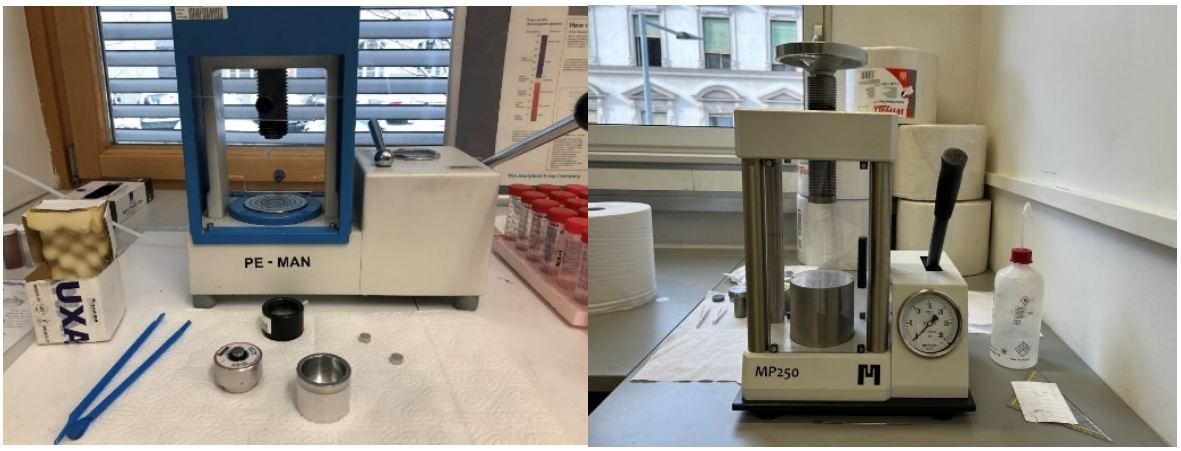


*Figure 12: Different presses for the pellet preparation: 11 mm pressing diameter (left image) and 31 mm pressing diameter (right image).*

*The larger press (MP 250; Maasen Spektroskopie) with 31 mm pressing element diameter, featured films that could be affixed to the upper and lower press components to avoid adherence of the pressed graphite to the metallic surfaces, as seen in*

Figure 13. Attempts without these films as separating elements between the pressing part and the material were unsuccessful, as the material adhered to the metal pressing element. While reducing the pressure could prevent material adhesion, it resulted in insufficient stability.

Several pressing experiments revealed ideal pressing parameters for the 31 mm diameter press as 4.5 g of graphite material, 12 t contact pressure and approx. 150 – 180 sec time. It is noteworthy that the pressing dynamics are influenced by grain/flake size and grain/flake morphology, with each material showing distinctly different behaviors during the pressing process. Flake graphite, notably, has better pressing characteristics when compared to the exceedingly fine-grained amorphous (semi-graphite) material, but also the certified reference material BAM S009. Small powder pellets were adopted for LA-ICP-MS analysis due to their capacity to accommodate a greater number of samples within the sample chamber, thereby optimizing analytical efficiency. A gradual and slow release of pressure after the pressing process is necessary, as rapid decompression can result in surface chipping of the pellet. For analytical purposes, only perfectly flat and smooth surfaces are suitable.

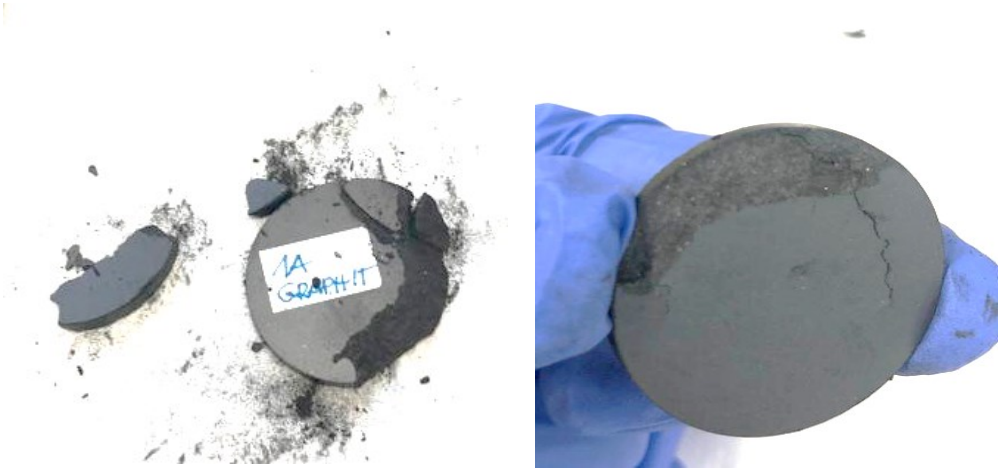


*Figure 13: Surface chipping or breaking apart of amorphous graphite material pressed into pellets*

### 5.2.4. Water suspension and Glass Plates

To facilitate Raman analysis, it was necessary to attach the graphite sample onto a smooth surface while ensuring a straightforward sample preparation process, given the need to analyze a substantial quantity of samples. The smooth, optically transparent surfaces of glass plates or glass slides were moistened with high purity water to establish a water interface. Subsequently, individual graphite flakes were dispersed onto this surface and allowed to air dry for a minimum of 24 hours. As the water evaporated, the graphite flakes adhered to the surface of the glass plate, eliminating their loose attachment.

For raw ores, graphite was selectively extracted from the ore using tweezers and spatulas, after which it was directly applied to the glass plate with the aid of high purity water, as described above. Further manipulation, such as fragmenting or milling the flakes, had the potential to modify the inherent structure of the graphite. Given that all the graphite flakes examined were sourced from processed flotation concentrates, that were milled and ground before, the resulting data remained comparable.

### 5.2.5. Preparation for Carbon Isotope Determination

The standard sample preparation method for measuring carbon isotope ratios involves placing the material within small tin capsules, which are subsequently subjected to combustion during the analytical procedure to liberate the material for analysis. It is inherent that the material is completely carbonate-free, as the presence of carbonates could potentially introduce variations in the carbon signature.

Highly pure graphite, either in the form of concentrates, or manually extracted from raw ores using tweezers or spatulas, is weighed into these pure tin capsules. The quantity of material typically falls within the range of 0.4 to 0.6 milligrams. Since individual flakes do not consistently possess the same weight, and each sample may not contain an identical quantity of material, any deviation from the prescribed amount of material (0.4 – 0.6 mg).is strictly prohibited.

Tin capsules, sample holders, a high-precision balance, spatula and tweezers, as well as an additional sample holder for the filled capsules, were the necessary tools and materials for sample preparation (Figure 14).

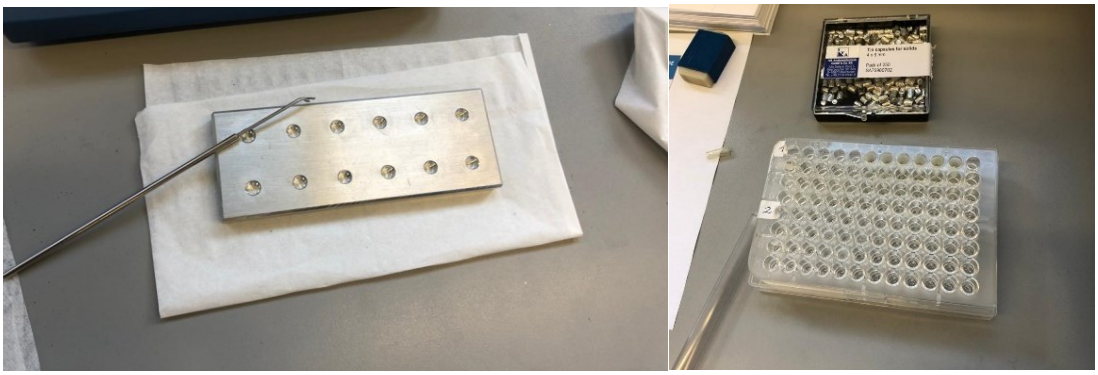

*Figure 14: left: Sample holder and a special spatula for the filling process and right: Necessary tools for the preparation as tin capsules and sample holder for final preparations*

### 5.2.6. SEM Specimen Pin Stubs

For the analysis of graphite concentrates using SEM, loose concentrate was applied to stub holders, to which a type of self-adhesive sticker had been previously affixed. This allowed the concentrate to adhere to the holder. In order to facilitate imaging through scanning electron microscopy and the associated visualization, the material on the specimen holder needs to be rendered conductive. This is achieved through a carbon coating, although it did not work effectively for graphite. An attempt was made to capture images and perform analysis without additional coating(conductivity), as graphite is a conductive material already. However, the resulting imaging was insufficient and blurred. Consequently, a shift was made to gold coating with a gold sputter vacuum coater (Agar Sputter Coater) at the Department of Functional Ceramics (Figure 15).

The gold coating parameters were defined as follows - working distance: 3 cm, electric current: 30 mA, time: 30 sec.

*Figure 15: Gold sputter vacuum coaters for SEM*

### 5.2.7. Polished Sections/Mounts

In the context of graphite imaging via light microscopy and its application for LA-ICP-MS, the creation of polished sections (Figure 16) was necessary and presented a notable challenge due to the softness of graphite, which contrasts with the considerably harder minerals present in the raw ore samples. The procedural approach involved the following steps assuming the material already being completely dry:

- ✓ Embedding samples in epoxy resin (epoxy casting resin "water-clear" and hardener W300 in a ratio of 100:30); curing time minimum 3 days
- ✓ Removing air from samples and resin in a vacuum chamber (Heraeus)
- ✓ Grinding with a 125 µm diamond grinding wheel

- ✓ Grinding with a 40 µm diamond grinding wheel
- ✓ Grinding with a 10 µm diamond grinding wheel
- ✓ Lapping: ATM Alpha polishing cloth and 120 mesh (approximately 9 µm) aluminum oxide abrasive
- ✓ Polishing Step 1: DP-Pan polishing cloth, 350 mm diameter, with 3 µm diamond suspension
- ✓ Polishing Step 2: MD-Dur polishing cloth, 350 mm diameter, with 1 µm diamond suspension
- ✓ Polishing Step 3: Buehler Metaserv polishing machine, Mambo Chen polishing cloth, 200 mm diameter, with 0.05 µm aluminum oxide polishing abrasive

Due to the softness of graphite, the polishing process was demanding, resulting in frequent incidents of breakage and relief occurrences and not achieving a perfectly flat and uniform polish, as typically attained with conventional rock samples.

In some cases, graphite flakes exhibited such low density that they failed to settle during the thick section preparation, remaining suspended and thus not emerging on the surface of the final thick section. Careful resin pouring ensured that the pre-introduced concentrates remained at the bottom and subsequently became visible on surface of the mount.

*Figure 16: Graphite concentrates (left image) and raw ore (right image) embedded into epoxy resin*

### 5.2.8. Sample Digestion

For the solution-based-ICP-MS analysis the ions of interest in the graphite samples had to be brought into a solution. Consequently, the development of a sample preparation and measurement procedure for ICP-MS measurement emerged as a pivotal component of this research study. The high resistance of graphite to digestion was a primary consideration and resulted in the main challenge for multi-element analysis. The aim of extensive laboratory experiments was to develop a complete digestion procedure method, for the natural, geogenic graphite samples. Understanding the elemental composition of carbon-rich samples, whether of geogenic, biogenic, or technological origin, is crucial for advancing technical applications and identifying their origin through elemental fingerprinting. The methods used for digestion are both microwave digestion procedures and both convert C to $CO_2$. In the MIC digestion procedure, the material is combusted in pressed form under oxygen in quartz glass vessels. In the MW methodology, the digestion procedure is performed in PTFE vessels with the sample material in loose form without the addition of oxygen.

High purity water (HPW) water was sourced from a Milli-Q element module (18.2 MΩ cm; Merck Millipore, Darmstadt, Germany). Nitric acid ($HNO_3$, w = 65 %, p.a. grade; Carl Roth GmbH, Karlsruhe, Germany) was purified in perfluoroalkoxy-polymer (PFA) sub-boiling units (DST-1000 and DST-4000, Savillex, Eden Prairie, MN, USA). Hydrogen peroxide solution ($H_2O_2$, w = 30 %; Merck KGaA, Darmstadt, Germany) for digestion assistance were purchased in ultra-pure quality. All plastic

consumables underwent cleaning by vaporization in $HNO_3$ (w= 65 %), followed by thorough rinsing with ultra-pure water.

### 5.2.8.1. Literature Review on Graphite Digestion Methods

As part of the preparation process for experiments aimed at achieving complete digestions of graphite material and to gather insights on how to tackle this challenge, a literature review on graphite sample preparation for various analytical methods was conducted. So far, graphite has not been dissolved for the purpose of element analysis for proof of origin methods. However, it has been addressed in the context of various technical and technological inquiries related to carbon-rich materials.

Synthetic graphite powders with varying purities were thoroughly analyzed by Bögershausen in 1997 using a range of techniques. ICP-MS was employed for the determination of elements including Al, Co, Cu, Cr, and Pb. The analysis involved a microwave digestion process and the addition of specific acids. The study aimed to establish reference values rather than compare methods and laboratories. Notably, techniques capable of direct solid analysis (INAA, XRF, and DC-OES) demonstrated superior consistency and fewer outliers compared to methods such as ICP-MS, ICP-OES, FAAS (flame atomic absorption spectroscopy), and ETAAS (electrothermal atomic absorption spectroscopy), which required various wet chemical sample preparation steps. The quality of the complicated sample preparation significantly influenced the overall accuracy and precision of the results. Among the acid digestion techniques, using water-free nitric acid and concentrated sulfuric acid produced the clearest solutions, while other methods left some solid particles behind (Bögershausen et al. 1997).

A digestion technique based on microwave-induced combustion, tailored for organic samples such as bovine liver, pig kidney, and skim milk was established and tested in 2004. The sample digestion was described as a vulnerable point in analytical processes, susceptible to errors, especially in trace element determinations, with potential systematic errors as high as 100%. Closed-system microwave digestion has gained widespread acceptance as an efficient sample preparation method. It reduces digestion time and reagent usage, minimizes contamination and loss of volatile substances and provides safety. The use of concentrated mineral acids in these systems may elevate blank values due to contaminant elements. High acid concentrations may also pose challenges for certain analytical techniques, necessitating a subsequent step to remove or dilute excess acid (Flores et al. 2004).

A review from 2007 focuses on combustion, oxygen flask, and microwave-induced combustion (MIC) techniques, discussing their operational conditions, characteristics, and limitations. MIC techniques are highlighted, particularly for samples challenging to digest using traditional microwave-assisted wet digestion, such as coal, and for subsequent halogen determination. Traditional techniques based on microwave-assisted acid digestion have certain limitations for specific applications, primarily due to the stability of organic materials like graphite, which hinders efficient digestion. In such cases, combustion methods emerge as the most effective and convenient approach to decompose organic materials. Combustion techniques, driven by high temperatures, can efficiently decompose almost all organic matrices, minimizing interference with subsequent analytical determinations. Moreover, there is a growing need for non-metal determination in various samples, where conventional acid digestion techniques are less suitable. In summary, sample digestion techniques can be broadly categorized into two major groups: wet digestion and combustion techniques (Flores et al. 2007).

The challenges associated with digesting graphite and the critical need for impurity control in industrial applications was assessed by Cruz et al. in 2015. Microwave-induced combustion as a method for graphite digestion and the subsequent determination of multiple elements was proposed. This approach involved burning a relatively high mass of graphite (400 mg) using a pressurized system with oxygen and diluted nitric acid solution. Remarkably, it achieved a high digestion efficiency (over 99%) and

excellent recovery rates for various elements, even with relatively low concentrations of nitric acid. The results were confirmed through both inductively coupled plasma optical emission spectrometry (ICP-OES) and inductively coupled plasma mass spectrometry (ICP-MS). Traditional combustion methods using sample pellets and filter paper led to inconsistent combustion and suspended solid residues, highlighting the unique challenges posed by graphite's resistance to oxidation, particularly at atmospheric pressure (Cruz et al. 2015).

Microwave digestion advantages were reported in another publication in terms of efficiency, reagent economy, and reduced risk of contamination and elemental loss. However, it is acknowledged that microwave digestion remains time-consuming despite these benefits (Botelho et al. 2001).

The MIC digestion method was identified as a suitable method for digesting up to 100 mg of the graphite sample. However, microwave-assisted digestion and dry-ashing methods resulted in insoluble residues and analyte losses. To ensure complete oxidation of the graphite material matrix, cellulose should be utilized as a combustion aid during MIC digestion. For MIC digestion, two independent absorbing solutions (4 mol $L^{-1}$ $HNO_3$ and inversed aqua regia) were necessary for the quantitative recovery of embrittling elements. The limits of detection achieved through MIC, coupled with ICP-OES and FI-CVG-AAS, were satisfactory for quantifying all potentially embrittling elements (Enders et al. 2016).

Nuclear-grade graphite is the core structural material for the high-temperature gas-cooled reactor systems. The quantification of trace and ultra-trace elements in nuclear grade manufactured graphites by fast flow glow discharge mass spectrometry and by inductively coupled plasma mass spectrometry after microwave induced combustion digestion have been successfully tested (Wang et al. 2010).

The analysis methods presented in the literature, such as FTIR and TGA, are indeed applied to graphite materials. However, they primarily serve the purpose of identifying the carbon content rather than the trace or minor elements in graphite (Zethof et al. 2019), and thus, they are not relevant for this study.

In 1960, Janda and Schroll analyzed various elements in graphite and graphite-containing rocks using an emission spectrographic method. They found that with increasing crystallization degree and generally higher carbon content, the concentration of trace elements decreases (Janda and Schroll 1960).

### 5.2.8.2. Microwave Induced Combustion Digestion Procedure

*Table 9: Combustion digestion procedure*

| | | | |
|---|---|---|---|
| **1** | **Sample material** | For the systematic comparison of different digestion procedures four samples had been chosen for method development. Also, the certified reference material BAM-S009 *("Medium Purity Graphite Powder"*) was used for method validation in this study. All graphite concentrate samples were available as loose powders. | 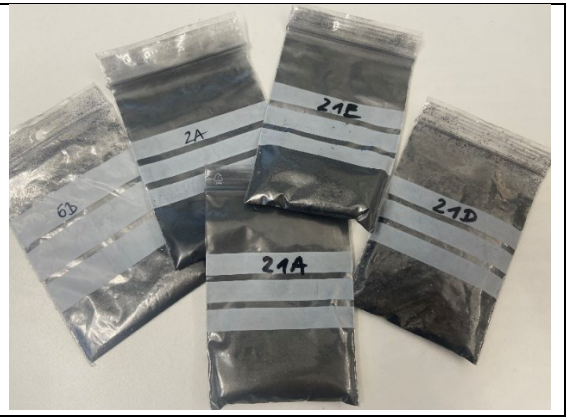 |
| **2** | **Pellet Pressing** | To place the samples in the quartz glass sample holder, the samples needed to be formed into a pellet shape and mixed beforehand with high-purity cellulose as a combustion aid in a 1:1 ratio. The pellet had to be pressed firmly enough with the cellulose to be stable in the MIC sample holder. If the pellet experienced too much pressure and became too firm, the complete combustion process would no longer work. Pressing was performed at 5 t contact pressure for max. 60 sec with a mixture of 100 mg powdered sample and 100 mg cellulose. | 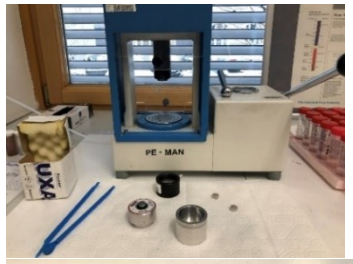 <br> 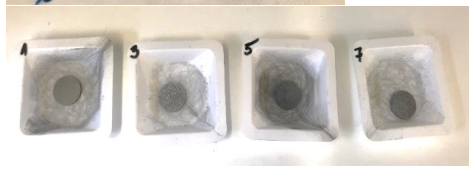 |

| | | | |
|---|---|---|---|
| **3** | **Preparing the sample holder and vessel** | The sample holders made of quartz glass were covered with cellulose filter paper (Macherey-Nagel, Grade MN 1640 de), which was precisely cut to the size of the sample tray. The samples were placed in the quartz glass tray on the filter paper. The filter paper around the sample was moistened with with 50 µl $NH_4NO_3$ solution (50 % w/v). Ammonium nitrate was used as a combustion aid (oxidizer).<br>The sample holder was placed into a quartz vessel containing 6 mL of 5 % nitric acid (or 8 mL 50% v/v). |    |
| **4** | **Gas-loading** | The vessels were sealed with a PTFE TFM lid and placed into the rotor (Rotor 8NXQ80, Multiwave Pro, Anton Paar). The vessels were prior filled with 20 bar oxygen (5.0) using a four-way valve station. When microwave irradiation is applied, the impregnated filter paper in the vessels, and thus the samples, are ignited by the microwave energy. |    |

| | | | |
|---|---|---|---|
| **5** | **Digestion process** | The microwave program was set to a maximum temperature of 280 ° and 80 bar, which was reached within a ramp time of 10 min and then held for 14 min. The maximum microwave power was 1800 W. After completing the digestion procedure and cooling down to 55°C, the vessels were vented, opened and their contents were transferred into 50 mL PP tubes. Successful digestion runs resulted in completely digested samples or an incomplete digestion leaving residues in the form of solid particles at the sample holder or in the solution. The operational conditions and the heating program followed the recommendations from the microwave oven manufacturer (Anton Paar, Graz, Austria). |  |
| **6** | **ICP-MS analysis** | Multi-element analysis using a 7500cx Agilent ICP-MS for the measurement of the diluted digestion solutions. |  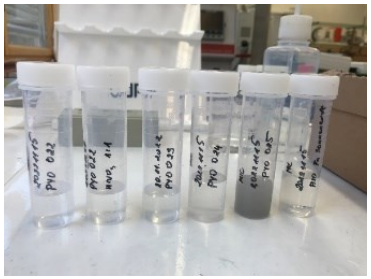 |

Following numerous tests aiming to achieve a complete dissolution of graphite material and subsequent analysis of the produced solutions, it has become apparent that the combustion process is not reproducible. It cannot be excluded that elements may be lost during the digestion procedure and de-gasing of the vessels, however, there was no way to verify this. The process does not facilitate the capture of the escaped gases.

During the MIC combustion digestion procedure, the following observations were made:

- *The digestion efficiency depends on the crystallinity and the grain sizes (amorphous (semi-graphites) are easier to digest, as well as the Reference Material BAM S009, which is a semi-graphite)*
- *Microwave induced combustion leads to a more complete digestion, however digestion results were not reproduceable and could not be successfully applied to each graphite concentrate (because of crystallinity and flake size differences)*

***Hypothesis***: Digestion rate depends on the structure and morphology of the carbon (Bandoniene et al. 2023)

### 5.2.8.3. Conventional Microwave Digestion Procedure

An Anton Paar Multiwave PRO closed-vessel digestion system, equipped with a 24HVT50 rotor (Anton Paar, Graz, Austria) and 30 mL PTFE vessels, was employed for the microwave digestion of natural graphite concentrates. Approximately 0.2 g of graphite sample was weighed into PTFE digestion vessels directly. After adding the chemicals, the microwave program was set to a maximum temperature of 200 °C, reached within a ramp time of 10 min, and held for 15 min. The maximum microwave power was 1500 W (Trimmel et al. 2023). After cooling down to 55 °C, the program concluded, and the vessels were vented and opened. The contents were transferred into 50 mL PP tubes, rinsed with ultrapure water to obtain a total digest volume of about 40 mL. The tubes were weighed empty and after adding the digest solution to determine exact masses.

The used reagent mixture was as follows: 5 mL $HNO_3$ and 1 mL $H_2O_2$ applied to each sample material. To determine the reproducibility of the digestions and eliminate outliers, three digestions of each sample were prepared in different digestion sessions. Alongside each batch, two procedural blanks were processed in the microwave using the same procedure and the same reagents. One cleaning digestion run with 5 mL of $HNO_3$ in each vessel was conducted between batches.

### 5.2.8.4. Comparison of the digestion procedures

Both digestion procedures were compared for five graphite samples and the certified reference material (BAMRM) for two elements (Figure 17). The digestions generated by conventional microwave procedure (MW) show higher precisions in general, compared to digestions from the microwave induced combustion digestion procedure (MIC). To ensure reproducible digestions and analyses, all samples must ultimately be processed with the same method. Since this was not feasible with the MIC method, the sample preparation for solution-based ICP-MS via MW was chosen.

BAM S009 (BAMRM) was digested using both methods. Results from MW and MIC for the elements Cr and Zn are quite close to the certified value for the respective element (Cr and Zn). Element concentrations for other elements with lower concentrations (in BAMRM) could not be reproduced properly (due to blank values higher than certified element concentrations).

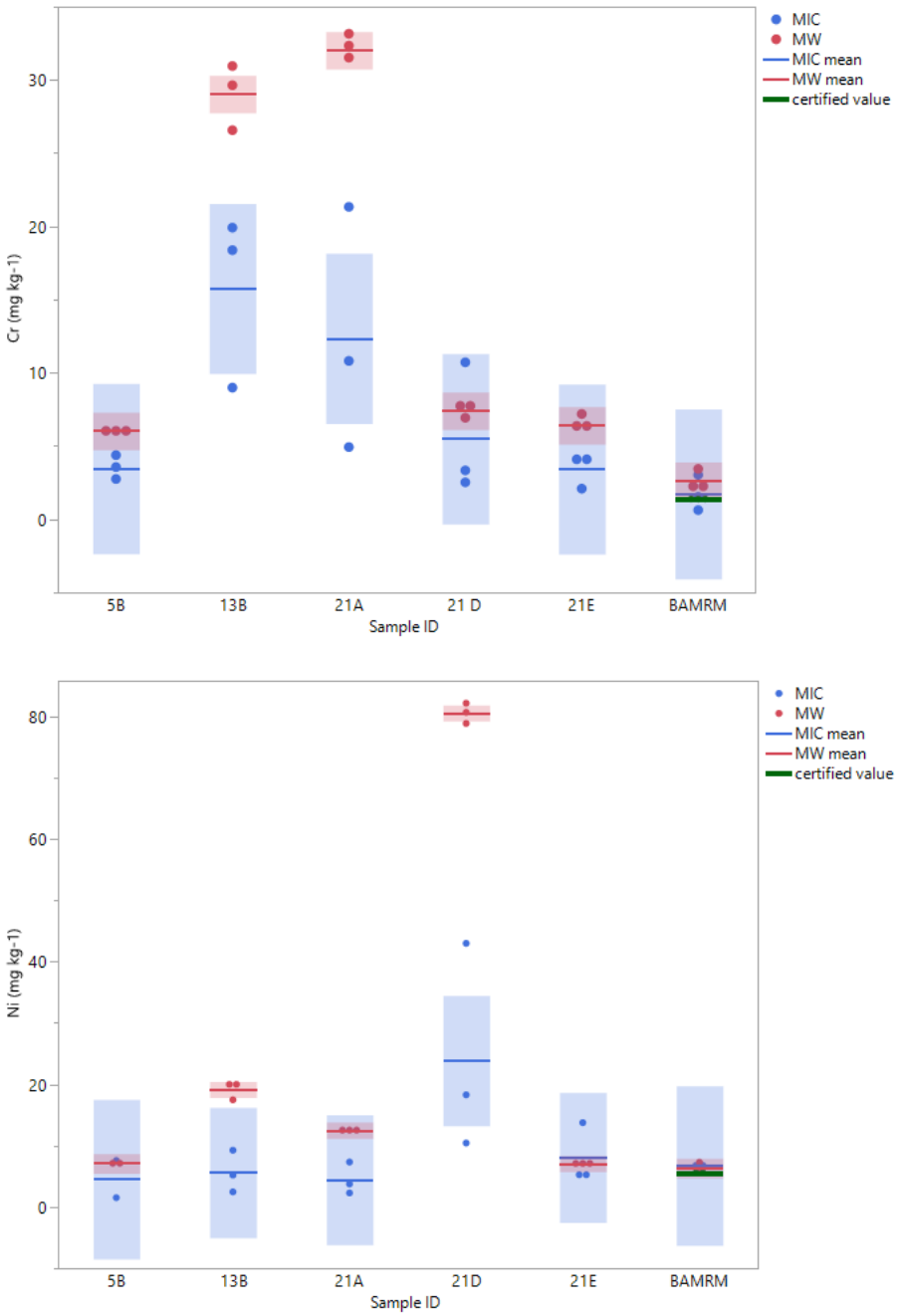


*Figure 17: Mass fractions (n=3) of selected trace elements (Cr and Ni) in graphite concentrate samples and in certified reference material (BAMRM) BAM-S009 determined using solution-based-ICP-MS analysis after different digestion methods (conventional MW – red, MIC – blue)*

## 5.3. Analytical Methods and Instrumental Procedure

### 5.3.1. Overview of the Analytical Methods

A broad range of analytical methods are used in natural sciences such as chemistry, metallurgy, archaeometry and geosciences. A common application in the latter is quantifying the composition of minerals and rocks, spanning from major elements in the percentage range to trace elements in the parts per million range. Isotope compositions and ratios often play an important role in these analyses. Simultaneously, diffraction techniques are essential for phase analysis and determining the geometric arrangement of atoms, ions, or molecules in minerals. Conventional microscopic methods are complemented by high-resolution scanning and electron microscopy. A wide array of spectroscopic

methods, employing the full electromagnetic spectrum, are deployed for investigating chemical bonding in minerals and crystals, as well as resolving structural issues. In this chapter, the analytical instruments applied for graphite are listed, in five groups, which are based on the excitation energy.

*Table 10: Overview of the analytical methods used for the Analytical Proof of Origin of natural graphite divided into 5 groups based on their excitation energy*

| Group 1: Emission and mass spectrometric techniques | Group 2: Electron beam methods | Group 3: X-ray methods | Group 4: laser induced methods | Group 5: Imaging and visual analysis |
|---|---|---|---|---|
| Inductively coupled plasma-mass spectrometry (ICP-MS) | Scanning electron microscopy (SEM) | Handheld XRF | Laser-ablation inductively coupled plasma-mass spectrometry (LA-ICP-MS) | (Digital) light microscopy |
| Gas isotope ratio mass spectrometry (Gas-IR-MS) | | | Raman spectroscopy | |

### 5.3.2. LA-ICP-MS (Laser-Ablation Single Collector Inductively Coupled Plasma Mass Spectrometry)

Laser ablation is used for quantitative analysis of major, minor and trace elements in solid samples without the necessity of dissolving the sample. Performance and application type depend on the choice of laser and mass spectrometer. Available options include quadrupole (Q), sector-field (SF), and multi-collector (MC) mass spectrometers. Additionally, time-of-flight (TOF) instruments are becoming increasingly important.

Laser ablation single collector ICP-MS analyses of natural graphite ore and concentrates were performed at the Geological Survey of Finland (GTK), using a Nu AttoM SC-ICP-MS (Nu Instruments Ltd., Wrexham, UK) coupled with an Excite 193nm ArF laser-ablation system (Photon Machines, San Diego, USA). The mass spectrometer was tuned with NIST612 glass using a 40 % output on 5mJ, a repetition rate of 10 Hz, a circle spot of 50 µm, yielding around 500,000 to 600,000 cps. The laser was run at a pulse frequency of 10 Hz and a pulse energy of 5 mJ to produce an energy flux of about 10-15 J/cm$^2$ on the sample surface in a line raster mode of 135 µm circle spot. Prior to analysis, each line was preablated with a rastering at 30 µm/s. With these instrument parameters, about 13,000,000 cps can be obtained on a baseline of 5,000,000 cps. Each analysis was initiated with a 20 second baseline measurement followed by switching on the laser for 60-90 seconds for signal acquisition. These analyses were made using time resolved analysis (TRA) with continuous acquisition of data for each set of lines (generally following the scheme of 2 primary standards and 15 unknowns). An in-house synthetic pressed nanopellet of graphite standard Gh20220218 was used for external standardization (the preparation process is described separately below). The isotope $^{13}C$ has been used as an internal standard assuming a content of 98 wt % carbon. The measurements were performed on 68 isotopes covering 61 elements at low resolution ($\Delta M/M = 300$) using the Fastscan mode. Data reduction was handled using the software GLITTER ™ (Van Achterbergh et al. 2001) which allows the baseline subtraction, the integration of the signal over a selected time resolve area and the quantification using known concentrations of the external and internal standards. Due to unavailability of a second good in-house pressed pellet as a quality control, the analytical precision and accuracy was monitored by treating Gh20220218 as an unknown. The results suggested a relative standard deviation (RSD) of 10-40 % for all elements except Li, Ni, Ba, Bi and an accuracy of ±5-10 % for most elements except for Li, Fe, Ni, Ba, and Bi.

The standard was prepared by spiking a high purity (≤0.0002 % total impurities) natural graphite powder (200 mesh) with multielement solution from LabKing. The spiked powder was then soaked with MilliQ water to make it slurry, which was then dried on a hot plate at 70 °C. The dried material was then grinded and pressed to a pellet. This process can produce relatively homogeneous element distributions.

The LOD values for the LA-ICP-MS methodology were determined for graphite concentrates and the corresponding pressed pellets. LOD values for graphite raw ore is not reported due to the highly variable grain sizes of the graphite in raw ore which required different spot sizes for each analysis/raw ore. LOD values were determined as the point where signal from the analyte becomes differentiable from inherent noise/background in the system and is defined as the lowest concentration of an analyte in a sample that can be detected reliably. The LOD value for the LA-ICP-MS methodology is composed of the mean value of all LOD values reported for each respective element/analyte. Element concentrations below detection limit were replaced by 0.5 times the detection limit for the respective element.

*Table 11: LOD values for LA-ICP-MS analysis for graphite concentrates*

| **LA-ICP-MS** | **concentrate** |
|---|---|
| **Analyte** | **LOD µg/g-1** |
| Mg | 0.0019 |
| Al | 0.0119 |
| Ca | 0.7314 |
| V | 0.0054 |
| Cr | 0.1059 |
| Mn | 0.1446 |
| Fe | 0.8656 |
| Co | 0.0403 |
| Cu | 0.0369 |
| Zn | 0.0891 |
| Ga | 0.0050 |
| As | 0.0384 |
| Rb | 0.0122 |
| Sr | 0.0014 |
| Y | 0.0010 |
| Zr | 0.0004 |
| Ce | 0.0003 |
| Th | 0.0006 |
| U | 0.0002 |

### 5.3.3. ICP-MS (Inductively Coupled Plasma Mass Spectrometry)

The trace element concentrations in the graphite concentrates were determined using an Agilent 7500cx ICP-QMS (Agilent Technologies, Tokyo, Japan) equipped with a 100 µL PFA nebulizer and a quartz glass spray chamber cooled to 2 °C. Isotopes at given m/z which were affected by spectral interferences (V, Cr, Mn, Co, Ni, Cu, Zn, As) were measured with He as collision gas, where most isotopes could be measured without significant interferences. Signal intensities on m/z 24 (Mg), 27 (Al), 43 (Ca), 51 (V), 53 (Cr), 55 (Mn), 57 (Fe), 59 (Co), 62 (Ni), 65 (Cu), 66 (Zn), 71 (Ga), 75 (As), 82 (Se), 85 (Rb), 88 (Sr), 97 (Mo), 107 (Ag), 111 (Cd), 137 (Ba), 205 (Tl), 207 (Pb), 238 (U), 89 (Y), 139 (La), 140 (Ce), 141 (Pr), 145 (Nd), 146 (Nd), 147 (Sm), 149 (Sm), 151 (Eu), 160 (Gd), 159 (Tb), 161 (Dy), 163 (Dy), 165 (Ho), 166 (Er), 167(Er) 169 (Tm), 172 (Yb), 173 (Yb), 175 (Lu), 232 (Th) were measured.

The establishment of an external calibration curve for the quantification of ICP-MS signals offers an extensive range of calibration solutions available in different concentrations for all elements, encompassing the REE. This versatility enables the calibration of the method, even with the absence of dedicated reference or calibration materials tailored for graphite itself. General calibration solutions designed for ICP-MS applications are universally adaptable and applicable also to this study.

The ICP-MS multi element standard solution Merck VI (Merck Certipur, Darmstadt, Germany) featured the following element concentrations: Ag, Al, , Ba, Bi, Cd, Co, Cr, Cu, Ga, In, K, Li, Mg, Mn, Mo, Na, Ni, Pb, Rb, Sr, Te, Tl, U and V, with 10.0 $mgL^{-1}$, As, B, Be, Fe, Se, Zn with 100 $mgL^{-1}$, Ca with 1000 $mgL^{-1}$ effective certified concentrations diluted in $HNO_3$ (*w*=6 %). 40 ng $mL^{-1}$ stock solution for Ag, Al, Ba, Bi, Cd, Co, Cr, Cu, Ga, In, K, Li, Mg, Mn, Mo, Na, Ni, Pb, Rb, Sr, Te, Tl, U, V, 400 ng $mL^{-1}$ for As, B, Be, Fe, Se, Zn and 4000 ng $mL^{-1}$ for Ca of ICP multi-element standard solution Merck VI in $HNO_3$ (w=1 %) was used for a calibration. Calibration ranges were diluted accordingly from 0 -1 $\mu g\ g^{-1}$, 0-10 $\mu g\ g^{-1}$ and 0-100 $\mu g\ g^{-1}$ for the respective groups of elements.

Given the uneven distribution of Rare Earth Element (REE) concentrations, with higher concentrations of light REE compared to heavier REE, and higher concentrations of even-numbered elements compared to odd-numbered elements as per the Oddo–Harkins rule, a custom-made calibration solution was used. This solution (REE multi-element standard AHF-CAL-7, Inorganic Ventures, NJ, USA) featured the following REE concentrations: 1000 µg $mL^{-1}$ Ce, 500 µg $mL^{-1}$ La, Nd, Y, 150 µg $mL^{-1}$ Th, 100 µg $mL^{-1}$ Pr,, 50 µg $mL^{-1}$ Dy, Gd, Sm, U, 20 µg $mL^{-1}$ Er, Eu, Yb, 10 µg $mL^{-1}$ Ho, Tb, and 5 µg $mL^{-1}$ Lu, Tm in 7 % (m/v) $HNO_3$. A 40 ng $mL^{-1}$ stock solution (calculated for Ce) was prepared and diluted with 1 % $HNO_3$ to establish a calibration range from 0 to 40 ng $mL^{-1}$.

100µL portions of a 100 ng $mL^{-1}$ In and Re internal standard solutions (CertiPur, Merch Darmstadt, Germany) were added to 5.0 mL of each sample solution and to the calibration solutions to correct instrumental drift. Three independent digestion replicates were analyzed for each sample. Additionally, total procedural blanks, containing the same amount of concentrated $HNO_3$ and $H_2O_2$ used for sample decomposition, prepared in the same manner as the samples, were analyzed. The calibration for this analytical method offers an extensive range of calibration solutions available in various concentrations for all elements, including the REE. This versatility enables the calibration of the method, even when working with graphite digests, despite the absence of dedicated reference or calibration materials tailored for graphite. Calibration solutions designed for ICP-MS applications are universally adaptable and applicable.

Two independent analysis runs were conducted, one for the analysis of non-Rare Earth Elements (Mg, Al, Ca, V, Cr, Mn, Fe, Co, Cu, Zn, Ga, As, Se, Rb, Sr, Mo, Ag, Cd, Ba, Tl, Pb, U) and the other for REE (Y, La, Ce, Pr, Nd, Sm, Eu, Gd, Tb, Dy, Ho ,Er, Tm, Yb, Lu, Th, U). The mean of mass fraction of two isotopes was calculated for Nd (145, 146), Sm (147, 149). Dy (161, 163), Er (166, 167) and Yb (172,173). The most commonly used REE mass fractions for normalization are derived from chondrite data (for bulk Earth, Earth's mantle rocks, and most magmatic rocks) and shale composite values, such as PAAS (post-Archean Australian shale, representing the average present-day continental crust), for normalizing crustal sediments and soils. In this study, the European shale composite (EUS) was used for normalization (Bau et al. 2018b).

The LOD and LOQ values were determined using six procedural blanks with LOD three times the standard deviation and LOQ ten times the standard deviation of the mean procedural blank concentrations.

*Table 12: LOD and LOQ values for solution-based-ICP-MS analysis for graphite concentrates for each analyte*

| ICP-MS Analyte | LOD µg/g-1 | LOQ µg/g-1 |
|---|---|---|
| Mg | 0.922 | 3.07 |
| Al | 1.37 | 4.56 |
| Fe | 2.16 | 7.21 |
| Cu | 0.366 | 1.22 |
| Zn | 1.82 | 6.05 |
| As | 0.431 | 1.44 |
| Se | 0.399 | 1.33 |
| Mo | 0.625 | 2.08 |
| **ICP-MS Analyte** | **LOD ng/g-1** | **LOQ ng/g-1** |
| Mn | 194 | 647 |
| V | 5.52 | 18.40 |
| Cr | 22 | 74 |
| Ni | 107 | 356 |
| Ga | 4.71 | 15.70 |
| Rb | 41 | 135 |
| Sr | 18 | 60 |
| Ag | 8.10 | 27 |
| Cd | 10 | 32 |
| Ba | 44 | 147 |
| Tl | 18 | 60 |
| Pb | 52 | 174 |
| Y | 3.98 | 13 |
| La | 20 | 67 |
| Ce | 27 | 89 |
| Pr | 0.656 | 2.19 |
| Nd | 2.625 | 8.75 |
| Sm | 0.703 | 2.34 |
| Eu | 0.158 | 0.526 |
| Gd | 0.342 | 1.140 |
| Tb | 0.0633 | 0.211 |
| Dy | 0.361 | 1.210 |
| Ho | 0.087 | 0.289 |
| Er | 0.248 | 0.828 |
| Tm | 0.0491 | 0.164 |
| Yb | 0.213 | 0.711 |
| Lu | 0.0015 | 0.005 |
| U | 2.57 | 8.58 |

### 5.3.4. Raman Spectroscopy

Raman spectroscopy is used to evaluate the lattice ordering of graphite. Raman spectra were obtained using a Horiba Labram HR Evolution instrument at the Chair of Resource Mineralogy equipped with a 100mW Nd:Yag (532nm) laser, a confocal microscope (hole aperture=100µm), a 1800 g/mm grating and a Peltier cooled CCD detector. Ca. 5-10 % of the full laser power of 100 mW was applied in order to avoid sample damage. For laser focusing and sample observation, an Olympus BX 40 microscope with a 100x objective lens was employed. In order to enhance signal-to-noise ratios, two scans were accumulated with an acquisition duration of 20 seconds within two distinct spectral regions: 700–2000 $cm^{-1}$ (first-order) and 2200–3200 $cm^{-1}$ (second-order). In total, 10–20 spectra were recorded for each sample and the calibration of band positions was achieved using a silicon wafer standard.

### 5.3.5. Microscopy

#### 5.3.5.1. Digital Light Microscopy

Graphite concentrates were analyzed and documented with a KEYENCE VHX 6000 digital light microscope.

Samples from raw ores were analyzed using a Keyence VHX-7000 equipped with an EA300 LIBS analyzer at GTK in Espoo, Finland. This allowed for the direct determination of mineral phases in the raw ore samples.

#### 5.3.5.2. Scanning Electron Microscopy

This microscopical method is mainly used for the assessment of microstructural characteristics. Non-destructive electron beam-based methods such as SEM offer the choice of simultaneously imaging and analyzing the chemical composition of points and areas in graphite samples. The ZEISS EVO10 SEM at the Cahir of Geology and Economic Geology was operated in standardless mode at 15 kV acceleration voltage and 8 seconds measurement time per spectrum. Detection limits using this setup are in the order of 0.1 wt%.

### 5.3.6. Gas-IR-MS (Gas Isotope Ratio Mass Spectrometry)

0.5 mg of graphite samples were placed into tin foil containers and subjected to combustion using an elemental analyzer (Flash EA 1112) at a temperature of 1020 °C, while ensuring an excess of oxygen. The resulting $CO_2$, meticulously isolated through column chromatography, underwent real-time analysis employing a ThermoFisher DELTA-V isotope ratio mass spectrometer. The isotope ratios ($^{13}C/^{12}C$) of the $CO_2$ were subsequently cross-referenced with those of a monitoring gas, calibrated against the Vienna-Pee Dee Belemnite (VPDB) standard. The overall analytical procedure is reproducible within the range of 0.2–0.4 ‰.

### 5.3.7. Standard and Reference Materials

Reference materials are used as benchmarks to validate methods and ensure measurement accuracy, whereas standard materials, also known as calibration materials, are used for instrument calibration and measurement standardization. For the present study both were required (Tab. 13).

*Table 13: Various standard and reference materials used for this study*

| Name | Description | Type | Parameter | Method | Comment |
|---|---|---|---|---|---|
| **AHF CAL 7** | REE multi-element standard, Inorganic Ventures, NJ, USA | Custom made standard material | REE | ICP-MS | For REE in solutions only |
| **BAM S009** | Medium purity graphite powder, Bundesanstalt für Materialforschung, Germany | Certified reference material | Trace elements | ICP-MS, LA-ICP-MS | TE values are too low and below LOD |
| **Gh20220218** | Spiked high purity graphite powder | Reference Material (in-house from GTK) | Trace elements | LA-ICP-MS | In-house material for TE analysis |
| **MERCK IV** | Multi-element standard solution | Standard Material | Trace elements | ICP-MS | For Digestion analysis only |
| **NIST 610/612** | Multi-element glasses | Standard Material | (Trace) elements | LA-ICP-MS | Instrument Calibration LA-ICP-MS |
| **Si wafer** | Artificial Si-monocrystal | Standard material | Crystallinity | Raman spectroscopy | Instrument Calibration |

## 5.4. Statistical Methods

For the present study, the workflow proposed by (Frenzel 2023) was used as a guideline starting from the conceptual preparation of the work, followed by data preparation and data analysis. The general workflow proposed is illustrated below (Figure 18).

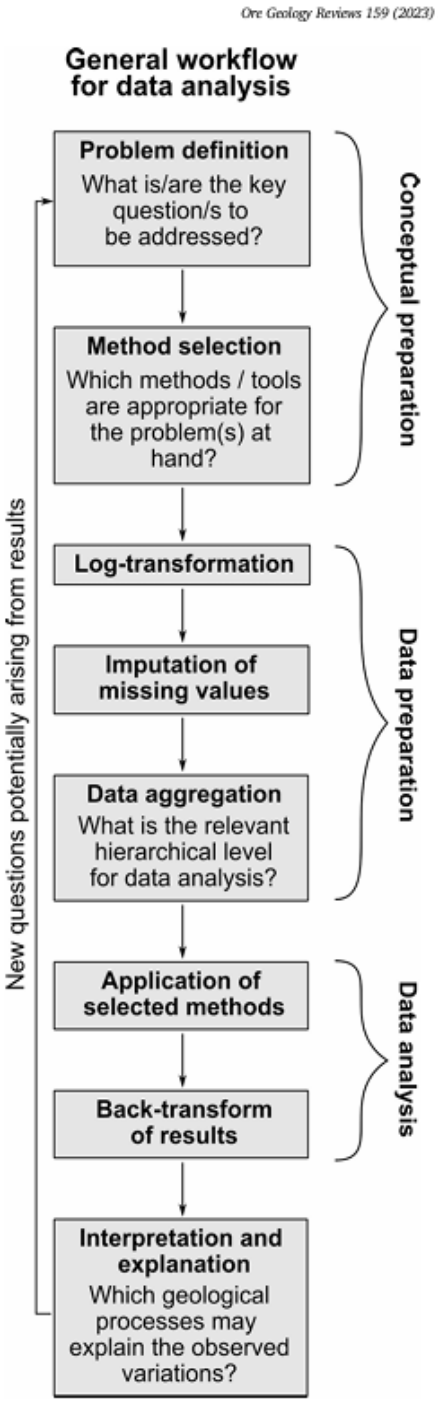


*Figure 18: General workflow for data analysis (Frenzel 2023)*

### I. CONCEPTUAL PREPARATION

**Problem definition:**

- (How) Can natural graphite concentrates be differentiated based on analytical methods? What are the parameters that allow differentiation?
- Can the analytical methods, that are usually applied to mineral phases also be applied to graphite concentrates?
- How do material properties influence the applicability and feasibility of the method?

**Method selection:**

- Which analytical methods can be used to identify parameters based on which graphite can be differentiated?
- Is the analytical method developed for the application in graphite?
- What needs to be done to apply the analytical methods to the graphite concentrates in form of loose powders?
- What is the respective sample preparation?
- Are there any standard, reference or calibration materials available?

### II. DATA PREPARATION

**Log transformation:**

Within the data types present in this study, the log transformation only had to be done for trace element data. The explanation and an example about data distribution before and after log transformation is provided in chapter 5.4.1.

**Imputation of missing values:**

The imputation of missing values was only relevant for the trace element data. Missing values in LA-ICP-MS data were supplemented by an average measurement value from the value before and after in the measurement series of the same sample. Elements with more than just individual values missing were excluded from this study and are not reported. Solution ICP-MS data for the selected elements showed no individual missing values. Elements that have not provided measurement results at all were excluded from this study.

**Data aggregation and relevant hierarchical level:**

As the aim of this work is the geographical differentiation of deposits, the main interest in the hierarchical level of the data is the mine/province level of the data. Most samples could be assigned to

one individual mine, however for some locations material aggregates could only be obtained. This is quite common because processing plants aggregate material from different mines in one place. Samples from China, Madagascar and Brazil are affected. All other samples refer to the mine site directly. Other hierarchical levels in this study are: continent and country of origin, organic vs. non-organic precursor material of the graphite (organic vs. hydrothermal), as well as vein, flake and amorphous graphite.

### III. DATA ANALYSIS

**Application of the selected methods for data analysis:**

Data analysis included describing the trace element data by reporting median values and standard deviations, as well as using scatter and box plots. For trace element data also PCA was applied. Data classification was conducted using LDA. For prediction purposes, the database still needs to be enlarged, as this study aimed at method development. More data for each parameter, as well as more samples per mine/province need to be obtained to enable reliable predictions of the geographic location for unknown samples. An outlook on data prediction is provided in the chapter on carbon isotopes. Log-transformed data is used for multivariate data analysis of trace element data.

### IV. INTERPRETATION AND EXPLANATION

Obtained data from the analytical methods were primarily used to identify certain patterns for each location to differentiate within the individual graphite samples and find common features for each location (mine/province).

## 5.4.1. Data Types and Structure

The choice of the applied statistical methods depends on the dataset, the number of samples and the specific features of the data (e.g. trace elements, isotope ratios and Raman spectra). Different types of data need to be treated separately from each other. Data preparation after Frenzel (2023) requires the log transformation of compositional. Compositional data (e.g. trace element data) refers to data that represents the relative proportions or a composition of parts within a sum and they are constrained in that the sum of the parts always equals a constant or a fixed whole (J. Aitchison 1982). There is a significant difference between unconstrained data in real Euclidean space and compositional data in sample space. Using the wrong data pre-processing methods can lead to serious misinterpretations (John Aitchison 2002; Filzmoser et al. 2010; Raič et al. 2022). To extract the relevant information from the elements being analyzed and convert the original data into Euclidean space, compositional data is treated by log transformation. Through the log transformation, the data becomes normally distributed (Figure 19).

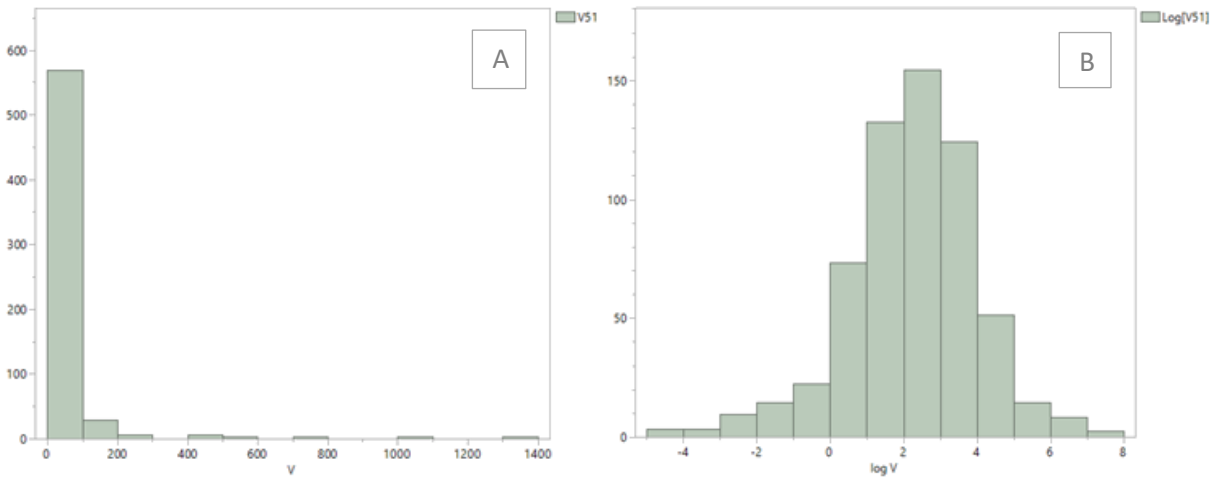


*Figure 19: An example for LA-ICP-MS trace element for V - data non-log transformed (A) and LA-ICP-MS log-transformed trace element data for V (normally distributed) (B)*

Carbon isotope ratios are not considered as compositional data, as they do not represent parts of a whole, but only ratios of an element or compound.

Raman spectra refer to spectral data. The information of the spectra is related to the interaction of light across different wavelengths with a sample. The relevant information in Raman spectra is dispersed across a spectrum (Hideyuki Shinzawa, Kimie Awa, Wataru Kanematsu, Yukihiro Ozaki 2009a, 2009b).

Another important part of data preparation is the treatment of missing values. Ignoring these would result in biased results (Frenzel 2023). For this study values below detection limit and values missing at random need to be differentiated. Missing individual values were observed in the LA-ICP-MS data. These missing values do not adhere with any discernible patterns associated to the sample and its properties, rather than occurring randomly. Such occurrences are typically attributed to external factors, such as human or machine errors leading to the absence of specific values during measurement (Frenzel 2023). Missing values at random for this study mainly occured within the LA-ICP-MS dataset and were replaced by mean values from the measurement before and after from the same sample. Another category of missing values was observed in this study, which represents the below detection limit values. These were replaced by 0.5x of the detection limit value for LA-ICP-MS data. All trace element data obtained from solution-based-ICP-MS data was above detection limit, except die element Lu, which is not reported, however included in the patterns for REE for completeness.

### 5.4.2. Tools and Methods for the Evaluation of the Dataset

After the selection and development of the appropriate analytical method, obtaining data and pre-processing it, relevant tools and methods for the statistical evaluation had to be identified. Most research questions related to the study of mineral/raw materials composition fall into one (or more) of the following categories, which have been proposed by Frenzel (2023): Description, Classification, Prediction, Simple hypothesis and explanation/interpretation. The following categories had been assessed for the respective study.

#### 5.4.2.1. Data Description

This category focuses on providing a descriptive data presentation approach without interpreting the data. Standard deviations and mean values of the dataset are reported, as well as displaying the individual data as histograms, scatter- and boxplots. Variables are also displayed as correlation matrix, which describes relationships between variables (Frenzel 2023). PCA is another method of data description which allows data presentation in new coordinates (Anderson 2003; Frenzel 2023).

Histograms are a graphical representation of the distribution of numerical values of a dataset, visualizing frequencies of values within different ranges. The horizontal axis of the histogram commonly represents the range of values and the vertical axis represents the frequency of observations falling within each range.

Boxplots, also known as box and whisker plots, show central tendencies, spreads and the overall distribution of the data. They are less affected by extreme values or outliers and provide a robust visualization of important statistical information, such as:

- Median: The line inside the box represents the median, which is the middle value of the dataset when it is ordered
- Quartiles (Q1 and Q3): The box itself represents the interquartile range (IQR), with the lower and upper edges representing the first quartile (Q1) and the third quartile (Q3). The IQR contains the central 50 % of the data
- Whiskers: The whiskers extend from the edges of the box to the minimum and maximum values within a specified range, typically 1.5 times the IQR

- Outliers: Individual data points beyond the whiskers are often plotted individually as dots and are considered as potential outliers

Trace element values displayed in box plots in this study show non-transformed data.

Principal Component Analysis (PCA) is a method for simplifying complex data. It reduces a large set of possibly interconnected variables to a smaller set of uncorrelated variables, helping to reveal relationships in elements (Macheyeki, Athanas S., Kafumu, Dalaly Peter et al. 2020) This technique simplifies the data but retains most of its variability (Reimann et al. 2009). The first principal component (PC1) delineates the direction of unit length that encapsulates the highest variance in the dataset, while the second principal component (PC2), orthogonal to PC1, encapsulates the maximum variance remaining within the dataset. This process can be extended to further components, each capturing maximal variance while remaining orthogonal to the other components. PCA methodology constructs an orthogonal basis that imposes a specific geometric structure on the set of variables (Dyer and Kording 2023).

#### 5.4.2.2. Data Classification

Linear Discriminant Analysis (LDA) is widely employed for addressing dimensionality reduction challenges in the context of machine learning and pattern classification applications. For optimal separation between distinct classes, LDA finds linear combinations of features, which is achieved by minimizing variance within each class, all the while incorporating class labels as crucial information during the dimensionality reduction process (Tharwat et al. 2017).

Canonicals or LD1 and LD2 as LDA axes refer to the primary and secondary transformed space that can maximize the separation between different groups (mines/provinces) in the data. Scoring coefficients represent most relevant information from the dataset to describe and classify data (e.g. key elements).

Multivariate statistical methods analyze multiple variables (the whole dataset) simultaneously. The diagrams in chapter 6.3.1.3. and 6.3.2.3. demonstrate the limitations of bivariate statistical methods. Even ratios considering four variables simultaneously are only partially suitable for distinguishing between all geographic origins. Some reasons for the application of multivariate statistical methods include the complexity of the data. The variables are interrelated and their relationships within the group (mine/province) are complex. Additionally, multivariate methods allow for dimensionality reduction. The interpretation of numerous variables, as well as analyzing and interpreting each variable individually without multivariate methods is highly challenging and for the number of individual variables for the different methods simply not feasible. The application of multivariate statistics was useful to identify patterns within the dataset and data visualization helped to reveal patterns that may be less visible/understandable in a tabular form or based on bivariate statistics only.

LDA serves as the first application of data classification for the underlying dataset on discriminating geographic origins of natural graphite deposits. More complex statistical data classification methods (such as support vector machines (SVM), random forests (RF), gaussian mixture models (GMM), partials least squares discriminant analysis (PLSDA), as proposed by Frenzel in 2023) are not applied within the frame of this work.

**Digression - PCA vs. LDA:** LDA is inapplicable to unlabelled data and is a supervised learning algorithm; it classifies labelled data. PCA in contrast, ignores class labels and preserves variance across the dataset.

#### 5.4.2.3. Data Prediction

Data prediction was applied to the carbon isotope dataset. Further analysis needs to be done, to enlarge the database and perform plausible data prediction on all parameters, as the dataset need to be split into a test and a training dataset with the respective amount of data for each group.

A logistic regression model is mainly used for prediction. The model is capable of predicting the value variables, such as the C isotopic values in the regions of Sri Lanka, Ukraine, or the Rest of the World. This is particularly useful when new data is introduced, and the corresponding output needs to be forecasted. Additionally, logistic regression models can be employed for outlier detection, quickly identifying data points that deviate from the general dataset.

#### 5.4.2.4. Explanation and Interpretation

A separate chapter is dedicated to the discussion, explanation, and interpretation of the data in this study (Chapter 7 Discussion).

### 5.4.3. Data Processing Software

The following software products were used for data processing and data presentation. This includes a mix of open-source programs and licensed programs.

ioGAS-64-8.1. is a software tool designed for geoscientists, especially those working in the fields of geochemistry and geostatistics. ioGAS was primarily used for the analysis and visualization of geochemical and geological data. The program allows users to import and manage various types of geochemical and geoscientific data, such as elemental concentrations, isotopic data, and geological information. The software offers a wide range of visualization options, including scatter plots, ternary diagrams, histograms, and more, which helps to gain insights into their data by visualizing the data. It is commonly used in mineral exploration, environmental monitoring, and other geoscientific applications and is an effective tool to make data-driven decisions and to communicate and visualize the findings.

GLITTER4.5. is a data reduction software tool designed for the analysis and visualization and to provide a simple and more consistent and faster reduction of LA-ICP-MS data. It represents a tool for real-time interactive data reduction for LA-ICP-MS analysis. One of the significant advantages of this software is the capacity to identify the optimal time intervals for background and signal measurement, which is achieved through the presentation of time-resolved data and allows a rapid identification of irregularities and data spikes.

JMP (student version) is a statistical data analysis software. It is designed to explore, analyze, and visualize data to make data-driven decisions in research, business, and various other industries. It provides a user-friendly interface for data visualization, such as the generation of graphs, histograms and scatter plots. It supports predictive modeling and (unsupervised) machine learning techniques.

Most of the programs mentioned above are complementary to each other. As a significant amount of this work focuses on data processing and analysis, various programs were tested and applied to the data. Apart from the more sophisticated applications and software products for data processing, reduction and displaying, Microsoft Excel was used as the basic program for data reduction and data pre-processing.

# 6. Results

## 6.1. Optical Properties

Microscopic as well as scanning electron microscopic images were taken from all graphite samples in this study to analyze the optical properties of the graphite concentrates. Mainly scanning electron microscopic images of the concentrates are presented in this chapter, as well as digital light microscopy images of the graphite raw ores, if available for the respective mine/deposit.

**Kaisersberg, Austria**

Sample 1A from Kaisersberg shows an irregular grain size distribution of an amorphous graphite concentrate with a notable presence of foreign components/impurities (quartz and mica). Sample 21G is a raw ore from Kaisersberg, with sub-parallel graphite (beige-grey-yellowish) embedded in a matrix of quartz and mica (Fig. 20).

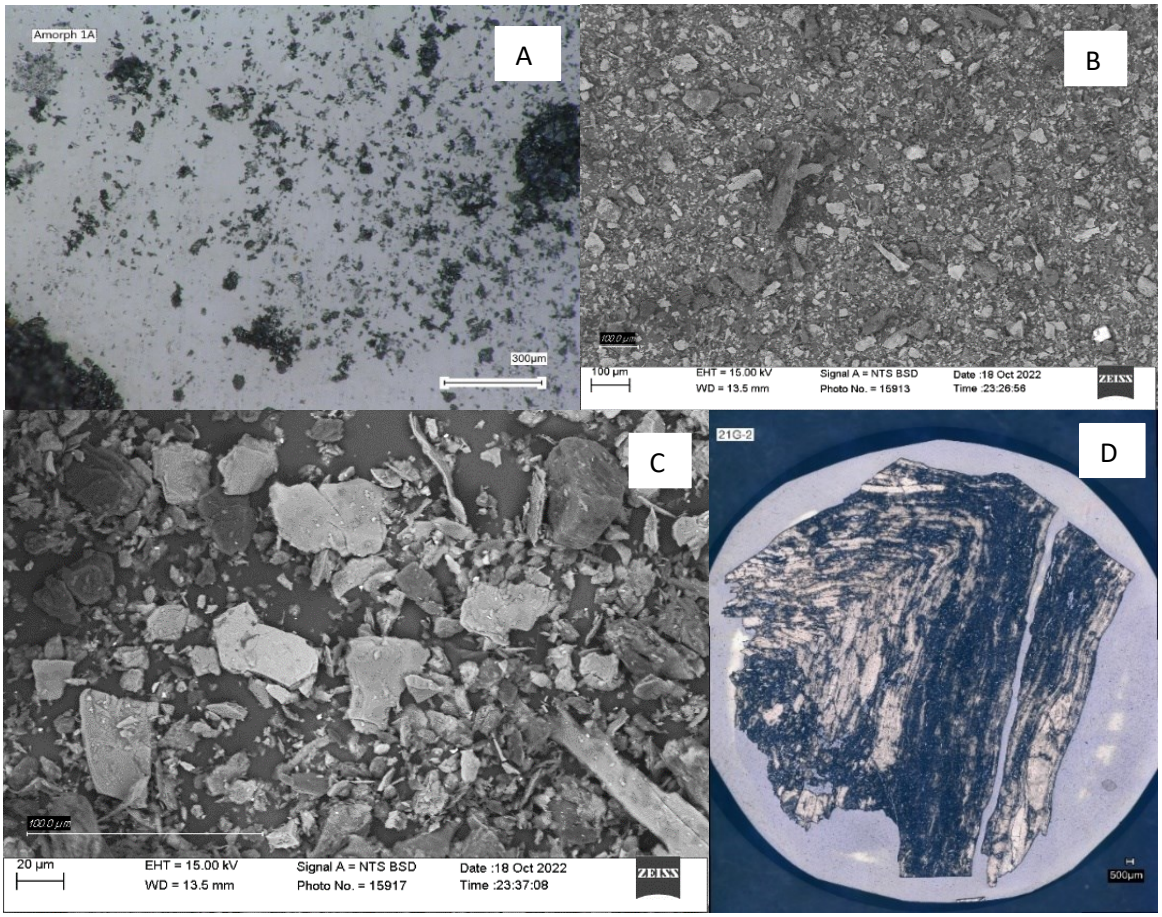


*Figure 20: A: digital light microscope image sample 1A, B: SEM image sample 1A 200x magnification C: SEM image sample 1A 1000x magnification, D: digital microscope image sample 21G showing disseminated graphite raw ore from Kaisersberg*

**Minas Gerais (Pedra Azul, Itapecerica, Salto da Divisa), Brazil, South America**

Samples from Minas Gerais province in Brazil are mixtures of material from the mines Pedra Azul, Itapecerica and Salto da Divisa. The material shows homogeneous grain size distributions with distinct flakes. Concentrates from Minas Gerais province show a relatively homogeneous grain size distribution ranging from 100 – 200 µm (Fig. 21).

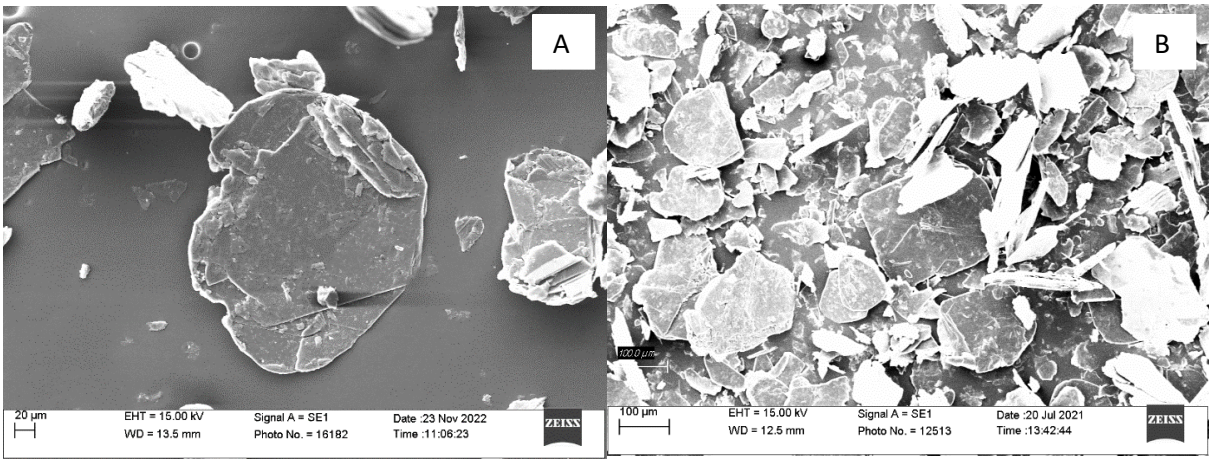


*Figure 21: A: Flake with 200 µm diameter in sample 3B, 250 x magnification, B: overview of flake distribution, SEM image from sample 21C, 50x magnification*

**China, Asia**

**Heilongjian**

Sample 7B exhibits significantly small, less idiomorphic flakes, partly aggregated and distributed inhomogeneously in terms of size. Individual flakes show sizes of up to 150 µm (Fig. 22).

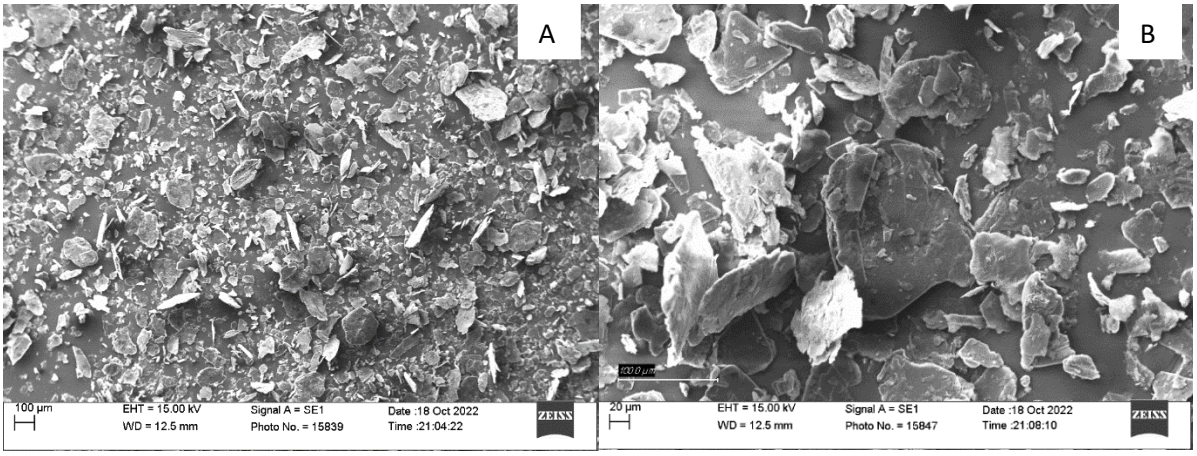


*Figure 22: A: sample 7B overview, 100x magnification, B: Flake sample 7B 500x magnification with flake sizes up to 250 µm and smaller flakes and fragments of 100 µm particles and smaller*

**Hunan Lutang**

Sample 4A (amorphous graphite sample) lacks a flake-like structure and is rather a loose aggregation of components without individual grain sizes (Fig. 23).

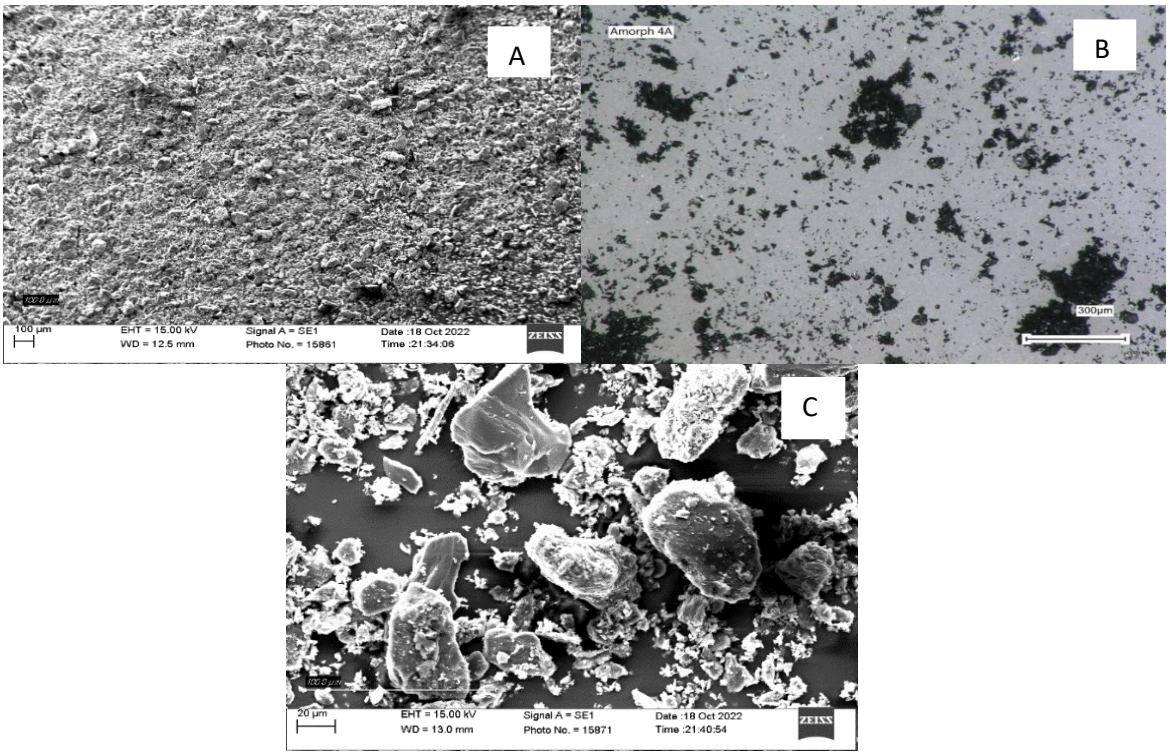


*Figure 23: A: sample 4A, SEM image overview, 100x magnification, B: Overview image sample 4A, digital light microscope without visible individual flakes/grains, C: detailed SEM image sample 4A 1000x magnification with grain sizes up to 80 um and smaller aggregates*

## Inner Mongolia

Sample 6B (Inner Mongolia, China) exhibits distinctly pronounced idiomorphic flakes with a size ranging from 350 to 450 µm and a very homogeneous grain size distribution. Even in digital light microscopy images, the idiomorphic flakes are identifiable (Fig. 24).

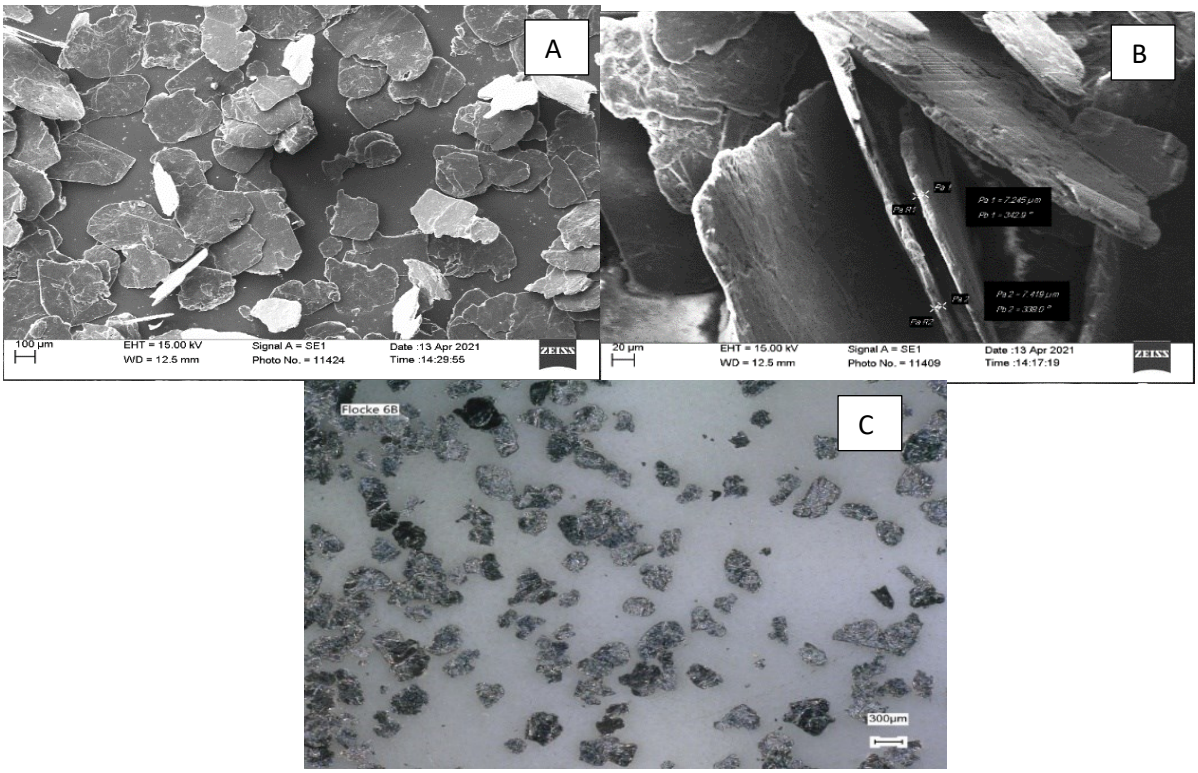


*Figure 24: A: sample 6B SEM image overview, 100x magnification, B: detailed SEM image sample 6B 550x magnification with a measurable flake thickness of almost 8 µm; C: overview digital light microscopy image sample 6B*

## Shandong

Samples 21A and 22A from Shandong, China exhibit idiomorphic flakes with a maximum grain size of approximately 250 µm down to small flakes and fragments of only 20 µm. The grain size distribution in this concentrate is relatively heterogeneous compared to other graphite concentrates (Fig. 25).

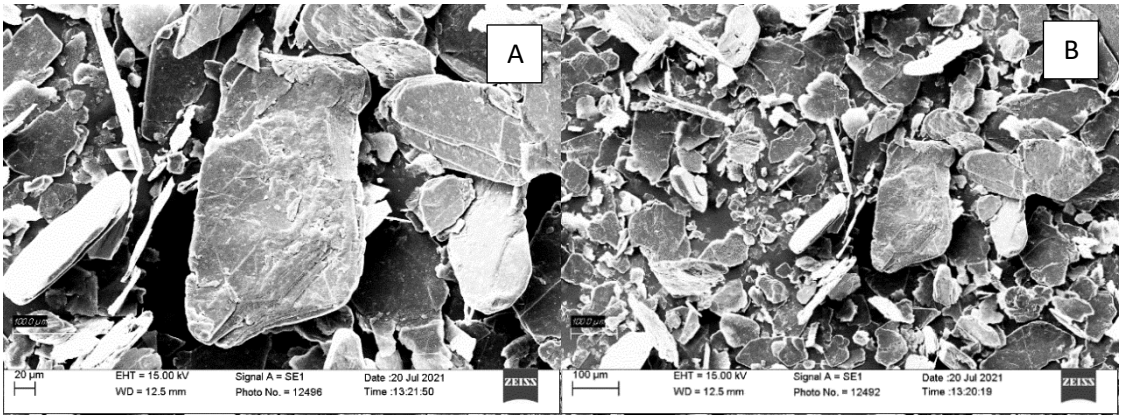


*Figure 25: A: SEM image, graphite flake in sample 21A, 550x magnification, B: sample 21A SEM image overview, 100x magnification*

**Kropfmühl, Germany, Europe**

Sample 13B from Kropfmühl, Germany exhibits idiomorphic flakes; however, the grain size distribution is very heterogeneous, ranging from a maximum grain size of approximately 400 µm down to a minimum grain size of 100 µm and below. Raw ore sample 14B shows disseminated graphite flakes (greyish-yellow) in a matrix of quartz (grey) and individual grains of pyrrhotite (white – light greyish) (Fig. 26).

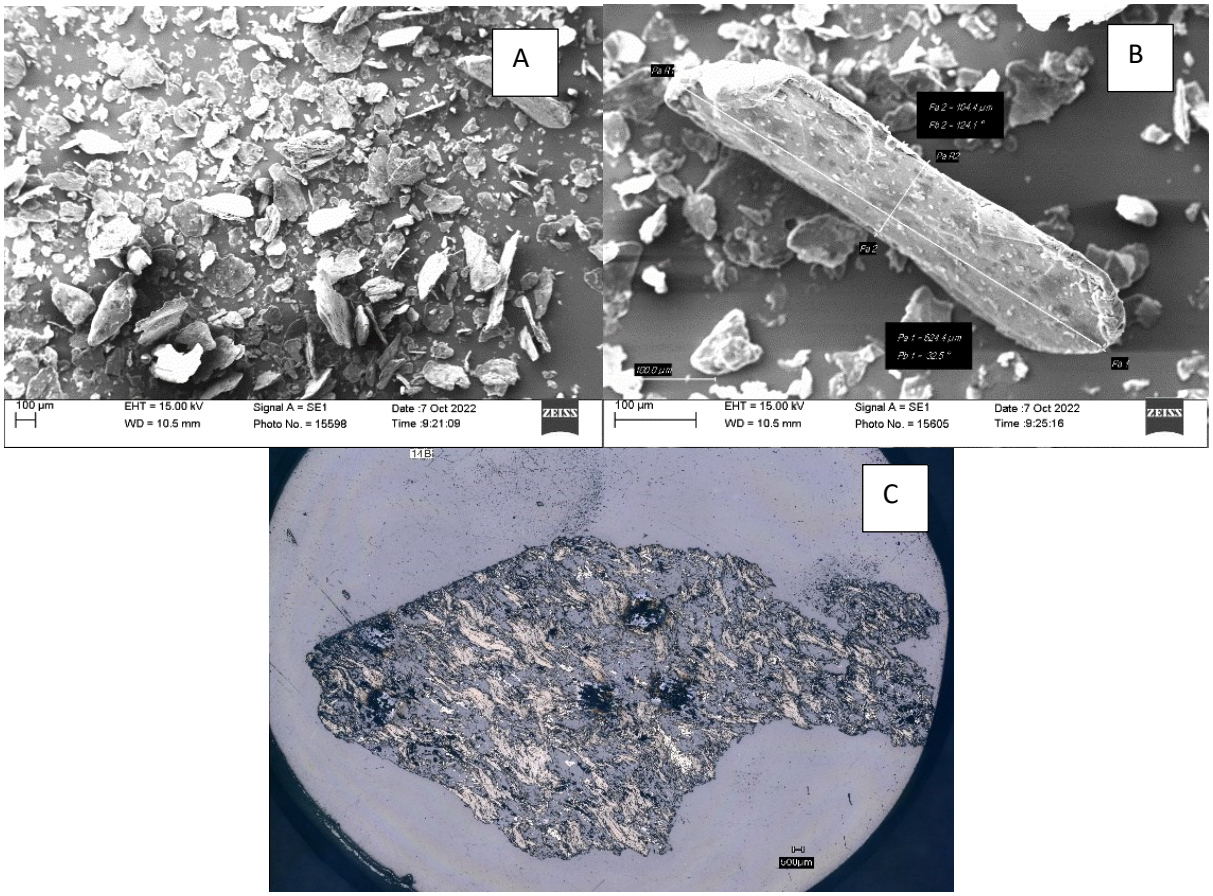


*Figure 26: A: Sample 13B overview SEM image with 100x magnification, B: sample 13B detailed SEM image sample 13B individual flake with 600 µm length and 400x magnification, C: raw ore sample 14B overview digital light microscope showing graphite flakes and pyrrhotite*

**Brickaville (Vatomina und Sahamamy Sahasoa), Madagascar, Africa**

Samples 11B, 21D and 22D from Brickaville province consist of idiomorphic graphite flakes with a maximum grain size of approximately 650 µm down to small flakes and fragments of only 20 µm. The grain size distribution in this concentrate is homogeneous and the flake size is among the largest in this study with flake diameter of up to 650 µm (Fig. 27).

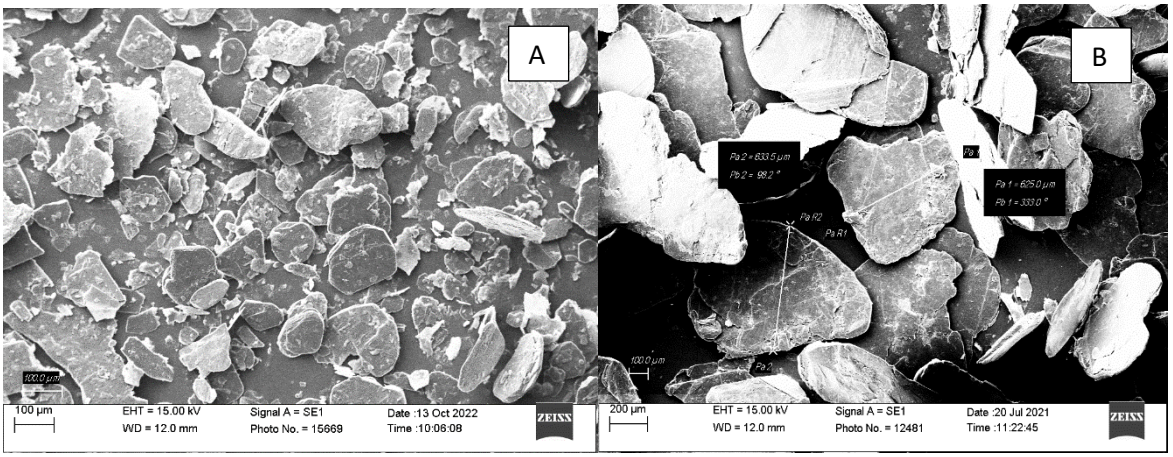


*Figure 27: A: sample 22D, overview SEM image 200x magnification, B: sample 21D, SEM image 1000x magnification and flake diameters of 500 – 600 µm*

**Balama, Cabo Delgado Province Mozambique, Africa**

Samples 1B, 21B, 21J, 21K, 21L and 22B from Balama mine consist of distinctly pronounced idiomorphic graphite flakes with a maximum identified flake size of 600 µm and average flake sizes of 200 µm and a flake thickness of up to 5 µm. Raw ore sample 22H from Balama mine shows disseminated graphite flake in a matrix consisting of quartz (grey), mica (light grey) and isolated titanite grains (bright white) (Fig. 28).

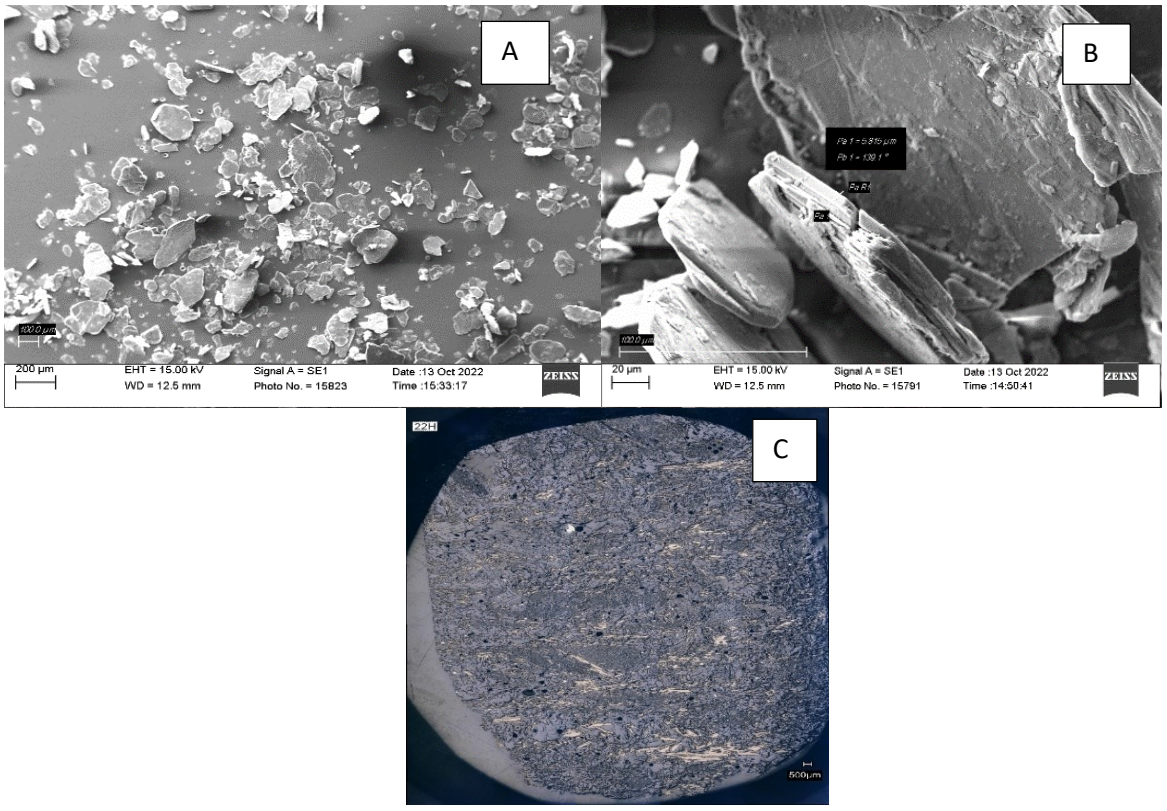


*Figure 28: A: sample 21J overview, 100x magnification, B: sample 21L detailed flake structure of individual components, C: 22H disseminated graphite raw ore sample from Balama*

**Skaland Norway**

Sample 2B, 15B and 16B, and 22G from Skaland mine in Norway exhibit well-defined graphite flakes with sizes ranging from 250 to 350 µm and fragments. Sample 16B (Skaland, Norway) presents a raw ore sample, predominantly composed of graphite, including pyrite, albite, and quartz (Fig. 29).

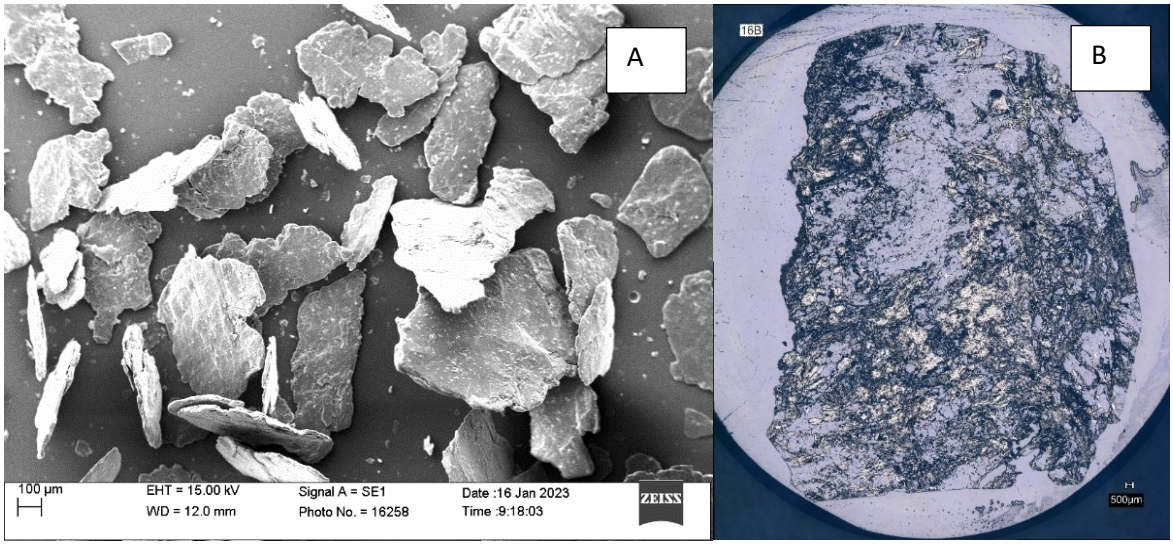


*Figure 29: A: individual flakes in sample 15B, magnification 100x, B: 16B disseminated graphite raw ore digital light microscope image (graphite particles too small for laser-ablation)*

**Taiginka, Chelyabinsk region, Russia, Asia**

Samples 5B, 21E and 22E from Tayginka exhibit idiomorphic flakes, with a relatively homogeneous grain size distribution, ranging from a maximum grain size of approximately 200 µm down to a minimum grain size of 100 µm and below (Fig. 30).

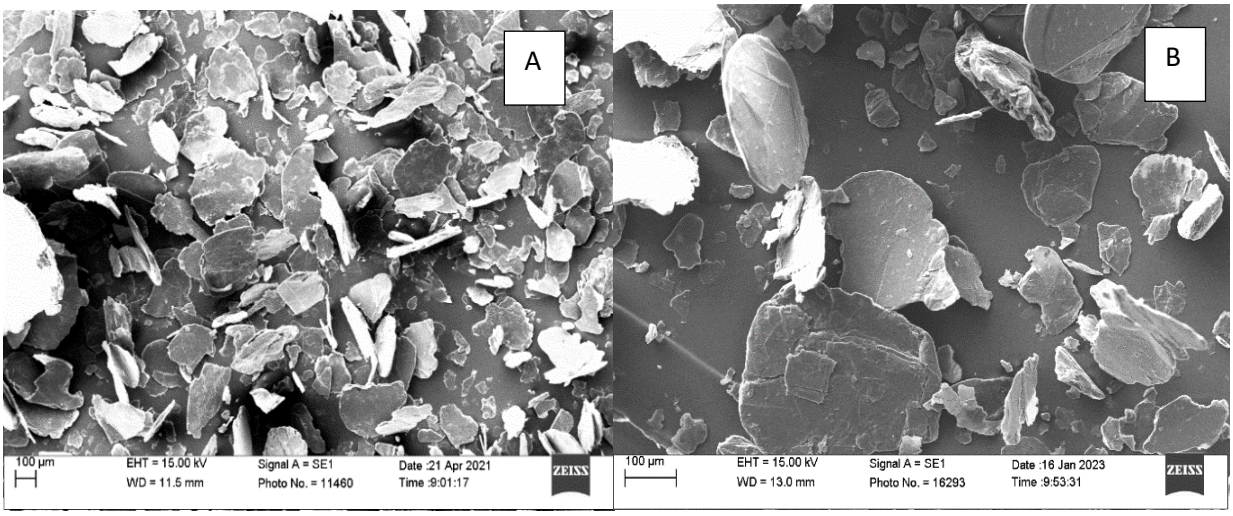


*Figure 30: A: SEM image sample 5B, 100x magnification, B: SEM image sample 21E, 250 x magnification*

**Ragedara, Sri Lanka, Asia**

Samples from Ragedara, Sri Lanka represent vein graphite and show highly pure graphite raw ore. Identified mineral phases are exclusively graphite. Black spots/areas on the sample only show relief phenomena due to polishing or uneven surfaces and laser ablation patterns from analysis (Fig. 31).


*Figure 31: Highly pure vein graphite (lump ore) (yellowish-grey) sample 10B*

**Zavallia, Ukraine, Europe**

Samples from Zavallia (UKR) show idiomorphic flakes with a relatively homogeneous grain size distribution and distinct idiomorphic flakes with sizes ranging from 100 µm to 200 µm. Even at lower magnification individual flakes can be identified. Through some flakes standing normal to the scanning surface, the flake thickness can be measured and is about 3 µm. Disseminated graphite flakes (yellowish-grey) in a raw ore (D) from Zavallia are embedded mainly in a quartz (grey) and mica (light grey) matrix (Fig. 32).

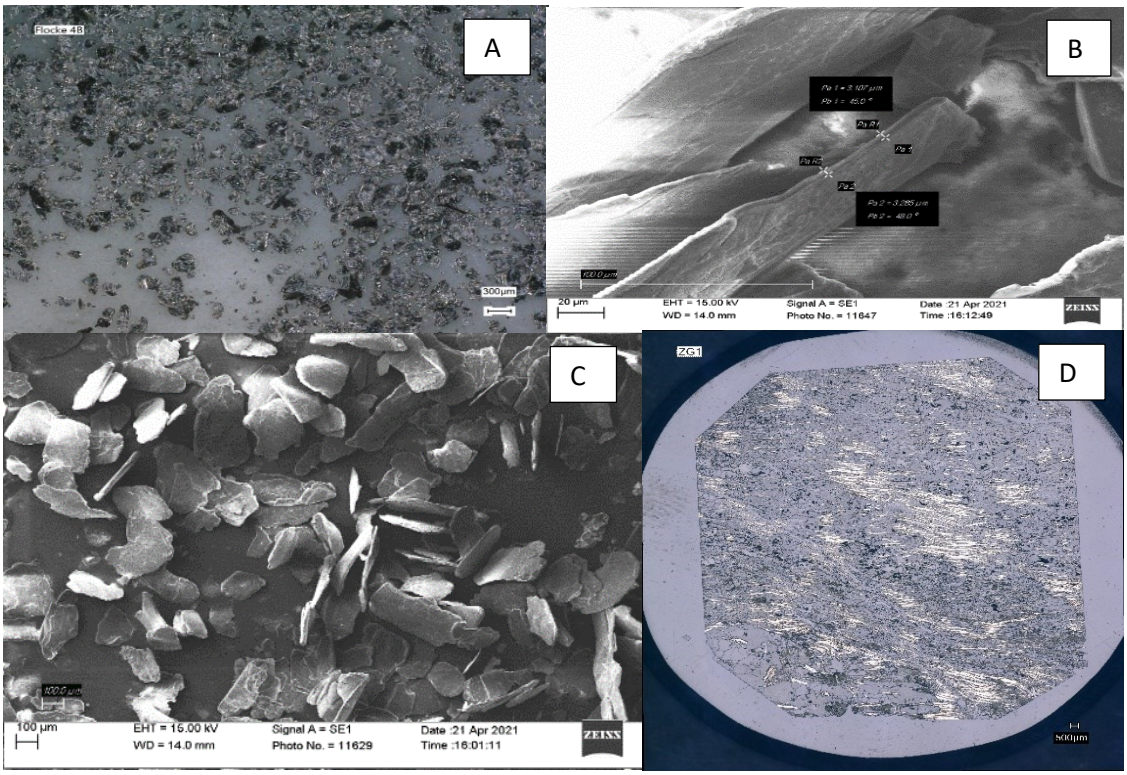


*Figure 32: A: digital light microscope image sample 4B, B: SEM image sample 4B 1200x magnification and flake thickness of 3 µm, C: overview SEM image sample 21E 100x magnification, D: digital light microscope image sample 22K-S disseminated graphite raw ore (graphite particles too small for laser-ablation)*

**Summary table:**

The optical properties of the samples are summarized in Table 14. All graphite concentrates under consideration are processing products, containing between 92-96+ % C, with the majority of impurities already removed by on-site processing. The flake size is mechanically manipulated and does not completely reflect the naturally occurring flake size. Accompanying mineral phases as residues and impurities in the concentrates represent mainly quartz and mica particles. Some deposits however are specified by their large flake sizes. Specific details are summarized in the table below.

*Table 14: Summary of optical properties of graphite concentrates assessed by SEM*

| mine/province | country | graphite type | av. flake size (µm) | concentrate properties |
|---|---|---|---|---|
| Kaisersberg | Austria | amorphous | 50 | no prominent flake-like structure, inhomogeneous |
| Minas Gerais | Brazil | flake | 150 | relatively homogeneous size distribution |
| Heilongjian | China | flake | 120 | inhomogeneous, less idiomorphic flakes |
| Hunan Lutang | China | amorphous | 30 | no prominent flake-like structure, inhomogeneous |
| Inner Mongolia | China | flake | 450 | very homogeneous size distribution, largest average flake sizes, thick flakes |
| Shandong | China | flake | 180 | inhomogeneous flake size distribution |
| Kropfmühl | Germany | flake | 200 | inhomogeneous flake size distribution |
| Brickaville | Madagascar | flake | 450 | homogeneous flake size distribution, large flakes |
| Balama | Mozambique | flake | 200 | rel. homogeneous flake size distribution |
| Skaland | Norway | flake | 300 | homogeneous flake size distribution |
| Taiginka | Russia | flake | 200 | inhomogeneous flake size distribution |
| Ragedara | Sri Lanka | vein/lump | -- | large chunks of pure graphite |
| Zavallia | Ukraine | flake | 200 | homogeneous flake size distribution |

## 6.2. Stable Carbon Isotope Ratios (δ13C)

There are three naturally occurring isotopes of carbon, namely $^{12}C$, $^{13}C$ and $^{14}C$. The latter is the radioactive isotope, with a half-life of 5730 years. It is generated by thermal neutrons from cosmic radiation in the upper atmosphere and is subsequently transported to Earth, where it is absorbed by living biological material. $^{12}C$ predominates as the most abundant isotope at 98.89 %, while the $^{13}C$ isotope occurs with a frequency of only 1.11 % (O'Leary et al. 1992). The isotopic ratios of $^{12}C$ and $^{13}C$ are quantified and expressed using the notation $\delta\,^{13}C$ in parts per thousand, called per mil (‰) and are calculated as follows:

$$\delta^{13}C = \left( \frac{\left(\frac{^{13}C}{^{12}C}\right)_{sample}}{\left(\frac{^{13}C}{^{12}C}\right)_{standard}} - 1 \right) \times 1000\ ‰$$

(O'Leary 1981)

The globally accepted standard is based upon carbon dioxide sourced from limestone within the Pee Dee formation in South Carolina and is denoted as PDB (Craig 1957).

A clear demarcation of the carbon signature is observed in graphite, indicating significantly heavier values for hydrothermal/vein graphite (Weis 1981). Within organic graphite (flake vs. amorphous), there are two trends, attributed to different source materials. Amorphous graphite is formed through regional or contact metamorphism of coal seams, while the flake type of graphite undergoes graphitization of organic precursors through regional metamorphism. Coals tend to include material enriched in $^{13}C$ (Weis 1981). The precursor material for coals is higher land plants, whereas the precursor material in disseminated graphite flakes is more likely composed of more primitive organisms (e.g. bacteria, algae).

### 6.2.1. Worldwide Database of Carbon Isotope Values ($\delta^{13}C$)

A database consisting of graphite stable carbon isotope data (n= 433) was developed in the frame of this project in collaboration with researchers from GTK, Finland. The database contains stable carbon isotope data obtained from samples within this study, but also literature data from various global graphite occurrences. The corresponding data table for Figure 33 can be found in the appendix, including references. Only values that could be assigned to a graphite type (amorphous, flake, vein) were included in the database. Potential outliers in the data may have been caused by mixture analyses, for example, by mixing/contaminating graphite material with carbonates, which have a $\delta^{13}C$ signature of ≈ 0 ‰. The figure presented below (Figure 33) illustrates the $\delta^{13}C$ values from global graphite occurrences. The values are associated with their respective mines/provinces, as well as the corresponding countries. Further differentiation could be made based on the graphite type (amorphous, flake, vein).

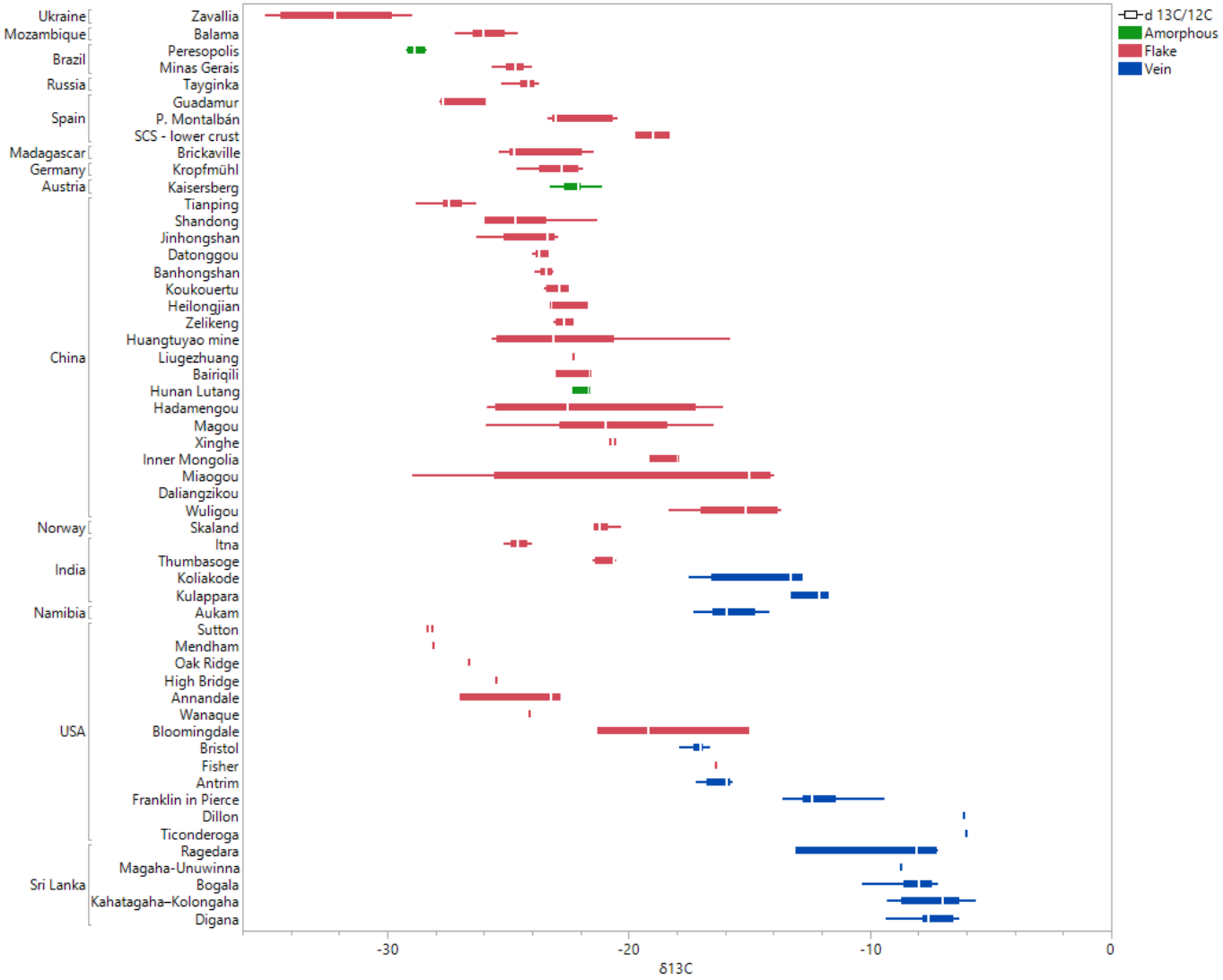


*Figure 33: Worldwide database of stable carbon isotope signatures in graphite (Data table and references can be found in in the Appendix)*

A representation of the $\delta^{13}C$ values sorted by continent and country is illustrated in Figure 34. Amorphous graphite in this study and in the database are limited to the continents of South America (Brazil), Europe (Austria), and Asia (China). Flake graphite is globally distributed. Vein graphite refers to North America (USA), Asia (Sri Lanka), and Africa (Namibia) in this study. The most common graphite type worldwide is flake graphite. The values of vein graphite are distinguishable (- 5 to -15 ‰), as are those of the Zavallia deposit in Ukraine, with a very light $\delta^{13}C$ value (-28 to -35 ‰). The $\delta^{13}C$ signatures of the remaining flake graphite overlap, and a distinction based on countries is not possible.

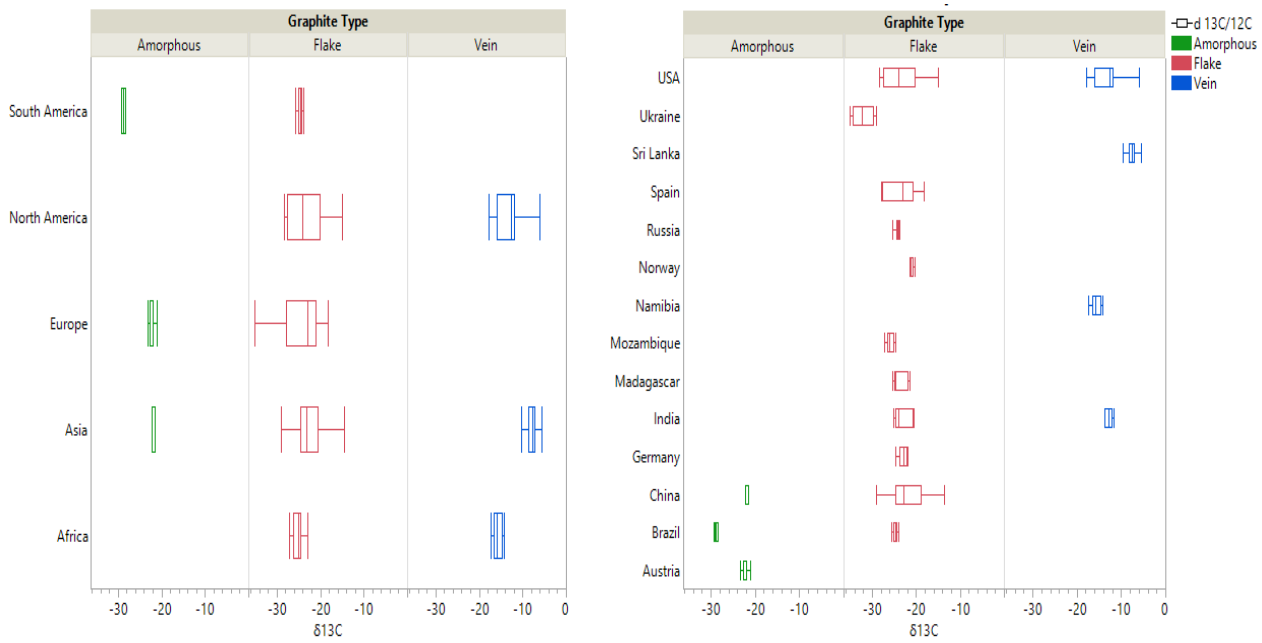


*Figure 34: Data distribution of δ13C values sorted by continent (left) and countries (right) and the respective graphite type (amorphous, flake, vein)*

### 6.2.2. Carbon Isotope Values from Sample Collection in this Project

The following data refers to $\delta^{13}C$ values from measurements of graphite concentrates, conducted in in-house laboratories at MUL. The data collection covers key countries in global graphite production, spanning South America, Europe, Africa and Asia. These measurements have also been associated with additional attributes.

Most of the isotope values correspond to flake graphite. Hydrothermal (vein) graphite was sampled from Asia (Sri Lanka) only and amorphous graphite was collected from Europe (Austria) and Asia (China). The analyzed graphite in Africa and South America can be assigned to as flake graphite. A geographical differentiation of continents based on carbon isotope values is not feasible, as carbon isotope signatures of the continents overlap (Fig. 35).

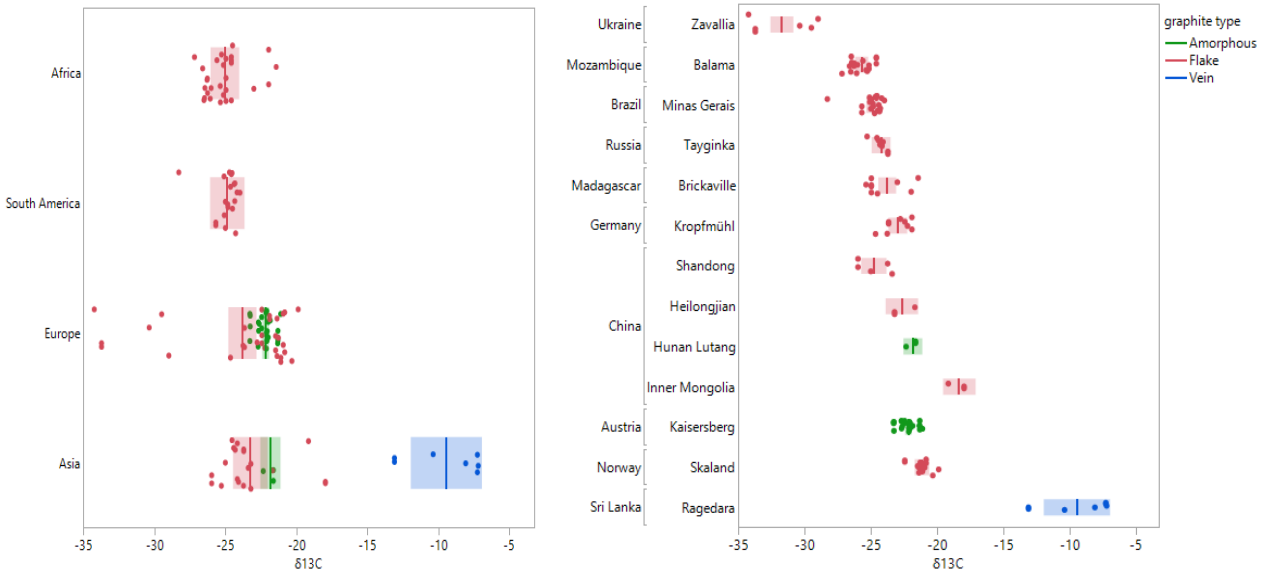


*Figure 35: Carbon isotope ratios categorized by graphite type (amorphous, flake, vein) and geographical origin across continents hierarchy (left) and mine/province and country hierarchy (right), vertical line in box represents mean value*

Another differentiation of $\delta^{13}C$ values was made based on geological ages (Fig. 36). The graphite samples from Africa and South America are classified as Proterozoic. The group of the oldest graphite (Archean) can be assigned to Ukraine. Geological ages ranging from Archean to Proterozoic and Paleozoic can be found in Europe. The graphites from Asia are classified as Proterozoic and Paleozoic. The measurement values across all continents overlap. The only clear distinction is observed in the Archean graphite in Europe (Ukraine).

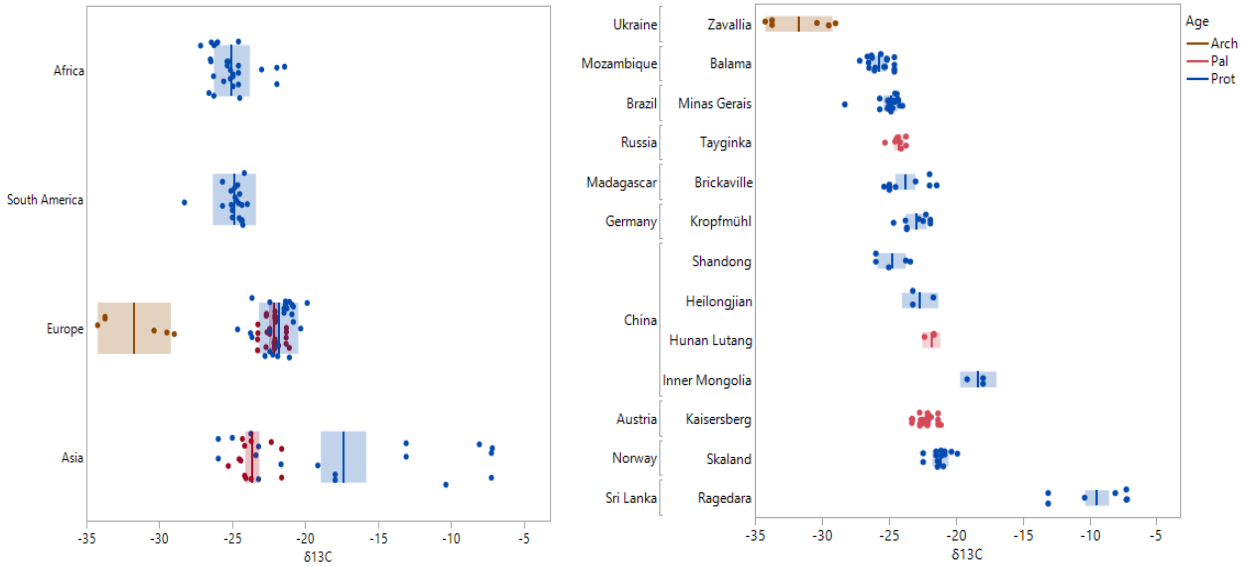


*Figure 36: Carbon isotope ratios categorized by geological age (Archean, Palaeozoic, Proterozoic) and geographical origin across continents hierarchy (left) and mine/province and country hierarchy (right); vertical line in box represents mean value*

**Variability of the data**

The data distribution of the $\delta^{13}C$ values shown below (Fig. 37) can be classified as follows: Vein graphite is categorized in a significantly heavier $\delta^{13}C$ range ( -7 ‰ to -13 ‰) and can be separated from the other two groups, which is flake type (-17 ‰ to -34 ‰) and amorphous type (-21 ‰ to -24 ‰). Amorphous and flake type overlap and cannot be differentiated.

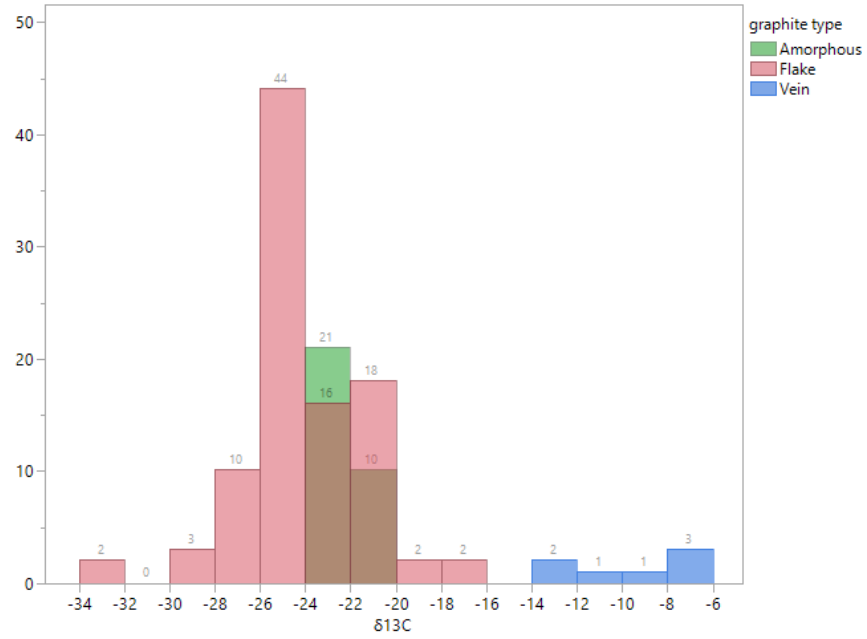


*Figure 37: General data distribution divided into three groups (amorphous, flake, and vein graphite).*

The geological age allows the distinction of Archean graphite, as shown in Fig 38. Paleozoic and Proterozoic $\delta^{13}C$ values overlap. Archean graphite shows a $\delta^{13}C$ range of -28 ‰ to -34 ‰, whereas Paleozoic graphite falls within a $\delta^{13}C$ range of -21 to -26 ‰ and the Proterozoic graphite lies within the values -7 ‰ to -28 ‰).

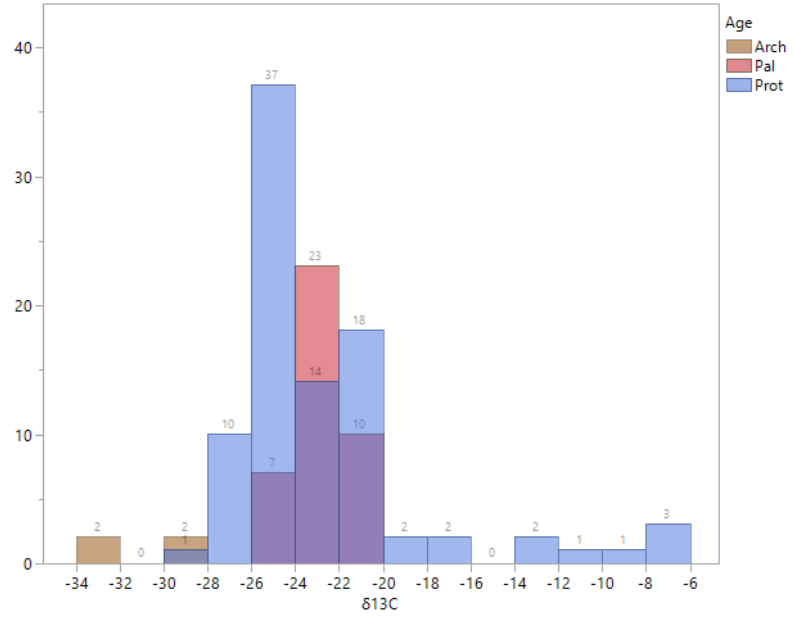


*Figure 38: General data distribution divided into three groups (Archean, Paleozoic and Proterozoic).*

### 6.2.3. Differentiation between country groups

The available data could be divided into three subgroups (Sri Lanka, Ukraine and the rest of the world (RoW)). A more detailed distinction within the RoW group is not feasible based on this parameter only.

The differentiation of the above-mentioned groups can be explained by additional attributes and is further illustrated (Fig. 39).

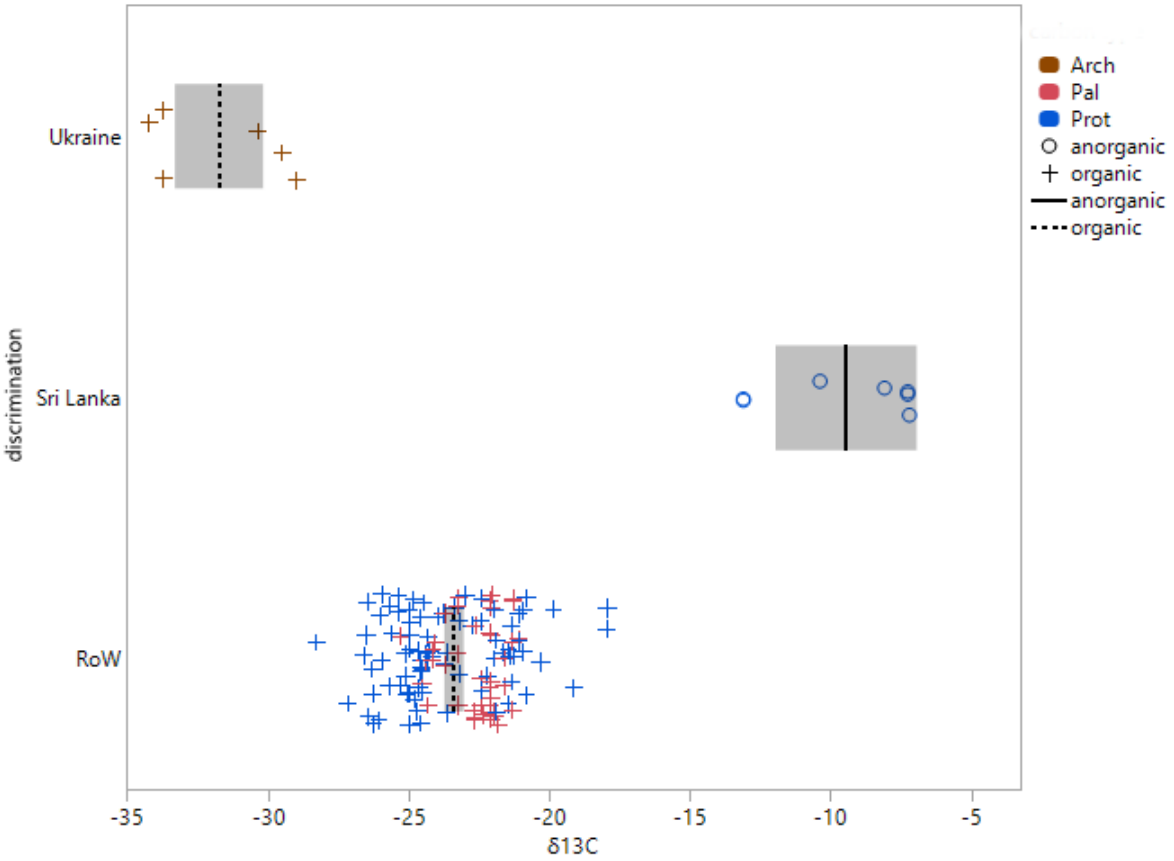


*Figure 39: Discrimination of samples into groups (Sri Lanka, Ukraine and rest of the world (RoW) with additional attributes related to the carbon source (organic or inorganic); vertical line in box represents mean value*

The data distribution of carbon isotopes within these three groups exhibits a significantly denser dataset for the RoW group. The Sri Lanka and Ukraine groups consequently display fewer data points; however, the existing data points fall within the defined groups and are therefore clearly distinguishable. Graphite within the group Ukraine is exclusively referred to as Archean organic graphite. The group RoW represents a mixed sample set, consisting of organic graphite, showing Paleozoic and Proterozoic ages and cannot be differentiated further. The group Sri Lanka consists only of anorganic (vein) graphite.

### 6.2.4. Supply Chain Consistency

To which extent carbon isotope values remain constant throughout the processing chain and what effect graphite processing has on the stable carbon isotope on the material was analyzed using samples from Finnish occurrences (Aitolampi, Emas, Koivuniemi and Raisjoki). The samples originate from the sample repository from GTK, as well as processing and intermediate materials. The stable carbon isotope data were analysed in the course of this study at MUL (Fig. 40).

Analyzing further products along the supply chain from the raw ore or flotation concentrates to the purified graphite is an advanced step in the analytical proof of origin study, focusing on the stability of individual parameters along the supply chain. Processing and intermediate products often represent

mixtures. The exact origin is often unclear, as processing steps may be carried out by different companies, possibly even at different locations.

Samples from the Aitolampi deposit were processed directly at the on-site pilot processing plant (Beowulf Mining) and at the GTK in-house facilities. Core and crushed core samples, flotation concentrates, by-products and residues, alkaline purified material and purified spherical graphite were analyzed. Samples from other Finnish occurrences (Emas, Raisjoki, and Koivuniemi) were processed by GTK in their in-house pilot processing plant. These samples include raw ore (flotation feed), flotation (rougher and cleaner) concentrates and the product (purified graphite).

The Aitolampi deposit exhibits a wider range of $\delta^{13}C$ values in the flotation feed, attributed to the increased (spatial) variability within the mine and the analyzed core samples from two different areas within the deposit (eastern and western zone), whereas the purified concentrates consistently show a significantly smaller range of isotopic values. A clear change in carbon isotopic composition is not observable throughout the graphite processing. Stable carbon isotope signatures from flotation concentrates and products typically overlap within a wide range within the same deposit. The majority of variability can be attributed to the (spatial) variability within the deposit, which may translate into temporal variability over the life of the mine and can be seen in flotation feed or crushed core material.

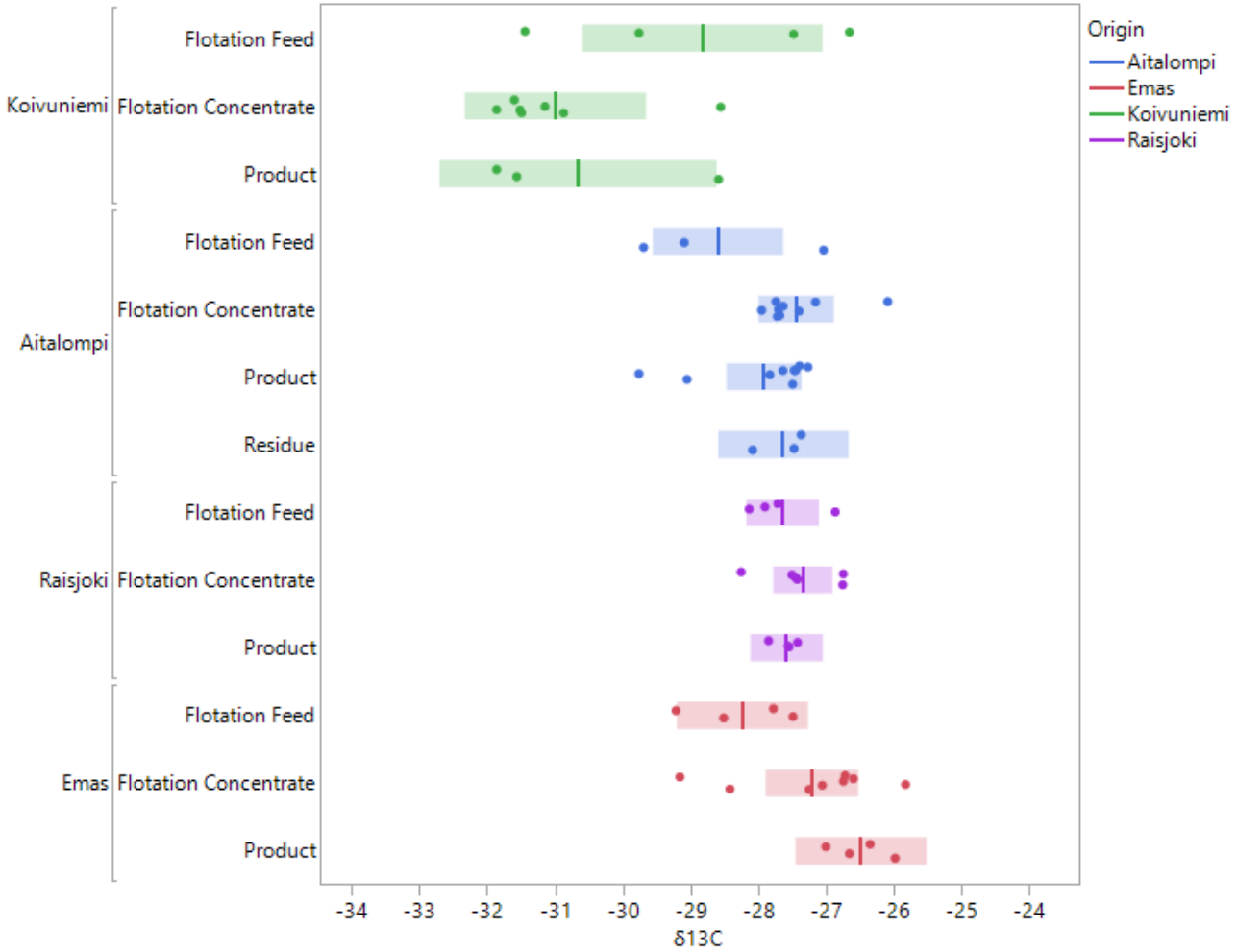


*Figure 40: Carbon isotope values from different occurrences in Finland and different intermediate products along the value chain; vertical line in box represents mean value*

## 6.3. Crystallinity and Spectral Data

The samples investigated are mainly graphite concentrates, with some graphite raw ore samples. The type of sample is important for the application of Raman spectroscopy. The concentrates have been ground and floated, with their Raman spectra representing a mixed signature of natural processes (organic maturation) and structural alteration through processing in the (processing) plant on the mine site itself. Previous work on Raman data quality showed that mechanical stress from shearing or polishing may influence the Raman spectra (Rantitsch et al. 2016b, Beyssac et al. 2004, Lünsdorf and Lünsdorf 2016), which however cannot be compared to the sample processing on the mine site. A study comparing Raman data from unprocessed, handpicked raw ore samples that suffered no mechanical stress and processed graphite concentrate both from the same mine (Kaisersberg (AUT)) showed that the discrepancies within the mean Raman parameters between these two samples types are lower compared to the variability of the within-sample data and also smaller than the variability observed among samples from different mines. These observations provide evidence that the graphite processing has an insignificant impact on the ordering properties (Rantitsch et al. 2016b). Evidence is provided with own data from this study. Figure 41 displays Raman spectra from Kropfmühl (GER). Spectrum 1 (red) shows a characteristic Raman spectrum of a graphite concentrate from this mine, while spectrum 2 (blue) represents a characteristic spectrum of a raw ore sample from the same mine. The two spectra do not differ from each other, apart from the varying intensity of the red (concentrate) spectrum. On-site sample processing does not induce significant spectral alterations into the sample.

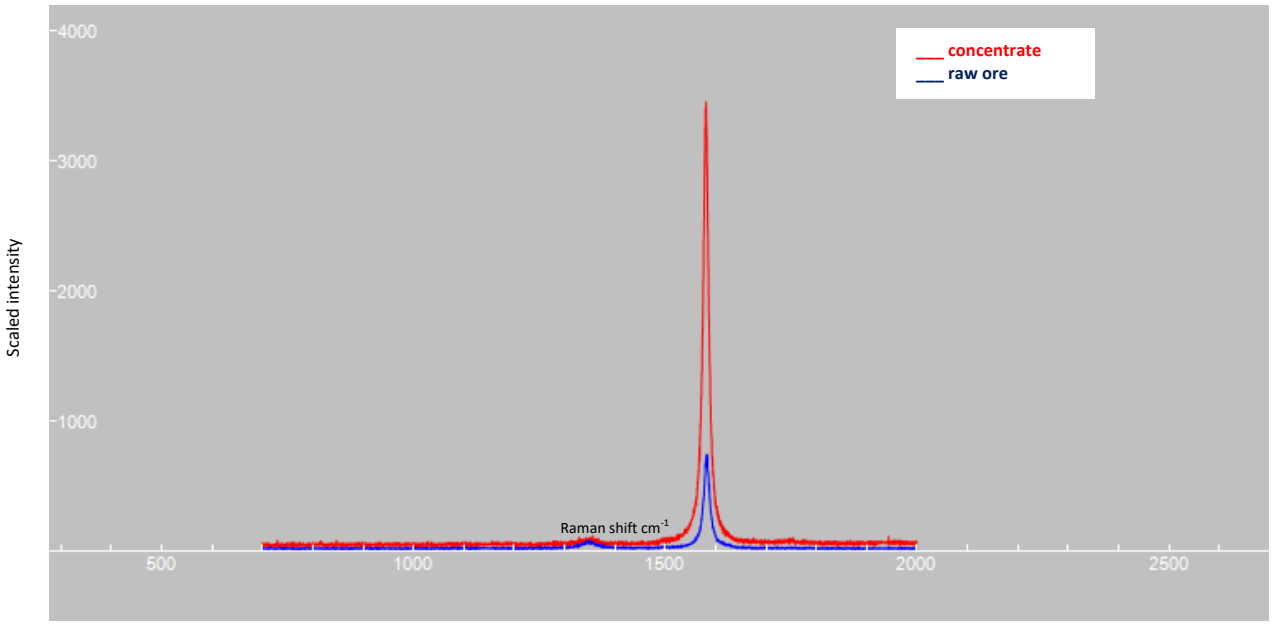


*Figure 41: Raman spectra from Passau (GER) - raw ore spectrum in blue and concentrate spectrum in red*

In order to avoid alteration of the graphite structure by sample preparation (polishing or shearing), samples were prepared as a water-suspension on a glass slide for the analysis. A variable number of spectra (10-20 spectra per sample) was recorded on different points (flakes). Each sample is assigned to a mine/province. Fig. 42 illustrates the total number of spectra per location. The Balama mine is overrepresented due to the presence of numerous individual samples. For the Chinese occurrences, mostly only one sample is available, hence the number of corresponding spectra is lower.

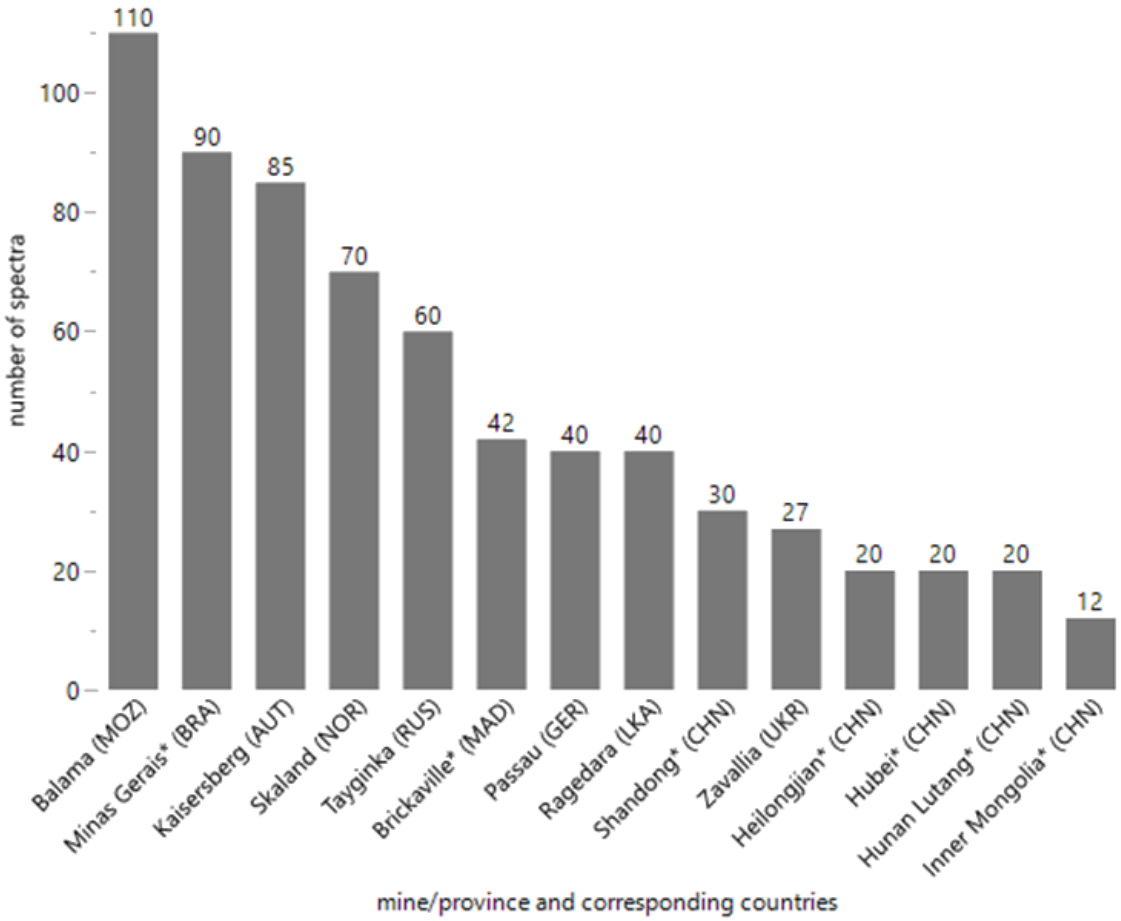


*Figure 42: Number of spectra per location (mine/province)*

Important parameters describing the spectra, were extracted using iFORS (iterative Fitting of Raman Spectra) (Rantitsch et al. 2014) by Dr. Ròbert Aratò. The extracted parameters, following (Lünsdorf et al. 2017) terminology, comprise the following features:

- D-band (disorder band): is associated with disordering or defects in the crystal lattice structure
- G-band (graphitic band): is associated with the crystalline structure of graphite and often used to describe the degree of graphitization
- Dmax and Gmax: D-band and G-band regions exhibit a central Raman band containing Dmax, with the G-band region characterized by the Raman band containing Gmax
- D_STA and G_STA: representing the area beneath the D-band/G-band; STA, an acronym for Scaled Total Area. D_STA is used to describe the evolution of organic matter during graphitization.
- G_shape_factor: indicating a mathematical descriptor of the fitted curve, the factor identifies the terminus of the transition zone, facilitating the connection between G_STA and D_STA.

Three Raman spectra are presented below (Figure 43), each of them representing one type of graphite (amorphous, flake, vein/hydrothermal) investigated in this study.

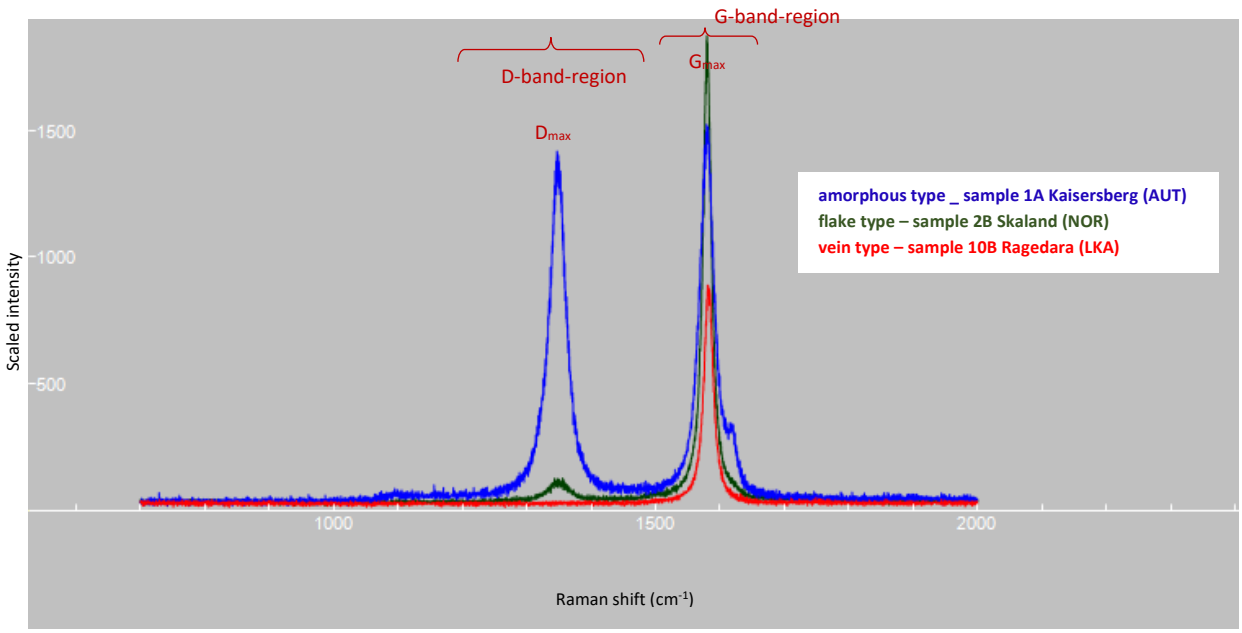


*Figure 43: Raman spectra of sample 1A from Kaisersberg (AUT, amorphous, green), sample 2B from Skaland (NOR, flake, blue) and sample 10B from Ragedara (LKA, hydrothermal, orange)*

The first order spectrum from sample 1A Kaisersberg (AUT) (green) reveals a prominent D-band and the G-band. First order spectrum from sample 2B from Skaland (NOR) (blue) reveals a sharp G-band with a high intensity and a weak D-band. Spectra from sample 10B from Ragedara (LKA) represent hydrothermal graphite with a pronounced G-band and missing D-band. Spectra from this sample hardly ever show any occurrence of a D-band.

The relevant parameters according to Lünsdorf et al (2017) were collected and analyzed in a Linear Discriminant Analysis (LDA). The first model (Figure 44) demonstrates the differentiation based on mine/province. Hunan Lutang (CHN) and Kaisersberg (AUT), representing amorphous (semi-) graphite can be distinguished from the rest of the samples. Two classes can be identified which represent the amorphous graphite type (Hunan Lutang and Kaisersberg) and the rest of the samples (flake and hydrothermal type), that overlap significantly. Further discrimination into individual mines/provinces is not feasible. Within the flake and vein graphite types, no further separation into subclasses (e.g. mine/province) is possible.

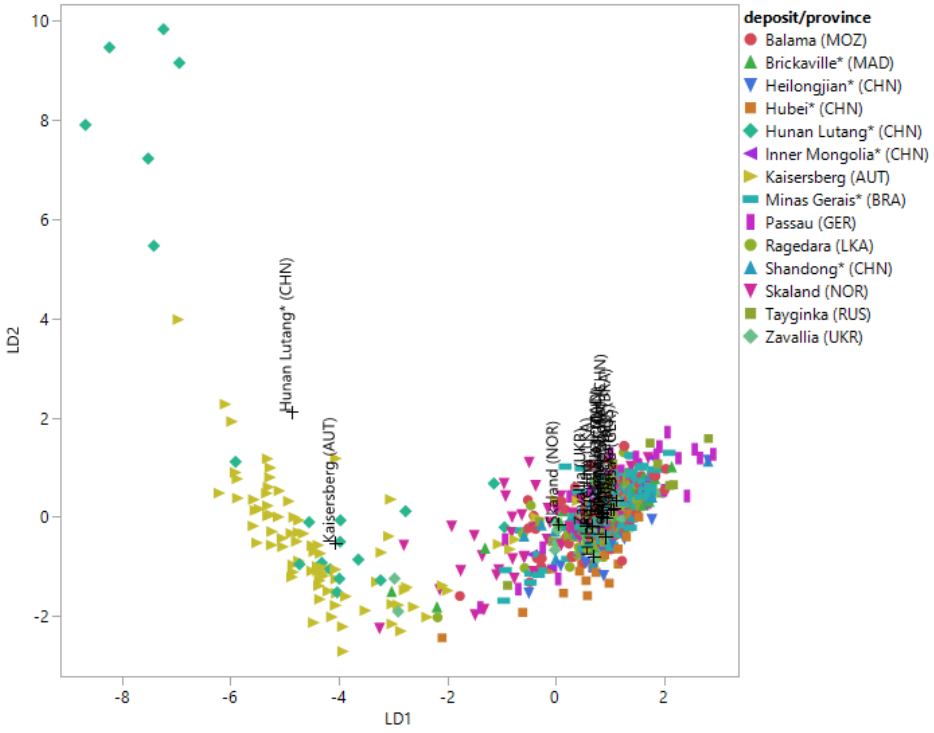


*Figure 44: LDA of the extracted parameters of graphite Raman spectra categorized into mines/provinces*

The same parameters were analyzed using Linear Discriminant Analysis (LDA), but this time classified by carbon type (Fig. 45). Discrimination based on the graphite type (amorphous – flake – hydrothermal) shows a clearer result. The group of amorphous graphite can be differentiated. However, the hydro and flake graphite groups overlap and cannot be separated from each other.

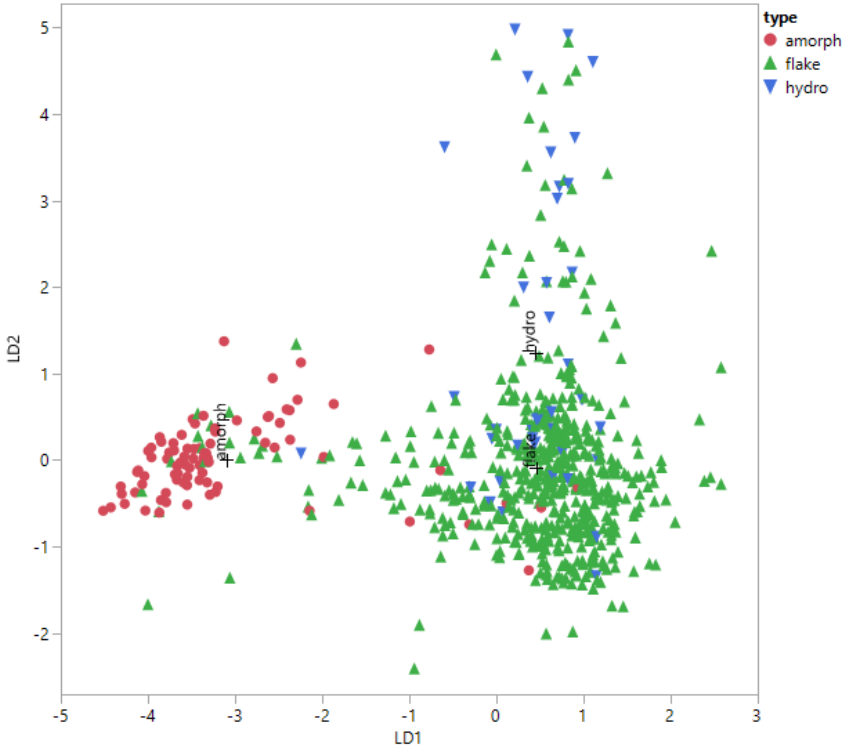


*Figure 45: LDA of the extracted parameters of graphite Raman spectra categorized into mines/provinces*

**Identification of important parameters for the discrimination (scoring coefficients):**

To interpret the result of the linear discriminant analysis (LDA) and to identify the contribution of each independent variable for the formation of the discriminant functions, the scoring coefficients of the canonicals were extracted from LDA, with LD1 and LD2 having the highest impact and class separability. Larger coefficients indicate stronger influence on the classes. G shape-factor and G_STA are the variables that are most important for discriminating between the graphite types (Tab. 15).
Canonicals 1 and 2 (expressed as LD1 and LD2) refer to linear combinations of the original variables that maximize the separation between groups. Canonical 1 of LD1 represents the linear combination of variables that provide the maximum discrimination between the graphite types (groups) and LD2 the most discriminative variable combination orthogonal to LD1 related to the same groups. In the matrix, there are further canonicals, but their significance gradually diminishes.

*Table 15: Standardized scoring coefficients from LDA (Fig. 60)*

| | ***D_STA*** | ***G_STA*** | ***G_shape_factor*** | ***Dmax_pos*** | ***Gmax_pos*** | ***Dmax/Gmax-ratio*** | ***D_shape_factor*** |
|---|---|---|---|---|---|---|---|
| *LD1* | *-0.3777* | *-0.3227* | ***0.9987*** | *0.0158* | *0.3254* | *0.0098* | *0.0025* |
| *LD2* | *-0.6420* | ***1.6246*** | *0.8693* | *0.0235* | *-0.4583* | *-0.6565* | *0.2312* |
| *LD3* | *0.1446* | *-0.5074* | *-0.2807* | *0.6562* | *-0.1466* | *0.4171* | *0.7157* |
| *LD4* | *0.9268* | *0.9521* | *-0.1353* | *-0.5172* | *0.5315* | *-0.8023* | *-0.2705* |
| *LD5* | *-0.6569* | *-0.3681* | *0.1847* | *0.2794* | *0.7349* | *0.5887* | *0.1465* |
| *LD6* | *-0.6382* | *-2.7770* | *-0.0446* | *-0.4761* | *-0.2646* | *2.7767* | *1.2758* |
| *LD7* | *0.6463* | *-1.1580* | *0.3262* | *0.1956* | *-0.0314* | *1.7492* | *-0.7205* |

## 6.4. Multi-Element-Analysis

### 6.4.1. Trace Element Concentrations Assessed by LA-ICP-MS

For each graphite concentrate a powder pressed pellet was prepared and approximately 15 to 20 line scans per pellet and five to ten points per raw ore, depending on the graphite flake size were carried out using LA-ICP-MS analysis. A total of 13 graphite mines/provinces are available for this study, divided into 37 individual graphite samples, which results into 17316 trace element data for this method. In some cases, distinguishing down to the level of the mine was not possible; therefore, samples marked with * will only be discussed at the province level as the material is likely a mixture from multiple mines from one province. In China, the exact mines are unknown and can partly be artisanal and small-scale mines. Brickaville* (MAD) samples are from the mines Vatomina and Sahamamy Sahasoa. In the province Minas Gerais* (BRA), samples originate from the mines Pedra Azul, Itapecerica and Salto da Divisa. All localities in China are referred to as provinces. For each mine/province, there was a varying number of samples available. The subsequent tables (Tab. 16 to 28) list the available samples for each location (concentrate/raw ore) and show median values for each element.

*Table 16: Median values Kaisersberg (AUT): 1A = concentrate; 21G, H and I are raw ore samples*

| Kaisersberg (AUT) | Analyte (µg g-1) | | | | | | | | | | | | | | | | |
|---|---|---|---|---|---|---|---|---|---|---|---|---|---|---|---|---|---|
| **sample ID** | **Mg** | **Al** | **Ca** | **V** | **Cr** | **Mn** | **Fe** | **Co** | **Cu** | **Zn** | **Ga** | **As** | **Rb** | **Sr** | **Zr** | **Ce** | **U** |
| 1A median | 396.04 | 5296.52 | 287.10 | 137.71 | 88.20 | 362.91 | 5084.70 | 4.45 | 26.34 | 52.00 | 101.21 | 19.76 | 149.71 | 112.08 | 11.64 | 57.28 | 3.80 |
| 21G median | 44.97 | 1479.72 | 45.17 | 15.42 | 35.14 | 6.30 | 101.94 | 0.20 | 0.36 | 5.11 | 11.34 | 3.37 | 11.34 | 16.06 | 5.12 | 1.60 | 0.68 |
| 21H median | 22.87 | 1777.98 | 23.22 | 17.01 | 27.52 | 3.36 | 58.63 | 0.06 | 0.62 | 3.85 | 10.66 | 4.08 | 17.38 | 14.87 | 5.45 | 1.51 | 0.48 |
| 21I median | 2.89 | 152.82 | 15.28 | 2.47 | 22.89 | 1.51 | 11.53 | 1.09 | 0.86 | 2.33 | 1.50 | 12.89 | 1.03 | 4.02 | 1.34 | 0.95 | 0.17 |

*Table 17: Median values Minas Gerais (BRA): all samples are concentrates*

| Minas Gerais (BRA) | Analyte (µg g-1) | | | | | | | | | | | | | | | | |
|---|---|---|---|---|---|---|---|---|---|---|---|---|---|---|---|---|---|
| **sample ID** | **Mg** | **Al** | **Ca** | **V** | **Cr** | **Mn** | **Fe** | **Co** | **Cu** | **Zn** | **Ga** | **As** | **Rb** | **Sr** | **Zr** | **Ce** | **U** |
| 21C median | 1.17 | 281.85 | 3.50 | 3.80 | 30.63 | 6.19 | 120.52 | 0.18 | 5.37 | 1.41 | 0.61 | 0.17 | 0.03 | 0.29 | 6.27 | 1.91 | 0.04 |
| 21N median | 0.93 | 317.90 | 3.74 | 3.81 | 29.10 | 5.04 | 128.26 | 0.19 | 5.10 | 1.30 | 0.53 | 0.17 | 0.02 | 0.29 | 6.53 | 1.95 | 0.04 |
| 3B median | 0.69 | 330.86 | 6.70 | 6.29 | 35.27 | 15.86 | 171.70 | 0.83 | 4.89 | 1.04 | 1.01 | 0.16 | 0.04 | 0.30 | 1.83 | 1.08 | 0.12 |
| 21M median | 1.32 | 361.06 | 5.27 | 4.85 | 30.17 | 8.27 | 158.62 | 0.34 | 5.68 | 1.60 | 0.90 | 0.13 | 0.04 | 0.53 | 7.08 | 2.39 | 0.06 |
| 22C median | 1.38 | 410.90 | 4.27 | 3.95 | 26.88 | 7.52 | 109.16 | 0.32 | 3.31 | 2.00 | 0.85 | 0.18 | 0.05 | 0.50 | 14.83 | 3.01 | 0.05 |

*Table 18: Median values Shandong (CHN)): all samples are concentrates*

| Shandong (CHN) | Analyte (µg g-1) | | | | | | | | | | | | | | | | |
|---|---|---|---|---|---|---|---|---|---|---|---|---|---|---|---|---|---|
| **sample ID** | **Mg** | **Al** | **Ca** | **V** | **Cr** | **Mn** | **Fe** | **Co** | **Cu** | **Zn** | **Ga** | **As** | **Rb** | **Sr** | **Zr** | **Ce** | **U** |
| 21A median | 1.47 | 397.79 | 13.77 | 34.85 | 45.12 | 2.41 | 461.04 | 0.16 | 8.76 | 9.90 | 1.53 | 0.28 | 0.10 | 1.71 | 1.64 | 0.85 | 0.31 |
| 22A median | 4.20 | 16.86 | 5.05 | 0.70 | 21.92 | 0.75 | 14.56 | 0.08 | 0.53 | 0.34 | 0.08 | 0.27 | 0.19 | 0.12 | 0.34 | 0.27 | 0.02 |

*Table 19: Median values Hunan Lutang (CHN): concentrate*

| Hunan Lutang* (CHN) | Analyte (µg g-1) | | | | | | | | | | | | | | | | |
|---|---|---|---|---|---|---|---|---|---|---|---|---|---|---|---|---|---|
| sample ID | Mg | Al | Ca | V | Cr | Mn | Fe | Co | Cu | Zn | Ga | As | Rb | Sr | Zr | Ce | U |
| 4A median | 37.47 | 977.16 | 51.64 | 16.96 | 27.79 | 41.35 | 496.97 | 2.66 | 7.65 | 15.98 | 6.35 | 36.72 | 13.54 | 16.41 | 21.41 | 4.60 | 0.59 |

*Table 20: Median values Inner Mongolia (CHN): concentrate*

| Inner Mongolia* (CHN) | Analyte (µg g-1) | | | | | | | | | | | | | | | | |
|---|---|---|---|---|---|---|---|---|---|---|---|---|---|---|---|---|---|
| Sample ID | Mg | Al | Ca | V | Cr | Mn | Fe | Co | Cu | Zn | Ga | As | Rb | Sr | Zr | Ce | U |
| 6B median | 2.42 | 2.76 | 14.85 | 0.14 | 30.73 | 0.75 | 41.25 | 0.13 | 0.37 | 0.31 | 0.04 | 0.17 | 0.08 | 0.41 | 1.59 | 0.89 | 0.02 |

*Table 21: Median values Heilongjian (CHN): concentrate*

| Heilongjian* (CHN) | Analyte (µg g-1) | | | | | | | | | | | | | | | | |
|---|---|---|---|---|---|---|---|---|---|---|---|---|---|---|---|---|---|
| sample ID | Mg | Al | Ca | V | Cr | Mn | Fe | Co | Cu | Zn | Ga | As | Rb | Sr | Zr | Ce | U |
| 7B median | 33.16 | 271.43 | 68.51 | 29.23 | 33.58 | 13.58 | 393.92 | 1.92 | 6.51 | 17.63 | 1.92 | 0.47 | 2.03 | 2.94 | 1.55 | 1.94 | 0.94 |

*Table 22: Median values Kropfmühl (GER): 14B is a raw ore, 13B a concentrate*

| Kropfmühl (GER) | Analyte (µg g-1) | | | | | | | | | | | | | | | | |
|---|---|---|---|---|---|---|---|---|---|---|---|---|---|---|---|---|---|
| sample ID | Mg | Al | Ca | V | Cr | Mn | Fe | Co | Cu | Zn | Ga | As | Rb | Sr | Zr | Ce | U |
| 13B median | 101.18 | 359.74 | 21.51 | 19.81 | 29.74 | 33.68 | 464.22 | 0.89 | 17.66 | 1.81 | 1.12 | 0.14 | 3.44 | 0.90 | 0.50 | 0.71 | 0.16 |
| 14B median | 136.80 | 538.99 | 20.94 | 63.30 | 63.18 | 35.46 | 697.79 | 0.49 | 7.56 | 7.73 | 2.80 | 0.43 | 21.02 | 1.05 | 0.59 | 0.14 | 0.12 |

*Table 23: Median values Brickaville (MAD): all samples are concentrates*

| Brickaville (MAD) | Analyte (µg g-1) | | | | | | | | | | | | | | | | |
|---|---|---|---|---|---|---|---|---|---|---|---|---|---|---|---|---|---|
| **sample ID** | **Mg** | **Al** | **Ca** | **V** | **Cr** | **Mn** | **Fe** | **Co** | **Cu** | **Zn** | **Ga** | **As** | **Rb** | **Sr** | **Zr** | **Ce** | **U** |
| 21D median | 2.01 | 194.76 | 2.67 | 13.08 | 22.58 | 19.06 | 134.60 | 0.61 | 5.04 | 5.15 | 0.39 | 0.36 | 0.07 | 0.06 | 0.03 | 2.55 | 0.11 |
| 11B median | 2.16 | 988.56 | 6.02 | 10.24 | 47.70 | 2.69 | 465.94 | 0.54 | 6.49 | 2.52 | 3.07 | 1.42 | 0.41 | 0.51 | 2.77 | 3.23 | 0.18 |
| 22D median | 7.08 | 345.51 | 8.56 | 8.04 | 25.46 | 16.05 | 397.01 | 0.79 | 5.72 | 6.36 | 0.80 | 0.41 | 0.78 | 0.45 | 0.74 | 11.62 | 0.22 |

*Table 24: Median values Balama (MOZ): sample 22H is a raw ore, rest of the samples are concentrates*

| Balama (MOZ) | Analyte (µg g-1) | | | | | | | | | | | | | | | | |
|---|---|---|---|---|---|---|---|---|---|---|---|---|---|---|---|---|---|
| **sample ID** | **Mg** | **Al** | **Ca** | **V** | **Cr** | **Mn** | **Fe** | **Co** | **Cu** | **Zn** | **Ga** | **As** | **Rb** | **Sr** | **Zr** | **Ce** | **U** |
| 1B median | 2.16 | 51.87 | 7.15 | 27.00 | 28.41 | 4.46 | 62.33 | 0.17 | 4.42 | 13.55 | 1.35 | 0.25 | 0.42 | 1.24 | 10.29 | 0.51 | 0.72 |
| 21B median | 0.93 | 143.39 | 9.35 | 11.84 | 34.54 | 6.21 | 200.28 | 0.28 | 4.56 | 9.60 | 1.06 | 0.24 | 0.16 | 0.75 | 2.12 | 0.91 | 0.25 |
| 21J median | 1.51 | 341.78 | 10.93 | 35.84 | 48.40 | 5.23 | 248.29 | 0.24 | 9.74 | 13.46 | 2.15 | 0.33 | 0.21 | 2.17 | 2.42 | 1.72 | 0.53 |
| 21K median | 1.07 | 396.58 | 13.27 | 44.48 | 36.95 | 4.03 | 202.35 | 0.15 | 6.70 | 11.26 | 3.41 | 0.30 | 0.17 | 4.15 | 4.93 | 1.90 | 0.42 |
| 21L median | 1.34 | 343.64 | 9.53 | 26.58 | 28.99 | 1.25 | 147.90 | 0.09 | 6.74 | 9.94 | 1.57 | 0.17 | 0.09 | 1.95 | 1.72 | 0.41 | 0.35 |
| 22B median | 0.99 | 341.60 | 10.50 | 45.89 | 36.31 | 4.87 | 181.91 | 0.15 | 6.08 | 14.07 | 1.44 | 0.28 | 0.14 | 1.20 | 4.12 | 1.61 | 0.41 |
| 22H median | 0.62 | 17.64 | 4.01 | 0.50 | 33.81 | 0.16 | 2.24 | 0.04 | 0.45 | 0.81 | 0.24 | 0.13 | 0.02 | 0.14 | 0.14 | 0.03 | 0.00 |

*Table 25: Median values Skaland (NOR): all samples are concentrates*

| Skaland (NOR) | Analyte (µg g-1) | | | | | | | | | | | | | | | | |
|---|---|---|---|---|---|---|---|---|---|---|---|---|---|---|---|---|---|
| **sample ID** | **Mg** | **Al** | **Ca** | **V** | **Cr** | **Mn** | **Fe** | **Co** | **Cu** | **Zn** | **Ga** | **As** | **Rb** | **Sr** | **Zr** | **Ce** | **U** |
| 15B median | 16.94 | 95.84 | 16.31 | 2.50 | 35.74 | 11.61 | 132.31 | 0.37 | 4.42 | 1.91 | 0.76 | 0.10 | 1.85 | 0.53 | 0.06 | 0.27 | 0.07 |
| 2B median | 37.97 | 213.82 | 38.77 | 16.91 | 26.45 | 17.81 | 267.89 | 0.76 | 3.94 | 6.12 | 1.05 | 0.57 | 2.07 | 3.13 | 0.57 | 2.04 | 0.49 |
| 22G median | 38.30 | 163.39 | 22.92 | 5.69 | 26.75 | 10.81 | 174.94 | 0.55 | 6.84 | 1.03 | 0.61 | 0.11 | 1.38 | 1.09 | 0.10 | 0.65 | 0.19 |

*Table 26: Median values Tayginka (RUS): all samples are concentrates*

| **Tayginka (RUS)** | **Analyte (µg g-1)** | | | | | | | | | | | | | | | | |
|---|---|---|---|---|---|---|---|---|---|---|---|---|---|---|---|---|---|
| **sample ID** | **Mg** | **Al** | **Ca** | **V** | **Cr** | **Mn** | **Fe** | **Co** | **Cu** | **Zn** | **Ga** | **As** | **Rb** | **Sr** | **Zr** | **Ce** | **U** |
| 21E median | 23.98 | 239.06 | 34.03 | 4.29 | 27.19 | 16.01 | 245.17 | 0.29 | 9.43 | 2.50 | 1.32 | 0.18 | 1.10 | 1.59 | 0.93 | 0.43 | 0.14 |
| 22E median | 11.24 | 65.48 | 15.77 | 1.49 | 25.77 | 9.36 | 138.66 | 0.23 | 3.92 | 1.98 | 0.34 | 0.13 | 0.28 | 0.58 | 0.37 | 0.44 | 0.07 |
| 5B median | 18.04 | 264.68 | 18.55 | 3.03 | 24.69 | 12.09 | 154.05 | 0.26 | 6.11 | 3.13 | 0.87 | 0.16 | 0.72 | 0.67 | 0.66 | 0.09 | 0.09 |

*Table 27: Median values Ragedara (LKA): all samples are raw ore (lumps/chunks)*

| **Ragedara (LKA)** | **Analyte (µg g-1)** | | | | | | | | | | | | | | | | |
|---|---|---|---|---|---|---|---|---|---|---|---|---|---|---|---|---|---|
| **sample ID** | **Mg** | **Al** | **Ca** | **V** | **Cr** | **Mn** | **Fe** | **Co** | **Cu** | **Zn** | **Ga** | **As** | **Rb** | **Sr** | **Zr** | **Ce** | **U** |
| 10B median | 9.23 | 43.06 | 20.91 | 1.90 | 37.71 | 14.21 | 502.60 | 2.85 | 55.83 | 16.41 | 2.20 | 0.82 | 0.09 | 1.50 | 0.08 | 0.44 | 0.20 |
| 21F median | 2.46 | 43.19 | 5.91 | 0.17 | 61.59 | 1.34 | 12.53 | 0.08 | 0.82 | 9.26 | 0.40 | 1.23 | 0.17 | 0.59 | 0.30 | 0.38 | 0.02 |

*Table 28: Median values Zavallia (UKR): sample 22K-S is a raw ore sample, rest of the samples are concentrates*

| **Zavallia (UKR)** | **Analyte (µg g-1)** | | | | | | | | | | | | | | | | |
|---|---|---|---|---|---|---|---|---|---|---|---|---|---|---|---|---|---|
| **sample ID** | **Mg** | **Al** | **Ca** | **V** | **Cr** | **Mn** | **Fe** | **Co** | **Cu** | **Zn** | **Ga** | **As** | **Rb** | **Sr** | **Zr** | **Ce** | **U** |
| 22F median | 94.70 | 355.38 | 23.50 | 13.78 | 27.25 | 14.92 | 831.34 | 0.55 | 7.80 | 26.01 | 6.04 | 1.22 | 1.99 | 1.94 | 3.23 | 0.28 | 0.15 |
| 4B median | 8.61 | 218.62 | 10.95 | 3.26 | 32.95 | 3.66 | 162.02 | 0.15 | 3.91 | 5.48 | 0.41 | 0.32 | 0.20 | 0.54 | 0.89 | 0.02 | 0.02 |

### 6.4.1.1. Laser-Ablation Signals and Ablation Marks

The ablation of graphite material using LA-ICP-MS is challenging. The properties of the graphite material (fine-grained/powdery, difficult to press into a stable form, generally unstable even as a powder pellet, partly heterogeneous grain sizes, conductivity of the material, etc.) complicated this application. To avoid the heterogeneity within the concentrates, lines with approximately 150 µm diameter were ablated for 72-75 seconds. This allowed for more stable signals (Figure 46) (compare signal Cr concentrate). Individual peaks in the intensities may also be attributed to accompanying mineral grains. Therefore, areas reflecting the graphite ablation signal only, were selected during data reduction. Data reduction was particularly important to eliminate outliers and choose stable areas of the signal for further data processing.

The analysis of graphite in raw ore was limited by the sometimes very small grain or flake sizes. The laser diameter for ablation was limited to about 50 µm; for smaller graphite grain sizes the analysis could not be performed.

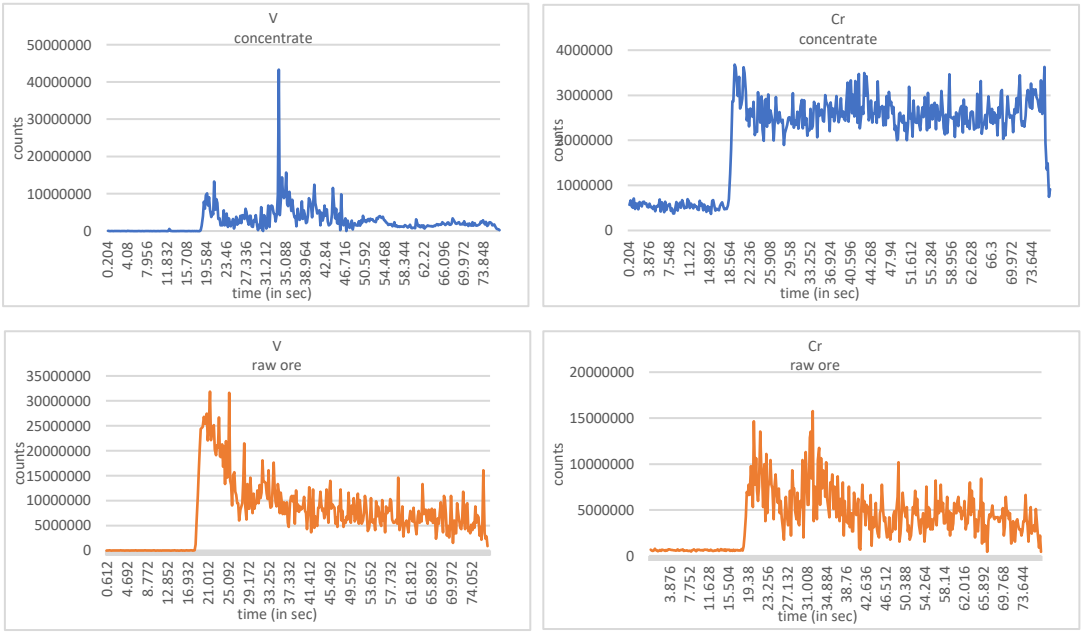


*Figure 46: Laser ablation signals for V and Cr for graphite concentrates (blue) and raw ore (orange)*

The remaining craters from the ablation were clearly visible after performing the analytical method. Figure 47 on the left shows the ablation of the lines in a powder pellet. The ablation lines are not directly visible, only the dark area of the ablation with the outer brownish area where the material burns out. Figure 47 right image shows the ablation crater in a raw ore graphite sample as remaining dark circle.


*Figure 47: Laser ablation craters in graphite concentrate, sample 15B (left) and raw ore sample 10B (right)*

### 6.4.1.2. Within Element Variability

Each of the following diagrams displays the variability of the respective element across all mines/provinces, allowing for the initial recognition of differences and the possibility of discriminations. A grouping of the individual graphite deposits for each element is not possible with the LA-ICP-MS data, as they show too few differences within the element.

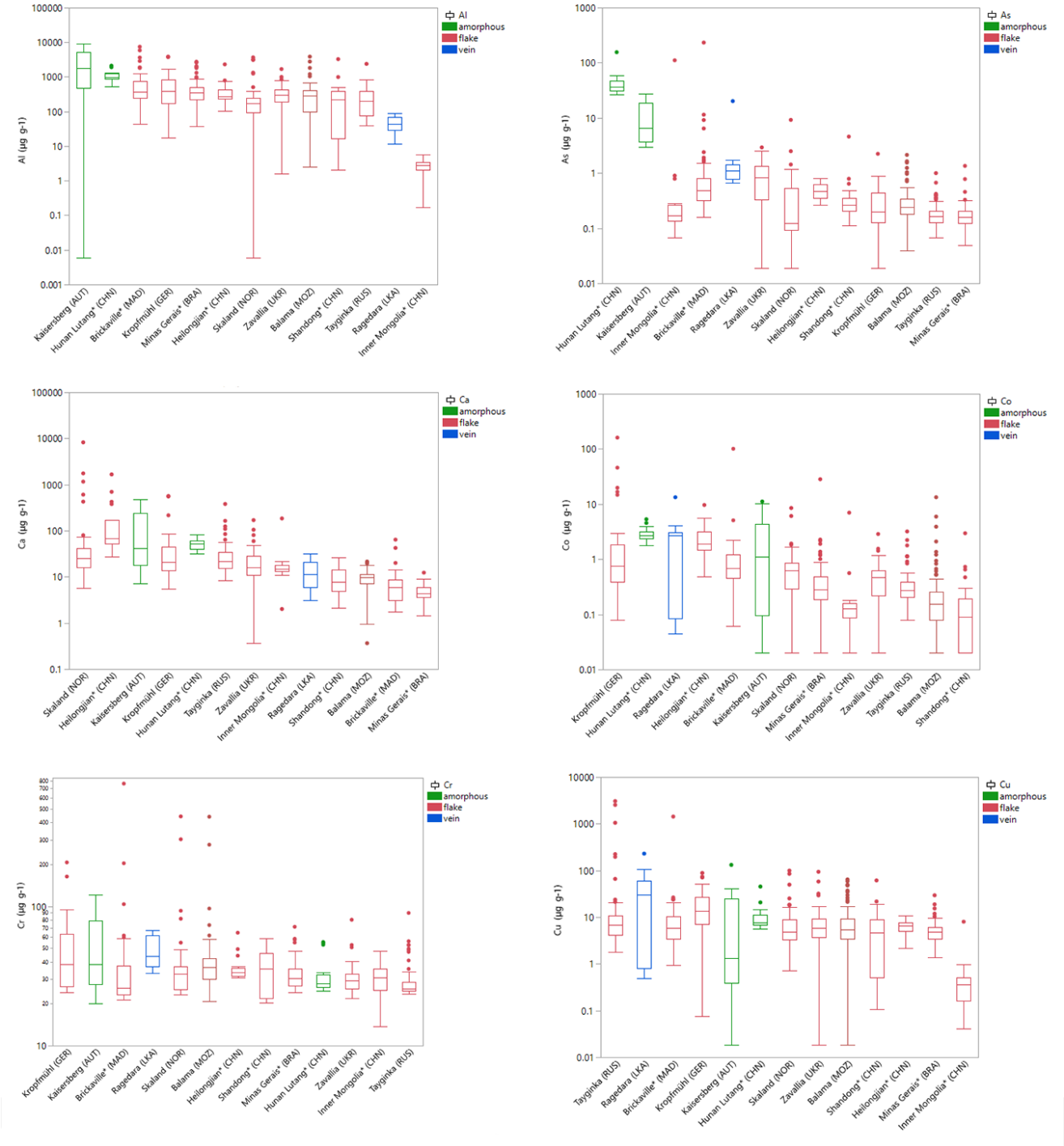


*Figure 48: Within element variability for Al, As, Ca, Co, Cr, Cu (LA-ICP-MS data) in µg $g^{-1}$*


*Figure 49: Within element variability for Fe, Ga, Mg, Mn, Rb (LA-ICP-MS data) in µg $g^{-1}$*

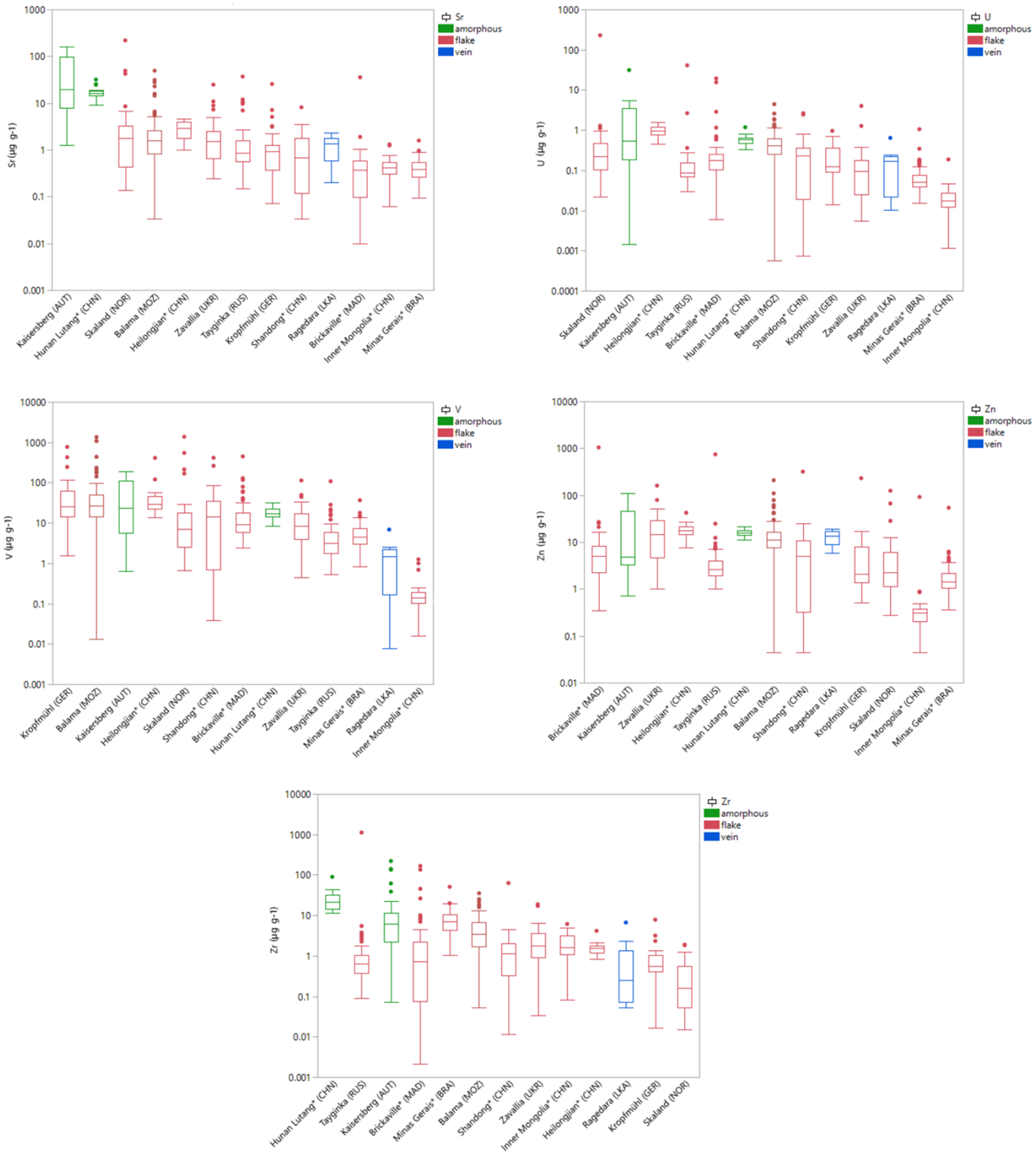


*Figure 50: Within element variability for Sr, U, V, Zn, Zr (LA-ICP-MS data) in $\mu g\ g^{-1}$*

### 6.4.1.3. Scatter Plots

The linear Al and Ga correlation is displayed in the scatter plot (Figure 51). A group of data points with higher Al and Ga is related to Kaisersberg. One group is associated to low Al and Ga levels, representing Inner Mongolia. Intermediate Ga and Al levels can be attributed to Ragedara, but interfere with other deposits. The rest of the samples cannot be differentiated based on these two elements. Aluminum (Al) and gallium (Ga) substitute for each other in silicate structures. High aluminum contents are usually associated with high gallium contents.

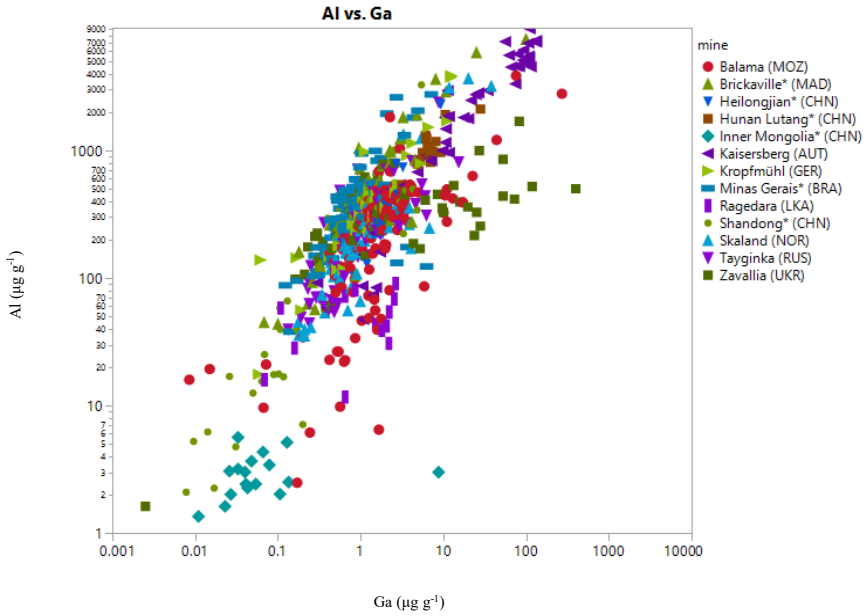


*Figure 51: Scatter plot of Al/Ga (log scale, LA-ICP-MS data) in µg g-1*

Scatter plot (Figure 52) shows the Al/Cr variation with overlapping data points for each deposit. Data from Kaisersberg show a group at higher Al and Cr levels, with outlying points at very low Al levels. Inner Mongolia also shows a set of data points located at lower Al levels, compared to other deposits. Overall, data points for Al/Cr do not allow a discrimination of individual deposits. There is no substitution between Al and Cr. Chromium might be incorporated into iron oxides, which in turn can occur as accompanying minerals in the graphite concentrate.

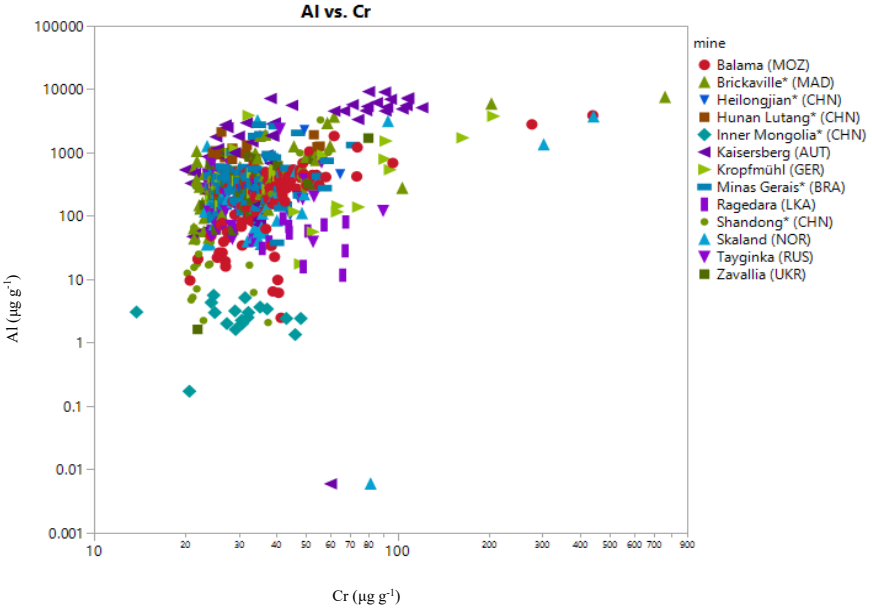


*Figure 52: Scatter plot of Al/Cr (log scale, LA-ICP-MS data) in µg g-1*

Al/Sr variation shows most data points are distributed across the graph (Fig. 53) with some data points at significant lower Al and Sr levels (Inner Mongolia), as well as some higher Al and Sr values for Kaisersberg. Most locations (data points) are located at intermediate Al and Sr levels. Strontium (Sr) can be incorporated into carbonates and feldspars, whereas aluminum (Al) can only be incorporated into feldspars.

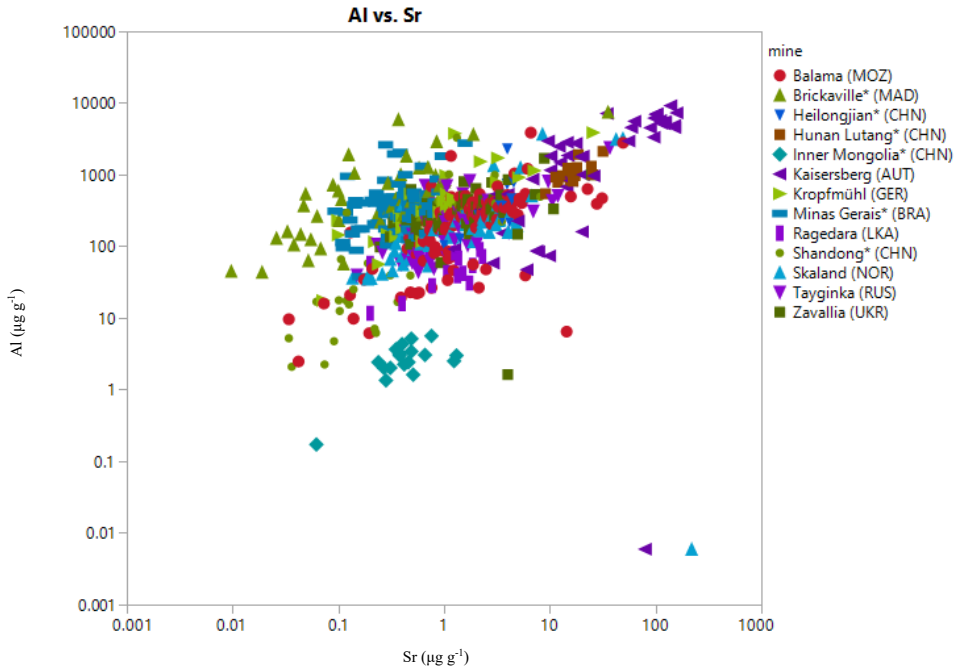


*Figure 53: Scatter plot of Al/Sr (log scale, LA-ICP-MS data) in µg g-1*

V/Ga element concentrations (Figure 54) demonstrate a linear correlation. Graphite deposits scatter across a large range of Ga and V levels. A differentiation of mines/provinces based on these elements is not feasibile. Inner Mongolia can be characterized by lower Ga and V levels, as well as Kaisersberg to higher Ga and V levels. Zavallia shows higher Ga levels, compared to other deposits.

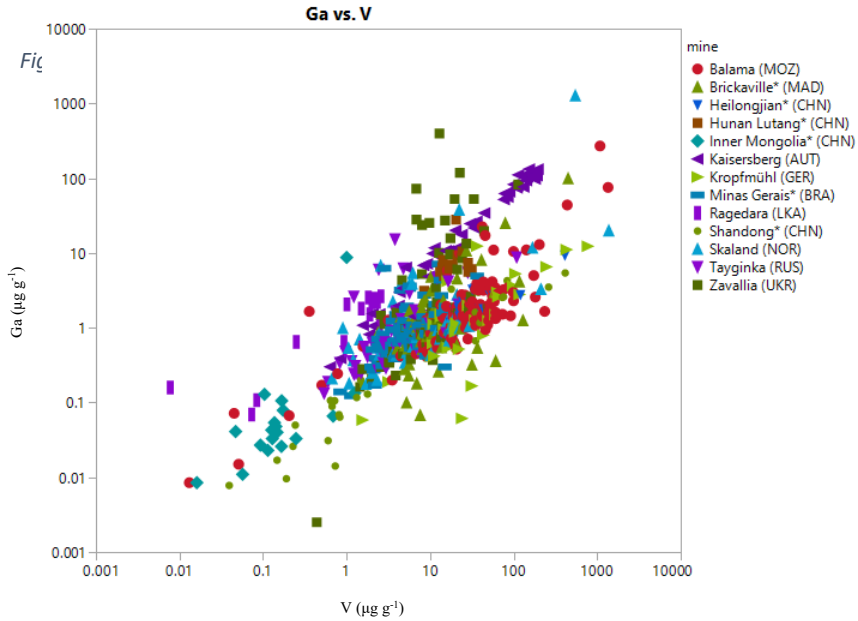


*Figure 54: Scatter plot of Ga/V (log scale, LA-ICP-MS data) in µg g-1*

As/U (Figure 55) are not linear correlated. Data points of this element ratio allow a discrimination of some deposits, with Hunan Lutang at higher As levels compared to other data points. Kaisersberg is also associated with higher As levels, however the grouping is not as precise as with Hunan Lutang province. The rest of the data points do not allow discrimination.

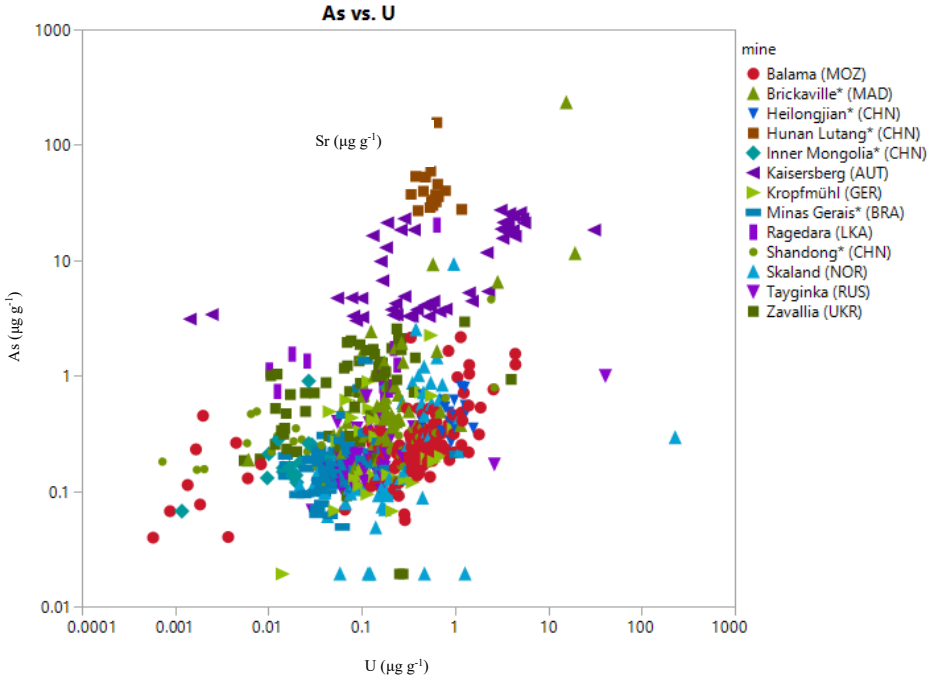


*Figure 55: Scatter plot As/U (log scale, LA-ICP-MS data)*

Rb/Sr (Figure 56) shows very densely distributed data points at intermediate Rb and Sr levels, with Kropfmühl at higher Rb levels and Kaisersberg at higher Sr levels, however scattered among data points from other deposits and therefore not clearly distinguishable. High rubidium (Rb) contents indicate the presence of silicates, while strontium (Sr) is incorporated into carbonates or feldspars.

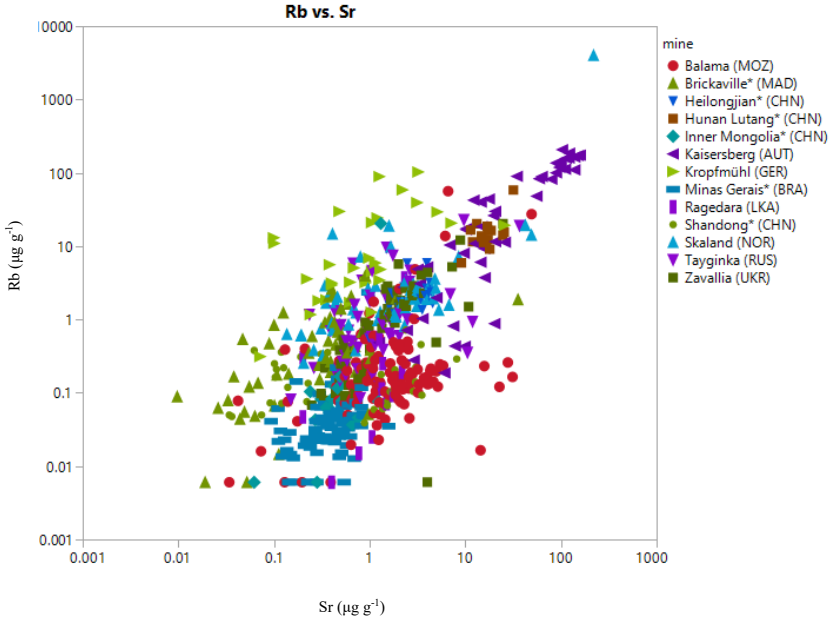


*Figure 56: Scatter plot Rb/Sr (log scale, LA-ICP-MS data) in µg g-1*

### 6.4.1.4. Factor Analysis

A factor analysis was performed using the trace element data from the LA-ICP-MS analysis to reduce a large number of variables (trace elements) to a smaller number of underlying factors and to better understand the structure within the dataset. These factors were then interpreted as component groups with potential mineral phases. The loadings (L %) assist in interpreting the data structure and understanding which variables are strongly associated with which factors. The table below (Tab. 28) provides an overview of the results of the factor analysis using the LA-ICP-MS trace element data. From the dataset, five component groups were interpreted and identified: K-Al silicates (Rb as a K proxy, plus Ga or Al), K-free Ca-Al silicates (Ca plus Ga/Al), Ca plus Ce (allanite), Al/Ga with Mg/Fe (chlorite), and Ca, Sr with Mn-Mg-Fe (carbonates).

*Table 28: Factor Analysis from LA-ICP-MS data; individual factors interpreted as component groups*

| mine/province | K-Al-Silicates (Rb as K proxy, plus Ga or Al) | L (%) | K-free Ca-Al-Silicates (Ca plus Ga/Al) | L (%) | Ca plus Ce (allanite?) | L (%) | Al/Ga mit Mg/Fe (chlorite?) | L (%) | Ca, Sr with Mn-Mg-Fe (carbonates?) | L (%) |
|---|---|---|---|---|---|---|---|---|---|---|
| Kaisersberg (AUT) | Sr, Ga, Rb, V, Ce, Ca, Cu, Fe, Mg, Mn, Zn, Cr | 34 | | | Sr, Ce, Ca, Cu, Mn, Zn, As, Co, Cr, | 20 | | | | |
| Minas Gerais (BRA) | | | Mn, Co , Ga, V, Fe, Ca | 16 | | | | | | |
| Shandong (CHN) | | | Cu, Al, Fe, V, Ga, Sr, Zn, ca, Cr, Mn, Ce | 54 | | | | | | |
| Hunan Lutang (CHN) | Rb, Ga, Al, Sr, Ce, Mg, V | 24 | | | | | | | | |
| Inner Mongolia (CHN) | Rb, Ga, ZN, As, Mg, Cu, Ca, Mn, Co , Sr, V | 36 | | | Ca, Al, Sr, V, Ce | 15 | | | As, Mg, Ca, Mn, Co , Sr, V | 19 |
| Heilongjian (CHN) | Al, V, Ga, Rb, Mg, Fe, Ce, Zn | 18 | Mn, Ca, Al, V, Ga, Mg, Sr, Co, Zn | 22 | Ca, Al, Ga, Mg, Sr, Fe, Ce | 12 | | | | |
| Kropfmühl (GER) | V, Mg, Mn, Rb, Cr, Ga, Al, Zn, AS | 32 | | | | | Mg, Rb, Sr, Ga, Al, Fe, As | 16 | | |
| Brickaville (MAD) | Rb, Mg, Al, Ce, Sr, Ca | 16 | | | | | V, Cr, As, Cu, Fe, Co, Al, Ga | 19 | | |
| Balama (MOZ) | V, Al, Mg, Rb, Cr, Ga | 18 | Zn, Fe, Cu, Al, Ca, Ce, Sr, Mn | 18 | | | | | | |
| Skaland (NOR) | Mn, Mg, Fe, V, Ca, Rb, Ga, Sr | 20 | Cr, Mn, Mg, Fe, V, Ca, Ga, Zn, As | 23 | | | | | | |
| Tayginka (RUS) | Ga, Rb, Al, Sr, V | 22 | V, Mg, Mn, Ca, Co, Fe | 14 | | | | | Sr, Mn, Ca | 7 |
| Ragedara (LKA) | Cu, Co, V, Sr, Zn, Ce, Al, Rb, As, Mg | 24 | Ga, Cu, Co, Mn, Ca, V, Cr, Sr, Zn, Al, Fe | 40 | | | | | | |
| Zavallia (UKR) | As, Zn, Fe, Ce, Mn, Rb, Ga, V, Cu | 25 | Zn, Co, Mg, Sr, Mn, Rb, V, Ca | 22 | Zn, Fe, Ce, Sr, Al, Rb, Ga, V, Cu | 20 | | | Sr, Ca | 7 |

### 6.4.1.5. Multivariate Statistical Analysis

Multivariate statistical methods analyze multiple variables simultaneously. In the diagrams in the previous chapters, the limitations of bivariate statistical methods are demonstrated. Reasons favoring the application of multivariate statistical methods include the complexity of the data. The variables are interrelated, and their relationships within the groups (mine/province) are complex. Data visualization in two or three dimensions helps to uncover patterns that may be less apparent in tabular form or uni-/bivariate statistics.

#### 6.4.1.5.1. Linear Discriminant Analysis (LDA)

Two models using LDA were created for the LA-ICP-MS trace element dataset. The data shows significantly more dispersion within each group/deposit, compared to the solution-based-ICP-MS trace element dataset, but also more available data points. The models are based on continents and mines/provinces and allow classification of the data. The input data consist of the trace element data as well as the categories on which the classification is based.

The first LDA (Fig. 57) demonstrates the discrimination of graphite samples based on continents. Through the multivariate analysis of trace element data obtained from LA-ICP-MS, data points from South America and Africa can be differentiated from each other, whereas data points related to Europe and Asia overlap. Confidence ellipses display 95 % confidence for the mean value of each group in the diagram and assume a normal distribution of the data.

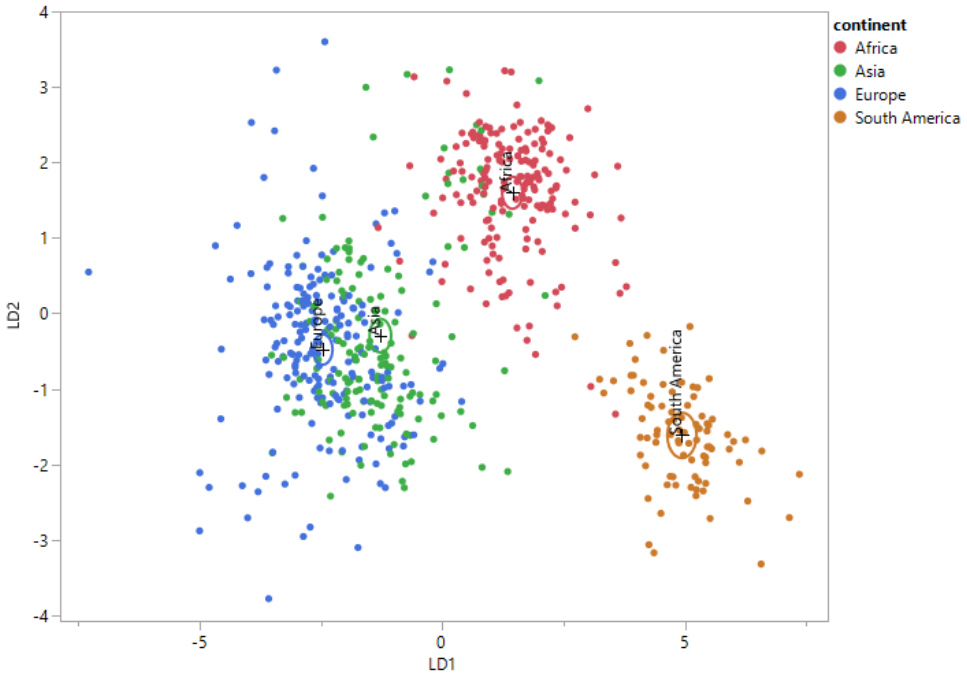


*Figure 57: LDA of LA-ICP-MS trace element data based on continents*

To identify **key elements** for differentiation, the scoring coefficients of the LDA were extracted and are presented in Table 29. The elements **V, Cr, Mn, Ga, Zn, Zr, Ce** contribute most for the classification of individual graphite samples based on continents (based on the scoring coefficients in Tab. 29).

*Table 29: Scoring coefficients from LDA based on continents*

| | Log[Mg] | Log[Al] | Log[Ca] | Log[V] | Log[Cr] | Log[Mn] | Log[Fe] | Log[Co] | Log[Cu] | Log[Zn] | Log[Ga] | Log[As] | Log[Rb] | Log[Sr] | Log[Zr] | Log[Ce] | Log[U] |
|---|---|---|---|---|---|---|---|---|---|---|---|---|---|---|---|---|---|
| LD1 | -0.48 | 0.05 | -0.43 | 0.28 | 0.27 | 0.49 | -0.34 | 0.24 | 0.08 | -0.09 | 0.37 | -0.32 | -0.51 | -0.25 | 0.51 | 0.41 | -0.41 |
| LD2 | -0.47 | -0.17 | -0.14 | 0.37 | 0.22 | -0.39 | -0.09 | -0.06 | -0.08 | 0.58 | -0.10 | -0.01 | 0.35 | -0.12 | -0.34 | 0.01 | 0.35 |
| LD3 | -0.31 | -0.15 | 0.70 | -0.41 | -0.05 | -0.32 | 0.07 | 0.04 | 0.37 | 0.14 | -0.38 | 0.09 | 0.15 | -0.18 | 0.17 | 0.04 | 0.10 |

A LDA based on the classification of LA-ICP-MS trace element data according to individual mines/provinces is displayed in Fig. 58. Minas Gerais can be clearly differentiated from the rest of the dataset, as well as amorphous graphite from Kaisersberg and Hunan Lutang. The rest of the data is scattered and no further discrimination can be done.
Confidence ellipses display 95 % confidence for the mean value of each group in the diagram.

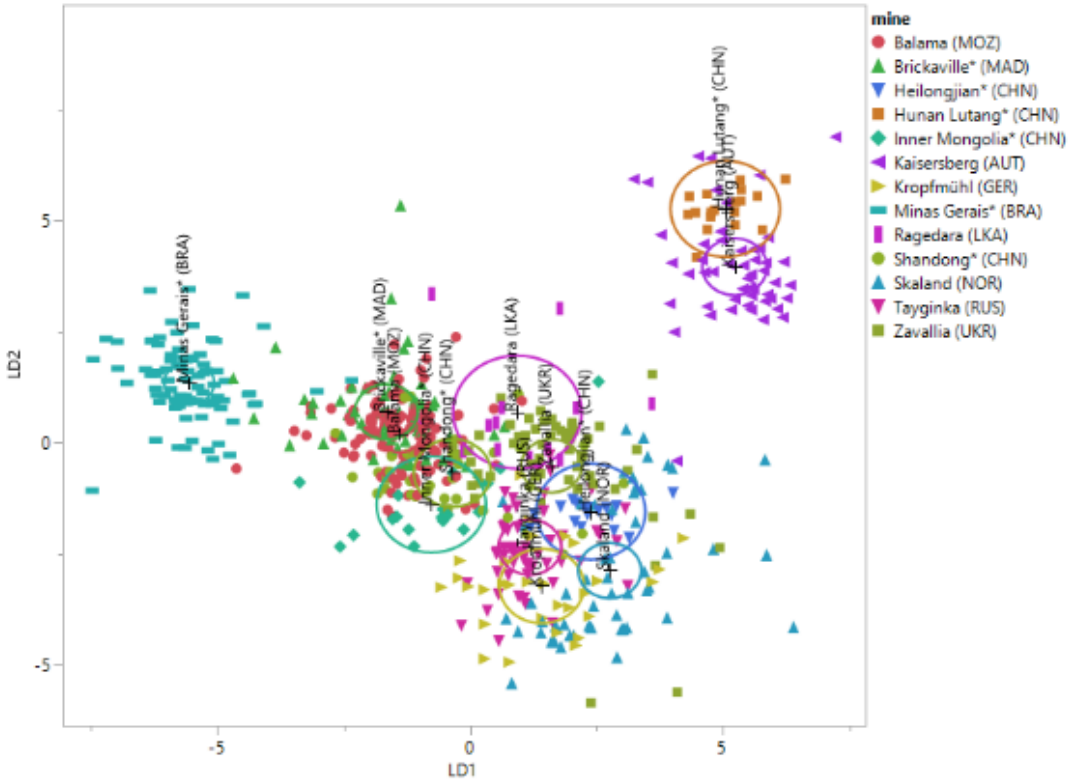


*Figure 58: LDA of LA-ICP-MS trace element data based on mines*

To identify **key elements** for differentiation, the scoring coefficients of this LDA were extracted and displayed in Table 30. The elements **Al, Ca, Mn, Zn, As, Rb, Sr and U** contribute most for the classification of individual graphite samples based on individual mines/provinces (based on the scoring coefficients in Tab. 30).

*Table 30: Scoring coefficients from LDA based on all mines/provinces*

| | Log[Mg] | Log[Al] | Log[Ca] | Log[V] | Log[Cr] | Log[Mn] | Log[Fe] | Log[Co] | Log[Cu] | Log[Zn] | Log[Ga] | Log[As] | Log[Rb] | Log[Sr] | Log[Ce] | Log[U] |
|---|---|---|---|---|---|---|---|---|---|---|---|---|---|---|---|---|
| **LD1** | 0.32 | 0.08 | 0.46 | -0.43 | -0.86 | -0.05 | 0.08 | -0.16 | -0.19 | 0.11 | -0.38 | 0.61 | 0.50 | 0.41 | -0.51 | 0.25 |
| **LD2** | -0.36 | 0.29 | -0.56 | 0.03 | -0.17 | 0.26 | -0.35 | 0.08 | -0.36 | 0.00 | 0.14 | 0.93 | -0.13 | 0.35 | 0.44 | -0.21 |
| **LD3** | -0.32 | -0.38 | 0.12 | 0.16 | 0.28 | -0.33 | -0.21 | -0.19 | -0.19 | 0.86 | 0.17 | -0.19 | -0.15 | 0.53 | -0.42 | 0.25 |
| **LD4** | -0.52 | -0.19 | 0.59 | 0.81 | 0.27 | -0.42 | 0.07 | 0.16 | -0.32 | -0.30 | -0.60 | -0.37 | 0.73 | -0.14 | 0.41 | 0.02 |
| **LD5** | -0.10 | 0.41 | -0.21 | 0.70 | -1.05 | 0.34 | -0.34 | -0.04 | 0.14 | 0.02 | -0.09 | 0.00 | 0.17 | -0.14 | -0.30 | -0.02 |
| **LD6** | -0.38 | 0.16 | 0.11 | -0.38 | 0.24 | 0.77 | -0.42 | -0.13 | 0.06 | -0.27 | 0.10 | -0.54 | 0.04 | 0.83 | -0.03 | 0.00 |
| **LD7** | -0.13 | 0.13 | 0.40 | -0.69 | 0.27 | 0.00 | -0.60 | 0.40 | 0.17 | 0.65 | 0.24 | -0.26 | 0.13 | -0.60 | 0.11 | 0.57 |
| **LD8** | -0.53 | -0.06 | -0.61 | -0.15 | 0.49 | 0.25 | -0.02 | -0.22 | 0.77 | -0.14 | -0.74 | 0.27 | 0.62 | 0.42 | -0.20 | 0.02 |
| **LD9** | 0.43 | -0.07 | -0.90 | -0.39 | 1.93 | -0.07 | -0.13 | -0.15 | -0.11 | 0.09 | 0.40 | -0.26 | 0.15 | -0.11 | 0.12 | 0.29 |
| **LD10** | -0.06 | -0.32 | -0.33 | 0.46 | 0.94 | 0.11 | -0.04 | 0.69 | -0.03 | -0.03 | -0.25 | -0.06 | -0.11 | 0.58 | -0.07 | -0.49 |
| **LD11** | -0.48 | -0.38 | -0.39 | -0.28 | -0.96 | 0.66 | 0.42 | -0.09 | -0.54 | 0.29 | 0.21 | -0.18 | 0.37 | -0.02 | -0.12 | 0.15 |
| **LD12** | 0.72 | -0.22 | -0.75 | 0.19 | -0.75 | 0.00 | -0.16 | 0.05 | 0.10 | -0.32 | -0.16 | 0.12 | -0.48 | 0.35 | 0.06 | 0.62 |

#### 6.4.1.5.2. Principal Component Analysis (PCA)

Based on the elements that have been identified as significant (key elements) in the LDA, a Principal Component Analysis (PCA) was performed, which refers to the same hierarchies (continents and mines/province). PCA is a method of dimension-reduced data projection, where data are summarized into new, simplified variables and expressed as PC1 and PC2.

PC1 (50 %) and PC2 (10.6 %) for the hierarchy of continents account most of the variance in the data. They are presented in a two-dimensional graph with corresponding elements displayed (Figure 59). Data points corresponding to South America (orange) are densely distributed, whereas the datapoints of the other continents are highly dispersed, with a subgroup of data for European samples.

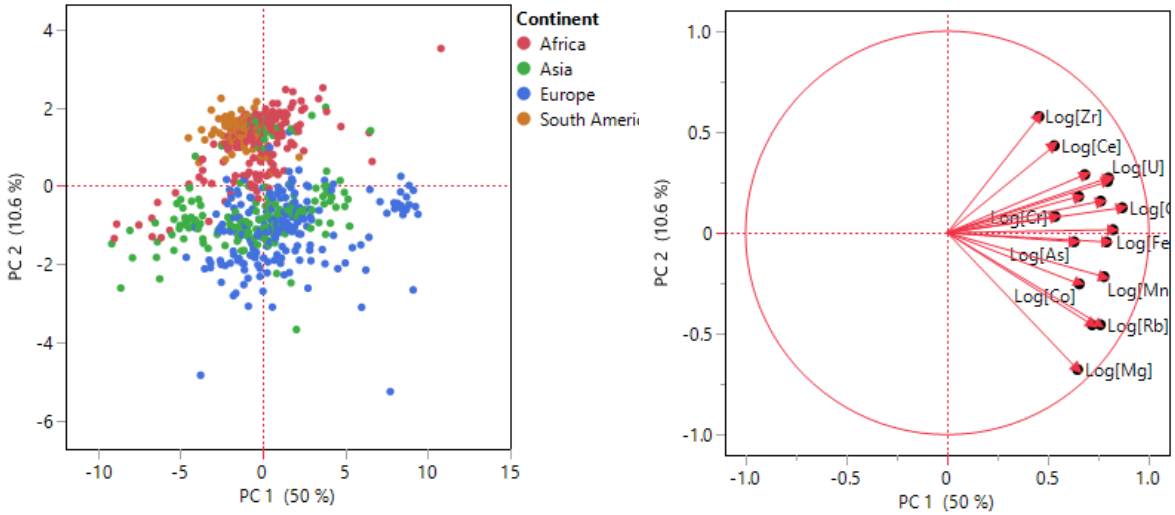


*Figure 59: PCA of LA-ICP-MS trace element data at continent level (left) with the indicated elements (right)*

PC1 (50 %) and PC2 (10 %) for the hierarchy of mines/provinces account for most of the variance in the data and are presented in a two-dimensional graph (Figure 60). The subgroup for European samples can be attributed to Kaisersberg, Inner Mongolia shows a densely distributed dataset, also Brickaville. The remaining data is not distinguishable based on the LA-trace element dataset only.

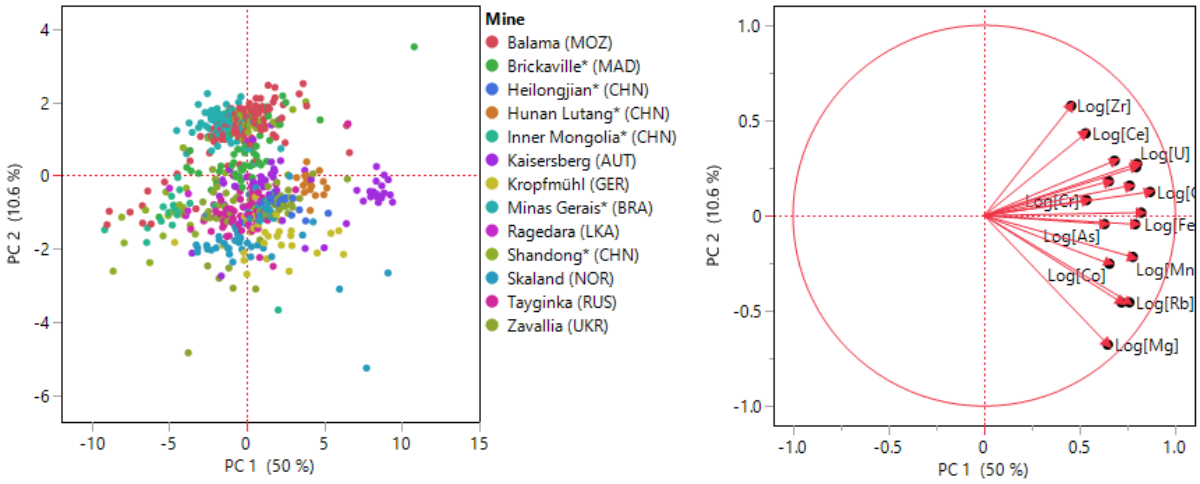


*Figure 60: PCA of LA-ICP-MS trace element data at mine level (left) with the indicated elements (right)*

### 6.4.2. Trace Element Concentrations Assessed by ICP-MS

For each available graphite sample three individual digestions were analyzed by solution-based-ICP-MS analysis. A total of 13 graphite mines/provinces are available for this study, divided into 38 individual samples, which results into 3990 trace element data for this method/parameter. In some cases, distinguishing down to the level of the mine was not possible; therefore, samples marked with * will only be discussed at the province level as the material is likely a mixture from multiple mines from one province. In China, the exact mines are unknown and can partly be artisanal and small-scale mines. Brickaville* (MAD) samples are from the mines Vatomina and Sahamamy Sahasoa. In the province Minas Gerais* (BRA), samples originate from the mines Pedra Azul, Itapecerica and Salto da Divisa. All localities in China are referred to as provinces. For each mine/province, there was a varying number of samples available. The subsequent tables (Tab. 31 to 43) list the number of samples available for each location and show median values of the measurements for each element.

*Table 31: Trace element concentrations Kaisersberg (Austria) with median, mean and standard deviation*

| Kaisersberg (AUT) | Analyte (µg g-1) | | | | | | | | | | | | | | | | | | | | |
|---|---|---|---|---|---|---|---|---|---|---|---|---|---|---|---|---|---|---|---|---|---|
| sample ID | Mg | Al | V | Cr | Mn | Fe | Ni | Cu | Zn | Ga | As | Se | Rb | Sr | Mo | Ag | Cd | Ba | Tl | Pb | U |
| 1A | 2235 | 28809 | 24.70 | 21.59 | 196.45 | 11993 | 7.80 | 16.13 | 31.48 | 8.45 | 10.51 | 1.92 | 22.37 | 47.87 | 3.40 | 0.13 | 0.07 | 77.34 | 0.18 | 29.46 | 3.22 |
| 1A | 2335 | 29475 | 25.21 | 22.31 | 207.05 | 12583 | 8.21 | 16.93 | 33.93 | 8.70 | 10.77 | 2.15 | 22.93 | 48.55 | 3.89 | 0.15 | 0.07 | 77.69 | 0.18 | 29.39 | 3.38 |
| 1A | 2257 | 29517 | 25.52 | 21.70 | 201.08 | 12029 | 8.27 | 16.32 | 33.18 | 8.61 | 10.97 | 1.88 | 23.23 | 48.72 | 3.44 | 0.14 | 0.08 | 80.12 | 0.18 | 29.63 | 3.28 |
| 2A | 1892 | 16091 | 18.95 | 20.82 | 128.57 | 10471 | 21.13 | 59.03 | 40.87 | 4.88 | 5.82 | 2.07 | 13.67 | 19.41 | 1.96 | 0.21 | 0.14 | 56.40 | 0.10 | 25.62 | 2.00 |
| 2A | 1995 | 14502 | 16.65 | 18.65 | 122.82 | 9999 | 21.19 | 45.30 | 47.16 | 4.34 | 7.41 | 1.82 | 11.74 | 17.28 | 1.98 | 0.16 | 0.17 | 51.93 | 0.10 | 26.97 | 1.88 |
| 2A | 1744 | 14088 | 17.19 | 19.60 | 113.74 | 8592 | 17.63 | 101.10 | 63.01 | 4.34 | 6.03 | 1.88 | 12.35 | 16.82 | 1.88 | 0.24 | 0.27 | 50.76 | 0.09 | 26.62 | 1.72 |
| median | 2115 | 22450 | 21.82 | 21.21 | 162.51 | 11232 | 12.95 | 31.12 | 37.40 | 6.66 | 8.96 | 1.90 | 18.02 | 33.64 | 2.69 | 0.15 | 0.11 | 66.87 | 0.14 | 28.18 | 2.61 |
| mean | 2076 | 22080 | 21.37 | 20.78 | 161.62 | 10945 | 14.04 | 42.47 | 41.60 | 6.55 | 8.59 | 1.95 | 17.72 | 33.11 | 2.76 | 0.17 | 0.13 | 65.71 | 0.14 | 27.95 | 2.58 |
| SD | 214 | 7216 | 3.84 | 1.28 | 40.26 | 1391 | 6.06 | 30.96 | 10.97 | 2.04 | 2.23 | 0.12 | 5.17 | 15.29 | 0.83 | 0.04 | 0.07 | 12.82 | 0.04 | 1.60 | 0.72 |

*Table 32: Trace element concentrations Minas Gerais (BRA) with median, mean and standard deviation*

| Minas Gerais (BRA) | Analyte (µg g-1) | | | | | | | | | | | | | | | | | | | | |
|---|---|---|---|---|---|---|---|---|---|---|---|---|---|---|---|---|---|---|---|---|---|
| sample ID | Mg | Al | V | Cr | Mn | Fe | Ni | Cu | Zn | Ga | As | Se | Rb | Sr | Mo | Ag | Cd | Ba | Tl | Pb | U |
| 21M | 22.71 | 3435 | 10.91 | 9.63 | 23.07 | 1797 | 3.06 | 12.53 | 3.75 | 1.08 | 0.05 | 1.76 | 0.15 | 1.41 | 3.61 | 0.12 | 0.02 | 5.54 | 0.02 | 0.30 | 0.13 |
| 21M | 19.43 | 3018 | 9.92 | 8.83 | 20.98 | 1669 | 2.89 | 11.72 | 3.48 | 0.96 | 0.06 | 1.36 | 0.14 | 1.20 | 2.51 | 0.11 | 0.02 | 5.07 | 0.01 | 0.26 | 0.12 |
| 21M | 18.58 | 2865 | 9.48 | 8.46 | 21.16 | 1678 | 2.65 | 11.43 | 3.53 | 0.92 | 0.04 | 1.57 | 0.13 | 1.16 | 3.02 | 0.11 | 0.02 | 5.08 | 0.01 | 0.26 | 0.13 |
| 21N | 24.10 | 2534 | 8.84 | 13.23 | 19.20 | 1409 | 2.64 | 13.86 | 3.24 | 0.84 | 0.04 | 1.28 | 0.10 | 1.19 | 2.28 | 0.10 | 0.02 | 4.60 | 0.02 | 0.20 | 0.12 |
| 21N | 24.45 | 2773 | 9.18 | 13.59 | 20.13 | 1420 | 2.88 | 13.93 | 4.54 | 0.89 | 0.03 | 1.01 | 0.10 | 1.12 | 2.17 | 0.09 | 0.02 | 4.86 | 0.02 | 0.21 | 0.13 |
| 21N | 22.85 | 2408 | 8.58 | 12.98 | 18.79 | 1415 | 2.53 | 13.75 | 4.01 | 0.80 | 0.04 | 1.06 | 0.10 | 1.10 | 2.61 | 0.09 | 0.02 | 4.67 | 0.02 | 0.19 | 0.11 |
| 22C | 21.64 | 3254 | 6.69 | 6.07 | 32.58 | 1311 | 2.43 | 8.96 | 4.01 | 0.95 | 0.06 | 0.30 | 0.11 | 1.29 | 1.80 | 0.08 | 0.01 | 7.31 | 0.03 | 0.31 | 0.11 |
| 22C | 21.33 | 3134 | 6.57 | 5.97 | 32.02 | 1286 | 2.47 | 9.02 | 4.39 | 0.92 | 0.04 | 0.41 | 0.10 | 1.35 | 1.51 | 0.08 | 0.01 | 7.13 | 0.03 | 0.30 | 0.10 |
| 3B | 17.56 | 4839 | 33.89 | 17.78 | 135.85 | 2897 | 3.22 | 13.66 | 2.80 | 1.27 | 0.19 | 0.65 | 0.10 | 1.61 | 6.01 | 0.08 | 0.03 | 34.71 | 0.08 | 0.60 | 0.55 |
| 3B | 15.01 | 3721 | 33.93 | 17.10 | 144.93 | 3016 | 3.29 | 13.85 | 3.93 | 1.04 | 0.19 | 0.57 | 0.09 | 1.50 | 5.62 | 0.08 | 0.03 | 43.86 | 0.09 | 0.64 | 0.55 |
| 3B | 16.12 | 4234 | 38.28 | 17.41 | 124.79 | 2999 | 3.45 | 13.70 | 3.77 | 1.15 | 0.19 | 0.60 | 0.10 | 1.76 | 5.95 | 0.08 | 0.03 | 33.48 | 0.08 | 0.59 | 0.58 |
| 21C | 25.78 | 2560 | 8.88 | 13.45 | 21.64 | 1482 | 2.68 | 14.11 | 2.90 | 0.84 | 0.03 | 1.08 | 0.10 | 1.83 | 2.55 | 0.09 | 0.02 | 4.96 | 0.02 | 0.19 | 0.12 |
| 21C | 25.37 | 2682 | 9.34 | 13.94 | 20.89 | 1480 | 2.71 | 15.03 | 3.14 | 0.87 | 0.07 | 1.30 | 0.11 | 1.88 | 2.59 | 0.09 | 0.02 | 4.91 | 0.02 | 0.18 | 0.12 |
| 21C | 25.13 | 2493 | 8.92 | 13.80 | 20.61 | 1464 | 2.61 | 14.63 | 2.92 | 0.82 | 0.05 | 1.16 | 0.10 | 2.19 | 2.25 | 0.10 | 0.02 | 4.74 | 0.02 | 0.33 | 0.13 |
| median | 22.17 | 2941 | 9.26 | 13.34 | 21.40 | 1481 | 2.70 | 13.72 | 3.64 | 0.92 | 0.05 | 1.07 | 0.10 | 1.38 | 2.57 | 0.09 | 0.02 | 5.08 | 0.02 | 0.28 | 0.13 |
| mean | 21.43 | 3139 | 14.53 | 12.30 | 46.90 | 1809 | 2.82 | 12.87 | 3.60 | 0.95 | 0.08 | 1.01 | 0.11 | 1.47 | 3.18 | 0.09 | 0.02 | 12.21 | 0.03 | 0.33 | 0.21 |
| SD | 3.43 | 687 | 10.98 | 3.79 | 46.44 | 622 | 0.31 | 1.85 | 0.53 | 0.13 | 0.06 | 0.43 | 0.02 | 0.32 | 1.48 | 0.01 | 0.01 | 13.33 | 0.03 | 0.16 | 0.18 |

*Table 33: Trace element concentrations Hunan Lutang (CHN) with median, mean and standard deviation*

| Hunan Lutang (CHN) | Analyte (µg g-1) | | | | | | | | | | | | | | | | | | | | |
|---|---|---|---|---|---|---|---|---|---|---|---|---|---|---|---|---|---|---|---|---|---|
| sample ID | Mg | Al | V | Cr | Mn | Fe | Ni | Cu | Zn | Ga | As | Se | Rb | Sr | Mo | Ag | Cd | Ba | Tl | Pb | U |
| 4A | 524 | 7891 | 20.42 | 5.55 | 92.25 | 4186 | 13.02 | 24.30 | 33.14 | 3.06 | 64.29 | 1.82 | 18.59 | 24.78 | 3.46 | 0.25 | 0.29 | 33.89 | 0.28 | 37.64 | 0.64 |
| 4A | 523 | 7498 | 20.73 | 5.26 | 94.62 | 4213 | 13.77 | 25.54 | 31.22 | 2.94 | 65.06 | 1.77 | 17.80 | 25.01 | 3.29 | 0.26 | 0.29 | 33.35 | 0.28 | 40.80 | 0.68 |
| 4A | 533 | 7885 | 21.54 | 5.45 | 96.02 | 4281 | 13.52 | 26.07 | 31.79 | 3.06 | 65.76 | 1.65 | 18.56 | 24.46 | 3.17 | 0.29 | 0.29 | 34.26 | 0.29 | 38.85 | 0.68 |
| median | 524 | 7885 | 20.73 | 5.45 | 94.62 | 4213 | 13.52 | 25.54 | 31.79 | 3.06 | 65.06 | 1.77 | 18.56 | 24.78 | 3.29 | 0.26 | 0.29 | 33.89 | 0.28 | 38.85 | 0.68 |
| mean | 526.79 | 7758 | 20.89 | 5.42 | 94.30 | 4227 | 13.44 | 25.30 | 32.05 | 3.02 | 65.04 | 1.75 | 18.32 | 24.75 | 3.31 | 0.27 | 0.29 | 33.83 | 0.28 | 39.09 | 0.66 |
| SD | 4.71 | 184 | 0.47 | 0.12 | 1.56 | 40 | 0.31 | 0.74 | 0.80 | 0.06 | 0.60 | 0.07 | 0.37 | 0.23 | 0.12 | 0.01 | 0.001 | 0.37 | 0.002 | 1.30 | 0.02 |

*Table 34: Trace element concentrations Inner Mongolia (CHN) with median, mean and standard deviation*

| Inner Mongolia (CHN) | Analyte (µg g-1) | | | | | | | | | | | | | | | | | | | | |
|---|---|---|---|---|---|---|---|---|---|---|---|---|---|---|---|---|---|---|---|---|---|
| sample ID | Mg | Al | V | Cr | Mn | Fe | Ni | Cu | Zn | Ga | As | Se | Rb | Sr | Mo | Ag | Cd | Ba | Tl | Pb | U |
| 6B | 60.22 | 53.91 | 0.62 | 21.11 | 4.19 | 891 | 6.54 | 1.17 | 1.57 | 0.08 | 0.17 | 0.05 | 0.18 | 0.97 | 1.76 | 0.08 | 0.01 | 3.41 | 0.01 | 0.33 | 0.06 |
| 6B | 56.94 | 49.93 | 0.50 | 16.31 | 4.23 | 829 | 5.39 | 0.98 | 0.84 | 0.08 | 0.10 | 0.01 | 0.16 | 0.91 | 1.08 | 0.07 | 0.01 | 0.98 | 0.02 | 0.31 | 0.06 |
| 6B | 57.81 | 52.38 | 0.54 | 16.91 | 4.20 | 1256 | 5.26 | 0.98 | 13.17 | 0.09 | 0.12 | 0.00 | 0.16 | 0.97 | 1.13 | 0.08 | 0.01 | 1.01 | 0.02 | 0.25 | 0.06 |
| median | 57.81 | 52.38 | 0.54 | 16.91 | 4.20 | 891 | 5.39 | 0.98 | 1.57 | 0.08 | 0.12 | 0.01 | 0.16 | 0.97 | 1.13 | 0.08 | 0.01 | 1.01 | 0.02 | 0.31 | 0.06 |
| mean | 58.33 | 52.07 | 0.55 | 18.11 | 4.21 | 992 | 5.73 | 1.04 | 5.20 | 0.08 | 0.13 | 0.02 | 0.17 | 0.95 | 1.32 | 0.08 | 0.01 | 1.80 | 0.02 | 0.29 | 0.06 |
| SD | 1.39 | 1.64 | 0.05 | 2.14 | 0.02 | 189 | 0.58 | 0.09 | 5.65 | 0.01 | 0.03 | 0.02 | 0.01 | 0.03 | 0.31 | 0.00 | 0.00 | 1.14 | 0.004 | 0.03 | 0.001 |

*Table 35: Trace element concentrations Heilongjian (CHN) with median, mean and standard deviation*

| Heilongjian (CHN) | Analyte (µg g-1) | | | | | | | | | | | | | | | | | | | | |
|---|---|---|---|---|---|---|---|---|---|---|---|---|---|---|---|---|---|---|---|---|---|
| sample ID | Mg | Al | V | Cr | Mn | Fe | Ni | Cu | Zn | Ga | As | Se | Rb | Sr | Mo | Ag | Cd | Ba | Tl | Pb | U |
| 7B | 650.14 | 3686.97 | 69.78 | 9.07 | 38.08 | 3728.04 | 16.78 | 19.33 | 51.96 | 1.31 | 0.48 | 4.48 | 4.11 | 10.79 | 28.65 | 0.23 | 0.73 | 18.61 | 0.12 | 7.18 | 2.40 |
| 7B | 642.97 | 3745.60 | 69.12 | 8.97 | 37.50 | 3694.67 | 16.67 | 19.04 | 51.67 | 1.34 | 0.49 | 4.86 | 4.27 | 10.80 | 28.07 | 0.23 | 0.74 | 18.47 | 0.12 | 6.71 | 2.45 |
| 7B | 627.25 | 3595.49 | 68.70 | 8.95 | 36.68 | 3597.35 | 16.58 | 18.16 | 50.25 | 1.29 | 0.51 | 4.59 | 4.02 | 10.30 | 26.45 | 0.22 | 0.70 | 18.50 | 0.12 | 6.58 | 2.65 |
| median | 642.97 | 3686.97 | 69.12 | 8.97 | 37.50 | 3694.67 | 16.67 | 19.04 | 51.67 | 1.31 | 0.49 | 4.59 | 4.11 | 10.79 | 28.07 | 0.23 | 0.73 | 18.50 | 0.12 | 6.71 | 2.45 |
| mean | 640.12 | 3676.02 | 69.20 | 9.00 | 37.42 | 3673.36 | 16.68 | 18.84 | 51.29 | 1.32 | 0.49 | 4.64 | 4.13 | 10.63 | 27.73 | 0.23 | 0.72 | 18.53 | 0.12 | 6.82 | 2 |
| SD | 9.56 | 61.77 | 0.44 | 0.05 | 0.57 | 55.44 | 0.08 | 0.50 | 0.74 | 0.02 | 0.01 | 0.16 | 0.10 | 0.23 | 0.93 | 0.01 | 0.02 | 0.06 | 0.00 | 0.26 | 0.11 |

*Table 36: Trace element concentrations Shandong (CHN) with median, mean and standard deviation*

| Shandong (CHN) | Analyte (µg g-1) | | | | | | | | | | | | | | | | | | | | |
|---|---|---|---|---|---|---|---|---|---|---|---|---|---|---|---|---|---|---|---|---|---|
| sample ID | Mg | Al | V | Cr | Mn | Fe | Ni | Cu | Zn | Ga | As | Se | Rb | Sr | Mo | Ag | Cd | Ba | Tl | Pb | U |
| 22A | 208 | 564.1 | 11.60 | 0.93 | 4.73 | 387 | 1.43 | 2.27 | 1.55 | 0.17 | 0.08 | 0.17 | 1.07 | 2.66 | 6.61 | 0.12 | 0.01 | 3.16 | 0.05 | 0.64 | 0.11 |
| 22A | 193 | 609.4 | 7.06 | 0.99 | 5.47 | 503 | 1.64 | 2.17 | 1.51 | 0.17 | 0.07 | 0.20 | 1.15 | 2.46 | 5.30 | 0.13 | 0.01 | 4.31 | 0.05 | 0.71 | 0.10 |
| 21A | 16.52 | 3298.9 | 70.20 | 27.80 | 5.34 | 5827 | 11.40 | 24.87 | 20.39 | 0.77 | 0.35 | 4.39 | 0.24 | 5.94 | 29.61 | 0.33 | 0.57 | 18.44 | 0.02 | 0.49 | 1.54 |
| 21A | 15.79 | 3464.5 | 70.54 | 28.26 | 4.27 | 6109 | 11.07 | 23.52 | 20.52 | 0.79 | 0.37 | 4.57 | 0.23 | 6.27 | 30.47 | 0.34 | 0.83 | 19.13 | 0.02 | 0.47 | 0.86 |
| 21A | 17.79 | 3377.7 | 70.41 | 28.11 | 4.28 | 5969 | 11.25 | 23.67 | 21.23 | 0.78 | 0.38 | 4.64 | 0.24 | 6.23 | 28.54 | 0.33 | 0.52 | 18.55 | 0.01 | 0.45 | 0.80 |
| median | 17.79 | 3299 | 70.20 | 27.80 | 4.73 | 5827 | 11.07 | 23.52 | 20.39 | 0.77 | 0.35 | 4.39 | 0.24 | 5.94 | 28.54 | 0.33 | 0.52 | 18.44 | 0.02 | 0.49 | 0.80 |
| mean | 90.23 | 2263 | 45.96 | 17.22 | 4.82 | 3759 | 7.36 | 15.30 | 13.04 | 0.54 | 0.25 | 2.79 | 0.59 | 4.71 | 20.11 | 0.25 | 0.39 | 12.72 | 0.03 | 0.55 | 0.68 |
| SD | 90.18 | 1370 | 29.95 | 13.27 | 0.51 | 2708 | 4.76 | 10.69 | 9.40 | 0.30 | 0.15 | 2.13 | 0.43 | 1.76 | 11.58 | 0.10 | 0.33 | 7.35 | 0.02 | 0.11 | 0.54 |

*Table 37: Trace element concentrations Kropfmühl (GER) with median, mean and standard deviation*

| Kropfmühl (GER) | Analyte (µg g-1) | | | | | | | | | | | | | | | | | | | | |
|---|---|---|---|---|---|---|---|---|---|---|---|---|---|---|---|---|---|---|---|---|---|
| sample ID | Mg | Al | V | Cr | Mn | Fe | Ni | Cu | Zn | Ga | As | Se | Rb | Sr | Mo | Ag | Cd | Ba | Tl | Pb | U |
| 13B | 4145 | 4331 | 82.05 | 23.92 | 186.48 | 10738 | 16.53 | 293.78 | 23.07 | 2.12 | 0.78 | 1.49 | 21.39 | 4.22 | 29.97 | 0.13 | 0.21 | 8.83 | 0.20 | 1.58 | 1.62 |
| 13B | 4271 | 4413 | 84.18 | 24.86 | 190.89 | 10841 | 15.90 | 305.17 | 16.81 | 2.12 | 0.50 | 1.14 | 22.20 | 3.95 | 26.11 | 0.13 | 0.19 | 8.93 | 0.21 | 1.41 | 1.41 |
| 13B | 4217 | 4331 | 85.53 | 25.06 | 191.27 | 10823 | 16.56 | 307.16 | 19.05 | 2.16 | 1.28 | 1.24 | 21.64 | 3.26 | 39.28 | 0.13 | 0.16 | 8.64 | 0.20 | 1.57 | 1.70 |
| median | 4217 | 4331 | 84.18 | 24.86 | 190.89 | 10823 | 16.53 | 305.17 | 19.05 | 2.12 | 0.78 | 1.24 | 21.64 | 3.95 | 29.97 | 0.13 | 0.19 | 8.83 | 0.20 | 1.57 | 1.62 |
| mean | 4211 | 4358 | 83.92 | 24.61 | 189.55 | 10801 | 16.33 | 302.04 | 19.64 | 2.13 | 0.85 | 1.29 | 21.74 | 3.81 | 31.79 | 0.13 | 0.19 | 8.80 | 0.21 | 1.52 | 1.58 |
| SD | 51.74 | 38.93 | 1.43 | 0.50 | 2.17 | 44.84 | 0.30 | 5.90 | 2.59 | 0.02 | 0.32 | 0.15 | 0.34 | 0.40 | 5.53 | 0.00 | 0.02 | 0.12 | 0.00 | 0.07 | 0.12 |

*Table 38: Trace element concentrations Brickaville (MAD) with median, mean and standard deviation*

| Brickaville (MAD) | Analyte (µg g-1) | | | | | | | | | | | | | | | | | | | | |
|---|---|---|---|---|---|---|---|---|---|---|---|---|---|---|---|---|---|---|---|---|---|
| sample ID | Mg | Al | V | Cr | Mn | Fe | Ni | Cu | Zn | Ga | As | Se | Rb | Sr | Mo | Ag | Cd | Ba | Tl | Pb | U |
| 11B | 34.65 | 21663 | 54.31 | 57.51 | 5.61 | 24561 | 7.76 | 45.87 | 4.73 | 11.42 | 15.00 | 6.71 | 1.57 | 4.18 | 15.57 | 0.14 | 0.03 | 15.19 | 0.02 | 12.81 | 1.53 |
| 11B | 35.51 | 21028 | 52.01 | 60.13 | 5.69 | 23321 | 7.70 | 48.06 | 6.43 | 11.53 | 15.49 | 4.78 | 1.59 | 4.04 | 15.41 | 0.12 | 0.03 | 15.19 | 0.02 | 12.67 | 1.43 |
| 11B | 37.44 | 21774 | 54.39 | 58.44 | 5.45 | 23398 | 8.49 | 52.13 | 6.10 | 10.95 | 15.38 | 4.85 | 1.68 | 5.49 | 15.32 | 0.11 | 0.03 | 14.91 | 0.02 | 13.32 | 1.53 |
| 22D | 128 | 4813 | 19.30 | 3.63 | 63.15 | 4883 | 9.24 | 21.11 | 28.76 | 1.59 | 0.79 | 0.43 | 3.42 | 1.54 | 4.39 | 0.09 | 0.46 | 9.07 | 0.14 | 6.28 | 0.50 |
| 22D | 119 | 4475 | 18.48 | 3.39 | 59.92 | 4638 | 8.58 | 21.80 | 28.51 | 1.48 | 0.82 | 0.25 | 3.18 | 1.46 | 4.87 | 0.09 | 0.44 | 8.30 | 0.13 | 5.88 | 0.49 |
| 21D | 160 | 3857 | 129.29 | 5.17 | 259.95 | 3989 | 60.20 | 143.38 | 29.61 | 1.55 | 2.48 | 0.66 | 2.65 | 0.71 | 1.91 | 0.02 | 0.11 | 19.09 | 0.17 | 2.42 | 0.90 |
| 21D | 140 | 3730 | 135.36 | 5.26 | 253.62 | 4130 | 55.56 | 34.88 | 27.89 | 1.52 | 2.64 | 0.50 | 2.57 | 0.72 | 1.78 | 0.02 | 0.10 | 14.02 | 0.18 | 2.46 | 0.89 |
| 21D | 174 | 3799 | 135.04 | 5.03 | 281.87 | 4277 | 64.68 | 39.24 | 31.16 | 1.55 | 3.58 | 0.75 | 3.34 | 0.99 | 2.03 | 0.02 | 0.13 | 12.25 | 0.20 | 2.66 | 0.94 |
| median | 124 | 4644 | 54.35 | 5.21 | 61.54 | 4761 | 8.91 | 42.55 | 28.20 | 1.57 | 3.11 | 0.70 | 2.61 | 1.50 | 4.63 | 0.09 | 0.11 | 14.46 | 0.13 | 6.08 | 0.92 |
| mean | 104 | 10642 | 74.77 | 24.82 | 116.91 | 11650 | 27.78 | 50.81 | 20.40 | 5.20 | 7.02 | 2.37 | 2.50 | 2.39 | 7.66 | 0.08 | 0.17 | 13.50 | 0.11 | 7.31 | 1.03 |
| SD | 54.85 | 8410 | 47.27 | 26.25 | 117.09 | 9391 | 25.18 | 36.60 | 11.39 | 4.73 | 6.46 | 2.45 | 0.74 | 1.76 | 6.11 | 0.05 | 0.17 | 3.31 | 0.07 | 4.57 | 0.40 |

*Table 39: Trace element concentrations Balama (MOZ) with median, mean and standard deviation*

| Balama (MOZ) | Analyte (µg g-1) | | | | | | | | | | | | | | | | | | | | |
|---|---|---|---|---|---|---|---|---|---|---|---|---|---|---|---|---|---|---|---|---|---|
| sample ID | Mg | Al | V | Cr | Mn | Fe | Ni | Cu | Zn | Ga | As | Se | Rb | Sr | Mo | Ag | Cd | Ba | Tl | Pb | U |
| 21K | 17.56 | 4371 | 102.10 | 30.91 | 13.75 | 3269 | 13.96 | 19.83 | 29.28 | 1.90 | 0.38 | 5.59 | 0.44 | 12.14 | 24.11 | 0.34 | 0.76 | 39.80 | 0.03 | 1.14 | 1.25 |
| 21K | 16.75 | 4148 | 99.95 | 30.45 | 12.43 | 3148 | 13.96 | 19.32 | 30.15 | 1.86 | 0.36 | 5.42 | 0.43 | 11.78 | 22.24 | 0.33 | 0.70 | 39.09 | 0.02 | 1.10 | 1.28 |
| 21K | 15.07 | 4122 | 101.20 | 30.97 | 12.23 | 3145 | 14.27 | 19.49 | 29.52 | 1.85 | 0.37 | 5.51 | 0.42 | 11.69 | 22.26 | 0.34 | 0.66 | 38.28 | 0.02 | 1.07 | 1.19 |
| 21L | 18.77 | 4806 | 74.66 | 18.46 | 4.39 | 2319 | 14.87 | 20.47 | 29.44 | 1.32 | 0.13 | 6.11 | 0.25 | 6.60 | 48.41 | 0.49 | 1.13 | 21.18 | 0.03 | 0.67 | 1.00 |
| 21L | 17.55 | 4714 | 73.52 | 18.26 | 4.51 | 2354 | 14.78 | 20.49 | 27.85 | 1.31 | 0.16 | 6.05 | 0.23 | 6.91 | 44.04 | 0.46 | 1.16 | 21.99 | 0.03 | 0.69 | 1.01 |
| 21L | 18.68 | 4802 | 75.45 | 19.03 | 5.04 | 2407 | 14.68 | 21.27 | 30.22 | 1.34 | 0.13 | 6.12 | 0.24 | 6.91 | 50.24 | 0.51 | 1.14 | 22.18 | 0.03 | 0.76 | 1.07 |
| 1B | 31.85 | 363 | 38.82 | 8.92 | 11.84 | 995 | 9.45 | 13.32 | 30.21 | 0.35 | 0.39 | 1.43 | 0.58 | 3.50 | 10.95 | 0.51 | 0.33 | 11.29 | 0.05 | 2.39 | 2.50 |
| 1B | 30.00 | 339 | 37.95 | 8.78 | 11.65 | 958 | 9.21 | 12.35 | 30.40 | 0.36 | 0.46 | 1.39 | 0.53 | 3.47 | 10.28 | 0.51 | 0.33 | 10.33 | 0.05 | 2.54 | 2.37 |
| 1B | 30.60 | 345 | 36.81 | 8.61 | 11.88 | 965 | 8.99 | 12.77 | 31.03 | 0.34 | 0.33 | 1.48 | 0.52 | 3.79 | 10.17 | 0.48 | 0.38 | 10.69 | 0.05 | 2.48 | 2.25 |
| 21B | 15.13 | 1980 | 53.26 | 16.45 | 29.83 | 4339 | 10.26 | 17.22 | 27.98 | 0.59 | 0.40 | 2.21 | 0.37 | 4.19 | 14.71 | 0.17 | 0.25 | 17.62 | 0.04 | 0.60 | 1.13 |
| 21B | 18.72 | 2030 | 54.74 | 16.91 | 31.81 | 4351 | 11.36 | 20.84 | 30.15 | 0.61 | 0.46 | 2.04 | 0.39 | 6.35 | 15.15 | 0.19 | 0.20 | 16.71 | 0.05 | 0.62 | 1.12 |
| 21B | 18.46 | 2010 | 58.82 | 17.36 | 29.00 | 4468 | 11.28 | 18.00 | 29.78 | 0.63 | 0.50 | 1.82 | 0.39 | 6.30 | 14.72 | 0.15 | 0.26 | 16.12 | 0.05 | 0.61 | 1.15 |
| 21J | 17.64 | 4169 | 79.96 | 37.06 | 10.61 | 2643 | 14.80 | 18.78 | 26.73 | 1.01 | 0.25 | 4.23 | 0.29 | 6.53 | 34.09 | 0.33 | 0.57 | 22.08 | 0.03 | 0.55 | 1.08 |
| 21J | 16.00 | 3982 | 77.95 | 36.28 | 10.57 | 2564 | 14.48 | 17.82 | 28.55 | 0.96 | 0.31 | 4.38 | 0.27 | 6.23 | 33.72 | 0.33 | 0.62 | 20.71 | 0.03 | 0.49 | 0.98 |
| 21J | 15.73 | 4136 | 80.32 | 37.13 | 10.45 | 2636 | 14.76 | 18.24 | 26.59 | 1.00 | 0.27 | 4.73 | 0.28 | 6.19 | 32.95 | 0.31 | 0.54 | 20.96 | 0.03 | 0.49 | 1.14 |
| 22B | 15.59 | 4052 | 102.71 | 28.76 | 17.72 | 2977 | 15.17 | 20.10 | 29.52 | 1.33 | 0.33 | 4.48 | 0.38 | 5.49 | 25.92 | 0.41 | 1.51 | 20.29 | 0.03 | 0.88 | 1.24 |
| 22B | 13.66 | 3794 | 100.02 | 26.84 | 16.31 | 2914 | 15.34 | 19.56 | 28.66 | 1.26 | 0.31 | 4.47 | 0.34 | 5.53 | 24.51 | 0.38 | 0.52 | 22.99 | 0.03 | 0.78 | 1.19 |
| median | 17.56 | 4052 | 75.45 | 19.03 | 11.88 | 2643 | 14.27 | 19.32 | 29.52 | 1.01 | 0.33 | 4.47 | 0.38 | 6.30 | 24.11 | 0.34 | 0.57 | 20.96 | 0.03 | 0.76 | 1.15 |
| mean | 19.28 | 3186 | 73.43 | 23.01 | 14.35 | 2732 | 13.04 | 18.23 | 29.18 | 1.06 | 0.33 | 3.97 | 0.37 | 6.68 | 25.79 | 0.37 | 0.65 | 21.90 | 0.03 | 1.05 | 1.35 |
| SD | 5.54 | 1585 | 22.68 | 9.65 | 8.15 | 1049 | 2.27 | 2.73 | 1.24 | 0.51 | 0.11 | 1.76 | 0.10 | 2.65 | 12.65 | 0.11 | 0.37 | 8.88 | 0.01 | 0.69 | 0.48 |

*Table 40: Trace element concentrations Skaland (NOR) with median, mean and standard deviation*

| Skaland (NOR) | Analyte (µg g-1) | | | | | | | | | | | | | | | | | | | | |
|---|---|---|---|---|---|---|---|---|---|---|---|---|---|---|---|---|---|---|---|---|---|
| sample ID | Mg | Al | V | Cr | Mn | Fe | Ni | Cu | Zn | Ga | As | Se | Rb | Sr | Mo | Ag | Cd | Ba | Tl | Pb | U |
| 2B | 816 | 2084 | 37.72 | 7.71 | 46.95 | 3488 | 19.97 | 12.68 | 15.89 | 0.75 | 0.94 | 3.11 | 5.71 | 8.96 | 52.41 | 0.48 | 0.19 | 10.42 | 0.08 | 19.49 | 1.89 |
| 2B | 774 | 1871 | 35.60 | 7.07 | 44.51 | 3396 | 19.19 | 12.23 | 14.69 | 0.71 | 0.89 | 3.10 | 4.88 | 8.56 | 48.84 | 0.47 | 0.18 | 8.03 | 0.07 | 19.39 | 1.75 |
| 2B | 776 | 1883 | 35.44 | 7.06 | 43.07 | 3407 | 18.70 | 12.18 | 14.01 | 0.72 | 0.91 | 3.31 | 5.02 | 8.60 | 51.25 | 0.47 | 0.18 | 7.65 | 0.07 | 19.05 | 1.97 |
| 15B | 560 | 1059 | 7.25 | 5.98 | 24.18 | 1857 | 5.70 | 23.50 | 5.01 | 0.56 | 0.11 | 0.80 | 3.68 | 1.95 | 4.63 | 0.08 | 0.01 | 6.08 | 0.02 | 0.51 | 0.21 |
| 15B | 514 | 962 | 7.01 | 5.56 | 22.78 | 2062 | 6.58 | 19.86 | 5.42 | 0.53 | 0.04 | 0.95 | 3.38 | 1.81 | 1.27 | 0.07 | 0.01 | 5.27 | 0.02 | 0.51 | 0.22 |
| 15B | 614 | 1089 | 7.89 | 6.35 | 25.95 | 1927 | 5.56 | 22.20 | 5.12 | 0.59 | 0.04 | 0.73 | 4.16 | 3.85 | 10.06 | 0.06 | 0.02 | 7.26 | 0.02 | 0.49 | 0.21 |
| 22G | 829 | 1560 | 11.02 | 7.11 | 23.11 | 3119 | 15.46 | 33.65 | 3.01 | 0.75 | 0.13 | 1.24 | 5.01 | 3.80 | 16.77 | 0.05 | 0.02 | 9.94 | 0.02 | 0.57 | 0.59 |
| 22G | 849 | 1518 | 11.11 | 7.29 | 23.24 | 3108 | 14.76 | 35.05 | 2.83 | 0.74 | 0.10 | 1.49 | 5.13 | 3.63 | 23.75 | 0.05 | 0.02 | 9.71 | 0.03 | 0.58 | 0.59 |
| median | 775 | 1539 | 11.06 | 7.07 | 25.06 | 3114 | 15.11 | 21.03 | 5.27 | 0.71 | 0.12 | 1.36 | 4.94 | 3.83 | 20.26 | 0.07 | 0.02 | 7.84 | 0.03 | 0.58 | 0.59 |
| mean | 717 | 1503 | 19.13 | 6.77 | 31.72 | 2796 | 13.24 | 21.42 | 8.25 | 0.67 | 0.40 | 1.84 | 4.62 | 5.15 | 26.12 | 0.22 | 0.08 | 8.04 | 0.04 | 7.58 | 0.93 |
| SD | 124 | 400 | 13.36 | 0.68 | 10.25 | 670 | 5.89 | 8.58 | 5.22 | 0.09 | 0.40 | 1.06 | 0.74 | 2.86 | 20.21 | 0.20 | 0.08 | 1.74 | 0.03 | 9.09 | 0.74 |

*Table 41: Trace element concentrations Tayginka (RUS) with median, mean and standard deviation*

| Tayginka (RUS) | Analyte (µg g-1) | | | | | | | | | | | | | | | | | | | |
|---|---|---|---|---|---|---|---|---|---|---|---|---|---|---|---|---|---|---|---|---|
| sample ID | Mg | Al | V | Cr | Mn | Fe | Ni | Cu | Zn | Ga | As | Se | Rb | Sr | Mo | Ag | Cd | Ba | Tl | Pb | U |
| 5B | 726 | 3189 | 14.90 | 4.91 | 52.14 | 2623 | 6.23 | 203.54 | 34.58 | 1.03 | 0.34 | 1.15 | 2.96 | 2.25 | 75.66 | 0.57 | 0.48 | 6.22 | 0.02 | 7.08 | 0.65 |
| 5B | 717 | 3331 | 15.22 | 5.01 | 51.53 | 2703 | 6.57 | 233.58 | 36.19 | 1.06 | 0.19 | 1.02 | 2.90 | 2.17 | 90.81 | 0.53 | 0.66 | 6.06 | 0.02 | 6.92 | 0.62 |
| 5B | 760 | 3520 | 15.72 | 5.05 | 52.31 | 2767 | 6.71 | 224.91 | 38.58 | 1.11 | 0.16 | 1.28 | 3.08 | 2.39 | 76.54 | 0.57 | 0.54 | 6.10 | 0.02 | 6.55 | 0.41 |
| 21E | 734 | 2107 | 14.94 | 4.82 | 77.42 | 3701 | 6.42 | 286.52 | 19.80 | 0.88 | 0.30 | 0.40 | 4.08 | 7.32 | 94.52 | 0.46 | 0.17 | 10.50 | 0.02 | 2.80 | 0.85 |
| 21E | 747 | 2194 | 15.39 | 5.11 | 77.13 | 3738 | 6.18 | 291.74 | 20.50 | 0.91 | 0.20 | 0.34 | 4.18 | 6.67 | 107.23 | 0.49 | 0.16 | 10.37 | 0.02 | 3.26 | 0.79 |
| 21E | 776 | 2350 | 16.28 | 5.25 | 81.39 | 3928 | 5.96 | 297.33 | 26.05 | 0.98 | 0.23 | 0.44 | 4.38 | 7.50 | 100.65 | 0.47 | 0.17 | 11.11 | 0.02 | 3.00 | 0.65 |
| 22E | 634 | 1797 | 13.93 | 6.21 | 45.62 | 2497 | 4.56 | 97.55 | 21.34 | 0.69 | 0.11 | 0.19 | 2.97 | 3.47 | 42.62 | 0.62 | 0.21 | 11.67 | 0.02 | 1.13 | 0.52 |
| 22E | 632 | 1769 | 13.88 | 5.80 | 45.77 | 2480 | 4.63 | 105.41 | 25.89 | 0.68 | 0.04 | 0.18 | 2.99 | 3.34 | 47.17 | 0.57 | 0.21 | 11.51 | 0.02 | 1.11 | 0.41 |
| median | 730 | 2272 | 15.08 | 5.08 | 52.23 | 2735 | 6.21 | 229.25 | 25.97 | 0.95 | 0.19 | 0.42 | 3.04 | 3.41 | 83.67 | 0.55 | 0.21 | 10.44 | 0.02 | 3.13 | 0.63 |
| mean | 716 | 2532 | 15.03 | 5.27 | 60.41 | 3055 | 5.91 | 217.57 | 27.87 | 0.92 | 0.20 | 0.63 | 3.44 | 4.39 | 79.40 | 0.54 | 0.32 | 9.19 | 0.02 | 3.98 | 0.61 |
| SD | 51 | 661 | 0.77 | 0.45 | 14.38 | 579 | 0.79 | 74.25 | 7.05 | 0.15 | 0.09 | 0.42 | 0.60 | 2.20 | 22.36 | 0.05 | 0.19 | 2.41 | 0.00 | 2.35 | 0.15 |

*Table 42: Trace element concentrations Ragedara (LKA) with median, mean and standard deviation*

| Ragedara (LKA) | Analyte (µg g-1) | | | | | | | | | | | | | | | | | | | |
|---|---|---|---|---|---|---|---|---|---|---|---|---|---|---|---|---|---|---|---|---|
| sample ID | Mg | Al | V | Cr | Mn | Fe | Ni | Cu | Zn | Ga | As | Se | Rb | Sr | Mo | Ag | Cd | Ba | Tl | Pb | U |
| 10B | 808 | 559 | 0.35 | 0.42 | 41.83 | 1909 | 1.41 | 1.63 | 1.43 | 0.42 | 0.08 | 0.04 | 0.06 | 1.97 | 0.00 | 0.01 | 0.00 | 0.30 | 0.01 | 0.59 | 0.04 |
| 10B | 162 | 158 | 0.13 | 0.36 | 64.12 | 1213 | 8.78 | 197.62 | 5.95 | 0.12 | 0.08 | 0.03 | 0.14 | 1.62 | 42.52 | 0.05 | 0.06 | 0.90 | 0.02 | 7.22 | 0.01 |
| 10B | 234 | 508 | 0.06 | 0.54 | 12.53 | 2416 | 3.87 | 33.03 | 3.81 | 0.24 | 0.05 | 0.05 | 0.08 | 0.36 | 0.21 | 0.04 | 0.01 | 0.39 | 0.02 | 2.24 | 0.02 |
| 21F | 121 | 102 | 0.12 | 0.34 | 57.29 | 891 | 8.39 | 186.65 | 7.71 | 0.09 | 0.07 | 0.10 | 0.16 | 1.64 | 56.73 | 0.05 | 0.07 | 0.94 | 0.02 | 6.82 | 0.04 |
| 21F | 146 | 42.15 | 0.05 | 0.19 | 226.07 | 9610 | 22.53 | 711.71 | 2.90 | 0.70 | 0.05 | 0.10 | 0.02 | 4.26 | 5.94 | 0.11 | 0.02 | 0.56 | 0.53 | 13.17 | 0.01 |
| median | 162 | 158 | 0.12 | 0.36 | 57.29 | 1909 | 8.39 | 186.65 | 3.81 | 0.24 | 0.07 | 0.05 | 0.08 | 1.64 | 5.94 | 0.05 | 0.02 | 0.56 | 0.02 | 6.82 | 0.02 |
| mean | 294 | 274 | 0.14 | 0.37 | 80.37 | 3208 | 9.00 | 226.13 | 4.36 | 0.32 | 0.07 | 0.06 | 0.09 | 1.97 | 21.08 | 0.05 | 0.03 | 0.62 | 0.12 | 6.01 | 0.02 |
| SD | 259 | 216 | 0.11 | 0.11 | 74.99 | 3245 | 7.31 | 255.28 | 2.22 | 0.23 | 0.01 | 0.03 | 0.05 | 1.27 | 23.83 | 0.03 | 0.03 | 0.26 | 0.20 | 4.40 | 0.01 |

*Table 43: Trace element concentrations Zavallia (UKR) with median, mean and standard deviation*

| **Zavallia (UKR)** | **Analyte (µg g-1)** | | | | | | | | | | | | | | | | | | | |
|---|---|---|---|---|---|---|---|---|---|---|---|---|---|---|---|---|---|---|---|---|
| **sample ID** | **Mg** | **Al** | **V** | **Cr** | **Mn** | **Fe** | **Ni** | **Cu** | **Zn** | **Ga** | **As** | **Se** | **Rb** | **Sr** | **Mo** | **Ag** | **Cd** | **Ba** | **Tl** | **Pb** | **U** |
| 4B | 284 | 3950 | 16.17 | 7.86 | 30.19 | 3179 | 4.86 | 15.05 | 16.39 | 1.20 | 1.08 | 0.49 | 1.25 | 2.42 | 3.26 | 1.17 | 0.06 | 7.28 | 0.02 | 1.08 | 0.11 |
| 4B | 275 | 4204 | 16.12 | 8.09 | 29.48 | 3041 | 4.71 | 14.40 | 18.37 | 1.27 | 0.58 | 0.51 | 1.17 | 2.17 | 1.57 | 1.11 | 0.06 | 5.65 | 0.02 | 1.10 | 0.10 |
| 4B | 278 | 3971 | 16.02 | 7.90 | 30.29 | 3012 | 4.37 | 15.22 | 16.48 | 1.22 | 0.49 | 0.39 | 1.17 | 2.20 | 1.56 | 1.10 | 0.06 | 6.37 | 0.02 | 1.05 | 0.11 |
| 22F | 1656 | 3076 | 29.31 | 9.22 | 48.36 | 9516 | 15.04 | 43.65 | 59.45 | 1.18 | 1.14 | 0.71 | 4.41 | 6.01 | 73.52 | 0.87 | 1.78 | 120.12 | 0.04 | 2.89 | 0.26 |
| 22F | 1510 | 2826 | 26.72 | 8.39 | 43.95 | 8805 | 14.31 | 39.99 | 54.63 | 1.10 | 1.02 | 0.71 | 4.01 | 7.09 | 65.84 | 0.89 | 1.53 | 106.39 | 0.03 | 2.70 | 0.28 |
| median | 284 | 3950 | 16.17 | 8.09 | 30.29 | 3179 | 4.86 | 15.22 | 18.37 | 1.20 | 1.02 | 0.51 | 1.25 | 2.42 | 3.26 | 1.10 | 0.06 | 7.28 | 0.02 | 1.10 | 0.11 |
| mean | 801 | 3606 | 20.87 | 8.29 | 36.45 | 5511 | 8.66 | 25.66 | 33.06 | 1.19 | 0.86 | 0.56 | 2.40 | 3.98 | 29.15 | 1.03 | 0.70 | 49.16 | 0.03 | 1.76 | 0.17 |
| SD | 640 | 547 | 5.89 | 0.50 | 8.05 | 2989 | 4.92 | 13.25 | 19.65 | 0.06 | 0.27 | 0.13 | 1.48 | 2.13 | 33.19 | 0.12 | 0.79 | 52.51 | 0.01 | 0.84 | 0.08 |

### 6.4.2.1. Within Element Variability

Each of the following diagrams (Fig. 61 – 63) displays the variability of the respective element across all mines/provinces, allowing for the recognition of differences and the possibility of discriminations. Trace element data obtained from solution-based-ICP-MS analysis allows a better discrimination of locations, even when only one variable (element) is used, due to smaller dispersion of the data resulting from the higher reproducibility of the analyses.

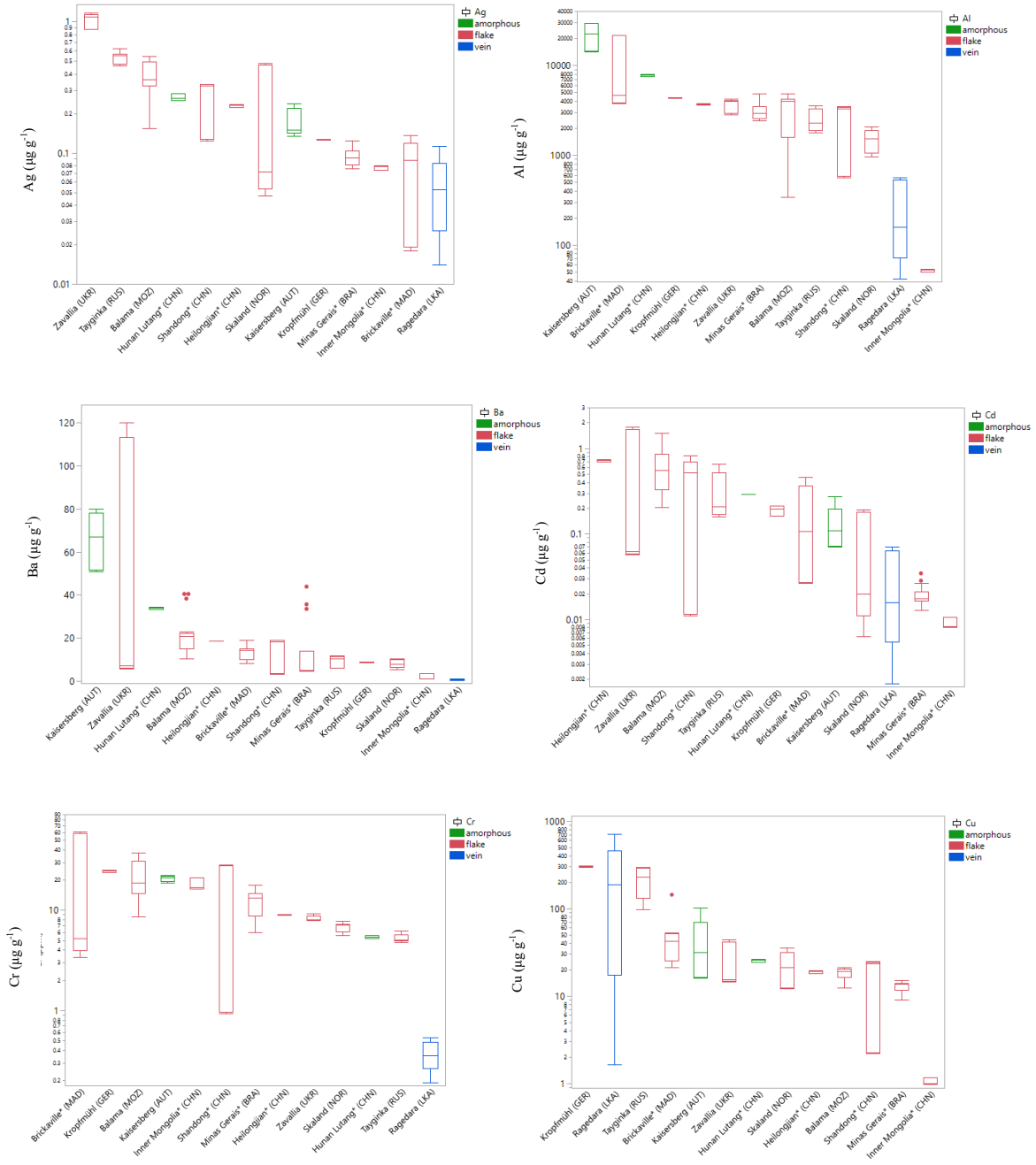


*Figure 61: Within element variability for Ag, Al, Ba Cd, Cr, Cu (solution-ICP-MS data) in µg $g^{-1}$*

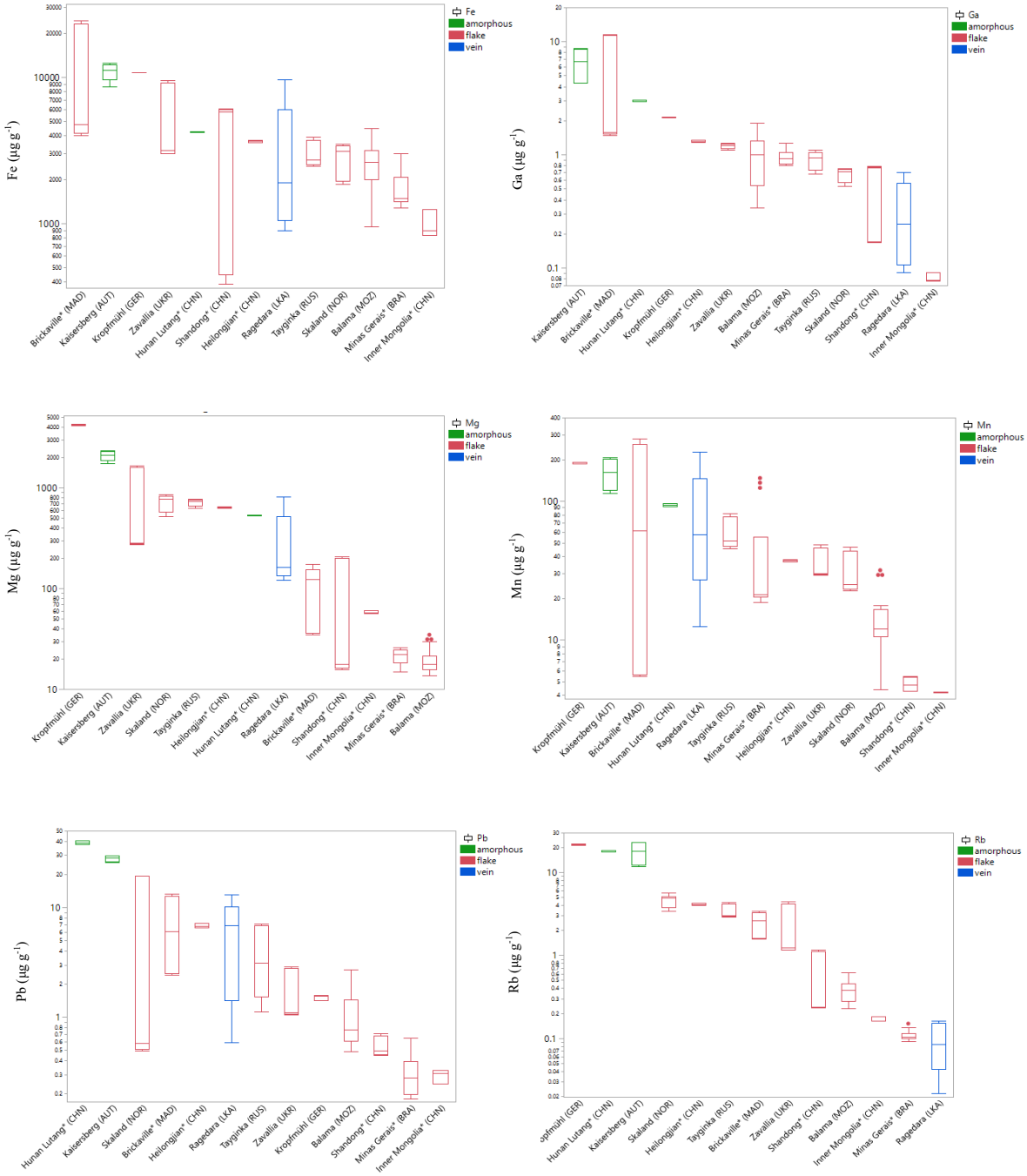


*Figure 62: Within element variability for Fe, Ga Mg, Mn, Pb, Rb (solution-ICP-MS data) in µg $g^{-1}$*

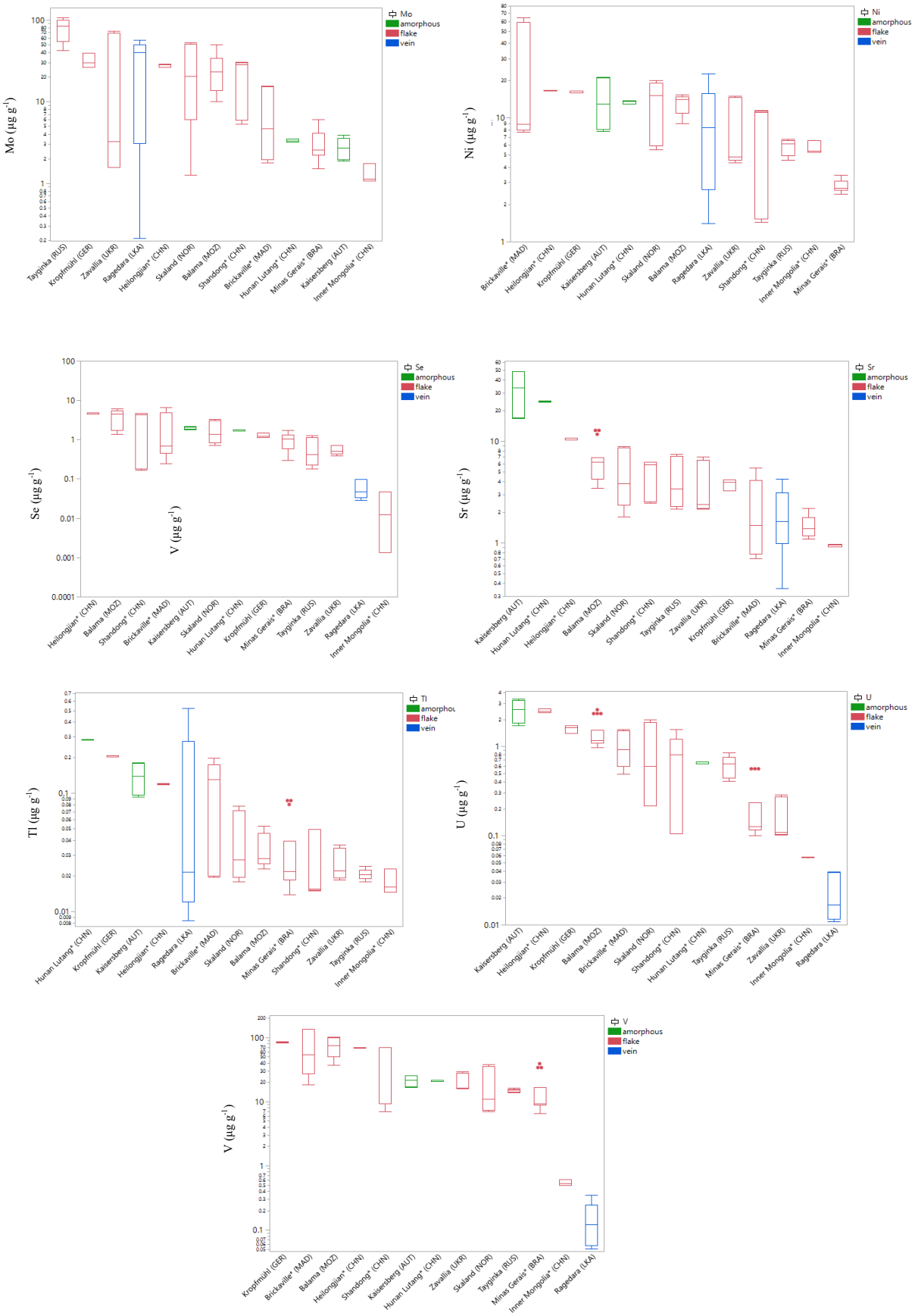


*Figure 63: Within element variability for Mn, Ni, Se, Sr, Tl, U, V (solution-ICP-MS data) in µg $g^{-1}$*

Diagrams displayed above (Fig. 61 to Fig. 63) were used for the initial qualitative differentiation of the individual locations. The mean element concentrations were divided into four groups per element, ranging from higher mean element concentrations (group 1) to lower mean element concentrations (group 4) (Tab. 44).
Kaisersberg (AUT) and Hunan Lutang* (CHN) as amorphous graphite stand out due to their high trace element content, which is attributed to their high impurity content and less precise processing.
Similarly, Kropfmühl (GER) is characterized by high trace element contents, despite being a flake graphite, which could be due to less processing. Balama (MOZ), Tayginka (RUS), and Zavallia (UKR) are characterized by their association with group 1 for the element Ag. Heilongjian* (CHN) stands out due to its higher Cd content related to the other mines/provinces. Skaland (NOR), Tayginka (RUS), Ragedara (LKA) and Zavallia (UKR) are characterized by their low trace element content. Samples from Shandong* (CHN) and Inner Mongolia* (CHN), Skaland (NOR) and Minas Gerais* (BRA) are not associated with group 1 at all. Inner Mongolia* (CHN) is predominantly associated with Group 4 in most cases, characterized by low trace element contents.

*Table 44: Grouping of elements and individual mines/provinces based on mean element concentrations, as seen in Fig. 62 - 64*

| Location | Ag | Al | Ba | Cd | Cr | Cu | Fe | Ga | Mg | Mn | Pb | Rb | Mo | Ni | Se | Sr | Tl | U | V |
|---|---|---|---|---|---|---|---|---|---|---|---|---|---|---|---|---|---|---|---|
| Kaisersberg (AUT) | 3 | 1 | 1 | 3 | 2 | 2 | 1 | 1 | 1 | 1 | 1 | 1 | 3 | 2 | 3 | 1 | 1 | 1 | 2 |
| Minas Gerais* (BRA) | 3 | 2 | 3 | 4 | 2 | 3 | 2 | 3 | 4 | 3 | 4 | 4 | 3 | 4 | 3 | 3 | 3 | 3 | 3 |
| Hunan Lutang* (CHN) | 2 | 2 | 2 | 3 | 3 | 3 | 2 | 2 | 2 | 2 | 1 | 1 | 3 | 2 | 3 | 1 | 1 | 2 | 2 |
| Heilongjian* (CHN) | 2 | 2 | 2 | 1 | 2 | 3 | 2 | 2 | 2 | 3 | 2 | 2 | 2 | 2 | 1 | 2 | 1 | 1 | 1 |
| Shandong* (CHN) | 2 | 3 | 3 | 2 | 2 | 3 | 2 | 3 | 3 | 4 | 3 | 3 | 2 | 2 | 2 | 2 | 4 | 2 | 2 |
| Inner Mongolia* (CHN) | 3 | 4 | 4 | 4 | 2 | 4 | 4 | 4 | 3 | 4 | 4 | 3 | 4 | 3 | 4 | 4 | 4 | 3 | 4 |
| Kropfmühl (GER) | 3 | 2 | 3 | 3 | 1 | 1 | 1 | 2 | 1 | 1 | 3 | 1 | 1 | 2 | 3 | 2 | 1 | 1 | 1 |
| Brickaville* (MAD) | 3 | 2 | 3 | 3 | 1 | 2 | 1 | 1 | 3 | 2 | 2 | 2 | 3 | 1 | 3 | 3 | 2 | 2 | 1 |
| Balama (MOZ) | 1 | 2 | 2 | 2 | 2 | 3 | 3 | 3 | 4 | 4 | 3 | 3 | 2 | 2 | 1 | 2 | 2 | 1 | 1 |
| Skaland (NOR) | 4 | 3 | 3 | 4 | 3 | 3 | 3 | 3 | 2 | 3 | 3 | 2 | 2 | 2 | 3 | 2 | 2 | 2 | 3 |
| Tayginka (RUS) | 1 | 2 | 3 | 3 | 3 | 1 | 3 | 3 | 2 | 2 | 2 | 2 | 1 | 3 | 3 | 2 | 4 | 2 | 2 |
| Ragedara (LKA) | 4 | 4 | 4 | 4 | 4 | 1 | 3 | 3 | 3 | 2 | 2 | 4 | 1 | 3 | 4 | 3 | 2 | 4 | 4 |
| Zavallia (UKR) | 1 | 2 | 2 | 3 | 3 | 3 | 2 | 3 | 2 | 3 | 3 | 3 | 3 | 3 | 3 | 2 | 3 | 3 | 2 |

### 6.4.2.2. Scatter Plots

Al/Ga element correlations are displayed in the graph below (Figure 64). There is a group of data points associated to higher Al and Ga levels related to Kaisersberg and Brickaville. One group is associated to low Al and Ga levels, representing Inner Mongolia. The rest of the samples cannot be differentiated based on these two elements only. Aluminum (Al) and gallium (Ga) substitute for each other in silicate structures. High aluminum contents are usually associated with high gallium contents.

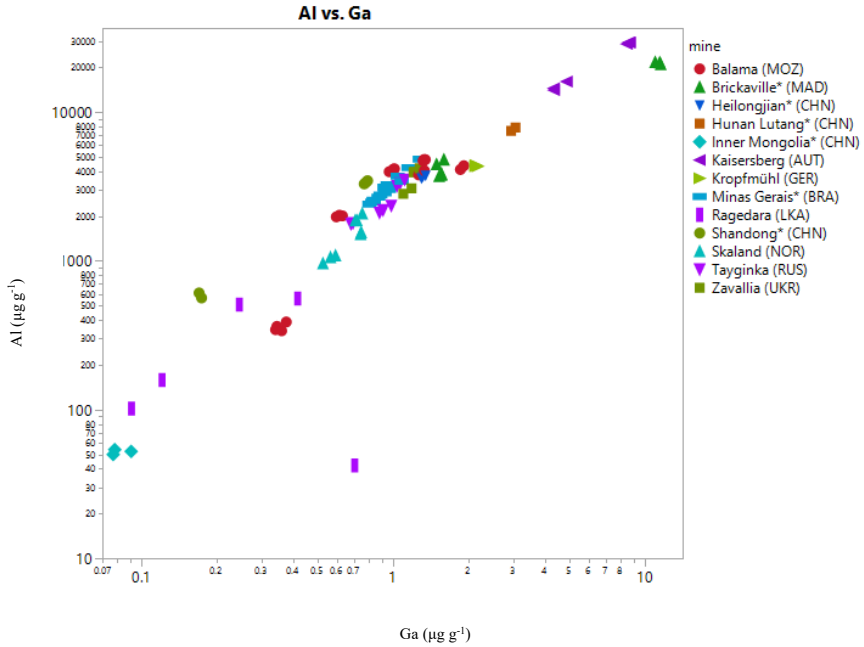


*Figure 64: Scatter plot of Al/Ga (log scale, solution-ICP-MS data) in µg g$^{-1}$*

The scatter plot (Figure 65) shows Al/Cr correlations and individual data points for Ragedara, Inner Mongolia, Kaisersberg and Hunan Lutang. They can clearly be distinguished from other provinces. The rest of the mines/provinces show similar ratios, that do not offer a distinct differentiation. Chromium might be incorporated into iron oxides, which in turn can occur as accompanying minerals in the graphite concentrate.

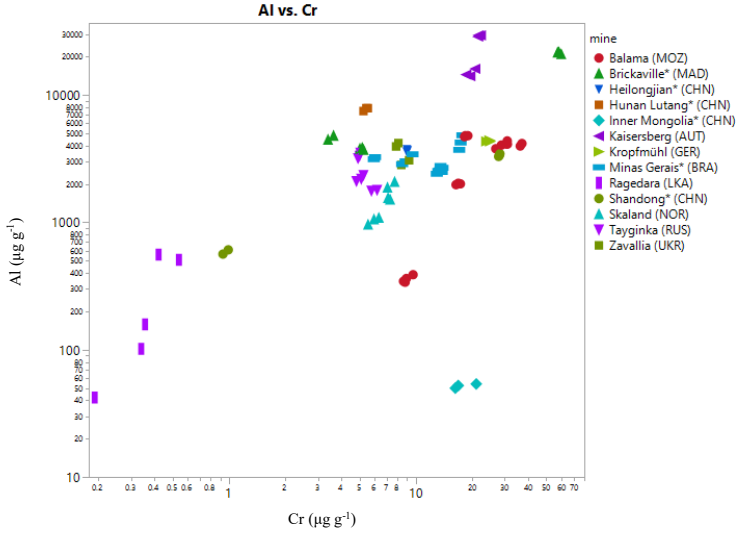


*Figure 65: Scatter plot of Al/Cr (log scale, solution-ICP-MS data) in µg g$^{-1}$*

Al/Sr correlations shows most data points scattered across the graph (Figure 66), with some data points at significant lower Al and Sr levels (Ragedara) as well as some higher Al and Sr values for Kaisersberg. Most locations (data points) are located at intermediate Al and Sr levels. Strontium can be incorporated into carbonates and feldspars, whereas aluminum (Al) can only be incorporated into feldspars.

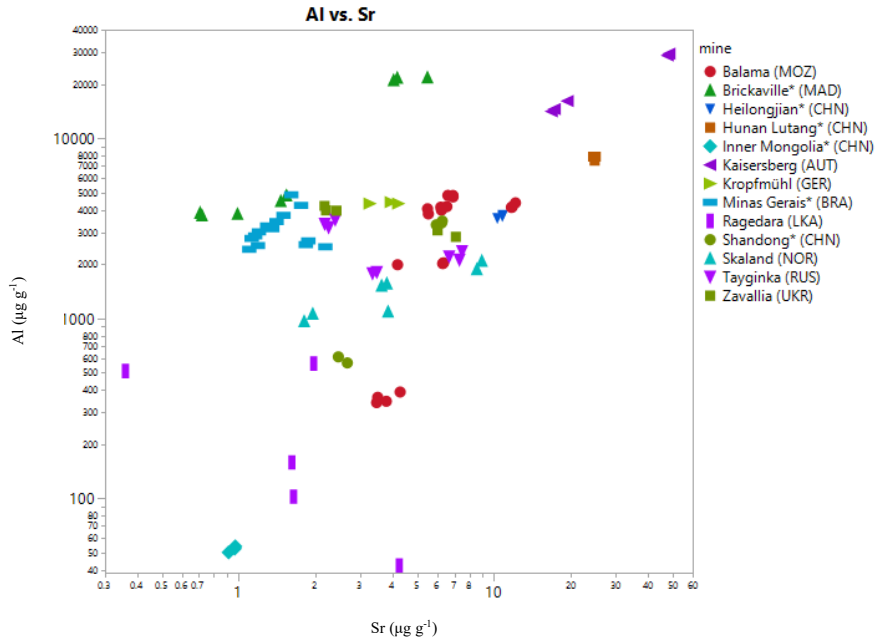


*Figure 66: Scatter plot of Al/Sr (log scale, solution-ICP-MS data) in µg g$^{-1}$*

V/Ga element concentrations (Figure 67) demonstrate a differentiation of some mines/provinces. Ragedara can be completely separated from other occurrences, as well as Inner Mongolia, along with Brickaville, which exhibits high V and Ga contents. In the range of intermediate Ga and high V content, a large number of data points are accumulated, leading to an overlap of the individual occurrences. Data points for Balama (MOZ) show a distinct correlation, which might be addressed to different V-bearing mica.

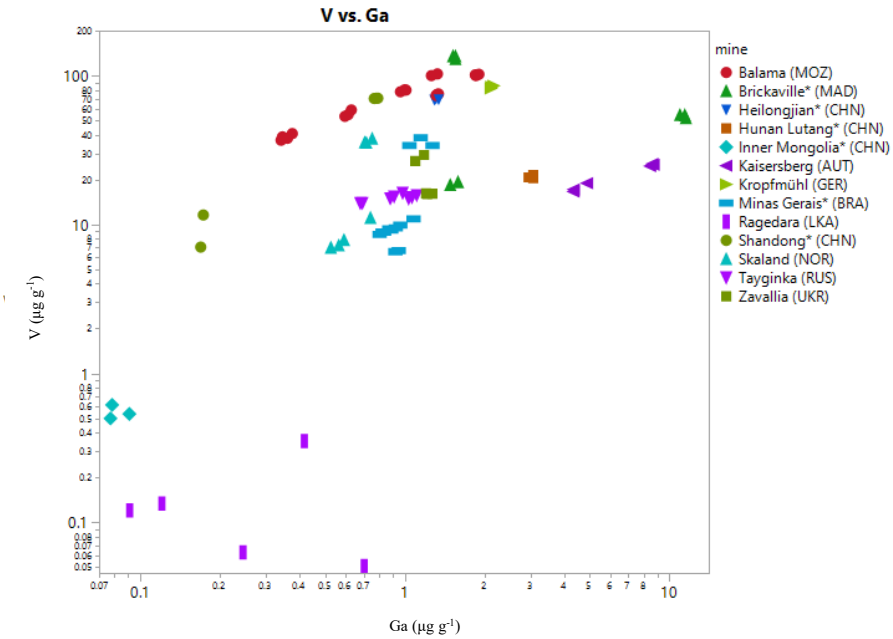


*Figure 67: Scatter plot of V/Ga (log scale, solution-ICP-MS data) in µg g$^{-1}$*

Fe/Ni element correlations (Figure 68) offer another parameter to differentiate between individual locations. Minas Gerais is characterized by lower Ni and intermediate Fe values. Some locations show two trends within the same location (e.g. Brickaville) at intermediate and high Fe values. Shandong province at low Ni and Fe concentrations scattered across datapoints from other locations. Kaisersberg shows two different trends, associated with different Ni levels at constant Fe levels.

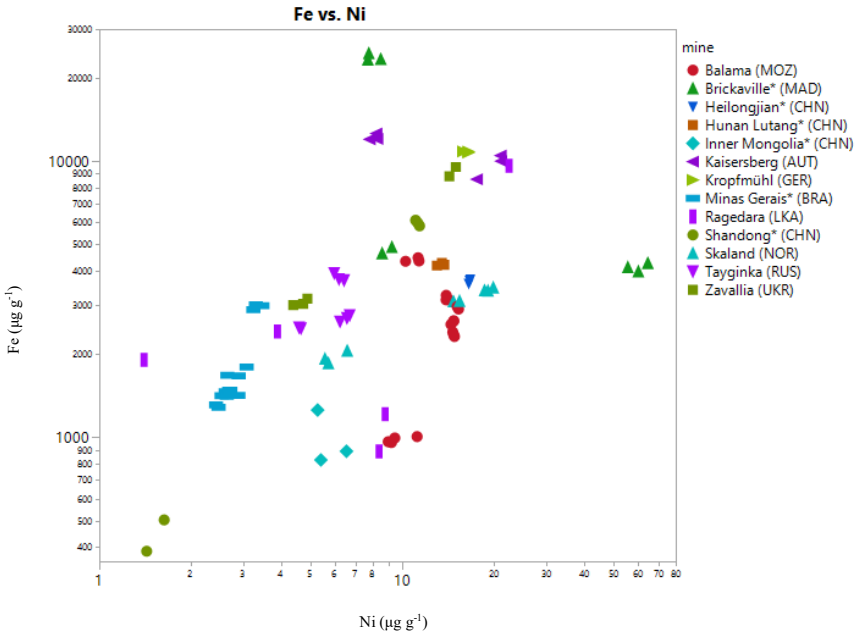


*Figure 68: Scatter plot of Fe/Ni (log scale, solution-ICP-MS data) in µg g$^{-1}$*

A potential for distinguishing individual mines/provinces is evident in the element correlation Rb/Sr (fig. 69). Samples from Minas Gerais form a distinctive group. Balama exhibits a relatively homogeneous grouping however influenced by some data points from Shandong.

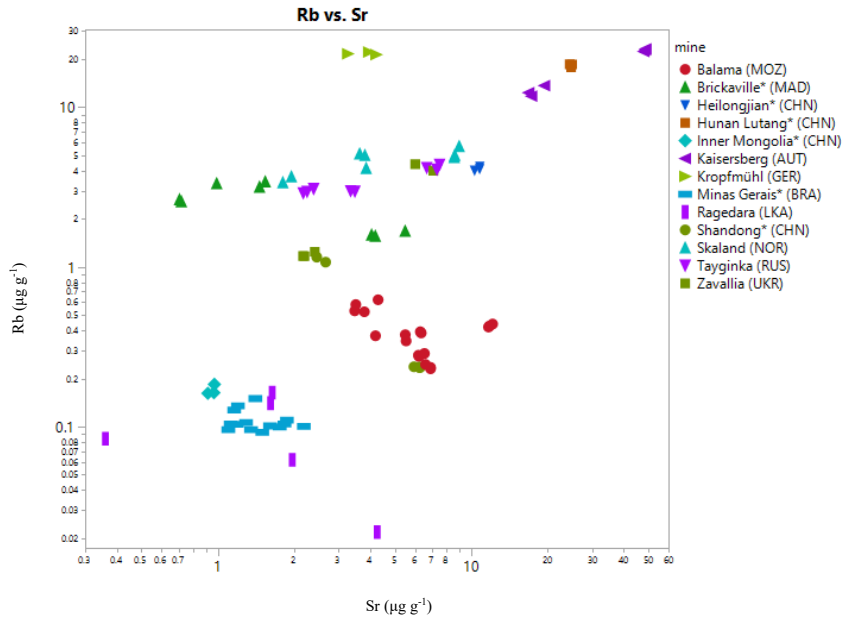


*Figure 69: Scatter plot of Rb/Sr (log scale, solution-ICP-MS data) in µg g$^{-1}$*

### 6.4.2.3. REE Patterns

REE concentrations from solution-based-ICP-MS analysis are presented below, due to the potential of reliably measuring all REE with this analytical method. The REE values were normalized to the EUS (Tab. 45). EUS refers to European Shale and serves as a standard reference material frequently employed to normalize REE concentrations across various samples to align with the compositional characteristics of European material analogous to Australian or North American shales (Bau et al. 2018). The diagrams below show log-normalized REE distributions of each mine/province individually and are later averaged and presented in a graph to compare the individual REE patterns of each mine/province with the others in this study. La-Eu can be indicated as LREE, Gd-Ho as MREE and Er-Lu as HREE.

*Table 45: REE concentrations used for REE normalisation for European Shale (EUS)*

| Recommended data set for European Shale (EUS) for REY normalisation (Bau et al. 2018) in mg $kg^{-1}$ | | | | | | | | | | | | | | |
|---|---|---|---|---|---|---|---|---|---|---|---|---|---|---|
| Y | La | Ce | Pr | Nd | Sm | Eu | Gd | Tb | Dy | Ho | Er | Tm | Yb | Lu |
| 31.9 | 44.3 | 88.5 | 10.6 | 39.5 | 7.30 | 1.48 | 6.34 | 0.944 | 5.86 | 1.17 | 3.43 | 0.492 | 3.26 | 0.485 |

The REE pattern (Fig. 70) from Kaisersberg shows a negative Eu anomaly and a depletion in heavy REE, as well as increasing LREE and decreasing MREE. The two patterns of samples 1A and 2A from Kaisersberg are similar and can be combined into a single curve without losing information, allowing for comparison with the REE patterns of other mines/provinces.

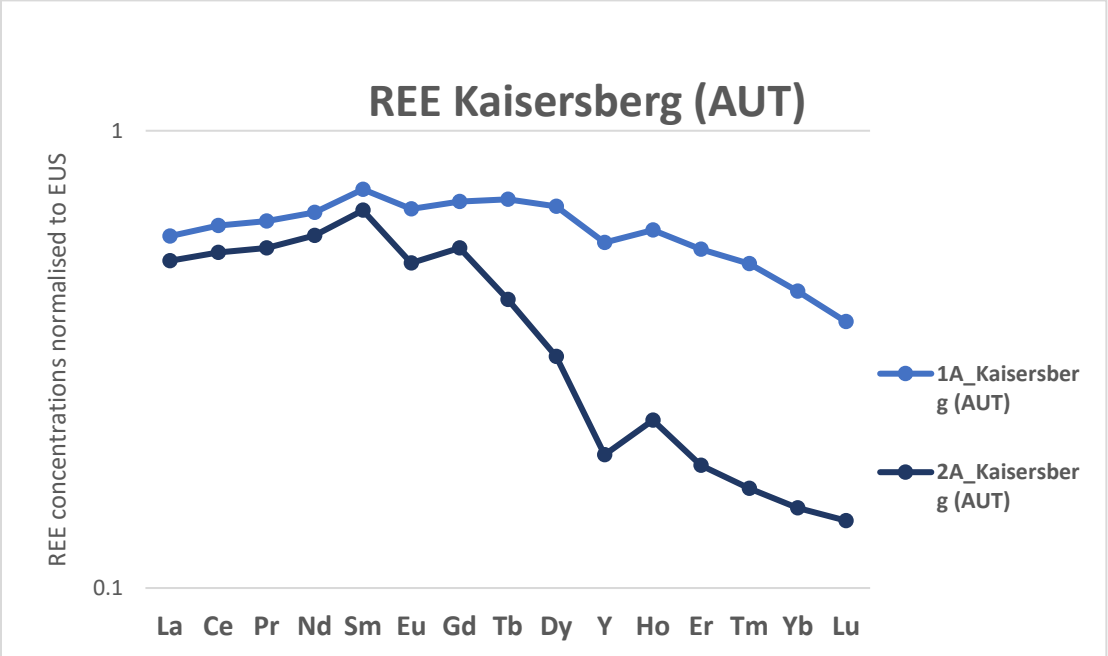


*Figure 70: REE patterns of sample 1A and 2A from Kaisersberg (AUT)*

REE patterns from the Minas Gerais (Fig. 71) province, including samples 21M, 21N, 22C, 3B and 21C, exhibit very homogeneous REE patterns, which can be combined for the comparison with REE patterns from other mines/provinces. The REE patterns shows a positive Ce anomaly, as well as enriched MREE and depleted HREE.

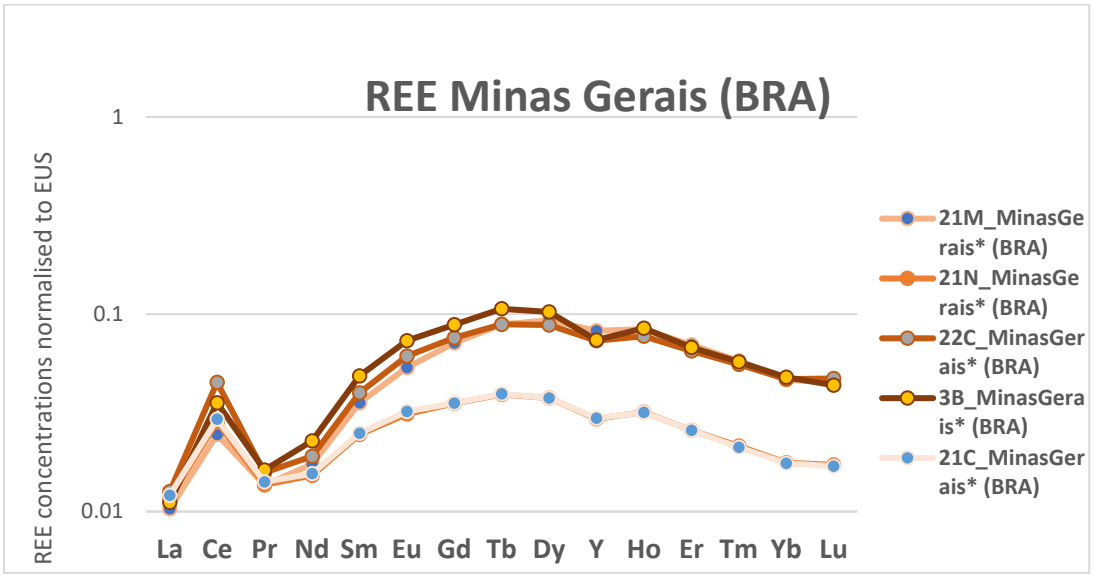


*Figure 71: REE patterns of sample 21M, 21N, 22C, 3B and 21C from the Minas Gerais province (BRA)*

From province Hunan Lutang (CHN) (Fig. 72) only one REE pattern was analyzed. The REE pattern shows a negative Eu anomaly, as well as depleted HREE. Positive outliers of Nd and Dy might be due to analytical errors and not related to natural processes.

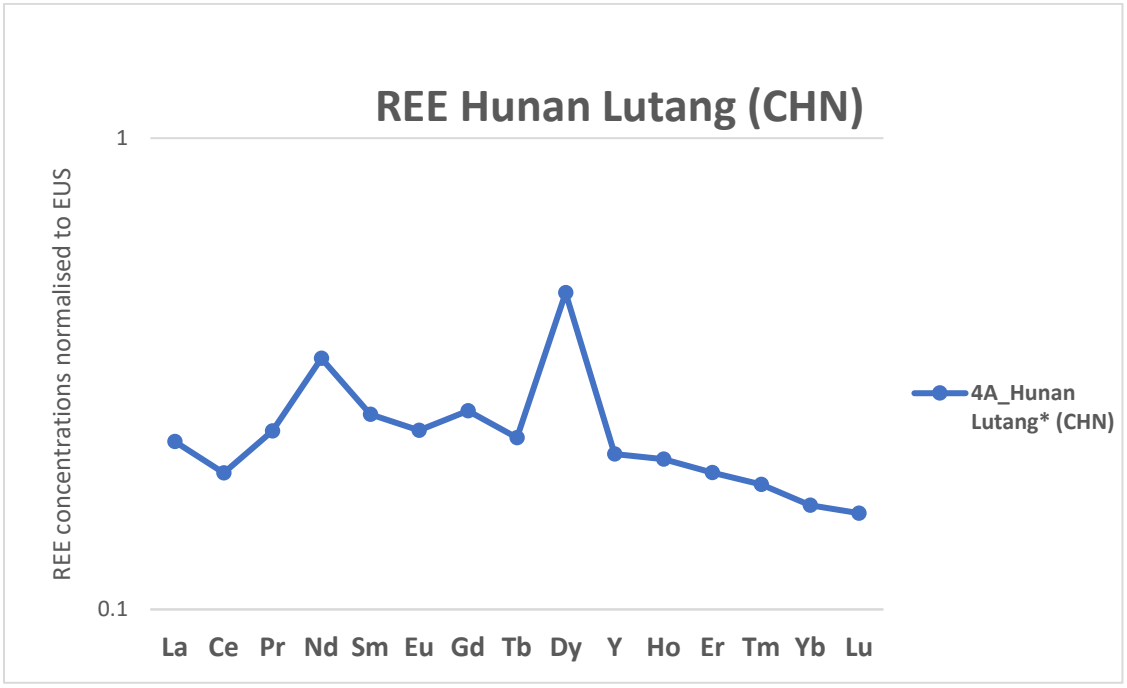


*Figure 72: REE pattern of sample 4A from the Hunan Lutang province (CHN)*

The REE pattern from sample 7B from Heilongjian(Fig. 73) province (CHN) shows a positive Ce anomaly, as well as increasing LREE and MREE and decreasing HREE.

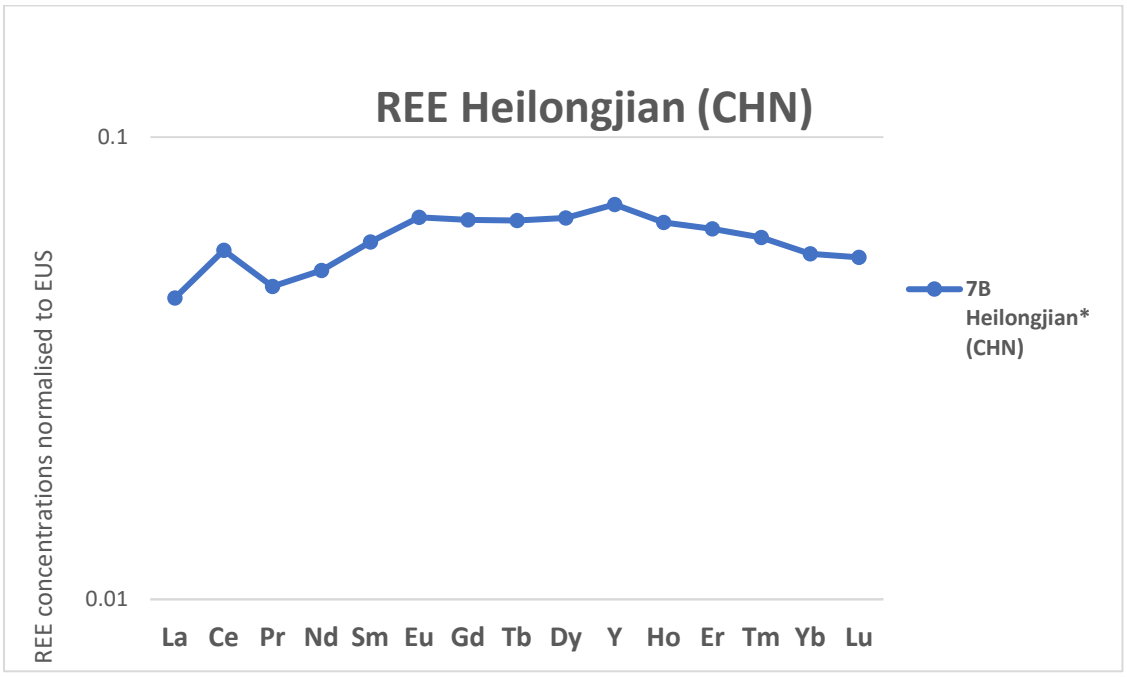


*Figure 73: REE pattern of sample 7B from the Heilongjian province (CHN)*

There are two available samples (21A and 22A) from Shandong province. Both samples exhibit different REE patterns (Fig. 74). Sample 21A shows a distinct negative Ce anomaly and positive Eu anomaly, with decreasing MREE and HREE. Sample 22A shows a positive Ce anomaly with decreasing LREE.

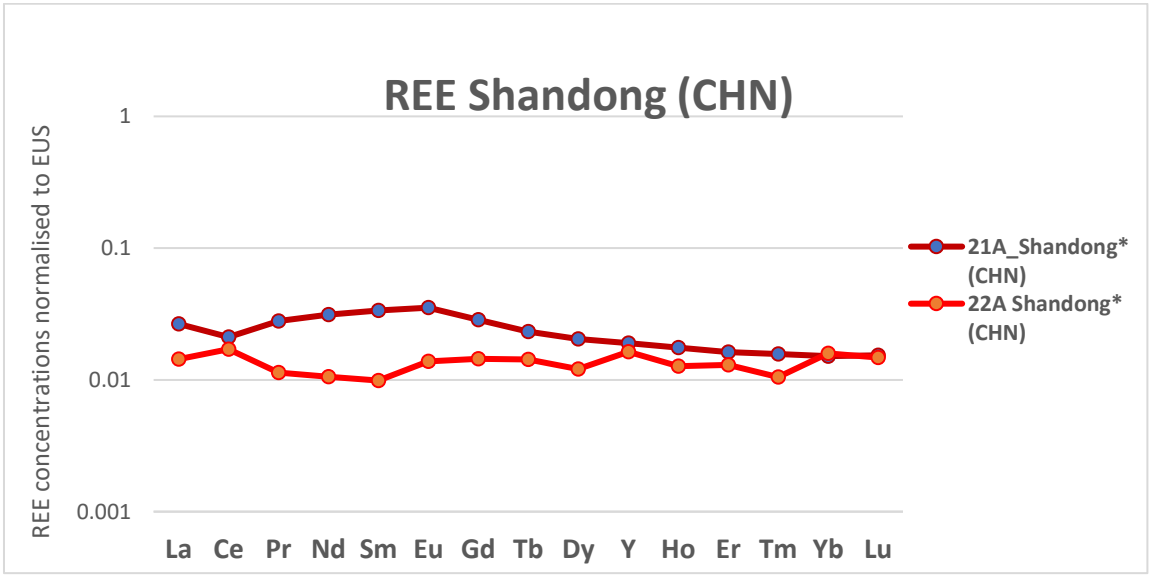


*Figure 74: REE patterns of sample 21A and 22A from the Shandong province (CHN)*

The REE pattern from sample 13B from Kropfmühl mine (GER) shows increasing LREE, a distinct negative Eu anomaly, as well as a depletion in MREE and HREE (Fig. 75).

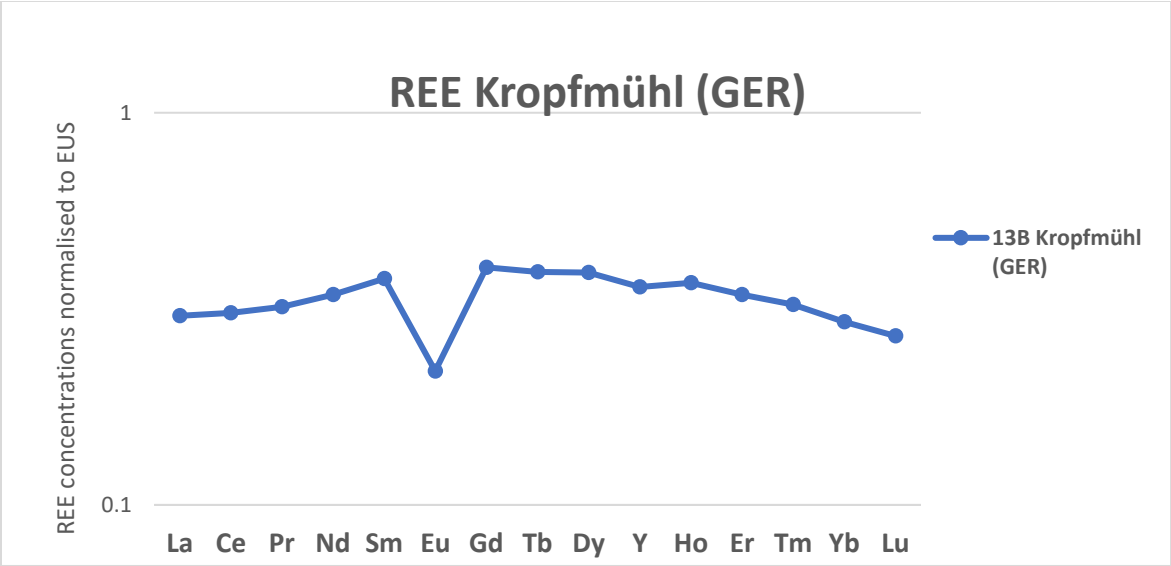


*Figure 75: REE pattern of sample 13B from Kropfmühl (GER)*

The REE pattern of sample 6B from Inner Mongolia (CHN) shows a distinct positive Ce anomaly with slightly decreasing LREE and MREE= HREE (Fig. 76).

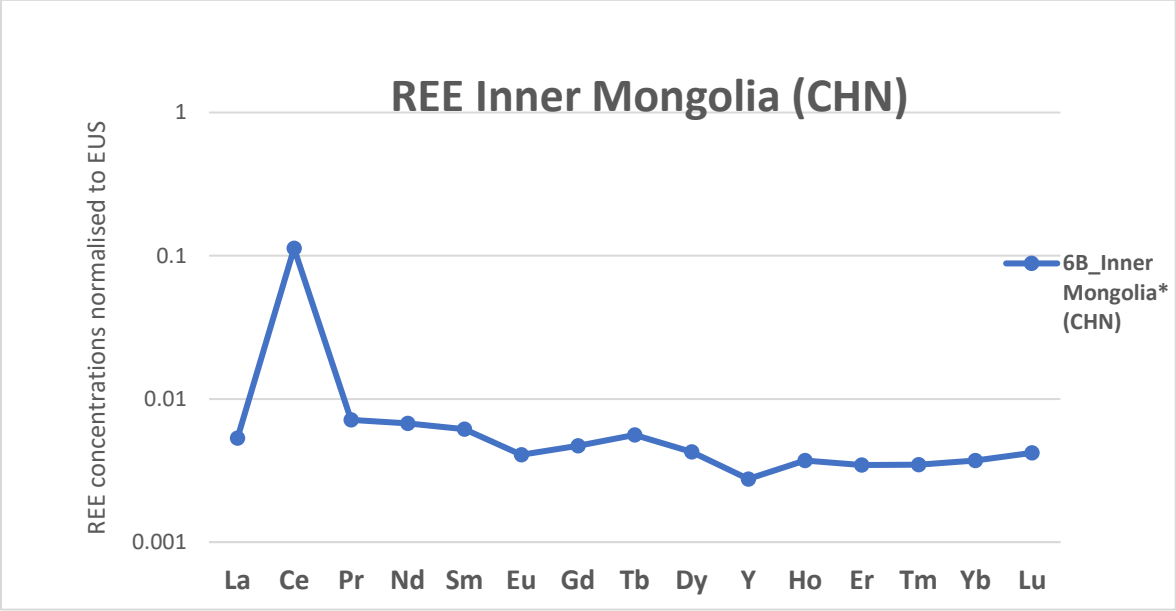


*Figure 76: REE pattern of sample 6B from Inner Mongolia province (CHN)*

From the Balama mine (MOZ), six samples were analyzed (21K, 21L, 1B, 21B, 21J, 22B), which exhibit relatively homogeneous REE patterns (Fig. 77). All samples, except for sample 21B, show a distinctly negative Ce anomaly. All samples from Balama mine show increasing LREE, as well as decreasing MREE and HREE. Sample 1B exhibits a slightly negative Eu anomaly in comparison to the other samples.

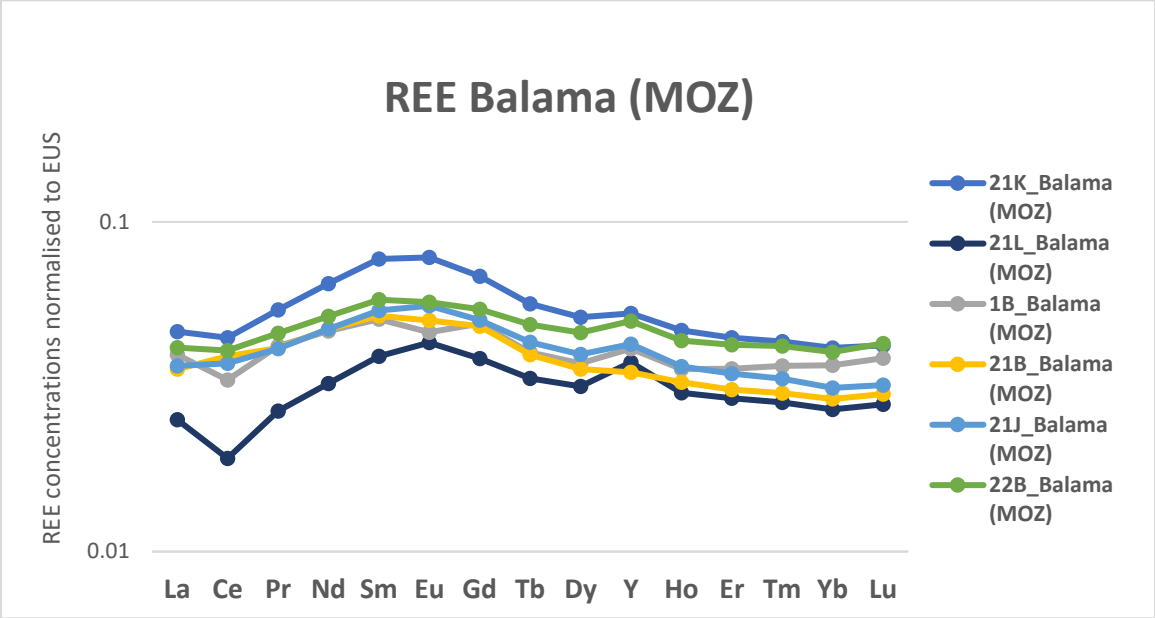


*Figure 77: REE patterns of sample 21K, 21L, 1B, 21B, 21J, 22B from Balama mine (MOZ)*

All three samples from the Brickaville deposit (MAD) exhibit a strongly positive Ce anomaly. The MREE and HREE are enriched in sample 21D, whereas they are relatively depleted in the other two samples, 11B and 22D (Fig. 78).

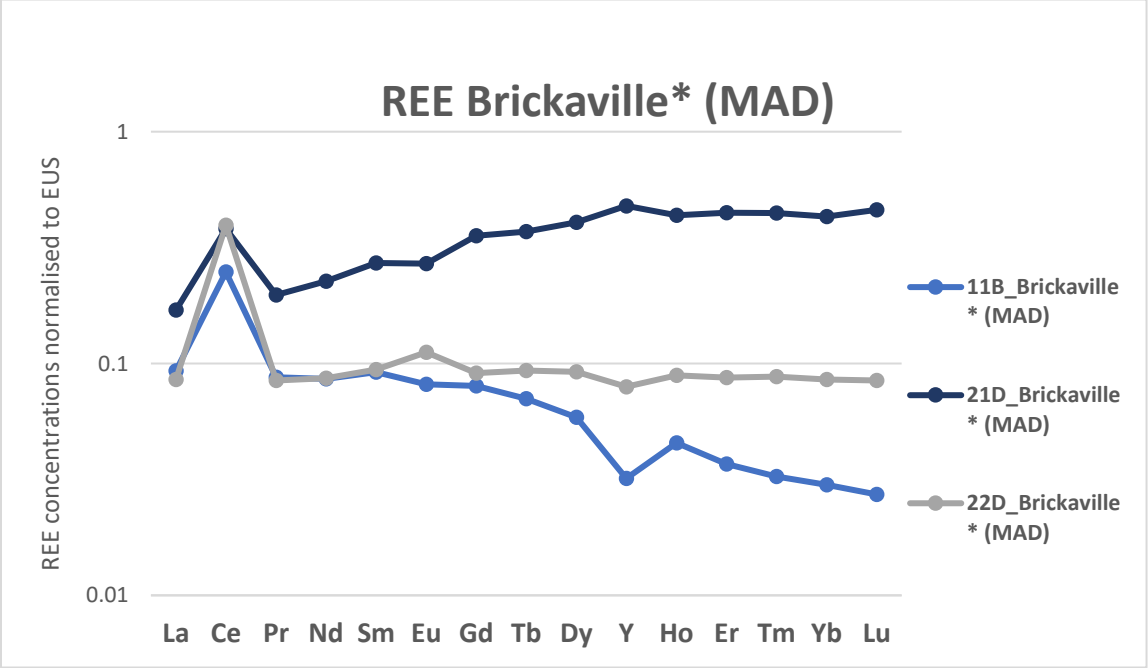


*Figure 78: REE patterns of sample 11B, 21D, 22D from Brickaville province (MAD)*

For the Skaland mine in Norway, three samples were analyzed (2B, 15B, and 22G), with samples 15B and 22G exhibiting similar REE patterns, displaying a distinct positive Eu anomaly and LREE = MREE = HREE. Sample 2B, in comparison, shows a distinctly positive Ce anomaly increasing LREE, MREE and HREE (Fig. 79).

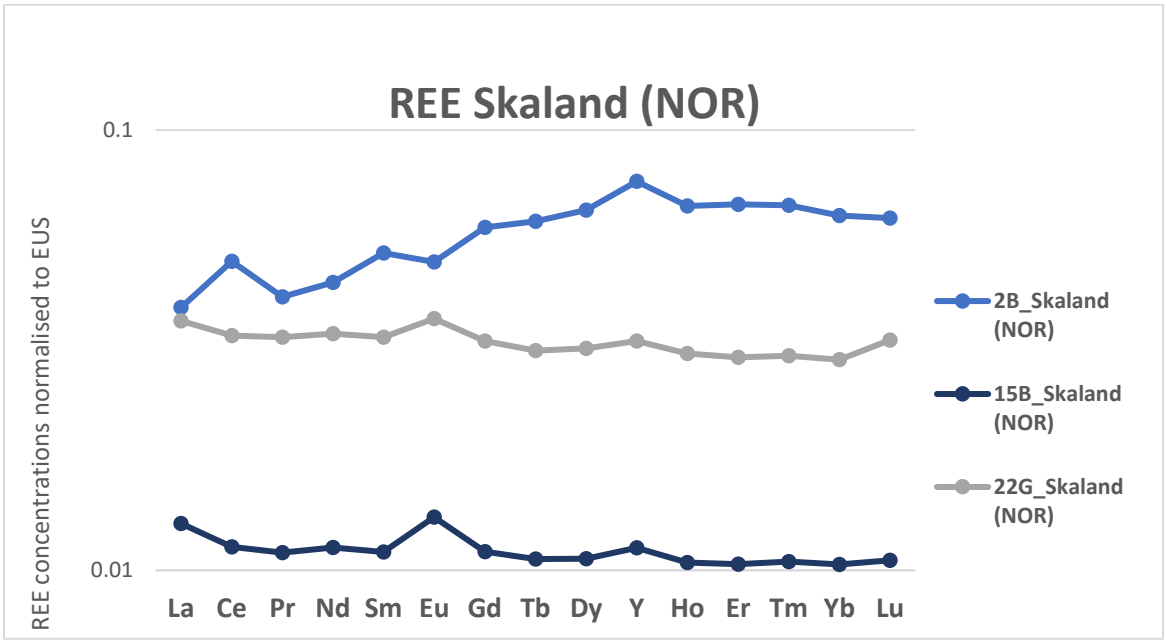


*Figure 79: REE patterns of sample 2B, 15B and22G from Skaland (NOR)*

Both available samples from Zavallia mine (UKR) show slightly decreasing LREE, an enrichment in MREE and HREE with sample 22F showing a positive Eu anomaly compared to sample 4B (Fig. 80).

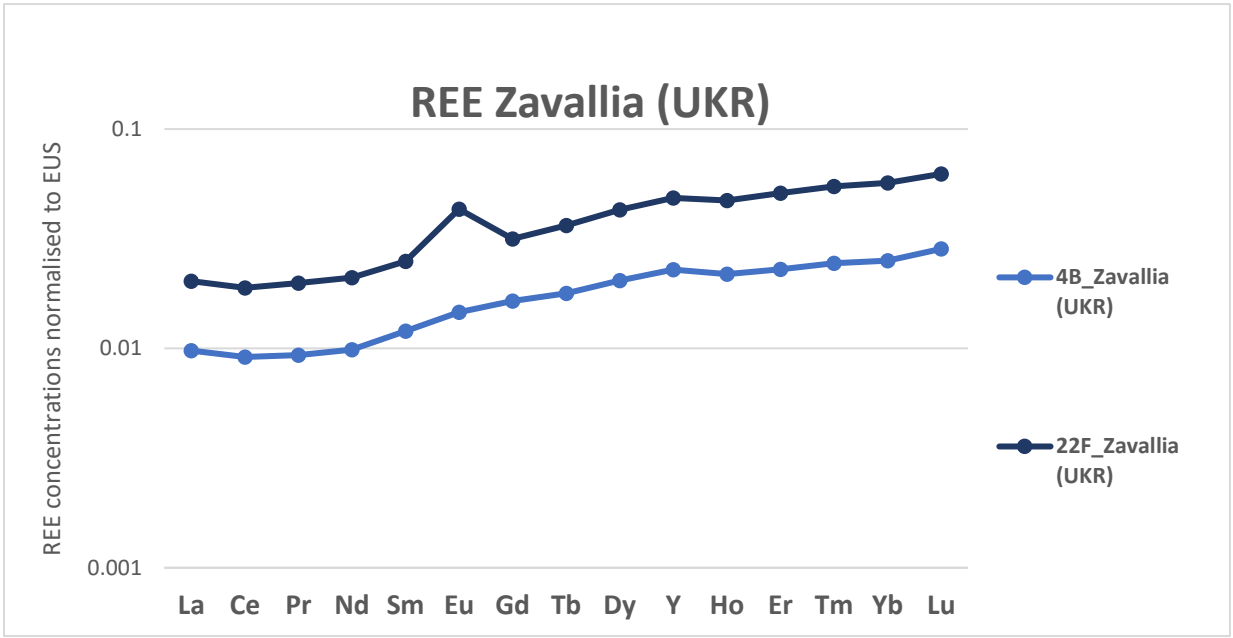


*Figure 80: REE patterns of sample 4B and 22F from Zavallia mine (UKR)*

Both samples from the Ragedara province (LKA) exhibit a distinct negative Eu anomaly, as well as decreasing HREE (Fig. 81). Sample 21F shows increasing MREE, whereas sample 10 B shows decreasing MREE.

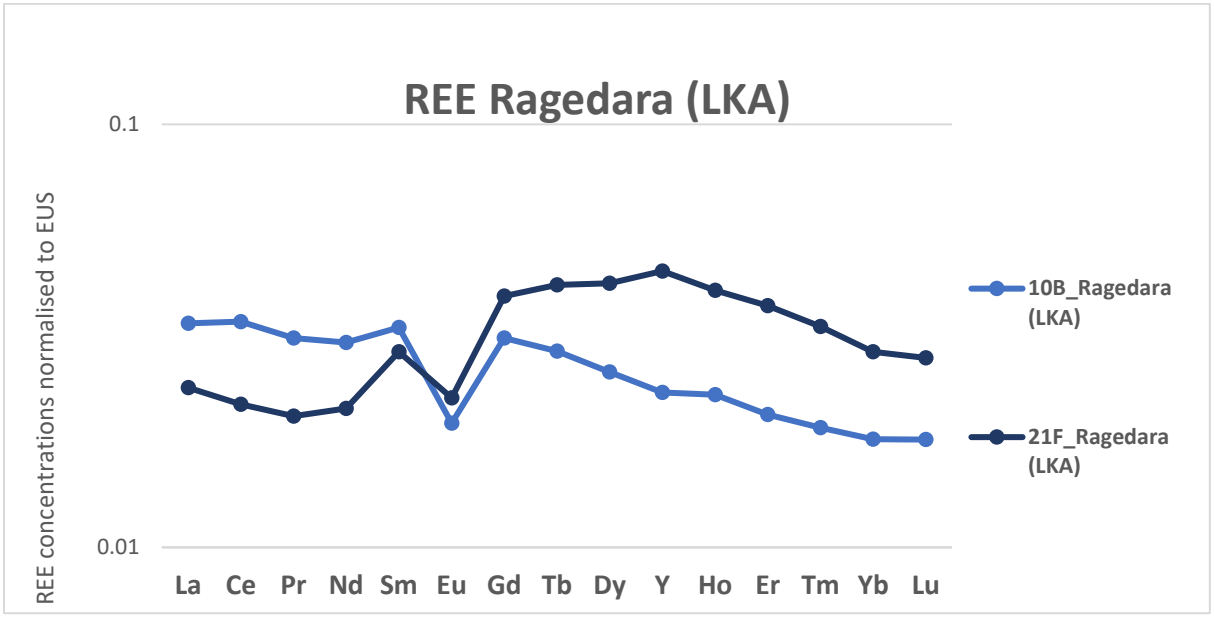


*Figure 81: REE patterns of sample 10B and 21F from Zavallia mine (UKR)*

Samples 5B and 21E from Tayginka mine (RUS) exhibit a distinct positive Eu anomaly. Samples 21E and 22E both show decreasing MREE and HREE. Sample 22E displays a negative Eu anomaly but otherwise follows a pattern very similar to that of sample 21E with depletion of MREE and HREE (Fig. 82).

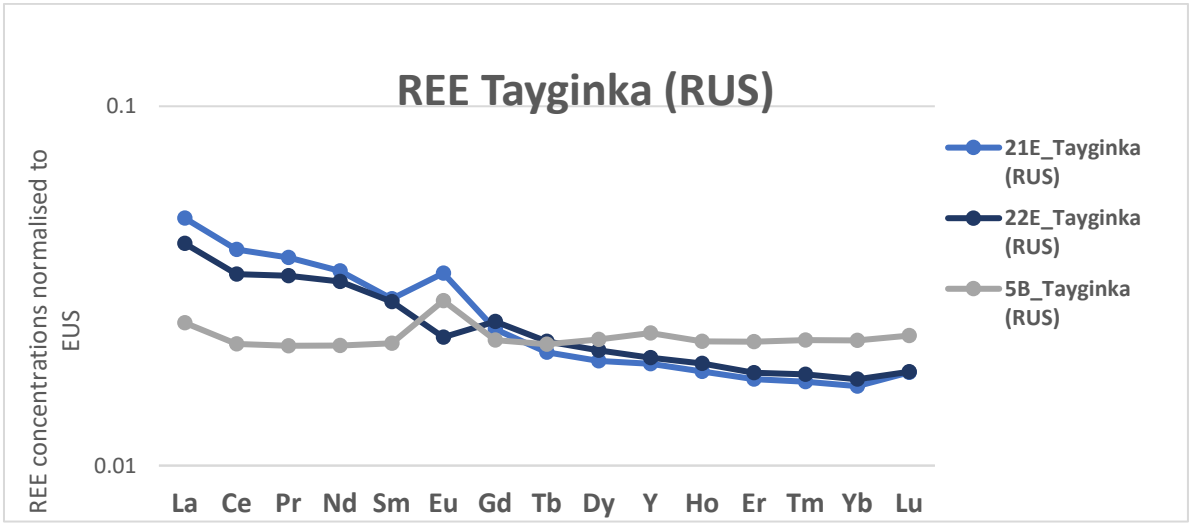


*Figure 82: REE patterns of sample 21E, 22E and 5B from Tayginka (RUS)*

**Comparison of REE patterns from all locations:**

Each individual location (mine/province) exhibits differences in the REE composition, even when represented as mean REE values from each location (Fig. 83). Brickaville (MAD), Inner Mongolia (CHN) and Minas Gerais (BRA) show positive Ce anomalies as a common feature. Kropfmühl (GER), Brickaville (MAD), Ragedara (LKA) and Inner Mongolia (CHN) show negative Eu anomalies. However REE patterns differ. Shandong REE patterns were different from sample 21A and 22A and could not be averaged into one pattern to represent the REE data from this province. The following figure (Fig. 84) shows two lines for Shandong, one representing sample 21A, the other sample 22A. Overall, we observe flat shale-normalized REE patterns, some with distinct to small Ce and Eu anomalies. In some samples, LREE prevail over HREE, but opposite patterns also occur (e.g., Zavallia).

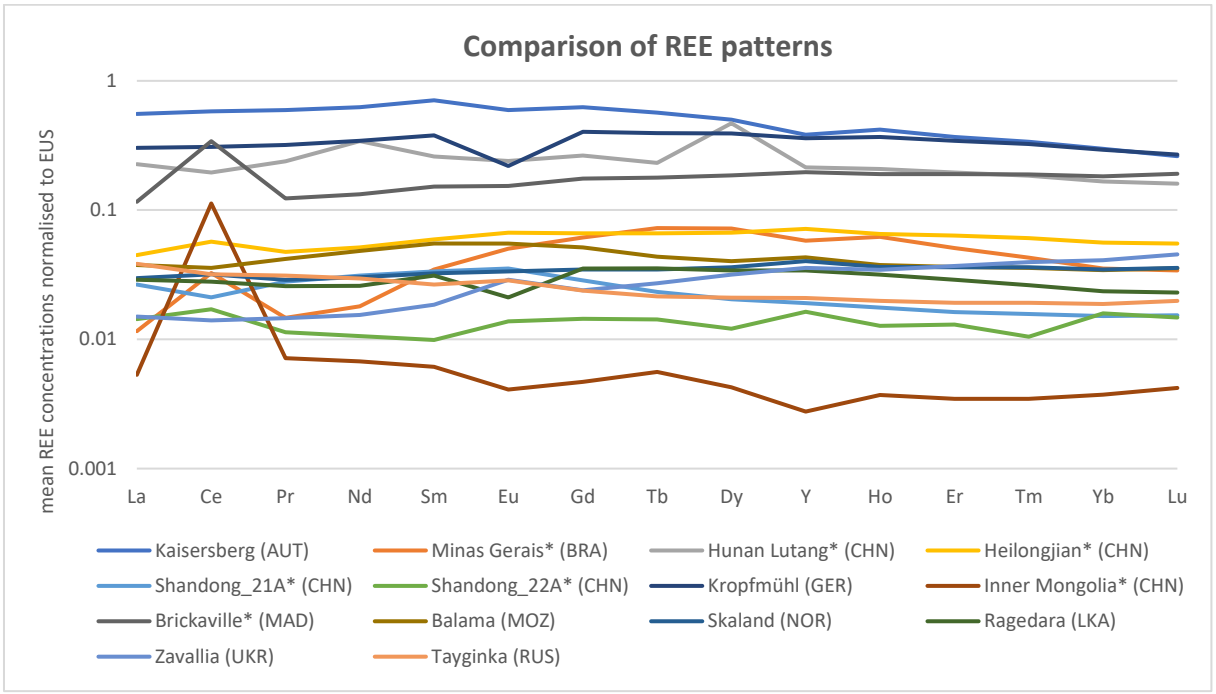


*Figure 83: Comparison of mean REE patterns across individual locations*

## 6.4.2.4. Multivariate Statistical Analysis and Key Elements

### 6.4.2.4.1. Linear Discriminant Analysis (LDA)

Two models using LDA were calculated using the solution-based-ICP-MS trace element data. The data shows significantly less dispersion within each group, as the measurements of the digestions vary little, producing almost identical values. The models are based on continents and on mines/provinces and allow classification of the data. The input data consist of the trace element data as well as the categories on which the classification is based.

The first LDA (Fig. 84) demonstrates the discrimination of graphite samples based on continents. Through the multivariate analysis of trace element data obtained from solution-ICP-MS, four continents can be clearly distinguished from each other. The mines/provinces from Asia and Europe are closer to each other, but there is minimal overlap in individual data points. Confidence ellipses display 95% confidence for the mean value of each group in the diagram assuming a normal distribution of the data. To identify **key elements** for differentiation, the scoring coefficients of this LDA were extracted (Table 46). The elements **Mg, Al, V, Fe, Ga, Sr, Ag, Cd, and U** contribute most to the classification of individual graphite samples (based on continents).

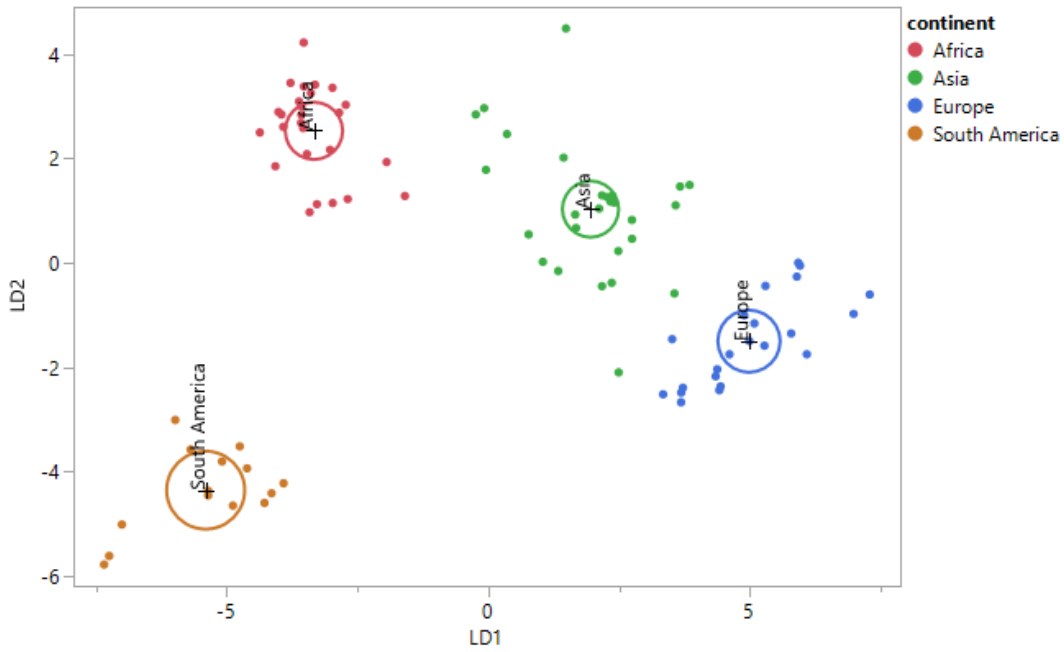


*Figure 84: LDA of solution-based-ICP-MS trace element data based on continents*

*Table 46: Scoring coefficients from LDA based on continents*

| | Log[Mg] | Log[Al] | Log[V] | Log[Cr] | Log[Mn] | Log[Fe] | Log[Ni] | Log[Cu] | Log[Zn] | Log[Ga] | Log[Se] | Log[Rb] | Log[Sr] | Log[Mo] | Log[Ag] | Log[Cd] | Log[Ba] | Log[Tl] | Log[Pb] | Log[U] |
|---|---|---|---|---|---|---|---|---|---|---|---|---|---|---|---|---|---|---|---|---|
| LD1 | 1.84 | 1.10 | 0.32 | -0.19 | -0.42 | 1.73 | 0.76 | -0.04 | -0.61 | -3.22 | -0.02 | 0.07 | 1.34 | -0.79 | 1.01 | -0.45 | -0.18 | -0.63 | -0.06 | -0.38 |
| LD2 | -1.04 | -1.16 | 1.05 | -1.47 | -1.32 | 0.39 | 0.48 | 0.16 | 0.20 | 1.42 | -1.82 | 0.97 | 0.88 | -0.05 | -0.69 | 1.13 | -1.00 | -0.69 | 0.09 | 0.83 |
| LD3 | -0.45 | -0.30 | -1.50 | -0.36 | 0.48 | 0.16 | 1.05 | -1.06 | 0.55 | 1.23 | 0.90 | 0.95 | -1.15 | 0.47 | 1.06 | -1.32 | 0.51 | 0.06 | -1.24 | 0.72 |

A second LDA, based on mines/provinces is displayed in Fig. 85. All occurrences can be differentiated from each other. Balama mine and Shandong province show a similar pattern in close proximity to each other. Ragedara mine is situated at the greatest distance from the other occurrences and differs most significantly, likely due to its hydrothermal graphite type and the non-organic origin of carbon in this mine.

Confidence ellipses display 95 % confidence for the mean value of each group in the diagram and assume a normal distribution of the data.

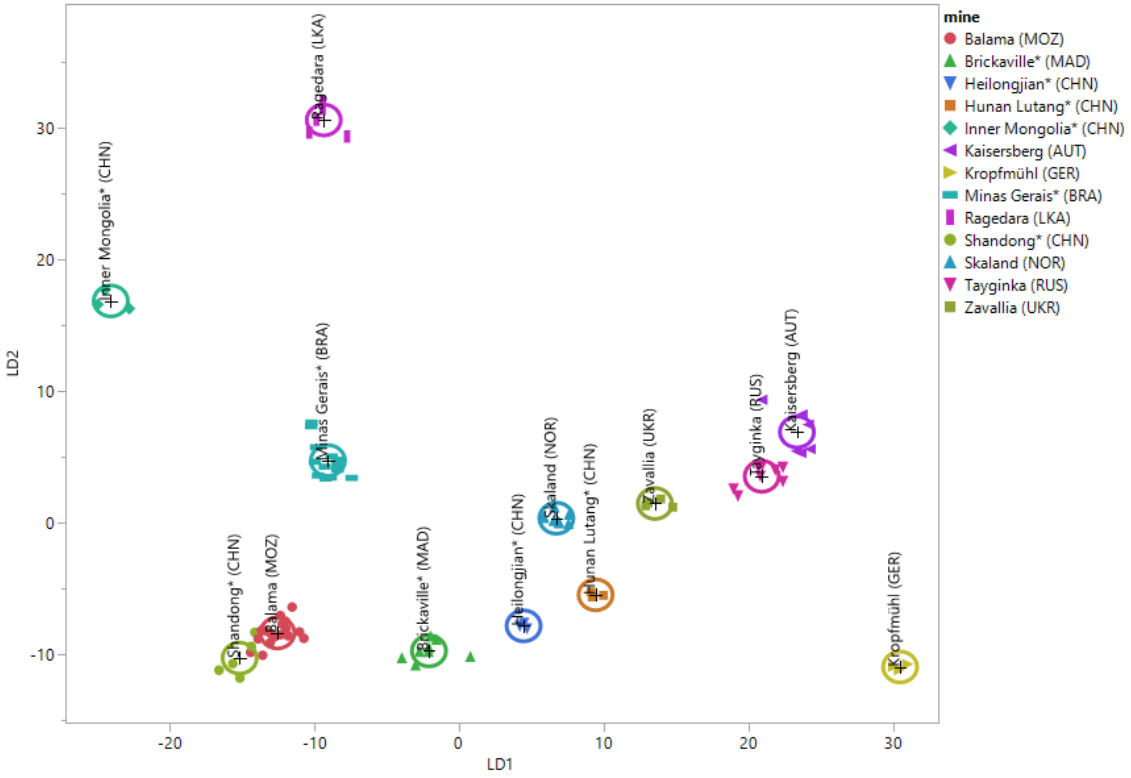


*Figure 85: LDA of solution-based-ICP-MS trace element data based on mines/provinces*

To identify **key elements** for differentiation, the scoring coefficients of this LDA were extracted and are displayed in Table 47. The elements **Mg, Al, Cr, Mn, Ni, Cu, Ga, Rb, Ag and U** contribute most for the classification of individual graphite samples based on individual mines/provinces.

*Table 47: Scoring coefficients from LDA based on mines/provinces*

| | Log[Mg] | Log[Al] | Log[V] | Log[Cr] | Log[Mn] | Log[Fe] | Log[Ni] | Log[Cu] | Log[Zn] | Log[Ga] | Log[Se] | Log[Rb] | Log[Sr] | Log[Mo] | Log[Ag] | Log[Cd] | Log[Ba] | Log[Tl] | Log[Pb] | Log[U] |
|---|---|---|---|---|---|---|---|---|---|---|---|---|---|---|---|---|---|---|---|---|
| LD1 | 2.04 | 1.55 | -1.08 | 0.95 | 2.42 | -0.69 | -0.56 | 1.86 | 0.26 | 0.95 | -0.05 | 0.77 | -0.74 | 0.03 | 2.36 | -1.11 | -0.43 | -0.55 | -1.23 | 1.00 |
| LD2 | 1.38 | 1.24 | -3.28 | 1.49 | 2.93 | -1.19 | 1.48 | -0.48 | -0.31 | -0.32 | -0.52 | -1.67 | 0.31 | 0.27 | 0.25 | -0.46 | 0.60 | -2.28 | 1.24 | 0.61 |
| LD3 | -0.82 | -0.31 | -1.62 | 2.00 | -0.55 | -0.59 | 2.00 | -1.69 | 0.27 | 1.20 | -0.36 | 1.08 | -0.13 | 0.23 | -1.33 | -0.01 | -0.40 | 1.07 | 0.72 | -0.14 |
| LD4 | 0.22 | 1.34 | -1.13 | -0.73 | 0.27 | -1.74 | -0.44 | 0.29 | 1.08 | -0.51 | 1.29 | -0.75 | 1.45 | -0.98 | -0.26 | -0.87 | 1.08 | 0.21 | -0.12 | 0.98 |
| LD5 | -0.45 | 0.24 | 0.65 | -1.84 | -0.70 | 0.45 | -0.92 | 1.11 | -0.11 | 0.67 | -0.21 | -0.13 | -0.08 | 0.03 | -1.71 | 0.85 | -0.88 | -0.10 | 0.90 | 0.64 |
| LD6 | 0.04 | 0.25 | 0.48 | -1.91 | -0.85 | 1.31 | 0.81 | -0.10 | -0.11 | -1.24 | -0.08 | 0.02 | 0.99 | -0.49 | 0.14 | -0.16 | 0.05 | -0.92 | 0.10 | 0.12 |
| LD7 | 0.59 | 0.19 | -0.43 | 1.10 | -0.47 | -0.69 | -0.56 | 0.73 | 0.10 | -0.67 | 0.32 | -0.34 | 0.64 | 0.26 | -0.71 | 0.36 | -1.00 | 1.14 | -0.59 | 0.98 |
| LD8 | -0.53 | -0.41 | -0.62 | 0.09 | 0.38 | -1.07 | 0.44 | 0.08 | 0.19 | 1.58 | -1.12 | 0.22 | -0.01 | 0.30 | 0.24 | 0.42 | -0.17 | -0.64 | -0.27 | 0.83 |
| LD9 | 0.72 | -0.17 | 1.35 | 0.53 | -0.93 | 0.53 | -1.40 | 0.72 | -0.07 | -0.57 | -0.85 | -0.64 | 0.91 | -1.10 | -0.83 | 1.51 | -0.34 | 0.38 | 0.81 | -0.83 |
| LD10 | 0.28 | -0.79 | -0.29 | 0.21 | 0.10 | -0.07 | 0.12 | -0.66 | 1.17 | 0.98 | 0.90 | -0.19 | -0.68 | 0.73 | 0.05 | -0.51 | 0.02 | 0.59 | -0.23 | -0.46 |
| LD11 | -0.71 | -0.22 | -0.26 | 0.28 | 0.57 | -0.40 | -0.07 | -0.12 | -0.15 | 0.29 | 0.31 | 0.64 | 0.24 | 0.45 | 0.16 | 0.33 | -0.46 | 0.48 | -0.22 | -0.77 |
| LD12 | 0.27 | -0.20 | 0.18 | 0.43 | -0.31 | -0.67 | -0.65 | -0.20 | 0.55 | 0.07 | 0.27 | -0.10 | -0.46 | 0.49 | -0.41 | -0.14 | 0.23 | 0.22 | 0.76 | -0.37 |

#### 6.4.2.4.2. Principal Component Analysis (PCA)

Based on the elements that have been identified as significant in the LDA shown in chapter 6.4.2.4.1., a Principal Component Analysis (PCA) was performed, which refers to the same hierarchies as above (continents and mines/province). PCA is a method of dimension-reduced data projection, where data are summarized into new, simplified variables and expressed as PC1 and PC2.

PC1 (48.3 %) and PC2 (15.6 %) for the hierarchy of continents account for most of the variance in the data and are presented in a two-dimensional graph with corresponding elements displayed in Fig. 86. Data points corresponding to South America (orange) are densely distributed, datapoints referring to Asia (green) show two sets of samples. A clear distinction of the data points based on the continents is therefore not entirely possible.

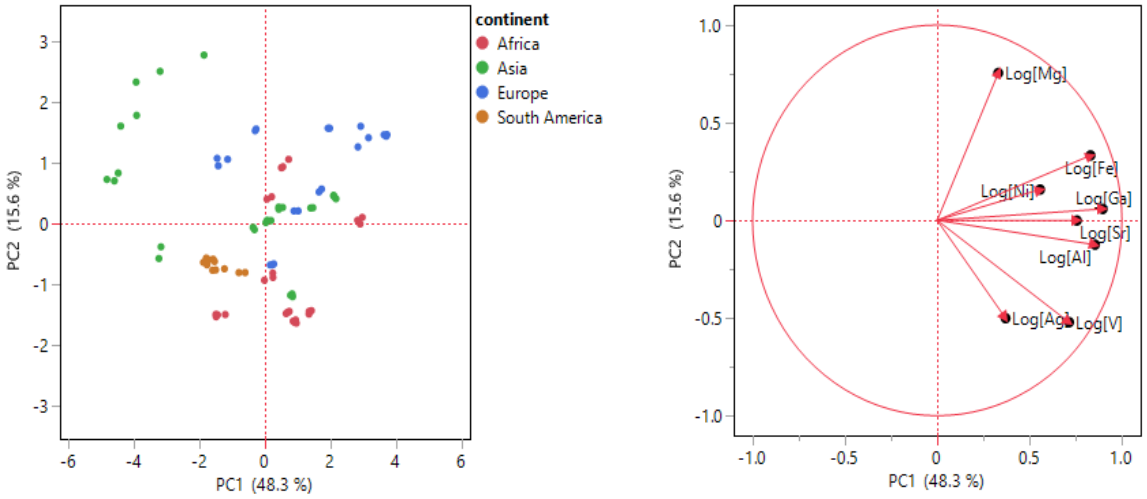


*Figure 86: PCA of solution-ICP-MS trace element data at continent level (left) with the indicated elements (right)*

PC1 (41.2 %) and PC2 (21.7 %) for the hierarchy of mines/provinces account for most of the variance in the data and are presented in a two-dimensional graph with corresponding elements displayed in Fig. 87. Data points referring to Ragedara (LKA) form a distinct group, as well as datapoints for Kaisersberg (AUT), Minas Gerais (BRA) and Inner Mongolia (CHN). Shandong (CHN) shows two sets of datapoints, which correlates to the REE pattern of this province, where two different patterns for the two samples from the same province were identified (see 6.4.2.3.)

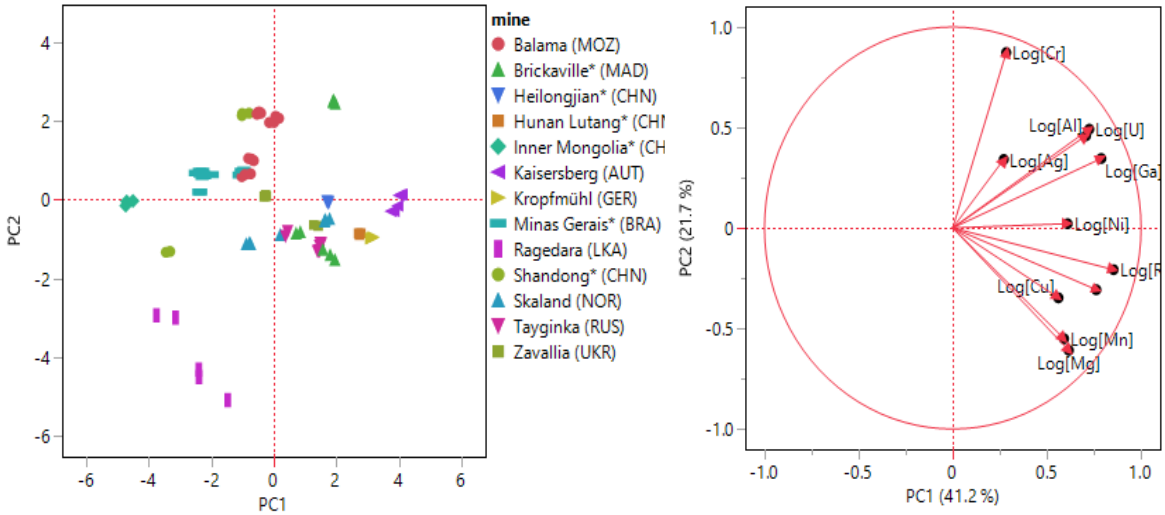


*Figure 87: PCA of solution-ICP-MS trace element data at mine/province level (left) with the indicated elements (right)*

## 6.5. Multi-Parameter Approach

The data generated in this study consist of various types, including compositional trace element data, stable carbon isotope ratios and dimensionless Raman data. For the multi-parameter approach, all data needed to be merged. Since a different number of measurements per sample was available for each method, standardization was necessary. Therefore, a 1:1:1 data fusion strategy was adopted, resulting in one value per sample for each parameter. The carbon isotope mean values, based on at least three measurements per sample, were used and the 10-20 Raman spectra, from which relevant information was extracted, as Raman parameters, were also averaged. Median values from the trace element data were used for each analytical method. This data fusion strategy was utilized for multivariate data analysis, which now includes multiple parameters. In the previous chapters, multidimensional data analyses only considered trace element or Raman data separately. This is an attempt to combine all parameters in a data analysis, since a single parameter, when used individually, could not achieve complete differentiation between the graphite deposits.

Linear discriminant model 1 (Fig. 88) uses the combination of trace element data obtained from solution-based-ICP-MS data with Raman parameters and δ $^{13}$C data. All analyzed trace elements have been selected for this purpose, as well as the Raman parameters related to the G-band (G_STA, G-shape-factor, Gmax, Dmax/Gmax ratio) and the stable carbon isotope ratios. The combination of solution-based-ICP-MS trace element data, selected Raman parameters and $\delta^{13}C$ clearly discriminates locations. Moreover, none of the locations overlap with each other. Balama and Heilongjian are in close proximity to each other and with a greater dispersion of the data, there might be an overlap between these two locations. The results of the trace element analysis using solution-based-ICP-MS show a greater difference in the elemental content between different locations (see grouping 6.4.2.1) and therefore also a larger difference between the individual deposits. Including all three parameters, the individual graphite deposits are clearly distinguishable.

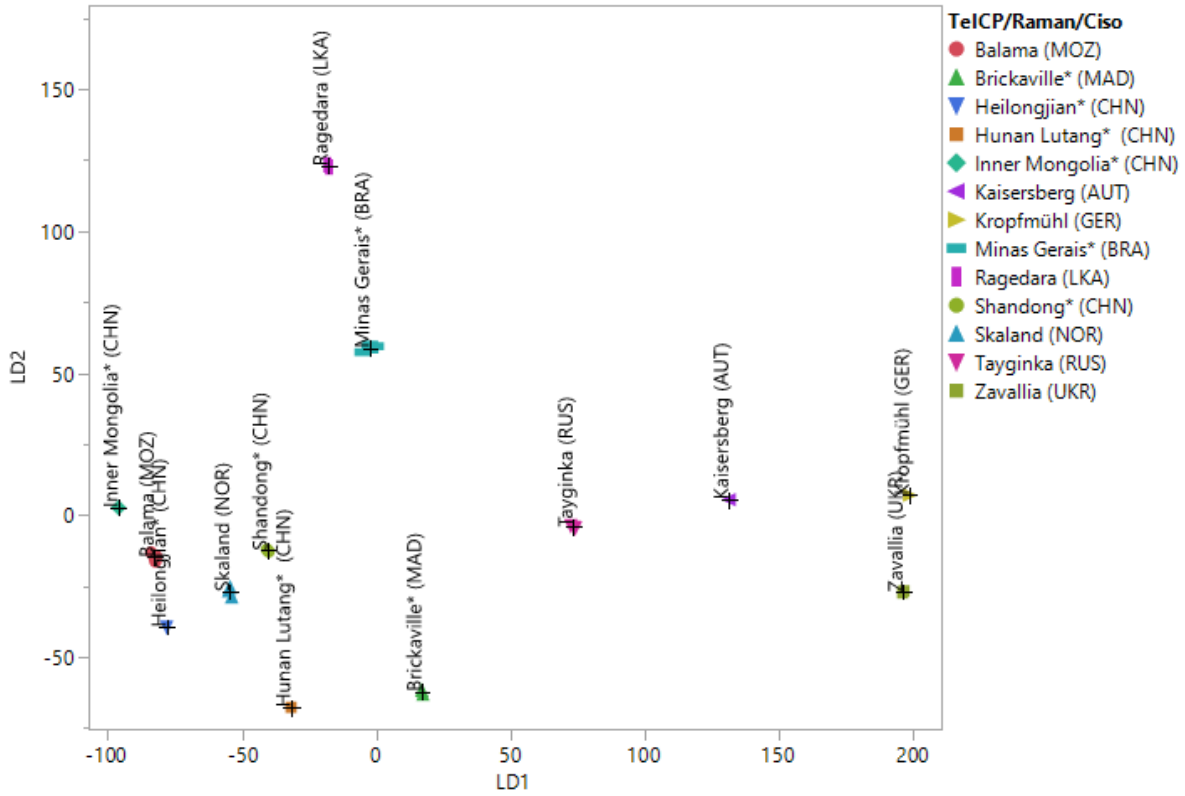


*Figure 88: LDA of trace element data from solution-based-ICP-MS analysis, Raman parameters and $\delta^{13}C$*

Model 2 (Figure 89) uses trace element data obtained from LA-ICP-MS analysis combined with Raman parameters and δ $^{13}$C data. The combination of trace element data from LA-ICP-MS analysis with Raman and δ $^{13}$C does not allow a clear discrimination of all locations. Ragedara and Minas Gerais are in a close proximity to each other, as well as Brickaville, Inner Mongolia and Skaland, but also Kropfmühl, Tayginka, Balama and Shandong.

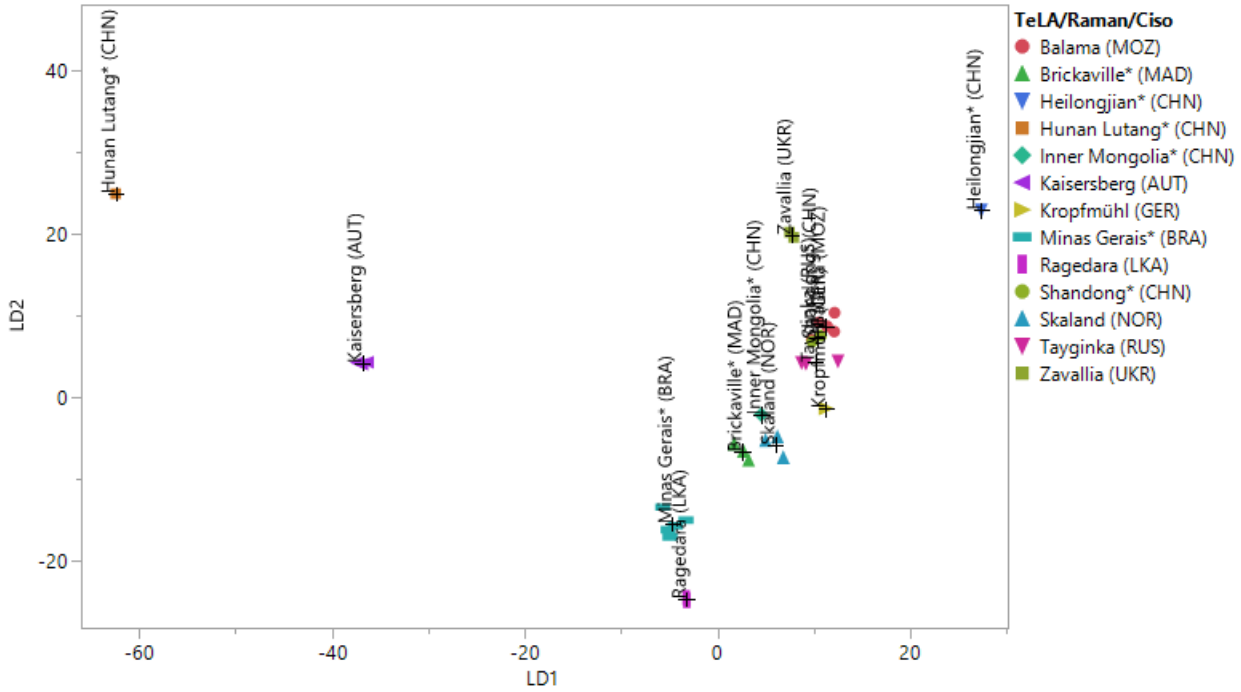


*Figure 89: LDA of trace element data from LA - ICP-MS analysis, Raman parameters and δ13C*

# 7. Discussion

## *7.1.* Stable Carbon Isotope Ratios (δ $^{13}$C)

The δ $^{13}$C values were divided into three major groups (related to the geographic origin): Ukraine, Sri Lanka and RoW (all occurrences except Ukraine and Sri Lanka). The δ $^{13}$C values within the RoW group overlap. The significant difference in the heavy δ$^{13}$C values from Sri Lanka is attributed to the inorganic origin of carbon. Hydrothermal graphite from Sri Lanka typically exhibits a significantly heavier signature (Luque et al. 2014a), than graphite deposits in other countries. Carbon isotope signatures of hydrothermal graphite from Sri Lanka are documented in literature and displayed in Fig. 90.
Reported δ$^{13}$C values for Bogala mine reach from -7.76 ‰ to – 10 ‰ (Touzain 2010, Weis et al, 1981, Dobner, 1978), for Digana mine between -7.6 ‰ and -8.5 ‰ (Binu-Lal et al. 2003; Touzain et al. (2010)) and δ$^{13}$C values for Kahatagaha–Kolongaha mine ranging from -5.61 ‰ to -9.29 ‰ (Weis et al. (1981); Touzain et al. (2010).

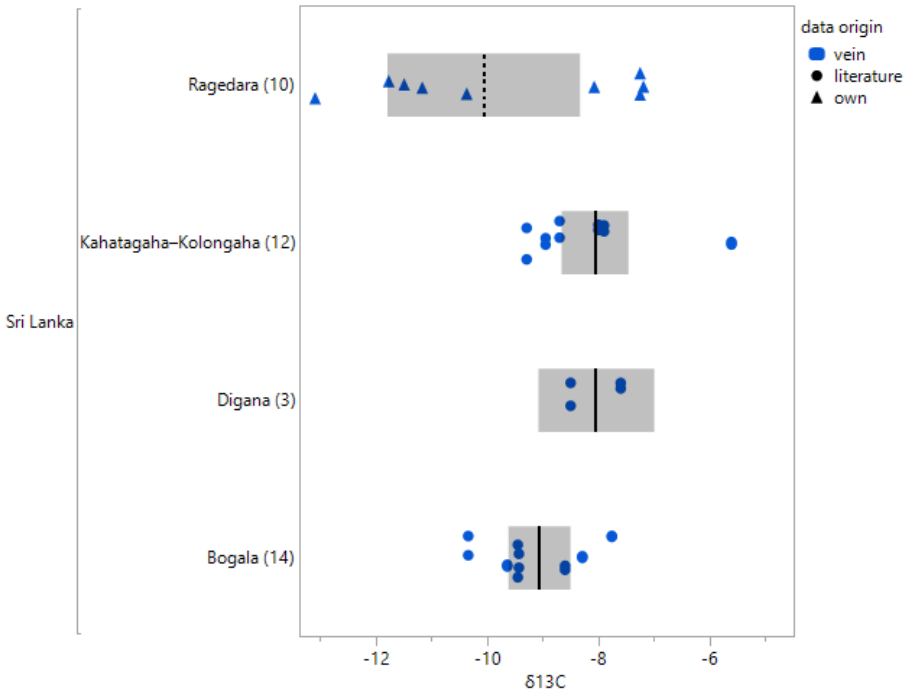


*Figure 90: Carbon isotope values from Sri Lankan graphite deposits, numbers in brackets represent number of available data; vertical line in box represents mean value*

Hydrothermal (vein) graphite from Sri Lanka (Ragedara) thus forms a distinct group for discrimination and is clearly distinguishable.

Within the database and worldwide collection of $\delta^{13}C$ values, more data could be referred to as hydrothermal (vein) graphite. Fig. 91 demonstrates $\delta^{13}C$ values from various hydrothermal graphite types worldwide which all fall within the range of -4.5 ‰ to -17.5 ‰. (references for $\delta^{13}C$ values can be found in the worldwide database table in the appendix)

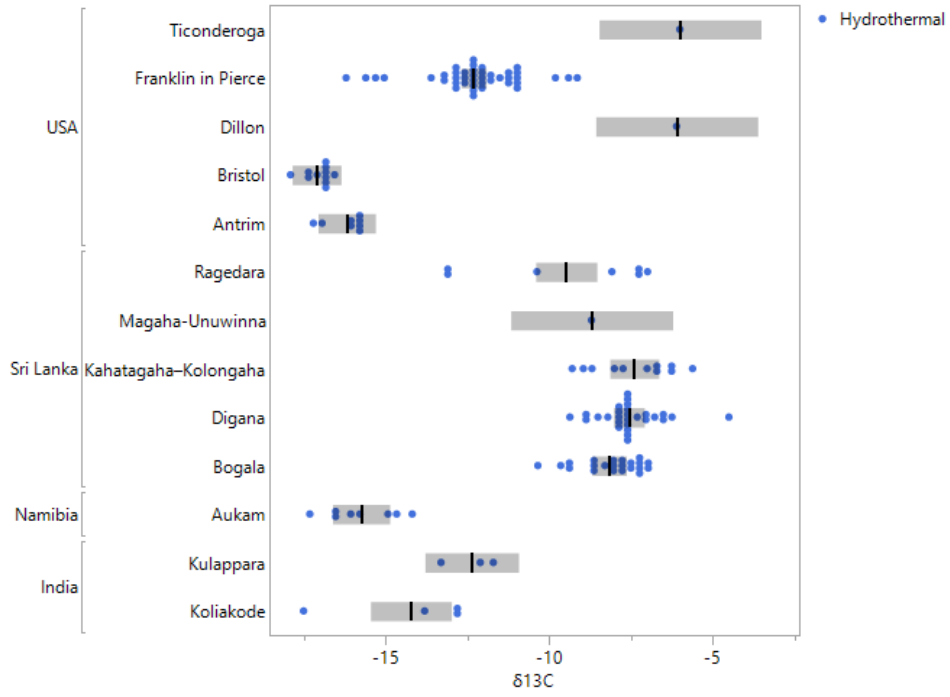


*Figure 91: Stable Carbon isotope values from worldwide hydrothermal graphite deposits (references see worldwide database table in appendix); vertical line in box represents mean value*

Another group that can be clearly discriminated using $\delta^{13}C$ values is Ukraine. These values are consistently very light and are well distinguishable from both RoW (rest of the world) and Sri Lanka. Graphite from Ukraine is considered the geologically oldest graphite (Archean) (Mykhailov, 2020). The source material for this graphite was exclusively organic. However, during this geological era, only very primitive organisms (Prokarya) with a simple metabolism prevailed. These organisms tend to absorb the more abundant $^{12}C$, explaining the light signature of this graphite material. (O Leary, 1992)
The group of samples from Ukraine differs significantly from the other deposits within the own sample collection. Literature $\delta^{13}C$ values for Zavallia, Ukraine range from -35,08 ‰ to -30,50‰ (Lyzhachenko, 2020).
Within the RoW group, more detailed distinctions could not be made. Available $\delta^{13}C$ values from literature confirm the data obtained in this study. All graphite samples from the RoW group are considered as organic material (both amorphous and flake). Within the RoW group, a trend can be observed that can be attributed to different source materials of the graphite (coal- amorphous) and thus different depositional environments.

**Biological isotope fractionation**

Organisms discriminate $^{12}C$ and $^{13}C$ uptake during photosynthetical processes, which reflect metabolic plant reactions, diffusion processes or other biochemical mechanisms and environment (O. Leary, 1992). More developed plants, such as higher land plants, e.g. leaves, roots and plant fragments can take up more $^{13}C$ (because they have a more advanced structure and metabolism) and are therefore more depleted in $^{12}C$. This influences the ratio towards heavier carbon isotope ratios (e.g. amorphous graphite from Kaisersberg originating from coal seams). More primitive organisms, such as prokaryotes and algae do not take up the heavier and less abundant $^{13}C$, but incorporate a higher amount of the more abundant $^{12}C$. Thus, they are enriched in $^{12}C$ ($\delta$ $^{13}C$ towards -35 ‰). This process is also known as biological isotope fractionation, occurring primarily during the photosynthetic process (O Leary, 1992). Vein graphite is clearly distinguishable due to the inorganic source of the material (Fig. 92).

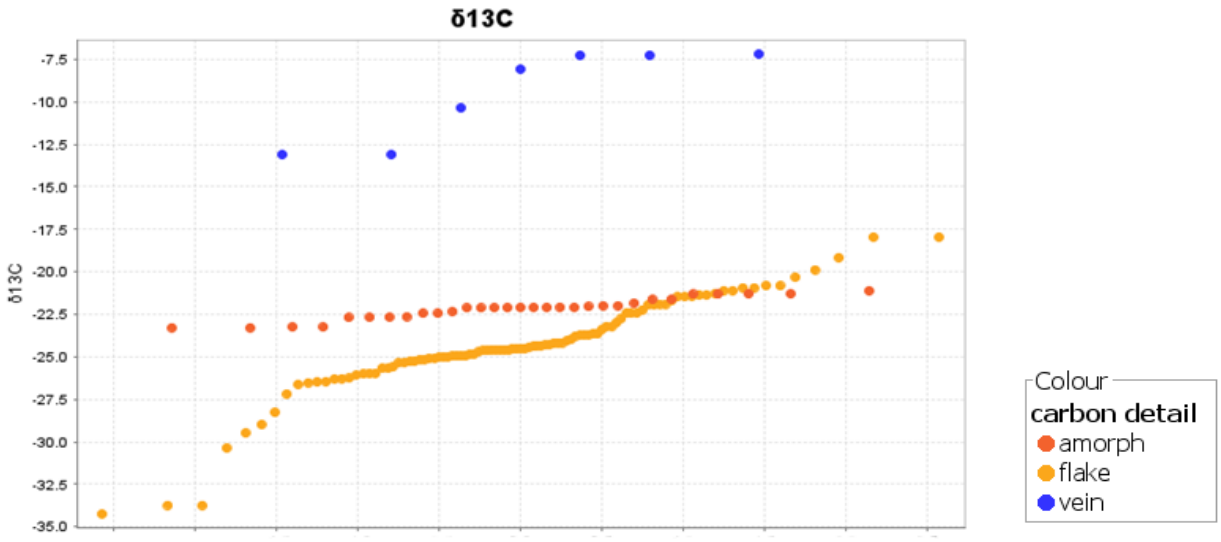


*Figure 92: Probability diagram of carbon isotope ratios divided into three groups based on the information about the graphite type (flake, vein, amorphous)*

**Depositional environment and geological ages**

More advanced life forms occur in a terrestrial environment, while more primitive life forms such as prokaryotes or algae are prevalent in aquatic environments. Where the signatures begin to overlap (at

approximately -22 ‰), a mixed environment can be assumed (e.g., river or limnic). The downward trend is an indicator of a marine deposition environment for the organic source material, while towards higher signatures, especially in amorphous graphite, a terrestrial depositional environment can be inferred. Carbon in non-organic graphite (vein graphite) exhibits a significantly heavier signature, clearly indicating this non-organic carbon and allowing for distinct separation.

The rapid evolution of organisms observed during the Proterozoic resulted in the initial deposition of carbonaceous material in sediments. Most significant carbon-containing material could form within this geological context (Parnell, 2021, Weber 2023). Most samples in this study could be attributed to the Proterozoic. The Great Oxidation Event led to an increase in the concentration of oxygen in the atmosphere and water at the Archean-Proterozoic boundary (Blaustein 2016), which explains the deposition of carbonaceous material in the Proterozoic era and thus assigns most graphite deposits to the Proterozoic.

Fig. 93 shows $\delta^{13}C$ signatures divided into geological ages. The group in the top right corner indicates the inorganic origin of carbon in the samples from Sri Lanka, which are, regardless their geological age, distinguishable. Values in the lower range of the diagram (-28 to -32 ‰) are labelled as Archean, thus representing the oldest graphites in this study. The rest of the data points are attributed to Paleozoic and Proterozoic ages. The Paleozoic graphites in this study are from Kaisersberg. The point in the diagram where Paleozoic values overlap with Proterozoic values can be seen as a change in depositional environments (e.g., marine - limnic - terrestrial) towards heavier values or as a result of the Great Oxidation Event.

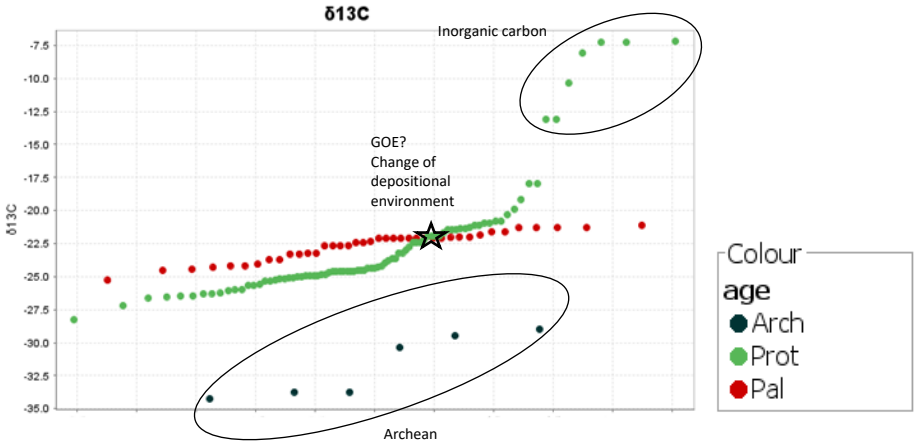


*Figure 93: Probability diagram of carbon isotope values divided into four groups based on their geological ages (Archean – Paleozoic and Proterozoic) and the carbon source (organic vs. inorganic)*

Carbon isotope analysis provides insights into the origin and precursor materials of graphite and consequently, the depositional environment. The parameter only is suitable to a limited extent for identifying the origin of graphite.

The study on graphite samples from Finnish deposits (Aitolampi, Raisjoki, Emas, and Koivuniemi) aimed to demonstrate that carbon isotope values do not undergo significant changes throughout the processing stages from raw ore to concentrates or purified graphite. The signatures do not change along the processing chain. Most of the variability is due to the (spatial) variability within the deposit which may translate into temporal variability over the life of the mine (different areas are mined within the years). The $\delta^{13}C$ values of the Finnish samples range from -25‰ to -32‰, which could overlap with the

$\delta^{13}C$ signature of the Zavallia deposit in Ukraine. The Ukrainian graphite is classified as Archean (Weber 2023), while the Finnish occurrences are classified as Paleoproterozoic (Weber 2023).

## 7.2. Crystallinity and Spectral Data

Raman spectroscopy serves as a standard application for the analysis of graphite, however it can only be used to a very limited extent for the determination of the geographic origin of graphite. A detailed discrimination based on mines/provinces is not feasible. Kaisersberg (Austria) and Hunan Lutang (China) stand out in this regard, both being identified as semi-graphite (amorphous graphite) with a more pronounced D-band and less intense G-band, indicating lower organic maturity of the material and associated lower crystallinity at lower formation temperatures. Other samples exhibit a weaker or almost non-existent D-band, indicating the higher maturity of organic material and the associated higher crystallinity and associated metamorphic temperatures. The crystallinity, especially in flake graphite, is crucial for the specific inherent properties that make this raw material highly demanded, particularly as anode material in the battery production. Hydrothermal graphite from Sri Lanka also shows very weak to no D-band at all and cannot be distinguished from other occurrences (flake graphites) by using Raman spectra only.

The G_STA and G_shape_factors had been identified as the most important variables for discrimination between amorphous graphite and the rest (flake and vein).
This method is not suitable to determine the geographic origin of graphite, but serves as a method to characterize the material and provides information about the type of the graphite material.

No temperature data were derived from the Raman data obtained within this study. The subsequent temperature data are literature values (Tab. 48) and serve as a comparison of the temperature conditions of the occurrences among each other.

*Table 48: Mines/provinces included in this study with respective formation temperatures*

| ***mine/province*** | ***Temperatures (°C)** (from Rantitsch et al., 2016)* |
|---|---|
| *Kaisersberg (AUT)* | *360° - 410°* |
| *Hubei (CHN)* | *700°* |
| *Balama (MOZ)* | *600°-850°* |
| *Minas Gerais (BRA)* | *> 750°* |
| *Taiginka (RUS)* | *650° - 750°* |
| *Inner Mongolia (CHN)* | *860° - 960°* |
| *Heilongjian (CHN)* | *800°- 850°* |
| *Brickaville (MAD)* | *700° - 880 °* |
| *Ragedara (LKA)* | *700° - 830 °* |
| *Zavallia (UKR)* | *640° - 800°* |
| *Kropfmühl (GER)* | *580° – 650°* |
| *Hunan Lutang (CHN)* | *300° – 450°* |
| *Skaland (NOR)* | *> 900°* |
| *Shandong (CHN)* | *< 500°* |

## 7.3. Multi-Element Analysis

**Comparison of trace element data obtained from LA-ICP-MS and solution-based-ICP-MS:**

Trace element data were analyzed using two different analytical methods, yielding non-uniform results. To provide an overview of the comparison of the entire dataset, a summary table was generated (Table 49). This table includes the median element concentrations for each deposit for elements measured by both analytical methods and the comparison factor, which is calculated by dividing the median solution-

based-ICP-MS value by the median LA-ICP-MS value and then collectively summarized to an average factor of comparison for each element. Fig. 94 shows the minimum, maximum and mean comparison factor for each element. The horizontal line indicates the same element concentrations in both analytical methods (e.g. Ga).

Generally, solution ICP-MS data shows higher values than LA-ICP-MS data, except for the values marked in red (in Tab. 49), which include some values for Ga, As, Rb, Zn, and V. Notably, for Cr, the measurements from the LA-ICP-MS analysis are consistently higher than those from solution-based-ICP-MS analysis.

The largest differences in measured values per analytical method and element are observed for Mg, Al, and Fe. For Mg, the average difference from solution-based-ICP-MS values compared to LA-ICP-MS values is 23 times as high, for Al approximately 12 times higher in solution-based-ICP-MS values and for Fe approximately 20 times higher in solution-based-ICP-MS data.

These observations allow the following conclusions for this study:

- Mg, Al and Fe occur in minerals that can be dissolved easily (e.g. silicates)
- Mg, Al and Fe are not distributed homogeneously within the pressed pellet (present in minerals)
- Cr (and Rb) are not soluble
- Ga and As show limited solubility, pointing to different host minerals

*Table 49: Comparison of median trace element data (in $\mu g\ g^{-1}$) obtained from solution-based-ICP-MS and LA-ICP-MS analysis*

| mine/province | Mg | Al | V | Cr | Mn | Fe | Co | Cu | Zn | Ga | As | Rb | Sr |
|---|---|---|---|---|---|---|---|---|---|---|---|---|---|
| S_Kaisersberg (AUT) | 2115.00 | 22449.80 | 21.82 | 21.21 | 162.51 | 11232.20 | 5.97 | 31.12 | 37.40 | 6.66 | 8.96 | 18.02 | 33.64 |
| LA_Kaisersberg (AUT) | 43.47 | 1824.35 | 23.63 | 38.19 | 6.20 | 118.80 | 1.09 | 1.33 | 4.92 | 17.72 | 6.67 | 26.19 | 19.88 |
| factor | 49 | 12 | 0.9 | 0.6 | 26 | 95 | 5 | 23 | 8 | 0.38 | 1.34 | 0.69 | 2 |
| S_Minas Gerais* (BRA) | 22.17 | 2941.37 | 9.26 | 13.34 | 21.40 | 1481.35 | 1.02 | 13.72 | 3.64 | 0.92 | 0.05 | 0.10 | 1.38 |
| LA_Minas Gerais* (BRA) | 1.18 | 355.35 | 4.57 | 30.35 | 7.60 | 128.26 | 0.28 | 4.89 | 1.46 | 0.77 | 0.16 | 0.03 | 0.39 |
| factor | 19 | 8 | 2 | 0.44 | 3 | 12 | 4 | 3 | 3 | 1.2 | 0.32 | 3 | 4 |
| S_Hunan Lutang* (CHN) | 523.93 | 7885.28 | 20.73 | 5.45 | 94.62 | 4213.17 | 5.93 | 25.54 | 31.79 | 3.06 | 65.06 | 18.56 | 24.78 |
| LA_Hunan Lutang* (CHN) | 37.47 | 977.16 | 16.96 | 27.79 | 41.35 | 496.97 | 2.66 | 7.65 | 15.98 | 6.35 | 36.72 | 13.54 | 16.41 |
| factor | 14 | 8 | 1.2 | 0.20 | 2 | 8 | 2 | 3 | 2 | 0.48 | 2 | 1.4 | 2 |
| S_Inner Mongolia* (CHN) | 57.81 | 52.38 | 0.54 | 16.91 | 4.20 | 891.07 | 0.63 | 0.98 | 1.57 | 0.08 | 0.12 | 0.16 | 0.97 |
| LA_Inner Mongolia* (CHN | 2.42 | 2.76 | 0.14 | 30.73 | 0.75 | 41.25 | 0.13 | 0.37 | 0.31 | 0.04 | 0.17 | 0.08 | 0.41 |
| factor | 24 | 19 | 4 | 0.6 | 6 | 22 | 5 | 3 | 5 | 2 | 0.70 | 2 | 2 |
| S_Heilongjian* (CHN) | 642.97 | 3686.97 | 69.12 | 8.97 | 37.50 | 3694.67 | 5.38 | 19.04 | 51.67 | 1.31 | 0.49 | 4.11 | 10.79 |
| LA_Heilongjian* (CHN) | 33.16 | 271.43 | 29.23 | 33.58 | 13.58 | 393.92 | 1.92 | 6.51 | 17.63 | 1.92 | 0.47 | 2.03 | 2.94 |
| factor | 19 | 14 | 2 | 0.27 | 3 | 9 | 3 | 3 | 3 | 0.68 | 1.04 | 2 | 4 |
| S_Shandong* (CHN) | 17.79 | 3298.89 | 70.20 | 27.80 | 4.73 | 5827.27 | 0.26 | 23.52 | 20.39 | 0.77 | 0.35 | 0.24 | 5.94 |
| LA_Shandong* (CHN) | 2.62 | 223.83 | 14.18 | 35.53 | 1.41 | 281.27 | 0.09 | 4.62 | 5.12 | 0.54 | 0.27 | 0.13 | 0.68 |
| factor | 7 | 15 | 5 | 0.8 | 3 | 21 | 3 | 5 | 4 | 1.43 | 1.33 | 2 | 9 |
| S_Kropfmühl (GER) | 4216.92 | 4331.01 | 84.18 | 24.86 | 190.89 | 10822.54 | 6.72 | 305.17 | 19.05 | 2.12 | 0.78 | 21.64 | 3.95 |
| LA_Kropfmühl (GER) | 103.79 | 399.44 | 26.11 | 38.35 | 34.84 | 581.87 | 0.77 | 13.40 | 2.13 | 1.26 | 0.20 | 5.33 | 0.94 |
| factor | 41 | 11 | 3 | 0.65 | 5 | 19 | 9 | 23 | 9 | 2 | 4 | 4 | 4 |
| S_Brickaville* (MAD) | 123.87 | 4643.94 | 54.35 | 5.21 | 61.54 | 4760.54 | 4.56 | 42.55 | 28.20 | 1.57 | 3.11 | 2.61 | 1.50 |
| LA_Brickaville* (MAD) | 3.90 | 368.47 | 9.11 | 26.07 | 13.77 | 276.72 | 0.70 | 5.76 | 5.06 | 0.94 | 0.49 | 0.39 | 0.37 |
| factor | 32 | 13 | 6 | 0.20 | 4 | 17 | 7 | 7 | 6 | 2 | 6 | 7 | 4 |
| S_Balama (MOZ) | 17.60 | 4016.79 | 75.05 | 18.74 | 12.05 | 2639.42 | 0.48 | 19.05 | 29.52 | 1.00 | 0.34 | 0.38 | 6.26 |
| LA_Balama (MOZ) | 1.20 | 290.36 | 27.07 | 36.43 | 4.18 | 153.96 | 0.15 | 5.48 | 11.25 | 1.50 | 0.24 | 0.15 | 1.59 |
| factor | 15 | 14 | 3 | 0.51 | 3 | 17 | 3 | 3 | 3 | 0.67 | 1.44 | 3 | 4 |
| S_Skaland (NOR) | 775.01 | 1539.23 | 11.06 | 7.07 | 25.06 | 3113.59 | 2.94 | 21.03 | 5.27 | 0.71 | 0.12 | 4.94 | 3.83 |
| LA_Skaland (NOR) | 36.91 | 174.92 | 6.96 | 32.82 | 13.95 | 233.61 | 0.62 | 4.82 | 2.22 | 0.92 | 0.12 | 1.81 | 1.76 |
| factor | 21 | 9 | 2 | 0.22 | 2 | 13 | 5 | 4 | 2 | 0.77 | 0.98 | 3 | 2 |
| S_Tayginka (RUS) | 729.98 | 2272.15 | 15.08 | 5.08 | 52.23 | 2735.34 | 1.02 | 229.25 | 25.97 | 0.95 | 0.19 | 3.04 | 3.41 |
| LA_Tayginka (RUS) | 18.92 | 204.57 | 3.14 | 25.75 | 12.27 | 150.23 | 0.27 | 6.80 | 2.63 | 0.64 | 0.16 | 0.68 | 0.86 |
| factor | 39 | 11 | 5 | 0.20 | 4 | 18 | 4 | 34 | 10 | 1.49 | 1.17 | 5 | 4 |
| S_Ragedara (LKA) | 161.99 | 158.05 | 0.12 | 0.36 | 57.29 | 1909.18 | 2.84 | 186.65 | 3.81 | 0.24 | 0.07 | 0.08 | 1.64 |
| LA_Ragedara (LKA) | 9.13 | 43.06 | 1.50 | 43.98 | 9.92 | 359.95 | 2.73 | 29.82 | 13.55 | 1.51 | 1.12 | 0.09 | 1.34 |
| factor | 18 | 4 | 0.08 | 0.01 | 6 | 5 | 1.0 | 6 | 0.28 | 0.16 | 0.06 | 0.89 | 1.2 |
| S_Zavallia (UKR) | 284.29 | 3950.09 | 16.17 | 8.09 | 30.29 | 3179.14 | 0.63 | 15.22 | 18.37 | 1.20 | 1.02 | 1.25 | 2.42 |
| LA_Zavallia (UKR) | 74.86 | 297.77 | 8.41 | 29.33 | 12.30 | 473.67 | 0.47 | 5.81 | 14.61 | 1.30 | 0.84 | 1.08 | 1.54 |
| factor | 4 | 13 | 2 | 0.28 | 2 | 7 | 1.3 | 3 | 1.26 | 0.93 | 1.23 | 1.16 | 2 |
| | | | | | | | | | | | | | |
| mean factor | 23 | 12 | 3 | 0.37 | 5 | 20 | 4 | 9 | 4 | 1.03 | 2 | 3 | 3 |

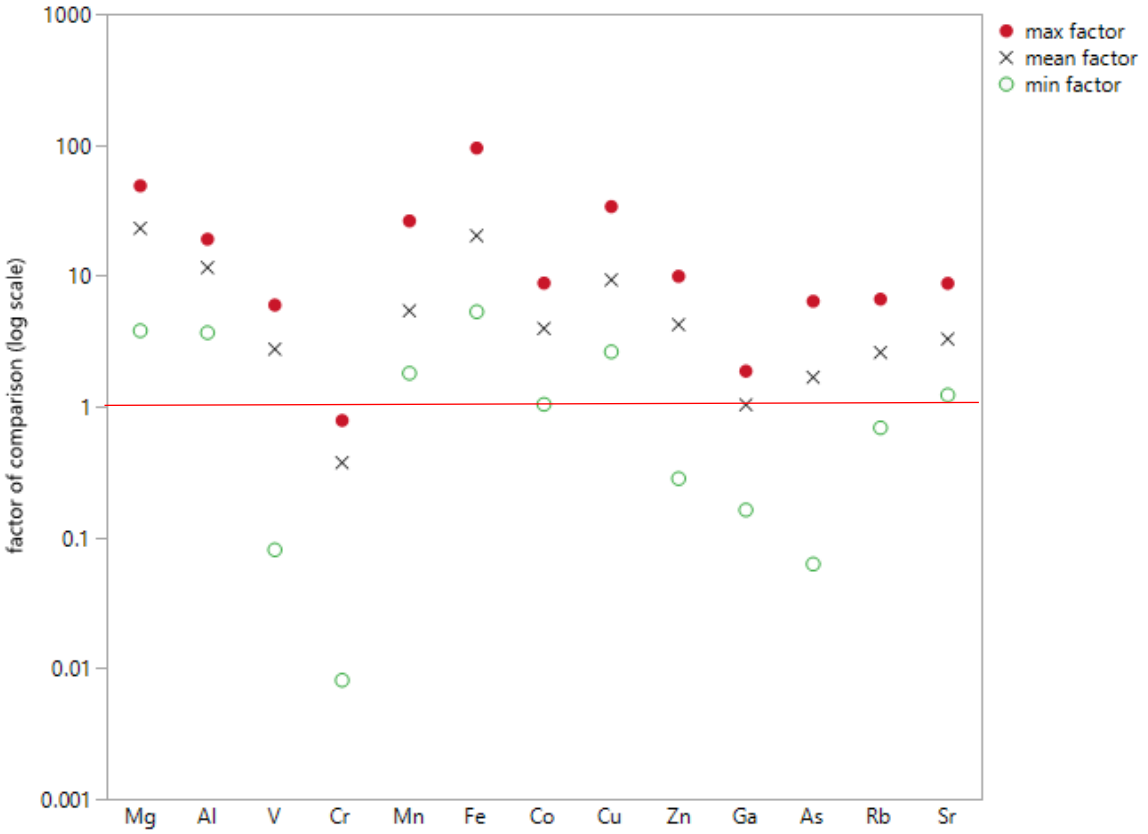


*Figure 94: Factor of comparison (log-scale) for solution-based-ICP-MS data and LA-ICP-MS data indicating minimum, maximum and mean comparison factors (data from Tab. 49)*

The primary difference between the methods are the sample preparation process and the sample condition during analysis. In the solution-based ICP-MS methodology, the digestions were measured, thus the measured fluid was homogeneous, with all dissolved substances present in the solution. This method also offers significantly lower detection limits. Calibration processes especially in the lower range, were feasible and the calibration in general is a standard method. With the availability of various calibration solutions this is a routine application. However, the sample preparation is considerably more complex, consuming more time and resources (personnel, consumables, acids, other). Another factor that must be considered is the current inability to precisely determine what exactly can be leached from the sample material and which elements/minerals may remain as a residue. A significant advantage of this methodology is the high reproducibility of the data. Measurements from each digestion (three digestions were made per sample) show minimal variation and high reproducibility.

The LA-ICP-MS methodology for trace element analysis in graphite proves to be a more time-efficient method, requiring the samples to be pressed into a stable form only. However, sample homogeneity plays a crucial role. Along the measured lines, impurity particles might be measured, likely contributing to the outliers in the data collection. The limits of detection are significantly higher than those in solution-based-ICP-MS analysis. Calibration, especially in the trace element range, is challenging due to the lack of suitable reference and calibration materials. In-house standard materials (provided by GTK) had to be used which were not certified and definitely need more testing and development of the production process of the material. The data are not reproducible to the same extent as the trace element data from ICP-MS analysis, partly because different areas in the pressed sample are analyzed and each area/line shows varying homogeneity. The graphite concentrates currently cannot be considered as routine material and should not be treated with the same ablation parameters as other minerals, likely due to the thermal conductivity of the material, the reaction (absorption and reflection) of the material

to the laser energy and the softness of the graphite material. Overall advantages and disadvantages of each method are summarized in Table 50.

*Table 50: Comparison of solution-based-ICP-MS and LA-ICP-MS method*

| **Solution-based-ICP-MS** | | **LA-ICP-MS** | |
|---|---|---|---|
| **Pro** | **Contra** | **Pro** | **Contra** |
| Availability of reference and calibration materials | Lack of knowledge what is being dissolved | Time efficient and easy sample preparation, reduced risk of contamination | No suitable reference and calibration materials available |
| High sensitivity, low LOD/LOQ | Time-consuming digestion process | Rapid analysis, high sample throughput, if method is developed and applicable | Not widely available |
| Analytical method is a standard application | Potential contamination (through chemicals or other consumables) | In-situ analysis, minimally destructive | Only the surface of the pellet is ablated, the centre of the pellet is not analysed |
| High precision and accuracy of results | Complex sample preparation | High spatial resolution and detailed mapping possible | Inhomogeneous sample material |
| Automated sample introduction | Memory effects | Own reference and calibration materials in production | Low precision of results |

The analyzed elements for the solution-based-ICP-MS analysis are collectively summarized in Fig. 95 and the analyzed element concentrations from the LA-ICP-MS analysis are collectively presented in Fig. 96. The median element concentrations for each element from each location were summarized to a median graphite element content across all locations for solution-based-ICP-MS and LA-ICP-MS values (Tab. 51). The median element concentrations for each location were then normalized to that mean element concentration listed in Tab. 51.

The two diagrams do not exhibit the same element patterns. However, common features between the two figures include generally higher element concentrations in the Kaisersberg, Hunan Lutang, and Kropfmühl provinces. Ragedara shows low V values in the measurements of both methods. Inner Mongolia generally exhibits very low element concentrations in the data from both methods. Ragedara shows high Cu values in both methods.

*Table 51: Average solution-based ICP-MS trace element concentrations (left) and av. LA-ICP-MS trace element concentrations (right) used for normalization of the data for Fig. 95 and Fig. 96*

| Average solution-based-ICP-MS element concentrations (µg $g^{-1}$) | | | Average LA-ICP-MS element concentrations (µg g-1) | |
|---|---|---|---|---|
| **Mg** | 745.33 | | **Mg** | 28.39 |
| **Al** | 4709.69 | | **Al** | 417.96 |
| **V** | 34.44 | | **Ca** | 23.10 |
| **Cr** | 12.54 | | **V** | 13.15 |
| **Mn** | 58.02 | | **Cr** | 32.99 |
| **Fe** | 4346.11 | | **Mn** | 13.24 |
| **Co** | 2.95 | | **Fe** | 283.88 |
| **Ni** | 10.49 | | **Co** | 0.91 |
| **Cu** | 71.76 | | **Cu** | 7.48 |
| **Zn** | 21.28 | | **Zn** | 7.45 |
| **Ga** | 1.58 | | **Ga** | 2.72 |
| **As** | 6.21 | | **As** | 3.66 |
| **Se** | 1.73 | | **Rb** | 3.96 |
| **Rb** | 5.78 | | **Sr** | 3.78 |
| **Sr** | 7.73 | | **Y** | 0.98 |
| **Mo** | 19.43 | | **Zr** | 3.58 |
| **Ag** | 0.27 | | **Ce** | 1.68 |
| **Cd** | 0.22 | | **Th** | 0.30 |
| **Ba** | 16.46 | | **U** | 0.28 |
| **Tl** | 0.08 | | | |
| **Pb** | 7.30 | | | |
| **Ce** | 12.42 | | | |
| **Th** | 1.97 | | | |
| **U** | 0.91 | | | |

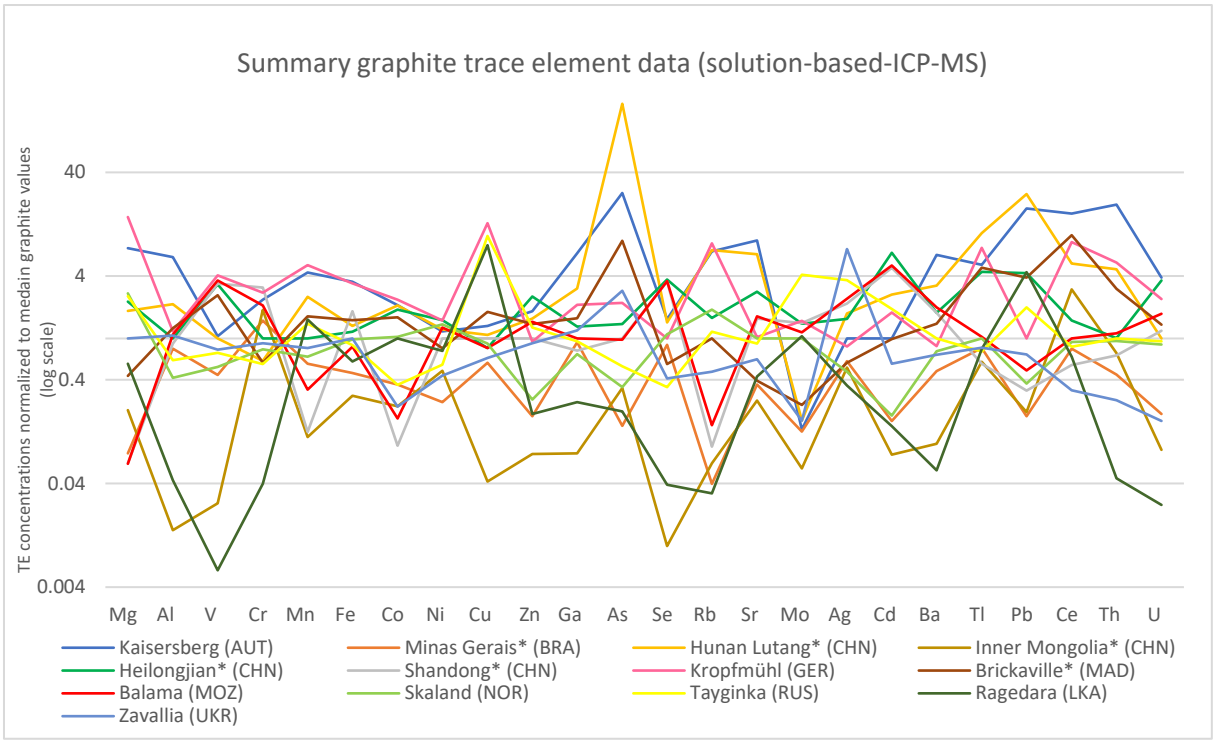


*Figure 95: Summary of graphite trace element data obtained from solution-based-ICP-MS analysis*

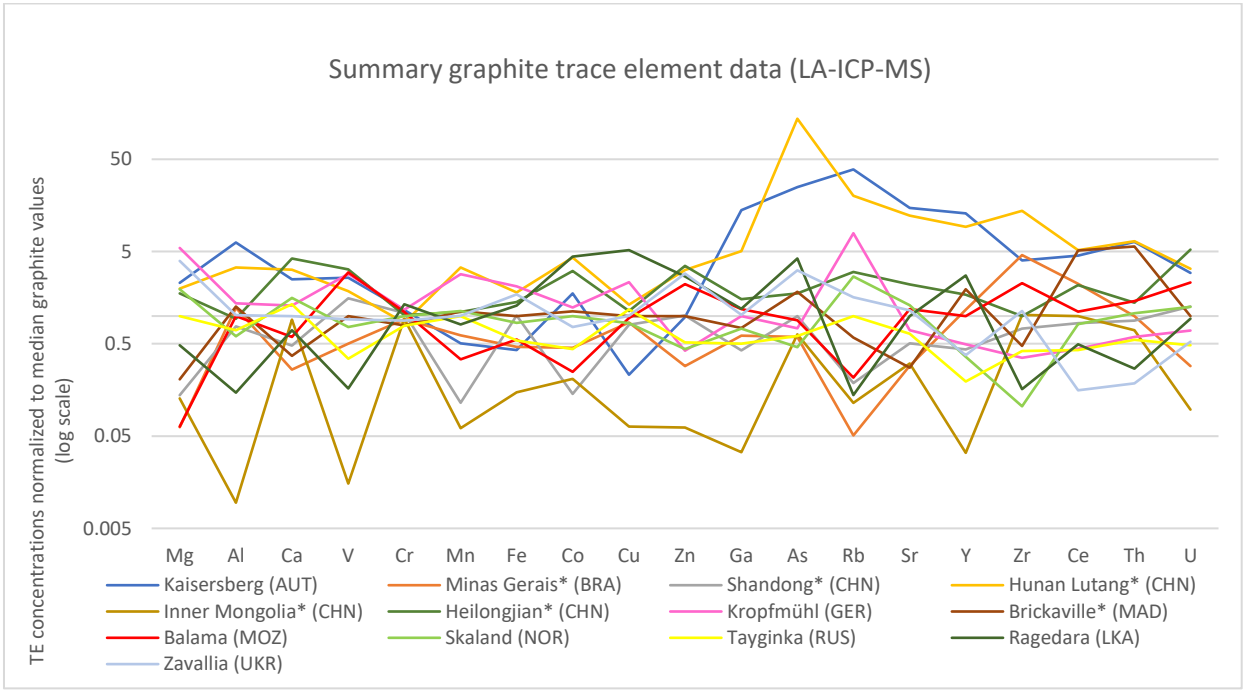


*Figure 96: Summary of graphite trace element data obtained from LA-ICP-MS analysis*

**Comparison of trace elements (based on solution-based-ICP-MS data):**

For the description and comparison of trace elements, data from solution-based-ICP-MS analysis was used due to lower dispersion and higher reproducibility of the data.

Magnesium, Al, and Fe are typical elements found in high concentrations and are bound to accessory minerals.

Vanadium: Inner Mongolia and Ragedara differ significantly from the V content of other occurrences, due to their low V content. Vanadium is considered a biophilic element that tends to accumulate in organic source materials (Schroll 1976). The hydrothermal graphite sample from Ragedara (LKA) exhibits the lowest V content (0.1 µg $g^{-1}$). Kropfmühl (GER) (84 µg $g^{-1}$) and Balama (MOZ) (75 µg $g^{-1}$) exhibit the highest values.

Chromium: The Ragedara mine is also distinguishable from the rest of the deposits due to its low Cr content (0.4 µg $g^{-1}$) compared to other locations. Shandong (27 µg $g^{-1}$) and Kropfmühl (24 µg $g^{-1}$) show the highest Cr values. Despite being both amorphous, Kaisersberg and Hunan Lutang exhibit different values of 21 µg $g^{-1}$ (Kaisersberg) and only 5 µg $g^{-1}$ (Hunan Lutang). According to Schroll (1976), Cr is bound to the lattice of the graphite.

Manganese: Shandong and Inner Mongolia (4 µg $g^{-1}$) have the lowest Mn contents among the locations. Kaisersberg and Hunan Lutang have high Mn contents, which can be attributed to impurities and lower carbon content compared to other samples. However, the sample from Kropfmühl contains even higher Mn contents. Mn might be bound to Mg and therefore associated with carbonates.

Iron: Inner Mongolia (891 µg $g^{-1}$) shows the lowest Fe concentrations, Kaisersberg (1.1 %) and Kropfmühl (1.08 %) the highest concentrations.

Cobalt: Cobalt values reach from very low values in Shandong (0.26 µg $g^{-1}$) to values up to 6.7 µg $g^{-1}$in Kropfmühl.

Nickel: Minas Gerais (2.6 µg $g^{-1}$) and Zavallia (4.8 µg $g^{-1}$) show the lowest Ni content of all graphite deposits in this study. Higher Ni values are associated with amorphous graphite, which generally contain the most impurities, but flake type graphite from Heilongjian (16.6 µg $g^{-1}$) and Kropfmühl (16.5 µg $g^{-1}$) show highest Ni values.

Copper: Inner Mongolia shows very low Cu contents (1 µg $g^{-1}$). Kropfmühl has the highest Cu contents (305 µg $g^{-1}$). The otherwise trace element-poor hydrothermal graphite from Ragedara also has high Cu contents, confirming that ash-free graphites are generally richer in copper (Janda & Schroll 1960).

Zinc: Inner Mongolia has the lowest Zn contents (1 µg $g^{-1}$). Heilongjian has the highest value (51 µg $g^{-1}$), followed by the impure amorphous graphite (Kaisersberg (37 µg $g^{-1}$) and Hunan Lutang (31 µg $g^{-1}$).

Gallium: Inner Mongolia (0.08 µg $g^{-1}$) and Ragedara (0.2 µg $g^{-1}$) clearly differentiate with the lowest Ga contents among the occurrences. Kaisersberg (6 µg $g^{-1}$) and Hunan Lutang (3 µg $g^{-1}$) show the highest values.

Selenium: The lowest values are found in Inner Mongolia (0.01 µg $g^{-1}$), followed by Ragedara (0.04 µg $g^{-1}$). Balama, Heilongjian and Shandong (4 µg $g^{-1}$) refer to the highest Se values.

Rubidium: Amorphous graphite (Kaisersberg and Hunan Lutang) has the highest values for this element (18 µg $g^{-1}$). Very low values are found in Minas Gerais (0.1 µg $g^{-1}$), Inner Mongolia (0.16 µg $g^{-1}$), Shandong (0.2 µg $g^{-1}$), Ragedara (0.08 µg $g^{-1}$), and Balama (0.3 µg $g^{-1}$).

Strontium: Minas Gerais (1.5 µg $g^{-1}$) and Inner Mongolia (0.9 µg $g^{-1}$) have the lowest contents, while Kaisersberg (33 µg $g^{-1}$) and Hunan Lutang (24 µg $g^{-1}$) show the highest values.

Molybdenum: A reversed pattern is observed for Mo. Tayginka has the highest contents of this element (84 µg $g^{-1}$), followed by Kropfmühl (29 µg $g^{-1}$), Shandong, and Heilongjian (28 µg $g^{-1}$). Schroll (1976) describe Mo as a characteristic trace element for graphite.

Silver: Highest silver values can be found in Zavallia (1 µg $g^{-1}$), compared to very low values in the Ragedara mine (0.05 µg $g^{-1}$).

Cadmium: Heilongjian (0.7 µg $g^{-1}$), Shandong, and Balama (0.5 µg $g^{-1}$) show the highest Cd values, while Inner Mongolia shows the lowest Cd values of all deposits (0.08 µg $g^{-1}$).

Barium: Ragedara mine shows the lowest Ba values (0.5 µg $g^{-1}$), as well as Inner Mongolia with 1 µg $g^{-1}$. Highest Ba values can be associated with Kaisersberg (66 µg $g^{-1}$) and Hunan Lutang (33 µg $g^{-1}$), both amorphous graphites.

Thallium: Generally, values for this element are very low with highest Tl values for Hunan Lutang (0.2 µg $g^{-1}$) and lowest values for Shandong (0.01 µg $g^{-1}$).

Lead: Amorphous graphite (Kaisersberg 28 µg $g^{-1}$) and Hunan Lutang (38 µg $g^{-1}$) are associated with high Pb levels, whereas Inner Mongolia (0.3 µg $g^{-1}$), Shandong (0.4 µg $g^{-1}$) and Skaland (0.5 µg $g^{-1}$) show low Pb levels.

Yttrium: The highest Y values are associated with Kaisersberg (12 µg $g^{-1}$) and Kropfmühl (11 µg $g^{-1}$). Inner Mongolia (0.08 µg $g^{-1}$) shows the lowest Y values. Most locations show Y values in the range of 1 to 2 µg $g^{-1}$.

Thorium: Kaisersberg (13 µg $g^{-1}$) is associated with the highest Th values, followed by Hunan Lutang and Kropfmühl (3 µg $g^{-1}$). Very low Th values (0.02 µg $g^{-1}$) are present in samples from Ragedara mine.

Uranium: Higher U values are associated with Kaisersberg (2.6 µg $g^{-1}$) and Heilongjian (2.4 µg $g^{-1}$) and low U values with Ragedara (0.01 µg $g^{-1}$).

Based on the scoring coefficients from LDA performed in chapter 6.4.2.4.1. and the assessment of the individual element values compared to each deposit the following elements could be identified as key elements for the discrimination of graphite deposits: **Mg, Al, V, Fe, Ga, Sr, Ag, Cd, U.**

**Comparison REE patterns:**

REE patterns of all locations differ from each other. Only Kaisersberg and Kropfmühl exhibit similarities. The individual patterns of each sample from Kaisersberg, Minas Gerais, Balama, Zavallia, and Ragedara, are very similar within the location, indicating little variability in the deposit, possibly also similar mining areas. The two individual samples from the Shandong province are distinct from each other. Also, one (sample 2B) of three available samples from the Skaland mine shows a different pattern. Sample 2B was collected before 2019, which could be an indication of a different mining area. For the Tayginka deposit, two samples show a positive Eu anomaly and one sample shows a negative Eu anomaly, which could also suggest different mining areas within the deposit. The comparison of REE patterns allows conclusions about the homogeneity of the deposit, meaning they are difficult to contaminate by sample preparation or similar processes. Normalizing the data resulted in smooth patterns that exclusively exhibit positive or negative anomalies. Anomalies could originate from fractionation due to variations in redox conditions during geochemical or biochemical cycles or from anthropogenic influences and contamination (e.g. dust) within the raw material processing.

## 7.4. Multi-Parameter Approach

Various parameters were tested for the development of an analytical proof of origin for natural graphite deposits. The analytical methods generated individual parameters, which, in a multidimensional model, allow to distinguish individual locations. Utilizing different parameters, such as carbon isotopes, crystallinity and trace elements, increases the number of individual variables for multivariate data analysis. The multi-parameter approach enables greater differentiability of the data, compared to uni- or bivariate data analysis. Crystallinity, measured by Raman spectroscopy mainly refers to the carbon type (amorphous/flake/vein). Carbon isotopes enable differentiation into groups related to the genesis and the geographic origin (Ukraine, Sri Lanka and rest of the world) but are not capable of distinguishing at the level of individual mines/provinces. Trace element data, obtained from both, ICP-MS and LA-ICP-MS does not allow a clear differentiation of mines/provinces, but allows for the highest individual level of differentiability, if combined with crystallinity data. In general, trace element data from ICP-MS shows a clearer differentiation of individual mines/provinces compared to data from LA-ICP-MS. Trace element data obtained from ICP-MS, when combined with the stable carbon isotope ratios, also demonstrates complete differentiation of individual graphite deposits, whereas trace element data obtained from LA-ICP-MS, along with stable carbon isotope data, exhibits overlaps in some occurrences. When all three parameters are combined, the results with trace element data from ICP-MS show a better outcome in terms of differentiation, compared to the multivariate analysis of all parameters, including trace element data from LA-ICP-MS. For the development of an analytical proof of origin (APO) for natural graphite, it made sense to use and analyze all three parameters. For a graphite APO database intended for comparing unknown graphite samples to, all three parameters should be analyzed and taken record of in the database.

## 7.5. Test Run with Unknown Samples

To verify and test the developed methodology with unknown samples, the attributes related to the origin were removed from three graphite samples in the present study. The identity of the samples only consisted of the Sample ID, along with the trace element data from the solution-based-ICP-MS analysis, stable carbon isotopes and Raman parameters.

Row 3 (in Fig. 97) represents Sample 21N from Minas Gerais (BRA). The study includes four more samples from this deposit. Row 17 (in Fig. 97) represents Sample 21B from Balama (MOZ). The study includes five more samples from this origin. Row 26 (in Fig. 97) represents Sample 4B from Zavallia (UKR). The study only contains one more sample from this deposit.

Through LDA, Sample 21N could be assigned to the correct origin (Minas Gerais, BRA) with 100% probability (Fig. 97 right column and Fig. 98). Sample 21B from Balama (MOZ) could only be assigned to the correct origin with 42 % probability, with 58 % of the probability for the wrong origin (Shandong) (Fig. 97 and 98). Sample 4B (Zavallia) in row 26 was assigned to a wrong origin (Brickaville, MAD) with 100 % probability (Fig. 97). The data basis and multiple samples from one origin (deposit/mine) are thus essential to assign unknown samples to an origin in the database. If a deposit is not stored in the database, it is also impossible to assign an unknown sample to that origin. APO databases constantly need to be enlarged and updated.

| | | | | | |
|---|---|---|---|---|---|
| 1 | ICP-MS | 1A | Kaisersberg (AUT) | Austria |
| 2 | ICP-MS | 21C | Minas Gerais* (BRA) | Brazil |
| X 3 | ICP-MS | 21N | | |
| 4 | ICP-MS | 3B | Minas Gerais* (BRA) | Brazil |
| 5 | ICP-MS | 21M | Minas Gerais* (BRA) | Brazil |
| 6 | ICP-MS | 22C | Minas Gerais* (BRA) | Brazil |
| 7 | ICP-MS | 21A | Shandong* (CHN) | China |
| 8 | ICP-MS | 22A | Shandong* (CHN) | China |
| 9 | ICP-MS | 4A | Hunan Lutang* (CHN) | China |
| 10 | ICP-MS | 6B | Inner Mongolia* (CHN) | China |
| 11 | ICP-MS | 7B | Heilongjian* (CHN) | China |
| 12 | ICP-MS | 13B | Kropfmühl (GER) | Germany |
| 13 | ICP-MS | 21D | Brickaville* (MAD) | Madagascar |
| 14 | ICP-MS | 11B | Brickaville* (MAD) | Madagascar |
| 15 | ICP-MS | 22D | Brickaville* (MAD) | Madagascar |
| 16 | ICP-MS | 1B | Balama (MOZ) | Mozambique |
| X 17 | ICP-MS | 21B | | |
| 18 | ICP-MS | 21J | Balama (MOZ) | Mozambique |
| 19 | ICP-MS | 21K | Balama (MOZ) | Mozambique |
| 20 | ICP-MS | 21L | Balama (MOZ) | Mozambique |
| 21 | ICP-MS | 22B | Balama (MOZ) | Mozambique |
| 22 | ICP-MS | 15B | Skaland (NOR) | Norway |
| 23 | ICP-MS | 2B | Skaland (NOR) | Norway |
| 24 | ICP-MS | 22G | Skaland (NOR) | Norway |
| 25 | ICP-MS | 22F | Zavallia (UKR) | Ukraine |
| X 26 | ICP-MS | 4B | | |

| Zeile | Beobachtet | Qu.Dist.(Beobachtet) | Wahrsch.(Beobachtet) | -Log(Wahrsch.) | Vorhersage | Wahrsch.(Vorhers.) | Sonstige |
|---|---|---|---|---|---|---|---|
| 1 | Kaisersberg (AUT) | 2.274e-13 | 1.0000 | 0.000 | Kaisersberg (AUT) | 1.0000 | |
| 2 | Minas Gerais* (BRA) | 11.2500 | 1.0000 | 0.000 | Minas Gerais* (BRA) | 1.0000 | |
| 3 | | | | | - Minas Gerais* (BRA) | 1.0000 | |
| 4 | Minas Gerais* (BRA) | 11.2500 | 1.0000 | 0.000 | Minas Gerais* (BRA) | 1.0000 | |
| 5 | Minas Gerais* (BRA) | 11.2500 | 1.0000 | 0.000 | Minas Gerais* (BRA) | 1.0000 | |
| 6 | Minas Gerais* (BRA) | 11.2500 | 1.0000 | 0.000 | Minas Gerais* (BRA) | 1.0000 | |
| 7 | Shandong* (CHN) | 7.5000 | 0.9805 | 0.020 | Shandong* (CHN) | 0.9805 | |
| 8 | Shandong* (CHN) | 7.5000 | 1.0000 | 0.000 | Shandong* (CHN) | 1.0000 | |
| 9 | Hunan Lutang* (CHN) | 9.095e-13 | 1.0000 | 0.000 | Hunan Lutang* (CHN) | 1.0000 | |
| 10 | Inner Mongolia* (CHN) | -2.27e-13 | 1.0000 | 0.000 | Inner Mongolia* (CHN) | 1.0000 | |
| 11 | Heilongjian* (CHN) | 2.842e-14 | 1.0000 | 0.000 | Heilongjian* (CHN) | 1.0000 | |
| 12 | Kropfmühl (GER) | 2.274e-13 | 1.0000 | 0.000 | Kropfmühl (GER) | 1.0000 | |
| 13 | Brickaville* (MAD) | 10.0000 | 1.0000 | 0.000 | Brickaville* (MAD) | 1.0000 | |
| 14 | Brickaville* (MAD) | 10.0000 | 1.0000 | 0.000 | Brickaville* (MAD) | 1.0000 | |
| 15 | Brickaville* (MAD) | 10.0000 | 1.0000 | 0.000 | Brickaville* (MAD) | 1.0000 | |
| 16 | Balama (MOZ) | 12.0000 | 1.0000 | 0.000 | Balama (MOZ) | 1.0000 | |
| 17 | | . | . | . | - Shandong* (CHN) | 0.5820 | Balama (MOZ) 0.42 |
| 18 | Balama (MOZ) | 12.0000 | 0.9963 | 0.004 | Balama (MOZ) | 0.9963 | |
| 19 | Balama (MOZ) | 12.0000 | 1.0000 | 0.000 | Balama (MOZ) | 1.0000 | |
| 20 | Balama (MOZ) | 12.0000 | 0.9996 | 0.000 | Balama (MOZ) | 0.9996 | |
| 21 | Balama (MOZ) | 12.0000 | 0.9978 | 0.002 | Balama (MOZ) | 0.9978 | |
| 22 | Skaland (NOR) | 10.0000 | 1.0000 | 0.000 | Skaland (NOR) | 1.0000 | |
| 23 | Skaland (NOR) | 10.0000 | 1.0000 | 0.000 | Skaland (NOR) | 1.0000 | |
| 24 | Skaland (NOR) | 10.0000 | 1.0000 | 0.000 | Skaland (NOR) | 1.0000 | |
| 25 | Zavallia (UKR) | 0.0000 | 1.0000 | 0.000 | Zavallia (UKR) | 1.0000 | |
| 26 | | . | . | . | - Brickaville* (MAD) | 1.0000 | |
| 27 | Tayginka (RUS) | 10.0000 | 1.0000 | 0.000 | Tayginka (RUS) | 1.0000 | |
| 28 | Tayginka (RUS) | 10.0000 | 1.0000 | 0.000 | Tayginka (RUS) | 1.0000 | |
| 29 | Tayginka (RUS) | 10.0000 | 1.0000 | 0.000 | Tayginka (RUS) | 1.0000 | |
| 30 | Ragedara (LKA) | 7.5000 | 1.0000 | 0.000 | Ragedara (LKA) | 1.0000 | |
| 31 | Ragedara (LKA) | 7.5000 | 1.0000 | 0.000 | Ragedara (LKA) | 1.0000 | |

*Figure 97: Test run with unknown samples (row 3, 17 and 26) left and estimated probabilities for the origin right*

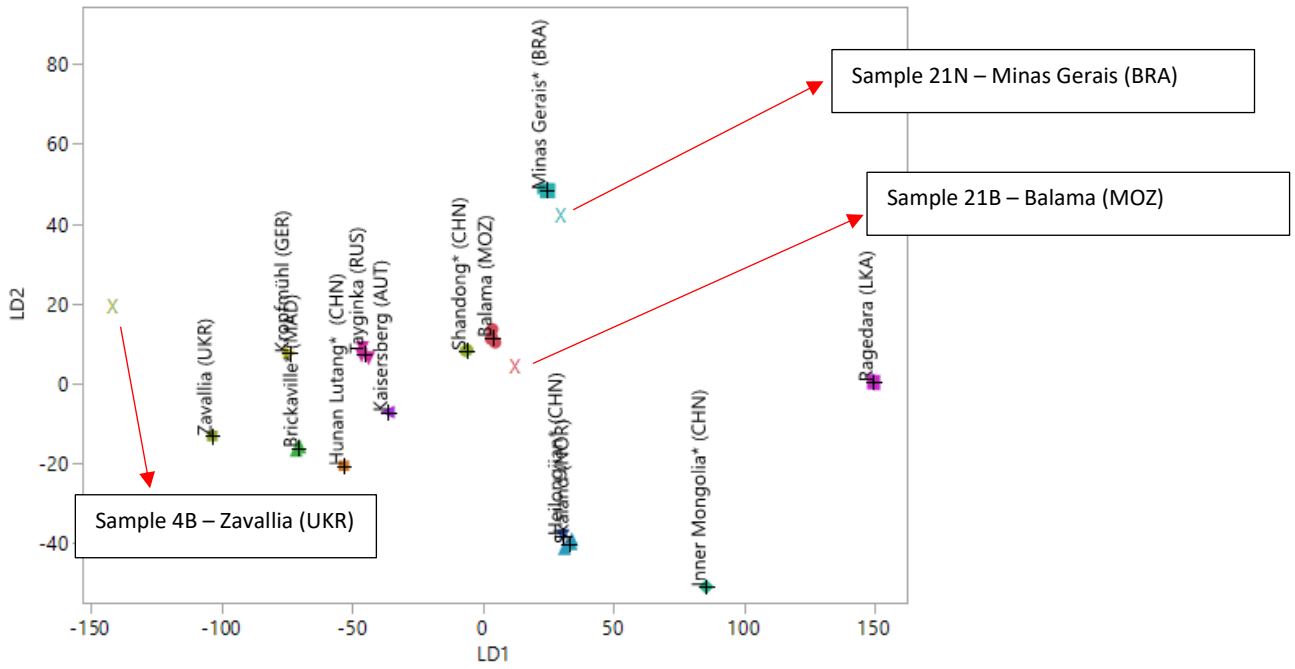


*Figure 98: Graphical presentation of unknown samples (X) related to their origin*

# 8. Conclusion and Perspectives

## 8.1. Analytical Method Evaluation – A Traffic Light System Perspective

The applied analytical methods used for the Analytical Proof of Origin (APO) for graphite are rated using a traffic light system to classify them into three performance levels (green: good/preferred, yellow: moderate/caution, red: poor/not recommended).

The rated categories are the following:

**1. Differentiating Power:** How meaningful are the results and to what extent can individual locations/origins be distinguished? Can specific deposits be identified, or can only broad categories (e.g. carbon type) be defined?

**2. Simplicity/Sample Throughput:** How straightforward is the method in its application and how many samples can be processed? How labor-intense is the sample preparation?

**3. Accessibility:** How accessible are the laboratory methods or laboratory equipment in general? This needs to be kept in mind for laboratories and analyses especially on processing sites and export hubs in developing countries. Does it require cleanrooms or certified laboratory facilities? Can the analysis also be conducted using portable devices? What about required gases and acids?

**4. Cost:** How cost-intense is the methodology? What is the acquisition, maintenance, and operational cost of the laboratory equipment?

The main factors considered are costs and simplicity/sample throughput.

| Carbon isotopes | | | |
|---|---|---|---|
| differentiating power | simplicity/sample throughput | accessibility | cost |

*Figure 99: Traffic light system for carbon isotopes*

The analysis of carbon isotopes is rated yellow for the categories of differentiating power, simplicity/sample throughput and cost, and red for the category of the accessibility (Fig. 99). None of the categories are marked in green. The differentiation power is limited to interpretations about the localities concerning Sri Lanka, Ukraine and "rest of the world". The methodology is complex, both in sample preparation and measurement, requiring high-end laboratory equipment with gas supply and exhaust. This laboratory equipment is only available in specialized laboratories. The costs are correspondingly high due to the sample preparation and measurement duration.

| Structure and Crystallinity | | | |
|---|---|---|---|
| differentiating power | simplicity/sample throughput | accessibility | cost |

*Figure 100: Traffic light system for structure and crystallinity*

The structural analysis is rated yellow for the category of differentiating power and green for the remaining categories of simplicity/sample throughput, cost and accessibility. (Fig. 100). The differentiating power is limited to the graphite type (amorphous, flake, hydrothermal type). HR Raman Spectroscopy can be performed fast and many samples can be analyzed in a short time. The methodology is available as a portable device also and in terms of handling, it requires no special preparation of the

sample. A high sample throughput is possible and the resulting costs are therefore reasonable and rated as green.

| Trace elements | | | |
|---|---|---|---|
| differentiating power | simplicity/sample throughput | accessibility | cost |

*Figure 101: Traffic light system for trace elements*

Trace element analysis using (LA)-ICP-MS exhibits a different pattern. The differentiating power is rated as green, allowing the differentiation of individual deposits. The rest of the categories remain yellow. The simplicity/sample throughput is moderate and the sample preparation is moderately complex (Fig. 101). The access to this laboratory methodology is limited and requires well-equipped facilities. The resulting costs are moderate due to the relatively large sample throughput. Acquiring trace elements using LA-ICP-MS in general is much less complicated and requires no special sample preparation (only pressing of the material), compared to solution analysis using ICP-MS, making it preferable for the determination of trace elements in graphite.

As a result, trace element analysis is identified as the method with the most significant information regarding the origin, with moderate assessments in the remaining categories of simplicity/sample throughput, accessibility and cost.

## 8.2. Feasibility and Costs

During the Analytical Proof of Origin (APO) study for graphite, the question of the costs associated and the applicability of this traceability method in the industry arose more frequently. For industrial applications, handheld options are best suited, which are quick and easy to apply directly at the site, without the need for advanced sample preparation, especially without trained personnel and expensive laboratory facilities. Currently it is not feasible to use portable methods for this application. This presented study on method development for an Analytical Proof of Origin (APO) for graphite is only a first step in the application of traceability through laboratory methods.

The APO can only be applied in special cases and does not constitute a routine method for everyday use. However, it is a method directly related to the raw material, making it highly tamper-resistant.

## 8.3. Conclusion

To conclude this study, a fish bone diagram, or cause and effect diagram or Ishikawa Diagram is used to organize information to see and understand various factors influencing the Analytical Proof of Origin (for graphite) (Fig. 102).

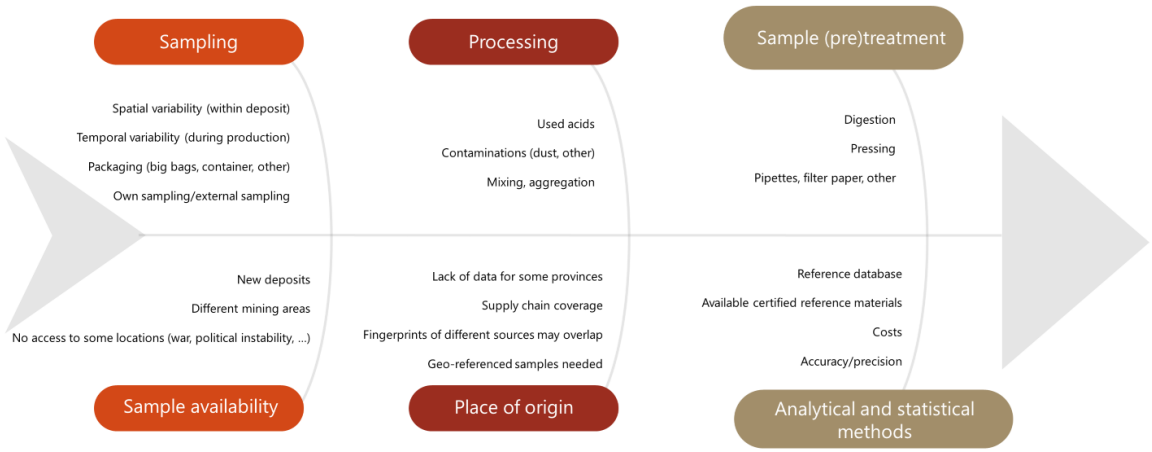


*Figure 102: Cause and effect diagram APO Method for Graphite*

An essential point at the beginning of the APO process is the availability of samples to conduct fingerprinting studies. Various areas of a deposit need to be covered to represent the spatial variability within the mine/deposit. Also, different sections of a deposit are mined and processed over time (temporal variability). New deposits (currently mostly in Europe and Canada) are also being developed, contributing to the diversification of global production, especially in the coming years due to increasing demand and the desire for a reduced dependence on China. The database needs to be kept up-to-date and new locations must be analyzed and documented. Some production locations are no longer accessible due to war and political instabilities, or production may be halted or exports restricted (see current situation in Ukraine and Russia).

The sampling process heavily relies on the availability of samples and the person taking samples. Efforts should always be made to achieve a representative sampling strategy. In many cases, sampling is conducted externally. Sampling also involves the process of mixing material from mining in the processing plant and determining which concentrate (quality) from the processing plant is filled into a big bag or container.

It is crucial to secure and geo-reference the origin of the samples. For some regions, the origin could only be specified up to the province level (for China, Madagascar and Brazil), not the exact mine site. In the case of China, achieving a more detailed level is not feasible unless samples are collected on-site. Processing plants from locations in Madagascar and Brazil process the material of more than one mine. Resulting concentrates are therefore mixtures of different mines within one province. Mixing and aggregation of material from different sources (countries) might harm the potential use of a geochemical fingerprint and needs to be investigated further.

Various acids are used in the processing process, which can vary between different plants (processing fingerprint!). Contaminations from the processing plant can be introduced, especially if other raw materials are processed in the same plant as well and external inputs (equipment abrasion, dust) can introduce contaminations. The potential supply chain coverage of this methodology needs to be considered and at which stage in the supply chain the geo-based traceability does stop working. Impurities (trace elements levels) are expected to decrease throughout the processing chain and no longer be present in battery-grade graphite concentrate.

Samples must undergo sample preparation, including dissolution, pressing into pellets and treatment of liquids with pipettes and filters. Additionally, the weighing process can introduce uncertainties and is highly operator-dependent.

The application of analytical and statistical methods at the very end of the APO brings certain uncertainties and data quality still needs to be improved by enhanced method development. Machine operators may cause differences in results due to different machine handling and tuning. The precision and accuracy of the produced data play a crucial role, as well as the availability of suitable certified calibration and reference materials. A reference database needs to be available to compare unknown samples and needs to be constantly updated.

The three tested and applied parameters to identify the origin of graphite deposits in this study provide information at various levels. Trace element analysis provided the most detailed information, allowing differentiation down to the level of the mine. However, this parameter is highly dependent on the processing and further investigation is needed to understand how the parameter behaves throughout the processing chain of graphite. The information provided by carbon isotope ratio parameter also provided information, to some extent, but is more related to the carbon source material. Therefore, Ukraine could be distinguished from the rest of the world and samples from Sri Lanka due to the non-organic (hydrothermal origin) of the graphite precursor material. The remaining samples could not be further differentiated from other deposits based solely on this parameter and were classified as RoW (rest of the world).

Using Raman spectroscopy, amorphous graphite is distinguished from other deposits based on the different crystallinity. Amorphous graphite in this study is limited to the deposits in Kaisersberg (Austria) and Hunan Lutang (China). Thus, these two deposits could be distinguished from all others.

A multi-parameter modeling approach at the end of the Results chapter, considering all three parameters, significantly increased the differentiation power of the three methods.

Overall, establishing a proof of origin method for mineral raw materials is an important part of supply chain management and can help ensure compliance with regulations/certifications and ethical sourcing practices.

## 8.4. Further research implications and aspects

### 1. Optimization and Automation:

**How can the developed method be further optimized for enhanced efficiency?**

The sample preparation process is the most error-prone. This is where the majority of errors occur, as impurities may be introduced and the material can become contaminated very easily. Portable analytical methods enable greater efficiency in analytics. Analysis can take place directly on-site without the need for standardized laboratory facilities and personnel can be trained for these applications. With the elimination of complicated sample preparation, the accuracy of results also increases simultaneously. Sample preparation processes can introduce impurities and overall biases through digestion methods. However, portable methods require method development and usually show lower limits of detection in comparison to stationary laboratory methods and can currently not be used for determining the origin of graphite. Portable LIBS and XRF methods had been tested, but need to undergo special method development for the use in APO techniques. Limitations using pLIBS and pXRF devices were inhomogeneous sample material, the analysis of small areas of the material only and the data processing and data reduction. The database of samples and analyzed parameters constantly needs to be enlarged and updated, as well as data quality must be improved.

**Are there opportunities for automation of the analytical and statistical process?**

The data evaluation process can be optimized. Machine-learning applications can assign unknown samples to known ones in the database. However, the entire process of analytical work always requires trained personnel. Complete automation is not possible, although some steps, such as in the sample preparation process, might be automated. Automated statistical data evaluation can save a significant amount of time.

**2. Exploration of New Analytical Techniques**

**What emerging analytical techniques could be explored to improve the precision and sensitivity of the analytical proof of origin method?**

LA-LIBS tandem systems can analyze samples even faster by generating more measurements in a shorter time. Advanced TOF-laser-(ablation) technologies and mass spectrometers enable increasingly higher sensitivities and speed.

Portable analytical applications can be combined or connected with processing facilities. This makes portable methods location-dependent again, but not tied to a certified laboratory. It allows for a rapid analysis without the need for specific sample preparation, potentially also on conveyor belts in the processing of raw materials. Sensitivities of those techniques still need to be improved to determine trace element levels.

If the sample preparation process can be automated or simplified and the application of analytical methods could become more user-friendly and less time-consuming in the future, analysis for industry applications could take place directly on-site. Note: Certified independent laboratory facilities will still be required in case of doubt for independent assessments (customs, certification systems, other).

**Are there any portable devices to be used for this application?**

Currently available on the market, handheld LIBS (Laser-Induced Breakdown Spectroscopy) devices could be applied after calibration and method development for the required application and raw material. Carbon isotope measurements still require well equipped laboratories. Trace element detection requires high sensitivities for the required limits of detection and need a sample preparation prior to applying the analytical method, which is currently not feasible with any portable device.

**3. Extension to Other Materials:**

**Can the developed method be adapted or extended to analyze the origin of other mineral raw materials? Or other carbon-based materials?**

The analytical proof of origin must be independently developed for each raw material. The parameters defining the APO are individual for each raw material and are influenced by geological formation processes, material properties, grain sizes and mineralogy. Trace elements are a parameter that can be used for many raw materials. However, their analysis is complex and material-dependent. Each material requires its own matrix-matched calibration materials, as well as various sample preparation and analytical methods.

The application of this methodology to other carbon-rich materials is very likely possible. Method development for graphite analysis was combined with the analysis of carbon-rich materials from methane pyrolysis at the Chair of General and Analytical Chemistry. Carbonaceous material from methane pyrolysis has a broad range of applications, spanning from various technological to agricultural applications. Also, by-products from the battery industry can be considered as carbon-rich materials due to the high graphite content (both synthetic and natural). Anode materials or black mass, a material

obtained from recycling Li-ion batteries might be a potential material using the developed analytical methodology.

**4. Real-world Application and Validation:**

**Can the method be validated and applied in real-world scenarios? Is there a potential for its application in industry and certification standards?**

In the present stage, APO for graphite is cost-intensive. The analytical proof of origin using laboratory methods is not likely to become a standard application due to its high costs, complexity, and time-consumption. APO can be applied in specific cases of doubt or questionable origin. This methodology directly refers to the raw material itself and thus might verify the origin of a raw material based on its inherent material properties. Most existing proof of origin methods refer to (digital) documents only, which can be falsified and are potentially vulnerable to fraud. The potential for industrial applications is more likely in on-site technologies. The approach developed in this study may be relevant for certified laboratory facilities involved in standardized certification systems.

**How consistent are the parameters along the value chain?**

This was tested and verified using carbon isotope ratios. The ratio remains consistent along the processing steps from flotation feed to purified graphite and only changes due to the natural spatial variability within a deposit. Trace elements in different (intermediate) products along the supply chain still need to be collected and analyzed. After each processing step, the content of impurities decreases and it is to be expected that the content of significant trace elements will therefore also decrease. If remaining elements are directly bound to the graphite structure still needs to be explored. However, effects of processing on fingerprinting results still needs to be understood.

**5. Environmental and Ethical Considerations:**

**Can the developed method be employed to address environmental and ethical concerns related to graphite production and sourcing?**

The $CO_2$ emissions of a raw material can be estimated and calculated by knowing the origin of the material and its trade routes.

Certain ethical problems or human rights violations are more prevalent in some regions than in others. For example, raw materials from Europe may receive less emphasis on ethical considerations, in comparison to raw materials originating from Africa. Chinese material is often criticized due to its strongly negative environmental impacts.

The analytical proof of origin (APO) of the critical raw material graphite marks a significant step towards securing and tracing graphite supply chains. The developed methodology does not only ensure the authenticity and origin verification of graphite but also aligns with the requirements of the EU supply chain law. By implementing traceability measures, industries can achieve greater transparency, reduce the risk of counterfeit materials and enhance the sustainability of their supply chains.

# References


Abduriyim A, Kitawaki H, Furuya M, Schwarz D, 2006. "Paraiba"-Type Copper-Bearing Tourmaline form Brazil, Nigeria, and Mozambique: Chemical Fingerprinting by LA-ICP-MS. Gems & Gemology, 42 (1), 4–21.

Aitchison, J, 2002. Biplots of compositional data. Appl. Statist, 51, 375–392.

Aitchison, J 1982. The Statistical Analysis of Compositional Data. J.R. Statist. Soc. B., 44 (2), 139–177.

Al-Ani T, Leinonen S, Ahtola T, Salvador D, 2020. High-Grade Flake Graphite Deposits in Metamorphic Schist Belt, Central Finland—Mineralogy and Beneficiation of Graphite for Lithium-Ion Battery Applications. Minerals, 10 (8), 680.

Aluminium Stewardship Initiative, 2022. ASI Home | Aluminium Stewardship Initiative, 06.12.2022. Accessed on 11.06.2024, https://aluminium-stewardship.org/

An, J.H., Tang, F.P., Li, J., 2016. Metallogenic rules and resource potential of the graphite deposit in Hunan Province. J. Geol. 40 (3), 433–437.

Anderson, T.W., 2003. An Introduction to multivariate statistical analysis, 3rd Ed. Wiley Interscience, Hoboken, NJ, p. 721.

Attanasio D, Bruno M, Prochaska W, Yavuz AB, 2013. The Asiatic marbles of the Hadrian's Villa at Tivoli. Journal of Archaeological Science, 40 (12), 4358–4368.

Attanasio D, Bruno M, Prochaska W, Yavuz AB, 2015. A Multi-Method Database of the Black and White Marbles of G öktepe (Aphrodisias), Including Isotopic, EPR Trace and Petrographic Data. Archaeometry, 57 (2), 217–245.

Aung MM, Chang YS, 2014. Traceability in a food supply chain: Safety and quality perspectives. Food Control, 39, 172–184.

Bacchetta AvB, Krümpel V, Cullen E, 2021. Transparency with Blockchain and Physical Tracking Technologies: Enabling Traceability in Raw Material Supply Chains. In: COM: Proposal for a Directive Of The European Parliament And Of Proposal for a Directive of the European Parliament and of the Council on Corporate Sustainability Due Diligence and amending Directive EU (2019/1937) ing Directive (EU) 2019/1937. MDPI, Basel Switzerland, p. 1.

Badia-Melis R, Mishra P, Ruiz-García L, 2015. Food traceability: New trends and recent advances. A review. Food Control, 57, 393–401.

Bandoniene D, Meisel T, Rachetti A, Walkner C, 2018a. A tool to assure the geographical origin of local food products (glasshouse tomatoes) using labeling with rare earth elements. Journal of the science of food and agriculture, 98 (12), 4769–4777.

Bandoniene D, Walkner C, Zettl D, Meisel T, 2018b. Rare Earth Element Labeling as a Tool for Assuring the Origin of Eggs and Poultry Products. Journal of agricultural and food chemistry, 66 (44), 11729–11738.

Bandoniene D, Zettl D, Meisel T, Maneiko M, 2013. Suitability of elemental fingerprinting for assessing the geographic origin of pumpkin (Cucurbita pepo var. styriaca) seed oil. Food Chemistry, 136, 1533–1542.

Barrera P, 2021. Europe’s Graphite Supply Chain — Key Facts. INN, 17.05.2021. Accessed on 12.06.2024, https://investingnews.com/daily/resource-investing/battery-metals-investing/graphite-investing/europes-graphite-supply-chain/

Bau M, Schmidt K, Pack A, Bendel V, Kraemer D, 2018a. The European Shale: An improved data set for normalisation of rare earth element and yttrium concentrations in environmental and biological samples from Europe. Applied Geochemistry, 90, 142–149.

Bendall C., Wigg-Wolf D, Lahaye Y, Kaenel H-M von, Brey GP, 2009. Detecting changes of celtic gold sources through the application of trace element and Pb isotope laser-ablation analysis of celtic gold coins. Archaeometry, 51 (4), 598–625.

Beowulf Mining plc, 2024. Home - Beowulf Mining plc, 29.05.2024. Accessed on 12.06.2024, https://beowulfmining.com/

BetterCoal. BettercoalCode2.0-English. Accessed on 11.06.2024, https://static1.squarespace.com/static/616d4f4a45c4cd5a0ed1a30d/t/61b757467619bc24846ecf9e/1639405383831/BettercoalCode2.0-English.pdf

Beyssac O, Brunet F, Petitet J-P, Goffé B, Rouzaud J-N, 2004. Experimental study of the microtextural and structural transformations of carbonaceous materials under pressure and temperature. European Journal of Mineralogy, 15 (6), 937–951.

Beyssac O, Rumble D, 2014. Graphitic Carbon: A Ubiquitous, Diverse, and Useful Geomaterial. Elements, 10 (6), 415–420.

Binu-Lal S, Kehelpannala K, Satish-Kumar M, Wada H, 2003. Multistage graphite precipitation through protracted fluid flow in sheared metagranitoid, Digana, Sri Lanka: evidence from stable isotopes. Chemical Geology, 197 (1-4), 253–270.

Blaustein R, 2016. The Great Oxidation Event. BioScience, 66 (3), 189–195.

Bonijoly, M, Oberlin, M, Oberlin A , 1982. A possible mechanism for natural graphite formation. International Journal of Coal Geology, 1, 283–312.

Bögershausen W, Cicciarelli R, Gercken B, König E, Krivan V, Müller-Käfer R, Pavel J, Seltner H, Schelcher J, 1997. Pure graphite as a reference material for the determination of trace elements - an interlaboratory collaborative study. Fresenius J Analytical Chemistry, 357, 266–273.

Botelho GM, Campos, Reinaldo, C., Jackson, Kenneth, W., 2001. Determination of Trace Elements in Carbonaceous Samples by Graphite Furnance Atomic Absorption Spectrometry: Microwave Digestion Versus Slurry Sampling. Mikrochim. Acta, 136, 43–48.

Brezina I, Pekár J, Čičková Z, Reiff M, 2016. Herfindahl–Hirschman index level of concentration values modification and analysis of their change. Central European Journal of Operations Research, 24 (1), 49–72.

Burlet C, Vanbrabant Y, Goethals H, Thys T, Dupin L, 2011. Raman spectroscopy as a tool to characterize heterogenite (CoO·OH) (Katanga Province, Democratic Republic of Congo). Spectrochimica acta. Part A, Molecular and biomolecular spectroscopy, 80 (1), 138–147.

Carrara S, Bobba S, Blagoeva D, Alves Dias P, Cavalli A, Georgitzikis K, Grohol M, Itul A, Kuzov T, Latunussa CEL, Lyons L, Malano G, Maury T, Prior Á, Somers J, Telsnig T, Veeh C, Wittmer DMAG, Black C, Pennington DW, Christou M, 2023. Supply chain analysis and material demand forecast in strategic technologies and sectors in the EU. A foresight study. Publications Office of the European Union, Luxembourg, 1266 p.

Christensen A-M, Holm PM, Schuessler U, Petrasch J, 2006. Indications of a major Neolithic trade route? An archaeometric geochemical and Sr, Pb isotope study on amphibolitic raw material from present day Europe. Applied Geochemistry, 21 (10), 1635–1655.

Clarke FW, Washington HS, 1924. Professional Paper. US Geological Survey.

COM: Proposal for a Directive Of The European Parliament And Of Proposal for a Directive of the European Parliament and of the Council on Corporate Sustainability Due Diligence and amending Directive EU (2019/1937) ing Directive (EU) 2019/1937, 2021. MDPI, Basel Switzerland.

Coney L, Moila AV, Quadling AG, 2012. Gem-quality diamonds: Source discriminations. South African Journal of Geology, 115 (1), 33–46.

Crespo E, Luque FJ, Rodas M, Wada H, Gervilla F, 2006. Graphite–sulfide deposits in Ronda and Beni Bousera peridotites (Spain and Morocco) and the origin of carbon in mantle-derived rocks. Gondwana Research, 9 (3), 279–290.

Cruz SM, Schmidt L, Dalla Nora FM, Pedrotti MF, Bizzi CA, Barin JS, Flores EM, 2015. Microwave-induced combustion method for the determination of trace and ultratrace element impurities in graphite samples by ICP-OES and ICP-MS. Microchemical Journal, 123, 28–32.

Cui N, Sun L, Bagas L, Xiao K, Xia J, 2017. Geological characteristics and analysis of known and undiscovered graphite resources of China. Ore Geology Reviews, 91, 1119–1129.
Dabbene F, Gay P, Tortia C, 2014. Traceability issues in food supply chain management: A review. Biosystems Engineering, 120, 65–80.
Dalpé C, Hudon P, Ballantyne DJ, Williams D, Marcotte D, 2010. Trace element analysis of rough diamond by LA-ICP-MS: a case of source discrimination? Journal of forensic sciences, 55 (6), 1443–1456.
Decree S, Deloule É, Putter T de, Dewaele S, Mees F, Baele J-M, Marignac C, 2014. Dating of U-rich heterogenite: New insights into U deposit genesis and U cycling in the Katanga Copperbelt. Precambrian Research, 241, 17–28.
Decrée S, Pourret O, Baele J-M, 2015. Rare earth element fractionation in heterogenite (CoOOH): implication for cobalt oxidized ore in the Katanga Copperbelt (Democratic Republic of Congo). Journal of Geochemical Exploration, 159, 290–301.
DERA, 2022. Natürlicher und synthetischer Graphit. Rohstoffwirtschaftliche Steckbriefe.
Desaulty A-M, Monfort Climent D, Lefebvre G, Cristiano-Tassi A, Peralta D, Perret S, Urban A, Guerrot C, 2022. Tracing the origin of lithium in Li-ion batteries using lithium isotopes. Nature communications, 13 (1), 4172.
Dietrich V, Melcher F, 2022. Mineral Raw Material Supply Chain Transparency and Traceability: Does Provenance Matter in the Supply Chain? Berg- und huttenmannische Monatshefte, 167 (12), 594–597.
Dissanayake, R.P. Gunawardena, D.M.S.K. Dinalankara, 1988. Trace elements in vein graphite of Sri Lanka. Chemical Geology, 68, 121–128.
Dixon R, Schouwstra R, 2017. The role of forensic geology in the illicit precious metals trade. Episodes, 40 (2), 132–140.
Dixon RD, 2014. Provenance of Illicit Gold with Emphasis on the Witwatersrand Basin, unpublished. University of Pretoria, Pretoria, South Africa, 180 p.
Dixon RD, Merkle RKW, 2019. Identifying the source of illicit gold from South America. Geological Society, London, Special Publications, 492 (1), 135–145.
Dobner A, Graf W, Hahn-Weinheimer P, Hirner A, 1978. Stable carbon isotopes of graphite from Bogala Mine, Sri Lanka. Lithos, 11 (3), 251–255, https://www.sciencedirect.com/science/article/pii/0024493778900257
Dodd-Frank Wall Street Reform and Consumer Protection Act. Accessed on 11.06.2024, https://www.congress.gov/111/plaws/publ203/PLAW-111publ203.pdf
Dyer EL, Kording K, 2023. Why the simplest explanation isn't always the best. Proceedings of the National Academy of Sciences of the United States of America, 120 (52), e2319169120.
Ebner F, Kovacs S, Schönlaub HP, 1991. Das klassische Karbon in Österreich und Ungarn - ein Vergleich der sedimentären fossilführenden Vorkommen. In Jubiläumsschrift 20 Jahre Geologische Zusammenarbeit Österreich – Ungarn 1 (H. Lobitzer & G. Csàsàr, eds.) (263-294)
Echtler HP, Ivanov KS, Ronkin YL, Karsten LA, Hetzel R, Noskov AG, 1997. The tectono-metamorphic evolution of gneiss complexes in the Middle Urals, Russia: a reappraisal. Tectonophysics, 276, 229-25.
Ehser A, Borg G, Pernicka E, 2011. Provenance of the gold of the Early Bronze Age Nebra Sky Disk, central Germany: geochemical characterization of natural gold from Cornwall. European Journal of Mineralogy, 23 (6), 895–910.
Enders MSP, Souza JP de, Balestrin P, Mello PdA, Duarte FA, Muller EI, 2016. Microwave-induced combustion of high purity nuclear flexible graphite for the determination of potentially embrittling elements using atomic spectrometric techniques. Microchemical Journal, 124, 321–325.

Fair Stone, 2018. Herzlich Willkommen bei Fair Stone e.V. - Fair Stone, 25.06.2018. Accessed on 11.06.2024, https://www.fairstone.org/

Feneyrol J, Giuliani G, Ohnenstetter D, Fallick, A.E., Martelat, J.E., Monié, P., Dubessy, J., Rollion-Bard, C., Le Goff, E., Malisa, E., Rakotondrazafy, A., Pardieu, V., Kahn, T., Ichang'i, D., Venance, E., Voarintsoa, N.R., Ranatsenho, M.M., Simonet, C., Omito, E., Nyamai, C., Saul, M., 2013. New aspects and perspectives on tsavorite deposits. Ore Geol. Rev. 53, 1–25.

Ferrari AC, Robertson J, 2000. Interpretation of Raman spectra of disordered and amorphous carbon. Physical Review B, 61 (20).

Filion, M. 2012. The Graphite Mine of Ragedara, Sri Lanka, accessed via https://cdn.website-editor.net/

Filzmoser P, Hron K, Reimann C, 2010. The bivariate statistical analysis of environmental (compositional) data. The Science of the total environment, 408 (19), 4230–4238.

Flores M, Barin JS, Mesko MF, Knapp G, 2007. Sample preparation techniques based on combustion reactions in closed vessels — A brief overview and recent applications. Spectrochimica Acta Part B: Atomic Spectroscopy, 62 (9), 1051–1064.

Flores EM, Barin JS, Paniz JNG, Medeiros JA, Knapp G, 2004. Microwave-assisted sample combustion: a technique for sample preparation in trace element determination. Analytical chemistry, 76 (13), 3525–3529.

Frenzel M, 2023. Making sense of mineral trace-element data – How to avoid common pitfalls in statistical analysis and interpretation. Ore Geology Reviews, 159, 105566.

Gäbler H-E, Melcher F, Graupner T, Bahr A, Sitnikova MA, Henjes-Kunst F, Oberthür T, Brätz H, Gerdes A, 2011. Speeding Up the Analytical Workflow for Coltan Fingerprinting by an Integrated Mineral Liberation Analysis/LA-ICP-MS Approach. Geostandards and Geoanalytical Research, 35 (4), 431–448.

Gäbler H-E, Rehder S, Bahr A, Melcher F, Goldmann S, 2013. Cassiterite fingerprinting by LA-ICP-MS. Journal of Analytical Atomic Spectrometry, 28 (8), 1247.

Gäbler H-E, Schink W, Goldmann S, Bahr A, Gawronski T, 2017. Analytical Fingerprint of Wolframite Ore Concentrates. Journal of forensic sciences, 62 (4), 881–888.

Gautneb H, Rønning JS, Engvik AK, Henderson IH, Larsen BE, Solberg JK, Ofstad F, Gellein J, Elvebakk H, Davidsen B, 2020. The Graphite Occurrences of Northern Norway, a Review of Geology, Geophysics, and Resources. Minerals, 10 (7), 626.

Gautneb H, 2015. Natural Graphite in Norway. Overview and latest exploration results, presentation, 5th graphite and graphene conference, December 8th and 9th, London, 24 p., via ResearchGate

Giuliani G, Fallick AE, Garnier V, France-Lanord C, Ohnenstetter D, Schwarz D, 2005. Oxygen isotope composition as a tracer for the origins of rubies and sapphires. Geology, 33 (4), 249.

Giuliani G, France-Lanord C, Coget P, Schwarz D, Cheilletz A, Branquet Y, Giard D, Martin-Izard A, Alexandrov P, Piat DH, 1998. Oxygen isotope systematics of emerald: relevance for its origin and geological significance. Mineralium Deposita, 33 (5), 513–519.

GNAA – ARCHAEOMETRIE e.V, 2024, 21.03.2024. Accessed on 21.03.2024, https://www.archaeometrie.de/

Grohol, Milan V, Constanze, DG GROW, European Commission, 2023. Study on the Critical Raw Materials for the EU 2023.

Hapuarachchi, D.J.A.C. (1977) Decarbonation Reactions and the origin of vein graphite in Sri Lanka. Journal of the National Science Council of Sri Lanka, 5, 29–32.

Hark RR, Remus JJ, East LJ, Harmon RS, Wise MA, Tansi BM, Shughrue KM, Dunsin KS, Liu C, 2012. Geographical analysis of “conflict minerals” utilizing laser-induced breakdown spectroscopy. Spectrochimica Acta Part B: Atomic Spectroscopy, 74-75, 131–136.

Harmon RS, Shughrue KM, Remus JJ, Wise MA, East LJ, Hark RR, 2011. Can the provenance of the conflict minerals columbite and tantalite be ascertained by laser-induced breakdown spectroscopy? Analytical and bioanalytical chemistry, 400 (10), 3377–3382.

Harmon C, 1957. Isotopic standards for carbon and oxygen and correction factors for mass-spectrometric analysis of carbon dioxide. Geochimica et Cosmochimica Acta, 12, 133–149.

Heike M-J, 2023. Österreichisches Montan-Handbuch 2023, 97.

Heritiana A. R, Riva R, Ralay R, Boni R, 2019. Evaluation of flake graphite ore using self-potential (SP), electrical resistivity tomography (ERT) and induced polarization (IP) methods in east coast of Madagascar. Journal of Applied Geophysics, 169, 134–141.

Hewathilake HS, Balasooriya N, Nakamura Y, Pitawala H, Wijayasinghe HAC, Satish-Kumar M, 2018. Geochemical, structural and morphological characterization of vein graphite deposits of Sri Lanka: Witness to carbon rich fluid activity. Journal of Mineralogical and Petrological Sciences, 113 (2), 96–105.

Hoernes S, Fiorentini E, Hoffbauer R, 1994. The role of fluids in granulite-facies metamorphism as deduced from oxygen and carbon isotopic compositions. Precambrian Research, 66 (1-4), 183–198.

https://lgi.earth, LGI Sustainable Innovation - Maditrace, 2024. MaDiTraCe Project, 21.03.2024. Accessed on 21.03.2024, https://maditrace.eu/cera4in1

Janda I, Schroll E, 1960. Geochemische Untersuchungen an Graphitgesteinen. Report International Geological Congress Part I, Kopenhagen, 40–53.

Jansen-Vullers, M.H., C.A. van Dorp, A.J.M. Beulens, 2003. Managing traceability information in manufacture. International Journal of Information Management, 23, 395–413.

Katz, M.B. (1987) Graphite deposits of Sri Lanka: a consequence of granulite facies metamorphism. Mineral Deposita, 22, 18 25.

Keegan E, Richter S, Kelly I, Wong H, Gadd P, Kuehn H, Alonso-Munoz A, 2008. The provenance of Australian uranium ore concentrates by elemental and isotopic analysis. Applied Geochemistry, 23 (4), 765–777.

Keeling J, 2017. Graphite: properties, uses and South Australian resources. MESA Journal, Issue 3, 28–41.

Krüger N, Lehrberger G, Hoffmann E, Reiser F, 2017. Das Graphitbergwerk Kropfmühl im Passauer Wald. Geologie und Petrographie der Graphitmineralisation mit Anmerkungen zur Aufbereitung, Veredelung und Verwendung von Flockengraphit. Exkursion D am 20. April 2017. Jber. Mitt. oberrhein. geol.Ver., 99, 125–164.

Kwiecińska B, Petersen H, 2004. Graphite, semi-graphite, natural coke, and natural char classification—ICCP system. International Journal of Coal Geology, 57 (2), 99–116.

Lahfid A, Beyssac O, Deville E, Negro F, Chopin C, Goffé B, 2010. Evolution of the Raman spectrum of carbonaceous material in low-grade metasediments of the Glarus Alps (Switzerland). Terra Nova, 22 (5), 354–360.

Lamming RC, Caldwell ND, Harrison DA, Phillips W, 2001. Transparency in Supply Relationships: Concept and Practice. Journal of Supply Chain Management, 37 (3), 4–10.

Lee C-T, 2019. Geochemical Classification of Elements. In: White WM (ed.). Encyclopedia of Geochemistry. A Comprehensive Reference Source on the Chemistry of the Earth. Springer, Cham, p. 1–5.

Lünsdorf NK, Dunkl I, Schmidt BC, Rantitsch G, Eynatten H von, 2017. Towards a Higher Comparability of Geothermometric Data Obtained by Raman Spectroscopy of Carbonaceous Material. Part 2: A Revised Geothermometer. Geostandards and Geoanalytical Research, 41 (4), 593–612.

Lünsdorf NK, Lünsdorf JO, 2016. Evaluating Raman spectra of carbonaceous matter by automated, iterative curve-fitting. International Journal of Coal Geology, 160-161, 51–62.

Luque, F.J. P, J.D. W, B. R, M. B, J.F., 1998. Natural fluid-deposited graphite: Mineralogical Characteristics and mechanisms of formation. American Journal of Science, 298, 471–498.
Luque FJ, Huizenga J-M, Crespo-Feo E, Wada H, Ortega L, Barrenechea JF, 2014. Vein graphite deposits: geological settings, origin, and economic significance. Mineralium Deposita, 49 (2), 261–277.
Lyzhachenko N.M., Zagnitko V.M., Kurylo S.I. Atypical manifestations of graphite of the Zavalivske deposit. Scientific Bulletin of the National Mining University. 2013. № 4. c. 10-17
Ma Y, Huang Y, Liu L, 2021. Genesis of the Tianping flake graphite deposit at the western margin of Yangtze Block, SW China. Ore Geology Reviews, 139, 104434.
Machado N, Schrank A, Noce CM, Gauthier G, 1996. Ages of detrital zircon from Archean-Paleoproterozoic sequences: Implications for Greenstone Belt setting and evolution of a Transamazonian foreland basin in Quadrilátero Ferrífero, southeast Brazil. Earth and Planetary Science Letters, 141 (1-4), 259–276.
Machault J, Barbanson L, Augé T, Bailly L, Orgeval J-J, 2014. Mineralogical and microtextural parameters in metals ores traceability studies. Ore Geology Reviews, 63, 307–327.
Machault J, 2012. Paramètres minéralogiques et microtexturaux utilisables dans les études de traçabilité des minerais métalliques. Doctoral Thesis, unpublished. Universite d'Orleans, 388 p.
Macheyeki, Athanas S., Kafumu, Dalaly Peter, Li X, Yuan F, 2020. Applied Geochemistry. Advances in Mineral Exploration Techniques. Elsevier, San Diego, 1212 p.
Maibam B, Sanyal P, Bhattacharya S, 2015. Geochronological Study of Metasediments and Carbon Isotopes in Associated Graphite from the Sargur Area, Dhwarwar Craton: Constraints on the Age and Nature of the Protoliths. Journal Geological Society of India, 85, 577–585.
Manoel TN, Dexheimer Leite JA, 2018. On the origin of the Neoproterozoic Peresopolis graphite deposit, Paraguay Belt, Brazil. Journal of South American Earth Sciences, 84, 104–112.
Martín-Méndez I, Boixereu E, Villaseca C, 2016. Mineralogical and isotopic characterization of graphite deposits from the Anatectic Complex of Toledo, central Spain. Mineralium Deposita, 51 (5), 575–590.
Martyna A, Gäbler H-E, Bahr A, Zadora G, 2018. Geochemical wolframite fingerprinting - the likelihood ratio approach for laser ablation ICP-MS data. Analytical and bioanalytical chemistry, 410 (13), 3073–3091.
Maslova OA, Ammar MR, Guimbretière G, Rouzaud J-N, Simon P, 2012. Determination of crystallite size in polished graphitized carbon by Raman spectroscopy. Physical Review B, 86 (13).
McManus CE, McMillan NJ, Dowe J, Bell J, 2020. Diamonds Certify Themselves: Multivariate Statistical Provenance Analysis. Minerals, 10 (10), 916.
Melcher F, Dietrich V, Gäbler H-E, 2021. Analytical Proof of Origin for Raw Materials. Minerals, 11 (5), 461.
Melcher, F.; Sitnikova, M.; Graupner, T.; Martin, N.; Oberthür, T.; Henjes-Kunst, F.; Gäbler, E.; Gerdes, A.; Brätz, H.; Davis, D.; et al. Fingerprinting of conflict minerals: Columbite-tantalite (“coltan”) ores. Sga News 2008, 23, 7–14.
Meng, H. (2016). The geochemical characteristics and deposit genesis analysis of Liugezhuang graphite deposit in Pingdu country of Shandong Province. Beijing: China University of Geosciences. (in Chinese)
Mineral Commodities Ltd, 2022a. Munglinup Graphite Project - Mineral Commodities Ltd, 02.06.2022. Accessed on 12.06.2024, https://www.mineralcommodities.com/operations-projects/graphite/munglinup-graphite-project/
Mineral deposits of national interest, 2024, 12.06.2024. Accessed on 12.06.2024, https://www.sgu.se/en/mineral-resources/legislation/mineral-deposits-of-national-interest/

Mining Technology, 2021. Balama Graphite Project, 10.11.2021. Accessed on 19.06.2024, https://www.mining-technology.com/projects/balama-graphite-project/
Miranda DA, Oliveira Chaves A , Campello MS, Ramos S, 2019. Origin and thermometry of graphites from Itapecerica supracrustal succession of the southern Sao Francisco Craton by C isotopes, X-ray diffraction, and Raman spectroscopy. International Geology Review, 61 (15), 1864–1875.
Modern Slavery Act 2015, 2024, 20.05.2024. Accessed on 11.06.2024, https://www.legislation.gov.uk/ukpga/2015/30/contents
Moe T, 1998. Perspectives on traceability in food manufacture. Trends in Food Science & Technology, 9, 211–214.
Moreira H, Lana C, Nalini HA, 2016. The detrital zircon record of an Archaean convergent basin in the Southern São Francisco Craton, Brazil. Precambrian Research, 275, 84–99.
Mykhailov VA, Hrinchenko OV, Malyuk BI, 2023. Exploration and mining perspectives of the critical elements for green technologies in Ukraine. Geological Society, London, Special Publications, 526 (1), 267–287.
Nacional de Grafite, 2024. Foundation of Nacional de Grafite - Nacional de Grafite, 19.06.2024. Accessed on 19.06.2024, https://www.grafite.com/en/a-nacional-de-grafite
Neubauer, F. & Vozàrovà, A. (1989): The Noetsch - Veitsch North Gemeric zone of Alps and Carpathians: correlation, paleogeography and significance for Variscan orogeny. In Thirty Years of Geological Cooperation Between Austria and Czechoslovakia (D. Manarikova & H. Lobitzer, eds.). Vydal Ustred. Ustav. Geol., Prague, Czechoslovakia (167-171)
Neubauer, F., Handler, R., Hermann, S. & Paulus, G. (1994): Revised lithostratigraphy and structure of the Eastern Greywacke Zone (Eastern Alps). Min. Österr. Geol. Ges. 86 (1993), 61-74
Nievoll, J. (1984): Der Südrand der Grauwackenzone zwischen Stübming und Neuberg (Obersteiermark, ÖK 103 Kindberg). Mitt. Osterr. Geol. Ges.77,63-71
NS Energy, 2024. Traelen Graphite Mining Project, 19.06.2024. Accessed on 19.06.2024, https://www.nsenergybusiness.com/projects/traelen-graphite-mining-project/
OECD, 2016. OECD Due Diligence Guidance for Responsible Supply Chains of Minerals from Conflict-Affected and High-Risk Areas (Third edition). OECD Publishing, Paris, 118 p.
O'Leary MH, 1981. Carbon isotope fractionation in plants. Phytochemistry, 20 (4), 553–567.
O'Leary MH, S. Madhavan, P. Paneth, 1992. Physical and chemical basis of carbon isotope fractionation in plants. Plant, Cell and Environment, 15, 1099–1104.
Olsen P and Borit M, 2013. How to define traceability. Trends in Food Science & Technology, 29, 142–150.
Olson DW, 2009. Graphite (natural).
Olson DW, 2020. Graphite (Natural).
Olson DW, 2021. Graphite (Natural).
Olson DW, 2022. Graphite (Natural).
Parnell J, Brolly C, Boyce AJ, 2021. Graphite from Palaeoproterozoic enhanced carbon burial, and its metallogenic legacy. Geological Magazine, 158 (9), 1711–1718.
Perelygin A, Kuchkin A, Kharkov N, Moskvina T, 2008. Criminalistic identification of PGM-containing products of mining and metallurgical companies. Forensic science international, 174 (1), 12–15.
Pochon A, Desaulty A-M, Bailly L, 2020. Handheld laser-induced breakdown spectroscopy (LIBS) as a fast and easy method to trace gold. Journal of Analytical Atomic Spectrometry, 35 (2), 254–264.
Pochon A, Desaulty A-M, Bailly L, Lach P, 2021. Challenging the traceability of natural gold by combining geochemical methods: French Guiana example. Applied Geochemistry, 129, 104952.
Prochaska W, 2013. A sculptural marble of prime quality in antiquity . the dolomitic marble of the sivec mountains in Macedonia. Archaeometry, 55 (2), 179–197.

Prochaska W, Grillo SM, 2010. A new method for the determination of the provenance of white marbles by chemical analyis of inclusion fluids. The marbles of the mausoleum of Belevi/Turkey. Archaeometry, 52 (1), 59–82.

Raič S, Molnár F, Cook N, O'Brien H, Lahaye Y, 2022. Application of lithogeochemical and pyrite trace element data for the determination of vectors to ore in the Raja Au–Co prospect, northern Finland. Solid Earth, 13 (2), 271–299.

Raith, Johann G., Vali, Hojatollah, 1998. Fibrous Chlorite and Muskovite from the Kaisersberg Graphite Mine, Styria, Austria. The Canadian Mineralogist, 36, 741–754.

Rantitsch G, Bhattacharyya A, Schenk J, Lünsdorf NK, 2014. Assessing the quality of metallurgical coke by Raman spectroscopy. International Journal of Coal Geology, 130, 1–7.

Rantitsch G, Lämmerer W, Fisslthaler E, Mitsche S, Kaltenböck H, 2016a. On the discrimination of semi-graphite and graphite by Raman spectroscopy. International Journal of Coal Geology, 159, 48–56.

Ratschbacher L, 1984. Beitrag zur Neugliederung der Veitscher Decke (Grauwackenzone) in ihrem Westabschnitt (Obersteiermark, Österreich). Jb. GeoI. B.-A. 127, 423-453

Ratschbacher L, 1985. Strukturgeologische Grundlagenforschungsaspekte als Propsektions- und Abbaurichtlinien am Beispiel Graphitbergbau Sunk/trieben (Paltental, Steiermark). Arch. f. Lagerst. Forsch. Geol. B.-A. 6, 81-84

Regelous & Holzförster, unknown year. Die drei Schätze im Passauer Land: 6. Rohstoff Grafit. Accessed on 27.02.2024, https://graphit-bbw.de/wp-content/uploads/2019/01/Kap_6-Rohstoff-Graphit.pdf

Reichl C., Schatz, M., 2024. World Mining Data 2024, 39.

Reimann C, Filzmoser P, Garrett RG, Dutter R (eds.), 2009. Statistical data analysis explained. Applied environmental statistics with R (Reprinted.). Wiley, Chichester, 343 p.

Responsible Jewellery Council, 2024. Home, 10.06.2024. Accessed on 11.06.2024, https://www.responsiblejewellery.com/

Roberts RJ, Dixon RD, Merkle RKW, 2016. Distinguishing Between Legally and Illegally Produced Gold in South Africa. Journal of forensic sciences, 61 Suppl 1, S230-6.

Robinson GR, Hammarstrom JM, Olson DW, Schulz KJ, DeYoung JH, Seal RR, Bradley DC, 2017. Graphite. Critical Mineral Resources of the United States - Economic and Environmental Geology and Prospects for Future Supply, 2017.

Rumble D, Hoering TC, 1986. Carbon isotope geochemistry of graphite vein deposits from New Hampshire, U.S.A. Geochimica et Cosmochimica Acta, 50 (6), 1239–1247.

Sattouf M, Kratz S, Diemer K, Fleckenstein J, Rienitz O, Schiel D, Schnug E, 2008. Significance of Uranium and Strontium Isotope Ratios for Retracing the Fate of Uranium during the Processing of Phosphate Fertilizers from Rock Phosphates. Loads and Fate of Fertilizer Derived Uranium, 191–202.

Scharfe G, 1981. Steirische Graphitvorkommen. Mitt. Abt. Geol. Paläont. Bergb. Landesmuseum Joanneum 42, 117-121

Scherba C, Montreuil J-F, Barrie CT, 2018. Geology and Economics of the Giant Molo Graphite Deposit, Southern Madagascar. In: Geology and Economics of the Giant Molo Deposit, Southern Madagascar. Society of Economic Geologists (SEG).

Schiebel D, 2022. Metamorphic and hydrothermal evolution of the Aukam graphite and fluorite mineralization in SW-Namibia. Master Thesis, unpublished. KIT Karlsruher Institut für Technologie, Karlsruhe, 76 p.

Schmiderer, A., 2008. Geochemische Charakterisierung von Goldvorkommen in Europa. Dissertation. 2009. Martin Luther Universität Halle-Wittenberg, Institut für Geowissenschaften

Schroll E, 1976. Grundlagen und Anwendungen. 79 Tabellen (1. Aufl.). Enke, Stuttgart, 374 p.

Shinzawa H, Wataru Kanematsu KA, Ozaki Y, 2009. Multivariate data analysis for Raman spectroscopic imaging. Journal of Raman Spectroscopy, 40, 1720–1725.
Silva, K.K.M.W. (1987) Mineralization and wall rock alteration at the Bogala graphite deposit, Bulathkohupitiya, Sri Lanka. Economical Geology, 82, 1710–1722.
Simandl GJ, Kenan WM, 1997. Microcrystalline Graphite, unpublished, 4 p.
Simandl GJ, Paradis S, Akam C. Graphite deposit types, their origin, and economic significance. In: Brit. Col. Geol. Surv. Paper, p. 163–171.
Sirven J-B, Pailloux A, M'Baye Y, Coulon N, Alpettaz T, Gossé S, 2009. Towards the determination of the geographical origin of yellow cake samples by laser-induced breakdown spectroscopy and chemometrics. Journal of Analytical Atomic Spectrometry, 24 (4), 451.
Skilton PF, Jessica L. Robinson, 2009. Traceability and normal accident theory: How does supply network complexity influence the traceability of adverse events? Journal of Supply Chain Management, 45 (3), 40–53.
Souali K, Rahmaoui O, Ouzzif M, 2017. An Overview of Traceability: Towards a general multi-domain model. Advances in Science, Technology and Engineering Systems Journal, 2 (3), 356–361.
Švedkauskaitė-LeGore J, Rasmussen G, Abousahl S, van Belle P, 2008. Investigation of the sample characteristics needed for the determination of the origin of uranium-bearing materials. Journal of Radioanalytical and Nuclear Chemistry, 278 (1), 201–209.
Syrah Resources, 2024. Balama Graphite Operation. "><meta name, 11.06.2024. Accessed on 19.06.2024, https://www.syrahresources.com.au/our-business/balama-graphite-operation
Taylor G, 2024. Africa's Growing Graphite Mining Potential, 12.06.2024. Accessed on 12.06.2024, https://www.spglobal.com/marketintelligence/en/news-insights/research/africa-s-growing-graphite-mining-potential
Teixeira W, Oliveira EP, Peng P, Dantas EL, Hollanda MH, 2017. U-Pb geochronology of the 2.0 Ga Itapecerica graphite-rich supracrustal succession in the São Francisco Craton: Tectonic matches with the North China Craton and paleogeographic inferences. Precambrian Research, 293, 91–111.
Tharwat A, Gaber T, Ibrahim A, Hassanien AE, 2017. Linear discriminant analysis: A detailed tutorial. AI Communications, 30 (2), 169–190.
The European Parliament and the council of the European Union. Regulation (EU) 2023/ of the European Union concerning batteries and waste batteries, amending Directive 2008/98/EC and Regulation (EU) 2019/1020 and repealing Directive 2006/66/EC. Accessed on 11.06.2024, https://eur-lex.europa.eu/legal-content/EN/TXT/PDF/?uri=CELEX:32023R1542
The Kimberley Process (KP) | KimberleyProcess, 2024, 11.06.2024. Accessed on 11.06.2024, https://www.kimberleyprocess.com/
Thrane K, Kalvig P, 2019. Graphite potential in Greenland. Reporting on the 9th Greenland mineral resource assessment workshop, November 2017, unpublished.
Touret JLT, Huizenga JM, Kehelpannala KVW, Piccoli F, 2019. Vein-type graphite deposits in Sri Lanka: The ultimate fate of granulite fluids. Chemical Geology, 508, 167–181.
Touzain P, Balasooriya N, Bandaranayake K, Descolas-Gros C, 2010. vein graphite from the Bogala and Kahatagaha-Kolongaha mines, Sri Lanka: A possible origin. The Canadian Mineralogist, 48 (6), 1373–1384.
Trimmel S, Meisel TC, Lancaster ST, Prohaska T, Irrgeher J, 2023. Determination of 48 elements in 7 plant CRMs by ICP-MS/MS with a focus on technology-critical elements. Analytical and bioanalytical chemistry, 415 (6), 1159–1172.
Tsuji K, 2022. Global Value Chains: Graphite in Lithium-ion Batteries for Electric Vehicles. Working Paper ID-090. Accessed on 11.06.2024, https://www.usitc.gov/publications/332/working_papers/gvc_paper.pdf

Uralgraphite - natural graphite producer and supplier, 2024, 18.06.2024. Accessed on 18.06.2024, http://uralgraphite.com/en/

Van Achterbergh, E., Ryan, C.G., Jackson, S.E., and Griffin, W.L. 2001. Data reduction software for LA-ICP-MS: appendix. *In* Laser Ablation – ICP-Mass Spectrometry in the Earth Sciences: Principles and Applications. *Edited by* P.J. Sylvester. Mineralogical Association of Canada Short Course Series, Ottawa, Ontario, Canada, 29, pp. 239–243

Van Ruth S, Visser R de, 2015. Provenancing Flower Bulbs by Analytical Fingerprinting: Convallaria Majalis. Agriculture, 5 (1), 17–29.

Volkert RA, Craig A. Johnson, Albert V. Tamashausky, 2000. Mesoproterozoic graphite deposits, New Jersey Highlands: geologic and stable isotopic evidence for possible algal origins. Can. J. Earth Sci., 37, 1665–1675.

Wang J, Liu J, Zhang H, Zhang H, Li Y, 2019. Metamorphism, geochemistry, and carbon source on sedimentary-metamorphic graphite deposits in eastern Shandong, China. Geological Journal, 55 (5), 3748–3769.

Wang X, Bhagat G, O´Brien K, Putyera K, 2010. Quantification of Trace and Ultra-trace Elements in Nuclear Grade Manufactured Graphites by Fast-Glow Discharge Mass Spectrometry and by Inductively-Coupled Plasma-Mass Spectrometry after Microwave - Induced Combustion Digestion. Mater. Res. Soc. Symp. Proc., 1215.

Wang X, Li H, Yao H, Zhu D, Liu N, 2018. Simulation analysis of the spread of a supply crisis based on the global natural graphite trade network. Resources Policy, 59, 200–209.

Watling R, Herbert HK, Delev D, Abell ID, 1994. Gold fingerprinting by laser ablation inductively coupled plasma mass spectrometry. Spectrochimica Acta Part B: Atomic Spectroscopy, 49 (2), 205–219.

Watling R.J., H.K. Herbert, I.S. Barrow, A.G. Thomas, 1995. Analyis of Diamonds and Indicator Minerals for Diamond Exploration by Laser-Ablation-Inductively-Coupled Plasma Mass Spectrometry. Analyst., 120, 1357–1364.

Weber GW, Lukeneder A, Harzhauser M, Mitteroecker P, Wurm L, Hollaus L-M, Kainz S, Haack F, Antl-Weiser W, Kern A, 2022. The microstructure and the origin of the Venus from Willendorf. Scientific reports, 12 (1), 2926.

Weber L, 2023. On the security of graphite supply. Mineralogy and Petrology, 117 (2), 387–399.

Weis, P.L., Friedman, I. & Gleason, J.P. 1981. The origin of epigenetic graphite: evidence from isotopes. Geochim. Cosmochim. Acta 45, 2325-2332.

Wright KE, Palmer CD, 2008. Geochemical Signatures as a Tool for Vermiculite Provenance Determination. Idaho National Laboratory, INL/EXT-08-14828, 157.

XertifiX, 2024. Home • XertifiX, 18.01.2024. Accessed on 11.06.2024, https://www.xertifix.de/?lang=en

Yan M, Zhang D, Huizenga JM, Wei J, Li H, Li G, Huang X, Zhang X, Zhao S, 2020. Mineralogical and isotopic characterization of graphite deposits in the western part of the North Qaidam Orogen and East Kunlun Orogen, northeast Tibetan Plateau, China. Ore Geology Reviews, 126, 103788.

Yang Q-Y, Santosh M, Wada H, 2014. Graphite mineralization in Paleoproterozoic khondalites of the North China Craton: A carbon isotope study. Precambrian Research, 255, 641–652.

Zavalievsky Graphite Operation – Volt Resources Limited, 2024, 12.06.2024. Accessed on 12.06.2024, https://voltresources.com/assets/zavalievsky-graphite/

Zethof JHT, Leue M, Vogel C, Stoner SW, Kalbitz K, 2019. Identifying and quantifying geogenic organic carbon in soils – the case of graphite. SOIL, 5 (2), 383–398.

Zhang C, Santosh M, 2019. Coupled laser Raman spectroscopy and carbon stable isotopes of graphite from the khondalite belt of Kerala, southern India. Lithos, 334-335, 245–253.

Zhou Q, Damm S, 2020. Supply and demand of natural graphite. DERA, Berlin, 132 p.
Zhu J, Liu F, Wang F, Xu W, Liu F, Shi C, 2021. Carbon isotope and geochemical characteristics of the Paleoproterozoic graphite deposits in the Jiao-Liao-Ji belt, North China Craton: Implications for genesis and depositional environment. Precambrian Research, 362, 106320.

# Appendix

## A. Worldwide Database of Graphite Carbon Isotope Values ($\delta^{13}C$)

| sample ID | continent | mine/province | country | type | $\delta^{13}C$ (‰) | Reference |
|---|---|---|---|---|---|---|
| Cx-07 | South America | Peresopolis | Brazil | Amorph | -28.7 | (Manoel and Dexheimer Leite 2018) |
| Cx-12 | South America | Peresopolis | Brazil | Amorph | -29.01 | (Manoel and Dexheimer Leite 2018) |
| Cx-15 | South America | Peresopolis | Brazil | Amorph | -29.23 | (Manoel and Dexheimer Leite 2018) |
| Cx-19 | South America | Peresopolis | Brazil | Amorph | -28.36 | (Manoel and Dexheimer Leite 2018) |
| 20TP01 | Asia | Tianping | China | Flake | -28.8 | (Ma et al. 2021) |
| 20TP02 | Asia | Tianping | China | Flake | -26.8 | (Ma et al. 2021) |
| 20TP03 | Asia | Tianping | China | Flake | -27.2 | (Ma et al. 2021) |
| 20TP04 | Asia | Tianping | China | Flake | -26.3 | (Ma et al. 2021) |
| 20TP05 | Asia | Tianping | China | Flake | -27.6 | (Ma et al. 2021) |
| 20TP06 | Asia | Tianping | China | Flake | -27.7 | (Ma et al. 2021) |
| 20TP07 | Asia | Tianping | China | Flake | -27.7 | (Ma et al. 2021) |
| 20TP08 | Asia | Tianping | China | Flake | -27.3 | (Ma et al. 2021) |
| PD-10 | Asia | Liugezhuang | China | Flake | -21.3 | (Wang et al. 2019) |
| PD-17 | Asia | Liugezhuang | China | Flake | -24.7 | (Wang et al. 2019, Meng 2016) |
| Z25 | Asia | Hadamengou | China | Flake | -25.86 | (Wang et al. 1988) |
| Z26 | Asia | Hadamengou | China | Flake | -24.55 | (Wang et al. 1988) |
| Z27 | Asia | Hadamengou | China | Flake | -16.1 | (Wang et al. 1988) |
| Z28 | Asia | Hadamengou | China | Flake | -20.54 | (Wang et al. 1988) |
| Z20 | Asia | Miaogou | China | Flake | -28.97 | (Wang et al. 1988) |
| Z21 | Asia | Miaogou | China | Flake | -14.6 | (Wang et al. 1988) |
| Z22 | Asia | Miaogou | China | Flake | -15.41 | (Wang et al. 1988) |
| Z23 | Asia | Miaogou | China | Flake | -13.95 | (Wang et al. 1988) |
| Z16 | Asia | Xinghe | China | Flake | -20.49 | (Wang et al. 1988) |
| Z17 | Asia | Xinghe | China | Flake | -20.78 | (Wang et al. 1988) |
| Z18 | Asia | Xinghe | China | Flake | -20.64 | (Wang et al. 1988) |
| DL-4 | Asia | Daliangziko u | China | Flake | -17.9 | (Wang et al. 2019) |
| DL-9 | Asia | Daliangziko u | China | Flake | -18 | (Wang et al. 2019) |
| LG-6 | Asia | Liugezhuang | China | Flake | -22.3 | (Wang et al. 2019) |
| B5304-1 | Asia | Bairiqili | China | Flake | -21.6 | (Yan et al. 2020) |
| B5304-3 | Asia | Bairiqili | China | Flake | -21.6 | (Yan et al. 2020) |
| B5304-2 | Asia | Bairiqili | China | Flake | -23 | (Yan et al. 2020) |
| B3458-1 | Asia | Banhongshan | China | Flake | -23.1 | (Yan et al. 2020) |
| B3461-1 | Asia | Banhongshan | China | Flake | -23.2 | (Yan et al. 2020) |
| B3461-2 | Asia | Banhongshan | China | Flake | -23.4 | (Yan et al. 2020) |

| | | | | | | |
|---|---|---|---|---|---|---|
| B3763-4 | Asia | Banhongshan | China | Flake | -23.4 | (Yan et al. 2020) |
| B3763-5 | Asia | Banhongshan | China | Flake | -23.9 | (Yan et al. 2020) |
| B20002-1 | Asia | Datonggou | China | Flake | -23.7 | (Yan et al. 2020) |
| B2103-1 | Asia | Datonggou | China | Flake | -23.3 | (Yan et al. 2020) |
| B2103-2 | Asia | Datonggou | China | Flake | -24 | (Yan et al. 2020) |
| B2103-3 | Asia | Datonggou | China | Flake | -23.8 | (Yan et al. 2020) |
| B2011TC1-1 | Asia | Datonggou | China | Flake | -23.7 | (Yan et al. 2020) |
| B2011TC1-2 | Asia | Datonggou | China | Flake | -23.3 | (Yan et al. 2020) |
| JHS-1 | Asia | Jinhongshan | China | Flake | -23.1 | (Yan et al. 2020) |
| JHS-2 | Asia | Jinhongshan | China | Flake | -26.3 | (Yan et al. 2020) |
| JHS-3 | Asia | Jinhongshan | China | Flake | -22.9 | (Yan et al. 2020) |
| JHS-4 | Asia | Jinhongshan | China | Flake | -23.6 | (Yan et al. 2020) |
| JHS-5 | Asia | Jinhongshan | China | Flake | -23.1 | (Yan et al. 2020) |
| JHS-6 | Asia | Jinhongshan | China | Flake | -24.8 | (Yan et al. 2020) |
| B2003-1 | Asia | Koukouertu | China | Flake | -22.5 | (Yan et al. 2020) |
| B2003-2 | Asia | Koukouertu | China | Flake | -23.5 | (Yan et al. 2020) |
| BTC2-1-3 | Asia | Koukouertu | China | Flake | -22.5 | (Yan et al. 2020) |
| BTC3-1-2 | Asia | Koukouertu | China | Flake | -23.2 | (Yan et al. 2020) |
| B6305-1 | Asia | Zelikeng | China | Flake | -22.3 | (Yan et al. 2020) |
| B6305-3 | Asia | Zelikeng | China | Flake | -22.3 | (Yan et al. 2020) |
| B6305-4 | Asia | Zelikeng | China | Flake | -22.8 | (Yan et al. 2020) |
| B6305-5 | Asia | Zelikeng | China | Flake | -22.5 | (Yan et al. 2020) |
| B6308-1 | Asia | Zelikeng | China | Flake | -23.1 | (Yan et al. 2020) |
| B6308-3 | Asia | Zelikeng | China | Flake | -23 | (Yan et al. 2020) |
| OY-XH-6a-1 | Asia | Huangtuyao | China | Flake | -25.5 | (Yang et al. 2014) |
| OY-XH-6a-2/1 | Asia | Huangtuyao | China | Flake | -25.48 | (Yang et al. 2014) |
| OY-XH-6a-2/2 | Asia | Huangtuyao | China | Flake | -25.5 | (Yang et al. 2014) |
| OY-XH-6b-1 | Asia | Huangtuyao | China | Flake | -15.77 | (Yang et al. 2014) |
| OY-XH-6b-2 | Asia | Huangtuyao | China | Flake | -16.77 | (Yang et al. 2014) |
| OY-XH-6c-1A2 | Asia | Huangtuyao | China | Flake | -19.05 | (Yang et al. 2014) |
| OY-XH-6c-1B1 | Asia | Huangtuyao | China | Flake | -20.63 | (Yang et al. 2014) |
| OY-XH-6c-1B2 | Asia | Huangtuyao | China | Flake | -20.93 | (Yang et al. 2014) |
| OY-XH-6c-1B3 | Asia | Huangtuyao | China | Flake | -20.76 | (Yang et al. 2014) |
| OY-XH-6c-1B4 | Asia | Huangtuyao | China | Flake | -20.72 | (Yang et al. 2014) |
| OY-XH-6d1-1 | Asia | Huangtuyao | China | Flake | -25.63 | (Yang et al. 2014) |
| OY-XH-6d1-2 | Asia | Huangtuyao | China | Flake | -25.66 | (Yang et al. 2014) |
| OY-XH-6d2 | Asia | Huangtuyao | China | Flake | -25.5 | (Yang et al. 2014) |
| OY-XH-6d3-1 | Asia | Huangtuyao | China | Flake | -25.28 | (Yang et al. 2014) |
| OY-XH-6d3-2 | Asia | Huangtuyao | China | Flake | -25.56 | (Yang et al. 2014) |
| OY-XH-6d4-1 | Asia | Huangtuyao | China | Flake | -20.6 | (Yang et al. 2014) |
| ZK7-4H25 | Asia | Magou | China | Flake | -18.65 | (Zhu et al. 2021) |
| ZK7-4H31 | Asia | Magou | China | Flake | -22.88 | (Zhu et al. 2021) |
| ZK7-4H42 | Asia | Magou | China | Flake | -25.93 | (Zhu et al. 2021) |
| ZK7-4H55 | Asia | Magou | China | Flake | -20.94 | (Zhu et al. 2021) |
| ZK7-4H66 | Asia | Magou | China | Flake | -18.63 | (Zhu et al. 2021) |
| ZK7-4H95 | Asia | Magou | China | Flake | -17.39 | (Zhu et al. 2021) |

| | | | | | | |
|---|---|---|---|---|---|---|
| ZK3-7H4 | Asia | Magou | China | Flake | -18.13 | (Zhu et al. 2021) |
| ZK3-7H9 | Asia | Magou | China | Flake | -22.47 | (Zhu et al. 2021) |
| ZK3-7H14 | Asia | Magou | China | Flake | -25 | (Zhu et al. 2021) |
| ZK3-7H24 | Asia | Magou | China | Flake | -25.72 | (Zhu et al. 2021) |
| ZK3-7H32 | Asia | Magou | China | Flake | -21.88 | (Zhu et al. 2021) |
| ZK3-7H32-rep | Asia | Magou | China | Flake | -21.78 | (Zhu et al. 2021) |
| ZK3-7H37 | Asia | Magou | China | Flake | -18.83 | (Zhu et al. 2021) |
| ZK3-7H101 | Asia | Magou | China | Flake | -18.39 | (Zhu et al. 2021) |
| ZK3-7H118 | Asia | Magou | China | Flake | -16.49 | (Zhu et al. 2021) |
| WLG-1–01 | Asia | Wuligou | China | Flake | -15.14 | (Zhu et al. 2021) |
| WLG-1–05 | Asia | Wuligou | China | Flake | -15.71 | (Zhu et al. 2021) |
| WLG-1–18 | Asia | Wuligou | China | Flake | -14.95 | (Zhu et al. 2021) |
| WLG-1–19 | Asia | Wuligou | China | Flake | -16.22 | (Zhu et al. 2021) |
| WLG-2–01 | Asia | Wuligou | China | Flake | -18.34 | (Zhu et al. 2021) |
| WLG-2–02 | Asia | Wuligou | China | Flake | -17.82 | (Zhu et al. 2021) |
| WLG-2–03 | Asia | Wuligou | China | Flake | -13.93 | (Zhu et al. 2021) |
| WLG-2–04 | Asia | Wuligou | China | Flake | -13.71 | (Zhu et al. 2021) |
| WLG-2–04-rep | Asia | Wuligou | China | Flake | -13.69 | (Zhu et al. 2021) |
| 15a2 | Asia | Itna | India | Flake | -24 | (B. Maibam, P. Sanyal, S. Bhattacharya 2015) |
| 15A1 | Asia | Itna | India | Flake | -24.6 | (Maibam et al. 2015) |
| 15A2 | Asia | Itna | India | Flake | -24.6 | (Maibam et al. 2015) |
| 15b1 | Asia | Itna | India | Flake | -24.9 | (Maibam et al. 2015) |
| 15b2 | Asia | Itna | India | Flake | -24.8 | (Maibam et al. 2015) |
| 15B1 | Asia | Itna | India | Flake | -25.2 | (Maibam et al. 2015) |
| 14a | Asia | Thumbasoge | India | Flake | -20.6 | (Maibam et al. 2015) |
| 14b | Asia | Thumbasoge | India | Flake | -21.3 | (Maibam et al. 2015) |
| 14A | Asia | Thumbasoge | India | Flake | -21.5 | (Maibam et al. 2015) |
| 14B | Asia | Thumbasoge | India | Flake | -20.5 | (Maibam et al. 2015) |
| 14C | Asia | Thumbasoge | India | Flake | -20.6 | (Maibam et al. 2015) |
| GR-KLD-1-3 | Asia | Koliakode | India | Vein | -17.5 | (Zhang and Santosh 2019) |
| GR-KLD-2-4 | Asia | Koliakode | India | Vein | -12.8 | (Zhang and Santosh 2019) |
| GR-KLD-3-3 | Asia | Koliakode | India | Vein | -12.8 | (Zhang and Santosh 2019) |
| GR-KLD-4-2 | Asia | Koliakode | India | Vein | -13.8 | (Zhang and Santosh 2019) |
| GR-KLP-3 | Asia | Kulappara | India | Vein | -11.7 | (Zhang and Santosh 2019) |
| GR-KLP-4-1 | Asia | Kulappara | India | Vein | -12.1 | (Zhang and Santosh 2019) |
| GR-KLP-4-3 | Asia | Kulappara | India | Vein | -13.3 | (Zhang and Santosh 2019) |
| 114400 | Europe | Guadamur | Spain | Flake | -20.59 | (Martín-Méndez et al. 2016) |
| 114632 | Europe | Guadamur | Spain | Flake | -27.76 | (Martin-Mendez et al. 2016) |
| 114633 | Europe | Guadamur | Spain | Flake | -20.92 | (Martin-Mendez et al. 2016) |
| 114428 | Europe | Guadamur mine site | Spain | Flake | -27.63 | (Martin-Mendez et al. 2016) |
| 114429 | Europe | Guadamur mine site | Spain | Flake | -27.86 | (Martin-Mendez et al. 2016) |
| 114430 | Europe | Guadamur mine site | Spain | Flake | -27.86 | (Martin-Mendez et al. 2016) |

| | | | | | | |
|---|---|---|---|---|---|---|
| 114431 | Europe | Guadamur mine site (trench) | Spain | Flake | -27.64 | (Martin-Mendez et al. 2016) |
| 114432 | Europe | Guadamur mine site (waste) | Spain | Flake | -27.78 | (Martin-Mendez et al. 2016) |
| 114433 | Europe | Guadamur mine site (waste) | Spain | Flake | -27.75 | (Martin-Mendez et al. 2016) |
| 114434 | Europe | Guadamur mine site (waste) | Spain | Flake | -27.59 | (Martin-Mendez et al. 2016) |
| 114568 | Europe | P. Montalbán mine | Spain | Flake | -20.91 | (Martin-Mendez et al. 2016) |
| 114554 | Europe | P. Montalbán mine | Spain | Flake | -23.15 | (Martin-Mendez et al. 2016) |
| 114555 | Europe | P. Montalbán mine | Spain | Flake | -23.03 | (Martin-Mendez et al. 2016) |
| 114556 | Europe | P. Montalbán mine | Spain | Flake | -23.13 | (Martin-Mendez et al. 2016) |
| 114557 | Europe | P. Montalbán mine | Spain | Flake | -23.01 | (Martin-Mendez et al. 2016) |
| 114571 | Europe | Puebla Montalbán | Spain | Flake | -23.38 | (Martin-Mendez et al. 2016) |
| 114566 | Europe | Puebla Montalbán | Spain | Flake | -20.58 | (Martin-Mendez et al. 2016) |
| 114567 | Europe | Puebla Montalbán | Spain | Flake | -20.46 | (Martin-Mendez et al. 2016) |
| U-10 | Europe | SCS lower crust | Spain | Flake | -18.28 | (Martin-Mendez et al. 2016) |
| U-10 | Europe | SCS lower crust | Spain | Flake | -19.7 | (Martin-Mendez et al. 2016) |
| 00S10115st1-4 | Asia | Digana | Sri Lanka | Vein | -7.6 | (Touzain et al. 2010) |
| 00S10115st1-3 | Asia | Digana | Sri Lanka | Vein | -8.5 | (Touzain et al. 2010) |
| 00Sl0115st-1-1 | Asia | Digana | Sri Lanka | Vein | -7.5 | (Binu-Lal et al. 2003) |
| 00Sl0115st-1-3 | Asia | Digana | Sri Lanka | Vein | -7.9 | (Binu-Lal et al. 2003) |
| 00Sl0115st-1-3 | Asia | Digana | Sri Lanka | Vein | -7.7 | (Binu-Lal et al. 2003) |
| 00Sl0115st-1-4 | Asia | Digana | Sri Lanka | Vein | -7.8 | (Binu-Lal et al. 2003) |
| 00Sl0115st-1-6-1 | Asia | Digana | Sri Lanka | Vein | -6.3 | (Binu-Lal et al. 2003) |
| 00Sl0115st-1-6-1 | Asia | Digana | Sri Lanka | Vein | -7 | (Binu-Lal et al. 2003) |
| 00Sl0115st-2-1 | Asia | Digana | Sri Lanka | Vein | -7.3 | (Binu-Lal et al. 2003) |
| 00Sl0115st-2-1 | Asia | Digana | Sri Lanka | Vein | -7.2 | (Binu-Lal et al. 2003) |
| 00Sl0115st-2-2 | Asia | Digana | Sri Lanka | Vein | -4.5 | (Binu-Lal et al. 2003) |
| 00Sl011st2-2 | Asia | Digana | Sri Lanka | Vein | -1.6 | (Binu-Lal et al. 2003) |
| 00Sl011st2-2 | Asia | Digana | Sri Lanka | Vein | -1.7 | (Binu-Lal et al. 2003) |

| | | | | | | |
|---|---|---|---|---|---|---|
| 00Sl011st2-2 | Asia | Digana | Sri Lanka | Vein | -2.3 | (Binu-Lal et al. 2003) |
| 00Sl0114st-5 | Asia | Magaha-Unuwinna | Sri Lanka | Vein | -8.7 | (Binu-Lal et al. 2003) |
| 00Sl0115st-1-4 Inta Crystalline | Asia | Digana | Sri Lanka | Vein | -7.64 | (Binu-Lal et al. 2003) |
| 00Sl0115st-1-4 Inta Crystalline | Asia | Digana | Sri Lanka | Vein | -7.65 | (Binu-Lal et al. 2003) |
| 00Sl0115st-1-4 Inta Crystalline | Asia | Digana | Sri Lanka | Vein | -7.67 | (Binu-Lal et al. 2003) |
| 00Sl0115st-1-4 Inta Crystalline | Asia | Digana | Sri Lanka | Vein | -7.61 | (Binu-Lal et al. 2003) |
| 00Sl0115st-1-4 Inta Crystalline | Asia | Digana | Sri Lanka | Vein | -7.59 | (Binu-Lal et al. 2003) |
| 00Sl0115st-1-4 Inta Crystalline | Asia | Digana | Sri Lanka | Vein | -7.59 | (Binu-Lal et al. 2003) |
| 00Sl0115st-1-4 Inta Crystalline | Asia | Digana | Sri Lanka | Vein | -7.59 | (Binu-Lal et al. 2003) |
| 00Sl0115st-1-3 Intra Crystalline | Asia | Digana | Sri Lanka | Vein | -8.92 | (Binu-Lal et al. 2003) |
| 00Sl0115st-1-3 Intra Crystalline | Asia | Digana | Sri Lanka | Vein | -8.81 | (Binu-Lal et al. 2003) |
| 00Sl0115st-1-3 Intra Crystalline | Asia | Digana | Sri Lanka | Vein | -8.2 | (Binu-Lal et al. 2003) |
| 00Sl0115st-1-3 Intra Crystalline | Asia | Digana | Sri Lanka | Vein | -9.36 | (Binu-Lal et al. 2003) |
| 00Sl0115st-1-3 Intra Crystalline | Asia | Digana | Sri Lanka | Vein | -7.98 | (Binu-Lal et al. 2003) |
| 00Sl0115st-1-3 Intra Crystalline | Asia | Digana | Sri Lanka | Vein | -7.82 | (Binu-Lal et al. 2003) |
| 00Sl0115st-1-6-1 Intra Crystalline | Asia | Digana | Sri Lanka | Vein | -7.8 | (Binu-Lal et al. 2003) |
| 00Sl0115st-1-6-1 Intra Crystalline | Asia | Digana | Sri Lanka | Vein | -6.91 | (Binu-Lal et al. 2003) |
| 00Sl0115st-1-6-1 Intra Crystalline | Asia | Digana | Sri Lanka | Vein | -6.65 | (Binu-Lal et al. 2003) |
| 00Sl0115st-1-6-1 Intra Crystalline | Asia | Digana | Sri Lanka | Vein | -6.65 | (Binu-Lal et al. 2003) |
| 00Sl0115st2-2 Intra Crystalline | Asia | Digana | Sri Lanka | Vein | -0.64 | (Binu-Lal et al. 2003) |
| 00Sl0115st2-2 Intra Crystalline | Asia | Digana | Sri Lanka | Vein | -1.37 | (Binu-Lal et al. 2003) |
| 00Sl0115st2-2 Intra Crystalline | Asia | Digana | Sri Lanka | Vein | -1.39 | (Binu-Lal et al. 2003) |
| 010W77 | Asia | Bogala | Sri Lanka | Vein | -7.76 | (Touzain et al. 2010) |
| BSSF | Asia | Bogala | Sri Lanka | Vein | -10.34 | (Touzain et al. 2010) |
| BNPG | Asia | Bogala | Sri Lanka | Vein | -9.64 | (Touzain et al. 2010) |
| BCSF | Asia | Bogala | Sri Lanka | Vein | -9.45 | (Touzain et al. 2010) |
| BCFR | Asia | Bogala | Sri Lanka | Vein | -9.43 | (Touzain et al. 2010) |
| Close to nuclei | Asia | Bogala | Sri Lanka | Vein | -8.29 | (Touzain et al. 2010) |
| na | Asia | Bogala | Sri Lanka | Vein | -7.79 | (Dobner et al. 1978) |
| na | Asia | Bogala | Sri Lanka | Vein | -8.61 | (Dobner et al. 1978) |
| na | Asia | Bogala | Sri Lanka | Vein | -7.42 | (Dobner et al. 1978) |

| | | | | | | |
|---|---|---|---|---|---|---|
| na | Asia | Bogala | Sri Lanka | Vein | -7.3 | (Dobner et al. 1978) |
| na | Asia | Bogala | Sri Lanka | Vein | -7.2 | (Dobner et al. 1978) |
| na | Asia | Bogala | Sri Lanka | Vein | -7.18 | (Dobner et al. 1978) |
| na | Asia | Bogala | Sri Lanka | Vein | -8.11 | (Dobner et al. 1978) |
| na | Asia | Bogala | Sri Lanka | Vein | -8.23 | (Dobner et al. 1978)) |
| na | Asia | Bogala | Sri Lanka | Vein | -7.35 | (Dobner et al. 1978) |
| na | Asia | Bogala | Sri Lanka | Vein | -8.66 | (Dobner et al. 1978) |
| na | Asia | Bogala | Sri Lanka | Vein | -7.3 | (Dobner et al. 1978) |
| na | Asia | Bogala | Sri Lanka | Vein | -7.49 | (Dobner et al. 1978) |
| BSL88-30-4a | Asia | Bogala | Sri Lanka | Vein | -8 | (Hoernes et al. 1994) |
| BSL88-30-4b | Asia | Bogala | Sri Lanka | Vein | -7.6 | (Hoernes et al. 1994) |
| BSL88-30-5 | Asia | Bogala | Sri Lanka | Vein | -7.9 | (Hoernes et al. 1994) |
| KSSF | Asia | Kahatagaha –Kolongaha | Sri Lanka | Vein | -8.7 | (Touzain et al. 2010) |
| KNPG | Asia | Kahatagaha –Kolongaha | Sri Lanka | Vein | -8.95 | (Touzain et al. 2010) |
| KCSF | Asia | Kahatagaha –Kolongaha | Sri Lanka | Vein | -5.61 | (Touzain et al. 2010) |
| KCFR | Asia | Kahatagaha –Kolongaha | Sri Lanka | Vein | -9.29 | (Touzain et al. 2010) |
| Close to nuclei | Asia | Kahatagaha –Kolongaha | Sri Lanka | Vein | -7.9 | (Touzain et al. 2010) |
| 010W76 | Asia | Bogala | Sri Lanka | Vein | -8.6 | (Weis et al. 1981; Touzain et al. 2010) |
| 009W76 | Asia | Kahatagaha –Kolongaha | Sri Lanka | Vein | -8 | (Weis et al. 1981; Touzain et al. 2010) |
| BSL88-31-1 | Asia | Kahatagaha –Kolongaha | Sri Lanka | Vein | -6.2 | (Hoernes et al. 1994) |
| BSL88-31-3a | Asia | Kahatagaha –Kolongaha | Sri Lanka | Vein | -6.3 | (Hoernes et al. 1994) |
| BSL88-31-3b | Asia | Kahatagaha –Kolongaha | Sri Lanka | Vein | -6.7 | (Hoernes et al. 1994) |
| BSL88-31-3c | Asia | Kahatagaha –Kolongaha | Sri Lanka | Vein | -7 | (Hoernes et al. 1994) |
| BSL88-31-4 | Asia | Kahatagaha –Kolongaha | Sri Lanka | Vein | -6.7 | (Hoernes et al. 1994) |
| Graphite Gneiss | Europe | Zavalje | Ukraine | Flake | -35.08 | (Zagnitko et al. 2013) |
| Garnet-graphite gneiss | Europe | Zavalje | Ukraine | Flake | -30.65 | (Zagnitko et al. 2013) |
| Graphite Garnet biotite gneiss | Europe | Zavalje | Ukraine | Flake | -30.5 | (Zagnitko et al. 2013) |
| Graphite Garnet biotite gneiss | Europe | Zavalje | Ukraine | Flake | -34.5 | (Zagnitko et al. 2013) |
| 82-14A-1 | North America | Antrim | USA | Vein | -15.8 | (Rumble and Hoering 1986) |
| 82-14A-2 | North America | Antrim | USA | Vein | -17 | (Rumble and Hoering 1986) |
| 82-14A-3 | North America | Antrim | USA | Vein | -15.7 | (Rumble and Hoering 1986) |

| | | | | | | |
|---|---|---|---|---|---|---|
| 82-14A-4 | North America | Antrim | USA | Vein | -16 | (Rumble and Hoering 1986) |
| 82-14A-5 | North America | Antrim | USA | Vein | -15.8 | (Rumble and Hoering 1986) |
| 82-14A-6 | North America | Antrim | USA | Vein | -16.1 | (Rumble and Hoering 1986) |
| 82-14A-7 | North America | Antrim | USA | Vein | -17.2 | (Rumble and Hoering 1986) |
| 82-14B | North America | Antrim | USA | Vein | -15.9 | (Rumble and Hoering 1986) |
| 81-8A | North America | Bristol | USA | Vein | -17 | (Rumble and Hoering 1986) |
| 8I-8B-1 | North America | Bristol | USA | Vein | -16.9 | (Rumble and Hoering 1986) |
| 81-8B-2 | North America | Bristol | USA | Vein | -16.6 | (Rumble and Hoering 1986) |
| 81-8C | North America | Bristol | USA | Vein | -17.2 | (Rumble and Hoering 1986) |
| 81-8F | North America | Bristol | USA | Vein | -17.4 | (Rumble and Hoering 1986) |
| 81-80 | North America | Bristol | USA | Vein | -17.3 | (Rumble and Hoering 1986) |
| 81-8P-1 | North America | Bristol | USA | Vein | -17 | (Rumble and Hoering 1986) |
| 81-8P-2 | North America | Bristol | USA | Vein | -17.9 | (Rumble and Hoering 1986) |
| 81-8P-3 | North America | Bristol | USA | Vein | -16.9 | (Rumble and Hoering 1986) |
| 81-8Q-1 | North America | Bristol | USA | Vein | -17 | (Rumble and Hoering 1986) |
| 81-8Q-2 | North America | Bristol | USA | Vein | -17 | (Rumble and Hoering 1986) |
| 80-41C-1 | North America | Franklin in Pierce | USA | Vein | -9.4 | (Rumble and Hoering 1986) |
| 80-41C-2 | North America | Franklin in Pierce | USA | Vein | -9.2 | (Rumble and Hoering 1986) |
| BO-41C-3 | North America | Franklin in Pierce | USA | Vein | -9.8 | (Rumble and Hoering 1986) |
| 80-41D-3 | North America | Franklin in Pierce | USA | Vein | -12.4 | (Rumble and Hoering 1986) |
| BO-41D-4 | North America | Franklin in Pierce | USA | Vein | -12.9 | (Rumble and Hoering 1986) |
| 80-41D-5 | North America | Franklin in Pierce | USA | Vein | -12.7 | (Rumble and Hoering 1986) |
| 80-41D-6 | North America | Franklin in Pierce | USA | Vein | -12.8 | (Rumble and Hoering 1986) |
| 80-41D-7 | North America | Franklin in Pierce | USA | Vein | -13.3 | (Rumble and Hoering 1986) |
| 80-41M-3 | North America | Franklin in Pierce | USA | Vein | -11 | (Rumble and Hoering 1986) |
| 80-41N-1 | North America | Franklin in Pierce | USA | Vein | -12.1 | (Rumble and Hoering 1986) |
| 80-41N-2 | North America | Franklin in Pierce | USA | Vein | -11.1 | (Rumble and Hoering 1986) |
| 80-41N-3 | North America | Franklin in Pierce | USA | Vein | -12 | (Rumble and Hoering 1986) |
| 80-41AA-4 | North America | Franklin in Pierce | USA | Vein | -11.5 | (Rumble and Hoering 1986) |
| 80-41AA-5 | North America | Franklin in Pierce | USA | Vein | -11.8 | (Rumble and Hoering 1986) |
| 80-41AA-6 | North America | Franklin in Pierce | USA | Vein | -12.6 | (Rumble and Hoering 1986) |

| | | | | | | |
|---|---|---|---|---|---|---|
| 80-41AA-7 | North America | Franklin in Pierce | USA | Vein | -12.4 | (Rumble and Hoering 1986) |
| 80-41AA-8 | North America | Franklin in Pierce | USA | Vein | -12.4 | (Rumble and Hoering 1986) |
| 80-41AA-9 | North America | Franklin in Pierce | USA | Vein | -11.2 | (Rumble and Hoering 1986) |
| 80-41AA-10 | North America | Franklin in Pierce | USA | Vein | -11.1 | (Rumble and Hoering 1986) |
| 80-41AA-11 | North America | Franklin in Pierce | USA | Vein | -11.1 | (Rumble and Hoering 1986) |
| 80-41AA-12 | North America | Franklin in Pierce | USA | Vein | -12.6 | (Rumble and Hoering 1986) |
| 80-41AA-13 | North America | Franklin in Pierce | USA | Vein | -12.4 | (Rumble and Hoering 1986) |
| 80-41AA-14 | North America | Franklin in Pierce | USA | Vein | -11.9 | (Rumble and Hoering 1986) |
| 80-41AA-15 | North America | Franklin in Pierce | USA | Vein | -11.4 | (Rumble and Hoering 1986) |
| 80-41BB-3 | North America | Franklin in Pierce | USA | Vein | -15.3 | (Rumble and Hoering 1986) |
| 80-41BB-4 | North America | Franklin in Pierce | USA | Vein | -12.4 | (Rumble and Hoering 1986) |
| 80-41BB-5 | North America | Franklin in Pierce | USA | Vein | -12.4 | (Rumble and Hoering 1986) |
| 80-41BB-6 | North America | Franklin in Pierce | USA | Vein | -12.2 | (Rumble and Hoering 1986) |
| 80-41BB-7 | North America | Franklin in Pierce | USA | Vein | -12.1 | (Rumble and Hoering 1986) |
| BO-41BB-8 | North America | Franklin in Pierce | USA | Vein | -12.4 | (Rumble and Hoering 1986) |
| 80-41BB-9 | North America | Franklin in Pierce | USA | Vein | -12 | (Rumble and Hoering 1986) |
| 80-41BB-10 | North America | Franklin in Pierce | USA | Vein | -12.8 | (Rumble and Hoering 1986) |
| 80-41BB-11 | North America | Franklin in Pierce | USA | Vein | -15.6 | (Rumble and Hoering 1986) |
| 80-41BB-12 | North America | Franklin in Pierce | USA | Vein | -15.1 | (Rumble and Hoering 1986) |
| 80-41BB-13 | North America | Franklin in Pierce | USA | Vein | -12.4 | (Rumble and Hoering 1986) |
| 80-41BB-14 | North America | Franklin in Pierce | USA | Vein | -16.2 | (Rumble and Hoering 1986) |
| 80-41A1-4 | North America | Franklin in Pierce | USA | Vein | -11.1 | (Rumble and Hoering 1986) |
| 80-41A1-6 | North America | Franklin in Pierce | USA | Vein | -11.4 | (Rumble and Hoering 1986) |
| 80-41A1-5 | North America | Franklin in Pierce | USA | Vein | -12.9 | (Rumble and Hoering 1986) |
| 80-41A1-7 | North America | Franklin in Pierce | USA | Vein | -13.6 | (Rumble and Hoering 1986) |
| 80-41A2-4 | North America | Franklin in Pierce | USA | Vein | -12.8 | (Rumble and Hoering 1986) |
| 80-41A2-5 | North America | Franklin in Pierce | USA | Vein | -13.1 | (Rumble and Hoering 1986) |
| 9220G-1 | North America | Annandale | USA | Flake | -23.2 | (Volkert et al. 2000) |
| 9220F-2 | North America | Annandale | USA | Flake | -27 | (Volkert et al. 2000) |
| 9220M | North America | Annandale | USA | Flake | -22.8 | (Volkert et al. 2000) |
| 9220D-1 | North America | Bloomingdale | USA | Flake | -19.2 | (Volkert et al. 2000) |

| | | | | | | |
|---|---|---|---|---|---|---|
| 9220K-3 | North America | Bloomingdale | USA | Flake | -21.3 | (Volkert et al. 2000) |
| 9220J-2 | North America | Bloomingdale | USA | Flake | -15 | (Volkert et al. 2000) |
| 9220C | North America | Fisher | USA | Flake | -16.4 | (Volkert et al. 2000) |
| 9220A | North America | High Bridge | USA | Flake | -25.5 | (Volkert et al. 2000) |
| 9220E | North America | Mendham | USA | Flake | -28.1 | (Volkert et al. 2000) |
| 9220N | North America | Oak Ridge | USA | Flake | -26.6 | (Volkert et al. 2000) |
| 9220B | North America | Sutton | USA | Flake | -28.4 | (Volkert et al. 2000) |
| 9220L | North America | Sutton | USA | Flake | -28.1 | (Volkert et al. 2000) |
| 9220I | North America | Wanaque | USA | Flake | -24.1 | (Volkert et al. 2000) |
| 006S75 | North America | Dillon | USA | Vein | -6.1 | (Paul L. Weis 1981); Touzain et al. 2010) |
| 001W76 | North America | Ticonderoga | USA | Vein | -6 | (Weis et al. 1981; Touzain et al. 2010) |
| AKIT17a | Africa | Aukam | Namibia | Vein | -16.5 | (Schiebel 2022) |
| AKIT17b | Africa | Aukam | Namibia | Vein | -15.78 | (Schiebel 2022) |
| AKIT15 | Africa | Aukam | Namibia | Vein | -16.54 | (Schiebel 2022) |
| AKIT14 | Africa | Aukam | Namibia | Vein | -16.06 | (Schiebel 2022) |
| AKIT13 | Africa | Aukam | Namibia | Vein | -14.68 | (Schiebel 2022) |
| AKIT12 | Africa | Aukam | Namibia | Vein | -14.92 | (Schiebel 2022) |
| AKIT11 | Africa | Aukam | Namibia | Vein | -14.18 | (Schiebel 2022) |
| AKIT08 | Africa | Aukam | Namibia | Vein | -17.31 | (Schiebel 2022) |

## B. Database of Graphite Carbon Isotope Values ($\delta^{13}C$) from Samples in this Project

| **sample ID** | **continent** | **mine/province** | **country** | **type** | **$\delta^{13}C$ (‰)** | | | | | | |
|---|---|---|---|---|---|---|---|---|---|---|---|
| 1A | Europe | Kaisersberg | Austria | amorph | -23.25 | -23.27 | -23.27 | | | | |
| 2A | Europe | Kaisersberg | Austria | amorph | -22.70 | -21.98 | -21.98 | -22.05 | | | |
| 1B | Africa | Balama | Mozambique | flake | -25.27 | -25.14 | -24.58 | -24.58 | | | |
| 2B | Europe | Skaland | Norway | flake | -21.09 | -21.09 | -20.93 | | | | |
| 3B | South America | Minas Gerais | Brazil | flake | -24.84 | -24.64 | -25.00 | -25.68 | -25.68 | -25.00 | |
| 4A | Asia | Hunan Lutang | China | amorph | -21.62 | -21.62 | -22.34 | | | | |
| 4B | Europe | Zavallia | Ukraine | flake | -33.73 | -33.25 | -34.24 | | | | |
| 5B | Asia | Taygink a | Russia | flake | -23.71 | -24.16 | -24.54 | -24.16 | | | |
| 6A | Europe | Kaisersberg | Austria | amorph | -22.45 | -21.10 | -22.45 | | | | |
| 6B | Asia | Inner Mongolia | China | flake | -17.96 | -17.95 | -19.15 | | | | |
| 7B | Asia | Heilongjian | China | flake | -23.21 | -23.21 | -21.67 | | | | |
| 10B | Asia | Ragedara | Sri Lanka | hydro (vein) | -7.25 | -13.09 | -7.19 | -8.08 | | | |

| | | | | | | | | | | | |
|---|---|---|---|---|---|---|---|---|---|---|---|
| 11B | Africa | Brickavil le | Madagasc ar | flake | -24.50 | -24.96 | -21.95 | -24.96 | | | |
| 13B | Europe | Kropfm ühl | Germany | flake | -23.66 | -23.76 | -23.66 | -24.64 | | | |
| 14B | Europe | Kropfm ühl | Germany | flake | -21.90 | -21.90 | -22.23 | -22.43 | -22.76 | | |
| 15B | Europe | Skaland | Norway | flake | -21.27 | -22.43 | -20.32 | | | | |
| 16B | Europe | Skaland | Norway | flake | -20.93 | -20.83 | -21.36 | -21.46 | | | |
| 21A | Asia | Shando ng | China | flake | -25.97 | -25.97 | -25.00 | | | | |
| 21B | Africa | Balama | Mozambi que | flake | -26.60 | -26.51 | -26.07 | -26.27 | | | |
| 21C | South America | Minas Gerais | Brazil | flake | -25.10 | -23.98 | -28.29 | | | | |
| 21D | Africa | Brickavil le | Madagasc ar | flake | -21.42 | -24.96 | -25.36 | | | | |
| 21E | Asia | Taygink a | Russia | flake | -23.71 | -25.28 | -24.42 | | | | |
| 21F | Asia | Ragedar a | Sri Lanka | hydro (vein) | -7.25 | -10.37 | -13.09 | | | | |
| 21G | Europe | Kaisersb erg | Austria | amorph | -21.32 | -21.32 | -21.30 | -21.30 | -21.84 | | |
| 21H | Europe | Kaisersb erg | Austria | amorph | -22.13 | -22.13 | -22.00 | -22.08 | -22.68 | -22.67 | |
| 21I | Europe | Kaisersb erg | Austria | amorph | -22.09 | -22.09 | -22.09 | -23.25 | -22.12 | -22.12 | -22.62 |
| 21K | Africa | Balama | Mozambi que | flake | -26.29 | -26.01 | -25.35 | | | | |
| 21L | Africa | Balama | Mozambi que | flake | -26.47 | -26.26 | -25.60 | | | | |
| 21M | South America | Minas Gerais | Brazil | flake | -24.33 | -24.34 | -24.50 | | | | |
| 21N | South America | Minas Gerais | Brazil | flake | -25.08 | -24.58 | -24.53 | | | | |
| 22A | Asia | Shando ng | China | flake | -23.39 | -23.73 | | | | | |
| 22B | Africa | Balama | Mozambi que | flake | -25.14 | -24.58 | -24.58 | | | | |
| 22C | South America | Minas Gerais | Brazil | flake | -24.28 | -24.18 | -24.39 | -24.82 | -24.72 | | |
| 22D | Africa | Brickavil le | Madagasc ar | flake | -21.95 | -24.96 | -23.00 | | | | |
| 22E | Asia | Taygink a | Russia | flake | -24.31 | -24.08 | | | | | |
| 22F | Europe | Zavallia | Ukraine | flake | -30.37 | -28.98 | -29.49 | | | | |
| 22G | Europe | Skaland | Norway | flake | -20.83 | -19.88 | -22.43 | -21.46 | -21.36 | | |
| 22H | Africa | Balama | Mozambi que | flake | -26.44 | -27.18 | | | | | |

## C. Finnish Graphite Samples (Supply Chain Coverage)

| Company | Origin | Sample type | Sample name | Sample ID | $\delta^{13}C$ (‰) |
|---|---|---|---|---|---|
| Beowulf Mining | Aitalompi, Finland | Ore | Typical ROM - Crushed core | 202100749 | -29.09 |
| Beowulf Mining | Aitalompi, Finland | Ore | Typical ROM - Crushed core | 202100749 | -29.69 |
| Beowulf Mining | Aitalompi, Finland | Ore | Typical ROM - Crushed core | 202100749 | -27.03 |
| Beowulf Mining | Aitalompi, Finland | Concentrate | Flotation concentrate - Fine Fraction | 202100752 | -27.70 |
| Beowulf Mining | Aitalompi, Finland | Concentrate | Flotation concentrate - Fine Fraction | 202100752 | -27.68 |
| Beowulf Mining | Aitalompi, Finland | Concentrate | Flotation concentrate - Fine Fraction | 202100752 | -27.72 |
| Beowulf Mining | Aitalompi, Finland | Concentrate | Flotation concentrate - Mid Fraction | 202100751 | -27.95 |
| Beowulf Mining | Aitalompi, Finland | Concentrate | Flotation concentrate - Mid Fraction | 202100751 | -27.39 |
| Beowulf Mining | Aitalompi, Finland | Concentrate | Flotation concentrate - Mid Fraction | 202100751 | -27.74 |
| Beowulf Mining | Aitalompi, Finland | Concentrate | Flotation concentrate - Coarse fraction | 202100750 | -27.15 |
| Beowulf Mining | Aitalompi, Finland | Concentrate | Flotation concentrate - Coarse fraction | 202100750 | -26.08 |
| Beowulf Mining | Aitalompi, Finland | Concentrate | Flotation concentrate - Coarse fraction | 202100750 | -27.63 |
| Beowulf Mining | Aitalompi, Finland | Product | Purifed spherical graphite (SPG) 2A | 202100754 | -27.63 |
| Beowulf Mining | Aitalompi, Finland | Product | Purifed spherical graphite (SPG) 2A | 202100754 | -27.39 |
| Beowulf Mining | Aitalompi, Finland | Product | Purifed spherical graphite (SPG) 2A | 202100754 | -27.83 |
| Beowulf Mining | Aitalompi, Finland | Product | Alkaline purified graphite | 202100755 | -27.45 |
| Beowulf Mining | Aitalompi, Finland | Product | Alkaline purified graphite | 202100755 | -27.49 |
| Beowulf Mining | Aitalompi, Finland | Product | Alkaline purified graphite | 202100755 | -29.05 |
| Beowulf Mining | Aitalompi, Finland | Product | Micronized graphite | 202100756 | -27.26 |
| Beowulf Mining | Aitalompi, Finland | Product | Micronized graphite | 202100756 | -27.47 |
| Beowulf Mining | Aitalompi, Finland | Product | Micronized graphite | 202100756 | -29.76 |
| Beowulf Mining | Aitalompi, Finland | Residue | By-product | 202100757 | -27.47 |
| Beowulf Mining | Aitalompi, Finland | Residue | By-product | 202100757 | -27.36 |
| Beowulf Mining | Aitalompi, Finland | Residue | By-product | 202100757 | -28.08 |
| Beowulf Mining | Aitalompi, Finland | Core | Core Samples (Easter Zone) | AITDD17007 | -30.58 |
| Beowulf Mining | Aitalompi, Finland | Core | Core Samples (Easter Zone) | AITDD17007 | -25.75 |
| Beowulf Mining | Aitalompi, Finland | Core | Core Samples (Easter Zone) | AITDD17008 | -27.77 |
| Beowulf Mining | Aitalompi, Finland | Core | Core Samples (Easter Zone) | AITDD17008 | -30.93 |
| Beowulf Mining | Aitalompi, Finland | Core | Core Samples (Easter Zone) | AITDD18012 | -27.23 |
| Beowulf Mining | Aitalompi, Finland | Core | Core Samples (Easter Zone) | AITDD18012 | -26.77 |
| Beowulf Mining | Aitalompi, Finland | Core | Core Samples (Western Zone) | AITDD18018 | -26.83 |
| Beowulf Mining | Aitalompi, Finland | Core | Core Samples (Western Zone) | AITDD18018 | -30.20 |

| | | | | | |
|---|---|---|---|---|---|
| Beowulf Mining | Aitalompi, Finland | Core | Core Samples (Western Zone) | AITDD18016A | -30.44 |
| Beowulf Mining | Aitalompi, Finland | Core | Core Samples (Western Zone) | AITDD18016A | -28.07 |
| Beowulf Mining | Aitalompi, Finland | Core | Core Samples (Western Zone) | AITDD18016B | -28.07 |
| Beowulf Mining | Aitalompi, Finland | Core | Core Samples (Western Zone) | AITDD18016B | -30.34 |
| Beowulf Mining | Aitalompi, Finland | Core | Core Samples (Western Zone) | AITDD18015 | -29.51 |
| Beowulf Mining | Aitalompi, Finland | Core | Core Samples (Western Zone) | AITDD18015 | -28.48814286 |
| GTK | Emas, Finland | Ore | Flotation Feed | 202301520 | -27.77 |
| GTK | Emas, Finland | Ore | Flotation Feed | 202301520 | -28.51 |
| GTK | Emas, Finland | Ore | Flotation Feed | 202301520 | -29.21 |
| GTK | Emas, Finland | Ore | Flotation Feed | 202301520 | -27.48 |
| GTK | Emas, Finland | Concentrate | Flotation Rougher Concentrate | 202301521 | -29.15 |
| GTK | Emas, Finland | Concentrate | Flotation Rougher Concentrate | 202301521 | -26.74 |
| GTK | Emas, Finland | Concentrate | Flotation Rougher Concentrate | 202301521 | -28.41 |
| GTK | Emas, Finland | Concentrate | Flotation Rougher Concentrate | 202301521 | -26.59 |
| GTK | Emas, Finland | Concentrate | Flotation Cleaner Concentrate | 202301522 | -27.05 |
| GTK | Emas, Finland | Concentrate | Flotation Cleaner Concentrate | 202301522 | -26.71 |
| GTK | Emas, Finland | Concentrate | Flotation Cleaner Concentrate | 202301522 | -27.25 |
| GTK | Emas, Finland | Concentrate | Flotation Cleaner Concentrate | 202301522 | -25.82 |
| GTK | Emas, Finland | Product | Purified graphite | 202301523 | -26.35 |
| GTK | Emas, Finland | Product | Purified graphite | 202301523 | -27.00 |
| GTK | Emas, Finland | Product | Purified graphite | 202301523 | -26.65 |
| GTK | Emas, Finland | Product | Purified graphite | 202301523 | -25.98 |
| GTK | Raisjoki, Finland | Ore | Flotation Feed | 202301524 | -27.71 |
| GTK | Raisjoki, Finland | Ore | Flotation Feed | 202301524 | -27.90 |
| GTK | Raisjoki, Finland | Ore | Flotation Feed | 202301524 | -28.13 |
| GTK | Raisjoki, Finland | Ore | Flotation Feed | 202301524 | -26.86 |
| GTK | Raisjoki, Finland | Concentrate | Flotation Rougher Concentrate | 202301525 Rough | -28.25 |
| GTK | Raisjoki, Finland | Concentrate | Flotation Rougher Concentrate | 202301525 Rough | -26.74 |
| GTK | Raisjoki, Finland | Concentrate | Flotation Rougher Concentrate | 202301525 Rough | -26.75 |
| GTK | Raisjoki, Finland | Concentrate | Flotation Cleaner Concentrate | 202301525 Clean | -27.42 |
| GTK | Raisjoki, Finland | Concentrate | Flotation Cleaner Concentrate | 202301525 Clean | -27.50 |
| GTK | Raisjoki, Finland | Concentrate | Flotation Cleaner Concentrate | 202301525 Clean | -27.45 |
| GTK | Raisjoki, Finland | Product | Purified graphite | 202301527 | -27.56 |
| GTK | Raisjoki, Finland | Product | Purified graphite | 202301527 | -27.85 |
| GTK | Raisjoki, Finland | Product | Purified graphite | 202301527 | -27.54 |
| GTK | Raisjoki, Finland | Product | Purified graphite | 202301527 | -27.42 |
| GTK | Koivuniemi, Finland | Ore | Flotation Feed | 202301528 | -27.48 |
| GTK | Koivuniemi, Finland | Ore | Flotation Feed | 202301528 | -26.65 |
| GTK | Koivuniemi, Finland | Ore | Flotation Feed | 202301528 | -31.44 |
| GTK | Koivuniemi, Finland | Ore | Flotation Feed | 202301528 | -29.76 |
| GTK | Koivuniemi, Finland | Concentrate | Flotation Rougher Concentrate | 202301529 | -31.15 |
| GTK | Koivuniemi, Finland | Concentrate | Flotation Rougher Concentrate | 202301529 | -31.49 |

| | | | | | |
|---|---|---|---|---|---|
| GTK | Koivuniemi, Finland | Concentrate | Flotation Rougher Concentrate | 202301529 | -30.87 |
| GTK | Koivuniemi, Finland | Concentrate | Flotation Rougher Concentrate | 202301529 | -28.55 |
| GTK | Koivuniemi, Finland | Concentrate | Flotation Cleaner Concentrate | 202301530 | -31.60 |
| GTK | Koivuniemi, Finland | Concentrate | Flotation Cleaner Concentrate | 202301530 | -31.52 |
| GTK | Koivuniemi, Finland | Concentrate | Flotation Cleaner Concentrate | 202301530 | -31.86 |
| GTK | Koivuniemi, Finland | Product | Purified graphite | 202301531 | -31.56 |
| GTK | Koivuniemi, Finland | Product | Purified graphite | 202301531 | -31.86 |
| GTK | Koivuniemi, Finland | Product | Purified graphite | 202301531 | -28.58 |

## C. Raman Spectroscopy Data Table

| analysis ID | sample ID | | continent | mine/province | country | type | D_STA (mean) | G_STA (mean) | G_shape_factor (mean) | Dmax_pos (mean) | Gmax_pos (mean) | Dmax/Gmax-ratio (mean) | D_shape_factor |
|---|---|---|---|---|---|---|---|---|---|---|---|---|---|
| fit_1A_01 | 1A | | Europe | Kaisersberg | Austria | amorph | 93.47 | 34.94 | 6.14 | 1348.13 | 1576.82 | 0.37 | 38.72 |
| fit_1A_02 | 1A | | Europe | Kaisersberg | Austria | amorph | 77.80 | 41.41 | 5.33 | 1349.40 | 1579.37 | 0.54 | 38.54 |
| fit_1A_03 | 1A | | Europe | Kaisersberg | Austria | amorph | 74.65 | 51.70 | 4.39 | 1345.59 | 1579.37 | 0.68 | 37.74 |
| fit_1A_04 | 1A | | Europe | Kaisersberg | Austria | amorph | 305.25 | 19.25 | 14.63 | 1357.02 | 1580.64 | 0.06 | 46.60 |
| fit_1A_05 | 1A | | Europe | Kaisersberg | Austria | amorph | 218.05 | 16.84 | 14.61 | 1346.86 | 1578.09 | 0.08 | 38.48 |
| fit_1A_06 | 1A | | Europe | Kaisersberg | Austria | amorph | 56.32 | 51.95 | 4.68 | 1346.86 | 1580.64 | 0.92 | 28.23 |
| fit_1A_07 | 1A | | Europe | Kaisersberg | Austria | amorph | 103.52 | 55.31 | 3.24 | 1343.05 | 1574.28 | 0.54 | 41.22 |
| fit_1A_08 | 1A | | Europe | Kaisersberg | Austria | amorph | 85.22 | 43.50 | 5.02 | 1350.69 | 1579.39 | 0.52 | 43.28 |
| fit_1A_09 | 1A | | Europe | Kaisersberg | Austria | amorph | 127.46 | 33.58 | 6.60 | 1343.07 | 1567.96 | 0.27 | 37.83 |
| fit_1A_10 | 1A | | Europe | Kaisersberg | Austria | amorph | 68.05 | 55.84 | 3.94 | 1343.07 | 1575.58 | 0.86 | 29.75 |
| fit_1A_11 | 1A | | Europe | Kaisersberg | Austria | amorph | 85.00 | 49.53 | 4.11 | 1354.50 | 1581.93 | 0.56 | 50.71 |
| fit_1A_12 | 1A | | Europe | Kaisersberg | Austria | amorph | 74.53 | 47.49 | 4.80 | 1341.80 | 1574.31 | 0.62 | 31.62 |
| fit_1A_13 | 1A | | Europe | Kaisersberg | Austria | amorph | 114.79 | 42.80 | 7.82 | 1344.34 | 1575.58 | 0.38 | 59.71 |
| fit_1A_14 | 1A | | Europe | Kaisersberg | Austria | amorph | 73.80 | 56.02 | 3.46 | 1341.80 | 1571.77 | 0.76 | 29.96 |
| fit_1A_15 | 1A | | Europe | Kaisersberg | Austria | amorph | 80.98 | 43.15 | 4.75 | 1343.07 | 1569.23 | 0.52 | 27.06 |
| fit_1A_16 | 1A | | Europe | Kaisersberg | Austria | amorph | 173.98 | 22.50 | 11.38 | 1345.61 | 1571.77 | 0.13 | 33.85 |
| fit_1A_17 | 1A | | Europe | Kaisersberg | Austria | amorph | 110.79 | 35.20 | 5.36 | 1337.99 | 1570.50 | 0.30 | 36.17 |
| fit_1A_18 | 1A | | Europe | Kaisersberg | Austria | amorph | 122.10 | 30.00 | 6.19 | 1346.88 | 1571.77 | 0.25 | 35.97 |

| | | | | | | | | | | | | | |
|---|---|---|---|---|---|---|---|---|---|---|---|---|---|
| fit_1A_19 | 1A | | Europe | Kaisersberg | Austria | amorph | 118.81 | 26.63 | 7.13 | 1348.15 | 1571.77 | 0.22 | 29.96 |
| fit_1A_20 | 1A | | Europe | Kaisersberg | Austria | amorph | 65.39 | 40.82 | 5.53 | 1351.96 | 1580.66 | 0.63 | 33.91 |
| fit_1B_01 | 1B | | Africa | Balama | Mozambique | flake | 5118.34 | 12.42 | 21.54 | 1350.69 | 1576.83 | 0.00 | 59.76 |
| fit_1B_02 | 1B | | Africa | Balama | Mozambique | flake | 5121.25 | 14.01 | 19.89 | 1346.88 | 1581.91 | 0.00 | 64.74 |
| fit_1B_03 | 1B | | Africa | Balama | Mozambique | flake | 5477.28 | 12.94 | 22.33 | 1353.23 | 1580.64 | 0.00 | 64.24 |
| fit_1B_04 | 1B | | Africa | Balama | Mozambique | flake | 5714.83 | 12.80 | 22.85 | 1349.42 | 1581.91 | 0.00 | 64.43 |
| fit_1B_05 | 1B | | Africa | Balama | Mozambique | flake | 969.10 | 12.83 | 22.58 | 1343.07 | 1578.10 | 0.01 | 56.98 |
| fit_1B_06 | 1B | | Africa | Balama | Mozambique | flake | 595.23 | 12.95 | 21.46 | 1344.34 | 1580.64 | 0.02 | 42.16 |
| fit_1B_07 | 1B | | Africa | Balama | Mozambique | flake | 527.01 | 13.25 | 22.34 | 1360.85 | 1578.10 | 0.02 | 52.55 |
| fit_1B_08 | 1B | | Africa | Balama | Mozambique | flake | 642.23 | 13.39 | 21.60 | 1357.04 | 1579.37 | 0.02 | 45.36 |
| fit_1B_09 | 1B | | Africa | Balama | Mozambique | flake | 812.72 | 13.59 | 21.38 | 1348.15 | 1579.37 | 0.02 | 55.01 |
| fit_1B_10 | 1B | | Africa | Balama | Mozambique | flake | 598.82 | 14.41 | 20.32 | 1349.42 | 1581.91 | 0.02 | 48.76 |
| fit_1B_11 | 1B | | Africa | Balama | Mozambique | flake | 5496.99 | 13.27 | 22.22 | 1353.23 | 1581.91 | 0.00 | 64.52 |
| fit_1B_12 | 1B | | Africa | Balama | Mozambique | flake | 5544.18 | 13.18 | 21.54 | 1337.98 | 1580.64 | 0.00 | 63.84 |
| fit_1B_13 | 1B | | Africa | Balama | Mozambique | flake | 402.82 | 15.10 | 19.37 | 1349.42 | 1578.10 | 0.04 | 41.14 |
| fit_1B_14 | 1B | | Africa | Balama | Mozambique | flake | 4904.18 | 13.13 | 20.02 | 1344.34 | 1575.56 | 0.00 | 60.13 |
| fit_1B_15 | 1B | | Africa | Balama | Mozambique | flake | 148.08 | 20.23 | 11.21 | 1345.61 | 1580.64 | 0.13 | 41.07 |
| fit_1B_16 | 1B | | Africa | Balama | Mozambique | flake | 336.45 | 15.21 | 19.70 | 1353.23 | 1581.91 | 0.05 | 44.76 |
| fit_1B_17 | 1B | | Africa | Balama | Mozambique | flake | 469.46 | 14.87 | 19.41 | 1343.07 | 1580.64 | 0.03 | 44.77 |
| fit_1B_18 | 1B | | Africa | Balama | Mozambique | flake | 5630.97 | 12.91 | 22.59 | 1354.50 | 1580.64 | 0.00 | 64.23 |
| fit_1B_19 | 1B | | Africa | Balama | Mozambique | flake | 579.08 | 13.82 | 21.15 | 1353.23 | 1580.64 | 0.02 | 48.82 |
| fit_1B_20 | 1B | | Africa | Balama | Mozambique | flake | 5680.58 | 12.42 | 24.39 | 1362.12 | 1579.37 | 0.00 | 63.60 |

| | | | | | | | | | | | | | |
|---|---|---|---|---|---|---|---|---|---|---|---|---|---|
| fit_2A_01 | 2A | | Europe | Kaisersberg | Austria | amorph | 134.20 | 39.53 | 5.26 | 1345.61 | 1571.74 | 0.29 | 45.40 |
| fit_2A_02 | 2A | | Europe | Kaisersberg | Austria | amorph | 86.02 | 45.14 | 4.89 | 1343.07 | 1569.20 | 0.54 | 32.24 |
| fit_2A_03 | 2A | | Europe | Kaisersberg | Austria | amorph | 113.47 | 55.05 | 4.43 | 1343.07 | 1570.47 | 0.49 | 47.12 |
| fit_2A_04 | 2A | | Europe | Kaisersberg | Austria | amorph | 78.34 | 49.79 | 4.43 | 1346.88 | 1580.63 | 0.63 | 42.66 |
| fit_2A_05 | 2A | | Europe | Kaisersberg | Austria | amorph | 94.60 | 41.67 | 5.50 | 1346.88 | 1578.09 | 0.44 | 42.13 |
| fit_2A_06 | 2A | | Europe | Kaisersberg | Austria | amorph | 126.46 | 45.66 | 5.02 | 1348.15 | 1573.01 | 0.35 | 48.67 |
| fit_2A_07 | 2A | | Europe | Kaisersberg | Austria | amorph | 80.85 | 59.11 | 3.65 | 1351.96 | 1581.91 | 0.72 | 47.30 |
| fit_2A_08 | 2A | | Europe | Kaisersberg | Austria | amorph | 115.94 | 47.01 | 4.62 | 1348.15 | 1576.82 | 0.40 | 48.93 |
| fit_2A_09 | 2A | | Europe | Kaisersberg | Austria | amorph | 91.86 | 51.83 | 3.70 | 1351.96 | 1585.72 | 0.57 | 52.41 |
| fit_2A_10 | 2A | | Europe | Kaisersberg | Austria | amorph | 76.94 | 50.83 | 4.33 | 1346.88 | 1581.91 | 0.67 | 41.43 |
| fit_2A_11 | 2A | | Europe | Kaisersberg | Austria | amorph | 99.76 | 50.94 | 4.07 | 1349.42 | 1581.91 | 0.51 | 49.14 |
| fit_2A_12 | 2A | | Europe | Kaisersberg | Austria | amorph | 93.10 | 51.82 | 4.04 | 1345.61 | 1583.18 | 0.56 | 48.11 |
| fit_2A_13 | 2A | | Europe | Kaisersberg | Austria | amorph | 95.03 | 45.76 | 4.35 | 1351.96 | 1584.45 | 0.49 | 53.86 |
| fit_2A_14 | 2A | | Europe | Kaisersberg | Austria | amorph | 101.21 | 35.65 | 5.62 | 1345.61 | 1573.01 | 0.36 | 36.17 |
| fit_2A_15 | 2A | | Europe | Kaisersberg | Austria | amorph | 68.14 | 79.20 | 2.68 | 1351.96 | 1581.91 | 1.15 | 44.27 |
| fit_2A_16 | 2A | | Europe | Kaisersberg | Austria | amorph | 65.44 | 76.69 | 2.44 | 1346.88 | 1581.91 | 1.17 | 42.81 |
| fit_2A_17 | 2A | | Europe | Kaisersberg | Austria | amorph | 90.16 | 63.01 | 3.56 | 1344.34 | 1583.18 | 0.70 | 51.53 |
| fit_2A_18 | 2A | | Europe | Kaisersberg | Austria | amorph | 71.12 | 51.42 | 3.93 | 1354.50 | 1584.45 | 0.71 | 42.94 |
| fit_2A_19 | 2A | | Europe | Kaisersberg | Austria | amorph | 68.41 | 50.09 | 4.49 | 1346.88 | 1578.09 | 0.73 | 33.87 |
| fit_2A_20 | 2A | | Europe | Kaisersberg | Austria | amorph | 94.26 | 49.14 | 4.14 | 1345.61 | 1576.82 | 0.52 | 46.26 |
| fit_2B_01 | 2B | | Europe | Skaland | Norway | flake | 265.95 | 15.54 | 14.84 | 1350.56 | 1579.26 | 0.06 | 38.21 |
| fit_2B_02 | 2B | | Europe | Skaland | Norway | flake | 207.30 | 24.19 | 9.98 | 1342.93 | 1576.72 | 0.12 | 40.83 |

| | | | | | | | | | | | | | |
|---|---|---|---|---|---|---|---|---|---|---|---|---|---|
| fit_2B_03 | 2B | | Europe | Skaland | Norway | flake | 246.80 | 17.32 | 13.05 | 1355.64 | 1579.26 | 0.07 | 50.17 |
| fit_2B_04 | 2B | | Europe | Skaland | Norway | flake | 198.17 | 21.03 | 11.39 | 1353.10 | 1580.54 | 0.11 | 50.53 |
| fit_2B_05 | 2B | | Europe | Skaland | Norway | flake | 216.83 | 17.33 | 13.48 | 1349.29 | 1580.54 | 0.08 | 46.48 |
| fit_2B_06 | 2B | | Europe | Skaland | Norway | flake | 5319.78 | 12.94 | 21.94 | 1346.75 | 1580.54 | 0.00 | 63.86 |
| fit_2B_07 | 2B | | Europe | Skaland | Norway | flake | 165.89 | 22.04 | 10.14 | 1350.56 | 1580.54 | 0.13 | 46.36 |
| fit_2B_08 | 2B | | Europe | Skaland | Norway | flake | 406.92 | 16.26 | 17.79 | 1342.93 | 1579.26 | 0.04 | 42.27 |
| fit_2B_09 | 2B | | Europe | Skaland | Norway | flake | 250.01 | 16.93 | 13.80 | 1355.64 | 1581.81 | 0.06 | 46.47 |
| fit_2B_10 | 2B | | Europe | Skaland | Norway | flake | 562.42 | 14.36 | 19.44 | 1349.29 | 1581.81 | 0.03 | 45.13 |
| fit_2B_11 | 2B | | Europe | Skaland | Norway | flake | 705.42 | 13.74 | 21.52 | 1350.56 | 1579.26 | 0.02 | 46.90 |
| fit_2B_12 | 2B | | Europe | Skaland | Norway | flake | 711.23 | 15.17 | 18.10 | 1350.56 | 1581.81 | 0.02 | 53.02 |
| fit_2B_13 | 2B | | Europe | Skaland | Norway | flake | 188.22 | 19.43 | 11.49 | 1346.75 | 1583.08 | 0.10 | 46.92 |
| fit_2B_14 | 2B | | Europe | Skaland | Norway | flake | 503.12 | 14.67 | 19.85 | 1349.29 | 1580.54 | 0.03 | 46.46 |
| fit_2B_15 | 2B | | Europe | Skaland | Norway | flake | 409.07 | 13.99 | 16.84 | 1341.66 | 1574.18 | 0.04 | 35.00 |
| fit_2B_16 | 2B | | Europe | Skaland | Norway | flake | 111.80 | 28.53 | 6.28 | 1348.02 | 1581.81 | 0.26 | 47.20 |
| fit_2B_17 | 2B | | Europe | Skaland | Norway | flake | 180.02 | 20.42 | 11.01 | 1349.29 | 1583.08 | 0.12 | 44.04 |
| fit_2B_18 | 2B | | Europe | Skaland | Norway | flake | 511.70 | 14.51 | 19.65 | 1353.10 | 1581.81 | 0.03 | 48.20 |
| fit_2B_19 | 2B | | Europe | Skaland | Norway | flake | 609.59 | 13.57 | 13.49 | 1346.75 | 1574.18 | 0.02 | 47.06 |
| fit_2B_20 | 2B | | Europe | Skaland | Norway | flake | 5769.93 | 13.07 | 22.33 | 1345.48 | 1581.81 | 0.00 | 64.49 |
| fit_3B_01 | 3B | | S_America | PedraAzul, Itaperica, Salta da Divisa | Brasil | flake | 647.56 | 13.37 | 22.09 | 1351.84 | 1581.81 | 0.02 | 47.90 |
| fit_3B_02 | 3B | | S_America | PedraAzul, Itaperica, Salta da Divisa | Brasil | flake | 5607.04 | 12.32 | 23.12 | 1353.11 | 1581.81 | 0.00 | 61.95 |
| fit_3B_03 | 3B | | S_America | PedraAzul, Itaperica, Salta da Divisa | Brasil | flake | 5203.10 | 12.74 | 22.49 | 1326.42 | 1581.81 | 0.00 | 53.00 |
| fit_3B_04 | 3B | | S_America | PedraAzul, Itaperica, Salta da Divisa | Brasil | flake | 5343.88 | 12.50 | 22.80 | 1345.48 | 1581.81 | 0.00 | 63.75 |

| | | | | | | | | | | | | | |
|---|---|---|---|---|---|---|---|---|---|---|---|---|---|
| fit_3B_05 | 3B | | S_America | PedraAzul, Itaperica, Salta da Divisa | Brasil | flake | 5500.60 | 12.38 | 22.52 | 1355.65 | 1581.81 | 0.00 | 58.37 |
| fit_3B_06 | 3B | | S_America | PedraAzul, Itaperica, Salta da Divisa | Brasil | flake | 737.24 | 13.33 | 21.90 | 1342.94 | 1580.54 | 0.02 | 43.99 |
| fit_3B_07 | 3B | | S_America | PedraAzul, Itaperica, Salta da Divisa | Brasil | flake | 5552.74 | 12.86 | 23.11 | 1351.84 | 1580.54 | 0.00 | 63.98 |
| fit_3B_08 | 3B | | S_America | PedraAzul, Itaperica, Salta da Divisa | Brasil | flake | 5556.50 | 12.69 | 23.43 | 1354.38 | 1581.81 | 0.00 | 63.68 |
| fit_3B_09 | 3B | | S_America | PedraAzul, Itaperica, Salta da Divisa | Brasil | flake | 402.43 | 13.60 | 22.51 | 1346.75 | 1580.54 | 0.03 | 34.48 |
| fit_3B_10 | 3B | | S_America | PedraAzul, Itaperica, Salta da Divisa | Brasil | flake | 1321.39 | 12.79 | 22.63 | 1353.11 | 1581.81 | 0.01 | 56.65 |
| fit_3B_11 | 3B | | S_America | PedraAzul, Itaperica, Salta da Divisa | Brasil | flake | 5542.16 | 12.72 | 22.91 | 1436.97 | 1580.54 | 0.00 | 64.03 |
| fit_3B_12 | 3B | | S_America | PedraAzul, Itaperica, Salta da Divisa | Brasil | flake | 331.55 | 14.15 | 21.39 | 1345.48 | 1581.81 | 0.04 | 39.50 |
| fit_3B_13 | 3B | | S_America | PedraAzul, Itaperica, Salta da Divisa | Brasil | flake | 628.53 | 13.41 | 21.69 | 1348.02 | 1581.81 | 0.02 | 48.78 |
| fit_3B_14 | 3B | | S_America | PedraAzul, Itaperica, Salta da Divisa | Brasil | flake | 206.72 | 16.42 | 14.76 | 1353.11 | 1581.81 | 0.08 | 37.56 |
| fit_3B_15 | 3B | | S_America | PedraAzul, Itaperica, Salta da Divisa | Brasil | flake | 599.11 | 14.38 | 19.92 | 1346.75 | 1581.81 | 0.02 | 45.23 |
| fit_3B_16 | 3B | | S_America | PedraAzul, Itaperica, Salta da Divisa | Brasil | flake | 848.57 | 14.08 | 20.23 | 1350.56 | 1580.54 | 0.02 | 58.28 |
| fit_3B_17 | 3B | | S_America | PedraAzul, Itaperica, Salta da Divisa | Brasil | flake | 297.62 | 15.19 | 15.90 | 1344.21 | 1580.54 | 0.05 | 42.48 |
| fit_3B_18 | 3B | | S_America | PedraAzul, Itaperica, Salta da Divisa | Brasil | flake | 153.40 | 17.32 | 13.13 | 1351.84 | 1581.81 | 0.11 | 39.29 |
| fit_3B_19 | 3B | | S_America | PedraAzul, Itaperica, Salta da Divisa | Brasil | flake | 213.35 | 16.31 | 15.28 | 1350.56 | 1581.81 | 0.08 | 39.31 |
| fit_3B_20 | 3B | | S_America | PedraAzul, Itaperica, Salta da Divisa | Brasil | flake | 5302.04 | 12.90 | 22.42 | 1339.13 | 1581.81 | 0.00 | 63.75 |
| fit_4A_01 | 4A | | Asia | Hunan Lutang | China | flake | 175.35 | 29.43 | 9.85 | 1344.34 | 1578.11 | 0.17 | 58.34 |
| fit_4A_02 | 4A | | Asia | Hunan Lutang | China | flake | 174.30 | 33.36 | 6.59 | 1351.96 | 1579.38 | 0.20 | 46.16 |
| fit_4A_03 | 4A | | Asia | Hunan Lutang | China | flake | 99.70 | 168.38 | 1.65 | 1345.61 | 1590.81 | 1.69 | 79.12 |
| fit_4A_04 | 4A | | Asia | Hunan Lutang | China | flake | 118.54 | 124.65 | 2.05 | 1344.34 | 1573.03 | 1.05 | 87.57 |
| fit_4A_05 | 4A | | Asia | Hunan Lutang | China | flake | 79.85 | 55.19 | 3.50 | 1348.15 | 1581.92 | 0.69 | 46.90 |
| fit_4A_06 | 4A | | Asia | Hunan Lutang | China | flake | 116.73 | 32.80 | 6.58 | 1349.42 | 1576.84 | 0.28 | 54.56 |

| | | | | | | | | | | | | | |
|---|---|---|---|---|---|---|---|---|---|---|---|---|---|
| fit_4A_07 | 4A | | Asia | Hunan Lutang | China | flake | 234.60 | 19.69 | 14.64 | 1344.34 | 1579.38 | 0.08 | 47.62 |
| fit_4A_08 | 4A | | Asia | Hunan Lutang | China | flake | 101.24 | 36.40 | 5.60 | 1353.24 | 1579.38 | 0.36 | 46.88 |
| fit_4A_09 | 4A | | Asia | Hunan Lutang | China | flake | 96.81 | 38.99 | 5.08 | 1350.69 | 1580.65 | 0.41 | 44.39 |
| fit_4A_10 | 4A | | Asia | Hunan Lutang | China | flake | 120.25 | 26.70 | 7.98 | 1351.96 | 1578.11 | 0.23 | 44.23 |
| fit_4A_11 | 4A | | Asia | Hunan Lutang | China | flake | 66.56 | 168.67 | 1.78 | 1345.61 | 1578.11 | 2.57 | 51.05 |
| fit_4A_12 | 4A | | Asia | Hunan Lutang | China | flake | 95.25 | 42.04 | 4.99 | 1349.42 | 1579.38 | 0.45 | 49.22 |
| fit_4A_13 | 4A | | Asia | Hunan Lutang | China | flake | 69.21 | 80.47 | 2.91 | 1345.61 | 1579.38 | 1.16 | 46.90 |
| fit_4A_14 | 4A | | Asia | Hunan Lutang | China | flake | 312.62 | 19.88 | 8.70 | 1345.61 | 1570.48 | 0.07 | 40.19 |
| fit_4A_15 | 4A | | Asia | Hunan Lutang | China | flake | 106.04 | 164.59 | 1.56 | 1348.15 | 1588.27 | 1.55 | 87.41 |
| fit_4A_16 | 4A | | Asia | Hunan Lutang | China | flake | 267.31 | 18.72 | 15.73 | 1351.96 | 1575.57 | 0.07 | 44.65 |
| fit_4A_17 | 4A | | Asia | Hunan Lutang | China | flake | 92.80 | 40.94 | 5.43 | 1348.15 | 1579.38 | 0.44 | 43.94 |
| fit_4A_18 | 4A | | Asia | Hunan Lutang | China | flake | 485.75 | 16.63 | 7.76 | 1348.15 | 1567.94 | 0.03 | 42.43 |
| fit_4A_19 | 4A | | Asia | Hunan Lutang | China | flake | 66.20 | 151.97 | 1.50 | 1353.24 | 1584.46 | 2.35 | 63.56 |
| fit_4A_20 | 4A | | Asia | Hunan Lutang | China | flake | 68.76 | 175.66 | 1.39 | 1354.51 | 1588.27 | 2.53 | 65.16 |
| fit_4B_01 | 4B | | Europe | Zavalje | Ukraine | flake | 5203.91 | 13.29 | 21.71 | 1355.76 | 1579.36 | 0.00 | 63.74 |
| fit_4B_02 | 4B | | Europe | Zavalje | Ukraine | flake | 5836.08 | 12.71 | 22.70 | 1351.95 | 1581.90 | 0.00 | 64.56 |
| fit_4B_03 | 4B | | Europe | Zavalje | Ukraine | flake | 4904.44 | 14.47 | 19.50 | 1350.68 | 1580.63 | 0.00 | 64.13 |
| fit_4B_04 | 4B | | Europe | Zavalje | Ukraine | flake | 527.61 | 14.06 | 20.51 | 1344.32 | 1581.90 | 0.03 | 40.09 |
| fit_4B_05 | 4B | | Europe | Zavalje | Ukraine | flake | 5902.30 | 13.99 | 23.70 | 1329.92 | 1581.90 | 0.00 | 65.10 |
| fit_4B_06 | 4B | | Europe | Zavalje | Ukraine | flake | 5562.82 | 12.85 | 22.78 | 1348.13 | 1580.63 | 0.00 | 64.30 |
| fit_4B_07 | 4B | | Europe | Zavalje | Ukraine | flake | 791.80 | 13.36 | 21.60 | 1349.40 | 1580.63 | 0.02 | 49.02 |
| fit_4B_08 | 4B | | Europe | Zavalje | Ukraine | flake | 917.68 | 13.65 | 20.61 | 1353.22 | 1581.90 | 0.02 | 55.41 |

| | | | | | | | | | | | | | |
|---|---|---|---|---|---|---|---|---|---|---|---|---|---|
| fit_4B_09 | 4B | | Europe | Zavalje | Ukraine | flake | 782.76 | 13.60 | 20.72 | 1348.13 | 1581.90 | 0.02 | 63.45 |
| fit_4B_10 | 4B | | Europe | Zavalje | Ukraine | flake | 5640.67 | 12.82 | 22.56 | 1339.24 | 1581.90 | 0.00 | 64.84 |
| fit_4B_11 | 4B | | Europe | Zavalje | Ukraine | flake | 5518.19 | 13.08 | 21.63 | 1354.49 | 1580.63 | 0.00 | 64.22 |
| fit_4B_12 | 4B | | Europe | Zavalje | Ukraine | flake | 731.75 | 14.07 | 19.91 | 1354.49 | 1580.63 | 0.02 | 63.24 |
| fit_4B_13 | 4B | | Europe | Zavalje | Ukraine | flake | 5748.87 | 13.19 | 21.76 | 1339.24 | 1580.63 | 0.00 | 64.09 |
| fit_4B_14 | 4B | | Europe | Zavalje | Ukraine | flake | 2432.34 | 13.47 | 21.79 | 1343.05 | 1580.63 | 0.01 | 61.20 |
| fit_4B_15 | 4B | | Europe | Zavalje | Ukraine | flake | 5587.14 | 13.03 | 22.34 | 1355.76 | 1581.90 | 0.00 | 64.76 |
| fit_4B_16 | 4B | | Europe | Zavalje | Ukraine | flake | 5355.74 | 13.77 | 20.85 | 1392.60 | 1583.17 | 0.00 | 64.77 |
| fit_4B_17 | 4B | | Europe | Zavalje | Ukraine | flake | 429.99 | 14.42 | 19.96 | 1353.22 | 1581.90 | 0.03 | 44.05 |
| fit_4B_18 | 4B | | Europe | Zavalje | Ukraine | flake | 5559.42 | 13.77 | 20.65 | 1346.86 | 1581.90 | 0.00 | 65.37 |
| fit_4B_19 | 4B | | Europe | Zavalje | Ukraine | flake | 5831.73 | 12.90 | 22.31 | 1411.66 | 1580.63 | 0.00 | 61.75 |
| fit_5B_01 | 5B | | Europe | Ural, Tayginka | Russia | flake | 6472.21 | 14.02 | 26.25 | 1355.75 | 1581.91 | 0.00 | 65.19 |
| fit_5B_02 | 5B | | Europe | Ural, Tayginka | Russia | flake | 5885.91 | 14.37 | 23.89 | 1353.21 | 1581.91 | 0.00 | 64.78 |
| fit_5B_03 | 5B | | Europe | Ural, Tayginka | Russia | flake | 5061.00 | 13.52 | 22.74 | 1442.15 | 1580.64 | 0.00 | 62.61 |
| fit_5B_04 | 5B | | Europe | Ural, Tayginka | Russia | flake | 4439.57 | 14.65 | 24.35 | 1368.46 | 1581.91 | 0.01 | 63.00 |
| fit_5B_05 | 5B | | Europe | Ural, Tayginka | Russia | flake | 5943.28 | 13.86 | 24.39 | 1418.01 | 1581.91 | 0.00 | 64.71 |
| fit_5B_06 | 5B | | Europe | Ural, Tayginka | Russia | flake | 5261.25 | 12.84 | 22.85 | 1367.19 | 1580.64 | 0.00 | 63.40 |
| fit_5B_07 | 5B | | Europe | Ural, Tayginka | Russia | flake | 7189.48 | 14.26 | 30.29 | 1351.94 | 1580.64 | 0.00 | 64.69 |
| fit_5B_08 | 5B | | Europe | Ural, Tayginka | Russia | flake | 6329.63 | 14.25 | 26.82 | 1328.65 | 1581.91 | 0.00 | 64.14 |
| fit_5B_09 | 5B | | Europe | Ural, Tayginka | Russia | flake | 5115.91 | 12.98 | 22.01 | 1387.94 | 1580.64 | 0.00 | 63.61 |
| fit_5B_10 | 5B | | Europe | Ural, Tayginka | Russia | flake | 304.32 | 14.38 | 21.37 | 1367.19 | 1580.64 | 0.04 | 54.94 |
| fit_5B_11 | 5B | | Europe | Ural, Tayginka | Russia | flake | 225.13 | 16.27 | 19.46 | 1362.11 | 1580.64 | 0.07 | 60.96 |

| | | | | | | | | | | | | | |
|---|---|---|---|---|---|---|---|---|---|---|---|---|---|
| fit_5B_12 | 5B | | Europe | Ural, Tayginka | Russia | flake | 210.08 | 15.51 | 20.45 | 1362.11 | 1580.64 | 0.07 | 55.98 |
| fit_5B_13 | 5B | | Europe | Ural, Tayginka | Russia | flake | 214.23 | 16.11 | 19.22 | 1364.65 | 1581.91 | 0.07 | 57.38 |
| fit_5B_14 | 5B | | Europe | Ural, Tayginka | Russia | flake | 6019.95 | 14.37 | 24.89 | 1346.86 | 1580.64 | 0.00 | 64.47 |
| fit_5B_15 | 5B | | Europe | Ural, Tayginka | Russia | flake | 5669.80 | 15.46 | 23.05 | 1346.86 | 1581.91 | 0.00 | 64.35 |
| fit_5B_16 | 5B | | Europe | Ural, Tayginka | Russia | flake | 6559.55 | 15.72 | 26.88 | 1350.67 | 1580.64 | 0.00 | 64.29 |
| fit_5B_17 | 5B | | Europe | Ural, Tayginka | Russia | flake | 5721.52 | 14.46 | 23.18 | 1397.68 | 1581.91 | 0.00 | 64.71 |
| fit_5B_18 | 5B | | Europe | Ural, Tayginka | Russia | flake | 5750.80 | 16.30 | 22.10 | 1353.21 | 1581.91 | 0.00 | 65.04 |
| fit_5B_19 | 5B | | Europe | Ural, Tayginka | Russia | flake | 5771.94 | 14.32 | 23.57 | 1351.94 | 1580.64 | 0.00 | 64.59 |
| fit_5B_20 | 5B | | Europe | Ural, Tayginka | Russia | flake | 6505.53 | 13.95 | 27.08 | 1343.05 | 1581.91 | 0.00 | 64.79 |
| fit_6A_01 | 6A | | Europe | Kaisersberg | Austria | amorph | 179.43 | 23.02 | 9.42 | 1355.77 | 1575.56 | 0.12 | 49.43 |
| fit_6A_02 | 6A | | Europe | Kaisersberg | Austria | amorph | 161.49 | 30.97 | 5.95 | 1351.96 | 1585.72 | 0.19 | 57.53 |
| fit_6A_03 | 6A | | Europe | Kaisersberg | Austria | amorph | 248.28 | 22.20 | 9.40 | 1348.15 | 1583.18 | 0.08 | 66.69 |
| fit_6A_04 | 6A | | Europe | Kaisersberg | Austria | amorph | 166.14 | 31.95 | 6.09 | 1358.31 | 1584.45 | 0.19 | 61.56 |
| fit_6A_05 | 6A | | Europe | Kaisersberg | Austria | amorph | 151.75 | 33.18 | 6.48 | 1349.42 | 1581.91 | 0.22 | 52.94 |
| fit_6A_06 | 6A | | Europe | Kaisersberg | Austria | amorph | 85.77 | 70.01 | 2.59 | 1354.50 | 1585.72 | 0.82 | 64.14 |
| fit_6A_07 | 6A | | Europe | Kaisersberg | Austria | amorph | 122.69 | 31.21 | 7.01 | 1353.23 | 1583.18 | 0.26 | 54.66 |
| fit_6A_08 | 6A | | Europe | Kaisersberg | Austria | amorph | 116.34 | 34.98 | 5.73 | 1348.15 | 1585.72 | 0.29 | 57.88 |
| fit_6A_09 | 6A | | Europe | Kaisersberg | Austria | amorph | 151.43 | 27.37 | 7.66 | 1353.23 | 1583.18 | 0.18 | 56.84 |
| fit_6A_10 | 6A | | Europe | Kaisersberg | Austria | amorph | 159.22 | 30.22 | 7.74 | 1350.69 | 1579.37 | 0.19 | 55.78 |
| fit_6A_11 | 6A | | Europe | Kaisersberg | Austria | amorph | 180.75 | 33.59 | 6.55 | 1357.04 | 1585.72 | 0.19 | 71.52 |
| fit_6A_12 | 6A | | Europe | Kaisersberg | Austria | amorph | 172.39 | 34.11 | 6.46 | 1350.69 | 1585.72 | 0.19 | 68.57 |
| fit_6A_13 | 6A | | Europe | Kaisersberg | Austria | amorph | 134.20 | 23.47 | 8.76 | 1351.96 | 1581.91 | 0.18 | 47.43 |

| | | | | | | | | | | | | | |
|---|---|---|---|---|---|---|---|---|---|---|---|---|---|
| fit_6A_14 | 6A | | Europe | Kaisersberg | Austria | amorph | 104.72 | 44.09 | 4.22 | 1349.42 | 1586.99 | 0.41 | 62.08 |
| fit_6A_15 | 6A | | Europe | Kaisersberg | Austria | amorph | 117.08 | 45.06 | 3.63 | 1358.31 | 1584.45 | 0.39 | 72.24 |
| fit_6B_01 | 6B | | Asia | Inner Mongolia | China | flake | 785.62 | 13.24 | 21.10 | 1342.94 | 1581.81 | 0.02 | 47.24 |
| fit_6B_02 | 6B | | Asia | Inner Mongolia | China | flake | 306.04 | 15.09 | 16.05 | 1351.83 | 1581.81 | 0.05 | 41.01 |
| fit_6B_03 | 6B | | Asia | Inner Mongolia | China | flake | 5359.13 | 12.63 | 22.24 | 1334.47 | 1581.81 | 0.00 | 64.56 |
| fit_6B_04 | 6B | | Asia | Inner Mongolia | China | flake | 313.15 | 15.35 | 15.51 | 1342.94 | 1580.54 | 0.05 | 45.47 |
| fit_6B_05 | 6B | | Asia | Inner Mongolia | China | flake | 1019.44 | 12.84 | 22.27 | 1355.64 | 1581.81 | 0.01 | 52.82 |
| fit_6B_06 | 6B | | Asia | Inner Mongolia | China | flake | 5368.85 | 13.23 | 20.30 | 1391.22 | 1581.81 | 0.00 | 65.08 |
| fit_6B_07 | 6B | | Asia | Inner Mongolia | China | flake | 721.21 | 13.53 | 21.25 | 1350.56 | 1581.81 | 0.02 | 49.18 |
| fit_6B_08 | 6B | | Asia | Inner Mongolia | China | flake | 845.05 | 13.39 | 21.28 | 1351.83 | 1580.54 | 0.02 | 49.89 |
| fit_6B_09 | 6B | | Asia | Inner Mongolia | China | flake | 431.44 | 16.77 | 16.52 | 1351.83 | 1581.81 | 0.04 | 46.97 |
| fit_6B_10 | 6B | | Asia | Inner Mongolia | China | flake | 764.33 | 13.42 | 21.30 | 1348.02 | 1581.81 | 0.02 | 52.60 |
| fit_6B_11 | 6B | | Asia | Inner Mongolia | China | flake | 1149.79 | 13.26 | 23.32 | 1348.02 | 1580.54 | 0.01 | 58.70 |
| fit_6B_12 | 6B | | Asia | Inner Mongolia | China | flake | 1182.81 | 13.27 | 21.19 | 1348.02 | 1581.81 | 0.01 | 57.30 |
| fit_7B_01 | 7B | | Asia | Heilongjian | China | flake | 5475.33 | 13.58 | 20.71 | 1355.35 | 1581.92 | 0.00 | 65.48 |
| fit_7B_02 | 7B | | Asia | Heilongjian | China | flake | 261.55 | 15.90 | 18.10 | 1348.15 | 1581.92 | 0.06 | 42.59 |
| fit_7B_03 | 7B | | Asia | Heilongjian | China | flake | 5307.25 | 12.86 | 23.33 | 1367.21 | 1579.38 | 0.00 | 62.55 |
| fit_7B_04 | 7B | | Asia | Heilongjian | China | flake | 5344.68 | 14.42 | 20.27 | 1362.13 | 1583.19 | 0.00 | 65.43 |
| fit_7B_05 | 7B | | Asia | Heilongjian | China | flake | 5559.66 | 14.65 | 21.13 | 1335.45 | 1581.92 | 0.00 | 65.56 |
| fit_7B_06 | 7B | | Asia | Heilongjian | China | flake | 3991.69 | 16.36 | 19.74 | 1348.15 | 1584.46 | 0.02 | 60.05 |
| fit_7B_07 | 7B | | Asia | Heilongjian | China | flake | 214.55 | 17.54 | 16.10 | 1353.24 | 1583.19 | 0.08 | 43.17 |
| fit_7B_08 | 7B | | Asia | Heilongjian | China | flake | 6417.07 | 14.25 | 23.27 | 1367.21 | 1583.19 | 0.00 | 66.67 |

| | | | | | | | | | | | | | |
|---|---|---|---|---|---|---|---|---|---|---|---|---|---|
| fit_7B_09 | 7B | | Asia | Heilongjian | China | flake | 4640.72 | 15.75 | 16.44 | 1349.42 | 1583.19 | 0.00 | 65.67 |
| fit_7B_10 | 7B | | Asia | Heilongjian | China | flake | 5907.10 | 13.93 | 21.12 | 1339.26 | 1584.46 | 0.00 | 66.55 |
| fit_7B_11 | 7B | | Asia | Heilongjian | China | flake | 2302.64 | 14.05 | 20.74 | 1357.05 | 1583.19 | 0.02 | 58.36 |
| fit_7B_12 | 7B | | Asia | Heilongjian | China | flake | 5603.36 | 16.72 | 20.64 | 1344.34 | 1581.92 | 0.00 | 65.62 |
| fit_7B_13 | 7B | | Asia | Heilongjian | China | flake | 4093.29 | 14.61 | 21.27 | 1360.86 | 1583.19 | 0.01 | 57.98 |
| fit_7B_14 | 7B | | Asia | Heilongjian | China | flake | 7435.08 | 14.22 | 29.79 | 1351.96 | 1581.92 | 0.00 | 65.60 |
| fit_7B_15 | 7B | | Asia | Heilongjian | China | flake | 6327.30 | 14.08 | 25.00 | 1348.15 | 1583.19 | 0.00 | 65.47 |
| fit_7B_16 | 7B | | Asia | Heilongjian | China | flake | 5804.86 | 14.02 | 22.74 | 1350.69 | 1581.92 | 0.00 | 65.37 |
| fit_7B_17 | 7B | | Asia | Heilongjian | China | flake | 5834.85 | 14.28 | 22.55 | 1302.42 | 1581.92 | 0.00 | 65.56 |
| fit_7B_18 | 7B | | Asia | Heilongjian | China | flake | 5690.03 | 14.23 | 21.52 | 1368.48 | 1583.19 | 0.00 | 65.74 |
| fit_7B_19 | 7B | | Asia | Heilongjian | China | flake | 5659.73 | 14.02 | 23.06 | 1337.99 | 1580.65 | 0.00 | 64.58 |
| fit_7B_20 | 7B | | Asia | Heilongjian | China | flake | 6106.25 | 13.33 | 25.81 | 1327.83 | 1580.65 | 0.00 | 64.38 |
| fit_8B_01 | 8B | | Asia | Hubei | China | flake | 5886.23 | 13.82 | 24.08 | 1331.64 | 1580.64 | 0.00 | 64.69 |
| fit_8B_02 | 8B | | Asia | Hubei | China | flake | 5912.76 | 12.92 | 25.11 | 1355.77 | 1579.37 | 0.00 | 63.74 |
| fit_8B_03 | 8B | | Asia | Hubei | China | flake | 6307.85 | 14.88 | 25.30 | 1349.42 | 1581.91 | 0.00 | 65.09 |
| fit_8B_04 | 8B | | Asia | Hubei | China | flake | 5658.51 | 13.42 | 23.07 | 1355.77 | 1581.91 | 0.00 | 64.29 |
| fit_8B_05 | 8B | | Asia | Hubei | China | flake | 6017.05 | 12.92 | 24.54 | 1340.53 | 1581.91 | 0.00 | 64.89 |
| fit_8B_06 | 8B | | Asia | Hubei | China | flake | 423.74 | 15.12 | 17.02 | 1346.88 | 1584.45 | 0.03 | 40.64 |
| fit_8B_07 | 8B | | Asia | Hubei | China | flake | 291.66 | 14.68 | 16.42 | 1362.13 | 1584.45 | 0.05 | 56.23 |
| fit_8B_08 | 8B | | Asia | Hubei | China | flake | 552.78 | 17.25 | 12.64 | 1353.23 | 1585.72 | 0.03 | 59.00 |
| fit_8B_09 | 8B | | Asia | Hubei | China | flake | 233.11 | 14.68 | 18.82 | 1359.59 | 1584.45 | 0.06 | 51.01 |
| fit_8B_10 | 8B | | Asia | Hubei | China | flake | 255.39 | 16.67 | 16.73 | 1358.31 | 1584.45 | 0.07 | 50.29 |

| | | | | | | | | | | | | | |
|---|---|---|---|---|---|---|---|---|---|---|---|---|---|
| fit_8B_11 | 8B | | Asia | Hubei | China | flake | 268.81 | 15.14 | 17.64 | 1355.51 | 1584.22 | 0.05 | 39.81 |
| fit_8B_12 | 8B | | Asia | Hubei | China | flake | 5278.67 | 14.65 | 18.41 | 1342.32 | 1584.22 | 0.00 | 66.95 |
| fit_8B_13 | 8B | | Asia | Hubei | China | flake | 713.33 | 13.65 | 20.40 | 1354.50 | 1583.18 | 0.02 | 58.48 |
| fit_8B_14 | 8B | | Asia | Hubei | China | flake | 210.63 | 17.77 | 15.54 | 1353.23 | 1583.18 | 0.08 | 45.38 |
| fit_8B_15 | 8B | | Asia | Hubei | China | flake | 5990.91 | 12.41 | 21.35 | 1350.69 | 1584.45 | 0.00 | 66.48 |
| fit_8B_16 | 8B | | Asia | Hubei | China | flake | 401.77 | 13.69 | 20.03 | 1346.88 | 1583.18 | 0.03 | 42.41 |
| fit_8B_17 | 8B | | Asia | Hubei | China | flake | 5621.42 | 12.72 | 19.85 | 1336.72 | 1584.45 | 0.00 | 66.69 |
| fit_8B_18 | 8B | | Asia | Hubei | China | flake | 5941.03 | 13.73 | 21.61 | 1401.51 | 1583.18 | 0.00 | 66.04 |
| fit_8B_19 | 8B | | Asia | Hubei | China | flake | 232.04 | 14.96 | 18.89 | 1351.96 | 1584.45 | 0.07 | 37.92 |
| fit_8B_20 | 8B | | Asia | Hubei | China | flake | 111.10 | 22.75 | 8.36 | 1367.21 | 1584.45 | 0.17 | 57.13 |
| fit_10B_01 | 10B | | Asia | Ragedara | Sri_Lanka | hydro | 5412.39 | 13.15 | 21.75 | 1348.15 | 1581.91 | 0.00 | 64.36 |
| fit_10B_02 | 10B | | Asia | Ragedara | Sri_Lanka | hydro | 5359.51 | 13.40 | 20.98 | 1345.61 | 1581.91 | 0.00 | 64.95 |
| fit_10B_03 | 10B | | Asia | Ragedara | Sri_Lanka | hydro | 5529.59 | 12.48 | 23.35 | 1391.34 | 1580.64 | 0.00 | 63.93 |
| fit_10B_04 | 10B | | Asia | Ragedara | Sri_Lanka | hydro | 5357.90 | 13.11 | 21.92 | 1387.53 | 1581.91 | 0.00 | 64.08 |
| fit_10B_05 | 10B | | Asia | Ragedara | Sri_Lanka | hydro | 5512.28 | 12.97 | 23.01 | 1369.75 | 1581.91 | 0.00 | 63.96 |
| fit_10B_06 | 10B | | Asia | Ragedara | Sri_Lanka | hydro | 5526.65 | 12.96 | 22.33 | 1407.86 | 1581.91 | 0.00 | 64.56 |
| fit_10B_07 | 10B | | Asia | Ragedara | Sri_Lanka | hydro | 4650.12 | 16.56 | 16.67 | 1412.94 | 1581.91 | 0.00 | 65.35 |
| fit_10B_08 | 10B | | Asia | Ragedara | Sri_Lanka | hydro | 6050.34 | 13.74 | 24.75 | 1348.15 | 1580.64 | 0.00 | 64.75 |
| fit_10B_09 | 10B | | Asia | Ragedara | Sri_Lanka | hydro | 5129.71 | 14.33 | 19.93 | 1330.36 | 1580.64 | 0.00 | 64.62 |
| fit_10B_10 | 10B | | Asia | Ragedara | Sri_Lanka | hydro | 347.05 | 16.09 | 17.16 | 1351.96 | 1581.91 | 0.05 | 53.53 |
| fit_10B_11 | 10B | | Asia | Ragedara | Sri_Lanka | hydro | 147.69 | 21.22 | 9.26 | 1346.88 | 1581.91 | 0.14 | 49.68 |
| fit_10B_12 | 10B | | Asia | Ragedara | Sri_Lanka | hydro | 5246.28 | 13.72 | 20.38 | 1329.09 | 1581.91 | 0.00 | 64.52 |

| | | | | | | | | | | | | | |
|---|---|---|---|---|---|---|---|---|---|---|---|---|---|
| fit_10B_13 | 10B | | Asia | Ragedara | Sri_Lanka | hydro | 5154.06 | 13.97 | 19.89 | 1348.15 | 1581.91 | 0.00 | 64.92 |
| fit_10B_14 | 10B | | Asia | Ragedara | Sri_Lanka | hydro | 604.56 | 17.03 | 16.27 | 1343.07 | 1579.37 | 0.03 | 58.90 |
| fit_10B_15 | 10B | | Asia | Ragedara | Sri_Lanka | hydro | 5341.27 | 13.02 | 21.02 | 1383.72 | 1581.91 | 0.00 | 64.91 |
| fit_10B_16 | 10B | | Asia | Ragedara | Sri_Lanka | hydro | 5485.09 | 12.97 | 22.23 | 1418.02 | 1580.64 | 0.00 | 64.49 |
| fit_10B_17 | 10B | | Asia | Ragedara | Sri_Lanka | hydro | 930.49 | 13.29 | 21.90 | 1360.85 | 1579.37 | 0.01 | 64.78 |
| fit_10B_18 | 10B | | Asia | Ragedara | Sri_Lanka | hydro | 5709.22 | 13.05 | 21.92 | 1346.88 | 1581.91 | 0.00 | 64.85 |
| fit_10B_19 | 10B | | Asia | Ragedara | Sri_Lanka | hydro | 5623.48 | 12.75 | 22.78 | 1355.77 | 1580.64 | 0.00 | 64.50 |
| fit_10B_20 | 10B | | Asia | Ragedara | Sri_Lanka | hydro | 5389.95 | 13.06 | 21.90 | 1365.93 | 1581.91 | 0.00 | 50.59 |
| fit_11B_01 | 11B | | Africa | Vatomina/Sahamamy Sahasoa | Madagascar | flake | 5271.67 | 13.81 | 20.63 | 1367.19 | 1583.18 | 0.00 | 64.64 |
| fit_11B_02 | 11B | | Africa | Vatomina/Sahamamy Sahasoa | Madagascar | flake | 5746.81 | 12.79 | 23.78 | 1320.18 | 1581.91 | 0.00 | 64.10 |
| fit_11B_03 | 11B | | Africa | Vatomina/Sahamamy Sahasoa | Madagascar | flake | 2483.15 | 14.54 | 22.32 | 1344.32 | 1581.91 | 0.02 | 52.85 |
| fit_11B_04 | 11B | | Africa | Vatomina/Sahamamy Sahasoa | Madagascar | flake | 423.88 | 16.43 | 17.49 | 1350.67 | 1580.64 | 0.04 | 54.78 |
| fit_11B_05 | 11B | | Africa | Vatomina/Sahamamy Sahasoa | Madagascar | flake | 5750.12 | 14.46 | 23.14 | 1348.13 | 1581.91 | 0.00 | 64.83 |
| fit_11B_06 | 11B | | Africa | Vatomina/Sahamamy Sahasoa | Madagascar | flake | 6414.91 | 13.93 | 26.49 | 1338.39 | 1580.64 | 0.00 | 64.86 |
| fit_11B_07 | 11B | | Africa | Vatomina/Sahamamy Sahasoa | Madagascar | flake | 5386.15 | 13.09 | 22.33 | 1346.86 | 1580.64 | 0.00 | 63.93 |
| fit_11B_08 | 11B | | Africa | Vatomina/Sahamamy Sahasoa | Madagascar | flake | 5569.88 | 12.87 | 22.53 | 1397.68 | 1581.91 | 0.00 | 64.34 |
| fit_11B_09 | 11B | | Africa | Vatomina/Sahamamy Sahasoa | Madagascar | flake | 6208.43 | 13.95 | 25.35 | 1355.75 | 1581.91 | 0.00 | 64.94 |
| fit_11B_10 | 11B | | Africa | Vatomina/Sahamamy Sahasoa | Madagascar | flake | 5656.90 | 13.17 | 21.61 | 1337.96 | 1581.91 | 0.00 | 64.58 |
| fit_11B_11 | 11B | | Africa | Vatomina/Sahamamy Sahasoa | Madagascar | flake | 5787.78 | 13.94 | 23.47 | 1353.21 | 1581.91 | 0.00 | 64.81 |
| fit_11B_12 | 11B | | Africa | Vatomina/Sahamamy Sahasoa | Madagascar | flake | 411.66 | 14.15 | 20.88 | 1351.94 | 1581.91 | 0.03 | 38.85 |
| fit_11B_13 | 11B | | Africa | Vatomina/Sahamamy Sahasoa | Madagascar | flake | 5878.82 | 13.92 | 24.14 | 1355.75 | 1580.64 | 0.00 | 64.62 |
| fit_11B_14 | 11B | | Africa | Vatomina/Sahamamy Sahasoa | Madagascar | flake | 400.74 | 14.58 | 20.05 | 1344.32 | 1581.91 | 0.04 | 40.90 |

| | | | | | | | | | | | | | |
|---|---|---|---|---|---|---|---|---|---|---|---|---|---|
| fit_11B_15 | 11B | | Africa | Vatomina/Sahamamy Sahasoa | Madagascar | flake | 6052.74 | 14.03 | 24.96 | 1341.78 | 1581.91 | 0.00 | 64.64 |
| fit_11B_16 | 11B | | Africa | Vatomina/Sahamamy Sahasoa | Madagascar | flake | 5784.49 | 13.65 | 24.24 | 1343.05 | 1579.37 | 0.00 | 63.95 |
| fit_11B_17 | 11B | | Africa | Vatomina/Sahamamy Sahasoa | Madagascar | flake | 6094.31 | 14.44 | 25.13 | 1343.05 | 1580.64 | 0.00 | 64.57 |
| fit_11B_18 | 11B | | Africa | Vatomina/Sahamamy Sahasoa | Madagascar | flake | 6500.81 | 13.79 | 27.54 | 1353.21 | 1580.64 | 0.00 | 64.45 |
| fit_11B_19 | 11B | | Africa | Vatomina/Sahamamy Sahasoa | Madagascar | flake | 5796.48 | 13.87 | 23.09 | 1341.78 | 1581.91 | 0.00 | 65.08 |
| fit_11B_20 | 11B | | Africa | Vatomina/Sahamamy Sahasoa | Madagascar | flake | 267.57 | 15.81 | 19.53 | 1344.32 | 1580.64 | 0.06 | 43.31 |
| fit_13B_01 | 13B | | Europe | Passau | Germany | flake | 618.58 | 14.52 | 20.33 | 1355.63 | 1580.51 | 0.02 | 61.54 |
| fit_13B_02 | 13B | | Europe | Passau | Germany | flake | 953.07 | 13.94 | 21.32 | 1350.54 | 1580.51 | 0.01 | 62.54 |
| fit_13B_03 | 13B | | Europe | Passau | Germany | flake | 720.81 | 14.20 | 21.00 | 1350.54 | 1580.51 | 0.02 | 53.44 |
| fit_13B_04 | 13B | | Europe | Passau | Germany | flake | 808.83 | 14.33 | 21.17 | 1354.35 | 1579.24 | 0.02 | 64.20 |
| fit_13B_05 | 13B | | Europe | Passau | Germany | flake | 697.16 | 13.48 | 23.33 | 1354.35 | 1580.51 | 0.02 | 55.23 |
| fit_13B_06 | 13B | | Europe | Passau | Germany | flake | 5719.31 | 12.96 | 23.17 | 1344.19 | 1580.51 | 0.00 | 63.49 |
| fit_13B_07 | 13B | | Europe | Passau | Germany | flake | 1269.19 | 13.19 | 24.32 | 1351.81 | 1580.51 | 0.01 | 69.99 |
| fit_13B_08 | 13B | | Europe | Passau | Germany | flake | 5478.12 | 12.71 | 22.50 | 1344.19 | 1580.51 | 0.00 | 64.11 |
| fit_13B_09 | 13B | | Europe | Passau | Germany | flake | 5656.29 | 13.09 | 23.22 | 1342.92 | 1577.97 | 0.00 | 63.22 |
| fit_13B_10 | 13B | | Europe | Passau | Germany | flake | 5360.16 | 13.39 | 21.92 | 1355.63 | 1580.51 | 0.00 | 64.07 |
| fit_13B_11 | 13B | | Europe | Passau | Germany | flake | 5501.26 | 12.65 | 24.16 | 1306.07 | 1579.24 | 0.00 | 62.86 |
| fit_13B_12 | 13B | | Europe | Passau | Germany | flake | 714.46 | 13.71 | 22.27 | 1349.27 | 1580.51 | 0.02 | 57.61 |
| fit_13B_13 | 13B | | Europe | Passau | Germany | flake | 656.73 | 13.68 | 21.57 | 1353.08 | 1580.51 | 0.02 | 55.10 |
| fit_13B_14 | 13B | | Europe | Passau | Germany | flake | 1171.13 | 13.59 | 22.33 | 1349.27 | 1580.51 | 0.01 | 67.31 |
| fit_13B_15 | 13B | | Europe | Passau | Germany | flake | 2550.21 | 13.10 | 22.61 | 1355.63 | 1580.51 | 0.01 | 63.58 |
| fit_13B_16 | 13B | | Europe | Passau | Germany | flake | 514.52 | 13.72 | 22.10 | 1354.35 | 1581.79 | 0.03 | 48.64 |

| | | | | | | | | | | | | | |
|---|---|---|---|---|---|---|---|---|---|---|---|---|---|
| fit_13B_17 | 13B | | Europe | Passau | Germany | flake | 5562.31 | 12.75 | 23.67 | 1355.63 | 1580.51 | 0.00 | 63.47 |
| fit_13B_18 | 13B | | Europe | Passau | Germany | flake | 5460.77 | 12.77 | 23.01 | 1345.46 | 1580.51 | 0.00 | 63.38 |
| fit_13B_19 | 13B | | Europe | Passau | Germany | flake | 5694.01 | 12.66 | 23.92 | 1340.38 | 1580.51 | 0.00 | 63.77 |
| fit_13B_20 | 13B | | Europe | Passau | Germany | flake | 953.52 | 13.59 | 23.66 | 1355.63 | 1580.51 | 0.01 | 59.67 |
| fit_14B_01 | 14B | | Europe | Passau | Germany | flake | 5781.37 | 15.49 | 22.17 | 1355.78 | 1581.93 | 0.00 | 65.40 |
| fit_14B_02 | 14B | | Europe | Passau | Germany | flake | 216.17 | 15.61 | 13.85 | 1359.59 | 1581.93 | 0.07 | 45.11 |
| fit_14B_03 | 14B | | Europe | Passau | Germany | flake | 6220.87 | 16.62 | 23.25 | 1343.07 | 1581.93 | 0.00 | 65.56 |
| fit_14B_04 | 14B | | Europe | Passau | Germany | flake | 195.65 | 18.86 | 15.70 | 1348.15 | 1581.93 | 0.09 | 46.52 |
| fit_14B_05 | 14B | | Europe | Passau | Germany | flake | 135.27 | 18.55 | 11.67 | 1355.78 | 1581.93 | 0.14 | 45.83 |
| fit_14B_06 | 14B | | Europe | Passau | Germany | flake | 5662.37 | 15.63 | 21.21 | 1433.28 | 1581.93 | 0.00 | 65.68 |
| fit_14B_07 | 14B | | Europe | Passau | Germany | flake | 6112.49 | 13.97 | 25.26 | 1346.88 | 1581.93 | 0.00 | 64.68 |
| fit_14B_08 | 14B | | Europe | Passau | Germany | flake | 5495.49 | 13.49 | 20.63 | 1357.05 | 1583.20 | 0.00 | 65.62 |
| fit_14B_09 | 14B | | Europe | Passau | Germany | flake | 6807.43 | 13.98 | 27.48 | 1343.92 | 1583.20 | 0.00 | 65.40 |
| fit_14B_10 | 14B | | Europe | Passau | Germany | flake | 367.58 | 19.03 | 14.07 | 1344.34 | 1580.66 | 0.05 | 53.91 |
| fit_14B_11 | 14B | | Europe | Passau | Germany | flake | 350.60 | 15.79 | 18.30 | 1355.78 | 1580.66 | 0.04 | 41.80 |
| fit_14B_12 | 14B | | Europe | Passau | Germany | flake | 7215.66 | 15.27 | 29.24 | 1351.96 | 1581.93 | 0.00 | 65.02 |
| fit_14B_13 | 14B | | Europe | Passau | Germany | flake | 4949.73 | 15.00 | 19.08 | 1334.18 | 1581.93 | 0.00 | 48.52 |
| fit_14B_14 | 14B | | Europe | Passau | Germany | flake | 243.80 | 15.85 | 19.12 | 1344.34 | 1581.93 | 0.06 | 40.90 |
| fit_14B_15 | 14B | | Europe | Passau | Germany | flake | 6536.51 | 14.17 | 26.17 | 1340.53 | 1580.66 | 0.00 | 65.36 |
| fit_14B_16 | 14B | | Europe | Passau | Germany | flake | 6852.26 | 14.02 | 29.16 | 1365.94 | 1580.66 | 0.00 | 64.51 |
| fit_14B_17 | 14B | | Europe | Passau | Germany | flake | 6893.79 | 14.61 | 28.29 | 1339.26 | 1580.66 | 0.00 | 64.95 |
| fit_14B_18 | 14B | | Europe | Passau | Germany | flake | 7055.48 | 14.21 | 29.79 | 1380.34 | 1581.93 | 0.00 | 64.69 |

| | | | | | | | | | | | | | |
|---|---|---|---|---|---|---|---|---|---|---|---|---|---|
| fit_14B_19 | 14B | | Europe | Passau | Germany | flake | 6422.57 | 14.14 | 26.44 | 1348.15 | 1581.93 | 0.00 | 64.86 |
| fit_14B_20 | 14B | | Europe | Passau | Germany | flake | 4737.21 | 13.91 | 21.15 | 1415.49 | 1578.12 | 0.00 | 61.97 |
| fit_15B_01 | 15B | | Europe | Skaland | Norway | flake | 2124.65 | 15.59 | 18.49 | 1350.69 | 1579.36 | 0.01 | 59.80 |
| fit_15B_02 | 15B | | Europe | Skaland | Norway | flake | 297.12 | 16.85 | 17.43 | 1351.96 | 1581.91 | 0.06 | 50.78 |
| fit_15B_03 | 15B | | Europe | Skaland | Norway | flake | 823.43 | 16.68 | 15.92 | 1340.53 | 1576.82 | 0.02 | 63.03 |
| fit_15B_04 | 15B | | Europe | Skaland | Norway | flake | 269.44 | 17.55 | 16.70 | 1348.15 | 1580.63 | 0.07 | 49.87 |
| fit_15B_05 | 15B | | Europe | Skaland | Norway | flake | 209.30 | 16.77 | 15.02 | 1343.07 | 1580.63 | 0.07 | 44.45 |
| fit_15B_06 | 15B | | Europe | Skaland | Norway | flake | 260.17 | 18.63 | 12.80 | 1350.69 | 1581.91 | 0.07 | 52.59 |
| fit_15B_07 | 15B | | Europe | Skaland | Norway | flake | 486.50 | 13.61 | 22.21 | 1344.34 | 1579.36 | 0.03 | 46.92 |
| fit_15B_08 | 15B | | Europe | Skaland | Norway | flake | 5197.45 | 14.06 | 20.81 | 1357.04 | 1580.63 | 0.00 | 64.01 |
| fit_15B_09 | 15B | | Europe | Skaland | Norway | flake | 5563.67 | 12.87 | 23.29 | 1343.07 | 1580.63 | 0.00 | 63.35 |
| fit_15B_10 | 15B | | Europe | Skaland | Norway | flake | 5552.93 | 12.89 | 22.61 | 1351.96 | 1580.63 | 0.00 | 64.40 |
| fit_15B_11 | 15B | | Europe | Skaland | Norway | flake | 5216.54 | 12.99 | 22.32 | 1346.88 | 1578.09 | 0.00 | 61.60 |
| fit_15B_12 | 15B | | Europe | Skaland | Norway | flake | 422.28 | 15.07 | 19.44 | 1349.42 | 1580.63 | 0.04 | 48.50 |
| fit_15B_13 | 15B | | Europe | Skaland | Norway | flake | 315.47 | 15.48 | 16.36 | 1349.42 | 1580.63 | 0.05 | 48.94 |
| fit_15B_14 | 15B | | Europe | Skaland | Norway | flake | 5635.38 | 12.62 | 23.70 | 1368.48 | 1579.36 | 0.00 | 62.71 |
| fit_15B_15 | 15B | | Europe | Skaland | Norway | flake | 5569.80 | 13.14 | 22.73 | 1359.58 | 1579.36 | 0.00 | 62.17 |
| fit_15B_16 | 15B | | Europe | Skaland | Norway | flake | 346.37 | 18.59 | 15.07 | 1351.96 | 1579.36 | 0.06 | 54.33 |
| fit_15B_17 | 15B | | Europe | Skaland | Norway | flake | 287.29 | 18.66 | 15.66 | 1346.88 | 1579.36 | 0.07 | 50.72 |
| fit_15B_18 | 15B | | Europe | Skaland | Norway | flake | 808.75 | 13.34 | 21.77 | 1350.69 | 1579.36 | 0.02 | 44.64 |
| fit_15B_19 | 15B | | Europe | Skaland | Norway | flake | 820.53 | 13.51 | 18.43 | 1348.15 | 1574.28 | 0.02 | 50.61 |
| fit_15B_20 | 15B | | Europe | Skaland | Norway | flake | 5424.00 | 13.52 | 21.85 | 1344.34 | 1579.36 | 0.00 | 63.66 |

| | | | | | | | | | | | | | |
|---|---|---|---|---|---|---|---|---|---|---|---|---|---|
| fit_16B_01 | 16B | | Europe | Skaland | Norway | flake | 5493.52 | 15.56 | 20.58 | 1379.93 | 1580.67 | 0.00 | 65.63 |
| fit_16B_02 | 16B | | Europe | Skaland | Norway | flake | 5037.10 | 15.51 | 21.13 | 1348.17 | 1578.13 | 0.00 | 61.39 |
| fit_16B_03 | 16B | | Europe | Skaland | Norway | flake | 5185.24 | 17.44 | 19.91 | 1362.14 | 1579.40 | 0.00 | 64.49 |
| fit_16B_04 | 16B | | Europe | Skaland | Norway | flake | 5635.51 | 16.22 | 22.24 | 1345.63 | 1581.94 | 0.00 | 64.77 |
| fit_16B_05 | 16B | | Europe | Skaland | Norway | flake | 217.78 | 20.18 | 14.46 | 1351.98 | 1580.67 | 0.09 | 54.01 |
| fit_16B_06 | 16B | | Europe | Skaland | Norway | flake | 4760.99 | 13.90 | 20.33 | 1390.09 | 1575.59 | 0.00 | 60.48 |
| fit_16B_07 | 16B | | Europe | Skaland | Norway | flake | 5522.36 | 17.38 | 20.35 | 1346.90 | 1581.94 | 0.00 | 65.32 |
| fit_16B_08 | 16B | | Europe | Skaland | Norway | flake | 4705.34 | 18.20 | 17.00 | 1346.90 | 1583.21 | 0.00 | 65.12 |
| fit_16B_09 | 16B | | Europe | Skaland | Norway | flake | 6206.85 | 16.44 | 23.74 | 1344.36 | 1583.21 | 0.00 | 65.28 |
| fit_16B_10 | 16B | | Europe | Skaland | Norway | flake | 172.70 | 19.59 | 15.79 | 1350.71 | 1580.67 | 0.11 | 50.29 |
| fit_16B_11 | 16B | | Europe | Skaland | Norway | flake | 250.36 | 19.94 | 13.98 | 1355.79 | 1583.21 | 0.08 | 58.78 |
| fit_16B_12 | 16B | | Europe | Skaland | Norway | flake | 4758.13 | 17.87 | 17.11 | 1354.52 | 1583.21 | 0.00 | 65.27 |
| fit_16B_13 | 16B | | Europe | Skaland | Norway | flake | 198.11 | 16.73 | 19.70 | 1351.98 | 1580.67 | 0.08 | 50.00 |
| fit_16B_14 | 16B | | Europe | Skaland | Norway | flake | 5912.51 | 16.09 | 22.83 | 1351.98 | 1581.94 | 0.00 | 65.18 |
| fit_16B_15 | 16B | | Europe | Skaland | Norway | flake | 441.34 | 15.32 | 18.12 | 1357.06 | 1581.94 | 0.03 | 58.42 |
| fit_16B_16 | 16B | | Europe | Skaland | Norway | flake | 5107.03 | 13.76 | 19.66 | 1391.36 | 1580.67 | 0.00 | 64.95 |
| fit_16B_17 | 16B | | Europe | Skaland | Norway | flake | 5934.74 | 14.59 | 23.53 | 1387.55 | 1581.94 | 0.00 | 65.16 |
| fit_16B_18 | 16B | | Europe | Skaland | Norway | flake | 6192.21 | 14.38 | 24.55 | 1350.71 | 1581.94 | 0.00 | 65.30 |
| fit_16B_19 | 16B | | Europe | Skaland | Norway | flake | 291.10 | 16.15 | 17.85 | 1351.98 | 1581.94 | 0.06 | 42.25 |
| fit_16B_20 | 16B | | Europe | Skaland | Norway | flake | 306.62 | 15.25 | 19.30 | 1344.36 | 1581.94 | 0.04 | 40.91 |
| fit_21A_01 | 21A | | Asia | Shandong | China | flake | 5363.33 | 12.82 | 22.75 | 1348.16 | 1580.65 | 0.00 | 63.34 |
| fit_21A_02 | 21A | | Asia | Shandong | China | flake | 335.45 | 14.63 | 20.58 | 1351.97 | 1580.65 | 0.04 | 44.27 |

| | | | | | | | | | | | | | |
|---|---|---|---|---|---|---|---|---|---|---|---|---|---|
| fit_21A_03 | 21A | | Asia | Shandong | China | flake | 401.68 | 15.26 | 17.76 | 1348.16 | 1580.65 | 0.04 | 47.11 |
| fit_21A_04 | 21A | | Asia | Shandong | China | flake | 307.45 | 16.13 | 15.58 | 1349.43 | 1579.38 | 0.05 | 46.19 |
| fit_21A_05 | 21A | | Asia | Shandong | China | flake | 1213.65 | 12.95 | 21.59 | 1348.16 | 1581.92 | 0.01 | 58.24 |
| fit_21A_06 | 21A | | Asia | Shandong | China | flake | 395.47 | 16.96 | 17.15 | 1349.43 | 1581.92 | 0.04 | 54.37 |
| fit_21A_07 | 21A | | Asia | Shandong | China | flake | 485.52 | 13.49 | 22.26 | 1349.43 | 1581.92 | 0.03 | 42.59 |
| fit_21A_08 | 21A | | Asia | Shandong | China | flake | 5196.58 | 13.94 | 20.15 | 1329.11 | 1579.38 | 0.00 | 64.08 |
| fit_21A_09 | 21A | | Asia | Shandong | China | flake | 354.05 | 15.72 | 18.62 | 1353.24 | 1580.65 | 0.04 | 49.46 |
| fit_21A_10 | 21A | | Asia | Shandong | China | flake | 360.58 | 15.61 | 18.77 | 1348.16 | 1581.92 | 0.04 | 43.96 |
| fit_21A_11 | 21A | | Asia | Shandong | China | flake | 5597.29 | 12.76 | 22.97 | 1411.68 | 1581.92 | 0.00 | 64.00 |
| fit_21A_12 | 21A | | Asia | Shandong | China | flake | 444.78 | 13.93 | 22.80 | 1340.54 | 1580.65 | 0.03 | 42.60 |
| fit_21A_13 | 21A | | Asia | Shandong | China | flake | 5441.70 | 12.77 | 22.79 | 1340.54 | 1580.65 | 0.00 | 63.68 |
| fit_21A_14 | 21A | | Asia | Shandong | China | flake | 493.96 | 13.93 | 20.80 | 1351.97 | 1580.65 | 0.03 | 46.23 |
| fit_21A_15 | 21A | | Asia | Shandong | China | flake | 362.23 | 16.12 | 18.00 | 1350.70 | 1580.65 | 0.04 | 48.02 |
| fit_21A_16 | 21A | | Asia | Shandong | China | flake | 5615.81 | 13.50 | 20.90 | 1339.27 | 1583.19 | 0.00 | 65.18 |
| fit_21A_17 | 21A | | Asia | Shandong | China | flake | 421.39 | 15.35 | 18.94 | 1345.62 | 1581.92 | 0.04 | 46.45 |
| fit_21A_18 | 21A | | Asia | Shandong | China | flake | 298.40 | 15.21 | 16.24 | 1351.97 | 1581.92 | 0.05 | 45.66 |
| fit_21A_19 | 21A | | Asia | Shandong | China | flake | 5151.30 | 12.79 | 22.62 | 1414.22 | 1580.65 | 0.00 | 62.86 |
| fit_21A_20 | 21A | | Asia | Shandong | China | flake | 461.64 | 14.84 | 19.11 | 1349.43 | 1580.65 | 0.03 | 52.95 |
| fit_21B_01 | 21B | | Africa | Balama | Mozambique | flake | 460.14 | 14.69 | 19.93 | 1354.49 | 1581.91 | 0.03 | 49.33 |
| fit_21B_02 | 21B | | Africa | Balama | Mozambique | flake | 288.03 | 17.72 | 16.31 | 1353.22 | 1579.37 | 0.06 | 47.61 |
| fit_21B_03 | 21B | | Africa | Balama | Mozambique | flake | 464.93 | 14.76 | 19.75 | 1346.87 | 1581.91 | 0.03 | 45.85 |
| fit_21B_04 | 21B | | Africa | Balama | Mozambique | flake | 5358.70 | 13.51 | 22.96 | 1346.87 | 1581.91 | 0.00 | 63.34 |

| | | | | | | | | | | | | | |
|---|---|---|---|---|---|---|---|---|---|---|---|---|---|
| fit_21B_05 | 21B | | Africa | Balama | Mozambique | flake | 451.02 | 14.36 | 21.36 | 1343.06 | 1580.64 | 0.03 | 46.36 |
| fit_21B_06 | 21B | | Africa | Balama | Mozambique | flake | 351.28 | 16.77 | 17.09 | 1350.68 | 1581.91 | 0.05 | 46.29 |
| fit_21B_07 | 21B | | Africa | Balama | Mozambique | flake | 628.07 | 13.73 | 21.17 | 1351.95 | 1580.64 | 0.02 | 50.55 |
| fit_21B_08 | 21B | | Africa | Balama | Mozambique | flake | 5678.50 | 13.34 | 22.44 | 1345.60 | 1581.91 | 0.00 | 64.42 |
| fit_21B_09 | 21B | | Africa | Balama | Mozambique | flake | 5381.74 | 13.24 | 21.95 | 1357.04 | 1581.91 | 0.00 | 64.12 |
| fit_21B_10 | 21B | | Africa | Balama | Mozambique | flake | 316.25 | 14.55 | 20.90 | 1345.60 | 1581.91 | 0.05 | 39.63 |
| fit_21B_11 | 21B | | Africa | Balama | Mozambique | flake | 662.35 | 14.11 | 20.03 | 1341.79 | 1581.91 | 0.02 | 43.53 |
| fit_21B_12 | 21B | | Africa | Balama | Mozambique | flake | 5457.96 | 13.40 | 22.34 | 1350.68 | 1581.91 | 0.00 | 64.25 |
| fit_21B_13 | 21B | | Africa | Balama | Mozambique | flake | 5722.88 | 13.28 | 22.72 | 1327.81 | 1580.64 | 0.00 | 63.96 |
| fit_21B_14 | 21B | | Africa | Balama | Mozambique | flake | 5797.94 | 13.77 | 24.16 | 1383.72 | 1579.37 | 0.00 | 64.08 |
| fit_21B_15 | 21B | | Africa | Balama | Mozambique | flake | 5582.49 | 13.60 | 22.63 | 1355.77 | 1581.91 | 0.00 | 64.50 |
| fit_21B_16 | 21B | | Africa | Balama | Mozambique | flake | 2091.64 | 15.77 | 20.11 | 1348.14 | 1580.64 | 0.04 | 54.57 |
| fit_21B_17 | 21B | | Africa | Balama | Mozambique | flake | 357.38 | 15.25 | 18.78 | 1351.95 | 1581.91 | 0.04 | 38.45 |
| fit_21B_18 | 21B | | Africa | Balama | Mozambique | flake | 5474.78 | 12.66 | 23.43 | 1350.68 | 1579.37 | 0.00 | 63.07 |
| fit_21B_19 | 21B | | Africa | Balama | Mozambique | flake | 277.45 | 16.82 | 14.35 | 1351.10 | 1582.75 | 0.06 | 45.91 |
| fit_21B_20 | 21B | | Africa | Balama | Mozambique | flake | 456.70 | 14.32 | 20.52 | 1348.17 | 1581.28 | 0.03 | 51.09 |
| fit_21C_01 | 21C | | S_America | PedraAzul, Itaperica, Salta da Divisa | Brasil | flake | 499.70 | 15.19 | 18.17 | 1340.54 | 1580.65 | 0.03 | 50.50 |
| fit_21C_02 | 21C | | S_America | PedraAzul, Itaperica, Salta da Divisa | Brasil | flake | 468.90 | 15.76 | 17.99 | 1343.08 | 1581.92 | 0.03 | 50.75 |
| fit_21C_03 | 21C | | S_America | PedraAzul, Itaperica, Salta da Divisa | Brasil | flake | 886.08 | 13.07 | 22.33 | 1348.16 | 1579.38 | 0.02 | 59.92 |
| fit_21C_04 | 21C | | S_America | PedraAzul, Itaperica, Salta da Divisa | Brasil | flake | 530.33 | 13.71 | 21.98 | 1354.51 | 1580.65 | 0.03 | 49.54 |
| fit_21C_05 | 21C | | S_America | PedraAzul, Itaperica, Salta da Divisa | Brasil | flake | 1049.02 | 13.72 | 21.22 | 1344.35 | 1580.65 | 0.01 | 65.54 |
| fit_21C_06 | 21C | | S_America | PedraAzul, Itaperica, Salta da Divisa | Brasil | flake | 537.89 | 13.53 | 21.75 | 1345.62 | 1579.38 | 0.03 | 45.09 |

| | | | | | | | | | | | | | |
|---|---|---|---|---|---|---|---|---|---|---|---|---|---|
| fit_21C_07 | 21C | | S_America | PedraAzul, Itaperica, Salta da Divisa | Brasil | flake | 523.78 | 14.47 | 19.68 | 1353.24 | 1580.65 | 0.03 | 55.75 |
| fit_21C_08 | 21C | | S_America | PedraAzul, Itaperica, Salta da Divisa | Brasil | flake | 805.26 | 13.54 | 20.55 | 1351.97 | 1579.38 | 0.02 | 55.43 |
| fit_21C_09 | 21C | | S_America | PedraAzul, Itaperica, Salta da Divisa | Brasil | flake | 327.26 | 16.16 | 19.02 | 1346.89 | 1579.38 | 0.05 | 46.74 |
| fit_21C_10 | 21C | | S_America | PedraAzul, Itaperica, Salta da Divisa | Brasil | flake | 5369.20 | 12.94 | 22.23 | 1341.81 | 1580.65 | 0.00 | 63.86 |
| fit_21C_11 | 21C | | S_America | PedraAzul, Itaperica, Salta da Divisa | Brasil | flake | 5295.61 | 12.93 | 22.50 | 1348.16 | 1580.65 | 0.00 | 63.38 |
| fit_21C_12 | 21C | | S_America | PedraAzul, Itaperica, Salta da Divisa | Brasil | flake | 506.33 | 14.07 | 20.87 | 1343.08 | 1580.65 | 0.03 | 47.73 |
| fit_21C_13 | 21C | | S_America | PedraAzul, Itaperica, Salta da Divisa | Brasil | flake | 306.17 | 14.76 | 20.74 | 1348.16 | 1580.65 | 0.05 | 39.74 |
| fit_21C_14 | 21C | | S_America | PedraAzul, Itaperica, Salta da Divisa | Brasil | flake | 1302.24 | 12.76 | 22.73 | 1349.43 | 1581.92 | 0.01 | 67.62 |
| fit_21C_15 | 21C | | S_America | PedraAzul, Itaperica, Salta da Divisa | Brasil | flake | 5434.33 | 13.23 | 21.93 | 1338.00 | 1581.92 | 0.00 | 64.28 |
| fit_21C_16 | 21C | | S_America | PedraAzul, Itaperica, Salta da Divisa | Brasil | flake | 609.18 | 13.40 | 22.17 | 1344.35 | 1580.65 | 0.02 | 46.43 |
| fit_21C_17 | 21C | | S_America | PedraAzul, Itaperica, Salta da Divisa | Brasil | flake | 912.25 | 13.45 | 21.82 | 1348.16 | 1580.65 | 0.02 | 60.15 |
| fit_21C_18 | 21C | | S_America | PedraAzul, Itaperica, Salta da Divisa | Brasil | flake | 5709.08 | 12.54 | 23.29 | 1344.35 | 1580.65 | 0.00 | 64.05 |
| fit_21C_19 | 21C | | S_America | PedraAzul, Itaperica, Salta da Divisa | Brasil | flake | 5849.67 | 12.31 | 23.83 | 1351.97 | 1581.92 | 0.00 | 64.24 |
| fit_21C_20 | 21C | | S_America | PedraAzul, Itaperica, Salta da Divisa | Brasil | flake | 1041.54 | 13.50 | 22.01 | 1355.78 | 1581.92 | 0.01 | 61.48 |
| fit_21D_01 | 21D | | Africa | Vatomina/Sahamamy Sahasoa | Madagascar | flake | 782.44 | 13.87 | 21.31 | 1349.41 | 1580.64 | 0.02 | 54.13 |
| fit_21D_02 | 21D | | Africa | Vatomina/Sahamamy Sahasoa | Madagascar | flake | 419.35 | 14.35 | 20.39 | 1344.33 | 1580.64 | 0.03 | 39.29 |
| fit_21D_03 | 21D | | Africa | Vatomina/Sahamamy Sahasoa | Madagascar | flake | 206.83 | 17.86 | 13.85 | 1349.41 | 1578.10 | 0.08 | 38.15 |
| fit_21D_04 | 21D | | Africa | Vatomina/Sahamamy Sahasoa | Madagascar | flake | 5548.37 | 13.00 | 23.27 | 1339.25 | 1580.64 | 0.00 | 63.49 |
| fit_21D_05 | 21D | | Africa | Vatomina/Sahamamy Sahasoa | Madagascar | flake | 547.43 | 14.56 | 20.39 | 1349.41 | 1580.64 | 0.03 | 50.21 |
| fit_21D_06 | 21D | | Africa | Vatomina/Sahamamy Sahasoa | Madagascar | flake | 492.79 | 15.60 | 18.07 | 1340.52 | 1581.91 | 0.03 | 48.49 |
| fit_21D_07 | 21D | | Africa | Vatomina/Sahamamy Sahasoa | Madagascar | flake | 471.64 | 14.94 | 19.33 | 1346.87 | 1580.64 | 0.03 | 46.43 |
| fit_21D_08 | 21D | | Africa | Vatomina/Sahamamy Sahasoa | Madagascar | flake | 2192.74 | 13.85 | 20.74 | 1348.14 | 1580.64 | 0.02 | 53.92 |

| | | | | | | | | | | | | | |
|---|---|---|---|---|---|---|---|---|---|---|---|---|---|
| fit_21D_09 | 21D | | Africa | Vatomina/Sahamamy Sahasoa | Madagascar | flake | 5396.64 | 12.88 | 23.18 | 1360.85 | 1581.91 | 0.00 | 63.48 |
| fit_21D_10 | 21D | | Africa | Vatomina/Sahamamy Sahasoa | Madagascar | flake | 1223.94 | 13.36 | 22.13 | 1343.06 | 1581.91 | 0.01 | 66.32 |
| fit_21D_11 | 21D | | Africa | Vatomina/Sahamamy Sahasoa | Madagascar | flake | 346.62 | 16.60 | 17.35 | 1344.33 | 1580.64 | 0.05 | 46.22 |
| fit_21D_12 | 21D | | Africa | Vatomina/Sahamamy Sahasoa | Madagascar | flake | 5510.18 | 12.98 | 21.65 | 1357.04 | 1580.64 | 0.00 | 64.86 |
| fit_21D_13 | 21D | | Africa | Vatomina/Sahamamy Sahasoa | Madagascar | flake | 139.83 | 22.26 | 9.93 | 1349.41 | 1580.64 | 0.16 | 37.49 |
| fit_21D_14 | 21D | | Africa | Vatomina/Sahamamy Sahasoa | Madagascar | flake | 5492.25 | 13.25 | 22.16 | 1352.57 | 1579.81 | 0.00 | 63.59 |
| fit_21D_15 | 21D | | Africa | Vatomina/Sahamamy Sahasoa | Madagascar | flake | 612.08 | 14.79 | 19.53 | 1342.30 | 1581.28 | 0.02 | 43.47 |
| fit_21D_16 | 21D | | Africa | Vatomina/Sahamamy Sahasoa | Madagascar | flake | 417.10 | 14.34 | 21.08 | 1348.17 | 1579.81 | 0.04 | 37.75 |
| fit_21D_17 | 21D | | Africa | Vatomina/Sahamamy Sahasoa | Madagascar | flake | 6004.25 | 12.95 | 23.43 | 1355.50 | 1581.28 | 0.00 | 64.77 |
| fit_21D_18 | 21D | | Africa | Vatomina/Sahamamy Sahasoa | Madagascar | flake | 415.30 | 14.83 | 20.31 | 1346.70 | 1581.28 | 0.04 | 42.17 |
| fit_21D_19 | 21D | | Africa | Vatomina/Sahamamy Sahasoa | Madagascar | flake | 5397.12 | 12.74 | 22.29 | 1368.69 | 1581.28 | 0.00 | 64.60 |
| fit_21D_20 | 21D | | Africa | Vatomina/Sahamamy Sahasoa | Madagascar | flake | 530.93 | 14.11 | 21.38 | 1342.30 | 1581.28 | 0.02 | 50.31 |
| fit_21E_01 | 21E | | Europe | Ural, Tayginka | Russia | flake | 5013.00 | 13.61 | 20.55 | 1345.61 | 1580.64 | 0.00 | 63.90 |
| fit_21E_02 | 21E | | Europe | Ural, Tayginka | Russia | flake | 5334.41 | 13.63 | 20.50 | 1358.31 | 1581.91 | 0.00 | 64.92 |
| fit_21E_03 | 21E | | Europe | Ural, Tayginka | Russia | flake | 825.75 | 14.00 | 20.86 | 1354.50 | 1580.64 | 0.02 | 56.94 |
| fit_21E_04 | 21E | | Europe | Ural, Tayginka | Russia | flake | 5385.96 | 12.91 | 23.10 | 1367.21 | 1581.91 | 0.00 | 63.47 |
| fit_21E_05 | 21E | | Europe | Ural, Tayginka | Russia | flake | 323.53 | 14.71 | 20.34 | 1362.12 | 1581.91 | 0.04 | 58.86 |
| fit_21E_06 | 21E | | Europe | Ural, Tayginka | Russia | flake | 5593.58 | 12.64 | 23.15 | 1350.69 | 1581.91 | 0.00 | 63.76 |
| fit_21E_07 | 21E | | Europe | Ural, Tayginka | Russia | flake | 5302.72 | 12.89 | 22.04 | 1339.26 | 1580.64 | 0.00 | 63.86 |
| fit_21E_08 | 21E | | Europe | Ural, Tayginka | Russia | flake | 5499.24 | 13.04 | 22.64 | 1397.27 | 1581.91 | 0.00 | 64.26 |
| fit_21E_09 | 21E | | Europe | Ural, Tayginka | Russia | flake | 5296.32 | 12.74 | 22.20 | 1340.53 | 1581.91 | 0.00 | 63.78 |
| fit_21E_10 | 21E | | Europe | Ural, Tayginka | Russia | flake | 5473.25 | 13.10 | 22.21 | 1355.77 | 1581.91 | 0.00 | 64.28 |

| | | | | | | | | | | | | | |
|---|---|---|---|---|---|---|---|---|---|---|---|---|---|
| fit_21E_11 | 21E | | Europe | Ural, Tayginka | Russia | flake | 5459.32 | 13.04 | 21.61 | 1351.96 | 1581.91 | 0.00 | 64.24 |
| fit_21E_12 | 21E | | Europe | Ural, Tayginka | Russia | flake | 5324.68 | 12.95 | 22.31 | 1340.53 | 1581.91 | 0.00 | 63.75 |
| fit_21E_13 | 21E | | Europe | Ural, Tayginka | Russia | flake | 5275.86 | 12.82 | 22.54 | 1354.50 | 1581.91 | 0.00 | 63.38 |
| fit_21E_14 | 21E | | Europe | Ural, Tayginka | Russia | flake | 917.23 | 14.02 | 20.10 | 1362.84 | 1581.29 | 0.01 | 72.63 |
| fit_21E_15 | 21E | | Europe | Ural, Tayginka | Russia | flake | 530.78 | 13.97 | 20.94 | 1349.65 | 1581.29 | 0.03 | 44.70 |
| fit_21E_16 | 21E | | Europe | Ural, Tayginka | Russia | flake | 230.69 | 17.02 | 13.37 | 1344.34 | 1581.91 | 0.07 | 46.70 |
| fit_21E_17 | 21E | | Europe | Ural, Tayginka | Russia | flake | 5560.47 | 12.96 | 22.11 | 1344.34 | 1580.64 | 0.00 | 64.75 |
| fit_21E_18 | 21E | | Europe | Ural, Tayginka | Russia | flake | 488.49 | 17.11 | 15.81 | 1346.72 | 1581.29 | 0.03 | 64.87 |
| fit_21E_19 | 21E | | Europe | Ural, Tayginka | Russia | flake | 926.04 | 14.28 | 19.74 | 1343.78 | 1581.29 | 0.02 | 70.34 |
| fit_21E_20 | 21E | | Europe | Ural, Tayginka | Russia | flake | 5690.64 | 12.96 | 22.92 | 1388.80 | 1581.91 | 0.00 | 64.10 |
| fit_21F_01 | 21F | | Asia | Ragedara | Sri_Lanka | hydro | 5006.46 | 13.82 | 19.98 | 1445.84 | 1581.79 | 0.00 | 64.38 |
| fit_21F_02 | 21F | | Asia | Ragedara | Sri_Lanka | hydro | 5099.09 | 13.95 | 21.34 | 1350.54 | 1581.79 | 0.00 | 63.44 |
| fit_21F_03 | 21F | | Asia | Ragedara | Sri_Lanka | hydro | 4915.41 | 13.43 | 21.77 | 1381.04 | 1581.79 | 0.00 | 63.07 |
| fit_21F_04 | 21F | | Asia | Ragedara | Sri_Lanka | hydro | 1186.14 | 13.72 | 21.87 | 1341.65 | 1580.51 | 0.01 | 56.99 |
| fit_21F_05 | 21F | | Asia | Ragedara | Sri_Lanka | hydro | 5230.56 | 13.16 | 23.58 | 1445.84 | 1580.51 | 0.00 | 61.95 |
| fit_21F_06 | 21F | | Asia | Ragedara | Sri_Lanka | hydro | 5423.15 | 12.91 | 22.82 | 1341.65 | 1580.51 | 0.00 | 63.64 |
| fit_21F_07 | 21F | | Asia | Ragedara | Sri_Lanka | hydro | 5267.33 | 14.05 | 20.67 | 1435.25 | 1581.79 | 0.00 | 64.64 |
| fit_21F_08 | 21F | | Asia | Ragedara | Sri_Lanka | hydro | 5400.57 | 13.09 | 22.67 | 1448.38 | 1580.51 | 0.00 | 63.77 |
| fit_21F_09 | 21F | | Asia | Ragedara | Sri_Lanka | hydro | 5002.66 | 12.59 | 23.17 | 1425.51 | 1579.24 | 0.00 | 62.20 |
| fit_21F_10 | 21F | | Asia | Ragedara | Sri_Lanka | hydro | 5510.66 | 13.40 | 21.90 | 1350.54 | 1580.51 | 0.00 | 64.07 |
| fit_21F_11 | 21F | | Asia | Ragedara | Sri_Lanka | hydro | 930.62 | 14.10 | 20.42 | 1350.54 | 1580.51 | 0.01 | 60.31 |
| fit_21F_12 | 21F | | Asia | Ragedara | Sri_Lanka | hydro | 581.74 | 13.85 | 21.49 | 1342.92 | 1581.79 | 0.02 | 46.01 |

| | | | | | | | | | | | | | |
|---|---|---|---|---|---|---|---|---|---|---|---|---|---|
| fit_21F_13 | 21F | | Asia | Ragedara | Sri_Lanka | hydro | 5472.02 | 13.22 | 22.71 | 1353.08 | 1580.51 | 0.00 | 63.60 |
| fit_21F_14 | 21F | | Asia | Ragedara | Sri_Lanka | hydro | 5408.11 | 12.66 | 23.87 | 1363.25 | 1580.51 | 0.00 | 62.47 |
| fit_21F_15 | 21F | | Asia | Ragedara | Sri_Lanka | hydro | 5045.37 | 13.31 | 22.31 | 1412.80 | 1580.51 | 0.00 | 62.73 |
| fit_21F_16 | 21F | | Asia | Ragedara | Sri_Lanka | hydro | 4867.50 | 15.11 | 19.16 | 1348.00 | 1583.06 | 0.00 | 63.76 |
| fit_21F_17 | 21F | | Asia | Ragedara | Sri_Lanka | hydro | 1008.52 | 14.30 | 19.87 | 1349.27 | 1581.79 | 0.01 | 68.78 |
| fit_21F_18 | 21F | | Asia | Ragedara | Sri_Lanka | hydro | 5435.78 | 14.60 | 21.90 | 1354.35 | 1580.51 | 0.00 | 64.53 |
| fit_21F_19 | 21F | | Asia | Ragedara | Sri_Lanka | hydro | 5185.81 | 13.14 | 22.78 | 1414.07 | 1580.51 | 0.00 | 62.65 |
| fit_21F_20 | 21F | | Asia | Ragedara | Sri_Lanka | hydro | 4695.04 | 16.10 | 18.04 | 1354.35 | 1579.24 | 0.00 | 63.69 |
| fit_21G_01 | 21G | | Europe | Kaisersberg | Austria | amorph | 85.80 | 52.65 | 3.72 | 1351.11 | 1576.89 | 0.61 | 45.83 |
| fit_21G_02 | 21G | | Europe | Kaisersberg | Austria | amorph | 93.95 | 68.13 | 2.45 | 1344.34 | 1586.99 | 0.72 | 58.88 |
| fit_21G_03 | 21G | | Europe | Kaisersberg | Austria | amorph | 111.72 | 47.43 | 3.87 | 1346.88 | 1575.56 | 0.43 | 53.63 |
| fit_21G_04 | 21G | | Europe | Kaisersberg | Austria | amorph | 87.22 | 66.70 | 2.87 | 1344.34 | 1586.99 | 0.75 | 55.84 |
| fit_21G_05 | 21G | | Europe | Kaisersberg | Austria | amorph | 63.11 | 52.90 | 4.12 | 1351.96 | 1585.72 | 0.87 | 38.56 |
| fit_21G_06 | 21G | | Europe | Kaisersberg | Austria | amorph | 75.10 | 55.62 | 3.70 | 1349.42 | 1579.37 | 0.75 | 45.56 |
| fit_21G_07 | 21G | | Europe | Kaisersberg | Austria | amorph | 68.38 | 75.16 | 2.73 | 1351.11 | 1581.29 | 1.09 | 44.15 |
| fit_21G_08 | 21G | | Europe | Kaisersberg | Austria | amorph | 74.34 | 50.84 | 3.96 | 1351.11 | 1582.76 | 0.68 | 43.12 |
| fit_21G_09 | 21G | | Europe | Kaisersberg | Austria | amorph | 97.98 | 46.09 | 4.39 | 1351.96 | 1583.18 | 0.47 | 53.09 |
| fit_21G_10 | 21G | | Europe | Kaisersberg | Austria | amorph | 69.38 | 72.12 | 2.72 | 1344.34 | 1585.72 | 1.03 | 43.13 |
| fit_21G_11 | 21G | | Europe | Kaisersberg | Austria | amorph | 65.87 | 73.19 | 2.66 | 1351.96 | 1583.18 | 1.09 | 42.10 |
| fit_21G_12 | 21G | | Europe | Kaisersberg | Austria | amorph | 84.28 | 62.65 | 3.12 | 1351.11 | 1587.16 | 0.76 | 53.32 |
| fit_21G_13 | 21G | | Europe | Kaisersberg | Austria | amorph | 81.90 | 56.13 | 3.61 | 1348.15 | 1584.45 | 0.69 | 48.46 |
| fit_21G_14 | 21G | | Europe | Kaisersberg | Austria | amorph | 85.55 | 59.62 | 3.18 | 1351.96 | 1585.72 | 0.70 | 53.09 |

| | | | | | | | | | | | | | |
|---|---|---|---|---|---|---|---|---|---|---|---|---|---|
| fit_21G_15 | 21G | | Europe | Kaisersberg | Austria | amorph | 83.57 | 52.61 | 3.68 | 1350.69 | 1585.72 | 0.65 | 50.03 |
| fit_21G_16 | 21G | | Europe | Kaisersberg | Austria | amorph | 86.59 | 57.01 | 2.97 | 1350.69 | 1578.10 | 0.64 | 50.17 |
| fit_21G_17 | 21G | | Europe | Kaisersberg | Austria | amorph | 97.08 | 58.55 | 3.77 | 1351.96 | 1579.37 | 0.59 | 51.14 |
| fit_21G_18 | 21G | | Europe | Kaisersberg | Austria | amorph | 415.94 | 15.98 | 19.01 | 1344.34 | 1579.37 | 0.04 | 39.93 |
| fit_21G_19 | 21G | | Europe | Kaisersberg | Austria | amorph | 562.62 | 15.28 | 19.17 | 1351.96 | 1580.64 | 0.03 | 49.42 |
| fit_21G_20 | 21G | | Europe | Kaisersberg | Austria | amorph | 83.21 | 64.25 | 2.58 | 1351.96 | 1583.18 | 0.77 | 50.92 |
| fit_21I_01 | 21I | | Europe | Kaisersberg | Austria | amorph | 97.22 | 80.49 | 3.07 | 1344.32 | 1571.74 | 0.83 | 52.13 |
| fit_21I_02 | 21I | | Europe | Kaisersberg | Austria | amorph | 95.22 | 66.41 | 2.53 | 1351.94 | 1581.91 | 0.72 | 63.08 |
| fit_21I_03 | 21I | | Europe | Kaisersberg | Austria | amorph | 773.99 | 13.50 | 20.62 | 1351.94 | 1581.91 | 0.02 | 57.56 |
| fit_21I_04 | 21I | | Europe | Kaisersberg | Austria | amorph | 86.51 | 58.06 | 3.17 | 1346.88 | 1579.39 | 0.67 | 51.94 |
| fit_21I_05 | 21I | | Europe | Kaisersberg | Austria | amorph | 71.09 | 59.78 | 2.78 | 1348.15 | 1583.20 | 0.82 | 48.79 |
| fit_21I_06 | 21I | | Europe | Kaisersberg | Austria | amorph | 81.67 | 87.88 | 2.11 | 1346.88 | 1581.93 | 1.09 | 58.85 |
| fit_21I_07 | 21I | | Europe | Kaisersberg | Austria | amorph | 184.12 | 19.12 | 16.51 | 1349.42 | 1579.39 | 0.10 | 42.07 |
| fit_21I_08 | 21I | | Europe | Kaisersberg | Austria | amorph | 301.38 | 16.25 | 18.20 | 1362.13 | 1578.12 | 0.04 | 35.69 |
| fit_21I_09 | 21I | | Europe | Kaisersberg | Austria | amorph | 151.03 | 20.46 | 10.71 | 1353.24 | 1579.39 | 0.13 | 42.43 |
| fit_21I_10 | 21I | | Europe | Kaisersberg | Austria | amorph | 4597.21 | 15.46 | 16.99 | 1362.13 | 1579.39 | 0.00 | 65.01 |
| fit_21J_01 | 21J | | Africa | Balama | Mozambique | flake | 5408.53 | 13.30 | 23.14 | 1332.89 | 1581.87 | 0.00 | 63.42 |
| fit_21J_02 | 21J | | Africa | Balama | Mozambique | flake | 5349.85 | 14.34 | 21.33 | 1335.43 | 1581.87 | 0.00 | 64.58 |
| fit_21J_03 | 21J | | Africa | Balama | Mozambique | flake | 658.94 | 15.61 | 17.71 | 1349.40 | 1580.60 | 0.02 | 58.37 |
| fit_21J_04 | 21J | | Africa | Balama | Mozambique | flake | 449.71 | 14.43 | 20.61 | 1353.21 | 1580.60 | 0.03 | 48.26 |
| fit_21J_05 | 21J | | Africa | Balama | Mozambique | flake | 204.22 | 16.43 | 19.09 | 1354.48 | 1581.87 | 0.08 | 49.19 |
| fit_21J_06 | 21J | | Africa | Balama | Mozambique | flake | 231.70 | 15.79 | 15.38 | 1357.02 | 1581.87 | 0.07 | 52.87 |

| | | | | | | | | | | | | | |
|---|---|---|---|---|---|---|---|---|---|---|---|---|---|
| fit_21J_07 | 21J | | Africa | Balama | Mozambique | flake | 5624.08 | 13.36 | 22.21 | 1344.32 | 1580.60 | 0.00 | 63.52 |
| fit_21J_08 | 21J | | Africa | Balama | Mozambique | flake | 2480.59 | 14.42 | 21.80 | 1344.32 | 1581.87 | 0.01 | 67.16 |
| fit_21J_09 | 21J | | Africa | Balama | Mozambique | flake | 450.62 | 14.67 | 19.75 | 1351.94 | 1580.60 | 0.03 | 45.16 |
| fit_21J_10 | 21J | | Africa | Balama | Mozambique | flake | 583.99 | 14.41 | 19.73 | 1349.40 | 1581.87 | 0.03 | 57.84 |
| fit_21J_11 | 21J | | Africa | Balama | Mozambique | flake | 5813.55 | 13.77 | 22.90 | 1360.84 | 1581.87 | 0.00 | 64.54 |
| fit_21J_12 | 21J | | Africa | Balama | Mozambique | flake | 5351.43 | 14.57 | 21.69 | 1348.13 | 1581.87 | 0.00 | 64.24 |
| fit_21J_13 | 21J | | Africa | Balama | Mozambique | flake | 526.68 | 14.96 | 18.77 | 1345.59 | 1581.87 | 0.03 | 51.14 |
| fit_21J_14 | 21J | | Africa | Balama | Mozambique | flake | 600.15 | 13.85 | 20.96 | 1348.13 | 1581.87 | 0.02 | 53.13 |
| fit_21J_15 | 21J | | Africa | Balama | Mozambique | flake | 533.86 | 14.20 | 20.40 | 1343.05 | 1581.87 | 0.03 | 45.63 |
| fit_21J_16 | 21J | | Africa | Balama | Mozambique | flake | 5617.58 | 14.62 | 22.54 | 1339.24 | 1580.60 | 0.00 | 64.82 |
| fit_21J_17 | 21J | | Africa | Balama | Mozambique | flake | 5053.99 | 13.79 | 20.03 | 1327.81 | 1581.87 | 0.00 | 63.92 |
| fit_21J_18 | 21J | | Africa | Balama | Mozambique | flake | 457.68 | 15.20 | 19.78 | 1343.05 | 1579.33 | 0.03 | 64.28 |
| fit_21J_19 | 21J | | Africa | Balama | Mozambique | flake | 707.61 | 16.25 | 15.94 | 1351.94 | 1580.60 | 0.02 | 57.48 |
| fit_21J_20 | 21J | | Africa | Balama | Mozambique | flake | 5384.83 | 12.61 | 22.92 | 1349.40 | 1579.33 | 0.00 | 48.67 |
| fit_21K_01 | 21K | | Africa | Balama | Mozambique | flake | 5332.62 | 12.82 | 21.80 | 1339.24 | 1581.87 | 0.00 | 64.02 |
| fit_21K_02 | 21K | | Africa | Balama | Mozambique | flake | 671.83 | 13.44 | 21.65 | 1348.13 | 1580.60 | 0.02 | 44.72 |
| fit_21K_03 | 21K | | Africa | Balama | Mozambique | flake | 279.54 | 16.60 | 15.20 | 1348.13 | 1581.87 | 0.06 | 50.55 |
| fit_21K_04 | 21K | | Africa | Balama | Mozambique | flake | 400.14 | 15.16 | 19.85 | 1351.94 | 1580.60 | 0.04 | 55.55 |
| fit_21K_05 | 21K | | Africa | Balama | Mozambique | flake | 6161.46 | 14.41 | 25.43 | 1348.13 | 1580.60 | 0.00 | 64.59 |
| fit_21K_06 | 21K | | Africa | Balama | Mozambique | flake | 5225.34 | 14.10 | 20.31 | 1345.59 | 1580.60 | 0.00 | 64.39 |
| fit_21K_07 | 21K | | Africa | Balama | Mozambique | flake | 601.11 | 15.23 | 18.80 | 1357.02 | 1581.87 | 0.02 | 52.45 |
| fit_21K_08 | 21K | | Africa | Balama | Mozambique | flake | 5469.42 | 13.99 | 20.13 | 1348.13 | 1581.87 | 0.00 | 64.92 |

| | | | | | | | | | | | | | |
|---|---|---|---|---|---|---|---|---|---|---|---|---|---|
| fit_21K_09 | 21K | | Africa | Balama | Mozambique | flake | 5387.45 | 12.95 | 22.80 | 1346.86 | 1579.33 | 0.00 | 63.56 |
| fit_21K_10 | 21K | | Africa | Balama | Mozambique | flake | 5642.12 | 14.60 | 22.99 | 1353.21 | 1580.60 | 0.00 | 64.54 |
| fit_21K_11 | 21K | | Africa | Balama | Mozambique | flake | 334.04 | 15.92 | 18.91 | 1348.13 | 1579.33 | 0.05 | 43.97 |
| fit_21K_12 | 21K | | Africa | Balama | Mozambique | flake | 693.00 | 14.10 | 20.08 | 1340.51 | 1581.87 | 0.02 | 48.32 |
| fit_21K_13 | 21K | | Africa | Balama | Mozambique | flake | 5469.18 | 13.23 | 22.02 | 1353.21 | 1580.60 | 0.00 | 64.27 |
| fit_21K_14 | 21K | | Africa | Balama | Mozambique | flake | 5527.29 | 12.90 | 22.84 | 1350.67 | 1580.60 | 0.00 | 63.32 |
| fit_21K_15 | 21K | | Africa | Balama | Mozambique | flake | 5386.12 | 13.13 | 22.02 | 1349.40 | 1579.33 | 0.00 | 64.29 |
| fit_21K_16 | 21K | | Africa | Balama | Mozambique | flake | 6200.02 | 14.35 | 26.32 | 1348.13 | 1580.60 | 0.00 | 64.13 |
| fit_21K_17 | 21K | | Africa | Balama | Mozambique | flake | 630.25 | 13.29 | 22.30 | 1351.94 | 1580.60 | 0.02 | 49.78 |
| fit_21K_18 | 21K | | Africa | Balama | Mozambique | flake | 975.67 | 13.99 | 19.94 | 1351.94 | 1581.87 | 0.01 | 58.80 |
| fit_21K_19 | 21K | | Africa | Balama | Mozambique | flake | 464.73 | 14.42 | 20.43 | 1346.86 | 1580.60 | 0.03 | 46.33 |
| fit_21K_20 | 21K | | Africa | Balama | Mozambique | flake | 357.47 | 15.58 | 18.83 | 1357.02 | 1580.60 | 0.04 | 46.95 |
| fit_21L_01 | 21L | | Africa | Balama | Mozambique | flake | 400.21 | 14.06 | 21.16 | 1348.02 | 1580.54 | 0.04 | 41.92 |
| fit_21L_02 | 21L | | Africa | Balama | Mozambique | flake | 722.75 | 13.59 | 21.25 | 1355.65 | 1580.54 | 0.02 | 55.34 |
| fit_21L_03 | 21L | | Africa | Balama | Mozambique | flake | 5640.49 | 12.58 | 23.31 | 1339.13 | 1581.81 | 0.00 | 39.54 |
| fit_21L_04 | 21L | | Africa | Balama | Mozambique | flake | 5554.10 | 12.95 | 22.87 | 1351.84 | 1581.81 | 0.00 | 64.18 |
| fit_21L_05 | 21L | | Africa | Balama | Mozambique | flake | 5526.05 | 12.58 | 23.08 | 1358.19 | 1580.54 | 0.00 | 63.96 |
| fit_21L_06 | 21L | | Africa | Balama | Mozambique | flake | 5398.11 | 13.06 | 22.44 | 1364.54 | 1581.81 | 0.00 | 50.87 |
| fit_21L_07 | 21L | | Africa | Balama | Mozambique | flake | 5619.58 | 12.57 | 22.83 | 1388.68 | 1581.81 | 0.00 | 63.86 |
| fit_21L_08 | 21L | | Africa | Balama | Mozambique | flake | 889.37 | 13.17 | 21.73 | 1355.65 | 1581.81 | 0.01 | 54.16 |
| fit_21L_09 | 21L | | Africa | Balama | Mozambique | flake | 5587.17 | 12.52 | 23.61 | 1364.54 | 1581.81 | 0.00 | 63.65 |
| fit_21L_10 | 21L | | Africa | Balama | Mozambique | flake | 1149.38 | 12.88 | 22.36 | 1354.38 | 1580.54 | 0.01 | 64.50 |

| | | | | | | | | | | | | | |
|---|---|---|---|---|---|---|---|---|---|---|---|---|---|
| fit_21L_11 | 21L | | Africa | Balama | Mozambique | flake | 5201.72 | 13.93 | 20.75 | 1344.21 | 1581.81 | 0.00 | 51.60 |
| fit_21L_12 | 21L | | Africa | Balama | Mozambique | flake | 283.80 | 15.86 | 15.45 | 1345.48 | 1581.81 | 0.05 | 44.55 |
| fit_21L_13 | 21L | | Africa | Balama | Mozambique | flake | 5981.90 | 13.87 | 24.84 | 1349.29 | 1580.54 | 0.00 | 64.51 |
| fit_21L_14 | 21L | | Africa | Balama | Mozambique | flake | 279.24 | 15.45 | 19.68 | 1351.84 | 1580.54 | 0.06 | 41.13 |
| fit_21L_15 | 21L | | Africa | Balama | Mozambique | flake | 400.75 | 14.26 | 20.83 | 1353.11 | 1580.54 | 0.04 | 45.30 |
| fit_21L_16 | 21L | | Africa | Balama | Mozambique | flake | 5667.54 | 12.72 | 23.44 | 1353.11 | 1580.54 | 0.00 | 63.88 |
| fit_21L_17 | 21L | | Africa | Balama | Mozambique | flake | 836.01 | 12.70 | 23.25 | 1348.02 | 1581.81 | 0.02 | 44.06 |
| fit_21L_18 | 21L | | Africa | Balama | Mozambique | flake | 255.56 | 15.68 | 17.94 | 1346.75 | 1580.54 | 0.06 | 43.68 |
| fit_21L_19 | 21L | | Africa | Balama | Mozambique | flake | 5377.32 | 12.86 | 22.91 | 1367.08 | 1581.81 | 0.00 | 64.01 |
| fit_21L_20 | 21L | | Africa | Balama | Mozambique | flake | 5553.84 | 12.81 | 22.83 | 1445.86 | 1580.54 | 0.00 | 64.31 |
| fit_21M_01 | 21M | | S_America | PedraAzul, Itaperica, Salta da Divisa | Brasil | flake | 691.47 | 13.39 | 21.19 | 1353.24 | 1580.63 | 0.02 | 47.55 |
| fit_21M_02 | 21M | | S_America | PedraAzul, Itaperica, Salta da Divisa | Brasil | flake | 256.70 | 15.63 | 15.97 | 1344.35 | 1578.09 | 0.06 | 40.08 |
| fit_21M_03 | 21M | | S_America | PedraAzul, Itaperica, Salta da Divisa | Brasil | flake | 398.45 | 13.96 | 21.91 | 1345.46 | 1580.51 | 0.04 | 41.41 |
| fit_21M_04 | 21M | | S_America | PedraAzul, Itaperica, Salta da Divisa | Brasil | flake | 5676.78 | 12.72 | 22.88 | 1346.73 | 1580.51 | 0.00 | 63.71 |
| fit_21M_05 | 21M | | S_America | PedraAzul, Itaperica, Salta da Divisa | Brasil | flake | 383.59 | 15.04 | 19.07 | 1349.27 | 1581.78 | 0.04 | 47.22 |
| fit_21M_06 | 21M | | S_America | PedraAzul, Itaperica, Salta da Divisa | Brasil | flake | 1021.18 | 13.10 | 21.59 | 1350.54 | 1581.78 | 0.01 | 51.08 |
| fit_21M_07 | 21M | | S_America | PedraAzul, Itaperica, Salta da Divisa | Brasil | flake | 564.02 | 13.25 | 22.21 | 1350.54 | 1581.78 | 0.02 | 43.37 |
| fit_21M_08 | 21M | | S_America | PedraAzul, Itaperica, Salta da Divisa | Brasil | flake | 5857.21 | 12.45 | 24.63 | 1345.46 | 1580.51 | 0.00 | 63.76 |
| fit_21M_09 | 21M | | S_America | PedraAzul, Itaperica, Salta da Divisa | Brasil | flake | 933.80 | 13.27 | 22.07 | 1350.54 | 1581.78 | 0.01 | 53.03 |
| fit_21M_10 | 21M | | S_America | PedraAzul, Itaperica, Salta da Divisa | Brasil | flake | 1116.02 | 13.19 | 22.54 | 1350.54 | 1580.51 | 0.01 | 58.15 |
| fit_21M_11 | 21M | | S_America | PedraAzul, Itaperica, Salta da Divisa | Brasil | flake | 958.45 | 12.96 | 22.55 | 1342.92 | 1579.24 | 0.01 | 57.22 |
| fit_21M_12 | 21M | | S_America | PedraAzul, Itaperica, Salta da Divisa | Brasil | flake | 5823.29 | 12.30 | 24.60 | 1361.98 | 1580.51 | 0.00 | 63.83 |

| | | | | | | | | | | | | | |
|---|---|---|---|---|---|---|---|---|---|---|---|---|---|
| fit_21M_13 | 21M | | S_America | PedraAzul, Itaperica, Salta da Divisa | Brasil | flake | 247.48 | 16.39 | 14.81 | 1354.35 | 1581.78 | 0.06 | 42.67 |
| fit_21M_14 | 21M | | S_America | PedraAzul, Itaperica, Salta da Divisa | Brasil | flake | 5515.86 | 12.51 | 23.70 | 1341.65 | 1580.51 | 0.00 | 63.56 |
| fit_21M_15 | 21M | | S_America | PedraAzul, Itaperica, Salta da Divisa | Brasil | flake | 1035.45 | 13.06 | 22.72 | 1351.81 | 1581.78 | 0.01 | 65.01 |
| fit_21M_16 | 21M | | S_America | PedraAzul, Itaperica, Salta da Divisa | Brasil | flake | 613.05 | 13.87 | 21.32 | 1349.27 | 1581.78 | 0.02 | 48.55 |
| fit_21M_17 | 21M | | S_America | PedraAzul, Itaperica, Salta da Divisa | Brasil | flake | 751.24 | 13.36 | 21.49 | 1345.46 | 1581.78 | 0.02 | 49.06 |
| fit_21M_18 | 21M | | S_America | PedraAzul, Itaperica, Salta da Divisa | Brasil | flake | 5497.39 | 12.64 | 23.28 | 1361.98 | 1581.78 | 0.00 | 63.83 |
| fit_21M_19 | 21M | | S_America | PedraAzul, Itaperica, Salta da Divisa | Brasil | flake | 837.81 | 12.98 | 24.21 | 1344.19 | 1580.51 | 0.02 | 52.00 |
| fit_21M_20 | 21M | | S_America | PedraAzul, Itaperica, Salta da Divisa | Brasil | flake | 5630.22 | 12.53 | 23.33 | 1355.62 | 1580.51 | 0.00 | 64.02 |
| fit_21N_01 | 21N | | S_America | PedraAzul, Itaperica, Salta da Divisa | Brasil | flake | 5363.76 | 13.14 | 22.44 | 1337.84 | 1580.51 | 0.00 | 63.47 |
| fit_21N_02 | 21N | | S_America | PedraAzul, Itaperica, Salta da Divisa | Brasil | flake | 778.86 | 13.10 | 22.20 | 1351.81 | 1581.78 | 0.02 | 46.47 |
| fit_21N_03 | 21N | | S_America | PedraAzul, Itaperica, Salta da Divisa | Brasil | flake | 284.04 | 15.38 | 15.60 | 1355.62 | 1581.78 | 0.05 | 40.90 |
| fit_21N_04 | 21N | | S_America | PedraAzul, Itaperica, Salta da Divisa | Brasil | flake | 800.11 | 13.46 | 21.79 | 1359.44 | 1580.51 | 0.02 | 55.04 |
| fit_21N_05 | 21N | | S_America | PedraAzul, Itaperica, Salta da Divisa | Brasil | flake | 5705.75 | 12.57 | 23.70 | 1348.00 | 1581.78 | 0.00 | 64.03 |
| fit_21N_06 | 21N | | S_America | PedraAzul, Itaperica, Salta da Divisa | Brasil | flake | 1195.22 | 13.01 | 23.02 | 1351.81 | 1581.78 | 0.01 | 63.46 |
| fit_21N_07 | 21N | | S_America | PedraAzul, Itaperica, Salta da Divisa | Brasil | flake | 624.89 | 13.29 | 22.28 | 1354.35 | 1581.78 | 0.02 | 46.43 |
| fit_21N_08 | 21N | | S_America | PedraAzul, Itaperica, Salta da Divisa | Brasil | flake | 492.86 | 14.29 | 20.62 | 1348.00 | 1581.78 | 0.03 | 49.39 |
| fit_21N_09 | 21N | | S_America | PedraAzul, Itaperica, Salta da Divisa | Brasil | flake | 463.33 | 13.85 | 21.54 | 1350.54 | 1580.51 | 0.03 | 40.85 |
| fit_21N_10 | 21N | | S_America | PedraAzul, Itaperica, Salta da Divisa | Brasil | flake | 442.35 | 13.95 | 20.27 | 1354.35 | 1580.51 | 0.03 | 46.61 |
| fit_21N_11 | 21N | | S_America | PedraAzul, Itaperica, Salta da Divisa | Brasil | flake | 767.52 | 13.72 | 20.83 | 1346.73 | 1581.78 | 0.02 | 51.75 |
| fit_21N_12 | 21N | | S_America | PedraAzul, Itaperica, Salta da Divisa | Brasil | flake | 239.18 | 16.61 | 13.86 | 1351.81 | 1580.51 | 0.07 | 44.49 |
| fit_21N_13 | 21N | | S_America | PedraAzul, Itaperica, Salta da Divisa | Brasil | flake | 332.81 | 14.52 | 21.34 | 1354.35 | 1580.51 | 0.04 | 42.31 |
| fit_21N_14 | 21N | | S_America | PedraAzul, Itaperica, Salta da Divisa | Brasil | flake | 677.86 | 14.92 | 18.31 | 1349.27 | 1583.05 | 0.02 | 47.21 |

| | | | | | | | | | | | | | |
|---|---|---|---|---|---|---|---|---|---|---|---|---|---|
| fit_21N_15 | 21N | | S_America | PedraAzul, Itaperica, Salta da Divisa | Brasil | flake | 5249.22 | 13.43 | 20.88 | 1425.50 | 1581.78 | 0.00 | 64.18 |
| fit_21N_16 | 21N | | S_America | PedraAzul, Itaperica, Salta da Divisa | Brasil | flake | 5530.33 | 12.81 | 22.65 | 1341.65 | 1581.78 | 0.00 | 64.26 |
| fit_21N_17 | 21N | | S_America | PedraAzul, Itaperica, Salta da Divisa | Brasil | flake | 5178.22 | 13.47 | 20.65 | 1361.98 | 1581.78 | 0.00 | 64.62 |
| fit_21N_18 | 21N | | S_America | PedraAzul, Itaperica, Salta da Divisa | Brasil | flake | 516.69 | 13.85 | 18.74 | 1354.35 | 1581.78 | 0.03 | 51.76 |
| fit_21N_19 | 21N | | S_America | PedraAzul, Itaperica, Salta da Divisa | Brasil | flake | 5384.20 | 13.24 | 21.76 | 1342.92 | 1580.51 | 0.00 | 64.28 |
| fit_21N_20 | 21N | | S_America | PedraAzul, Itaperica, Salta da Divisa | Brasil | flake | 769.84 | 14.53 | 19.55 | 1344.19 | 1580.51 | 0.02 | 47.84 |
| fit_22A_01 | 22A | | Asia | Shandong | China | flake | 362.34 | 15.89 | 17.61 | 1350.70 | 1581.93 | 0.04 | 48.68 |
| fit_22A_02 | 22A | | Asia | Shandong | China | flake | 5732.28 | 16.08 | 22.69 | 1372.29 | 1579.39 | 0.00 | 64.68 |
| fit_22A_03 | 22A | | Asia | Shandong | China | flake | 5564.95 | 15.72 | 22.14 | 1340.53 | 1581.93 | 0.00 | 64.63 |
| fit_22A_04 | 22A | | Asia | Shandong | China | flake | 7103.17 | 13.71 | 29.35 | 1406.60 | 1581.93 | 0.00 | 65.16 |
| fit_22A_05 | 22A | | Asia | Shandong | China | flake | 6051.25 | 13.57 | 25.28 | 1382.46 | 1580.66 | 0.00 | 64.48 |
| fit_22A_06 | 22A | | Asia | Shandong | China | flake | 6225.02 | 14.44 | 25.28 | 1374.84 | 1581.93 | 0.00 | 64.96 |
| fit_22A_07 | 22A | | Asia | Shandong | China | flake | 5900.32 | 13.39 | 23.95 | 1391.35 | 1581.93 | 0.00 | 64.49 |
| fit_22A_08 | 22A | | Asia | Shandong | China | flake | 5525.45 | 14.72 | 23.05 | 1355.78 | 1580.66 | 0.00 | 63.77 |
| fit_22A_09 | 22A | | Asia | Shandong | China | flake | 252.79 | 17.95 | 16.20 | 1341.80 | 1580.66 | 0.07 | 51.17 |
| fit_22A_10 | 22A | | Asia | Shandong | China | flake | 6076.71 | 14.46 | 24.56 | 1348.15 | 1579.39 | 0.00 | 64.93 |
| fit_22B_01 | 22B | | Africa | Balama | Mozambique | flake | 6024.41 | 15.72 | 24.73 | 1341.80 | 1578.12 | 0.00 | 64.25 |
| fit_22B_02 | 22B | | Africa | Balama | Mozambique | flake | 241.19 | 15.14 | 20.51 | 1348.15 | 1580.66 | 0.06 | 36.66 |
| fit_22B_03 | 22B | | Africa | Balama | Mozambique | flake | 230.58 | 17.24 | 15.89 | 1349.42 | 1579.39 | 0.08 | 46.18 |
| fit_22B_04 | 22B | | Africa | Balama | Mozambique | flake | 5121.61 | 13.34 | 21.54 | 1346.88 | 1579.39 | 0.00 | 63.54 |
| fit_22B_05 | 22B | | Africa | Balama | Mozambique | flake | 5839.10 | 14.11 | 24.64 | 1349.42 | 1580.66 | 0.00 | 63.96 |
| fit_22B_06 | 22B | | Africa | Balama | Mozambique | flake | 5784.97 | 12.75 | 23.43 | 1359.59 | 1581.93 | 0.00 | 64.20 |

| | | | | | | | | | | | | | |
|---|---|---|---|---|---|---|---|---|---|---|---|---|---|
| fit_22B_07 | 22B | | Africa | Balama | Mozambique | flake | 6310.13 | 14.13 | 27.10 | 1348.15 | 1580.66 | 0.00 | 64.00 |
| fit_22B_08 | 22B | | Africa | Balama | Mozambique | flake | 242.44 | 17.12 | 17.23 | 1345.61 | 1581.93 | 0.07 | 40.74 |
| fit_22B_09 | 22B | | Africa | Balama | Mozambique | flake | 6361.01 | 14.27 | 26.51 | 1339.26 | 1580.66 | 0.00 | 64.58 |
| fit_22B_10 | 22B | | Africa | Balama | Mozambique | flake | 399.28 | 13.89 | 21.28 | 1350.70 | 1581.93 | 0.04 | 37.70 |
| fit_22C_01 | 22C | | S_America | PedraAzul, Itaperica, Salta da Divisa | | flake | 1000.03 | 14.56 | 19.01 | 1348.17 | 1578.13 | 0.01 | 67.60 |
| fit_22C_02 | 22C | | S_America | PedraAzul, Itaperica, Salta da Divisa | Brasil | flake | 5122.24 | 13.93 | 19.30 | 1438.37 | 1581.94 | 0.00 | 64.08 |
| fit_22C_03 | 22C | | S_America | PedraAzul, Itaperica, Salta da Divisa | Brasil | flake | 1247.75 | 12.75 | 22.61 | 1351.98 | 1580.67 | 0.01 | 63.65 |
| fit_22C_04 | 22C | | S_America | PedraAzul, Itaperica, Salta da Divisa | Brasil | flake | 5732.92 | 13.81 | 24.21 | 1353.25 | 1580.67 | 0.00 | 63.91 |
| fit_22C_05 | 22C | | S_America | PedraAzul, Itaperica, Salta da Divisa | Brasil | flake | 260.06 | 16.32 | 18.96 | 1348.17 | 1581.94 | 0.07 | 34.35 |
| fit_22C_06 | 22C | | S_America | PedraAzul, Itaperica, Salta da Divisa | Brasil | flake | 5947.68 | 13.99 | 24.69 | 1378.66 | 1580.67 | 0.00 | 64.45 |
| fit_22C_07 | 22C | | S_America | PedraAzul, Itaperica, Salta da Divisa | Brasil | flake | 5484.33 | 13.97 | 23.08 | 1391.36 | 1580.67 | 0.00 | 63.70 |
| fit_22C_08 | 22C | | S_America | PedraAzul, Itaperica, Salta da Divisa | Brasil | flake | 5750.78 | 14.14 | 23.14 | 1345.63 | 1580.67 | 0.00 | 64.86 |
| fit_22C_09 | 22C | | S_America | PedraAzul, Itaperica, Salta da Divisa | Brasil | flake | 262.86 | 17.81 | 18.61 | 1360.87 | 1580.67 | 0.05 | 70.07 |
| fit_22C_10 | 22C | | S_America | PedraAzul, Itaperica, Salta da Divisa | Brasil | flake | 263.14 | 16.27 | 18.43 | 1348.17 | 1580.67 | 0.06 | 39.32 |
| fit_22D_01 | 22D | | Africa | Vatomina/Sahamamy Sahasoa | Madagascar | flake | 122.03 | 26.42 | 8.03 | 1350.69 | 1579.39 | 0.22 | 44.90 |
| fit_22D_02 | 22D | | Africa | Vatomina/Sahamamy Sahasoa | Madagascar | flake | 5722.35 | 14.23 | 23.30 | 1343.07 | 1580.66 | 0.00 | 64.60 |
| fit_22E_01 | 22E | | Europe | Ural, Tayginka | Russia | flake | 687.47 | 13.08 | 22.06 | 1344.32 | 1580.64 | 0.02 | 47.92 |
| fit_22E_02 | 22E | | Europe | Ural, Tayginka | Russia | flake | 587.75 | 13.42 | 21.33 | 1357.02 | 1580.64 | 0.02 | 54.37 |
| fit_22E_03 | 22E | | Europe | Ural, Tayginka | Russia | flake | 703.10 | 13.41 | 21.01 | 1358.29 | 1580.64 | 0.02 | 60.13 |
| fit_22E_04 | 22E | | Europe | Ural, Tayginka | Russia | flake | 888.30 | 13.16 | 21.51 | 1348.13 | 1580.64 | 0.02 | 54.89 |
| fit_22E_05 | 22E | | Europe | Ural, Tayginka | Russia | flake | 1190.16 | 12.67 | 23.73 | 1340.51 | 1579.37 | 0.01 | 60.56 |
| fit_22E_06 | 22E | | Europe | Ural, Tayginka | Russia | flake | 5423.09 | 12.71 | 21.95 | 1359.56 | 1581.91 | 0.00 | 64.46 |

| | | | | | | | | | | | | | |
|---|---|---|---|---|---|---|---|---|---|---|---|---|---|
| fit_22E_07 | 22E | | Europe | Ural, Tayginka | Russia | flake | 780.64 | 13.33 | 21.20 | 1346.86 | 1579.37 | 0.02 | 62.19 |
| fit_22E_08 | 22E | | Europe | Ural, Tayginka | Russia | flake | 5447.27 | 13.15 | 22.11 | 1353.21 | 1581.91 | 0.00 | 64.35 |
| fit_22E_09 | 22E | | Europe | Ural, Tayginka | Russia | flake | 5349.27 | 13.12 | 21.57 | 1424.36 | 1581.91 | 0.00 | 64.20 |
| fit_22E_10 | 22E | | Europe | Ural, Tayginka | Russia | flake | 756.65 | 13.58 | 21.01 | 1358.29 | 1581.91 | 0.02 | 64.55 |
| fit_22E_11 | 22E | | Europe | Ural, Tayginka | Russia | flake | 734.96 | 13.62 | 19.97 | 1367.19 | 1581.91 | 0.02 | 72.72 |
| fit_22E_12 | 22E | | Europe | Ural, Tayginka | Russia | flake | 312.24 | 15.50 | 18.63 | 1351.94 | 1581.91 | 0.05 | 43.54 |
| fit_22E_13 | 22E | | Europe | Ural, Tayginka | Russia | flake | 5307.67 | 13.18 | 21.88 | 1351.94 | 1580.64 | 0.00 | 64.02 |
| fit_22E_14 | 22E | | Europe | Ural, Tayginka | Russia | flake | 6106.76 | 13.85 | 24.82 | 1386.25 | 1581.91 | 0.00 | 64.99 |
| fit_22E_15 | 22E | | Europe | Ural, Tayginka | Russia | flake | 4940.76 | 14.34 | 20.15 | 1357.02 | 1580.64 | 0.00 | 63.58 |
| fit_22E_16 | 22E | | Europe | Ural, Tayginka | Russia | flake | 4722.97 | 14.85 | 19.03 | 1386.25 | 1580.64 | 0.00 | 63.73 |
| fit_22E_17 | 22E | | Europe | Ural, Tayginka | Russia | flake | 5536.35 | 12.77 | 23.05 | 1315.10 | 1580.64 | 0.00 | 64.05 |
| fit_22E_18 | 22E | | Europe | Ural, Tayginka | Russia | flake | 639.33 | 14.42 | 20.08 | 1348.13 | 1580.64 | 0.02 | 52.20 |
| fit_22E_19 | 22E | | Europe | Ural, Tayginka | Russia | flake | 384.44 | 14.75 | 19.57 | 1348.13 | 1580.64 | 0.04 | 42.50 |
| fit_22E_20 | 22E | | Europe | Ural, Tayginka | Russia | flake | 5599.68 | 13.04 | 22.75 | 1359.56 | 1580.64 | 0.00 | 64.15 |
| fit_22F_01 | 22F | | Europe | Zavalje | Ukraine | flake | 320.04 | 16.42 | 17.10 | 1348.15 | 1580.66 | 0.05 | 44.71 |
| fit_22F_02 | 22F | | Europe | Zavalje | Ukraine | flake | 116.03 | 26.13 | 7.80 | 1349.42 | 1580.66 | 0.23 | 44.35 |
| fit_22F_03 | 22F | | Europe | Zavalje | Ukraine | flake | 6390.58 | 13.99 | 26.29 | 1353.24 | 1581.93 | 0.00 | 64.91 |
| fit_22F_04 | 22F | | Europe | Zavalje | Ukraine | flake | 161.06 | 16.52 | 19.90 | 1360.86 | 1579.39 | 0.10 | 48.16 |
| fit_22F_05 | 22F | | Europe | Zavalje | Ukraine | flake | 414.60 | 16.39 | 17.04 | 1348.15 | 1580.66 | 0.04 | 50.13 |
| fit_22F_06 | 22F | | Europe | Zavalje | Ukraine | flake | 5923.21 | 14.45 | 24.05 | 1354.51 | 1580.66 | 0.00 | 64.76 |
| fit_22F_07 | 22F | | Europe | Zavalje | Ukraine | flake | 321.45 | 17.01 | 16.37 | 1349.42 | 1581.93 | 0.05 | 43.16 |
| fit_22F_08 | 22F | | Europe | Zavalje | Ukraine | flake | 145.85 | 26.82 | 8.27 | 1348.15 | 1579.39 | 0.19 | 47.05 |

| | | | | | | | | | | | | | |
|---|---|---|---|---|---|---|---|---|---|---|---|---|---|
| fit_22G_01 | 22G | | Europe | Skaland | Norway | flake | 157.74 | 23.54 | 13.01 | 1348.17 | 1579.40 | 0.15 | 46.09 |
| fit_22G_02 | 22G | | Europe | Skaland | Norway | flake | 5585.12 | 14.48 | 22.35 | 1350.71 | 1581.94 | 0.00 | 64.77 |
| fit_22G_03 | 22G | | Europe | Skaland | Norway | flake | 232.31 | 17.17 | 18.00 | 1355.79 | 1580.67 | 0.07 | 46.17 |
| fit_22G_04 | 22G | | Europe | Skaland | Norway | flake | 5875.03 | 14.46 | 24.73 | 1362.14 | 1579.40 | 0.00 | 63.98 |
| fit_22G_05 | 22G | | Europe | Skaland | Norway | flake | 296.47 | 16.10 | 18.76 | 1346.90 | 1579.40 | 0.05 | 47.33 |
| fit_22G_06 | 22G | | Europe | Skaland | Norway | flake | 5535.25 | 14.33 | 21.33 | 1387.55 | 1579.40 | 0.00 | 64.06 |
| fit_22G_07 | 22G | | Europe | Skaland | Norway | flake | 6141.09 | 14.90 | 25.06 | 1360.87 | 1580.67 | 0.00 | 64.75 |
| fit_22G_08 | 22G | | Europe | Skaland | Norway | flake | 6568.65 | 14.89 | 26.83 | 1343.08 | 1579.40 | 0.00 | 64.91 |
| fit_22G_09 | 22G | | Europe | Skaland | Norway | flake | 163.25 | 16.60 | 20.22 | 1350.71 | 1580.67 | 0.10 | 43.61 |
| fit_22G_10 | 22G | | Europe | Skaland | Norway | flake | 5785.29 | 13.76 | 24.80 | 1340.54 | 1579.40 | 0.00 | 63.57 |

## D. LA-ICP-MS Trace Element Data, Correlation Matrices and Factor Analysis

*Correlation matrix for LA-ICP-MS trace element data for Kaisersberg (AUT)*

| *Kaisersberg (AUT)* | Mg | Al | Ca | V | Cr | Mn | Fe | Co | Cu | Zn | Ga | As | Rb | Sr | Zr | Ce | Th | U |
|---|---|---|---|---|---|---|---|---|---|---|---|---|---|---|---|---|---|---|
| **Mg** | 1.00 | | | | | | | | | | | | | | | | | |
| **Al** | 0.82 | 1.00 | | | | | | | | | | | | | | | | |
| **Ca** | 0.74 | 0.72 | 1.00 | | | | | | | | | | | | | | | |
| **V** | 0.83 | 0.88 | 0.93 | 1.00 | | | | | | | | | | | | | | |
| **Cr** | 0.75 | 0.80 | 0.92 | 0.95 | 1.00 | | | | | | | | | | | | | |
| **Mn** | 0.80 | 0.73 | 0.86 | 0.90 | 0.85 | 1.00 | | | | | | | | | | | | |
| **Fe** | 0.91 | 0.77 | 0.87 | 0.91 | 0.85 | 0.97 | 1.00 | | | | | | | | | | | |
| **Co** | 0.86 | 0.69 | 0.78 | 0.80 | 0.72 | 0.83 | 0.90 | 1.00 | | | | | | | | | | |
| **Cu** | 0.47 | 0.36 | 0.77 | 0.62 | 0.62 | 0.57 | 0.58 | 0.50 | 1.00 | | | | | | | | | |
| **Zn** | 0.80 | 0.72 | 0.91 | 0.92 | 0.90 | 0.95 | 0.94 | 0.81 | 0.68 | 1.00 | | | | | | | | |
| **Ga** | 0.80 | 0.91 | 0.90 | 0.98 | 0.94 | 0.85 | 0.85 | 0.73 | 0.60 | 0.87 | 1.00 | | | | | | | |
| **As** | 0.55 | 0.49 | 0.75 | 0.72 | 0.77 | 0.72 | 0.69 | 0.67 | 0.58 | 0.75 | 0.71 | 1.00 | | | | | | |
| **Rb** | 0.80 | 0.87 | 0.92 | 0.99 | 0.94 | 0.87 | 0.88 | 0.76 | 0.62 | 0.90 | 0.98 | 0.72 | 1.00 | | | | | |
| **Sr** | 0.77 | 0.84 | 0.95 | 0.95 | 0.94 | 0.83 | 0.84 | 0.75 | 0.64 | 0.87 | 0.96 | 0.72 | 0.95 | 1.00 | | | | |
| **Y** | 0.15 | 0.04 | 0.44 | 0.23 | 0.23 | 0.16 | 0.19 | 0.18 | 0.86 | 0.29 | 0.22 | 0.24 | 0.23 | 0.29 | | | | |
| **Zr** | 0.38 | 0.56 | 0.46 | 0.41 | 0.39 | 0.28 | 0.31 | 0.41 | 0.21 | 0.31 | 0.46 | 0.24 | 0.39 | 0.51 | 1.00 | | | |
| **Ce** | 0.31 | 0.14 | 0.61 | 0.42 | 0.42 | 0.38 | 0.40 | 0.37 | 0.93 | 0.51 | 0.37 | 0.41 | 0.41 | 0.45 | 0.10 | 1.00 | | |
| **Th** | 0.41 | 0.50 | 0.57 | 0.55 | 0.59 | 0.49 | 0.47 | 0.38 | 0.39 | 0.50 | 0.58 | 0.43 | 0.55 | 0.60 | 0.48 | 0.36 | 1.00 | |
| **U** | 0.29 | 0.18 | 0.59 | 0.40 | 0.41 | 0.34 | 0.35 | 0.31 | 0.95 | 0.47 | 0.40 | 0.40 | 0.40 | 0.45 | 0.18 | 0.95 | 0.33 | 1.00 |

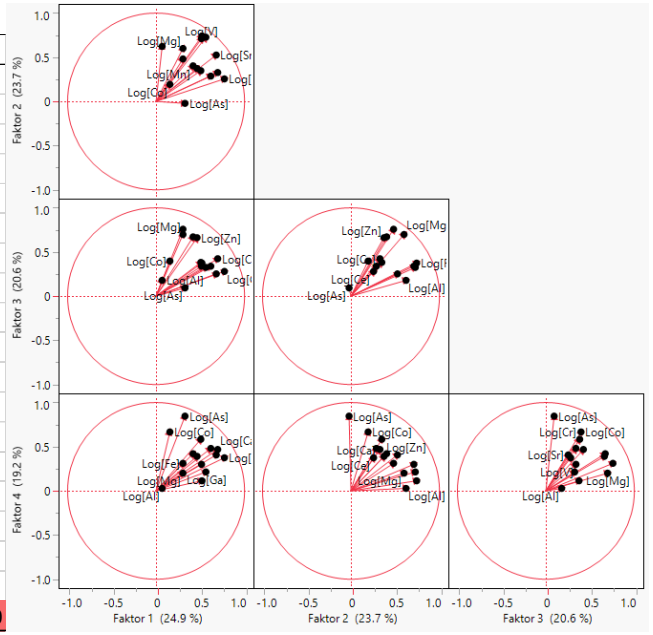

*Correlation matrix for LA-ICP-MS trace element data for Minas Gerais* (BRA)*

| *Minas Gerais* (BRA)* | Mg | Al | Ca | V | Cr | Mn | Fe | Co | Cu | Zn | Ga | As | Rb | Sr | Zr | Ce | Th | U |
|---|---|---|---|---|---|---|---|---|---|---|---|---|---|---|---|---|---|---|
| **Mg** | 1.00 | | | | | | | | | | | | | | | | | |
| **Al** | 0.67 | 1.00 | | | | | | | | | | | | | | | | |
| **Ca** | 0.25 | 0.29 | 1.00 | | | | | | | | | | | | | | | |
| **V** | 0.25 | 0.61 | 0.38 | 1.00 | | | | | | | | | | | | | | |
| **Cr** | 0.24 | 0.30 | 0.55 | 0.31 | 1.00 | | | | | | | | | | | | | |
| **Mn** | 0.00 | -0.04 | 0.16 | 0.16 | 0.02 | 1.00 | | | | | | | | | | | | |
| **Fe** | 0.46 | 0.50 | 0.38 | 0.52 | 0.21 | 0.21 | 1.00 | | | | | | | | | | | |
| **Co** | 0.02 | 0.02 | 0.15 | 0.31 | 0.05 | 0.52 | 0.17 | 1.00 | | | | | | | | | | |
| **Cu** | 0.57 | 0.48 | 0.29 | 0.43 | 0.11 | 0.33 | 0.62 | 0.44 | 1.00 | | | | | | | | | |
| **Zn** | 0.65 | 0.37 | 0.26 | 0.23 | 0.01 | 0.07 | 0.47 | 0.13 | 0.76 | 1.00 | | | | | | | | |
| **Ga** | 0.58 | 0.66 | 0.33 | 0.48 | 0.24 | 0.52 | 0.48 | 0.06 | 0.41 | 0.31 | 1.00 | | | | | | | |
| **As** | 0.33 | 0.35 | 0.14 | 0.37 | 0.00 | 0.35 | 0.28 | 0.81 | 0.47 | 0.17 | 0.29 | 1.00 | | | | | | |
| **Rb** | 0.62 | 0.31 | 0.26 | 0.19 | 0.02 | 0.07 | 0.48 | 0.06 | 0.70 | 0.98 | 0.30 | 0.09 | 1.00 | | | | | |
| **Sr** | 0.56 | 0.38 | 0.21 | 0.13 | 0.12 | 0.07 | 0.31 | -0.01 | 0.27 | 0.27 | 0.50 | 0.21 | 0.26 | 1.00 | | | | |
| **Zr** | 0.16 | 0.12 | -0.15 | -0.09 | -0.25 | 0.10 | 0.18 | -0.09 | 0.04 | 0.17 | 0.17 | -0.01 | 0.17 | 0.31 | 1.00 | | | |
| **Ce** | 0.08 | 0.05 | -0.09 | -0.08 | -0.21 | -0.04 | 0.04 | -0.08 | -0.03 | 0.03 | 0.02 | 0.02 | 0.02 | 0.38 | 0.48 | 1.00 | | |
| **Th** | 0.17 | 0.11 | 0.16 | 0.03 | 0.04 | 0.09 | 0.21 | 0.07 | 0.19 | 0.24 | 0.16 | 0.15 | 0.23 | 0.30 | 0.36 | 0.33 | 1.00 | |
| **U** | 0.03 | 0.06 | 0.20 | 0.13 | 0.03 | 0.16 | 0.18 | 0.08 | 0.05 | 0.03 | 0.16 | 0.09 | 0.04 | 0.27 | 0.18 | 0.79 | 0.26 | 1.00 |

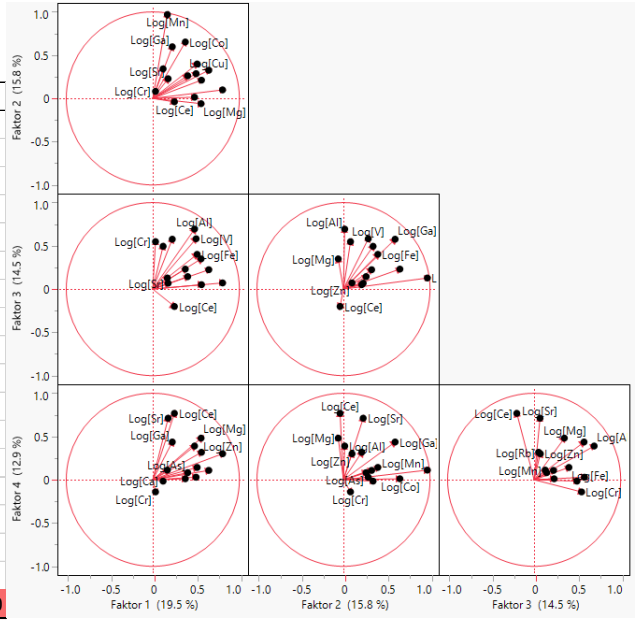

*Correlation matrix for LA-ICP-MS trace element data for Shandong* (CHN)*

| *Shandong (CHN)* | Mg | Al | Ca | V | Cr | Mn | Fe | Co | Cu | Zn | Ga | As | Rb | Sr | Zr | Ce | Th | U |
|---|---|---|---|---|---|---|---|---|---|---|---|---|---|---|---|---|---|---|
| **Mg** | 1.00 | | | | | | | | | | | | | | | | | |
| **Al** | -0.06 | 1.00 | | | | | | | | | | | | | | | | |
| **Ca** | 0.09 | 0.66 | 1.00 | | | | | | | | | | | | | | | |
| **V** | -0.09 | 0.88 | 0.73 | 1.00 | | | | | | | | | | | | | | |
| **Cr** | -0.28 | 0.61 | 0.73 | 0.56 | 1.00 | | | | | | | | | | | | | |
| **Mn** | 0.04 | 0.68 | 0.46 | 0.65 | 0.33 | 1.00 | | | | | | | | | | | | |
| **Fe** | -0.09 | 0.86 | 0.75 | 0.99 | 0.53 | 0.66 | 1.00 | | | | | | | | | | | |
| **Co** | 0.00 | 0.12 | 0.07 | 0.13 | -0.08 | 0.35 | 0.14 | 1.00 | | | | | | | | | | |
| **Cu** | -0.12 | 0.93 | 0.78 | 0.93 | 0.64 | 0.68 | 0.95 | 0.12 | 1.00 | | | | | | | | | |
| **Zn** | -0.03 | 0.92 | 0.53 | 0.86 | 0.37 | 0.63 | 0.86 | 0.15 | 0.89 | 1.00 | | | | | | | | |
| **Ga** | -0.17 | 0.70 | 0.78 | 0.72 | 0.77 | 0.53 | 0.72 | 0.04 | 0.78 | 0.55 | 1.00 | | | | | | | |
| **As** | -0.04 | 0.16 | 0.46 | 0.58 | 0.21 | 0.23 | 0.58 | 0.04 | 0.34 | 0.15 | 0.34 | 1.00 | | | | | | |
| **Rb** | 0.28 | -0.04 | 0.16 | 0.07 | 0.00 | -0.01 | 0.08 | 0.08 | 0.04 | -0.01 | 0.32 | 0.18 | 1.00 | | | | | |
| **Sr** | -0.18 | 0.27 | 0.69 | 0.53 | 0.63 | 0.29 | 0.55 | -0.03 | 0.48 | 0.11 | 0.71 | 0.74 | 0.17 | 1.00 | | | | |
| **Zr** | -0.02 | -0.03 | -0.01 | -0.03 | -0.07 | 0.03 | -0.03 | -0.04 | -0.04 | -0.02 | -0.05 | 0.00 | 0.08 | -0.02 | 1.00 | | | |
| **Ce** | -0.05 | -0.08 | -0.14 | -0.05 | -0.16 | -0.01 | -0.05 | -0.06 | -0.08 | -0.04 | -0.08 | 0.02 | -0.11 | -0.06 | -0.01 | 1.00 | | |
| **Th** | -0.07 | 0.34 | 0.65 | 0.56 | 0.48 | 0.40 | 0.59 | 0.03 | 0.52 | 0.23 | 0.61 | 0.68 | 0.17 | 0.85 | 0.41 | -0.02 | 1.00 | |
| **U** | -0.11 | 0.76 | 0.74 | 0.95 | 0.51 | 0.60 | 0.96 | 0.10 | 0.87 | 0.74 | 0.70 | 0.72 | 0.09 | 0.65 | 0.02 | 0.12 | 0.69 | 1.00 |

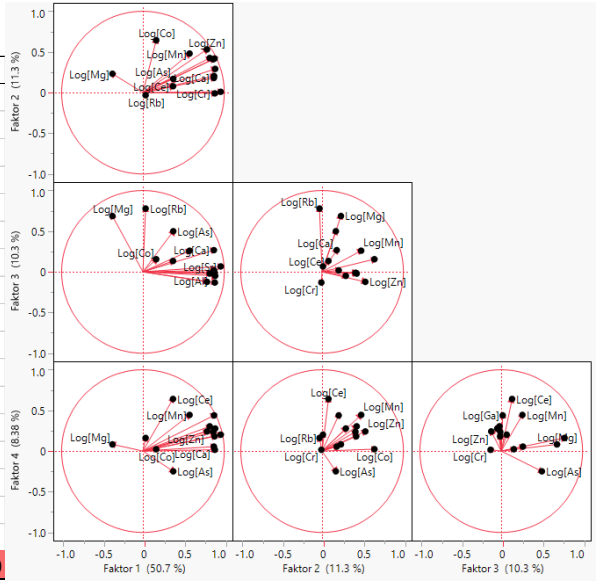

*Correlation matrix for LA-ICP-MS trace element data for Hunan Lutang* (CHN)*

| *Hunan Lutang* (CHN)* | Mg | Al | Ca | V | Cr | Mn | Fe | Co | Cu | Zn | Ga | As | Rb | Sr | Zr | Ce | Th | U |
|---|---|---|---|---|---|---|---|---|---|---|---|---|---|---|---|---|---|---|
| **Mg** | 1.00 | | | | | | | | | | | | | | | | | |
| **Al** | 0.72 | 1.00 | | | | | | | | | | | | | | | | |
| **Ca** | 0.59 | 0.39 | 1.00 | | | | | | | | | | | | | | | |
| **V** | 0.22 | 0.38 | 0.21 | 1.00 | | | | | | | | | | | | | | |
| **Cr** | 0.26 | 0.42 | 0.41 | 0.04 | 1.00 | | | | | | | | | | | | | |
| **Mn** | 0.78 | 0.61 | 0.51 | 0.10 | 0.37 | 1.00 | | | | | | | | | | | | |
| **Fe** | 0.14 | 0.06 | 0.28 | 0.17 | 0.18 | 0.34 | 1.00 | | | | | | | | | | | |
| **Co** | 0.34 | 0.33 | 0.68 | 0.22 | 0.57 | 0.33 | 0.23 | 1.00 | | | | | | | | | | |
| **Cu** | 0.05 | 0.10 | 0.20 | -0.12 | -0.10 | 0.30 | -0.07 | 0.08 | 1.00 | | | | | | | | | |
| **Zn** | 0.72 | 0.36 | 0.36 | 0.25 | 0.05 | 0.55 | -0.18 | 0.18 | -0.09 | 1.00 | | | | | | | | |
| **Ga** | 0.41 | 0.79 | 0.04 | 0.20 | -0.02 | 0.29 | 0.01 | -0.07 | 0.02 | 0.07 | 1.00 | | | | | | | |
| **As** | 0.30 | 0.24 | 0.42 | 0.59 | 0.08 | 0.19 | 0.20 | 0.70 | 0.11 | 0.16 | -0.05 | 1.00 | | | | | | |
| **Rb** | 0.32 | 0.72 | -0.06 | 0.20 | -0.14 | 0.15 | -0.09 | -0.12 | 0.05 | 0.01 | 0.98 | -0.04 | 1.00 | | | | | |
| **Sr** | 0.40 | 0.72 | 0.31 | 0.49 | 0.03 | 0.19 | 0.13 | 0.29 | 0.05 | 0.16 | 0.72 | 0.39 | 0.70 | 1.00 | | | | |
| **Zr** | -0.10 | -0.08 | -0.25 | -0.15 | -0.17 | 0.01 | -0.24 | -0.25 | 0.57 | 0.00 | -0.06 | -0.15 | 0.04 | -0.20 | 1.00 | | | |
| **Ce** | 0.26 | 0.63 | -0.05 | 0.09 | -0.17 | 0.09 | -0.09 | -0.12 | 0.01 | -0.07 | 0.93 | -0.06 | 0.94 | 0.63 | -0.09 | 1.00 | | |
| **Th** | -0.07 | 0.30 | -0.15 | -0.05 | 0.33 | -0.21 | -0.15 | 0.23 | -0.10 | -0.36 | 0.27 | 0.03 | 0.33 | 0.10 | 0.11 | 0.36 | 1.00 | |
| **U** | -0.15 | -0.04 | -0.34 | 0.05 | 0.00 | -0.15 | -0.29 | -0.14 | 0.28 | -0.02 | -0.14 | -0.03 | -0.03 | -0.20 | 0.82 | -0.13 | 0.46 | 1.00 |

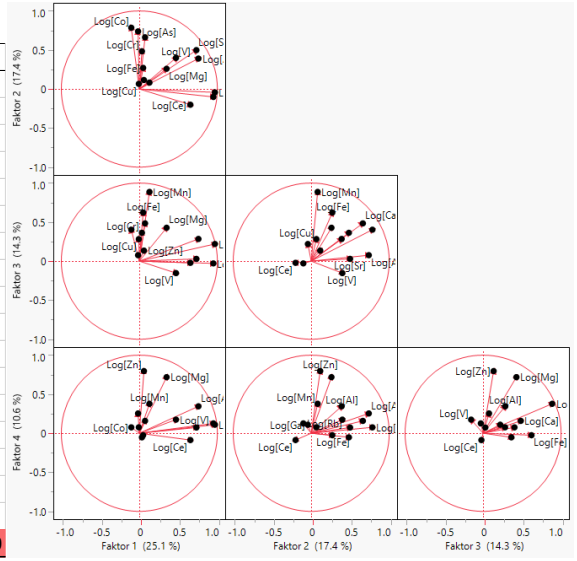

*Correlation matrix for LA-ICP-MS trace element data for Inner Mongolia* (CHN)*

| *Inner Mongolia* (CHN)* | Mg | Al | Ca | V | Cr | Mn | Fe | Co | Cu | Zn | Ga | As | Rb | Sr | Zr | Ce | Th | U |
|---|---|---|---|---|---|---|---|---|---|---|---|---|---|---|---|---|---|---|
| **Mg** | 1.00 | | | | | | | | | | | | | | | | | |
| **Al** | 0.04 | 1.00 | | | | | | | | | | | | | | | | |
| **Ca** | 1.00 | 0.08 | 1.00 | | | | | | | | | | | | | | | |
| **V** | 0.54 | 0.18 | 0.56 | 1.00 | | | | | | | | | | | | | | |
| **Cr** | -0.18 | -0.13 | -0.15 | -0.19 | 1.00 | | | | | | | | | | | | | |
| **Mn** | 1.00 | 0.03 | 1.00 | 0.58 | -0.17 | 1.00 | | | | | | | | | | | | |
| **Fe** | 0.16 | -0.01 | 0.18 | 0.83 | -0.01 | 0.21 | 1.00 | | | | | | | | | | | |
| **Co** | 1.00 | 0.03 | 1.00 | 0.58 | -0.17 | 1.00 | 0.21 | 1.00 | | | | | | | | | | |
| **Cu** | 0.99 | 0.07 | 0.99 | 0.55 | -0.20 | 0.99 | 0.17 | 0.99 | 1.00 | | | | | | | | | |
| **Zn** | 1.00 | 0.04 | 0.99 | 0.53 | -0.18 | 1.00 | 0.15 | 1.00 | 0.99 | 1.00 | | | | | | | | |
| **Ga** | 1.00 | 0.04 | 0.99 | 0.54 | -0.18 | 1.00 | 0.16 | 1.00 | 0.99 | 1.00 | 1.00 | | | | | | | |
| **As** | 1.00 | 0.03 | 0.99 | 0.53 | -0.18 | 1.00 | 0.15 | 1.00 | 0.99 | 1.00 | 1.00 | 1.00 | | | | | | |
| **Rb** | 1.00 | 0.03 | 0.99 | 0.53 | -0.18 | 1.00 | 0.15 | 1.00 | 0.99 | 1.00 | 1.00 | 1.00 | 1.00 | | | | | |
| **Sr** | 0.64 | 0.32 | 0.68 | 0.84 | -0.21 | 0.67 | 0.71 | 0.67 | 0.66 | 0.63 | 0.64 | 0.63 | 0.63 | 1.00 | | | | |
| **Zr** | -0.15 | 0.37 | -0.13 | -0.07 | 0.34 | -0.16 | 0.10 | -0.15 | -0.11 | -0.16 | -0.15 | -0.16 | -0.16 | 0.03 | 1.00 | | | |
| **Ce** | -0.07 | 0.37 | -0.05 | -0.01 | 0.01 | -0.08 | 0.06 | -0.06 | -0.04 | -0.07 | -0.07 | -0.07 | -0.07 | 0.10 | 0.39 | 1.00 | | |
| **Th** | -0.10 | 0.28 | -0.08 | 0.64 | 0.09 | -0.08 | 0.61 | -0.08 | -0.10 | -0.11 | -0.10 | -0.11 | -0.11 | 0.35 | 0.22 | 0.27 | 1.00 | |
| **U** | -0.08 | 0.07 | -0.06 | 0.68 | 0.12 | -0.03 | 0.95 | -0.03 | -0.07 | -0.09 | -0.09 | -0.09 | -0.10 | 0.55 | 0.30 | 0.15 | 0.67 | 1.00 |

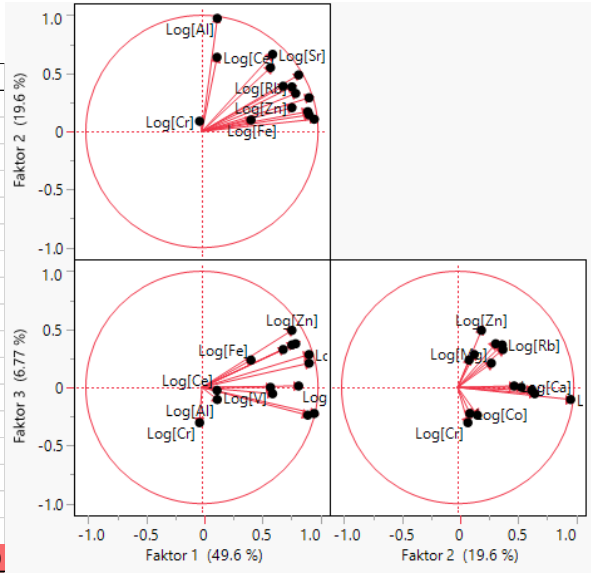

*Correlation matrix for LA-ICP-MS trace element data for Heilongjian* (CHN)*

| *Heilongjian* (CHN)* | Mg | Al | Ca | V | Cr | Mn | Fe | Co | Cu | Zn | Ga | As | Rb | Sr | Zr | Ce | Th | U |
|---|---|---|---|---|---|---|---|---|---|---|---|---|---|---|---|---|---|---|
| **Mg** | 1.00 | | | | | | | | | | | | | | | | | |
| **Al** | 0.62 | 1.00 | | | | | | | | | | | | | | | | |
| **Ca** | 0.56 | 0.97 | 1.00 | | | | | | | | | | | | | | | |
| **V** | 0.50 | 0.94 | 0.94 | 1.00 | | | | | | | | | | | | | | |
| **Cr** | 0.18 | 0.41 | 0.52 | 0.56 | 1.00 | | | | | | | | | | | | | |
| **Mn** | 0.57 | 0.93 | 0.96 | 0.88 | 0.38 | 1.00 | | | | | | | | | | | | |
| **Fe** | 0.62 | 0.55 | 0.44 | 0.44 | 0.07 | 0.45 | 1.00 | | | | | | | | | | | |
| **Co** | 0.36 | 0.45 | 0.51 | 0.30 | 0.09 | 0.64 | 0.35 | 1.00 | | | | | | | | | | |
| **Cu** | 0.50 | 0.50 | 0.47 | 0.49 | 0.24 | 0.49 | 0.63 | 0.32 | 1.00 | | | | | | | | | |
| **Zn** | 0.68 | 0.80 | 0.77 | 0.82 | 0.30 | 0.79 | 0.58 | 0.38 | 0.57 | 1.00 | | | | | | | | |
| **Ga** | 0.65 | 0.98 | 0.92 | 0.95 | 0.43 | 0.87 | 0.63 | 0.34 | 0.57 | 0.84 | 1.00 | | | | | | | |
| **As** | 0.10 | 0.45 | 0.50 | 0.50 | 0.32 | 0.44 | 0.26 | 0.17 | 0.39 | 0.51 | 0.46 | 1.00 | | | | | | |
| **Rb** | 0.67 | 0.67 | 0.56 | 0.66 | 0.24 | 0.51 | 0.58 | 0.09 | 0.45 | 0.69 | 0.76 | 0.37 | 1.00 | | | | | |
| **Sr** | 0.54 | 0.45 | 0.46 | 0.32 | 0.31 | 0.42 | 0.62 | 0.39 | 0.36 | 0.34 | 0.48 | 0.34 | 0.35 | 1.00 | | | | |
| **Zr** | 0.68 | 0.93 | 0.89 | 0.87 | 0.34 | 0.90 | 0.66 | 0.52 | 0.55 | 0.84 | 0.91 | 0.33 | 0.59 | 0.46 | 1.00 | | | |
| **Ce** | 0.70 | 0.30 | 0.24 | 0.11 | -0.19 | 0.36 | 0.60 | 0.56 | 0.36 | 0.39 | 0.30 | 0.00 | 0.48 | 0.55 | 0.44 | 1.00 | | |
| **Th** | 0.53 | 0.28 | 0.20 | 0.12 | -0.06 | 0.20 | 0.82 | 0.22 | 0.37 | 0.35 | 0.36 | 0.21 | 0.44 | 0.77 | 0.34 | 0.62 | 1.00 | |
| **U** | 0.46 | 0.41 | 0.40 | 0.30 | 0.07 | 0.43 | 0.54 | 0.41 | 0.24 | 0.43 | 0.45 | 0.16 | 0.28 | 0.81 | 0.51 | 0.58 | 0.67 | 1.00 |

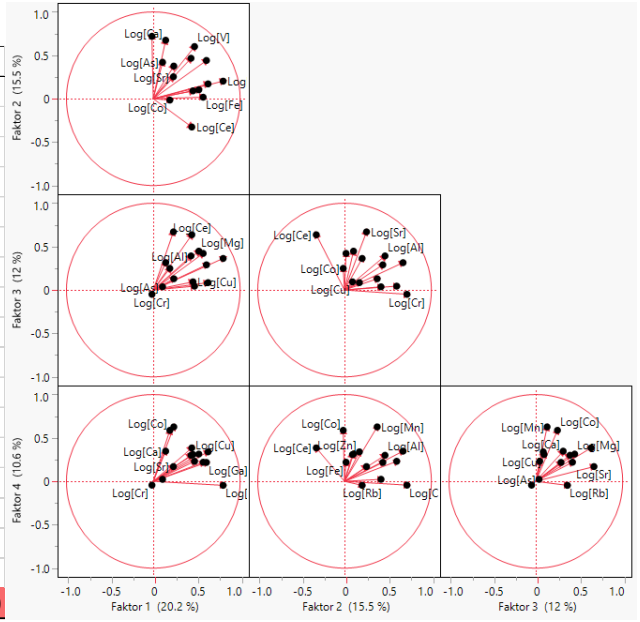

*Correlation matrix for LA-ICP-MS trace element data for Kropfmühl (GER)*

| *Kropfmühl (GER)* | *Mg* | *Al* | *Ca* | *V* | *Cr* | *Mn* | *Fe* | *Co* | *Cu* | *Zn* | *Ga* | *As* | *Rb* | *Sr* | *Zr* | *Ce* | *Th* | *U* |
|---|---|---|---|---|---|---|---|---|---|---|---|---|---|---|---|---|---|---|
| **Mg** | 1.00 | | | | | | | | | | | | | | | | | |
| **Al** | 0.73 | 1.00 | | | | | | | | | | | | | | | | |
| **Ca** | -0.05 | 0.19 | 1.00 | | | | | | | | | | | | | | | |
| **V** | 0.97 | 0.69 | -0.08 | 1.00 | | | | | | | | | | | | | | |
| **Cr** | 0.87 | 0.56 | -0.15 | 0.92 | 1.00 | | | | | | | | | | | | | |
| **Mn** | 0.98 | 0.71 | -0.04 | 0.94 | 0.84 | 1.00 | | | | | | | | | | | | |
| **Fe** | 0.05 | 0.66 | 0.39 | -0.02 | -0.08 | 0.04 | 1.00 | | | | | | | | | | | |
| **Co** | 0.04 | 0.64 | 0.37 | -0.05 | -0.10 | 0.04 | 0.99 | 1.00 | | | | | | | | | | |
| **Cu** | -0.02 | 0.29 | 0.01 | -0.09 | -0.25 | -0.01 | 0.48 | 0.51 | 1.00 | | | | | | | | | |
| **Zn** | 0.01 | -0.04 | 0.01 | 0.03 | 0.13 | 0.12 | -0.03 | 0.05 | -0.04 | 1.00 | | | | | | | | |
| **Ga** | 0.78 | 0.94 | 0.05 | 0.76 | 0.68 | 0.72 | 0.52 | 0.49 | 0.19 | -0.05 | 1.00 | | | | | | | |
| **As** | 0.26 | 0.75 | 0.18 | 0.23 | 0.21 | 0.25 | 0.83 | 0.83 | 0.32 | 0.19 | 0.69 | 1.00 | | | | | | |
| **Rb** | 0.87 | 0.66 | -0.10 | 0.90 | 0.89 | 0.80 | 0.03 | 0.01 | -0.15 | 0.04 | 0.84 | 0.33 | 1.00 | | | | | |
| **Sr** | 0.08 | 0.70 | 0.20 | 0.02 | -0.03 | 0.05 | 0.90 | 0.89 | 0.45 | -0.05 | 0.63 | 0.85 | 0.15 | 1.00 | | | | |
| **Zr** | 0.44 | 0.28 | 0.02 | 0.28 | 0.24 | 0.43 | 0.06 | 0.10 | -0.07 | -0.08 | 0.35 | 0.09 | 0.41 | 0.12 | 1.00 | | | |
| **Ce** | 0.00 | -0.02 | -0.04 | -0.02 | -0.02 | 0.04 | 0.03 | 0.03 | 0.05 | 0.10 | -0.06 | -0.03 | -0.11 | 0.00 | -0.04 | 1.00 | | |
| **Th** | 0.14 | 0.50 | 0.12 | 0.10 | 0.15 | 0.21 | 0.65 | 0.67 | 0.29 | 0.30 | 0.40 | 0.71 | 0.08 | 0.62 | -0.01 | 0.23 | 1.00 | |
| **U** | 0.35 | 0.32 | 0.02 | 0.20 | 0.11 | 0.40 | 0.28 | 0.36 | 0.25 | 0.28 | 0.26 | 0.26 | 0.15 | 0.21 | 0.61 | 0.27 | 0.44 | 1.00 |

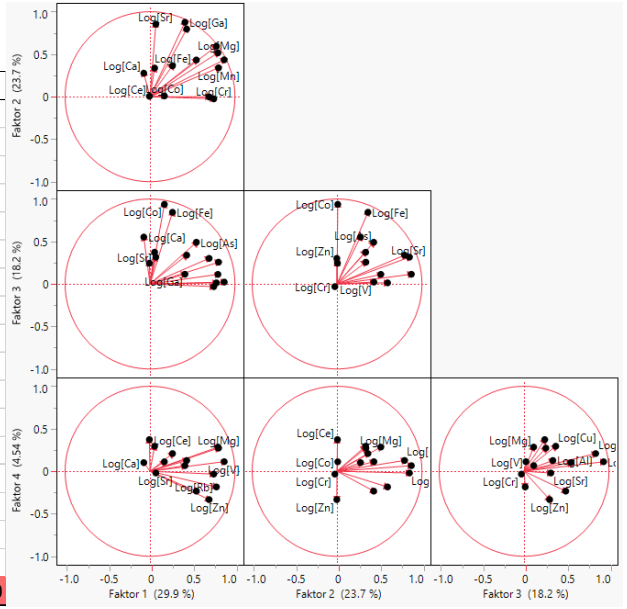

*Correlation matrix for LA-ICP-MS trace element data for Brickaville* (MAD)*

| *Brickaville* (MAD)* | Mg | Al | Ca | V | Cr | Mn | Fe | Co | Cu | Zn | Ga | As | Rb | Sr | Zr | Ce | Th | U |
|---|---|---|---|---|---|---|---|---|---|---|---|---|---|---|---|---|---|---|
| **Mg** | 1.00 | | | | | | | | | | | | | | | | | |
| **Al** | 0.13 | 1.00 | | | | | | | | | | | | | | | | |
| **Ca** | 0.24 | 0.81 | 1.00 | | | | | | | | | | | | | | | |
| **V** | 0.10 | 0.73 | 0.53 | 1.00 | | | | | | | | | | | | | | |
| **Cr** | 0.08 | 0.81 | 0.66 | 0.94 | 1.00 | | | | | | | | | | | | | |
| **Mn** | -0.02 | 0.01 | 0.02 | 0.17 | 0.09 | 1.00 | | | | | | | | | | | | |
| **Fe** | 0.09 | 0.69 | 0.48 | 0.92 | 0.96 | 0.11 | 1.00 | | | | | | | | | | | |
| **Co** | 0.10 | 0.69 | 0.49 | 0.92 | 0.96 | 0.16 | 1.00 | 1.00 | | | | | | | | | | |
| **Cu** | 0.10 | 0.69 | 0.49 | 0.92 | 0.97 | 0.12 | 1.00 | 1.00 | 1.00 | | | | | | | | | |
| **Zn** | 0.10 | 0.69 | 0.48 | 0.92 | 0.96 | 0.13 | 1.00 | 1.00 | 1.00 | 1.00 | | | | | | | | |
| **Ga** | 0.11 | 0.84 | 0.67 | 0.93 | 0.99 | 0.09 | 0.96 | 0.96 | 0.97 | 0.96 | 1.00 | | | | | | | |
| **As** | 0.09 | 0.71 | 0.52 | 0.93 | 0.98 | 0.11 | 1.00 | 1.00 | 1.00 | 1.00 | 0.97 | 1.00 | | | | | | |
| **Rb** | 0.77 | 0.39 | 0.46 | 0.29 | 0.29 | -0.04 | 0.21 | 0.22 | 0.22 | 0.21 | 0.30 | 0.23 | 1.00 | | | | | |
| **Sr** | 0.11 | 0.71 | 0.49 | 0.91 | 0.96 | 0.10 | 1.00 | 1.00 | 1.00 | 1.00 | 0.97 | 1.00 | 0.24 | 1.00 | | | | |
| **Zr** | 0.19 | 0.53 | 0.41 | 0.72 | 0.75 | 0.07 | 0.75 | 0.75 | 0.75 | 0.75 | 0.74 | 0.76 | 0.38 | 0.76 | 1.00 | | | |
| **Ce** | 0.43 | 0.48 | 0.38 | 0.57 | 0.62 | 0.05 | 0.66 | 0.66 | 0.66 | 0.66 | 0.64 | 0.66 | 0.60 | 0.67 | 0.52 | 1.00 | | |
| **Th** | 0.08 | 0.72 | 0.50 | 0.92 | 0.97 | 0.09 | 1.00 | 0.99 | 0.99 | 0.99 | 0.97 | 1.00 | 0.23 | 1.00 | 0.75 | 0.67 | 1.00 | |
| **U** | 0.10 | 0.84 | 0.92 | 0.69 | 0.78 | 0.08 | 0.61 | 0.62 | 0.62 | 0.61 | 0.77 | 0.65 | 0.37 | 0.61 | 0.52 | 0.37 | 0.63 | 1.00 |

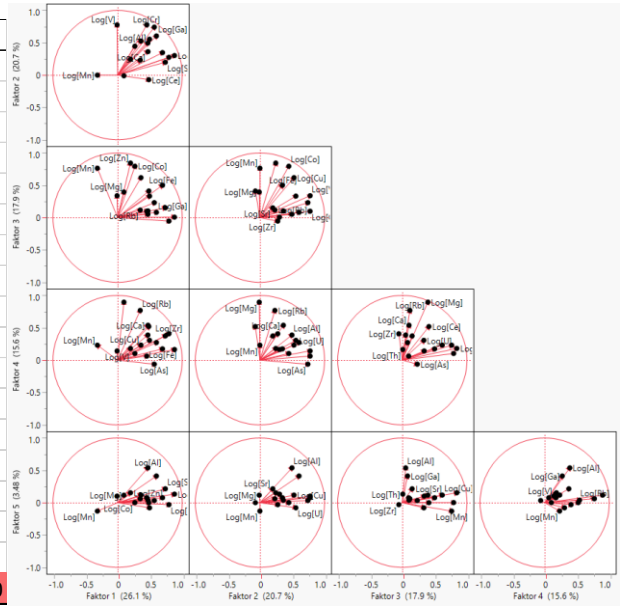

*Correlation matrix for LA-ICP-MS trace element data for Balama (MOZ)*

| Balama (MOZ) | Mg | Al | Ca | V | Cr | Mn | Fe | Co | Cu | Zn | Ga | As | Rb | Sr | Zr | Ce | Th | U |
|---|---|---|---|---|---|---|---|---|---|---|---|---|---|---|---|---|---|---|
| Mg | 1.00 | | | | | | | | | | | | | | | | | |
| Al | 0.84 | 1.00 | | | | | | | | | | | | | | | | |
| Ca | 0.18 | 0.44 | 1.00 | | | | | | | | | | | | | | | |
| V | 0.92 | 0.91 | 0.32 | 1.00 | | | | | | | | | | | | | | |
| Cr | 0.94 | 0.90 | 0.30 | 0.96 | 1.00 | | | | | | | | | | | | | |
| Mn | 0.48 | 0.50 | 0.33 | 0.59 | 0.58 | 1.00 | | | | | | | | | | | | |
| Fe | 0.05 | 0.13 | 0.30 | 0.14 | 0.13 | 0.48 | 1.00 | | | | | | | | | | | |
| Co | 0.34 | 0.26 | 0.09 | 0.29 | 0.34 | 0.67 | 0.11 | 1.00 | | | | | | | | | | |
| Cu | 0.24 | 0.39 | 0.45 | 0.41 | 0.38 | 0.58 | 0.69 | 0.11 | 1.00 | | | | | | | | | |
| Zn | 0.25 | 0.29 | 0.32 | 0.29 | 0.30 | 0.56 | 0.88 | 0.18 | 0.68 | 1.00 | | | | | | | | |
| Ga | 0.56 | 0.69 | 0.33 | 0.79 | 0.70 | 0.40 | 0.08 | 0.12 | 0.37 | 0.06 | 1.00 | | | | | | | |
| As | 0.49 | 0.49 | 0.34 | 0.52 | 0.55 | 0.52 | 0.52 | 0.22 | 0.72 | 0.52 | 0.30 | 1.00 | | | | | | |
| Rb | 0.98 | 0.86 | 0.19 | 0.95 | 0.96 | 0.50 | 0.06 | 0.34 | 0.25 | 0.22 | 0.66 | 0.49 | 1.00 | | | | | |
| Sr | 0.27 | 0.47 | 0.55 | 0.50 | 0.41 | 0.27 | 0.12 | 0.01 | 0.36 | 0.06 | 0.73 | 0.27 | 0.35 | 1.00 | | | | |
| Zr | 0.54 | 0.57 | 0.35 | 0.67 | 0.58 | 0.43 | 0.20 | 0.12 | 0.35 | 0.31 | 0.63 | 0.36 | 0.59 | 0.50 | 1.00 | | | |
| Ce | -0.01 | 0.18 | 0.64 | 0.13 | 0.09 | 0.24 | 0.25 | -0.01 | 0.38 | 0.21 | 0.14 | 0.32 | 0.00 | 0.60 | 0.22 | 1.00 | | |
| Th | 0.22 | 0.42 | 0.70 | 0.42 | 0.37 | 0.58 | 0.53 | 0.10 | 0.67 | 0.52 | 0.38 | 0.54 | 0.24 | 0.63 | 0.49 | 0.78 | 1.00 | |
| U | 0.14 | 0.25 | 0.46 | 0.28 | 0.22 | 0.56 | 0.74 | 0.07 | 0.71 | 0.76 | 0.15 | 0.56 | 0.13 | 0.38 | 0.41 | 0.60 | 0.78 | 1 |

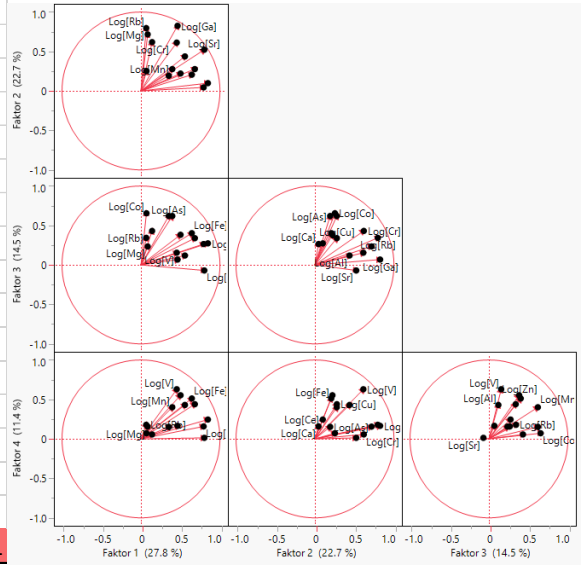


XL

*Correlation matrix for LA-ICP-MS trace element data for Skaland (NOR)*

| *Skaland (NOR)* | Mg | Al | Ca | V | Cr | Mn | Fe | Co | Cu | Zn | Ga | As | Rb | Sr | Zr | Ce | Th | U |
|---|---|---|---|---|---|---|---|---|---|---|---|---|---|---|---|---|---|---|
| **Mg** | 1.00 | | | | | | | | | | | | | | | | | |
| **Al** | 0.51 | 1.00 | | | | | | | | | | | | | | | | |
| **Ca** | 0.79 | 0.71 | 1.00 | | | | | | | | | | | | | | | |
| **V** | 0.91 | 0.62 | 0.95 | 1.00 | | | | | | | | | | | | | | |
| **Cr** | 0.70 | 0.65 | 0.82 | 0.87 | 1.00 | | | | | | | | | | | | | |
| **Mn** | 0.98 | 0.53 | 0.87 | 0.97 | 0.78 | 1.00 | | | | | | | | | | | | |
| **Fe** | 0.99 | 0.42 | 0.74 | 0.88 | 0.63 | 0.97 | 1.00 | | | | | | | | | | | |
| **Co** | 0.92 | 0.49 | 0.84 | 0.92 | 0.71 | 0.95 | 0.92 | 1.00 | | | | | | | | | | |
| **Cu** | 0.69 | 0.46 | 0.72 | 0.74 | 0.58 | 0.73 | 0.69 | 0.73 | 1.00 | | | | | | | | | |
| **Zn** | 0.71 | 0.52 | 0.86 | 0.86 | 0.72 | 0.79 | 0.69 | 0.78 | 0.62 | 1.00 | | | | | | | | |
| **Ga** | 0.69 | -0.04 | 0.13 | 0.36 | 0.09 | 0.58 | 0.75 | 0.54 | 0.32 | 0.17 | 1.00 | | | | | | | |
| **As** | 0.82 | 0.13 | 0.34 | 0.56 | 0.29 | 0.73 | 0.86 | 0.71 | 0.44 | 0.36 | 0.94 | 1.00 | | | | | | |
| **Rb** | 0.68 | -0.06 | 0.11 | 0.34 | 0.08 | 0.57 | 0.74 | 0.53 | 0.31 | 0.16 | 1.00 | 0.94 | 1.00 | | | | | |
| **Sr** | 0.71 | 0.16 | 0.18 | 0.37 | 0.11 | 0.58 | 0.75 | 0.55 | 0.33 | 0.17 | 0.97 | 0.93 | 0.96 | 1.00 | | | | |
| **Zr** | 0.36 | 0.39 | 0.49 | 0.49 | 0.42 | 0.41 | 0.34 | 0.49 | 0.27 | 0.46 | 0.02 | 0.21 | 0.01 | 0.07 | 1.00 | | | |
| **Ce** | 0.08 | 0.09 | 0.03 | 0.08 | 0.05 | 0.07 | 0.09 | 0.12 | 0.12 | 0.04 | 0.09 | 0.18 | 0.09 | 0.11 | 0.26 | 1.00 | | |
| **Th** | -0.03 | 0.03 | -0.02 | -0.01 | 0.00 | -0.03 | -0.03 | -0.01 | 0.12 | -0.04 | -0.02 | -0.02 | -0.02 | 0.00 | -0.05 | 0.80 | 1.00 | |
| **U** | -0.03 | 0.03 | -0.02 | -0.01 | 0.00 | -0.03 | -0.02 | -0.01 | 0.12 | -0.04 | -0.02 | -0.02 | -0.02 | 0.00 | -0.05 | 0.80 | 1.00 | 1.00 |

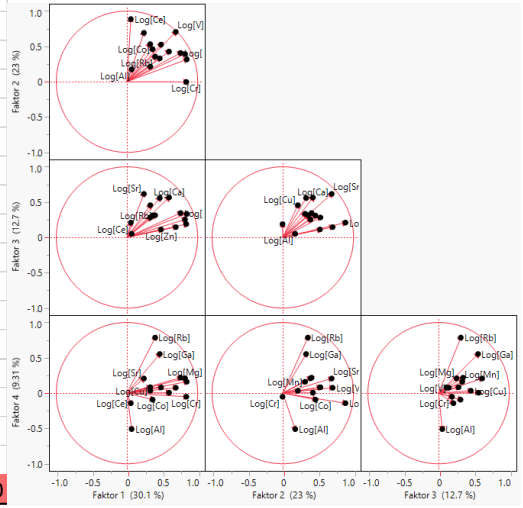

*Correlation matrix for LA-ICP-MS trace element data for Tayginka (RUS)*

| Tayginka (RUS) | Mg | Al | Ca | V | Cr | Mn | Fe | Co | Cu | Zn | Ga | As | Rb | Sr | Zr | Ce | Th | U |
|---|---|---|---|---|---|---|---|---|---|---|---|---|---|---|---|---|---|---|
| **Mg** | 1.00 | | | | | | | | | | | | | | | | | |
| **Al** | 0.26 | 1.00 | | | | | | | | | | | | | | | | |
| **Ca** | 0.65 | 0.24 | 1.00 | | | | | | | | | | | | | | | |
| **V** | 0.35 | 0.86 | 0.30 | 1.00 | | | | | | | | | | | | | | |
| **Cr** | 0.65 | 0.11 | 0.35 | 0.19 | 1.00 | | | | | | | | | | | | | |
| **Mn** | 0.49 | 0.29 | 0.91 | 0.38 | 0.14 | 1.00 | | | | | | | | | | | | |
| **Fe** | 0.28 | 0.56 | 0.32 | 0.66 | 0.20 | 0.39 | 1.00 | | | | | | | | | | | |
| **Co** | 0.34 | 0.31 | 0.30 | 0.43 | 0.42 | 0.33 | 0.51 | 1.00 | | | | | | | | | | |
| **Cu** | -0.05 | 0.08 | -0.05 | 0.00 | -0.02 | -0.06 | 0.16 | 0.14 | 1.00 | | | | | | | | | |
| **Zn** | 0.00 | 0.06 | 0.01 | 0.08 | 0.23 | 0.01 | 0.08 | 0.71 | 0.24 | 1.00 | | | | | | | | |
| **Ga** | 0.09 | 0.65 | 0.09 | 0.45 | 0.05 | 0.10 | 0.25 | 0.24 | 0.02 | 0.17 | 1.00 | | | | | | | |
| **As** | 0.17 | 0.59 | 0.15 | 0.68 | -0.02 | 0.20 | 0.48 | 0.19 | 0.13 | -0.04 | 0.30 | 1.00 | | | | | | |
| **Rb** | 0.17 | 0.76 | 0.11 | 0.64 | 0.04 | 0.16 | 0.39 | 0.28 | 0.04 | 0.10 | 0.91 | 0.45 | 1.00 | | | | | |
| **Sr** | 0.26 | 0.84 | 0.26 | 0.83 | 0.12 | 0.24 | 0.56 | 0.30 | -0.01 | 0.04 | 0.59 | 0.64 | 0.65 | 1.00 | | | | |
| **Zr** | 0.30 | 0.81 | 0.22 | 0.93 | 0.12 | 0.27 | 0.64 | 0.34 | 0.02 | 0.01 | 0.38 | 0.73 | 0.56 | 0.89 | 1.00 | | | |
| **Ce** | 0.18 | 0.50 | 0.15 | 0.45 | 0.01 | 0.12 | 0.27 | 0.12 | -0.05 | -0.02 | 0.28 | 0.44 | 0.37 | 0.40 | 0.41 | 1.00 | | |
| **Th** | 0.34 | 0.78 | 0.24 | 0.91 | 0.15 | 0.27 | 0.62 | 0.33 | 0.00 | 0.00 | 0.36 | 0.73 | 0.53 | 0.88 | 0.98 | 0.42 | 1.00 | |
| **U** | 0.30 | 0.81 | 0.22 | 0.93 | 0.13 | 0.27 | 0.64 | 0.34 | 0.01 | 0.01 | 0.38 | 0.73 | 0.56 | 0.91 | 1.00 | 0.41 | 0.98 | 1.00 |

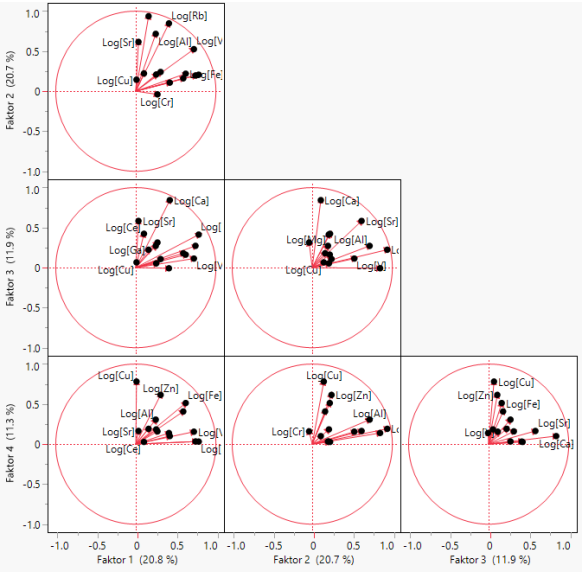

*Correlation matrix for LA-ICP-MS trace element data for Ragedara (LKA)*

| *Ragedara (LKA)* | Mg | Al | Ca | V | Cr | Mn | Fe | Co | Cu | Zn | Ga | As | Rb | Sr | Zr | Ce | Th | U |
|---|---|---|---|---|---|---|---|---|---|---|---|---|---|---|---|---|---|---|
| **Mg** | 1.00 | | | | | | | | | | | | | | | | | |
| **Al** | 0.44 | 1.00 | | | | | | | | | | | | | | | | |
| **Ca** | 0.09 | 0.15 | 1.00 | | | | | | | | | | | | | | | |
| **V** | -0.11 | 0.59 | 0.27 | 1.00 | | | | | | | | | | | | | | |
| **Cr** | -0.29 | -0.02 | -0.67 | 0.02 | 1.00 | | | | | | | | | | | | | |
| **Mn** | 0.21 | 0.18 | 0.89 | 0.19 | -0.75 | 1.00 | | | | | | | | | | | | |
| **Fe** | 0.26 | 0.24 | 0.82 | 0.18 | -0.86 | 0.93 | 1.00 | | | | | | | | | | | |
| **Co** | -0.20 | 0.47 | 0.20 | 0.96 | 0.04 | 0.12 | 0.11 | 1.00 | | | | | | | | | | |
| **Cu** | 0.15 | 0.52 | 0.61 | 0.24 | -0.47 | 0.58 | 0.70 | 0.08 | 1.00 | | | | | | | | | |
| **Zn** | 0.43 | 0.57 | 0.73 | 0.49 | -0.49 | 0.73 | 0.67 | 0.34 | 0.55 | 1.00 | | | | | | | | |
| **Ga** | 0.18 | 0.35 | 0.82 | 0.36 | -0.73 | 0.93 | 0.96 | 0.27 | 0.74 | 0.73 | 1.00 | | | | | | | |
| **As** | -0.31 | 0.39 | -0.18 | 0.85 | 0.45 | -0.30 | -0.32 | 0.89 | -0.16 | 0.02 | -0.15 | 1.00 | | | | | | |
| **Rb** | 0.79 | 0.36 | -0.27 | 0.01 | 0.27 | -0.20 | -0.22 | -0.04 | -0.15 | 0.15 | -0.19 | 0.05 | 1.00 | | | | | |
| **Sr** | 0.62 | 0.60 | 0.62 | 0.42 | -0.42 | 0.63 | 0.66 | 0.30 | 0.62 | 0.78 | 0.70 | 0.01 | 0.45 | 1.00 | | | | |
| **Zr** | 0.00 | 0.60 | -0.12 | 0.83 | 0.43 | -0.25 | -0.28 | 0.80 | 0.02 | 0.21 | -0.10 | 0.91 | 0.35 | 0.28 | 1.00 | | | |
| **Ce** | 0.76 | 0.55 | -0.02 | 0.21 | 0.16 | -0.02 | -0.05 | 0.11 | 0.14 | 0.40 | 0.00 | 0.14 | 0.92 | 0.67 | 0.50 | 1.00 | | |
| **Th** | 0.71 | 0.37 | -0.31 | 0.06 | 0.36 | -0.28 | -0.31 | 0.01 | -0.16 | 0.12 | -0.27 | 0.14 | 0.99 | 0.42 | 0.45 | 0.94 | 1.00 | |
| **U** | -0.01 | 0.62 | 0.27 | 0.99 | -0.01 | 0.22 | 0.22 | 0.96 | 0.23 | 0.51 | 0.39 | 0.83 | 0.12 | 0.50 | 0.83 | 0.30 | 0.16 | 1.00 |

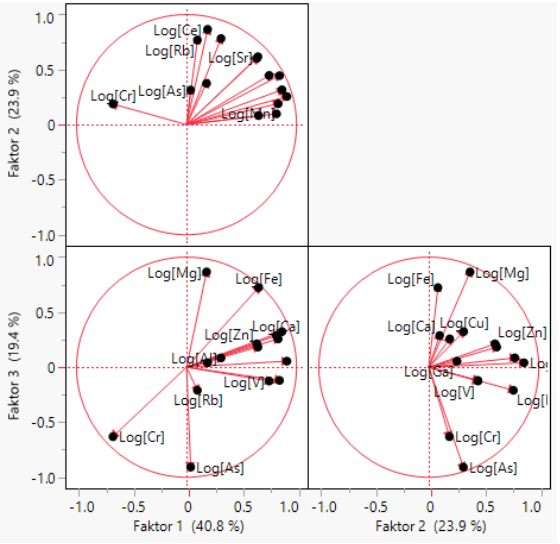

*Correlation matrix for LA-ICP-MS trace element data for Zavallia (UKR)*

| *Zavallia (UKR)* | Mg | Al | Ca | V | Cr | Mn | Fe | Co | Cu | Zn | Ga | As | Rb | Sr | Zr | Ce | Th | U |
|---|---|---|---|---|---|---|---|---|---|---|---|---|---|---|---|---|---|---|
| **Mg** | 1.00 | | | | | | | | | | | | | | | | | |
| **Al** | 0.18 | 1.00 | | | | | | | | | | | | | | | | |
| **Ca** | 0.49 | 0.15 | 1.00 | | | | | | | | | | | | | | | |
| **V** | 0.26 | 0.73 | 0.25 | 1.00 | | | | | | | | | | | | | | |
| **Cr** | 0.04 | 0.59 | 0.04 | 0.56 | 1.00 | | | | | | | | | | | | | |
| **Mn** | 0.32 | 0.66 | 0.56 | 0.80 | 0.47 | 1.00 | | | | | | | | | | | | |
| **Fe** | 0.07 | 0.49 | 0.18 | 0.68 | 0.20 | 0.67 | 1.00 | | | | | | | | | | | |
| **Co** | 0.64 | 0.57 | 0.53 | 0.74 | 0.47 | 0.80 | 0.42 | 1.00 | | | | | | | | | | |
| **Cu** | 0.15 | 0.63 | 0.20 | 0.82 | 0.55 | 0.68 | 0.49 | 0.63 | 1.00 | | | | | | | | | |
| **Zn** | 0.16 | 0.74 | 0.27 | 0.89 | 0.50 | 0.86 | 0.79 | 0.67 | 0.74 | 1.00 | | | | | | | | |
| **Ga** | 0.05 | 0.28 | 0.04 | 0.20 | 0.06 | 0.25 | 0.13 | 0.19 | 0.25 | 0.28 | 1.00 | | | | | | | |
| **As** | -0.08 | 0.41 | 0.10 | 0.68 | 0.20 | 0.54 | 0.65 | 0.40 | 0.61 | 0.66 | 0.18 | 1.00 | | | | | | |
| **Rb** | 0.17 | 0.72 | 0.18 | 0.51 | 0.22 | 0.47 | 0.35 | 0.42 | 0.44 | 0.49 | 0.23 | 0.33 | 1.00 | | | | | |
| **Sr** | 0.41 | 0.52 | 0.40 | 0.31 | 0.07 | 0.38 | 0.24 | 0.43 | 0.22 | 0.29 | 0.09 | 0.12 | 0.87 | 1.00 | | | | |
| **Zr** | 0.17 | 0.69 | 0.25 | 0.76 | 0.39 | 0.73 | 0.73 | 0.59 | 0.63 | 0.84 | 0.16 | 0.48 | 0.47 | 0.34 | 1.00 | | | |
| **Ce** | 0.07 | 0.57 | 0.35 | 0.52 | 0.24 | 0.47 | 0.41 | 0.37 | 0.51 | 0.56 | 0.14 | 0.39 | 0.70 | 0.60 | 0.46 | 1.00 | | |
| **Th** | 0.21 | 0.77 | 0.27 | 0.81 | 0.62 | 0.76 | 0.44 | 0.69 | 0.83 | 0.77 | 0.18 | 0.43 | 0.62 | 0.42 | 0.76 | 0.62 | 1.00 | |
| **U** | 0.20 | 0.44 | 0.18 | 0.43 | 0.19 | 0.43 | 0.27 | 0.42 | 0.43 | 0.42 | 0.15 | 0.18 | 0.27 | 0.19 | 0.72 | 0.28 | 0.66 | 1.00 |

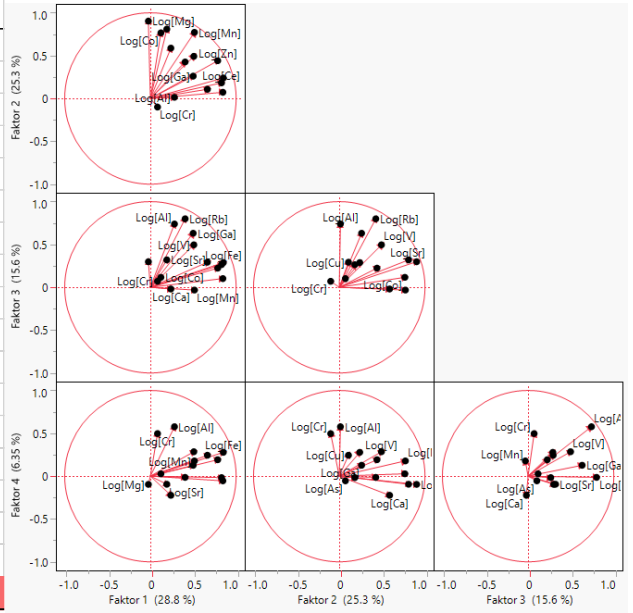

## LA ICP MS trace element data

| LA-ICP-MS | Analyte (µg g-1) | | | | | | | | | | | | | | | | |
|---|---|---|---|---|---|---|---|---|---|---|---|---|---|---|---|---|---|
| sample ID | Mg | Al | Ca | V | Cr | Mn | Fe | Co | Cu | Zn | Ga | As | Rb | Sr | Zr | Ce | U |
| 1A.1 | 426.71 | 6961.64 | 193.59 | 128.66 | 94.98 | 417.94 | 4410.92 | 2.66 | 25.75 | 49.48 | 107.21 | 21.63 | 126.83 | 100.15 | 9.81 | 34.4 | 3.66 |
| 1A.2 | 347.58 | 9029.64 | 231.29 | 113.45 | 90.92 | 270.05 | 3493.79 | 4.21 | 23.09 | 39.3 | 111.23 | 16.17 | 110.18 | 139.3 | 134.27 | 44.96 | 4.41 |
| 1A.3 | 519.91 | 7312.21 | 400.04 | 152.65 | 108.31 | 232.7 | 3817.1 | 4.14 | 26.69 | 59.24 | 132.78 | 22.95 | 174.8 | 158.67 | 139.7 | 36.62 | 5.32 |
| 1A_1 | 445.27 | 7091.84 | 293.33 | 194.33 | 108.26 | 434.23 | 6332.85 | 5.77 | 32.45 | 69.2 | 132.79 | 25.54 | 207.34 | 103.28 | 10.45 | 65.62 | 3.86 |
| 1A_10 | 371.14 | 5715.44 | 266.58 | 111.18 | 71.18 | 311.52 | 5107.68 | 5.95 | 20.89 | 27.77 | 79.84 | 17.95 | 112.4 | 110.87 | 11.74 | 57.93 | 3.45 |
| 1A_11 | 317.63 | 4597.6 | 222.18 | 131.17 | 78.87 | 441.39 | 5472.79 | 4.57 | 33.02 | 46.9 | 76.67 | 21.11 | 136.39 | 89.4 | 21.71 | 89.3 | 5.56 |
| 1A_12 | 206.67 | 4563.44 | 187.9 | 100.04 | 66.68 | 174.33 | 3165.35 | 3.06 | 16.64 | 26.06 | 82.92 | 11.66 | 83.18 | 59.32 | 11.12 | 27.49 | 2.21 |
| 1A_13 | 367.95 | 4540.975 | 425.28 | 163.54 | 91.21 | 383.86 | 5891.16 | 5.35 | 25.42 | 41.79 | 114.34 | 18.2 | 171.45 | 151.49 | 38.75 | 89.1 | 4.2 |
| 1A_14 | 348.76 | 4518.51 | 191.27 | 89.1 | 61.95 | 334.81 | 4237.66 | 3.8 | 21.91 | 29.48 | 66.05 | 15.49 | 100.15 | 89.3 | 6.17 | 41.61 | 3.27 |
| 1A_15 | 650.5 | 9189.16 | 410.94 | 167.63 | 80.51 | 465.45 | 7523.88 | 11.13 | 27.08 | 61.05 | 107.17 | 17.8 | 164.41 | 138.97 | 220.09 | 46.78 | 4.09 |
| 1A_2 | 420.93 | 5357.57 | 308.35 | 134.22 | 79.66 | 341.95 | 5061.71 | 4.33 | 25.77 | 62.43 | 109.33 | 27.25 | 182.9 | 124 | 12.02 | 56.63 | 3.11 |
| 1A_3 | 539.26 | 5235.46 | 280.86 | 145.43 | 92.42 | 497.66 | 7279.63 | 6.53 | 25.98 | 86.52 | 104.31 | 20.42 | 158.4 | 113.28 | 11.57 | 60.8 | 3.73 |
| 1A_4 | 367.87 | 3339.72 | 240.41 | 108.89 | 74.24 | 305.56 | 4751.46 | 4.01 | 27.16 | 47.38 | 74.53 | 18.7 | 118.88 | 96.65 | 22.21 | 40.11 | 3.17 |
| 1A_5 | 354.46 | 5124.24 | 374.01 | 141.69 | 120.61 | 206.61 | 4165.33 | 4.15 | 29.82 | 51.18 | 92.19 | 19.09 | 159.64 | 120.95 | 8.57 | 65.43 | 3.55 |
| 1A_6 | 568.43 | 4882 | 395.78 | 179.31 | 103.88 | 517.26 | 8156.98 | 10.23 | 39.81 | 90.8 | 98.1 | 25.94 | 172.02 | 150.87 | 8.63 | 227.14 | 5.03 |
| 1A_7 | 561.23 | 5525.465 | 478.32 | 189.32 | 107.01 | 957.84 | 12042.55 | 9.23 | 41.55 | 112.06 | 108.51 | 24.11 | 185.8 | 122.43 | 9.11 | 102.53 | 4.23 |
| 1A_8 | 456.93 | 6168.93 | 261.3 | 141.19 | 85.47 | 581.67 | 6968.51 | 6.06 | 22.29 | 88 | 93.3 | 21.28 | 141.02 | 97.55 | 6.57 | 47.33 | 3.34 |
| 1A_9 | 203.54 | 0.00595 | 393.57 | 76.42 | 60.29 | 146.39 | 2795.32 | 2.95 | 131.83 | 52.81 | 52.1 | 18.32 | 82.12 | 79.73 | 11.7 | 534.71 | 31.27 |
| 21G.1 | 10.85 | 91.81 | 7.17 | 0.635 | 35.13 | 2.58 | 42.41 | 0.02015 | 0.078 | 4.53 | 0.301 | 3.1 | 0.486 | 1.26 | 0.0707 | 0.063 | 0.00145 |
| 21G.2 | 75.69 | 328.62 | 12 | 1.87 | 35.14 | 7.49 | 280.12 | 0.204 | 0.01845 | 6.48 | 0.818 | 3.39 | 0.713 | 2.46 | 0.099 | 0.105 | 0.00249 |
| 21G.3 | 44.97 | 2836.78 | 16.66 | 36.13 | 38.79 | 3.48 | 101.94 | 0.02015 | 0.203 | 4.72 | 26.61 | 3.37 | 40.02 | 14.59 | 5.5 | 1.59 | 0.238 |
| 21G.4 | 8.46 | 921.78 | 63.75 | 5.15 | 37.2 | 3.25 | 33.49 | 0.051 | 0.255 | 4.18 | 6.44 | 4.43 | 3.73 | 16.06 | 61.72 | 84.72 | 1.53 |
| 21G_1 | 43.47 | 2956.85 | 59.69 | 44.66 | 39.42 | 5.93 | 98.15 | 0.52 | 3.74 | 9.23 | 34.35 | 3.78 | 48.11 | 55.9 | 12.78 | 7 | 0.8 |
| 21G_2 | 81.25 | 5592.1 | 77.64 | 78.15 | 44.95 | 6.3 | 184.59 | 0.41 | 2.64 | 4.92 | 62.5 | 4 | 89.32 | 63.39 | 11.64 | 6.86 | 0.55 |
| 21G_3 | 72.12 | 1479.72 | 40.9 | 15.42 | 33.24 | 13.38 | 486.52 | 0.63 | 0.82 | 12.78 | 10.77 | 4.72 | 10.89 | 12.66 | 2.85 | 0.56 | 0.078 |
| 21G_4 | 16.37 | 965.73 | 51.49 | 11.35 | 30.02 | 19.83 | 39.74 | 0.02015 | 2.02 | 5.11 | 11.73 | 3.28 | 11.34 | 26.08 | 8.18 | 5.39 | 0.32 |

| | | | | | | | | | | | | | | | | | |
|---|---|---|---|---|---|---|---|---|---|---|---|---|---|---|---|---|---|
| 21G_5 | 15.39 | 1000.97 | 45.17 | 10.76 | 29.11 | 3.23 | 36.83 | 0.166 | 0.21 | 3.35 | 9.85 | 3.36 | 11.56 | 20.63 | 5.12 | 11.24 | 0.221 |
| 21G_6 | 788.06 | 2956.93 | 29.98 | 23.63 | 31.85 | 134.59 | 5683.49 | 6.77 | 0.36 | 20.46 | 11.34 | 3.29 | 8.03 | 9.68 | 2.18 | 1.6 | 0.082 |
| 21G_7 | 731.56 | 7163.03 | 46.09 | 84.69 | 38.19 | 120.8 | 4428.45 | 5.26 | 0.87 | 15.88 | 56.19 | 3.21 | 89.85 | 34.75 | 3.99 | 0.7 | 0.102 |
| 21H.1 | 35.26 | 1854.88 | 16.99 | 21.04 | 38.52 | 3.87 | 132.43 | 0.081 | 1.08 | 3.16 | 11.73 | 3.26 | 18.54 | 14.87 | 1.93 | 0.311 | 0.347 |
| 21H.2 | 4.17 | 160.32 | 33.6 | 10.44 | 39.24 | 4 | 15.1 | 0.02015 | 0.72 | 4.71 | 1.73 | 5.23 | 0.88 | 20.27 | 11.56 | 4.03 | 1.42 |
| 21H.3 | 8.47 | 677.92 | 18.1 | 9.68 | 38.3 | 1.49 | 13.95 | 0.02015 | 1.47 | 2.24 | 4.89 | 3.73 | 6.06 | 14.5 | 1.46 | 0.358 | 0.393 |
| 21H.4 | 22.87 | 1824.35 | 26.1 | 17.01 | 38.97 | 2.79 | 44.11 | 0.096 | 0.92 | 3.47 | 10.56 | 3.26 | 17.38 | 10.25 | 16.2 | 2.27 | 0.53 |
| 21H_1 | 39.37 | 2480.62 | 21.51 | 33.64 | 27.52 | 4.6 | 95.21 | 0.061 | 0.332 | 2.37 | 21.75 | 5.38 | 42.47 | 12.25 | 11.22 | 6.21 | 2.29 |
| 21H_2 | 48.43 | 2748.74 | 27.32 | 30.16 | 27.13 | 4.23 | 118.8 | 0.087 | 0.405 | 3.85 | 24.77 | 4.86 | 44.09 | 17.75 | 5.43 | 1.2 | 0.29 |
| 21H_3 | 20.42 | 1158.56 | 20.85 | 16.43 | 25.63 | 2.36 | 44.26 | 0.061 | 0.391 | 3.65 | 10.66 | 4.08 | 16.87 | 10.21 | 6.13 | 1.13 | 0.477 |
| 21H_4 | 37.35 | 1777.98 | 20.02 | 20.13 | 25.27 | 3.01 | 78.51 | 0.058 | 1.17 | 4.32 | 20.12 | 4.43 | 26.19 | 19.88 | 5.45 | 1.14 | 0.59 |
| 21H_5 | 20.17 | 867.06 | 23.22 | 8.31 | 23.78 | 3.36 | 58.63 | 0.225 | 0.287 | 4.45 | 6.83 | 3.74 | 10.37 | 6.91 | 4.88 | 6.07 | 0.211 |
| 21H_6 | 28.31 | 1818.14 | 28.87 | 23.99 | 29.99 | 3.54 | 77.46 | 0.041 | 0.62 | 4.32 | 17.72 | 3.6 | 29.9 | 20.62 | 9.47 | 1.51 | 0.69 |
| 21H_7 | 14.91 | 830.46 | 52.18 | 9.18 | 27.33 | 3.22 | 32.49 | 0.145 | 0.52 | 4.57 | 7.17 | 4.23 | 9.32 | 15.83 | 4.57 | 3.3 | 0.233 |
| 21I.1 | 1.85 | 86.56 | 15.28 | 2.09 | 35.19 | 0.3 | 7.22 | 0.316 | 1 | 2.49 | 1.06 | 21.15 | 0.815 | 7.53 | 2.92 | 0.97 | 0.189 |
| 21I.2 | 1.36 | 73.65 | 14.6 | 6.49 | 34.99 | 1.76 | 4.7 | 1.19 | 0.333 | 2.36 | 1.42 | 18.38 | 0.432 | 9.93 | 0.603 | 0.95 | 0.365 |
| 21I.3 | 1.53 | 84.25 | 17.9 | 2.05 | 35.02 | 0.188 | 0.4325 | 2.37 | 0.86 | 0.71 | 1.55 | 22.94 | 0.435 | 7.83 | 1.67 | 1.2 | 0.288 |
| 21I.4 | 2.89 | 152.82 | 14.69 | 5.59 | 34.97 | 0.372 | 9.32 | 2.11 | 0.01845 | 1.05 | 1.09 | 18.38 | 1.03 | 3.6 | 0.97 | 0.501 | 0.264 |
| 21I_1 | 3.58 | 226.32 | 25.21 | 2.44 | 23.8 | 1.51 | 19.99 | 0.099 | 1.59 | 2.62 | 1.5 | 9.8 | 1.98 | 5.03 | 1.34 | 1.03 | 0.161 |
| 21I_2 | 2.13 | 58.4 | 15.82 | 0.85 | 22.89 | 1.15 | 15.33 | 0.26 | 2.67 | 2.33 | 0.39 | 16.35 | 0.28 | 2.91 | 0.41 | 0.7 | 0.132 |
| 21I_3 | 43.01 | 472.93 | 17.2 | 4.22 | 21.5 | 7.91 | 402.21 | 0.52 | 1.33 | 4.37 | 1.99 | 4.7 | 3.09 | 3.39 | 1.51 | 0.57 | 0.1 |
| 21I_4 | 20.82 | 539.86 | 11.21 | 4.33 | 20.99 | 2.55 | 79.78 | 1.09 | 0.2 | 2.27 | 2.99 | 4.71 | 4.87 | 3.19 | 1.03 | 0.65 | 0.055 |
| 21I_5 | 3.7 | 329.65 | 7.44 | 2.47 | 20.92 | 0.4 | 11.23 | 0.81 | 0.166 | 1.36 | 1.53 | 6.67 | 2.76 | 2.26 | 3.13 | 0.75 | 0.168 |
| 21I_6 | 1.5 | 47.47 | 18.94 | 1.57 | 21.19 | 6.2 | 11.53 | 6.77 | 0.53 | 0.75 | 1.08 | 12.89 | 0.187 | 6.08 | 0.79 | 0.98 | 0.184 |
| 21I_7 | 12.34 | 536.15 | 13.89 | 4.73 | 20.06 | 1.71 | 29.74 | 1.44 | 3.3 | 6.66 | 3.4 | 3 | 5.21 | 4.02 | 3.3 | 3.98 | 0.088 |
| 21C.1 | 2 | 133.31 | 3.62 | 8.94 | 41.34 | 5.25 | 69.41 | 0.102 | 4.86 | 2.82 | 0.418 | 0.078 | 0.096 | 0.297 | 4.15 | 1.11 | 0.0372 |
| 21C.2 | 1.54 | 150.58 | 3.31 | 3.78 | 42.56 | 6.18 | 106.67 | 0.068 | 5.43 | 1.78 | 0.383 | 0.177 | 0.0466 | 0.68 | 8.01 | 1.99 | 0.0556 |
| 21C.3 | 1.52 | 264.91 | 3.92 | 3.52 | 41.14 | 6.92 | 124.78 | 0.02015 | 5.74 | 1.53 | 0.526 | 0.102 | 0.027 | 0.529 | 6.13 | 1.63 | 0.0448 |
| 21C_1 | 0.74 | 123.18 | 2.86 | 2.83 | 26.18 | 209.06 | 108.66 | 0.48 | 5.64 | 1.19 | 6.27 | 0.112 | 0.057 | 0.46 | 4.94 | 1.94 | 0.0377 |
| 21C_10 | 0.71 | 113.15 | 3.01 | 1.97 | 31.03 | 2.87 | 73.57 | 0.043 | 3.18 | 0.62 | 0.3 | 0.093 | 0.061 | 0.11 | 3.14 | 0.96 | 0.0202 |

| | | | | | | | | | | | | | | | | | |
|---|---|---|---|---|---|---|---|---|---|---|---|---|---|---|---|---|---|
| 21C_11 | 0.85 | 298.78 | 4.59 | 6.09 | 26.6 | 15.46 | 139.91 | 0.206 | 5.3 | 1.33 | 0.78 | 0.147 | 0.033 | 0.6 | 8.45 | 2.3 | 0.049 |
| 21C_12 | 0.89 | 95.43 | 2.26 | 2.18 | 24.81 | 2.44 | 67.36 | 0.171 | 2.85 | 1.13 | 0.17 | 0.095 | 0.0218 | 0.111 | 3.12 | 1.01 | 0.0259 |
| 21C_13 | 1.31 | 431.44 | 3.78 | 6.54 | 32.57 | 8.71 | 294.17 | 0.5 | 9.67 | 2.16 | 0.68 | 0.247 | 0.0253 | 0.34 | 7.79 | 3.69 | 0.074 |
| 21C_14 | 1.56 | 947 | 3.57 | 10.43 | 37.65 | 10.5 | 83.29 | 0.108 | 5.79 | 1.39 | 1.03 | 0.189 | 0.0135 | 0.122 | 3.1 | 1.05 | 0.0274 |
| 21C_15 | 4.27 | 2621.82 | 6.99 | 13.61 | 39.63 | 9.52 | 233.08 | 0.43 | 15.38 | 6.35 | 2.71 | 0.266 | 0.064 | 0.28 | 8.11 | 1.88 | 0.069 |
| 21C_2 | 0.67 | 105.95 | 1.51 | 2.68 | 24.89 | 7.54 | 81.85 | 0.198 | 3.43 | 1.21 | 0.31 | 0.093 | 0.0262 | 0.29 | 4.35 | 1.63 | 0.024 |
| 21C_3 | 1.51 | 515.79 | 3.76 | 9.17 | 33.15 | 9.09 | 197.69 | 0.269 | 6.25 | 1.43 | 0.81 | 0.175 | 0.045 | 0.42 | 9.03 | 2.61 | 0.066 |
| 21C_4 | 0.91 | 436.86 | 3.75 | 3.81 | 31.88 | 4.55 | 126.05 | 0.186 | 4.85 | 1.51 | 0.62 | 0.204 | 0.019 | 0.208 | 7.68 | 2.11 | 0.0348 |
| 21C_5 | 0.91 | 207.03 | 3.23 | 3.44 | 30.22 | 4.61 | 138.46 | 0.175 | 4.69 | 1.05 | 0.44 | 0.221 | 0.0215 | 0.22 | 4.74 | 1.68 | 0.052 |
| 21C_6 | 0.42 | 87.76 | 2.85 | 1.13 | 24.92 | 1.46 | 49.09 | 0.02015 | 1.37 | 0.43 | 0.123 | 0.202 | 0.0146 | 0.148 | 2.22 | 0.78 | 0.0152 |
| 21C_7 | 1.03 | 370.66 | 2.41 | 5.86 | 28.02 | 5.4 | 140.78 | 0.193 | 7.13 | 1.63 | 0.64 | 0.165 | 0.025 | 0.29 | 6.4 | 2.09 | 0.0407 |
| 21C_8 | 3.27 | 424.05 | 3.71 | 5.57 | 28.44 | 4.99 | 116.26 | 0.113 | 4.58 | 1.27 | 0.67 | 0.174 | 0.0238 | 0.22 | 7.17 | 2.07 | 0.0353 |
| 21C_9 | 1.88 | 439.23 | 3.42 | 3.49 | 27.75 | 6.19 | 135.25 | 0.195 | 5.5 | 2.08 | 0.59 | 0.141 | 0.032 | 0.27 | 7.92 | 2 | 0.056 |
| 21N.1 | 1.45 | 741.93 | 4.47 | 4.97 | 58.5 | 3.78 | 144.11 | 1.25 | 5.14 | 1.05 | 0.984 | 0.0616 | 0.0391 | 0.372 | 6.49 | 1.59 | 0.0459 |
| 21N.2 | 0.938 | 211.02 | 6.55 | 2.51 | 47.62 | 2.28 | 67.18 | 0.28 | 4.14 | 1.21 | 0.517 | 0.0708 | 0.018 | 0.239 | 5.5 | 0.881 | 0.0336 |
| 21N.3 | 1.61 | 275.69 | 12.33 | 2.83 | 57.59 | 5.71 | 147.68 | 0.186 | 5.17 | 1.14 | 0.545 | 0.156 | 0.0241 | 0.295 | 6.56 | 1.52 | 0.0419 |
| 21N_1 | 0.7 | 175.25 | 1.91 | 2.4 | 26.88 | 4.09 | 102.43 | 0.05 | 4.34 | 1.4 | 0.36 | 0.184 | 0.00605 | 0.168 | 4.52 | 1.63 | 0.0286 |
| 21N_10 | 0.54 | 103.84 | 2.15 | 2.09 | 25.89 | 3.14 | 79.53 | 0.235 | 3.75 | 0.85 | 0.27 | 0.157 | 0.0224 | 0.31 | 3.33 | 1.22 | 0.0255 |
| 21N_11 | 0.91 | 404.42 | 3.14 | 5.89 | 26.76 | 6.48 | 334.86 | 0.7 | 5.05 | 1.58 | 0.53 | 0.175 | 0.143 | 0.17 | 6.18 | 1.92 | 0.049 |
| 21N_12 | 0.92 | 284.41 | 3.92 | 3.05 | 30.45 | 5.37 | 124.71 | 0.149 | 4.33 | 0.8 | 0.44 | 0.176 | 0.0153 | 0.28 | 6.35 | 2.53 | 0.0352 |
| 21N_13 | 0.87 | 351.39 | 3.93 | 3.58 | 27.93 | 4.44 | 111.29 | 0.222 | 4.71 | 1.37 | 0.56 | 0.23 | 0.029 | 0.27 | 10.17 | 3.08 | 0.0347 |
| 21N_14 | 1.84 | 995.73 | 3.98 | 11.6 | 28.79 | 4.9 | 123.51 | 0.178 | 6.06 | 2.03 | 1.51 | 0.139 | 0.0214 | 0.43 | 10.33 | 1.98 | 0.0421 |
| 21N_15 | 1.87 | 588.79 | 3.72 | 6.44 | 31.45 | 7.65 | 187.22 | 0.259 | 8 | 2.17 | 0.92 | 0.144 | 0.048 | 0.43 | 8.39 | 2.72 | 0.056 |
| 21N_2 | 7.94 | 538.41 | 3.39 | 5.47 | 29.67 | 8.21 | 176.96 | 0.188 | 7.28 | 1.68 | 1 | 0.275 | 0.0127 | 0.69 | 8.57 | 3.5 | 0.06 |
| 21N_3 | 0.86 | 142.51 | 3.32 | 3.37 | 26.94 | 5.41 | 109.91 | 0.237 | 5.15 | 1.33 | 0.46 | 0.169 | 0.00605 | 0.54 | 8.15 | 2.38 | 0.0419 |
| 21N_4 | 0.98 | 435.25 | 1.9 | 2.77 | 24.24 | 4.02 | 130.4 | 0.16 | 5.36 | 1.27 | 0.52 | 0.304 | 0.029 | 0.146 | 5.92 | 1.54 | 0.0395 |
| 21N_5 | 1.86 | 1947.16 | 3.76 | 11.52 | 35.54 | 7.46 | 263.04 | 0.2 | 7.41 | 2.45 | 2.07 | 0.21 | 0.071 | 0.34 | 10.32 | 2.37 | 0.079 |
| 21N_6 | 0.73 | 174.28 | 5.61 | 14.95 | 27.39 | 3.17 | 152.28 | 0.16 | 3.73 | 0.61 | 0.3 | 0.049 | 0.00605 | 0.155 | 4.25 | 1.43 | 0.062 |
| 21N_7 | 0.63 | 149.2 | 3.24 | 2.16 | 25.4 | 2.42 | 81.81 | 0.02015 | 2.6 | 0.76 | 0.28 | 0.169 | 0.0165 | 0.136 | 2.93 | 0.99 | 0.0157 |
| 21N_8 | 2.23 | 485.84 | 3.88 | 8.99 | 30.35 | 8.76 | 163.25 | 0.373 | 9.24 | 6.29 | 0.84 | 0.226 | 0.064 | 0.31 | 7.57 | 2.47 | 0.053 |

| | | | | | | | | | | | | | | | | | |
|---|---|---|---|---|---|---|---|---|---|---|---|---|---|---|---|---|---|
| 21N_9 | 0.78 | 174.28 | 1.43 | 4.04 | 29.4 | 5.18 | 126.12 | 0.167 | 4.74 | 0.99 | 0.44 | 0.145 | 0.00605 | 0.28 | 11.58 | 2.38 | 0.052 |
| 22C.1 | 1.21 | 252.55 | 4.65 | 2.82 | 36.26 | 4.02 | 60.11 | 0.38 | 2.22 | 1.97 | 0.507 | 0.096 | 0.0336 | 0.396 | 12.63 | 2.8 | 0.039 |
| 22C.2 | 1.18 | 282.11 | 3.54 | 2.53 | 35.2 | 4.92 | 58.51 | 0.202 | 2.11 | 2.23 | 0.54 | 0.113 | 0.0353 | 0.82 | 11.71 | 2.71 | 0.0515 |
| 22C.3 | 4.15 | 871.3 | 5.34 | 5.12 | 38.31 | 7.5 | 120.47 | 0.39 | 3.19 | 2.98 | 1.77 | 0.243 | 0.0521 | 0.86 | 20.12 | 4.68 | 0.072 |
| 3B.3 | 0.857 | 425.78 | 6.53 | 15.28 | 54.99 | 21.04 | 357.39 | 0.87 | 5 | 1.04 | 1.93 | 0.157 | 0.0495 | 0.689 | 4.83 | 1.76 | 0.185 |
| 3B_1 | 0.647 | 301.64 | 8.67 | 4.81 | 33.6 | 16.1 | 201.61 | 0.52 | 2.67 | 0.91 | 1.08 | 0.27 | 0.0635 | 0.82 | 1.69 | 1.94 | 0.154 |
| 3B_10 | 0.498 | 166.96 | 5.49 | 3.48 | 32.11 | 15.16 | 139.21 | 0.47 | 11.87 | 0.367 | 0.94 | 0.1591 | 0.0134 | 0.481 | 1.94 | 1.25 | 0.0685 |
| 3B_11 | 0.89 | 351.74 | 6.27 | 17.85 | 33.38 | 191.67 | 200.21 | 28.24 | 18.87 | 5.82 | 0.85 | 1.351 | 0.0437 | 0.32 | 1.2 | 0.66 | 0.1093 |
| 3B_12 | 0.678 | 233.68 | 6 | 3.81 | 32.58 | 12.43 | 123.95 | 0.52 | 5.85 | 1.55 | 0.66 | 0.176 | 0.023 | 0.129 | 7.25 | 0.93 | 0.144 |
| 3B_13 | 0.58 | 131.56 | 6.67 | 8.51 | 34.9 | 65.21 | 159.42 | 1.9 | 4.45 | 1.03 | 2.74 | 0.154 | 0.0192 | 0.573 | 1.58 | 1.19 | 0.344 |
| 3B_14 | 2.19 | 833.28 | 6.72 | 14.33 | 39.17 | 23.43 | 229.32 | 0.9 | 4.91 | 3.04 | 1.58 | 0.227 | 0.041 | 0.274 | 3.76 | 1.17 | 0.174 |
| 3B_15 | 0.566 | 400.21 | 5.45 | 6.82 | 32.29 | 8.65 | 89.91 | 0.295 | 1.54 | 0.82 | 0.91 | 0.1232 | 0.00605 | 0.224 | 1.078 | 0.57 | 0.0348 |
| 3B_2 | 0.521 | 196.67 | 8.22 | 2.6 | 31.84 | 10.68 | 122.35 | 0.184 | 2.29 | 0.673 | 0.7 | 0.1343 | 0.00605 | 0.228 | 1.38 | 0.87 | 0.0697 |
| 3B_3 | 0.692 | 553.11 | 6.84 | 8.31 | 33.76 | 12.95 | 151.08 | 0.83 | 4.87 | 0.97 | 1.42 | 0.1687 | 0.022 | 0.229 | 6.03 | 0.99 | 0.145 |
| 3B_4 | 9.57 | 1318.71 | 8.22 | 5.59 | 71.34 | 28.69 | 181.6 | 1.01 | 5.54 | 1.5 | 3.38 | 0.218 | 0.0426 | 0.621 | 3.18 | 1.61 | 0.1234 |
| 3B_5 | 0.765 | 378.19 | 6.51 | 4.33 | 36.1 | 15.62 | 193.59 | 0.83 | 3.33 | 1.48 | 0.84 | 0.19 | 0.00605 | 0.142 | 1.71 | 0.92 | 0.1023 |
| 3B_6 | 0.61 | 175.29 | 7.57 | 5.71 | 37.41 | 259.19 | 171.3 | 2.17 | 10.37 | 1.09 | 3.62 | 0.1518 | 0.0536 | 0.461 | 2.65 | 1.53 | 0.164 |
| 3B_7 | 0.62 | 309.97 | 6.12 | 7.44 | 35.63 | 9.42 | 172.09 | 0.68 | 3.46 | 0.96 | 0.76 | 0.1161 | 0.0412 | 0.093 | 1.21 | 0.5 | 0.0759 |
| 3B_9 | 1.27 | 2057.8 | 8 | 36.53 | 47.02 | 26.94 | 221.94 | 1.18 | 6.59 | 1.61 | 4.92 | 0.329 | 0.052 | 0.384 | 4.38 | 1.29 | 0.1144 |
| 3B_8 | 0.82 | 296.27 | 8.46 | 5.75 | 37.18 | 12.8 | 114.19 | 0.15 | 2.76 | 0.516 | 0.61 | 0.1491 | 0.0302 | 0.117 | 1.038 | 0.62 | 0.0497 |
| 21M_11 | 0.75 | 160.92 | 4.73 | 2.23 | 29.99 | 4.04 | 83.99 | 0.145 | 4.45 | 0.83 | 0.39 | 0.097 | 0.0222 | 0.38 | 5.01 | 1.74 | 0.032 |
| 21M_12 | 1.71 | 363.16 | 5.66 | 7.31 | 30.7 | 20.64 | 194.79 | 0.43 | 5.75 | 1.4 | 1.06 | 0.144 | 0.065 | 0.55 | 11.06 | 2.64 | 0.069 |
| 21M_13 | 1.28 | 262.8 | 5.81 | 7.35 | 28.85 | 6.3 | 127.59 | 0.3 | 4.44 | 4.43 | 0.56 | 0.122 | 0.035 | 0.36 | 7.24 | 2.97 | 0.05 |
| 21M_14 | 1.4 | 358.96 | 5.9 | 5.03 | 30.34 | 8.2 | 158.89 | 0.28 | 4.95 | 2.24 | 0.92 | 0.155 | 0.069 | 0.6 | 6.28 | 2.62 | 0.041 |
| 21M_15 | 1.13 | 244.83 | 4.31 | 4.23 | 26.79 | 10.02 | 240.86 | 0.41 | 6.41 | 2.57 | 0.63 | 0.116 | 0.05 | 0.47 | 7.1 | 2.65 | 0.07 |
| 21M_2 | 14.29 | 2756.34 | 5.49 | 12.64 | 34.96 | 16.84 | 258.94 | 0.78 | 9.11 | 3.11 | 7.14 | 0.78 | 0.035 | 1.58 | 10.34 | 2.74 | 0.096 |
| 21M_3 | 1.08 | 257.12 | 3.02 | 3.68 | 26.51 | 6.62 | 119.8 | 0.217 | 6.22 | 1.95 | 0.65 | 0.114 | 0.0152 | 0.51 | 6.32 | 1.85 | 0.039 |
| 21M_4 | 1.18 | 466.34 | 6.23 | 3.91 | 27.83 | 10.29 | 165.78 | 0.181 | 8.95 | 1.36 | 1.51 | 0.286 | 0.0253 | 0.63 | 6.81 | 1.98 | 0.051 |
| 21M_5 | 1.43 | 343.73 | 4.4 | 4.67 | 29.04 | 6.91 | 141.41 | 0.37 | 4.88 | 1.06 | 0.7 | 0.22 | 0.028 | 0.47 | 6.54 | 2.02 | 0.074 |
| 21M_6 | 1.75 | 413.15 | 5.05 | 5.79 | 28.84 | 8.34 | 162.02 | 0.39 | 4.86 | 1.16 | 0.88 | 0.121 | 0.118 | 0.82 | 6.53 | 2.21 | 0.06 |

| | | | | | | | | | | | | | | | | | |
|---|---|---|---|---|---|---|---|---|---|---|---|---|---|---|---|---|---|
| 21M_7 | 1.29 | 301.18 | 4.69 | 3.92 | 29.15 | 7.74 | 152.73 | 0.37 | 5.61 | 1.69 | 0.67 | 0.103 | 0.031 | 0.51 | 9.01 | 3.1 | 0.081 |
| 21M_8 | 2 | 531.71 | 5.98 | 9.45 | 35.25 | 11.35 | 205.53 | 0.47 | 8.79 | 3.94 | 1.23 | 0.179 | 0.22 | 0.45 | 7.07 | 2.57 | 0.104 |
| 21M_9 | 1.87 | 366.9 | 6.93 | 12.02 | 35.56 | 11.17 | 190.64 | 0.58 | 8.74 | 4.02 | 0.99 | 0.156 | 0.075 | 0.72 | 8.69 | 3.01 | 0.087 |
| 21M.1 | 1.35 | 573.44 | 5.74 | 4.38 | 43.27 | 8.95 | 158.35 | 0.165 | 7.04 | 1.05 | 1.06 | 0.115 | 0.0484 | 0.89 | 7.08 | 1.84 | 0.0492 |
| 21M.2 | 0.653 | 37.99 | 3.74 | 0.838 | 40.11 | 3.65 | 47.94 | 0.189 | 1.7 | 0.52 | 0.139 | 0.135 | 0.013 | 0.159 | 2.43 | 0.504 | 0.0153 |
| 21M.3 | 1.22 | 462.91 | 5.04 | 7.71 | 42.07 | 5.07 | 112.93 | 0.25 | 4.91 | 1.5 | 1.1 | 0.103 | 0.0389 | 0.54 | 7.38 | 1.13 | 0.043 |
| 22C_1 | 1.54 | 333.02 | 3.67 | 4.46 | 26 | 142.21 | 312.35 | 1.37 | 6.06 | 2.02 | 3.19 | 0.17 | 0.131 | 0.4 | 50.75 | 3.08 | 0.13 |
| 22C_10 | 1.08 | 238.66 | 3.7 | 2.38 | 25.52 | 6.48 | 93.43 | 0.195 | 3.25 | 1.49 | 0.71 | 0.127 | 0.0398 | 0.52 | 14.13 | 3.22 | 0.0425 |
| 22C_11 | 1.18 | 413.78 | 4.67 | 4.4 | 25.8 | 22.08 | 127 | 0.56 | 3.83 | 1.14 | 0.98 | 0.208 | 0.0498 | 0.85 | 19.99 | 18.4 | 1.05 |
| 22C_12 | 0.97 | 246.81 | 4.27 | 3.52 | 28.35 | 7.18 | 101.71 | 0.245 | 2.74 | 1.66 | 0.5 | 0.306 | 0.0248 | 0.39 | 12.86 | 2.74 | 0.071 |
| 22C_13 | 1.4 | 292 | 4.18 | 2.05 | 24.38 | 9.54 | 112.68 | 0.282 | 3.25 | 1.94 | 0.51 | 0.185 | 0.0458 | 0.32 | 11.68 | 2.75 | 0.0383 |
| 22C_14 | 1.49 | 408.01 | 4.26 | 2.39 | 27.36 | 6.76 | 90.87 | 0.185 | 2.38 | 1.16 | 0.56 | 0.19 | 0.0219 | 0.36 | 13.64 | 2.43 | 0.0292 |
| 22C_15 | 1.21 | 298.86 | 3.96 | 3.54 | 26.94 | 5.05 | 83.71 | 0.19 | 2.22 | 1.18 | 1.23 | 0.135 | 0.0494 | 0.68 | 12.53 | 2.65 | 0.056 |
| 22C_2 | 1.38 | 538.91 | 6.02 | 5.29 | 26.9 | 20.63 | 162.27 | 0.323 | 4.27 | 2.21 | 1.96 | 0.149 | 0.0358 | 0.66 | 16.54 | 3.31 | 0.055 |
| 22C_3 | 1.54 | 414.92 | 4.29 | 5.18 | 26.15 | 7.54 | 109.68 | 0.5 | 4.68 | 3.6 | 0.78 | 0.182 | 0.155 | 0.46 | 19.29 | 3.32 | 0.121 |
| 22C_4 | 15.71 | 1815.76 | 9.16 | 13.28 | 33.88 | 36.78 | 422.01 | 2.27 | 29.51 | 54.11 | 4.33 | 0.318 | 2.35 | 0.96 | 15.67 | 2.27 | 0.109 |
| 22C_5 | 1.37 | 594.41 | 4.05 | 4.35 | 26.53 | 6.34 | 108.1 | 0.293 | 3.41 | 2.26 | 0.87 | 0.204 | 0.0485 | 0.46 | 14.46 | 2.93 | 0.0429 |
| 22C_6 | 1.59 | 568.15 | 4.6 | 4.87 | 26.86 | 12.28 | 121.25 | 0.412 | 4.89 | 4.75 | 1.25 | 0.143 | 0.068 | 0.52 | 18.84 | 3.91 | 0.0452 |
| 22C_7 | 1.06 | 361.35 | 3.78 | 2.71 | 25.68 | 7.67 | 87.52 | 0.314 | 3.06 | 1.28 | 0.83 | 0.063 | 0.0251 | 0.48 | 13.07 | 2.57 | 0.033 |
| 22C_8 | 1.36 | 509.25 | 3.73 | 6.14 | 28.65 | 12.31 | 128.93 | 0.368 | 6.16 | 3.73 | 1.09 | 0.152 | 0.067 | 0.53 | 15.89 | 3.5 | 0.047 |
| 22C_9 | 1.5 | 489.11 | 4.33 | 2.61 | 25.08 | 6.3 | 108.64 | 0.286 | 3.36 | 1.71 | 0.64 | 0.456 | 0.0394 | 0.33 | 15.19 | 4.23 | 0.064 |
| 21A.1 | 1.41 | 264.62 | 8.03 | 19.58 | 49.39 | 1.28 | 281.55 | 0.077 | 9.75 | 6.7 | 1.27 | 0.166 | 0.105 | 2.85 | 3.17 | 0.84 | 0.263 |
| 21A.2 | 1.13 | 297.05 | 7.61 | 33.54 | 49.2 | 2.42 | 356.9 | 0.078 | 8.32 | 7.02 | 1.19 | 0.245 | 0.104 | 1.64 | 1.24 | 0.54 | 0.226 |
| 21A.3 | 1.44 | 418.2 | 16.01 | 40.08 | 47.88 | 2.17 | 759.4 | 0.262 | 11.05 | 11.11 | 1.45 | 0.348 | 0.206 | 1.84 | 2.67 | 0.6 | 0.347 |
| 21A_1 | 10.75 | 992.6 | 13.72 | 73 | 47.64 | 5.22 | 905.31 | 0.24 | 14.13 | 13.97 | 2.55 | 0.468 | 0.141 | 3.01 | 4.42 | 2.12 | 0.675 |
| 21A_10 | 0.71 | 429.09 | 12.68 | 35.02 | 35.29 | 1.05 | 458.14 | 0.163 | 5.98 | 11.35 | 0.67 | 0.163 | 0.039 | 0.88 | 1.16 | 0.5 | 0.279 |
| 21A_11 | 1.66 | 493.64 | 23.65 | 261.82 | 47.44 | 5.17 | 3404.22 | 0.301 | 21.78 | 25.27 | 3.51 | 4.59 | 0.29 | 8.12 | 1.69 | 4.21 | 2.44 |
| 21A_12 | 1.14 | 358.49 | 18.08 | 34.68 | 49.18 | 3.42 | 606.57 | 0.02015 | 15.55 | 9.93 | 1.61 | 0.345 | 0.108 | 1.78 | 2.19 | 1.08 | 0.373 |
| 21A_13 | 2.6 | 1013.38 | 12.83 | 75.61 | 59.18 | 2.59 | 325.16 | 0.122 | 5.99 | 7.33 | 2.6 | 0.223 | 0.0594 | 1.11 | 1.58 | 0.72 | 0.202 |
| 21A_14 | 1.51 | 396.71 | 15.19 | 34.01 | 41.19 | 2.41 | 866.28 | 0.158 | 9.2 | 15.82 | 1.04 | 0.293 | 0.0607 | 1.37 | 1.29 | 0.77 | 0.41 |

| | | | | | | | | | | | | | | | | | |
|---|---|---|---|---|---|---|---|---|---|---|---|---|---|---|---|---|---|
| 21A_15 | 0.86 | 364.13 | 11 | 39.45 | 38.67 | 2.35 | 463.94 | 0.02015 | 8.21 | 7.83 | 1.17 | 0.303 | 0.066 | 1.36 | 1.45 | 0.86 | 0.25 |
| 21A_2 | 1.07 | 416.81 | 9.04 | 23.99 | 35.77 | 0.91 | 389.19 | 0.107 | 7.6 | 9.86 | 1.02 | 0.1267 | 0.0513 | 1.25 | 1.09 | 0.84 | 0.229 |
| 21A_3 | 1.5 | 398.86 | 14.75 | 37.59 | 42.68 | 3.6 | 678.07 | 0.202 | 14.05 | 8.59 | 2.99 | 0.356 | 0.224 | 3.04 | 2.78 | 1.74 | 0.436 |
| 21A_4 | 2.64 | 341.82 | 13.79 | 34 | 50.49 | 1.98 | 299.9 | 0.02015 | 6.98 | 4.64 | 4.8 | 0.202 | 0.72 | 2.39 | 1.51 | 1.14 | 0.258 |
| 21A_5 | 3.68 | 3279.83 | 26.05 | 413.3 | 55.73 | 11.95 | 5443.82 | 0.65 | 61.34 | 318.86 | 5.42 | 0.79 | 0.178 | 1.32 | 2.38 | 1.04 | 2.64 |
| 21A_6 | 2.67 | 498.68 | 15.81 | 83.5 | 42.8 | 4.72 | 1542.15 | 0.47 | 19.28 | 17.61 | 4.28 | 0.64 | 0.456 | 3.44 | 2.58 | 1.98 | 0.791 |
| 21A_7 | 1.11 | 222.53 | 12.69 | 17.91 | 38.41 | 2.4 | 453.91 | 0.02015 | 7.61 | 7.95 | 3.29 | 0.241 | 0.093 | 3.51 | 1.02 | 2.45 | 0.227 |
| 21A_8 | 0.89 | 312.58 | 14.17 | 32.96 | 37.65 | 2.3 | 405.28 | 0.172 | 7.4 | 11.4 | 1.21 | 0.264 | 0.077 | 1.54 | 1.24 | 0.83 | 0.375 |
| 21A_9 | 4.14 | 225.13 | 13.74 | 17.73 | 39.92 | 1.4 | 340.71 | 0.282 | 8.24 | 5.59 | 1.1 | 0.227 | 0.067 | 1.53 | 2.41 | 0.82 | 0.273 |
| 22A.1 | 1.38 | 2.09 | 2.51 | 0.0393 | 37.44 | 0.072 | 6.09 | 0.08 | 0.106 | 0.0445 | 0.0078 | 0.18 | 0.0476 | 0.0362 | 0.0115 | 0.035 | 0.00073 |
| 22A.2 | 6.08 | 16.8 | 7.01 | 1.32 | 32.5 | 0.63 | 13.73 | 0.02015 | 0.41 | 0.0445 | 0.117 | 0.162 | 0.356 | 0.363 | 0.647 | 0.214 | 0.0329 |
| 22A.3 | 3.48 | 6.21 | 7.06 | 0.731 | 33.56 | 0.69 | 5.44 | 0.05 | 0.119 | 0.0445 | 0.0142 | 0.466 | 0.135 | 0.227 | 0.043 | 0.0481 | 0.0065 |
| 22A_1 | 7.95 | 294.37 | 3.3 | 10.63 | 21.65 | 13.22 | 280.99 | 0.73 | 3.25 | 14.7 | 0.4 | 0.112 | 0.072 | 0.12 | 0.135 | 3.31 | 0.041 |
| 22A_10 | 1.06 | 2.25 | 3.29 | 0.147 | 22.93 | 0.205 | 4.08 | 0.02015 | 0.11 | 0.181 | 0.017 | 0.153 | 0.05 | 0.074 | 0.049 | 0.043 | 0.00171 |
| 22A_11 | 3.51 | 39.3 | 7.06 | 1.58 | 24.23 | 2.27 | 32.15 | 0.086 | 0.85 | 0.52 | 0.17 | 0.35 | 0.24 | 0.48 | 63.09 | 2.73 | 0.229 |
| 22A_12 | 34.44 | 39.53 | 16.78 | 0.64 | 21.75 | 0.98 | 78.71 | 0.071 | 1.11 | 0.57 | 0.107 | 0.35 | 0.34 | 0.31 | 0.68 | 0.32 | 0.0197 |
| 22A_13 | 4.15 | 25.14 | 5.78 | 0.81 | 22.11 | 1.26 | 23.63 | 0.111 | 0.72 | 0.68 | 0.069 | 0.3 | 0.119 | 0.139 | 0.66 | 0.35 | 0.0124 |
| 22A_14 | 4.82 | 16.91 | 3.74 | 0.228 | 23.83 | 0.48 | 17.77 | 0.145 | 0.35 | 0.4 | 0.026 | 0.49 | 0.38 | 0.062 | 0.238 | 0.13 | 0.0075 |
| 22A_15 | 7.28 | 58.24 | 6.31 | 0.72 | 21.95 | 0.74 | 14.99 | 0.15 | 0.62 | 0.23 | 0.106 | 0.28 | 0.31 | 0.19 | 0.87 | 0.54 | 0.0227 |
| 22A_2 | 4.78 | 66.1 | 3.2 | 1.78 | 21.34 | 1.22 | 24.56 | 0.092 | 1.39 | 0.47 | 0.13 | 0.25 | 0.21 | 0.106 | 0.36 | 0.67 | 0.037 |
| 22A_3 | 6.48 | 15.49 | 5.92 | 0.83 | 21.35 | 1.18 | 30.53 | 0.081 | 1.19 | 0.42 | 0.064 | 0.64 | 0.22 | 0.126 | 0.222 | 0.28 | 0.255 |
| 22A_4 | 3.53 | 17.7 | 7.21 | 0.67 | 21.88 | 3.25 | 17.82 | 2.96 | 0.83 | 0.49 | 0.102 | 0.22 | 0.25 | 0.101 | 1.03 | 0.26 | 0.0261 |
| 22A_5 | 1.47 | 4.75 | 2.74 | 0.6 | 20.89 | 0.171 | 5.63 | 0.065 | 0.259 | 0.24 | 0.031 | 0.26 | 0.073 | 0.091 | 0.323 | 0.099 | 0.0059 |
| 22A_6 | 4.81 | 17.47 | 5.19 | 0.67 | 24.06 | 0.57 | 14.12 | 0.02015 | 0.57 | 0.38 | 0.089 | 0.22 | 0.36 | 0.119 | 0.251 | 0.24 | 0.0108 |
| 22A_7 | 2.3 | 7.1 | 3.93 | 1.48 | 21.8 | 1.42 | 10.76 | 0.02015 | 0.147 | 0.115 | 0.2 | 0.32 | 0.076 | 0.22 | 0.48 | 85.58 | 0.62 |
| 22A_8 | 4.24 | 12.54 | 4.9 | 0.243 | 20.28 | 0.76 | 10.49 | 0.02015 | 0.48 | 0.3 | 0.05 | 0.27 | 0.164 | 0.103 | 1.24 | 1.42 | 0.0186 |
| 22A_9 | 1.73 | 5.23 | 2.15 | 0.19 | 21.14 | 0.072 | 5.84 | 0.02015 | 0.164 | 0.0445 | 0.0096 | 0.155 | 0.05 | 0.034 | 0.167 | 0.17 | 0.00205 |
| 4A.1 | 52.2 | 1262.54 | 75.07 | 16.89 | 55.43 | 49.83 | 693.45 | 3.92 | 6.69 | 16.11 | 6.18 | 52.74 | 9.12 | 17.99 | 13.3 | 3.83 | 0.483 |
| 4A.2 | 94.91 | 1916.52 | 59.98 | 24.26 | 53.01 | 105.89 | 1255.65 | 3.21 | 12.37 | 21.62 | 10.55 | 45.7 | 16.37 | 18.59 | 24.66 | 4.88 | 0.653 |
| 4A.3 | 31.12 | 1240.54 | 58.86 | 13.97 | 54.41 | 32.51 | 459.16 | 4.54 | 6.85 | 13.3 | 6.26 | 35.68 | 13.78 | 14.73 | 16.96 | 4.46 | 0.666 |

L

| | | | | | | | | | | | | | | | | | |
|---|---|---|---|---|---|---|---|---|---|---|---|---|---|---|---|---|---|
| 4A_1 | 43.66 | 1177.8 | 65.52 | 14.24 | 28.57 | 66.82 | 481.71 | 3.05 | 45.33 | 15.59 | 8.14 | 40.08 | 18.63 | 16.99 | 89.5 | 7.56 | 0.79 |
| 4A_10 | 31.25 | 831.64 | 40.62 | 15.91 | 26.97 | 27.64 | 464.36 | 2.07 | 20.77 | 11.36 | 5.24 | 37.04 | 11.12 | 15.55 | 21.27 | 5.73 | 0.62 |
| 4A_11 | 40.87 | 926.7 | 31.85 | 15.66 | 26.48 | 29.38 | 431.58 | 1.76 | 8.16 | 15.93 | 5.97 | 27.66 | 16.62 | 11.35 | 89.77 | 7.08 | 1.18 |
| 4A_12 | 32.56 | 966.34 | 36.42 | 21.25 | 31.6 | 40.67 | 431.96 | 2.05 | 5.66 | 14.4 | 9.3 | 29.84 | 20.25 | 13.18 | 43.82 | 3.4 | 0.58 |
| 4A_13 | 34.07 | 938.45 | 43.97 | 13.14 | 25.95 | 41.23 | 574.05 | 2.4 | 9.97 | 14.82 | 5.6 | 53.33 | 13.3 | 14.71 | 11.87 | 3.94 | 0.379 |
| 4A_14 | 27.02 | 996.68 | 41.18 | 18.66 | 28.75 | 22.86 | 340.41 | 2.55 | 7.11 | 16.93 | 7.03 | 32.01 | 15.58 | 25.46 | 35.91 | 3.63 | 0.63 |
| 4A_15 | 19.45 | 540.72 | 40.45 | 8.47 | 25.73 | 41.47 | 329.77 | 2.78 | 9.22 | 13.7 | 3.14 | 31.91 | 5.94 | 9.11 | 21.54 | 6.93 | 0.56 |
| 4A_2 | 41.15 | 935.74 | 47.29 | 17.02 | 27.06 | 58.14 | 560.24 | 2.88 | 10.83 | 19.79 | 6.7 | 33.13 | 12.18 | 15.49 | 30.33 | 4.03 | 0.59 |
| 4A_3 | 91.78 | 1070.35 | 81.23 | 13.96 | 25.14 | 62.89 | 877.56 | 3.11 | 6.78 | 21.63 | 6.43 | 37.27 | 11.34 | 16.24 | 11.88 | 3.29 | 0.338 |
| 4A_4 | 65.29 | 1314.83 | 69.59 | 31.46 | 31.89 | 58.14 | 1546.52 | 5.32 | 14.49 | 17.5 | 6.12 | 156.04 | 14.12 | 24.67 | 23 | 3.05 | 0.64 |
| 4A_5 | 26.49 | 987.97 | 52.78 | 28.38 | 24.61 | 28.18 | 386.78 | 2.18 | 7.13 | 16.99 | 7.4 | 36.4 | 16.44 | 17.22 | 17.53 | 5.54 | 0.65 |
| 4A_6 | 43.46 | 781.97 | 35.24 | 14.6 | 28.52 | 39.08 | 512.23 | 2.65 | 6.57 | 18.24 | 4.93 | 28.64 | 11.48 | 11.91 | 22.22 | 3.85 | 0.54 |
| 4A_7 | 33.69 | 966.17 | 53.03 | 28.54 | 26.89 | 28.06 | 378.35 | 2.67 | 6.9 | 16.03 | 5.59 | 59.14 | 12.37 | 17.27 | 16.02 | 10.71 | 0.55 |
| 4A_8 | 71.65 | 2118.14 | 50.5 | 20.46 | 26.28 | 55.99 | 590.2 | 2.64 | 9.45 | 15.69 | 28.09 | 39.63 | 58.39 | 31.81 | 14.46 | 57.26 | 0.458 |
| 4A_9 | 25.56 | 809.09 | 54.02 | 17.81 | 33.52 | 49.47 | 3411.1 | 2.65 | 6.87 | 11.02 | 6.98 | 26.93 | 11.37 | 16.58 | 11.48 | 4.74 | 0.402 |
| 6B.1 | 1.7 | 1.35 | 15.22 | 0.0569 | 46.01 | 0.71 | 13.18 | 0.161 | 0.071 | 0.0445 | 0.011 | 0.13 | 0.00605 | 0.282 | 1.16 | 0.291 | 0.0097 |
| 6B.2 | 1.31 | 2.42 | 15.43 | 0.0469 | 43.01 | 0.79 | 0.88 | 0.1255 | 0.0405 | 0.0445 | 0.0411 | 0.136 | 0.104 | 0.239 | 1.007 | 0.124 | 0.0181 |
| 6B.3 | 3.06 | 2.42 | 16.22 | 0.137 | 48 | 0.287 | 64.53 | 0.09 | 0.09 | 0.209 | 0.054 | 0.259 | 0.116 | 0.46 | 2.99 | 1.08 | 0.027 |
| 6B_1 | 0.43 | 0.172 | 2.01 | 0.0161 | 20.62 | 0.072 | 38.87 | 0.02015 | 0.051 | 0.209 | 0.0085 | 0.067 | 0.00605 | 0.062 | 0.083 | 0.103 | 0.00118 |
| 6B_10 | 2.81 | 2.26 | 21.83 | 0.127 | 30.66 | 0.89 | 35 | 0.132 | 0.53 | 0.26 | 0.043 | 0.137 | 0.126 | 0.42 | 3.84 | 0.72 | 0.0198 |
| 6B_11 | 2.79 | 3.42 | 17.3 | 0.174 | 37.16 | 0.95 | 43.63 | 0.156 | 0.98 | 0.318 | 0.079 | 0.9 | 0.124 | 0.49 | 3.44 | 1.14 | 0.027 |
| 6B_12 | 1.69 | 2.01 | 12.61 | 0.093 | 27.38 | 0.443 | 31.73 | 0.091 | 0.38 | 0.248 | 0.027 | 0.147 | 0.043 | 0.27 | 1.41 | 1 | 0.0144 |
| 6B_13 | 3.5 | 5.63 | 20.75 | 0.248 | 24.78 | 0.89 | 52.58 | 0.133 | 0.37 | 0.88 | 0.033 | 0.161 | 0.046 | 0.76 | 1.12 | 1.03 | 0.0168 |
| 6B_14 | 2.03 | 3.18 | 14.34 | 0.129 | 29.14 | 0.443 | 27.39 | 0.126 | 0.31 | 0.313 | 0.033 | 0.119 | 0.061 | 0.38 | 2.15 | 3.25 | 0.0201 |
| 6B_15 | 2.34 | 3.01 | 14.48 | 0.147 | 32.24 | 0.83 | 44.88 | 0.157 | 0.296 | 0.316 | 0.04 | 0.151 | 0.054 | 0.38 | 2.36 | 0.9 | 0.0152 |
| 6B_2 | 1.8 | 2.02 | 11.1 | 0.167 | 30.79 | 0.83 | 27.77 | 0.077 | 0.39 | 0.182 | 0.106 | 0.159 | 0.082 | 0.31 | 1.77 | 0.29 | 0.0144 |
| 6B_3 | 3.25 | 1.62 | 16.72 | 0.114 | 29.27 | 0.89 | 29.59 | 0.139 | 0.39 | 0.345 | 0.023 | 0.28 | 0.078 | 0.51 | 1.39 | 0.88 | 0.0127 |
| 6B_4 | 233.33 | 3 | 184.5 | 1 | 25 | 30 | 179 | 7 | 8 | 92.05 | 8.75 | 111.31 | 20.43 | 1.31 | 1.15 | 0.7 | 0.0114 |
| 6B_5 | 2.5 | 3.06 | 13.18 | 0.166 | 13.795 | 0.56 | 22.23 | 0.107 | 0.36 | 0.191 | 0.026 | 0.21 | 0.0368 | 0.66 | 1.07 | 0.52 | 0.0101 |
| 6B_6 | 5.44 | 2.51 | 19.77 | 1.25 | 32.09 | 2.59 | 729.3 | 0.56 | 0.51 | 0.49 | 0.135 | 0.79 | 0.076 | 1.24 | 2.78 | 1.05 | 0.186 |

LI

| | | | | | | | | | | | | | | | | | |
|---|---|---|---|---|---|---|---|---|---|---|---|---|---|---|---|---|---|
| 6B_7 | 1.68 | 4.32 | 13.77 | 0.69 | 24.35 | 0.61 | 55.48 | 0.049 | 0.186 | 0.325 | 0.066 | 0.176 | 0.082 | 0.4 | 0.78 | 0.56 | 0.0216 |
| 6B_8 | 2.17 | 3.66 | 12.5 | 0.142 | 35.25 | 0.58 | 52.48 | 0.181 | 0.211 | 0.315 | 0.048 | 0.198 | 0.063 | 0.35 | 6.12 | 1.35 | 0.047 |
| 6B_9 | 2.77 | 5.15 | 14.15 | 0.104 | 31.45 | 0.072 | 43.77 | 0.02015 | 0.57 | 0.85 | 0.129 | 0.252 | 0.167 | 0.49 | 4.99 | 1.29 | 0.0293 |
| 7B.1 | 17.59 | 103.45 | 27.76 | 13.5 | 44.25 | 5.64 | 148.1 | 0.49 | 2.2 | 7.56 | 0.83 | 0.398 | 0.54 | 1.01 | 0.899 | 0.84 | 0.448 |
| 7B.2 | 44.39 | 2318.03 | 1664.82 | 410.02 | 49.32 | 150.08 | 734.84 | 5.08 | 10.68 | 42.35 | 9.3 | 0.8 | 5.92 | 3.96 | 4.15 | 2.06 | 1.27 |
| 7B.3 | 34.37 | 461.03 | 424.87 | 120.4 | 64.69 | 23.27 | 349.98 | 1.97 | 7.89 | 20.7 | 2.76 | 0.62 | 2.4 | 4.37 | 1.58 | 1.39 | 0.98 |
| 7B_1 | 37.7 | 244.84 | 70.73 | 39.11 | 30.74 | 30.39 | 464.81 | 2.69 | 7.49 | 21.87 | 1.8 | 0.268 | 1.45 | 2.04 | 1.99 | 2.04 | 0.908 |
| 7B_10 | 31.73 | 270.34 | 48.81 | 22.59 | 30.84 | 12.41 | 383.76 | 1.93 | 6.27 | 26.93 | 1.59 | 0.619 | 1.54 | 1.6 | 1.61 | 1.81 | 0.766 |
| 7B_11 | 26.98 | 221.54 | 88.18 | 26.99 | 30.77 | 12.74 | 433.95 | 1.23 | 3.76 | 19.24 | 1.84 | 0.811 | 2.34 | 4.16 | 1.02 | 1.61 | 1.16 |
| 7B_12 | 33.62 | 272.52 | 56.04 | 29.85 | 33.57 | 18.49 | 340.38 | 2.7 | 5.87 | 18.4 | 2.19 | 0.359 | 2.77 | 2.29 | 1.19 | 1.97 | 0.991 |
| 7B_13 | 37.9 | 791.53 | 696.05 | 57.61 | 36.8 | 88.21 | 404.08 | 9.63 | 7.14 | 21.86 | 2.68 | 0.556 | 1.68 | 4.55 | 2.14 | 3.1 | 1.28 |
| 7B_14 | 26.35 | 244.75 | 53.69 | 21.98 | 31.75 | 12.37 | 262.94 | 1.39 | 4.01 | 14.76 | 1.82 | 0.353 | 1.37 | 3.54 | 1.62 | 2.04 | 1.57 |
| 7B_15 | 24.68 | 216.68 | 49.05 | 22.26 | 33.85 | 12.97 | 342.54 | 5.61 | 5.5 | 16.08 | 1.43 | 0.486 | 1.2 | 1.83 | 1.34 | 1.44 | 0.865 |
| 7B_2 | 19.87 | 129.33 | 42.95 | 17.29 | 31.49 | 10.07 | 188.46 | 1.07 | 9.6 | 11.34 | 1.19 | 0.682 | 1.15 | 1.42 | 0.846 | 1.11 | 0.451 |
| 7B_3 | 39.9 | 742.44 | 378.82 | 32 | 33.45 | 22.26 | 495.34 | 1.82 | 5.55 | 14.49 | 3.24 | 0.403 | 2.68 | 3.94 | 1.74 | 1.9 | 1.059 |
| 7B_4 | 33.63 | 435.4 | 98.62 | 34.17 | 36.05 | 17.91 | 779.14 | 2.81 | 10.97 | 22.95 | 3.37 | 0.497 | 3.21 | 4.27 | 1.68 | 2.37 | 1.33 |
| 7B_5 | 40.68 | 397.49 | 63.86 | 51.83 | 34.54 | 12.81 | 467.37 | 1.61 | 6.75 | 21.85 | 2.72 | 0.538 | 5.9 | 2.47 | 1.51 | 2.88 | 0.782 |
| 7B_6 | 32.7 | 268.86 | 66.8 | 28.6 | 34.16 | 11.92 | 285.95 | 1.8 | 5.34 | 16.85 | 1.57 | 0.334 | 1.73 | 2.13 | 1.32 | 1.54 | 0.727 |
| 7B_7 | 36.81 | 377.89 | 70.21 | 24.43 | 32.28 | 14.29 | 414.06 | 1.9 | 7.08 | 15.38 | 2.22 | 0.403 | 1.93 | 3.41 | 1.33 | 2.06 | 0.881 |
| 7B_8 | 30.45 | 372.18 | 73.74 | 22.07 | 33.58 | 14.19 | 743.93 | 4.13 | 7.23 | 13.91 | 2 | 0.45 | 2.12 | 3.81 | 1.92 | 2.42 | 0.99 |
| 7B_9 | 23.57 | 268.77 | 52.3 | 43.34 | 32.05 | 8.14 | 246.73 | 1.51 | 3.92 | 15.76 | 1.79 | 0.299 | 2.31 | 1.72 | 1.09 | 1.44 | 0.596 |
| 13B.2 | 14.18 | 56.24 | 15.42 | 3.15 | 52.53 | 12.43 | 201.68 | 0.98 | 11.39 | 0.566 | 0.19 | 0.0676 | 1.17 | 0.24 | 0.1684 | 0.098 | 0.0512 |
| 13B.2 | 1140.9 | 1526.37 | 39.71 | 245.65 | 91.39 | 423.51 | 6383.36 | 19.78 | 13.33 | 9.25 | 6.56 | 0.346 | 58.67 | 2.2 | 7.82 | 0.83 | 0.96 |
| 13B.3 | 6.9 | 17.56 | 10.08 | 1.545 | 47.75 | 2.3 | 32.76 | 0.08 | 0.075 | 0.572 | 0.0586 | 0.01915 | 0.313 | 0.0715 | 0.0594 | 0.341 | 0.0141 |
| 13B.3 | 43.9 | 117.01 | 21.51 | 10.71 | 45.67 | 25.84 | 401.45 | 0.307 | 14.68 | 1.12 | 0.62 | 0.119 | 1.71 | 0.62 | 0.437 | 14.71 | 0.348 |
| 13B_1 | 104.92 | 378.51 | 565.83 | 20.29 | 26.53 | 40.71 | 350.8 | 0.51 | 9.4 | 1.41 | 1.16 | 0.094 | 4.51 | 1.05 | 1.08 | 0.73 | 0.114 |
| 13B_10 | 102.65 | 420.37 | 44.68 | 21.91 | 26.04 | 39.98 | 553.15 | 0.89 | 37.04 | 1.81 | 1.08 | 0.145 | 4.83 | 1.29 | 0.44 | 0.36 | 0.103 |
| 13B_11 | 2083.59 | 3756.41 | 47.67 | 767.96 | 206.75 | 851.84 | 3408.77 | 1.45 | 24.48 | 17.22 | 12.34 | 0.72 | 89.31 | 1.26 | 1.03 | 2 | 0.43 |
| 13B_12 | 50.92 | 977.57 | 552.45 | 10.9 | 28.16 | 30.15 | 29176.89 | 45.85 | 13.47 | 1.62 | 1.12 | 0.42 | 1.26 | 1.04 | 0.43 | 0.43 | 0.16 |
| 13B_13 | 49.55 | 147.07 | 13.12 | 11.13 | 26.18 | 21.89 | 369.98 | 0.62 | 70.91 | 1.26 | 0.42 | 0.128 | 1.81 | 0.29 | 0.66 | 0.55 | 0.084 |

| | | | | | | | | | | | | | | | | | |
|---|---|---|---|---|---|---|---|---|---|---|---|---|---|---|---|---|---|
| 13B_14 | 117.85 | 262.78 | 11.42 | 42.96 | 37.39 | 57.96 | 464.22 | 0.53 | 17.66 | 1.84 | 0.8 | 0.152 | 5.6 | 0.38 | 0.48 | 0.71 | 0.107 |
| 13B_15 | 57.85 | 449.08 | 26.57 | 13.24 | 26.7 | 23.84 | 328.91 | 0.41 | 19.24 | 1.1 | 1.54 | 0.134 | 3.44 | 1.26 | 0.5 | 0.4 | 0.097 |
| 13B_2 | 66.14 | 301.79 | 18.22 | 13.48 | 24.91 | 23.75 | 403.32 | 0.64 | 52.38 | 1.9 | 1.43 | 0.134 | 3.19 | 0.9 | 0.68 | 0.57 | 0.138 |
| 13B_3 | 101.18 | 308.26 | 13.64 | 14.54 | 25.61 | 33.68 | 325.82 | 0.36 | 71.62 | 1.74 | 0.97 | 0.112 | 3.23 | 0.62 | 0.41 | 0.14 | 0.094 |
| 13B_4 | 52.16 | 178.64 | 14.63 | 16.23 | 24.23 | 21.6 | 766.25 | 0.97 | 16.34 | 2.1 | 0.54 | 0.192 | 3.15 | 0.4 | 0.4 | 1.5 | 0.5 |
| 13B_5 | 278.48 | 3865.08 | 215.95 | 36.36 | 32.28 | 95.99 | 88943.11 | 160.77 | 88.33 | 7.79 | 12.4 | 2.24 | 19.28 | 25.67 | 1.15 | 1.88 | 0.55 |
| 13B_6 | 111.55 | 359.74 | 25.89 | 28.27 | 29.74 | 58.58 | 4156.05 | 16.71 | 73.7 | 6.5 | 1.99 | 0.2 | 5.91 | 1.14 | 0.5 | 0.85 | 0.7 |
| 13B_7 | 151.8 | 427.62 | 78.67 | 60.11 | 40.54 | 58.86 | 515.1 | 1 | 5.76 | 2.16 | 1.5 | 0.181 | 6.88 | 0.98 | 3.16 | 1.56 | 0.59 |
| 13B_8 | 62.56 | 238.43 | 13.36 | 19.81 | 25.36 | 23.85 | 341.66 | 0.61 | 10.7 | 1.23 | 0.88 | 0.138 | 2.96 | 0.4 | 0.8 | 0.26 | 0.189 |
| 13B_9 | 212.7 | 479.08 | 15.01 | 34.32 | 33.33 | 93.62 | 1004.02 | 1.6 | 34.58 | 1.95 | 1.27 | 0.127 | 5.06 | 0.68 | 0.65 | 5.62 | 0.288 |
| 14b.1 | 71.3 | 144.19 | 84.28 | 31.4 | 63.41 | 133.67 | 770.7025 | 14.72 | 17.99 | 231.1 | 0.167 | 0.67 | 10.95 | 0.1 | 0.17 | 2.8375 | 0.56 |
| 14b.2 | 57.93 | 116.27 | 5.5 | 21.99 | 63.18 | 17.4 | 712.373125 | 2.51 | 3 | 5.84 | 0.52 | 0.067 | 3.59 | 0.22 | 0.0166 | 0.055 | 0.21 |
| 14b.3 | 51.92 | 138.66 | 20.94 | 23.95 | 74.2 | 18.43 | 697.7907813 | 3 | 4.35 | 4.07 | 0.0615 | 0.413 | 1.86 | 0.35 | 0.0354 | 0.027 | 0.131 |
| 14b.4 | 254.66 | 792.16 | 5.5 | 104.29 | 90.58 | 175.51 | 694.1451953 | 1.5 | 4.865 | 0.5 | 5.29 | 0.52 | 39.34 | 3.12 | 2.33 | 0.0225 | 0.119 |
| 14B_1 | 156.07 | 471.55 | 24.7 | 65.15 | 39.31 | 34.22 | 610.58 | 0.49 | 5.38 | 10.49 | 2.62 | 0.89 | 24.34 | 1.2 | 0.59 | 0.386 | 0.117 |
| 14B_2 | 211.41 | 917.77 | 44.2 | 97.69 | 56.8 | 56.8 | 733.27 | 0.393 | 17.57 | 8.6 | 3.63 | 0.617 | 29.38 | 5.08 | 1.36 | 0.216 | 0.068 |
| 14B_3 | 268.47 | 538.99 | 13.59 | 116.76 | 94.35 | 61.76 | 734.94 | 0.276 | 8.04 | 7.73 | 2.8 | 0.432 | 29.87 | 0.48 | 0.8 | 0.148 | 0.078 |
| 14B_4 | 1026.23 | 1715.59 | 39.97 | 427.13 | 163.67 | 276.37 | 2602.74 | 1 | 9.08 | 14.83 | 11.12 | 0.488 | 102.99 | 3.21 | 1.08 | 0.214 | 0.0449 |
| 14B_5 | 136.8 | 543.98 | 16.6 | 63.3 | 39.52 | 35.46 | 375.48 | 0.234 | 7.56 | 8.12 | 2.99 | 0.298 | 21.02 | 1.05 | 0.412 | 0.098 | 0.139 |
| 14B_6 | 46.38 | 1142.59 | 49.91 | 16.08 | 29.09 | 10.05 | 277.63 | 0.197 | 7.92 | 4.56 | 4.21 | 0.269 | 20.69 | 7.11 | 0.95 | 0.142 | 0.0544 |
| 14B_7 | 118.15 | 231.13 | 7.32 | 49.4 | 33.36 | 29.12 | 339.34 | 0.137 | 4.25 | 5.85 | 1.25 | 0.332 | 13.08 | 0.099 | 0.063 | 0.045 | 0.096 |
| 21D.1 | 2.46 | 261.68 | 3.36 | 9.82 | 37.59 | 27.11 | 124.5 | 0.58 | 2.32 | 2.33 | 0.424 | 0.186 | 0.0481 | 0.063 | 0.1258 | 1.52 | 0.149 |
| 21D.2 | 4.03 | 229.26 | 3.15 | 13.62 | 35.41 | 20.59 | 193.42 | 0.395 | 6.41 | 8.26 | 0.547 | 0.452 | 0.067 | 0.101 | 0.0447 | 2.75 | 0.208 |
| 21D.3 | 1.92 | 124.25 | 2.3 | 5.61 | 37.46 | 17.97 | 69.38 | 0.6 | 1.41 | 2.89 | 0.325 | 0.392 | 0.121 | 0.055 | 0.0139 | 2.76 | 0.0699 |
| 21D_1 | 3.5 | 452.47 | 2.65 | 36.75 | 23.06 | 12.06 | 230.88 | 0.48 | 10.46 | 6.35 | 0.54 | 0.42 | 0.176 | 0.107 | 0.0366 | 2.3 | 0.253 |
| 21D_10 | 0.71 | 56.75 | 2.31 | 4.92 | 22.97 | 4.91 | 49.11 | 0.228 | 1.43 | 1.32 | 0.28 | 0.21 | 0.0145 | 0.112 | 0.017 | 1.88 | 0.061 |
| 21D_11 | 3.5 | 536.74 | 1.78 | 4.25 | 21.26 | 11.93 | 104.59 | 0.68 | 7.57 | 16.42 | 1.3 | 0.174 | 0.055 | 0.049 | 0.0201 | 1.37 | 0.089 |
| 21D_12 | 0.65 | 43.53 | 2.56 | 5.22 | 21.36 | 10.67 | 49.33 | 0.39 | 1.18 | 1.4 | 0.1 | 0.32 | 0.00605 | 0.019 | 0.0298 | 2.82 | 0.059 |
| 21D_13 | 5.21 | 1043.44 | 4.54 | 16.59 | 21.78 | 36.6 | 251.39 | 1.53 | 11.15 | 26.87 | 0.95 | 0.65 | 0.181 | 0.142 | 0.095 | 3.8 | 0.18 |
| 21D_14 | 1.16 | 130.14 | 2.82 | 31.64 | 22.39 | 280.94 | 234.47 | 5.08 | 16.22 | 10.55 | 0.32 | 0.81 | 0.062 | 0.026 | 0.0289 | 2.6 | 0.226 |

| | | | | | | | | | | | | | | | | | |
|---|---|---|---|---|---|---|---|---|---|---|---|---|---|---|---|---|---|
| 21D_15 | 1.77 | 146.38 | 3.42 | 60.88 | 22.21 | 36.78 | 258.88 | 1.45 | 6.8 | 6.74 | 0.36 | 0.83 | 0.044 | 0.044 | 0.113 | 3.64 | 0.188 |
| 21D_2 | 0.6 | 63.01 | 2.62 | 5.53 | 21.3 | 4.7 | 106.66 | 0.144 | 1.18 | 1.57 | 0.23 | 0.161 | 0.00605 | 0.052 | 0.078 | 1.22 | 0.087 |
| 21D_3 | 5.23 | 369.88 | 2.39 | 20.83 | 21.72 | 20.14 | 247.69 | 0.77 | 7.2 | 8.87 | 0.58 | 0.51 | 0.54 | 0.047 | 0.05 | 4.42 | 0.154 |
| 21D_4 | 9.75 | 720.23 | 6.56 | 23.62 | 21.84 | 20.83 | 144.69 | 1.34 | 7.5 | 11.6 | 0.98 | 0.3 | 0.47 | 0.089 | 0.093 | 2.14 | 0.108 |
| 21D_5 | 1.14 | 160.25 | 2.57 | 6.91 | 22.77 | 5.5 | 64.45 | 0.223 | 2.39 | 1.96 | 0.18 | 0.31 | 0.079 | 0.033 | 0.033 | 1.28 | 0.067 |
| 21D_6 | 6.13 | 589.9 | 3.32 | 128.98 | 48.59 | 55.27 | 187.14 | 1.86 | 15.82 | 8.06 | 1.26 | 0.3 | 0.84 | 0.1 | 0.0069 | 4.43 | 0.05 |
| 21D_7 | 0.57 | 44.91 | 2.63 | 7.59 | 23.85 | 2.15 | 11.65 | 0.062 | 0.93 | 0.35 | 0.068 | 0.186 | 0.089 | 0.0097 | 0.00215 | 0.27 | 0.0061 |
| 21D_8 | 1.1 | 92.77 | 2.69 | 12.54 | 23.07 | 25.48 | 107.9 | 1 | 2.99 | 2.5 | 0.26 | 0.68 | 0.136 | 0.068 | 0.0258 | 2.5 | 0.104 |
| 21D_9 | 2.1 | 284.56 | 2.87 | 14.37 | 22.26 | 17.61 | 169.63 | 0.61 | 3.67 | 3.94 | 2.3 | 0.55 | 0.051 | 0.97 | 0.065 | 10.7 | 0.278 |
| 11B_1 | 0.465 | 105.12 | 2.52 | 2.37 | 26.36 | 0.93 | 168.15 | 0.6 | 3.09 | 5.97 | 0.86 | 1.54 | 0.166 | 0.038 | 0.97 | 1.09 | 0.1 |
| 11B.1 | 3.11 | 1260.59 | 20.06 | 10.25 | 59.93 | 2.47 | 274.89 | 0.657 | 5.5 | 2.15 | 3.13 | 1.29 | 0.43 | 0.704 | 2.56 | 2.43 | 0.174 |
| 11B.2 | 1.67 | 758.64 | 10.28 | 7.93 | 53.83 | 1.89 | 956.91 | 0.369 | 3.88 | 1.25 | 1.83 | 0.575 | 0.239 | 0.294 | 2.04 | 1.96 | 0.18 |
| 11B.3 | 1.43 | 1002.79 | 11.95 | 8.15 | 54.24 | 1.25 | 93.31 | 0.175 | 2.52 | 1.34 | 2.25 | 0.552 | 0.191 | 0.389 | 2.04 | 2.15 | 0.166 |
| 11B_10 | 6.6 | 1903.43 | 5.56 | 10.23 | 36.69 | 6.1 | 941.71 | 0.45 | 23.81 | 3.57 | 4.8 | 2.4 | 1.24 | 0.125 | 10.07 | 72.57 | 0.126 |
| 11B_11 | 1.66 | 1823.77 | 5.1 | 11.37 | 35.21 | 4.15 | 405.37 | 0.44 | 5.63 | 1.52 | 3.26 | 1.62 | 0.453 | 0.44 | 2.98 | 5.21 | 0.64 |
| 11B_12 | 2.01 | 799.69 | 6.2 | 8.96 | 34.59 | 4.24 | 1525.94 | 1.33 | 19.59 | 2.72 | 2.24 | 1.91 | 0.384 | 1.01 | 1.66 | 3.61 | 0.268 |
| 11B_13 | 7.51 | 7476.66 | 42.34 | 447.88 | 760.48 | 53.44 | 160912.98 | 100.8 | 1428.54 | 1047.3 | 99.54 | 233.01 | 1.88 | 35.53 | 166.31 | 132.83 | 15.56 |
| 11B_14 | 1.03 | 342.78 | 4.17 | 6.12 | 37.9 | 1.47 | 331.98 | 0.51 | 9.47 | 2.7 | 1.18 | 0.77 | 0.152 | 0.3 | 1.09 | 1.51 | 0.09 |
| 11B_15 | 1.32 | 586.96 | 3.86 | 5.67 | 30.26 | 2.1 | 139.1 | 0.172 | 1.64 | 0.82 | 1.69 | 0.54 | 0.193 | 0.71 | 3.83 | 27.14 | 0.083 |
| 11B_2 | 7.48 | 2895.34 | 14.26 | 27.14 | 58.68 | 4.07 | 648.25 | 1.37 | 12.55 | 6.33 | 10.73 | 1.74 | 0.7 | 0.85 | 9.03 | 6.01 | 0.229 |
| 11B_3 | 2.3 | 974.33 | 4.81 | 8.53 | 33.99 | 2.4 | 2010.75 | 0.432 | 3.53 | 1.72 | 2.31 | 0.8 | 0.68 | 0.83 | 1.61 | 1.68 | 0.106 |
| 11B_4 | 7.35 | 3634.23 | 6.59 | 41.02 | 61.77 | 8.05 | 336.96 | 0.56 | 7.35 | 4.65 | 8.06 | 1.3 | 1.96 | 1.89 | 6.97 | 8.5 | 0.277 |
| 11B_5 | 2.69 | 1237.14 | 5.84 | 58.51 | 45.54 | 1.41 | 194.14 | 0.46 | 3.94 | 2.34 | 3.01 | 1.01 | 0.351 | 0.58 | 2.13 | 2.39 | 0.136 |
| 11B_6 | 1.12 | 461.17 | 3.45 | 6.46 | 29.96 | 1.08 | 65.35 | 0.133 | 1.76 | 0.86 | 1.13 | 0.487 | 0.297 | 0.35 | 1.17 | 1.71 | 0.06 |
| 11B_7 | 1.5 | 845.36 | 4.46 | 20.99 | 49.85 | 2.9 | 4836.03 | 2.2 | 24.37 | 25.48 | 4.55 | 9.17 | 0.295 | 1.02 | 8.03 | 5.29 | 0.58 |
| 11B_8 | 5.46 | 5877.58 | 64.05 | 79.23 | 203.79 | 24.18 | 526.5 | 2.07 | 20.56 | 7.94 | 25.09 | 11.45 | 2.08 | 0.37 | 8.56 | 2.85 | 19.36 |
| 11B_9 | 6.56 | 275.3 | 6.89 | 117.09 | 103.66 | 3.98 | 571.75 | 1.02 | 20.03 | 2.21 | 4.16 | 6.45 | 2.08 | 0.41 | 45.35 | 4.69 | 2.86 |
| 22D_1 | 11.89 | 319.84 | 5.11 | 7.98 | 23.9 | 14.54 | 459.16 | 0.74 | 26.51 | 8.82 | 0.85 | 0.488 | 0.91 | 0.34 | 1.91 | 9.75 | 0.182 |
| 22D_10 | 15.99 | 701.81 | 13.81 | 10.63 | 24.1 | 19.4 | 413.34 | 0.89 | 4.6 | 5.57 | 1.61 | 0.416 | 3.97 | 0.9 | 1.7 | 122.11 | 0.221 |
| 22D_11 | 5.79 | 355.75 | 7.38 | 7.7 | 25.82 | 15.86 | 331.74 | 0.71 | 5.15 | 4.89 | 0.66 | 0.276 | 0.294 | 0.32 | 1.02 | 16.67 | 0.19 |

| | | | | | | | | | | | | | | | | | |
|---|---|---|---|---|---|---|---|---|---|---|---|---|---|---|---|---|---|
| 22D_12 | 6.23 | 257.1 | 8.51 | 5.46 | 24.31 | 13.02 | 312.39 | 0.61 | 10.18 | 8.88 | 0.53 | 0.296 | 0.51 | 0.37 | 0.55 | 10.07 | 0.183 |
| 22D_13 | 5.67 | 276.51 | 8.64 | 4.99 | 24.09 | 15.56 | 278.54 | 0.77 | 3.66 | 7.64 | 0.58 | 0.283 | 0.405 | 0.62 | 0.52 | 10.87 | 0.158 |
| 22D_14 | 3.77 | 207.4 | 6.99 | 4.05 | 24.41 | 80.18 | 258.25 | 1.4 | 2.62 | 6.94 | 0.53 | 0.257 | 0.268 | 0.39 | 0.344 | 7.32 | 0.136 |
| 22D_15 | 11.63 | 425.77 | 10.69 | 9.18 | 25.67 | 20.07 | 386.72 | 0.8 | 10.36 | 21.05 | 1.31 | 0.357 | 1.4 | 0.5 | 0.87 | 16.28 | 0.209 |
| 22D_2 | 19.41 | 449.13 | 7.36 | 12.63 | 24.54 | 22.71 | 601.42 | 1.24 | 10.86 | 7.58 | 1.35 | 0.485 | 2.62 | 0.4 | 26.21 | 11.56 | 0.7 |
| 22D_3 | 4.54 | 262.53 | 6.73 | 5.51 | 25.24 | 11.33 | 240.01 | 0.42 | 5.05 | 3.85 | 0.62 | 0.54 | 0.92 | 0.43 | 4.56 | 8.14 | 0.146 |
| 22D_4 | 8.43 | 266.93 | 10.18 | 5.69 | 23.24 | 9.3 | 223.34 | 0.46 | 5.02 | 4.74 | 0.56 | 0.272 | 0.35 | 0.231 | 0.367 | 5.92 | 0.151 |
| 22D_5 | 6.95 | 335.26 | 7.15 | 10.74 | 26.32 | 23.4 | 612.1 | 0.78 | 5.41 | 9.24 | 0.84 | 0.68 | 0.62 | 0.5 | 0.56 | 12.05 | 0.246 |
| 22D_6 | 8.59 | 325.75 | 9.55 | 8.41 | 25.68 | 15.65 | 428.41 | 0.82 | 10.8 | 5.04 | 0.83 | 0.411 | 0.69 | 0.49 | 0.77 | 19.5 | 0.242 |
| 22D_7 | 7.06 | 358.81 | 8.6 | 9.94 | 25.51 | 21.97 | 556.43 | 0.73 | 7.08 | 5.52 | 0.77 | 0.399 | 0.68 | 0.46 | 0.66 | 11.67 | 0.234 |
| 22D_8 | 9.38 | 401.37 | 10.07 | 5.51 | 26.59 | 14.51 | 298.95 | 0.63 | 6.51 | 7.19 | 1.15 | 0.42 | 2.08 | 0.64 | 0.61 | 8.76 | 0.173 |
| 22D_9 | 11.08 | 421.36 | 9.48 | 9.67 | 25.41 | 16.23 | 502.57 | 0.97 | 6.17 | 13.36 | 0.92 | 0.49 | 0.86 | 0.48 | 0.7 | 23.47 | 0.321 |
| 22D.1 | 3.47 | 218.8 | 7.05 | 8.09 | 35.5 | 10.48 | 355.05 | 0.87 | 5.56 | 2.39 | 0.52 | 0.412 | 0.59 | 0.25 | 0.367 | 5.26 | 0.249 |
| 22D.2 | 7.09 | 434.63 | 8.6 | 6.99 | 36.43 | 21.42 | 407.29 | 1.19 | 5.88 | 5.07 | 1.03 | 0.37 | 1.63 | 0.58 | 134.43 | 14.84 | 1.15 |
| 22D.3 | 6.38 | 367.06 | 7.18 | 9.04 | 35.03 | 21.35 | 435.52 | 1.31 | 4.38 | 5.78 | 0.77 | 0.365 | 1.06 | 0.385 | 1.15 | 22.72 | 0.377 |
| 1B.1 | 186.26 | 3870.91 | 14.16 | 1346.87 | 439.75 | 55.38 | 816.86 | 5.94 | 23.07 | 78.68 | 75.57 | 2.16 | 56.34 | 6.6 | 25.18 | 0.69 | 1.15 |
| 1B.2 | 2.14 | 33.79 | 13.61 | 14.69 | 38.37 | 6.1 | 51.21 | 0.175 | 5.12 | 24.68 | 0.86 | 0.224 | 0.218 | 1.08 | 11.71 | 0.65 | 0.622 |
| 1B.3 | 1.89 | 22.67 | 7.15 | 11.73 | 39.33 | 9.66 | 44.57 | 0.219 | 3.47 | 12.87 | 0.65 | 0.251 | 0.201 | 0.58 | 18.3 | 0.49 | 1.17 |
| 1B_1 | 2.63 | 72.83 | 5.98 | 26.93 | 26.19 | 7.46 | 56.02 | 0.187 | 4.25 | 12.8 | 1.24 | 0.133 | 0.581 | 1.24 | 15.93 | 0.52 | 0.54 |
| 1B_10 | 1.34 | 26.51 | 5.54 | 12.16 | 25.84 | 2.28 | 39.46 | 0.156 | 2.94 | 9.59 | 0.54 | 0.315 | 0.145 | 0.76 | 6.87 | 0.32 | 0.53 |
| 1B_11 | 8.69 | 276.88 | 8.12 | 141.79 | 43.17 | 5.3 | 63.88 | 0.09 | 4.94 | 15.28 | 11.02 | 0.23 | 2.63 | 2.04 | 17.52 | 0.59 | 0.8 |
| 1B_12 | 2.18 | 55.87 | 8.93 | 22.16 | 27.49 | 3.82 | 46.66 | 0.138 | 3.33 | 13.06 | 1.5 | 0.217 | 0.431 | 1.88 | 11.7 | 0.62 | 1.4 |
| 1B_13 | 1.64 | 46.32 | 5.38 | 28.99 | 27.85 | 3.61 | 94.35 | 0.02015 | 4.52 | 17.94 | 1.03 | 0.313 | 0.316 | 1.23 | 9.42 | 0.44 | 0.97 |
| 1B_14 | 1.18 | 22.06 | 4.68 | 9.89 | 25.44 | 6.87 | 41.73 | 0.136 | 3.44 | 9.08 | 0.63 | 0.273 | 0.168 | 0.55 | 7.51 | 0.45 | 0.453 |
| 1B_15 | 2.73 | 80.27 | 5.16 | 31.86 | 30.69 | 30.89 | 89.11 | 0.94 | 6.44 | 18.2 | 2.23 | 0.314 | 0.63 | 0.81 | 8.34 | 0.28 | 0.9 |
| 1B_2 | 1.04 | 22.84 | 5.13 | 8.88 | 25.97 | 2.77 | 36.07 | 0.072 | 2.36 | 8.8 | 0.42 | 0.179 | 0.273 | 0.48 | 5.41 | 0.24 | 0.276 |
| 1B_3 | 1.65 | 39.3 | 7.14 | 18.97 | 26.71 | 2.89 | 69.78 | 0.138 | 4.69 | 19.36 | 1.59 | 0.252 | 0.235 | 5.86 | 6.76 | 1.09 | 0.72 |
| 1B_4 | 5.02 | 168.31 | 7.4 | 45.9 | 28.88 | 3.7 | 226.11 | 0.188 | 16.86 | 55.37 | 0.95 | 0.433 | 1.75 | 1.1 | 10.17 | 0.78 | 1.09 |
| 1B_5 | 1.13 | 26.53 | 6.6 | 20.78 | 26.45 | 2.47 | 67.72 | 0.085 | 4.31 | 8.1 | 0.52 | 0.232 | 0.133 | 2.13 | 7.28 | 0.66 | 0.54 |
| 1B_6 | 1.85 | 47.86 | 7.3 | 27.07 | 27.94 | 4.18 | 80.12 | 0.215 | 3.85 | 14.04 | 1.77 | 0.186 | 0.414 | 2.49 | 10.41 | 1.2 | 0.87 |

LV

| | | | | | | | | | | | | | | | | | |
|---|---|---|---|---|---|---|---|---|---|---|---|---|---|---|---|---|---|
| 1B_7 | 12.21 | 421.47 | 7.84 | 202.55 | 73.36 | 4.74 | 56.96 | 0.217 | 4.64 | 19.77 | 12.99 | 0.249 | 4.84 | 3 | 11.87 | 0.49 | 0.54 |
| 1B_8 | 2.22 | 67.89 | 7.2 | 29.62 | 30.57 | 2.91 | 60.77 | 0.125 | 4.89 | 11.99 | 1.46 | 0.318 | 0.6 | 1.1 | 9.1 | 0.39 | 0.72 |
| 1B_9 | 33.67 | 1212.56 | 7.06 | 437.04 | 73.69 | 6.5 | 67.1 | 0.283 | 4.04 | 10.99 | 43.99 | 0.201 | 13.79 | 6.16 | 15.91 | 0.34 | 0.54 |
| 21B.1 | 0.89 | 121.82 | 4.35 | 8.5 | 36.78 | 4.36 | 75.28 | 0.27 | 1.56 | 4.32 | 0.61 | 0.104 | 0.126 | 0.73 | 1.93 | 0.585 | 0.221 |
| 21B.2 | 0.76 | 62.72 | 6.37 | 6.8 | 36.81 | 2.15 | 72.64 | 0.174 | 1.13 | 2.96 | 0.449 | 0.11 | 0.129 | 0.64 | 2.19 | 0.967 | 0.158 |
| 21B.3 | 1.23 | 217.44 | 6.91 | 28.25 | 41.71 | 5.49 | 516.5 | 0.61 | 10.23 | 14.82 | 0.71 | 1.24 | 0.109 | 0.69 | 2.54 | 0.599 | 1.42 |
| 21B_1 | 1.95 | 155.6 | 9.18 | 14.13 | 39.43 | 9.62 | 360.79 | 0.42 | 5.48 | 14.62 | 1.4 | 0.52 | 0.247 | 0.96 | 1.66 | 1.29 | 0.307 |
| 21B_10 | 1.37 | 170.22 | 8.83 | 21.3 | 42.56 | 7.4 | 1153.07 | 0.178 | 58.92 | 10.84 | 1.98 | 2.14 | 0.54 | 0.9 | 3.58 | 0.7 | 0.335 |
| 21B_11 | 1.39 | 181.94 | 9.97 | 13.4 | 34.22 | 8.07 | 199.97 | 0.127 | 4.37 | 9.08 | 2.03 | 0.24 | 0.38 | 2 | 3.21 | 2.45 | 0.341 |
| 21B_12 | 0.69 | 131.18 | 9.51 | 9.27 | 31.95 | 2.53 | 138.72 | 0.02015 | 2.78 | 5.77 | 0.47 | 0.158 | 0.078 | 0.47 | 0.78 | 0.45 | 0.226 |
| 21B_13 | 0.68 | 77.22 | 11.71 | 8.34 | 33.8 | 3.65 | 109.12 | 0.285 | 2.31 | 6.18 | 0.5 | 0.188 | 0.073 | 0.55 | 2.04 | 1.39 | 0.166 |
| 21B_14 | 0.94 | 171.12 | 10.45 | 10.27 | 32.1 | 55.09 | 284.04 | 13.34 | 5.29 | 10.12 | 1.51 | 0.21 | 0.184 | 1.03 | 3.25 | 0.99 | 0.239 |
| 21B_15 | 0.69 | 93.52 | 11.08 | 8.88 | 32.31 | 5.15 | 175.73 | 1.36 | 2.18 | 4.47 | 0.56 | 0.24 | 0.121 | 0.45 | 0.63 | 0.63 | 0.152 |
| 21B_2 | 1.45 | 184.25 | 6.73 | 15.69 | 37.64 | 6.8 | 200.58 | 0.36 | 5.37 | 11.05 | 1.94 | 0.25 | 0.42 | 1.04 | 1.71 | 0.85 | 0.253 |
| 21B_3 | 0.76 | 98.77 | 5.81 | 10.11 | 34.86 | 6.76 | 187.43 | 0.17 | 4.74 | 11.58 | 0.85 | 0.23 | 0.214 | 0.82 | 3.51 | 0.63 | 0.244 |
| 21B_4 | 0.37 | 34.35 | 4.71 | 3.51 | 30.77 | 1.65 | 56.59 | 0.108 | 1.5 | 2.41 | 0.2 | 0.069 | 0.041 | 0.175 | 0.241 | 0.23 | 0.066 |
| 21B_5 | 0.91 | 119.84 | 9.05 | 18.14 | 34.2 | 5.66 | 233.66 | 0.223 | 3.48 | 11.47 | 0.75 | 0.23 | 0.26 | 0.72 | 1.97 | 1.11 | 0.31 |
| 21B_6 | 2.56 | 352.95 | 16.64 | 74.55 | 44.32 | 40.23 | 12971.71 | 1.21 | 64.38 | 208.71 | 3.23 | 1.55 | 0.49 | 1.78 | 12.87 | 2.36 | 4.42 |
| 21B_7 | 0.64 | 116.65 | 9.98 | 8.98 | 32.47 | 28.32 | 131.97 | 3.89 | 3.76 | 7.54 | 1.27 | 0.21 | 0.08 | 0.65 | 0.74 | 0.7 | 0.18 |
| 21B_8 | 0.98 | 205.29 | 11.51 | 14.87 | 33.97 | 4.75 | 398.54 | 0.162 | 5.41 | 7.52 | 1.34 | 0.32 | 0.181 | 2.79 | 4.81 | 1.97 | 0.462 |
| 21B_9 | 1.54 | 687.02 | 9.99 | 234.65 | 96.48 | 54.58 | 3929.05 | 2.1 | 47.91 | 109.84 | 1.66 | 0.76 | 0.121 | 0.76 | 7.41 | 1.41 | 2.58 |
| 21J.1 | 15.34 | 423.08 | 10.86 | 58.38 | 53.83 | 7.42 | 525.14 | 0.41 | 17.06 | 25.79 | 2.24 | 0.31 | 0.393 | 2.53 | 2.46 | 1.54 | 1.81 |
| 21J.2 | 0.97 | 412.25 | 10.23 | 36.91 | 58.04 | 4.72 | 202.75 | 0.255 | 8.88 | 14.26 | 1.27 | 0.29 | 0.131 | 1.86 | 1.76 | 1.06 | 0.468 |
| 21J.3 | 1.19 | 310.29 | 11.21 | 30.37 | 55.13 | 5.64 | 282.6 | 0.36 | 9.59 | 12.34 | 1.44 | 0.342 | 0.134 | 2.62 | 2.36 | 1.58 | 0.527 |
| 21J_1 | 1.26 | 535.88 | 10.92 | 181.19 | 47.78 | 46.82 | 870.45 | 0.02015 | 26.01 | 20.16 | 2.58 | 0.53 | 0.174 | 2.17 | 4.2 | 2.8 | 1.88 |
| 21J_10 | 1.91 | 305.85 | 11.16 | 34.77 | 50.23 | 4.74 | 225.75 | 0.434 | 9.24 | 15.03 | 3.28 | 0.288 | 0.46 | 2.09 | 1.98 | 2.03 | 0.527 |
| 21J_11 | 1.62 | 368.22 | 10.94 | 43.34 | 54.32 | 7.01 | 270.82 | 0.123 | 37.2 | 16.68 | 3.17 | 0.46 | 0.251 | 2.36 | 2.64 | 2.04 | 0.623 |
| 21J_12 | 0.78 | 261.43 | 8.33 | 21.6 | 41.54 | 3.29 | 138.66 | 0.21 | 4.58 | 7.47 | 1.38 | 0.177 | 0.095 | 1.86 | 1.85 | 1.6 | 0.275 |
| 21J_13 | 0.76 | 345.54 | 10.83 | 60.73 | 41.25 | 7.34 | 1963.59 | 0.52 | 9.88 | 14.33 | 1.33 | 1.64 | 0.074 | 1.26 | 1.31 | 1.16 | 0.85 |
| 21J_14 | 1.79 | 444.88 | 18.1 | 58.11 | 52.41 | 17.72 | 1000.4 | 0.61 | 15.93 | 24.98 | 2.66 | 0.71 | 0.278 | 2.16 | 4.57 | 1.73 | 1.24 |

| | | | | | | | | | | | | | | | | | |
|---|---|---|---|---|---|---|---|---|---|---|---|---|---|---|---|---|---|
| 21J_15 | 3.66 | 444.85 | 13.25 | 99.48 | 54.01 | 7.37 | 810.4 | 0.172 | 29.84 | 24.99 | 10.52 | 0.46 | 1.02 | 2.92 | 3.9 | 1.68 | 0.94 |
| 21J_2 | 2.12 | 336.19 | 9.74 | 26.97 | 43.14 | 4.81 | 198.44 | 0.231 | 21.33 | 11.75 | 2.27 | 0.52 | 0.169 | 1.85 | 2.01 | 1.73 | 0.401 |
| 21J_3 | 7.5 | 238.39 | 8.71 | 20.69 | 38.31 | 3.03 | 170.94 | 0.53 | 10.7 | 8.33 | 1.87 | 0.219 | 0.118 | 2.18 | 2.53 | 2.05 | 0.412 |
| 21J_4 | 1.1 | 338.02 | 11.96 | 26.92 | 42.54 | 3.66 | 131.86 | 0.158 | 6.37 | 9.52 | 2.05 | 0.37 | 0.131 | 4.05 | 2.37 | 4.84 | 0.434 |
| 21J_5 | 1.4 | 299.33 | 11.47 | 26.15 | 41.49 | 5.96 | 185.53 | 0.67 | 9.12 | 12.66 | 2.74 | 0.29 | 0.5 | 2.48 | 3.72 | 2.84 | 0.463 |
| 21J_6 | 5.49 | 300.63 | 9.96 | 24.5 | 39.51 | 2.33 | 186.37 | 0.02015 | 7.24 | 9.71 | 1.45 | 0.204 | 0.258 | 0.92 | 1.06 | 0.87 | 0.377 |
| 21J_7 | 1.27 | 455.24 | 17.66 | 39.85 | 49.02 | 4.78 | 346.61 | 0.02015 | 7.7 | 16.23 | 2.06 | 0.183 | 0.252 | 1.64 | 2.47 | 1.71 | 0.573 |
| 21J_8 | 0.71 | 170.54 | 8.47 | 17.65 | 39.43 | 2.86 | 142.76 | 0.02015 | 4.78 | 6.42 | 1.04 | 0.226 | 0.084 | 1.08 | 1.33 | 1.34 | 0.256 |
| 21J_9 | 66.82 | 2793.39 | 21.5 | 1079.63 | 276.98 | 43.08 | 1412.34 | 0.83 | 49.57 | 12.2 | 270.69 | 1.04 | 27.4 | 49.23 | 35.24 | 3.13 | 1.42 |
| 21K.1 | 0.83 | 252.76 | 8.59 | 28.91 | 36.43 | 2.57 | 129.03 | 0.104 | 4.44 | 8.46 | 1.41 | 0.192 | 0.115 | 2.56 | 3.74 | 0.99 | 0.383 |
| 21K.2 | 1.49 | 403.82 | 15.66 | 63.54 | 47.84 | 5.52 | 441.69 | 0.3 | 14.8 | 17.48 | 2.81 | 0.48 | 0.245 | 5.43 | 11.61 | 2.37 | 1.17 |
| 21K.3 | 0.5 | 84.58 | 5.29 | 19.92 | 32.86 | 1.7 | 73.23 | 0.078 | 2.24 | 5.15 | 0.59 | 0.172 | 0.053 | 1.1 | 1.09 | 0.438 | 0.244 |
| 21K_1 | 1.09 | 400.53 | 19.73 | 53.04 | 32.08 | 6 | 216.91 | 0.168 | 6.99 | 11.25 | 3.38 | 0.136 | 0.19 | 2.71 | 3.56 | 1.44 | 0.392 |
| 21K_10 | 0.86 | 631.63 | 15.5 | 41.93 | 33.6 | 1.35 | 100.4 | 0.1018 | 3.66 | 14.03 | 22.53 | 0.118 | 0.121 | 22.71 | 1.73 | 1.88 | 0.25 |
| 21K_11 | 2.76 | 496.71 | 16.92 | 57.46 | 41.3 | 5.08 | 274 | 0.122 | 8.2 | 16.54 | 11.01 | 0.51 | 0.232 | 15.77 | 21.89 | 4.4 | 0.593 |
| 21K_12 | 1.33 | 470 | 19.69 | 173.68 | 47.73 | 22.67 | 2647.34 | 0.388 | 34.74 | 42.63 | 5.01 | 1.25 | 0.165 | 31.15 | 8.61 | 12.46 | 4.44 |
| 21K_13 | 1.03 | 77.54 | 8.62 | 7.84 | 26.47 | 1.47 | 51.25 | 0.02015 | 2.11 | 3.47 | 0.81 | 0.34 | 0.0362 | 1.19 | 1.39 | 0.517 | 0.118 |
| 21K_14 | 0.72 | 256.48 | 7.55 | 14.33 | 26.89 | 1.89 | 73.88 | 0.059 | 3.47 | 3.51 | 0.93 | 0.335 | 0.0434 | 1.45 | 1.11 | 0.445 | 0.159 |
| 21K_15 | 0.97 | 238.42 | 10.99 | 23.73 | 33.42 | 3.07 | 133.53 | 0.166 | 5.24 | 7.49 | 2.78 | 0.209 | 0.209 | 3.17 | 4.11 | 1.75 | 0.402 |
| 21K_2 | 1.37 | 392.63 | 20.12 | 45.54 | 40.78 | 7.43 | 521.18 | 0.327 | 13.15 | 16.02 | 17.18 | 0.55 | 0.26 | 27.82 | 7.41 | 4.99 | 1.4 |
| 21K_3 | 1.21 | 275.98 | 14.69 | 40.52 | 37.94 | 3.67 | 242.71 | 0.154 | 7.14 | 8.61 | 3.74 | 0.266 | 0.197 | 4.98 | 5.08 | 2.12 | 0.476 |
| 21K_4 | 0.94 | 463.06 | 12.33 | 38.28 | 31.31 | 4.22 | 137.51 | 0.0913 | 4.16 | 9.66 | 3.2 | 0.164 | 0.122 | 5.15 | 3.39 | 1.71 | 0.35 |
| 21K_5 | 2.18 | 356.65 | 13.04 | 59.69 | 37.47 | 6.88 | 216.58 | 0.17 | 8.77 | 12.77 | 3.47 | 0.397 | 0.13 | 3.27 | 9.12 | 2.7 | 0.631 |
| 21K_6 | 1.33 | 471.54 | 13.5 | 55.25 | 42.12 | 5.57 | 299.9 | 0.163 | 7.02 | 11.41 | 4.14 | 0.52 | 0.214 | 4.35 | 6.96 | 2.16 | 0.527 |
| 21K_7 | 1.31 | 361.23 | 14.31 | 84.77 | 42.9 | 6.46 | 438.16 | 0.343 | 11.2 | 18.77 | 3.43 | 0.325 | 0.199 | 4.3 | 5.15 | 2.04 | 0.94 |
| 21K_8 | 1.05 | 401.43 | 10.26 | 55.59 | 34.09 | 3.25 | 162.26 | 0.152 | 4.66 | 9.32 | 2.69 | 0.144 | 0.166 | 2.57 | 9.86 | 1.39 | 0.417 |
| 21K_9 | 1 | 520.38 | 12.41 | 43.42 | 42.13 | 3.83 | 188.12 | 0.126 | 6.41 | 11.27 | 4.11 | 0.242 | 0.165 | 3.99 | 4.78 | 1.91 | 0.422 |
| 21L.1 | 2.56 | 1041.32 | 12.58 | 99.11 | 51.24 | 3.82 | 435.82 | 0.02015 | 12.63 | 29.95 | 2.98 | 0.408 | 0.142 | 4.63 | 8.96 | 1.43 | 1.2 |
| 21L.2 | 1.95 | 541.81 | 12.29 | 36.12 | 45.38 | 1.81 | 146.7 | 0.02015 | 9.47 | 17.18 | 3.92 | 0.214 | 0.235 | 5.86 | 2.43 | 1 | 0.498 |
| 21L.3 | 3.26 | 686.22 | 10.89 | 99.42 | 48.76 | 4.38 | 439.43 | 0.168 | 14.98 | 61.78 | 2.3 | 0.217 | 0.101 | 3.2 | 1.87 | 0.7 | 0.99 |

| | | | | | | | | | | | | | | | | | |
|---|---|---|---|---|---|---|---|---|---|---|---|---|---|---|---|---|---|
| 21L_1 | 0.84 | 291.76 | 8.31 | 26.55 | 26.34 | 1.14 | 121.14 | 0.0855 | 5.19 | 10.2 | 1 | 0.091 | 0.0508 | 1.28 | 0.92 | 0.35 | 0.249 |
| 21L_10 | 0.68 | 120.14 | 6.83 | 8.36 | 24.82 | 0.345 | 54.13 | 0.0502 | 2.51 | 4.17 | 0.5 | 0.12 | 0.0196 | 0.637 | 0.615 | 0.146 | 0.14 |
| 21L_11 | 0.87 | 168.65 | 6.95 | 8.18 | 28.62 | 1.08 | 38.37 | 0.1046 | 2.41 | 6.05 | 0.6 | 0.11 | 0.072 | 0.736 | 0.522 | 0.126 | 0.126 |
| 21L_12 | 1.26 | 357.32 | 9.2 | 18.85 | 28.64 | 1.41 | 149.09 | 0.132 | 6.05 | 7.21 | 1.41 | 0.218 | 0.113 | 1.9 | 1.95 | 0.41 | 0.272 |
| 21L_13 | 1.2 | 302.97 | 10.39 | 26.6 | 31.9 | 1.12 | 136.04 | 0.0798 | 7.44 | 7.74 | 1.34 | 0.148 | 0.081 | 2.01 | 2.16 | 0.54 | 0.348 |
| 21L_14 | 0.75 | 197.55 | 7.6 | 13.42 | 25.82 | 0.714 | 68.23 | 0.0673 | 5 | 5.35 | 0.76 | 0.127 | 0.0229 | 1.24 | 0.74 | 0.254 | 0.186 |
| 21L_15 | 1.56 | 293.19 | 10.19 | 21.41 | 29.96 | 1.42 | 153.96 | 0.163 | 9.12 | 7.83 | 1.53 | 0.185 | 0.07 | 2.29 | 12.68 | 0.608 | 0.42 |
| 21L_2 | 2.85 | 306.86 | 7.67 | 24.97 | 27.94 | 1.19 | 123.25 | 0.109 | 7.22 | 9.85 | 1.94 | 0.056 | 0.141 | 1.99 | 1.5 | 0.479 | 0.29 |
| 21L_3 | 1 | 338.95 | 7.7 | 48.42 | 27.93 | 1.3 | 161.34 | 0.02015 | 6.57 | 13.37 | 1.2 | 0.167 | 0.104 | 1.45 | 1.05 | 0.349 | 0.454 |
| 21L_4 | 2.13 | 507.25 | 9.29 | 32.84 | 29.89 | 0.95 | 121.46 | 0.0924 | 6.66 | 10.03 | 1.82 | 0.176 | 0.094 | 1.59 | 1.75 | 0.36 | 0.341 |
| 21L_5 | 18.77 | 360.55 | 10.24 | 41.88 | 29.33 | 1.46 | 170.89 | 0.0784 | 5.66 | 8.92 | 1.49 | 0.192 | 0.075 | 2.11 | 7.11 | 0.39 | 0.345 |
| 21L_6 | 1.23 | 348.33 | 9.77 | 24.58 | 28.01 | 1.05 | 163.39 | 0.1079 | 11.63 | 9.79 | 1.86 | 0.17 | 0.0451 | 2.6 | 1.37 | 0.51 | 0.379 |
| 21L_7 | 1.03 | 325.54 | 6.66 | 22.6 | 25.6 | 1.34 | 159.16 | 0.125 | 5.8 | 10.39 | 10 | 0.063 | 0.15 | 1.73 | 1.22 | 0.355 | 0.286 |
| 21L_8 | 3.37 | 442.24 | 9.88 | 42.45 | 29.56 | 3.71 | 133.58 | 0.0916 | 6.81 | 10.19 | 1.88 | 0.179 | 0.112 | 2.22 | 1.68 | 0.41 | 0.507 |
| 21L_9 | 1.41 | 492.31 | 10.21 | 49.98 | 45.37 | 1.07 | 485.03 | 0.293 | 7.39 | 22.67 | 1.61 | 0.242 | 0.072 | 1.4 | 2.07 | 0.412 | 0.5 |
| 22B.1 | 1.05 | 332.83 | 10.49 | 50.02 | 41.95 | 4.32 | 131.93 | 0.262 | 5.92 | 9.99 | 1.25 | 0.171 | 0.198 | 1.74 | 3.89 | 1.47 | 0.349 |
| 22B.2 | 0.71 | 213.16 | 6.69 | 19.15 | 37.24 | 2.37 | 152.12 | 0.111 | 4.47 | 5.47 | 0.65 | 0.193 | 0.093 | 0.76 | 8.59 | 0.596 | 0.325 |
| 22B.3 | 1.31 | 424.04 | 14.54 | 60.82 | 43.68 | 6.63 | 220.95 | 0.149 | 7.77 | 14.11 | 1.61 | 0.271 | 0.282 | 2.16 | 5.63 | 1.66 | 0.62 |
| 22B_1 | 0.96 | 388.55 | 14.81 | 52 | 39.91 | 6.95 | 232.71 | 0.243 | 8.65 | 23.7 | 1.95 | 0.32 | 0.189 | 1.63 | 5.06 | 2.01 | 0.6 |
| 22B_10 | 0.94 | 288.95 | 9.31 | 28.46 | 36.97 | 3.7 | 197.19 | 0.147 | 8.06 | 16.16 | 1.4 | 0.34 | 0.135 | 1.17 | 3.87 | 1.58 | 0.404 |
| 22B_11 | 0.57 | 104.95 | 8.72 | 9.2 | 29.07 | 2.55 | 58.32 | 0.145 | 1.96 | 6.77 | 0.49 | 0.193 | 0.05 | 0.59 | 1.6 | 0.75 | 0.132 |
| 22B_12 | 1.02 | 490.56 | 11.73 | 48.74 | 36.91 | 6.24 | 245.4 | 0.074 | 6.73 | 24.43 | 1.97 | 0.244 | 0.167 | 2.17 | 5.89 | 2.83 | 0.55 |
| 22B_13 | 9.47 | 390.3 | 9.7 | 48.82 | 31.77 | 3.67 | 234.15 | 0.076 | 6.08 | 16.27 | 1.1 | 0.187 | 0.087 | 1.13 | 3.16 | 1.58 | 0.49 |
| 22B_14 | 3.69 | 350.36 | 10.53 | 29.75 | 31.28 | 3.11 | 147.55 | 0.148 | 10.46 | 12.9 | 2.13 | 0.38 | 0.16 | 3.7 | 6.69 | 2.32 | 0.59 |
| 22B_15 | 1.07 | 1830.48 | 10.51 | 54.95 | 61.8 | 4.89 | 270.19 | 0.216 | 6.08 | 11.04 | 2.26 | 0.46 | 0.142 | 1.16 | 6.33 | 1.47 | 0.447 |
| 22B_2 | 0.91 | 408.28 | 12.16 | 56.1 | 34.68 | 5.58 | 185.5 | 0.194 | 6.21 | 17.1 | 1.64 | 0.281 | 0.134 | 1.29 | 4.23 | 1.61 | 0.41 |
| 22B_3 | 0.76 | 302.69 | 11.61 | 27.26 | 30.46 | 4.93 | 161.31 | 0.048 | 5 | 13.03 | 2.43 | 0.229 | 0.138 | 4.47 | 3.83 | 1.68 | 0.378 |
| 22B_4 | 17.82 | 491.56 | 9.64 | 73.44 | 32 | 7.91 | 424.53 | 0.236 | 12.69 | 28.07 | 1.52 | 0.38 | 0.106 | 1.16 | 4.15 | 1.6 | 0.85 |
| 22B_5 | 0.93 | 354.21 | 10.27 | 43.03 | 35.84 | 6.69 | 178.32 | 0.23 | 5.53 | 14.27 | 1.42 | 0.252 | 0.14 | 1.28 | 4.01 | 2.18 | 0.419 |
| 22B_6 | 1.07 | 293.44 | 13.78 | 34.33 | 31.81 | 4.3 | 116.82 | 0.02015 | 4.44 | 14.02 | 1.26 | 0.286 | 0.119 | 1.23 | 3.84 | 1.91 | 0.336 |

| | | | | | | | | | | | | | | | | | |
|---|---|---|---|---|---|---|---|---|---|---|---|---|---|---|---|---|---|
| 22B_7 | 1.19 | 271.03 | 8.52 | 91.73 | 36.77 | 9.3 | 637.31 | 0.332 | 15.57 | 41.1 | 1.45 | 0.97 | 0.28 | 1.14 | 4.56 | 1.7 | 1.06 |
| 22B_8 | 0.55 | 141.11 | 6.98 | 17.82 | 30.6 | 2.5 | 73.69 | 0.053 | 2.77 | 7.94 | 0.73 | 0.235 | 0.086 | 0.67 | 1.19 | 1.02 | 0.177 |
| 22B_9 | 0.84 | 271.47 | 10.53 | 35.06 | 46.45 | 4.85 | 172.82 | 0.135 | 4.99 | 13.21 | 1.08 | 0.31 | 0.146 | 0.94 | 4.09 | 1.37 | 0.326 |
| 22H.1 | 0.62 | 6.47 | 5.02 | 0.357 | 38.83 | 0.163 | 9.97 | 0.05 | 1.91 | 0.34 | 1.66 | 0.259 | 0.0165 | 14.41 | 0.6 | 1 | 0.129 |
| 22H.2 | 0.86 | 9.8 | 0.3655 | 1.57 | 40.3 | 0.309 | 8.72 | 0.216 | 0.01845 | 0.308 | 0.565 | 0.113 | 0.076 | 0.139 | 0.139 | 0.00194 | 0.00136 |
| 22H.3 | 0.67 | 6.14 | 3.69 | 0.78 | 40.55 | 0.71 | 0.89 | 0.0445 | 0.58 | 0.125 | 0.244 | 0.129 | 0.00605 | 0.196 | 1.84 | 0.0044 | 0.006 |
| 22H.4 | 0.61 | 2.48 | 6.52 | 0.504 | 41.29 | 0.072 | 2.4 | 0.243 | 0.445 | 0.81 | 0.171 | 0.171 | 0.078 | 0.042 | 0.113 | 0.0177 | 0.0083 |
| 22H_1 | 0.7 | 48.57 | 4.01 | 3.16 | 24.27 | 1.13 | 4.7 | 0.02015 | 0.31 | 0.0445 | 1.27 | 0.04 | 0.4 | 0.21 | 4.38 | 0.031 | 0.0037 |
| 22H_2 | 0.41 | 19.33 | 6.71 | 0.051 | 27.06 | 0.57 | 0.4325 | 0.02015 | 0.62 | 1.45 | 0.015 | 0.0395 | 0.00605 | 0.39 | 0.125 | 0.05 | 0.00058 |
| 22H_3 | 0.37 | 21.01 | 8.89 | 0.045 | 21.98 | 0.162 | 2.24 | 0.063 | 0.195 | 1.94 | 0.072 | 0.262 | 0.00605 | 0.129 | 0.132 | 0.057 | 0.0045 |
| 22H_4 | 2.45 | 86.14 | 0.95 | 16.14 | 33.81 | 0.072 | 0.88 | 0.0425 | 0.49 | 1.63 | 5.86 | 0.0765 | 1.22 | 0.99 | 0.98 | 0.0174 | 0.00185 |
| 22H_5 | 1.64 | 156.74 | 2.89 | 4.44 | 38.7 | 4.34 | 3.5 | 0.84 | 0.84 | 8.13 | 0.42 | 0.45 | 0.39 | 0.13 | 0.224 | 0.064 | 0.00199 |
| 22H_6 | 0.29 | 9.62 | 1.36 | 0.205 | 20.7 | 0.149 | 0.4325 | 0.02015 | 0.01845 | 1.78 | 0.067 | 0.067 | 0.00605 | 0.034 | 0.053 | 0.0074 | 0.00088 |
| 22H_7 | 0.33 | 15.95 | 4.28 | 0.0131 | 27.13 | 0.072 | 0.4325 | 0.02015 | 0.01845 | 0.13 | 0.0085 | 0.23 | 0.016 | 0.073 | 0.098 | 0.071 | 0.00167 |
| 15B.1 | 186.7 | 382.73 | 17.09 | 20.9 | 54.89 | 49.67 | 452.95 | 0.1055 | 3.13 | 4.75 | 2.76 | 0.01915 | 14.69 | 0.408 | 0.0796 | 0.148 | 0.0585 |
| 15B.2 | 13.21 | 109.94 | 11.1 | 1.052 | 48.41 | 4 | 128.81 | 0.219 | 0.73 | 0.652 | 0.537 | 0.106 | 1.68 | 0.349 | 0.0565 | 0.0905 | 0.0734 |
| 15B.3 | 22.18 | 217.32 | 31.49 | 2.36 | 49.25 | 6.98 | 131.96 | 1.39 | 2.71 | 2.03 | 0.542 | 0.01915 | 0.82 | 2.31 | 0.544 | 0.252 | 0.123 |
| 15B_1 | 5766.38 | 0.00595 | 1160.79 | 545.61 | 81.51 | 2376.6 | 14737.02 | 6.09 | 49.81 | 28.36 | 1275.25 | 9.22 | 4013.13 | 219.02 | 0.378 | 2.96 | 0.97 |
| 15B_10 | 12.69 | 55.47 | 14.62 | 1.43 | 34.66 | 4.9 | 111.93 | 0.48 | 5.52 | 1.09 | 0.7 | 0.116 | 0.72 | 0.41 | 0.0364 | 0.47 | 0.083 |
| 15B_11 | 67.17 | 355.23 | 25.53 | 5.65 | 36.88 | 33.23 | 484.69 | 0.84 | 18.57 | 3.68 | 3.87 | 0.073 | 9.83 | 1.66 | 0.069 | 0.73 | 0.165 |
| 15B_12 | 36.49 | 263.36 | 36.83 | 6.09 | 32.18 | 13.93 | 376.99 | 1.03 | 8.39 | 3.44 | 3.88 | 0.141 | 3.36 | 2.36 | 0.06 | 0.72 | 0.151 |
| 15B_13 | 6.83 | 39.46 | 12.95 | 0.67 | 32 | 3.86 | 65.06 | 0.063 | 3.93 | 0.94 | 0.21 | 0.11 | 0.61 | 0.193 | 0.0238 | 0.179 | 0.0301 |
| 15B_14 | 38.57 | 151.58 | 25.82 | 6.87 | 34.04 | 14.08 | 132.66 | 0.152 | 3.25 | 1.82 | 0.76 | 0.129 | 2.87 | 1.15 | 0.057 | 0.51 | 0.259 |
| 15B_15 | 15.71 | 246.45 | 16.72 | 2.56 | 33.81 | 11.46 | 239.32 | 0.58 | 16.41 | 1.28 | 6.78 | 0.095 | 18.94 | 1.59 | 0.087 | 0.32 | 0.076 |
| 15B_2 | 7.58 | 65.64 | 7.56 | 0.9 | 33.84 | 7.61 | 91.31 | 0.02015 | 1.13 | 1.47 | 0.99 | 0.111 | 2.02 | 0.46 | 0.72 | 0.126 | 0.0216 |
| 15B_3 | 43.84 | 83.78 | 16.63 | 6.93 | 40.03 | 11.75 | 259.46 | 0.77 | 4.9 | 2.24 | 0.76 | 0.091 | 2.89 | 0.34 | 0.121 | 0.38 | 0.151 |
| 15B_4 | 46.04 | 170.85 | 14.41 | 4.56 | 36.58 | 20.4 | 108.61 | 0.135 | 0.88 | 2.2 | 4.07 | 0.141 | 7.15 | 0.8 | 0.0407 | 0.23 | 0.0331 |
| 15B_5 | 17.47 | 107.89 | 13.76 | 2.53 | 35.87 | 10.37 | 127.81 | 0.8 | 5.15 | 2 | 0.9 | 0.208 | 0.85 | 0.6 | 0.0252 | 0.34 | 0.0567 |
| 15B_6 | 16.4 | 65.71 | 15.21 | 2.46 | 35.61 | 15.37 | 283.73 | 0.178 | 9.36 | 2.11 | 0.44 | 0.103 | 0.75 | 0.31 | 0.0239 | 0.26 | 0.086 |
| 15B_7 | 10.23 | 40.88 | 16.62 | 2.03 | 34.9 | 6.28 | 103.59 | 0.302 | 1.61 | 1.23 | 0.25 | 0.097 | 0.38 | 0.26 | 0.0383 | 0.174 | 0.0401 |

| | | | | | | | | | | | | | | | | | |
|---|---|---|---|---|---|---|---|---|---|---|---|---|---|---|---|---|---|
| 15B_8 | 7.53 | 35.79 | 14.62 | 1.07 | 35.4 | 25.74 | 114.01 | 0.232 | 1.94 | 1.62 | 0.18 | 0.06 | 0.256 | 0.204 | 0.056 | 0.167 | 0.043 |
| 15B_9 | 8.48 | 53.47 | 16 | 1.2 | 36.5 | 6.95 | 157.6 | 0.44 | 6.86 | 1.14 | 0.37 | 0.078 | 0.38 | 0.71 | 0.0154 | 0.27 | 0.067 |
| 2B.1 | 38.41 | 234.32 | 37.19 | 17.48 | 40.64 | 19.68 | 312.72 | 1.11 | 4.5 | 5.98 | 1.28 | 0.449 | 3.57 | 4.81 | 0.519 | 1.81 | 0.472 |
| 2B.2 | 40.24 | 195.53 | 80.08 | 18.17 | 38.94 | 20.05 | 293.39 | 1.19 | 5.96 | 6.21 | 1.12 | 0.531 | 2.66 | 4.9 | 0.794 | 2.63 | 0.443 |
| 2B.3 | 30.68 | 157.3 | 54.39 | 12.31 | 38.51 | 16.15 | 229.07 | 0.66 | 4.73 | 4.86 | 0.94 | 0.567 | 1.9 | 4.02 | 0.551 | 1.31 | 0.438 |
| 2B_1 | 22.34 | 164.73 | 45.78 | 18.59 | 28.56 | 10.89 | 222.17 | 0.41 | 2.64 | 6.5 | 0.99 | 0.01915 | 1.71 | 2.19 | 1.89 | 2.49 | 1.28 |
| 2B_10 | 920.84 | 1334.84 | 41.53 | 211.91 | 303.03 | 473.65 | 1138.12 | 0.9 | 3.88 | 7.03 | 3.3 | 0.71 | 1.91 | 2.93 | 0.531 | 2.31 | 0.458 |
| 2B_11 | 25.25 | 116.98 | 20.68 | 10.15 | 23.18 | 11.73 | 172.25 | 0.71 | 5.01 | 4.19 | 0.43 | 0.58 | 1.09 | 1.89 | 0.438 | 1.59 | 0.273 |
| 2B_12 | 29.7 | 228.32 | 35.67 | 18.55 | 25.5 | 18.5 | 263.5 | 0.63 | 3.75 | 6.39 | 1.4 | 0.86 | 2.42 | 3.28 | 0.528 | 2.61 | 0.55 |
| 2B_13 | 31.55 | 231.56 | 27.89 | 16.04 | 25.41 | 19.23 | 396.05 | 1.53 | 4.08 | 6.02 | 1.25 | 1.43 | 2.55 | 2.67 | 0.77 | 2.03 | 0.64 |
| 2B_14 | 88.31 | 386.19 | 40.68 | 21.8 | 27.04 | 28.56 | 436.9 | 1.27 | 6.65 | 12.36 | 1.23 | 0.01915 | 2.85 | 3.19 | 0.73 | 2.03 | 0.47 |
| 2B_15 | 28.91 | 184.37 | 34.95 | 17.03 | 27.52 | 15.91 | 330.09 | 0.61 | 3.51 | 7 | 0.98 | 0.57 | 1.92 | 4.63 | 0.58 | 2.2 | 0.56 |
| 2B_2 | 37.53 | 234.83 | 40.34 | 22.42 | 26.82 | 17.41 | 254.16 | 1.92 | 4 | 5.26 | 0.99 | 0.226 | 1.92 | 3.38 | 1.26 | 3.11 | 1.13 |
| 2B_3 | 41.86 | 156.14 | 33.57 | 16.78 | 26.07 | 14.16 | 224.64 | 0.92 | 3.3 | 7.8 | 0.68 | 0.83 | 2.22 | 2.67 | 0.61 | 3.46 | 0.73 |
| 2B_4 | 48.44 | 274.16 | 28.88 | 19.85 | 25.46 | 19.15 | 337.19 | 0.246 | 3.41 | 6.46 | 1.45 | 1 | 3.04 | 2.85 | 0.547 | 8.86 | 0.407 |
| 2B_5 | 51.43 | 178.98 | 30.07 | 16.11 | 25.2 | 11.39 | 202.18 | 0.263 | 1.67 | 7.08 | 0.63 | 0.326 | 1.17 | 1.85 | 0.295 | 1.04 | 0.5 |
| 2B_6 | 37.33 | 306.92 | 54.15 | 16.04 | 28.7 | 18.21 | 272.28 | 0.72 | 11.75 | 4.91 | 1.24 | 1.19 | 3.05 | 4.27 | 0.69 | 2.04 | 0.465 |
| 2B_7 | 40.62 | 268.51 | 53.74 | 13.46 | 25.31 | 13.96 | 225.79 | 0.85 | 3.81 | 4.64 | 1.1 | 0.087 | 2.55 | 3.15 | 0.445 | 2.01 | 0.448 |
| 2B_8 | 22.57 | 199.31 | 40.51 | 13.02 | 24.76 | 12.82 | 238.14 | 0.7 | 3.43 | 5.75 | 0.71 | 0.305 | 1.51 | 3.1 | 0.88 | 1.76 | 0.54 |
| 2B_9 | 55.13 | 181.72 | 21.18 | 13.28 | 24.43 | 21.19 | 373.49 | 0.79 | 10.85 | 2.85 | 0.75 | 0.62 | 1.42 | 1.92 | 0.471 | 1.19 | 0.68 |
| 22G_1 | 32.19 | 200.57 | 19.44 | 3.85 | 25.4 | 7.32 | 181.76 | 0.61 | 8.58 | 1.3 | 0.69 | 0.112 | 1.38 | 1.59 | 0.073 | 0.93 | 0.169 |
| 22G_10 | 115.26 | 1250.87 | 605.71 | 6.2 | 23.59 | 36.32 | 292.7 | 0.369 | 6.77 | 1.05 | 5.37 | 0.149 | 1.35 | 5.28 | 0.204 | 1.97 | 0.29 |
| 22G_11 | 1991.25 | 3106.1 | 1751.9 | 168.05 | 92.97 | 506.78 | 2600.85 | 1.7 | 13.97 | 9.6 | 11.75 | 0.86 | 19.32 | 42.32 | 0.44 | 0.92 | 0.35 |
| 22G_12 | 5745.6 | 3673.73 | 8250.13 | 1373.73 | 442.14 | 3293.12 | 12847.29 | 8.49 | 99.28 | 124.8 | 20.05 | 2.5 | 7.18 | 8.52 | 1.83 | 1.83 | 0.38 |
| 22G_13 | 115.45 | 158.9 | 73.06 | 18.97 | 30.45 | 26.5 | 260.63 | 0.49 | 6.9 | 1.13 | 0.66 | 0.127 | 1.37 | 0.67 | 0.29 | 0.68 | 0.197 |
| 22G_14 | 114.34 | 3197.99 | 427.42 | 22.26 | 34.57 | 27.24 | 259.64 | 0.4 | 13.35 | 2.15 | 37.94 | 0.43 | 14.23 | 49.05 | 0.55 | 1.42 | 1.11 |
| 22G_15 | 32.07 | 248.64 | 27.31 | 3.58 | 25.43 | 8.92 | 168.11 | 0.43 | 6.65 | 1 | 2.23 | 0.091 | 1.43 | 2.36 | 0.076 | 0.6 | 0.189 |
| 22G_2 | 38.51 | 73.54 | 20.82 | 4.97 | 24.88 | 10.48 | 162.31 | 0.71 | 4.4 | 0.99 | 0.34 | 0.096 | 0.89 | 0.4 | 0.055 | 0.61 | 0.186 |
| 22G_3 | 13.05 | 35.12 | 5.73 | 1.92 | 23.53 | 5.29 | 55.55 | 0.73 | 3.39 | 0.277 | 0.21 | 0.01915 | 0.6 | 0.19 | 0.028 | 0.19 | 0.117 |
| 22G_4 | 54.19 | 167.88 | 17.98 | 6.98 | 26.52 | 9.94 | 166.04 | 0.318 | 3.61 | 0.75 | 0.95 | 0.069 | 2.62 | 0.96 | 0.115 | 0.55 | 0.176 |

LX

| | | | | | | | | | | | | | | | | | |
|---|---|---|---|---|---|---|---|---|---|---|---|---|---|---|---|---|---|
| 22G_5 | 27.71 | 102.73 | 13.3 | 3.63 | 24.64 | 5.91 | 158.36 | 0.65 | 5.08 | 66.8 | 0.47 | 0.048 | 1.24 | 0.72 | 0.05 | 0.51 | 0.141 |
| 22G_6 | 33.54 | 225.31 | 25.01 | 5.21 | 26.98 | 11.16 | 246.8 | 0.54 | 84.96 | 0.89 | 0.47 | 0.099 | 1.26 | 1.29 | 0.148 | 0.72 | 0.248 |
| 22G_7 | 49.8 | 99.7 | 25.28 | 6.17 | 24.69 | 10.12 | 123.48 | 0.276 | 5.18 | 1.78 | 0.56 | 0.104 | 1.72 | 0.44 | 0.043 | 0.37 | 0.107 |
| 22G_8 | 21.6 | 36.11 | 11.02 | 2.31 | 24.07 | 4.2 | 53.09 | 0.158 | 1.15 | 0.45 | 0.2 | 0.118 | 0.63 | 0.136 | 0.045 | 0.23 | 0.051 |
| 22G.1 | 38.09 | 507.19 | 57.82 | 29.39 | 46.22 | 14.38 | 283.43 | 0.8 | 25.26 | 1.01 | 1.06 | 0.291 | 1.57 | 6.74 | 0.177 | 14.87 | 228.79 |
| 22G.2 | 13.3 | 45.32 | 9.27 | 1.71 | 33.46 | 5.63 | 146.44 | 1.83 | 18.17 | 0.74 | 0.177 | 0.092 | 0.324 | 0.325 | 0.0444 | 0.294 | 0.165 |
| 22G.3 | 27.07 | 133.04 | 14.54 | 3.95 | 33.91 | 11.13 | 127.53 | 0.55 | 9.97 | 0.92 | 0.437 | 0.098 | 0.97 | 1.21 | 0.116 | 0.767 | 0.204 |
| 22G_9 | 71.25 | 137.48 | 20.65 | 10.64 | 37.06 | 13.35 | 406.81 | 0.268 | 1.9 | 3.31 | 0.49 | 0.25 | 2.41 | 0.39 | 0.048 | 0.33 | 0.31 |
| 21E.1 | 12.08 | 187.13 | 31.36 | 3.01 | 48.67 | 6.22 | 138.67 | 0.374 | 6.9 | 2.91 | 0.611 | 0.152 | 0.39 | 1.38 | 0.981 | 0.498 | 0.144 |
| 21E.2 | 36.16 | 201.29 | 36.94 | 9.81 | 47.11 | 21.85 | 509.55 | 2.23 | 9.15 | 1.5 | 1.15 | 0.175 | 1.6 | 0.694 | 0.798 | 0.352 | 0.174 |
| 21E.3 | 26.78 | 382.27 | 35.82 | 12.1 | 49.64 | 16.01 | 420.47 | 3.19 | 1049.89 | 744.83 | 4.62 | 0.133 | 4.68 | 2.65 | 1.314 | 0.27 | 0.167 |
| 22E.1 | 41.69 | 512.48 | 63.9 | 7.41 | 33.27 | 25.01 | 268.48 | 0.235 | 2.37 | 2.23 | 1.33 | 0.172 | 0.94 | 11.9 | 1.2 | 0.367 | 2.64 |
| 22E.2 | 324.31 | 122.11 | 163.6 | 3.91 | 89.64 | 25.09 | 256.66 | 0.91 | 4.91 | 3.04 | 0.51 | 0.118 | 0.55 | 1 | 0.82 | 0.77 | 0.084 |
| 22E.3 | 13.59 | 311 | 15.57 | 4.77 | 34.12 | 8.72 | 148.38 | 0.46 | 4.87 | 2.2 | 6.23 | 0.173 | 2.24 | 6.96 | 0.275 | 0.494 | 0.087 |
| 21E_1 | 20.43 | 239.06 | 47.71 | 3.89 | 24.6 | 12.39 | 133.73 | 0.251 | 10.54 | 2.21 | 1.56 | 0.42 | 1.01 | 2.48 | 0.64 | 3.29 | 0.169 |
| 21E_10 | 14.43 | 486.05 | 21.27 | 1.63 | 25.32 | 7.48 | 125.77 | 0.218 | 3.95 | 1.81 | 0.56 | 0.144 | 0.49 | 0.67 | 0.98 | 0.11 | 0.066 |
| 21E_11 | 139.36 | 2392.03 | 124.2 | 108.4 | 40.9 | 66.41 | 2045.27 | 1.78 | 196.06 | 24.7 | 8.79 | 1 | 19.01 | 36.87 | 1115.7 | 7.32 | 40.93 |
| 21E_12 | 15.5 | 110.71 | 109.76 | 2.84 | 26.34 | 19.13 | 180.38 | 0.21 | 17.96 | 2.21 | 0.59 | 0.201 | 0.6 | 2.04 | 3.76 | 4.23 | 0.277 |
| 21E_13 | 31.81 | 233.79 | 34.28 | 4.5 | 26.97 | 22.16 | 224.63 | 0.38 | 20.83 | 3.05 | 1.32 | 0.124 | 0.97 | 1.65 | 1.54 | 0.8 | 0.174 |
| 21E_14 | 24.6 | 813.97 | 46.33 | 3.79 | 27.77 | 15.47 | 245.17 | 0.291 | 9.05 | 3.08 | 15.3 | 0.21 | 22.88 | 9.66 | 2.25 | 0.35 | 0.088 |
| 21E_15 | 23.98 | 269.88 | 27.61 | 4.58 | 25.62 | 21.79 | 257.19 | 0.33 | 9.43 | 4.96 | 0.97 | 0.36 | 2.09 | 1.47 | 0.93 | 0.31 | 0.36 |
| 21E_2 | 25.21 | 220.4 | 30.97 | 6.57 | 24.92 | 29.87 | 290.84 | 0.272 | 10.8 | 2.5 | 1.73 | 0.154 | 2.14 | 1.02 | 0.51 | 0.37 | 0.105 |
| 21E_3 | 20.22 | 208.54 | 38.49 | 4.29 | 27.33 | 19.96 | 239.2 | 0.38 | 66.04 | 3.1 | 0.68 | 0.209 | 0.65 | 1.59 | 1.81 | 0.37 | 0.184 |
| 21E_4 | 14.83 | 103.84 | 23.85 | 2.9 | 25.11 | 10.88 | 143.6 | 0.215 | 9.64 | 2.22 | 0.64 | 0.183 | 0.59 | 1.67 | 0.356 | 0.44 | 0.084 |
| 21E_5 | 32.01 | 545.84 | 29.67 | 28.26 | 25.76 | 14.37 | 251.14 | 0.25 | 7.96 | 2.24 | 5.49 | 0.211 | 9.64 | 1.5 | 0.38 | 0.4 | 0.087 |
| 21E_6 | 53.69 | 829.23 | 34.03 | 16.46 | 27.35 | 23.8 | 360.47 | 0.42 | 6.7 | 7.43 | 4.19 | 0.306 | 7.53 | 1.75 | 3.18 | 14.09 | 0.208 |
| 21E_7 | 13.79 | 79.17 | 17.7 | 3.26 | 26.18 | 11.55 | 112.18 | 0.211 | 5.43 | 1.92 | 0.48 | 0.112 | 0.51 | 0.57 | 0.5 | 0.7 | 0.083 |
| 21E_8 | 19.74 | 387.68 | 23.57 | 3.88 | 27.19 | 9.6 | 505.47 | 0.269 | 3064.83 | 3.06 | 1.66 | 0.39 | 3.42 | 0.83 | 0.44 | 0.43 | 0.121 |
| 21E_9 | 14.49 | 202.49 | 24.29 | 2.04 | 25.5 | 11.71 | 146.2 | 0.25 | 10.1 | 1.92 | 0.63 | 0.155 | 1.1 | 0.75 | 0.5 | 0.21 | 0.083 |
| 22E_1 | 14.15 | 67.24 | 22.41 | 1.82 | 25.54 | 13.25 | 193.32 | 0.51 | 6.28 | 2.32 | 0.45 | 0.352 | 0.42 | 0.75 | 0.98 | 1.08 | 0.089 |

| | | | | | | | | | | | | | | | | | |
|---|---|---|---|---|---|---|---|---|---|---|---|---|---|---|---|---|---|
| 22E_10 | 9.61 | 69.2 | 16.39 | 2.74 | 25.67 | 9.08 | 137.27 | 0.16 | 21.34 | 1.8 | 0.34 | 0.67 | 0.178 | 1.07 | 5.47 | 0.71 | 0.112 |
| 22E_11 | 11.24 | 62.89 | 15.77 | 1.24 | 25.65 | 7.46 | 138.66 | 0.282 | 4.19 | 7.09 | 0.24 | 0.108 | 0.212 | 0.74 | 0.339 | 0.43 | 0.06 |
| 22E_12 | 51.27 | 70.71 | 13.79 | 2.95 | 28.27 | 8.62 | 137.05 | 0.295 | 4.91 | 2.14 | 0.29 | 0.146 | 0.265 | 0.52 | 0.61 | 0.47 | 0.145 |
| 22E_13 | 41.06 | 147.68 | 13.16 | 7.01 | 29.28 | 22.34 | 225.6 | 0.33 | 2.88 | 3.85 | 0.93 | 0.098 | 1.31 | 0.5 | 0.213 | 0.52 | 0.072 |
| 22E_14 | 7.43 | 125 | 18.69 | 1.49 | 27.12 | 6.42 | 137.87 | 0.179 | 3.01 | 3.53 | 0.25 | 0.132 | 0.123 | 1.26 | 0.342 | 0.91 | 0.071 |
| 22E_15 | 12.6 | 56.21 | 13.8 | 1.78 | 27.28 | 13.52 | 160.72 | 0.298 | 3.66 | 1.31 | 0.41 | 0.4 | 0.7 | 0.39 | 0.67 | 0.39 | 0.055 |
| 22E_2 | 93.89 | 44.33 | 12.97 | 1.46 | 28.55 | 9.36 | 142.84 | 0.56 | 11.21 | 1.76 | 0.24 | 0.199 | 0.303 | 0.57 | 0.374 | 0.62 | 0.058 |
| 22E_3 | 6.81 | 54.31 | 16.3 | 0.96 | 24.85 | 6.37 | 117.33 | 0.121 | 2.33 | 2.42 | 0.48 | 0.132 | 0.175 | 0.56 | 0.6 | 0.37 | 0.079 |
| 22E_4 | 10.05 | 70.94 | 16.37 | 1.27 | 25.73 | 7.05 | 113.76 | 0.172 | 3.47 | 1.18 | 0.31 | 0.164 | 0.276 | 0.58 | 0.93 | 0.32 | 0.055 |
| 22E_5 | 6.78 | 49.3 | 13.61 | 0.6 | 24.33 | 10.58 | 79.33 | 0.132 | 1.81 | 1.1 | 0.19 | 0.156 | 0.086 | 0.8 | 0.331 | 0.39 | 0.045 |
| 22E_6 | 23.39 | 59.49 | 13.69 | 2.86 | 24.52 | 12.28 | 127.17 | 0.199 | 3.37 | 2.9 | 0.38 | 0.122 | 0.85 | 0.5 | 0.372 | 0.41 | 0.075 |
| 22E_7 | 26.39 | 63.31 | 21.55 | 4 | 29.34 | 20.02 | 148.79 | 0.273 | 3.92 | 1.98 | 0.53 | 0.113 | 0.71 | 0.6 | 0.212 | 0.43 | 0.061 |
| 22E_8 | 10.74 | 437.04 | 84.86 | 1.22 | 25.77 | 10.62 | 151.67 | 0.206 | 23.81 | 1.78 | 2.61 | 0.101 | 0.354 | 10.53 | 0.52 | 1.84 | 0.069 |
| 22E_9 | 7 | 65.48 | 15.03 | 0.83 | 25.8 | 9.32 | 140.05 | 0.227 | 12.21 | 1.53 | 0.34 | 0.124 | 0.177 | 0.45 | 0.161 | 0.44 | 0.063 |
| 5B.1 | 28.94 | 712.41 | 31.2 | 21.68 | 56.19 | 21.2 | 270.37 | 0.0875 | 6.33 | 5.28 | 2.06 | 0.158 | 1.78 | 1 | 2.91 | 0.126 | 0.165 |
| 5B.2 | 4.25 | 39.79 | 14.14 | 0.537 | 52.66 | 2.75 | 41.34 | 0.095 | 5 | 1.03 | 0.133 | 0.0682 | 0.082 | 0.15 | 0.0903 | 0.03 | 0.0293 |
| 5B.3 | 12.23 | 206.64 | 49.29 | 4.77 | 53.02 | 17.02 | 1010.53 | 0.467 | 7 | 12.35 | 0.918 | 0.2 | 0.85 | 0.89 | 0.478 | 0.482 | 0.134 |
| 5B_1 | 27.85 | 106.63 | 8.52 | 7.15 | 25.58 | 10.79 | 146.93 | 0.15 | 2.93 | 2.27 | 0.49 | 0.331 | 1.17 | 0.234 | 2.61 | 0.053 | 0.157 |
| 5B_10 | 17.63 | 712.43 | 22.35 | 3.44 | 24.14 | 11.01 | 190.33 | 0.193 | 224.18 | 8.27 | 0.92 | 0.123 | 0.509 | 0.66 | 3.52 | 0.201 | 0.107 |
| 5B_11 | 14.15 | 699.7 | 17.82 | 2.1 | 24.42 | 12.48 | 135.36 | 0.222 | 7.18 | 2.93 | 2.51 | 0.189 | 4.64 | 1.06 | 0.676 | 0.068 | 0.061 |
| 5B_12 | 17.99 | 224.55 | 18.92 | 2.32 | 24.64 | 12.34 | 136.19 | 0.306 | 4.82 | 2.76 | 0.5 | 0.102 | 0.394 | 0.67 | 0.691 | 0.35 | 0.163 |
| 5B_13 | 154.41 | 327.95 | 380.31 | 15.44 | 35.56 | 185.56 | 773.08 | 1.14 | 7.59 | 9.41 | 0.86 | 0.201 | 0.456 | 1.14 | 0.81 | 0.148 | 0.086 |
| 5B_14 | 10.18 | 89.61 | 18.17 | 1.22 | 24.64 | 8.81 | 104.43 | 0.155 | 4.18 | 1.88 | 0.243 | 0.128 | 0.215 | 0.48 | 0.236 | 0.063 | 0.051 |
| 5B_15 | 18.09 | 256.52 | 17.61 | 5.65 | 24.51 | 11.73 | 147.19 | 0.284 | 10.5 | 2.32 | 2.92 | 0.127 | 1.22 | 2.07 | 0.689 | 0.116 | 0.069 |
| 5B_2 | 25.74 | 273.21 | 19.18 | 2.62 | 25 | 12.26 | 112.17 | 0.17 | 5.06 | 3.31 | 1.08 | 0.212 | 0.583 | 1.04 | 0.653 | 0.094 | 0.093 |
| 5B_3 | 7.26 | 82.81 | 8.26 | 1.37 | 24.74 | 8.19 | 83.82 | 0.08 | 3.27 | 1.8 | 0.23 | 0.169 | 0.22 | 0.261 | 0.199 | 0.044 | 0.06 |
| 5B_4 | 45.44 | 299.84 | 56.58 | 5.66 | 23.9 | 32.96 | 223.65 | 0.388 | 5.88 | 4.43 | 0.87 | 0.161 | 0.88 | 1.36 | 0.61 | 0.35 | 0.175 |
| 5B_5 | 11.02 | 124.6 | 26.1 | 2.26 | 23.82 | 11.91 | 124.83 | 0.295 | 3.72 | 2.75 | 0.304 | 0.164 | 0.323 | 0.55 | 0.452 | 0.094 | 0.073 |
| 5B_6 | 13.15 | 272.84 | 12.84 | 1.15 | 23.51 | 8.47 | 548.83 | 0.275 | 2543.98 | 7.22 | 0.36 | 0.177 | 0.148 | 0.49 | 0.613 | 0.049 | 0.078 |
| 5B_7 | 22.73 | 440.04 | 15 | 2.42 | 25.39 | 10.51 | 160.91 | 0.25 | 13.19 | 5.02 | 6.02 | 0.184 | 3.29 | 2.6 | 1.01 | 1 | 0.124 |

| | | | | | | | | | | | | | | | | | |
|---|---|---|---|---|---|---|---|---|---|---|---|---|---|---|---|---|---|
| 5B_8 | 40.87 | 461.69 | 22.22 | 20.01 | 23.65 | 28.36 | 196.14 | 0.84 | 7.04 | 4.6 | 1.67 | 0.105 | 5.87 | 0.67 | 1.07 | 0.093 | 0.085 |
| 5B_9 | 20.93 | 165.41 | 12.15 | 6.19 | 25.48 | 14.83 | 1950.9 | 1.12 | 5.87 | 2.94 | 0.6 | 0.156 | 1.31 | 0.43 | 0.354 | 0.094 | 0.107 |
| 10B_1 | 10.17 | 90.53 | 23.7 | 2.58 | 41.96 | 16.1 | 527.51 | 2.68 | 229.97 | 19.34 | 2.65 | 1.24 | 0.192 | 2.18 | 2.09 | 1.67 | 0.24 |
| 10B_2 | 9.23 | 54.19 | 20.91 | 2.33 | 43.98 | 14.21 | 503.71 | 2.8 | 105.19 | 14.27 | 2.22 | 1.72 | 0.094 | 1.86 | 0.25 | 0.49 | 0.22 |
| 10B_3 | 9.78 | 68.56 | 15.48 | 1.82 | 43.77 | 20.92 | 496.5 | 2.95 | 55.83 | 16.41 | 2.55 | 0.8 | 0.25 | 1.37 | 0.08 | 0.44 | 0.214 |
| 10B_4 | 7.84 | 38.92 | 21.25 | 1.5 | 37.71 | 12.85 | 390.01 | 4.14 | 40.27 | 12.41 | 1.81 | 1.22 | 0.113 | 1.34 | 0.058 | 0.33 | 0.164 |
| 10B_5 | 9.13 | 30.73 | 31.76 | 2.01 | 35.84 | 23.69 | 502.6 | 3.21 | 35.06 | 19.13 | 2.2 | 0.75 | 0.092 | 1.74 | 0.63 | 0.95 | 0.197 |
| 10B_6 | 9.62 | 43.06 | 11.44 | 1.9 | 33.82 | 9.92 | 359.95 | 2.73 | 29.82 | 17.62 | 1.51 | 0.66 | 0.025 | 1.06 | 0.072 | 0.35 | 0.173 |
| 10B_7 | 8.53 | 42.02 | 11.88 | 1.01 | 33.13 | 12.99 | 536.99 | 2.85 | 65.6 | 9.11 | 2.06 | 0.82 | 0.071 | 1.5 | 0.071 | 0.39 | 0.169 |
| 10BA_1 | 0.7 | 80.35 | 8.03 | 6.87 | 67.53 | 0.8 | 2.5 | 13.32 | 4.07 | 13.55 | 0.86 | 20.23 | 0.56 | 1.26 | 6.66 | 1.27 | 0.64 |
| 10BA_2 | 1.1 | 28.28 | 9.74 | 0.00775 | 67.22 | 2.26 | 8.45 | 0.075 | 0.93 | 9.97 | 0.159 | 1.34 | 0.015 | 0.77 | 0.34 | 0.47 | 0.026 |
| 10BA_3 | 0.88 | 11.68 | 3.11 | 0.25 | 65.93 | 1.87 | 11.88 | 0.0555 | 0.6 | 5.78 | 0.65 | 1.54 | 0.3 | 0.2 | 0.052 | 0.098 | 0.018 |
| 10BA_4 | 29.25 | 72.18 | 5.69 | 0.93 | 57.25 | 3.73 | 107.3 | 0.71 | 8.3 | 15.2 | 0.65 | 0.96 | 3.68 | 2.31 | 2.35 | 3.91 | 0.168 |
| 10BA_5 | 11.42 | 58.1 | 5.24 | 0.084 | 50.6 | 0.2 | 59.02 | 0.092 | 0.7 | 8.54 | 0.108 | 1.12 | 0.047 | 0.2 | 0.16 | 0.117 | 0.0102 |
| 10BA_7 | 3.82 | 15.92 | 6.13 | 0.073 | 48.9 | 0.072 | 13.17 | 0.045 | 0.49 | 5.97 | 0.069 | 0.73 | 0.00605 | 0.4 | 0.26 | 0.29 | 0.0125 |
| 22F.1 | 94.7 | 326.28 | 24.34 | 21.53 | 50.78 | 27.18 | 1394.87 | 1.42 | 9.1 | 27.98 | 1.57 | 1.43 | 1.63 | 2.28 | 4.19 | 0.211 | 0.375 |
| 22F.2 | 226.79 | 300.27 | 29.38 | 7.7 | 52.92 | 14.92 | 331.95 | 0.562 | 3.66 | 17.19 | 1.14 | 0.87 | 0.9 | 1.84 | 1.77 | 0.063 | 0.0415 |
| 22F.3 | 101.72 | 780.66 | 29.3 | 20.3 | 52.81 | 17.21 | 1082.74 | 0.647 | 12.33 | 35.51 | 1.87 | 0.718 | 1.99 | 2.82 | 4.09 | 0.0837 | 0.094 |
| 22F_1 | 32.95 | 186.6 | 10.26 | 4.61 | 24.68 | 6.41 | 324.41 | 0.141 | 13.08 | 11.69 | 4.35 | 0.71 | 0.92 | 0.9 | 0.9 | 0.119 | 0.0311 |
| 22F_1 | 189.29 | 853.94 | 40.1 | 33.36 | 32.51 | 33.75 | 1564.51 | 1.039 | 29.36 | 51.48 | 52.73 | 0.93 | 4.38 | 4.03 | 18.82 | 0.663 | 4 |
| 22F_10 | 102.11 | 355.38 | 27.19 | 17.25 | 29.48 | 14.09 | 649.5 | 0.59 | 7.63 | 40.19 | 9.69 | 1.69 | 1.62 | 2.01 | 2.73 | 0.45 | 0.133 |
| 22F_10 | 163.51 | 522.51 | 31.32 | 22.67 | 29.04 | 20.53 | 1105.06 | 0.896 | 6.2 | 32.6 | 118.37 | 1.08 | 4.04 | 3.45 | 4.2 | 0.352 | 0.181 |
| 22F_11 | 63.61 | 327.54 | 80.54 | 9.79 | 24.93 | 9.15 | 818.24 | 0.344 | 10.5 | 26.01 | 25.25 | 0.92 | 1.82 | 2.11 | 1.99 | 2.94 | 0.238 |
| 22F_11 | 79.05 | 1000.2 | 27.43 | 15.08 | 27.41 | 14.23 | 561.81 | 0.462 | 6.48 | 16.02 | 27.18 | 0.81 | 20.26 | 24.75 | 3.24 | 2.48 | 0.201 |
| 22F_12 | 49.17 | 286.67 | 16.12 | 49.56 | 25.46 | 14.28 | 2472.77 | 0.69 | 5.82 | 45.75 | 1.78 | 2.11 | 1.16 | 1.42 | 6.44 | 0.32 | 0.266 |
| 22F_12 | 44.04 | 148.75 | 16.09 | 12.01 | 25.79 | 12.45 | 896.6 | 0.525 | 17.25 | 24.66 | 1.14 | 1.68 | 1.08 | 1.73 | 4.3 | 0.651 | 0.265 |
| 22F_13 | 40.73 | 196.03 | 9.86 | 9.58 | 25.78 | 12.77 | 1238.72 | 0.214 | 4.26 | 18.1 | 0.82 | 0.86 | 0.66 | 0.88 | 1.55 | 0.2 | 0.097 |
| 22F_13 | 109.13 | 328.28 | 36.76 | 12.78 | 27.12 | 16.02 | 741.47 | 0.561 | 9.27 | 21.15 | 10.05 | 1.73 | 2.27 | 2.77 | 3.51 | 0.377 | 0.21 |
| 22F_14 | 46.22 | 361.4 | 15.6 | 44.26 | 31.44 | 11.66 | 1567.03 | 0.61 | 58.07 | 27.87 | 19.74 | 2.54 | 2.61 | 1.47 | 3.99 | 0.43 | 0.238 |
| 22F_14 | 147.04 | 532.08 | 48.46 | 27.15 | 25.36 | 33.69 | 4998.56 | 0.651 | 6.55 | 79.23 | 13.34 | 1.2 | 5.23 | 7.27 | 17.12 | 0.646 | 0.152 |

| | | | | | | | | | | | | | | | | | |
|---|---|---|---|---|---|---|---|---|---|---|---|---|---|---|---|---|---|
| 22F_15 | 83.92 | 244.1 | 12.07 | 13.78 | 25.66 | 24.67 | 703.31 | 0.382 | 5.14 | 22.21 | 1.04 | 0.65 | 0.72 | 0.98 | 2.25 | 0.16 | 0.104 |
| 22F_15 | 74.74 | 359.77 | 23.5 | 10.45 | 27.08 | 17.81 | 864.6 | 0.553 | 32.01 | 24.42 | 1.82 | 1 | 2.88 | 2.87 | 3.7 | 0.282 | 0.145 |
| 22F_2 | 74.98 | 415.77 | 18.47 | 6.83 | 25.7 | 7.82 | 385.22 | 0.237 | 7.02 | 17.52 | 72.38 | 1.16 | 2.4 | 1.68 | 1.64 | 0.53 | 0.065 |
| 22F_2 | 440.75 | 1694.19 | 82.02 | 113.34 | 80.14 | 92.14 | 4114.18 | 2.87 | 93.76 | 160.66 | 82.82 | 2.93 | 12.14 | 8.86 | 18.77 | 2.6 | 1.27 |
| 22F_3 | 94.38 | 328.55 | 15.79 | 7.66 | 25.26 | 16.8 | 409.19 | 0.283 | 4.53 | 46.83 | 0.82 | 0.54 | 0.76 | 1.34 | 2.49 | 0.18 | 0.084 |
| 22F_3 | 180.8 | 453.33 | 33.6 | 24.19 | 29.18 | 36.93 | 1623.31 | 0.869 | 9.76 | 40.04 | 8.5 | 1.29 | 2.14 | 2.94 | 3.79 | 0.285 | 0.167 |
| 22F_4 | 95.16 | 409 | 28.33 | 21.1 | 25.16 | 29.57 | 5464.64 | 0.334 | 13.19 | 47.29 | 6.04 | 2.09 | 1.52 | 2.41 | 4.41 | 0.74 | 0.248 |
| 22F_4 | 62.2 | 216.03 | 19.76 | 7.99 | 26.62 | 12.19 | 831.34 | 0.578 | 10.42 | 10.53 | 23.67 | 2.01 | 2.49 | 1.94 | 1.53 | 0.24 | 0.077 |
| 22F_5 | 86.27 | 394.61 | 18.92 | 17.52 | 29.87 | 15.44 | 1227.68 | 0.51 | 5.79 | 37.79 | 15.83 | 1.53 | 1.84 | 1.66 | 3.23 | 0.28 | 0.138 |
| 22F_5 | 153.35 | 170.03 | 20.54 | 7.97 | 25.85 | 12.52 | 726 | 0.401 | 6.35 | 11.62 | 5.23 | 0.72 | 1.19 | 1.73 | 2.4 | 0.279 | 0.363 |
| 22F_6 | 58.11 | 208.24 | 25.48 | 8.83 | 25.06 | 10.03 | 542.92 | 0.308 | 7.8 | 21 | 0.87 | 1.94 | 1.07 | 1.62 | 1.8 | 0.095 | 0.07 |
| 22F_6 | 112.35 | 295.27 | 59.56 | 12 | 28.66 | 13.91 | 676.53 | 0.452 | 6.55 | 20.26 | 2.2 | 0.98 | 2.29 | 3.67 | 2.87 | 0.95 | 0.152 |
| 22F_7 | 112.34 | 502.48 | 16.5 | 12.94 | 29.58 | 20.38 | 689.6 | 0.51 | 16.83 | 34.03 | 398.14 | 1 | 2.85 | 1.54 | 1.48 | 0.095 | 0.173 |
| 22F_7 | 164.06 | 440.17 | 26.79 | 19.62 | 27.25 | 24.71 | 1768.11 | 0.927 | 12.75 | 37.19 | 52.73 | 1.32 | 2.68 | 2.36 | 4.59 | 0.356 | 0.157 |
| 22F_8 | 100.88 | 235.79 | 10.29 | 29.1 | 30.25 | 14.62 | 555.83 | 0.195 | 5.09 | 18.5 | 1.82 | 1.34 | 3.38 | 0.89 | 1.62 | 0.134 | 0.094 |
| 22F_8 | 142.05 | 451.39 | 21.06 | 11.76 | 28.2 | 14.87 | 538.14 | 0.587 | 5.51 | 23.09 | 3.45 | 1.22 | 1.24 | 1.68 | 2.56 | 0.177 | 0.0704 |
| 22F_9 | 56.35 | 799.61 | 15.81 | 30.61 | 34.1 | 23.16 | 1845.37 | 0.55 | 4.94 | 32.62 | 2.6 | 1.66 | 1.41 | 1.54 | 4.09 | 0.16 | 0.111 |
| 22F_9 | 53.66 | 255.75 | 21.67 | 6.86 | 25.47 | 11.65 | 784.4 | 0.754 | 11.8 | 13.2 | 27.96 | 1.86 | 2.13 | 2.99 | 1.75 | 0.158 | 0.096 |
| 4B.1 | 13.18 | 170.26 | 10.9 | 4.72 | 36.79 | 6.12 | 215.29 | 0.257 | 7.13 | 9 | 0.448 | 0.335 | 0.396 | 1 | 0.9 | 0.0103 | 0.0138 |
| 4B.2 | 16.98 | 498.2 | 20.05 | 5.1 | 39.17 | 9.6 | 160.32 | 0.105 | 3.28 | 5.48 | 0.97 | 0.687 | 0.247 | 0.5 | 2.12 | 0.011 | 0.0172 |
| 4B.3 | 8.66 | 620.97 | 6.36 | 2.83 | 40.3 | 2.61 | 163.72 | 0.02015 | 3.92 | 6.08 | 1.12 | 0.19 | 0.382 | 0.486 | 2.47 | 0.00413 | 0.00814 |
| 4B_1 | 6.1 | 193.12 | 10.14 | 3.2 | 33.07 | 7.29 | 154.7 | 0.02015 | 5.07 | 4.85 | 0.35 | 0.311 | 0.099 | 0.44 | 0.479 | 0.49 | 0.0147 |
| 4B_10 | 9.62 | 225.81 | 11.37 | 3.59 | 31.35 | 12.27 | 269.85 | 0.49 | 8.55 | 3.97 | 0.51 | 0.73 | 0.099 | 0.7 | 1.58 | 0.029 | 0.074 |
| 4B_11 | 3.21 | 239.18 | 7.2 | 6.08 | 32.67 | 2.43 | 59.84 | 0.067 | 2.85 | 1.92 | 0.53 | 0.23 | 0.219 | 0.34 | 1.72 | 0.088 | 0.0582 |
| 4B_12 | 9.97 | 175.51 | 10.51 | 3.87 | 33.09 | 4.35 | 188.56 | 0.095 | 6.26 | 6.52 | 0.23 | 0.3 | 0.47 | 0.54 | 0.82 | 0.145 | 0.075 |
| 4B_13 | 5.21 | 212.13 | 9.3 | 1.55 | 32.39 | 2.61 | 128.87 | 0.413 | 2.36 | 2.36 | 0.28 | 0.232 | 0.079 | 0.33 | 0.632 | 0.0076 | 0.0157 |
| 4B_14 | 13.78 | 421.14 | 11.27 | 7.97 | 34.08 | 3.35 | 145.49 | 0.08 | 4.07 | 5.92 | 0.8 | 0.52 | 0.53 | 0.53 | 1.35 | 0.0151 | 0.0119 |
| 4B_15 | 15.17 | 466.8 | 12.35 | 8.94 | 34.73 | 4.42 | 171.51 | 0.55 | 2.32 | 10.14 | 0.63 | 0.3 | 0.37 | 0.69 | 1.75 | 0.0051 | 0.0445 |
| 4B_2 | 12.55 | 361.11 | 12.82 | 6.41 | 33.9 | 6.25 | 265.41 | 0.421 | 5.91 | 6.42 | 0.82 | 0.71 | 0.177 | 0.87 | 1.37 | 0.083 | 0.0249 |
| 4B_3 | 6.74 | 238.36 | 9.61 | 2.57 | 32.83 | 3.97 | 125.04 | 0.02015 | 4.76 | 7.53 | 1.46 | 1.03 | 0.092 | 0.55 | 1.1 | 0.027 | 0.0124 |

| | | | | | | | | | | | | | | | | | |
|---|---|---|---|---|---|---|---|---|---|---|---|---|---|---|---|---|---|
| 4B_4 | 5.43 | 106.82 | 10.51 | 2 | 32.12 | 2.92 | 121.41 | 0.186 | 3.78 | 3.74 | 0.21 | 0.254 | 0.161 | 0.48 | 0.457 | 0.053 | 0.0118 |
| 4B_5 | 5.78 | 152.94 | 11.01 | 3.27 | 31.49 | 3.24 | 201.16 | 0.305 | 5.32 | 3.69 | 0.37 | 0.49 | 0.128 | 0.6 | 0.577 | 0.042 | 0.025 |
| 4B_6 | 3.26 | 98.11 | 11 | 1.45 | 32.81 | 2.12 | 50.97 | 0.02015 | 1.26 | 1.01 | 0.162 | 0.184 | 0.068 | 0.248 | 0.403 | 0.0112 | 0.0055 |
| 4B_7 | 11.47 | 225.11 | 12.44 | 2.58 | 31.83 | 2.86 | 183.8 | 0.105 | 2.94 | 5.47 | 0.3 | 1 | 0.23 | 0.56 | 0.88 | 0.0146 | 0.0106 |
| 4B_8 | 8.56 | 143.84 | 12.82 | 3.25 | 34.78 | 7.12 | 166.25 | 0.215 | 3.89 | 8.45 | 0.34 | 0.35 | 0.41 | 0.58 | 0.564 | 0.032 | 0.0149 |
| 4B_9 | 3.5 | 135.53 | 6.89 | 2.63 | 31.39 | 2.57 | 60.87 | 0.333 | 2.84 | 1.35 | 0.31 | 0.22 | 0.098 | 0.31 | 0.83 | 0.0212 | 0.0201 |

## E. Solution-based-ICP-MS Trace Element Data and Correlation Matrices

| **ICP-MS** | Analyte (µg g-1) | | | | | | | | | | | | | | | | | | | | |
|---|---|---|---|---|---|---|---|---|---|---|---|---|---|---|---|---|---|---|---|---|---|
| **sample ID** | **Mg** | **Al** | **V** | **Cr** | **Mn** | **Fe** | **Ni** | **Cu** | **Zn** | **Ga** | **As** | **Se** | **Rb** | **Sr** | **Mo** | **Ag** | **Cd** | **Ba** | **Tl** | **Pb** | **U** |
| 1A | 2235 | 28809 | 24.70 | 21.59 | 196.45 | 11993 | 7.80 | 16.13 | 31.48 | 8.45 | 10.51 | 1.92 | 22.37 | 47.87 | 3.40 | 0.13 | 0.07 | 77.34 | 0.18 | 29.46 | 3.22 |
| 1A | 2335 | 29475 | 25.21 | 22.31 | 207.05 | 12583 | 8.21 | 16.93 | 33.93 | 8.70 | 10.77 | 2.15 | 22.93 | 48.55 | 3.89 | 0.15 | 0.07 | 77.69 | 0.18 | 29.39 | 3.38 |
| 1A | 2257 | 29517 | 25.52 | 21.70 | 201.08 | 12029 | 8.27 | 16.32 | 33.18 | 8.61 | 10.97 | 1.88 | 23.23 | 48.72 | 3.44 | 0.14 | 0.08 | 80.12 | 0.18 | 29.63 | 3.28 |
| 1B | 33.96 | 389 | 40.81 | 9.68 | 13.05 | 1007 | 11.19 | 12.99 | 30.71 | 0.38 | 0.44 | 1.37 | 0.62 | 4.29 | 10.10 | 0.55 | 0.36 | 11.80 | 0.05 | 2.71 | 2.34 |
| 1B | 31.85 | 363 | 38.82 | 8.92 | 11.84 | 995 | 9.45 | 13.32 | 30.21 | 0.35 | 0.39 | 1.43 | 0.58 | 3.50 | 10.95 | 0.51 | 0.33 | 11.29 | 0.05 | 2.39 | 2.50 |
| 1B | 30.00 | 339 | 37.95 | 8.78 | 11.65 | 958 | 9.21 | 12.35 | 30.40 | 0.36 | 0.46 | 1.39 | 0.53 | 3.47 | 10.28 | 0.51 | 0.33 | 10.33 | 0.05 | 2.54 | 2.37 |
| 1B | 30.60 | 345 | 36.81 | 8.61 | 11.88 | 965 | 8.99 | 12.77 | 31.03 | 0.34 | 0.33 | 1.48 | 0.52 | 3.79 | 10.17 | 0.48 | 0.38 | 10.69 | 0.05 | 2.48 | 2.25 |
| 2A | 1892 | 16091 | 18.95 | 20.82 | 128.57 | 10471 | 21.13 | 59.03 | 40.87 | 4.88 | 5.82 | 2.07 | 13.67 | 19.41 | 1.96 | 0.21 | 0.14 | 56.40 | 0.10 | 25.62 | 2.00 |
| 2A | 1995 | 14502 | 16.65 | 18.65 | 122.82 | 9999 | 21.19 | 45.30 | 47.16 | 4.34 | 7.41 | 1.82 | 11.74 | 17.28 | 1.98 | 0.16 | 0.17 | 51.93 | 0.10 | 26.97 | 1.88 |
| 2A | 1744 | 14088 | 17.19 | 19.60 | 113.74 | 8592 | 17.63 | 101.10 | 63.01 | 4.34 | 6.03 | 1.88 | 12.35 | 16.82 | 1.88 | 0.24 | 0.27 | 50.76 | 0.09 | 26.62 | 1.72 |
| 2B | 816 | 2084 | 37.72 | 7.71 | 46.95 | 3488 | 19.97 | 12.68 | 15.89 | 0.75 | 0.94 | 3.11 | 5.71 | 8.96 | 52.41 | 0.48 | 0.19 | 10.42 | 0.08 | 19.49 | 1.89 |
| 2B | 774 | 1871 | 35.60 | 7.07 | 44.51 | 3396 | 19.19 | 12.23 | 14.69 | 0.71 | 0.89 | 3.10 | 4.88 | 8.56 | 48.84 | 0.47 | 0.18 | 8.03 | 0.07 | 19.39 | 1.75 |
| 2B | 776 | 1883 | 35.44 | 7.06 | 43.07 | 3407 | 18.70 | 12.18 | 14.01 | 0.72 | 0.91 | 3.31 | 5.02 | 8.60 | 51.25 | 0.47 | 0.18 | 7.65 | 0.07 | 19.05 | 1.97 |
| 3B | 17.56 | 4839 | 33.89 | 17.78 | 135.85 | 2897 | 3.22 | 13.66 | 2.80 | 1.27 | 0.19 | 0.65 | 0.10 | 1.61 | 6.01 | 0.08 | 0.03 | 34.71 | 0.08 | 0.60 | 0.55 |
| 3B | 15.01 | 3721 | 33.93 | 17.10 | 144.93 | 3016 | 3.29 | 13.85 | 3.93 | 1.04 | 0.19 | 0.57 | 0.09 | 1.50 | 5.62 | 0.08 | 0.03 | 43.86 | 0.09 | 0.64 | 0.55 |
| 3B | 16.12 | 4234 | 38.28 | 17.41 | 124.79 | 2999 | 3.45 | 13.70 | 3.77 | 1.15 | 0.19 | 0.60 | 0.10 | 1.76 | 5.95 | 0.08 | 0.03 | 33.48 | 0.08 | 0.59 | 0.58 |

| | | | | | | | | | | | | | | | | | | | | | |
|---|---|---|---|---|---|---|---|---|---|---|---|---|---|---|---|---|---|---|---|---|---|
| 4A | 523 | 7498 | 20.73 | 5.26 | 94.62 | 4213 | 13.77 | 25.54 | 31.22 | 2.94 | 65.06 | 1.77 | 17.80 | 24.78 | 3.46 | 0.26 | 0.29 | 33.35 | 0.28 | 40.80 | 0.68 |
| 4A | 533 | 7885 | 21.54 | 5.45 | 96.02 | 4281 | 13.52 | 26.07 | 31.79 | 3.06 | 65.76 | 1.65 | 18.56 | 25.01 | 3.29 | 0.29 | 0.29 | 34.26 | 0.29 | 38.85 | 0.68 |
| 4A | 524 | 7891 | 20.42 | 5.55 | 92.25 | 4186 | 13.02 | 24.30 | 33.14 | 3.06 | 64.29 | 1.82 | 18.59 | 24.46 | 3.17 | 0.25 | 0.29 | 33.89 | 0.28 | 37.64 | 0.64 |
| 4B | 284 | 3950 | 16.17 | 7.86 | 30.19 | 3179 | 4.86 | 15.05 | 16.39 | 1.20 | 1.08 | 0.49 | 1.25 | 2.42 | 3.26 | 1.17 | 0.06 | 7.28 | 0.02 | 1.08 | 0.11 |
| 4B | 275 | 4204 | 16.12 | 8.09 | 29.48 | 3041 | 4.71 | 14.40 | 18.37 | 1.27 | 0.58 | 0.51 | 1.17 | 2.17 | 1.57 | 1.11 | 0.06 | 5.65 | 0.02 | 1.10 | 0.10 |
| 4B | 278 | 3971 | 16.02 | 7.90 | 30.29 | 3012 | 4.37 | 15.22 | 16.48 | 1.22 | 0.49 | 0.39 | 1.17 | 2.20 | 1.56 | 1.10 | 0.06 | 6.37 | 0.02 | 1.05 | 0.11 |
| 5B | 726 | 3189 | 14.90 | 4.91 | 52.14 | 2623 | 6.23 | 203.54 | 34.58 | 1.03 | 0.34 | 1.15 | 2.96 | 2.25 | 75.66 | 0.57 | 0.48 | 6.22 | 0.02 | 7.08 | 0.65 |
| 5B | 717 | 3331 | 15.22 | 5.01 | 51.53 | 2703 | 6.57 | 233.58 | 36.19 | 1.06 | 0.19 | 1.02 | 2.90 | 2.17 | 90.81 | 0.53 | 0.66 | 6.06 | 0.02 | 6.92 | 0.62 |
| 5B | 760 | 3520 | 15.72 | 5.05 | 52.31 | 2767 | 6.71 | 224.91 | 38.58 | 1.11 | 0.16 | 1.28 | 3.08 | 2.39 | 76.54 | 0.57 | 0.54 | 6.10 | 0.02 | 6.55 | 0.41 |
| 6B | 60.22 | 53.91 | 0.62 | 21.11 | 4.19 | 891 | 6.54 | 1.17 | 1.57 | 0.08 | 0.17 | 0.05 | 0.18 | 0.97 | 1.76 | 0.08 | 0.01 | 3.41 | 0.01 | 0.33 | 0.06 |
| 6B | 56.94 | 49.93 | 0.50 | 16.31 | 4.23 | 829 | 5.39 | 0.98 | 0.84 | 0.08 | 0.10 | 0.01 | 0.16 | 0.91 | 1.08 | 0.07 | 0.01 | 0.98 | 0.02 | 0.31 | 0.06 |
| 6B | 57.81 | 52.38 | 0.54 | 16.91 | 4.20 | 1256 | 5.26 | 0.98 | 13.17 | 0.09 | 0.12 | 0.00 | 0.16 | 0.97 | 1.13 | 0.08 | 0.01 | 1.01 | 0.02 | 0.25 | 0.06 |
| 7B | 650 | 3687 | 69.78 | 9.07 | 38.08 | 3728 | 16.78 | 19.33 | 51.96 | 1.31 | 0.48 | 4.48 | 4.11 | 10.79 | 28.65 | 0.23 | 0.73 | 18.61 | 0.12 | 7.18 | 2.40 |
| 7B | 643 | 3746 | 69.12 | 8.97 | 37.50 | 3695 | 16.67 | 19.04 | 51.67 | 1.34 | 0.49 | 4.86 | 4.27 | 10.80 | 28.07 | 0.23 | 0.74 | 18.47 | 0.12 | 6.71 | 2.45 |
| 7B | 627 | 3595 | 68.70 | 8.95 | 36.68 | 3597 | 16.58 | 18.16 | 50.25 | 1.29 | 0.51 | 4.59 | 4.02 | 10.30 | 26.45 | 0.22 | 0.70 | 18.50 | 0.12 | 6.58 | 2.65 |
| 10B | 808 | 559 | 0.35 | 0.42 | 41.83 | 1909 | 1.41 | 1.63 | 1.43 | 0.42 | 0.08 | 0.04 | 0.06 | 1.97 | 40.00 | 0.01 | 0.00 | 0.30 | 0.01 | 0.59 | 0.04 |
| 10B | 162 | 158 | 0.13 | 0.36 | 64.12 | 1213 | 8.78 | 197.62 | 5.95 | 0.12 | 0.08 | 0.03 | 0.14 | 1.62 | 42.52 | 0.05 | 0.06 | 0.90 | 0.02 | 7.22 | 0.01 |
| 10B | 234 | 508 | 0.06 | 0.54 | 12.53 | 2416 | 3.87 | 33.03 | 3.81 | 0.24 | 0.05 | 0.05 | 0.08 | 0.36 | 0.21 | 0.04 | 0.01 | 0.39 | 0.02 | 2.24 | 0.02 |
| 11B | 34.65 | 21663 | 54.31 | 57.51 | 5.61 | 24561 | 7.76 | 45.87 | 4.73 | 11.42 | 15.00 | 6.71 | 1.57 | 4.18 | 15.57 | 0.14 | 0.03 | 15.19 | 0.02 | 12.81 | 1.53 |
| 11B | 35.51 | 21028 | 52.01 | 60.13 | 5.69 | 23321 | 7.70 | 48.06 | 6.43 | 11.53 | 15.49 | 4.78 | 1.59 | 4.04 | 15.41 | 0.12 | 0.03 | 15.19 | 0.02 | 12.67 | 1.43 |
| 11B | 37.44 | 21774 | 54.39 | 58.44 | 5.45 | 23398 | 8.49 | 52.13 | 6.10 | 10.95 | 15.38 | 4.85 | 1.68 | 5.49 | 15.32 | 0.11 | 0.03 | 14.91 | 0.02 | 13.32 | 1.53 |
| 13B | 4145 | 4331 | 82.05 | 23.92 | 186.48 | 10738 | 16.53 | 293.78 | 23.07 | 2.12 | 0.78 | 1.49 | 21.39 | 4.22 | 29.97 | 0.13 | 0.21 | 8.83 | 0.20 | 1.58 | 1.62 |
| 13B | 4271 | 4413 | 84.18 | 24.86 | 190.89 | 10841 | 15.90 | 305.17 | 16.81 | 2.12 | 0.50 | 1.14 | 22.20 | 3.95 | 26.11 | 0.13 | 0.19 | 8.93 | 0.21 | 1.41 | 1.41 |
| 13B | 4217 | 4331 | 85.53 | 25.06 | 191.27 | 10823 | 16.56 | 307.16 | 19.05 | 2.16 | 1.28 | 1.24 | 21.64 | 3.26 | 39.28 | 0.13 | 0.16 | 8.64 | 0.20 | 1.57 | 1.70 |
| 15B | 560 | 1059 | 7.25 | 5.98 | 24.18 | 1857 | 5.70 | 23.50 | 5.01 | 0.56 | 0.11 | 0.80 | 3.68 | 1.95 | 4.63 | 0.08 | 0.01 | 6.08 | 0.02 | 0.51 | 0.21 |
| 15B | 514 | 962 | 7.01 | 5.56 | 22.78 | 2062 | 6.58 | 19.86 | 5.42 | 0.53 | 0.04 | 0.95 | 3.38 | 1.81 | 1.27 | 0.07 | 0.01 | 5.27 | 0.02 | 0.51 | 0.22 |
| 15B | 614 | 1089 | 7.89 | 6.35 | 25.95 | 1927 | 5.56 | 22.20 | 5.12 | 0.59 | 0.04 | 0.73 | 4.16 | 3.85 | 10.06 | 0.06 | 0.02 | 7.26 | 0.02 | 0.49 | 0.21 |
| 21A | 16.52 | 3299 | 70.20 | 27.80 | 5.34 | 5827 | 11.40 | 24.87 | 20.39 | 0.77 | 0.35 | 4.39 | 0.24 | 5.94 | 29.61 | 0.33 | 0.57 | 18.44 | 0.02 | 0.49 | 1.54 |
| 21A | 15.79 | 3465 | 70.54 | 28.26 | 4.27 | 6109 | 11.07 | 23.52 | 20.52 | 0.79 | 0.37 | 4.57 | 0.23 | 6.27 | 30.47 | 0.34 | 0.83 | 19.13 | 0.02 | 0.47 | 0.86 |
| 21A | 17.79 | 3378 | 70.41 | 28.11 | 4.28 | 5969 | 11.25 | 23.67 | 21.23 | 0.78 | 0.38 | 4.64 | 0.24 | 6.23 | 28.54 | 0.33 | 0.52 | 18.55 | 0.01 | 0.45 | 0.80 |

| | | | | | | | | | | | | | | | | | | | | | |
|---|---|---|---|---|---|---|---|---|---|---|---|---|---|---|---|---|---|---|---|---|---|
| 21B | 15.13 | 1980 | 53.26 | 16.45 | 29.83 | 4339 | 10.26 | 17.22 | 27.98 | 0.59 | 0.40 | 2.21 | 0.37 | 4.19 | 14.71 | 0.17 | 0.25 | 17.62 | 0.04 | 0.60 | 1.13 |
| 21B | 18.72 | 2030 | 54.74 | 16.91 | 31.81 | 4351 | 11.36 | 20.84 | 30.15 | 0.61 | 0.46 | 2.04 | 0.39 | 6.35 | 15.15 | 0.19 | 0.20 | 16.71 | 0.05 | 0.62 | 1.12 |
| 21B | 18.46 | 2010 | 58.82 | 17.36 | 29.00 | 4468 | 11.28 | 18.00 | 29.78 | 0.63 | 0.50 | 1.82 | 0.39 | 6.30 | 14.72 | 0.15 | 0.26 | 16.12 | 0.05 | 0.61 | 1.15 |
| 21C | 25.78 | 2560 | 8.88 | 13.45 | 21.64 | 1482 | 2.68 | 14.11 | 2.90 | 0.84 | 0.03 | 1.08 | 0.10 | 1.83 | 2.55 | 0.09 | 0.02 | 4.96 | 0.02 | 0.19 | 0.12 |
| 21C | 25.37 | 2682 | 9.34 | 13.94 | 20.89 | 1480 | 2.71 | 15.03 | 3.14 | 0.87 | 0.07 | 1.30 | 0.11 | 1.88 | 2.59 | 0.09 | 0.02 | 4.91 | 0.02 | 0.18 | 0.12 |
| 21C | 25.13 | 2493 | 8.92 | 13.80 | 20.61 | 1464 | 2.61 | 14.63 | 2.92 | 0.82 | 0.05 | 1.16 | 0.10 | 2.19 | 2.25 | 0.10 | 0.02 | 4.74 | 0.02 | 0.33 | 0.13 |
| 21D | 160 | 3857 | 129.29 | 5.17 | 259.95 | 3989 | 60.20 | 143.38 | 29.61 | 1.55 | 2.48 | 0.66 | 2.65 | 0.71 | 1.91 | 0.02 | 0.11 | 19.09 | 0.17 | 2.42 | 0.90 |
| 21D | 140 | 3730 | 135.36 | 5.26 | 253.62 | 4130 | 55.56 | 34.88 | 27.89 | 1.52 | 2.64 | 0.50 | 2.57 | 0.72 | 1.78 | 0.02 | 0.10 | 14.02 | 0.18 | 2.46 | 0.89 |
| 21D | 174 | 3799 | 135.04 | 5.03 | 281.87 | 4277 | 64.68 | 39.24 | 31.16 | 1.55 | 3.58 | 0.75 | 3.34 | 0.99 | 2.03 | 0.02 | 0.13 | 12.25 | 0.20 | 2.66 | 0.94 |
| 21E | 734 | 2107 | 14.94 | 4.82 | 77.42 | 3701 | 6.42 | 286.52 | 19.80 | 0.88 | 0.30 | 0.40 | 4.08 | 7.32 | 94.52 | 0.46 | 0.17 | 10.50 | 0.02 | 2.80 | 0.85 |
| 21E | 747 | 2194 | 15.39 | 5.11 | 77.13 | 3738 | 6.18 | 291.74 | 20.50 | 0.91 | 0.20 | 0.34 | 4.18 | 6.67 | 107.23 | 0.49 | 0.16 | 10.37 | 0.02 | 3.26 | 0.79 |
| 21E | 776 | 2350 | 16.28 | 5.25 | 81.39 | 3928 | 5.96 | 297.33 | 26.05 | 0.98 | 0.23 | 0.44 | 4.38 | 7.50 | 100.65 | 0.47 | 0.17 | 11.11 | 0.02 | 3.00 | 0.65 |
| 21F | 121 | 102 | 0.12 | 0.34 | 57.29 | 891 | 8.39 | 186.65 | 7.71 | 0.09 | 0.07 | 0.10 | 0.16 | 1.64 | 56.73 | 0.05 | 0.07 | 0.94 | 0.02 | 6.82 | 0.04 |
| 21F | 146 | 42.15 | 0.05 | 0.19 | 226.07 | 9610 | 22.53 | 711.71 | 2.90 | 0.70 | 0.05 | 0.10 | 0.02 | 4.26 | 5.94 | 0.11 | 0.02 | 0.56 | 0.53 | 13.17 | 0.01 |
| 21J | 17.64 | 4169 | 79.96 | 37.06 | 10.61 | 2643 | 14.80 | 18.78 | 26.73 | 1.01 | 0.25 | 4.23 | 0.29 | 6.53 | 34.09 | 0.33 | 0.57 | 22.08 | 0.03 | 0.55 | 1.08 |
| 21J | 16.00 | 3982 | 77.95 | 36.28 | 10.57 | 2564 | 14.48 | 17.82 | 28.55 | 0.96 | 0.31 | 4.38 | 0.27 | 6.23 | 33.72 | 0.33 | 0.62 | 20.71 | 0.03 | 0.49 | 0.98 |
| 21J | 15.73 | 4136 | 80.32 | 37.13 | 10.45 | 2636 | 14.76 | 18.24 | 26.59 | 1.00 | 0.27 | 4.73 | 0.28 | 6.19 | 32.95 | 0.31 | 0.54 | 20.96 | 0.03 | 0.49 | 1.14 |
| 21K | 17.56 | 4371 | 102.10 | 30.91 | 13.75 | 3269 | 13.96 | 19.83 | 29.28 | 1.90 | 0.38 | 5.59 | 0.44 | 12.14 | 24.11 | 0.34 | 0.76 | 39.80 | 0.03 | 1.14 | 1.25 |
| 21K | 16.75 | 4148 | 99.95 | 30.45 | 12.43 | 3148 | 13.96 | 19.32 | 30.15 | 1.86 | 0.36 | 5.42 | 0.43 | 11.78 | 22.24 | 0.33 | 0.70 | 39.09 | 0.02 | 1.10 | 1.28 |
| 21K | 15.07 | 4122 | 101.20 | 30.97 | 12.23 | 3145 | 14.27 | 19.49 | 29.52 | 1.85 | 0.37 | 5.51 | 0.42 | 11.69 | 22.26 | 0.34 | 0.66 | 38.28 | 0.02 | 1.07 | 1.19 |
| 21L | 18.77 | 4806 | 74.66 | 18.46 | 4.39 | 2319 | 14.87 | 20.47 | 29.44 | 1.32 | 0.13 | 6.11 | 0.25 | 6.60 | 48.41 | 0.49 | 1.13 | 21.18 | 0.03 | 0.67 | 1.00 |
| 21L | 17.55 | 4714 | 73.52 | 18.26 | 4.51 | 2354 | 14.78 | 20.49 | 27.85 | 1.31 | 0.16 | 6.05 | 0.23 | 6.91 | 44.04 | 0.46 | 1.16 | 21.99 | 0.03 | 0.69 | 1.01 |
| 21L | 18.68 | 4802 | 75.45 | 19.03 | 5.04 | 2407 | 14.68 | 21.27 | 30.22 | 1.34 | 0.13 | 6.12 | 0.24 | 6.91 | 50.24 | 0.51 | 1.14 | 22.18 | 0.03 | 0.76 | 1.07 |
| 21M | 22.71 | 3435 | 10.91 | 9.63 | 23.07 | 1797 | 3.06 | 12.53 | 3.75 | 1.08 | 0.05 | 1.76 | 0.15 | 1.41 | 3.61 | 0.12 | 0.02 | 5.54 | 0.02 | 0.30 | 0.13 |
| 21M | 19.43 | 3018 | 9.92 | 8.83 | 20.98 | 1669 | 2.89 | 11.72 | 3.48 | 0.96 | 0.06 | 1.36 | 0.14 | 1.20 | 2.51 | 0.11 | 0.02 | 5.07 | 0.01 | 0.26 | 0.12 |
| 21M | 18.58 | 2865 | 9.48 | 8.46 | 21.16 | 1678 | 2.65 | 11.43 | 3.53 | 0.92 | 0.04 | 1.57 | 0.13 | 1.16 | 3.02 | 0.11 | 0.02 | 5.08 | 0.01 | 0.26 | 0.13 |
| 21N | 24.10 | 2534 | 8.84 | 13.23 | 19.20 | 1409 | 2.64 | 13.86 | 3.24 | 0.84 | 0.04 | 1.28 | 0.10 | 1.19 | 2.28 | 0.10 | 0.02 | 4.60 | 0.02 | 0.20 | 0.12 |
| 21N | 24.45 | 2773 | 9.18 | 13.59 | 20.13 | 1420 | 2.88 | 13.93 | 4.54 | 0.89 | 0.03 | 1.01 | 0.10 | 1.12 | 2.17 | 0.09 | 0.02 | 4.86 | 0.02 | 0.21 | 0.13 |
| 21N | 22.85 | 2408 | 8.58 | 12.98 | 18.79 | 1415 | 2.53 | 13.75 | 4.01 | 0.80 | 0.04 | 1.06 | 0.10 | 1.10 | 2.61 | 0.09 | 0.02 | 4.67 | 0.02 | 0.19 | 0.11 |
| 22A | 208 | 564 | 11.60 | 0.93 | 4.73 | 387 | 1.43 | 2.27 | 1.55 | 0.17 | 0.08 | 0.17 | 1.07 | 2.66 | 6.61 | 0.12 | 0.01 | 3.16 | 0.05 | 0.64 | 0.11 |

| | | | | | | | | | | | | | | | | | | | | | |
|---|---|---|---|---|---|---|---|---|---|---|---|---|---|---|---|---|---|---|---|---|---|
| 22A | 193 | 609 | 7.06 | 0.99 | 5.47 | 503 | 1.64 | 2.17 | 1.51 | 0.17 | 0.07 | 0.20 | 1.15 | 2.46 | 5.30 | 0.13 | 0.01 | 4.31 | 0.05 | 0.71 | 0.10 |
| 22B | 15.59 | 4052 | 102.71 | 28.76 | 17.72 | 2977 | 15.17 | 20.10 | 29.52 | 1.33 | 0.33 | 4.48 | 0.38 | 5.49 | 25.92 | 0.41 | 1.51 | 20.29 | 0.03 | 0.88 | 1.24 |
| 22B | 13.66 | 3794 | 100.02 | 26.84 | 16.31 | 2914 | 15.34 | 19.56 | 28.66 | 1.26 | 0.31 | 4.47 | 0.34 | 5.53 | 24.51 | 0.38 | 0.52 | 22.99 | 0.03 | 0.78 | 1.19 |
| 22C | 21.64 | 3254 | 6.69 | 6.07 | 32.58 | 1311 | 2.43 | 8.96 | 4.01 | 0.95 | 0.06 | 0.30 | 0.11 | 1.29 | 1.80 | 0.08 | 0.01 | 7.31 | 0.03 | 0.31 | 0.11 |
| 22C | 21.33 | 3134 | 6.57 | 5.97 | 32.02 | 1286 | 2.47 | 9.02 | 4.39 | 0.92 | 0.04 | 0.41 | 0.10 | 1.35 | 1.51 | 0.08 | 0.01 | 7.13 | 0.03 | 0.30 | 0.10 |
| 22D | 128 | 4813 | 19.30 | 3.63 | 63.15 | 4883 | 9.24 | 21.11 | 28.76 | 1.59 | 0.79 | 0.43 | 3.42 | 1.54 | 4.39 | 0.09 | 0.46 | 9.07 | 0.14 | 6.28 | 0.50 |
| 22D | 119 | 4475 | 18.48 | 3.39 | 59.92 | 4638 | 8.58 | 21.80 | 28.51 | 1.48 | 0.82 | 0.25 | 3.18 | 1.46 | 4.87 | 0.09 | 0.44 | 8.30 | 0.13 | 5.88 | 0.49 |
| 22E | 634 | 1797 | 13.93 | 6.21 | 45.62 | 2497 | 4.56 | 97.55 | 21.34 | 0.69 | 0.11 | 0.19 | 2.97 | 3.47 | 42.62 | 0.62 | 0.21 | 11.67 | 0.02 | 1.13 | 0.52 |
| 22E | 632 | 1769 | 13.88 | 5.80 | 45.77 | 2480 | 4.63 | 105.41 | 25.89 | 0.68 | 0.04 | 0.18 | 2.99 | 3.34 | 47.17 | 0.57 | 0.21 | 11.51 | 0.02 | 1.11 | 0.41 |
| 22F | 1656 | 3076 | 29.31 | 9.22 | 48.36 | 9516 | 15.04 | 43.65 | 59.45 | 1.18 | 1.14 | 0.71 | 4.41 | 6.01 | 73.52 | 0.87 | 1.78 | 120.12 | 0.04 | 2.89 | 0.26 |
| 22F | 1510 | 2826 | 26.72 | 8.39 | 43.95 | 8805 | 14.31 | 39.99 | 54.63 | 1.10 | 1.02 | 0.71 | 4.01 | 7.09 | 65.84 | 0.89 | 1.53 | 106.39 | 0.03 | 2.70 | 0.28 |
| 22G | 829 | 1560 | 11.02 | 7.11 | 23.11 | 3119 | 15.46 | 33.65 | 3.01 | 0.75 | 0.13 | 1.24 | 5.01 | 3.80 | 16.77 | 0.05 | 0.02 | 9.94 | 0.02 | 0.57 | 0.59 |
| 22G | 849 | 1518 | 11.11 | 7.29 | 23.24 | 3108 | 14.76 | 35.05 | 2.83 | 0.74 | 0.10 | 1.49 | 5.13 | 3.63 | 23.75 | 0.05 | 0.02 | 9.71 | 0.03 | 0.58 | 0.59 |

## Solution-based ICP-MS REE Data

| | Analyte (ng g-1) | | | | | | | | | | | | | | |
|---|---|---|---|---|---|---|---|---|---|---|---|---|---|---|---|
| Sample ID | La | Ce | Pr | Nd | Sm | Eu | Gd | Tb | Dy | Y | Ho | Er | Tm | Yb | Lu |
| 1A | 25171 | 52792 | 6478 | 25396 | 5268 | 971 | 4318 | 649 | 3739 | 17291 | 685 | 1818 | 242 | 1396 | 178 |
| 1A | 26698 | 56283 | 6897 | 26786 | 5571 | 1023 | 4562 | 684 | 3958 | 18658 | 726 | 1938 | 259 | 1499 | 191 |
| 1A | 26336 | 55497 | 6812 | 26353 | 5465 | 1001 | 4439 | 671 | 3904 | 18578 | 717 | 1910 | 254 | 1466 | 187 |
| 1B | 1326 | 2383 | 336 | 1372 | 280 | 59 | 254 | 34 | 199 | 1282 | 41 | 124 | 19 | 125 | 20 |
| 1B | 1303 | 2346 | 336 | 1384 | 289 | 59 | 257 | 34 | 202 | 1317 | 41 | 125 | 19 | 123 | 19 |
| 1B | 2977 | 4561 | 756 | 3169 | 618 | 99 | 476 | 51 | 251 | 1405 | 45 | 126 | 18 | 117 | 18 |
| 1B | 1401 | 2448 | 353 | 1456 | 293 | 58 | 258 | 33 | 192 | 1257 | 40 | 117 | 17 | 114 | 18 |
| 2A | 23920 | 49840 | 6029 | 24103 | 4951 | 787 | 3532 | 401 | 1811 | 6276 | 273 | 636 | 81 | 489 | 68 |
| 2A | 20206 | 41758 | 5121 | 20187 | 4239 | 681 | 3062 | 356 | 1642 | 5740 | 252 | 599 | 77 | 468 | 66 |
| 2A | 24909 | 52344 | 6458 | 25667 | 5479 | 811 | 3941 | 452 | 1992 | 6694 | 292 | 674 | 85 | 507 | 70 |
| 2B | 1757 | 4496 | 448 | 1806 | 393 | 75 | 390 | 60 | 379 | 2450 | 80 | 238 | 34 | 214 | 31 |
| 2B | 1732 | 4476 | 442 | 1768 | 377 | 73 | 374 | 58 | 366 | 2419 | 77 | 228 | 33 | 203 | 30 |
| 2B | 1763 | 4382 | 439 | 1766 | 380 | 75 | 379 | 58 | 372 | 2446 | 79 | 232 | 33 | 208 | 30 |
| 3B | 462 | 2902 | 160 | 859 | 352 | 109 | 570 | 101 | 584 | 2348 | 99 | 233 | 28 | 157 | 21 |
| 3B | 471 | 3134 | 165 | 860 | 344 | 107 | 551 | 99 | 575 | 2368 | 99 | 232 | 28 | 155 | 21 |

| | | | | | | | | | | | | | | | |
|---|---|---|---|---|---|---|---|---|---|---|---|---|---|---|---|
| 3B | 543 | 3412 | 190 | 981 | 371 | 110 | 567 | 102 | 584 | 2373 | 100 | 235 | 28 | 157 | 22 |
| 4A | 10330 | 17282 | 2494 | 12195 | 1850 | 359 | 1670 | 218 | 2542 | 6753 | 241 | 663 | 89 | 537 | 77 |
| 4A | 10004 | 17311 | 2590 | 14126 | 1952 | 356 | 1718 | 222 | 2540 | 6874 | 248 | 683 | 92 | 553 | 80 |
| 4A | 9851 | 17145 | 2518 | 14124 | 1880 | 349 | 1628 | 216 | 2894 | 6815 | 242 | 663 | 90 | 539 | 76 |
| 4B | 407 | 787 | 98 | 385 | 87 | 22 | 99 | 16 | 111 | 696 | 24 | 75 | 12 | 79 | 14 |
| 4B | 325 | 603 | 79 | 327 | 79 | 22 | 99 | 16 | 111 | 692 | 25 | 76 | 12 | 80 | 13 |
| 4B | 568 | 1037 | 119 | 459 | 96 | 22 | 114 | 18 | 124 | 802 | 27 | 85 | 13 | 87 | 14 |
| 5B | 1172 | 2056 | 244 | 903 | 164 | 38 | 141 | 21 | 125 | 747 | 25 | 74 | 11 | 70 | 11 |
| 5B | 1120 | 1950 | 230 | 859 | 162 | 47 | 144 | 20 | 128 | 752 | 26 | 77 | 11 | 75 | 12 |
| 5B | 1024 | 1778 | 212 | 797 | 153 | 43 | 140 | 20 | 128 | 738 | 26 | 76 | 11 | 73 | 11 |
| 6B | 232 | 9701 | 76 | 265 | 45 | 6 | 30 | 5 | 25 | 96 | 5 | 13 | 2 | 13 | 2 |
| 6B | 232 | 9734 | 72 | 255 | 42 | 6 | 28 | 5 | 23 | 80 | 4 | 11 | 2 | 12 | 2 |
| 6B | 244 | 10450 | 80 | 279 | 47 | 6 | 32 | 6 | 25 | 88 | 4 | 12 | 2 | 12 | 2 |
| 7B | 2091 | 5374 | 536 | 2179 | 462 | 102 | 442 | 65 | 387 | 2315 | 78 | 217 | 30 | 180 | 27 |
| 7B | 1920 | 4850 | 486 | 1961 | 418 | 98 | 408 | 61 | 374 | 2273 | 76 | 216 | 30 | 182 | 27 |
| 7B | 1951 | 4884 | 489 | 1961 | 420 | 97 | 410 | 61 | 375 | 2258 | 76 | 218 | 30 | 184 | 27 |
| 10B | 2739 | 5703 | 614 | 2182 | 400 | 52 | 270 | 32 | 152 | 666 | 25 | 63 | 8 | 54 | 8 |
| 10B | 1321 | 2480 | 280 | 1058 | 242 | 25 | 248 | 38 | 220 | 1212 | 42 | 113 | 15 | 88 | 13 |
| 10B | 443 | 887 | 101 | 373 | 84 | 10 | 76 | 12 | 69 | 344 | 13 | 36 | 5 | 35 | 5 |
| 11B | 4136 | 22413 | 945 | 3486 | 687 | 121 | 523 | 68 | 337 | 1042 | 53 | 127 | 16 | 96 | 13 |
| 11B | 3157 | 22008 | 719 | 2671 | 565 | 111 | 436 | 59 | 298 | 902 | 48 | 118 | 15 | 95 | 13 |
| 11B | 5053 | 21420 | 1109 | 4001 | 756 | 129 | 562 | 73 | 361 | 1110 | 58 | 135 | 17 | 103 | 14 |
| 13B | 13683 | 27922 | 3467 | 13877 | 2816 | 320 | 2606 | 375 | 2238 | 11564 | 434 | 1183 | 160 | 956 | 130 |
| 13B | 11617 | 23579 | 2918 | 11699 | 2415 | 317 | 2271 | 337 | 2053 | 10836 | 406 | 1129 | 155 | 930 | 129 |
| 13B | 15076 | 30551 | 3781 | 15128 | 3039 | 337 | 2796 | 401 | 2356 | 12011 | 453 | 1224 | 164 | 979 | 133 |
| 15B | 558 | 982 | 114 | 433 | 77 | 19 | 65 | 9 | 55 | 329 | 11 | 32 | 5 | 31 | 5 |
| 15B | 579 | 1040 | 121 | 467 | 89 | 22 | 80 | 12 | 73 | 440 | 15 | 44 | 6 | 42 | 6 |
| 15B | 561 | 978 | 114 | 434 | 75 | 18 | 64 | 9 | 52 | 308 | 10 | 30 | 4 | 28 | 4 |
| 21A | 1167 | 1843 | 293 | 1213 | 243 | 51 | 178 | 22 | 115 | 605 | 20 | 55 | 8 | 49 | 7 |
| 21A | 1226 | 1949 | 310 | 1292 | 255 | 54 | 191 | 23 | 117 | 605 | 21 | 56 | 8 | 50 | 7 |
| 21A | 1134 | 1810 | 287 | 1192 | 237 | 52 | 176 | 21 | 115 | 610 | 21 | 56 | 8 | 49 | 7 |
| 21B | 1303 | 3181 | 368 | 1593 | 336 | 69 | 279 | 35 | 195 | 1114 | 38 | 107 | 15 | 95 | 15 |
| 21B | 1330 | 3099 | 365 | 1545 | 316 | 66 | 261 | 33 | 186 | 1038 | 36 | 101 | 14 | 92 | 14 |
| 21B | 2121 | 4111 | 585 | 2464 | 485 | 87 | 378 | 44 | 227 | 1197 | 41 | 111 | 15 | 97 | 15 |
| 21C | 545 | 2618 | 153 | 626 | 188 | 47 | 229 | 37 | 215 | 953 | 38 | 90 | 11 | 58 | 8 |
| 21C | 539 | 2650 | 150 | 620 | 182 | 48 | 223 | 37 | 214 | 953 | 37 | 89 | 10 | 57 | 8 |
| 21C | 522 | 2538 | 145 | 602 | 177 | 47 | 223 | 37 | 210 | 942 | 37 | 87 | 10 | 56 | 8 |
| 21D | 9174 | 36380 | 2559 | 10924 | 2412 | 491 | 2668 | 412 | 2680 | 17107 | 582 | 1727 | 246 | 1566 | 246 |
| 21D | 6444 | 33918 | 1745 | 7345 | 1618 | 320 | 1843 | 287 | 1902 | 13220 | 428 | 1299 | 188 | 1214 | 195 |
| 21D | 6956 | 30965 | 1977 | 8537 | 1906 | 385 | 2247 | 349 | 2323 | 15482 | 522 | 1570 | 225 | 1431 | 229 |
| 21E | 2157 | 3739 | 434 | 1506 | 235 | 53 | 166 | 21 | 118 | 640 | 23 | 63 | 9 | 57 | 9 |

| | | | | | | | | | | | | | | | |
|---|---|---|---|---|---|---|---|---|---|---|---|---|---|---|---|
| 21E | 1576 | 2564 | 298 | 1037 | 173 | 48 | 128 | 17 | 98 | 557 | 19 | 54 | 8 | 50 | 9 |
| 21E | 2753 | 4290 | 474 | 1585 | 230 | 51 | 162 | 21 | 116 | 639 | 22 | 62 | 9 | 56 | 9 |
| 21F | 1164 | 2181 | 243 | 924 | 218 | 22 | 226 | 34 | 201 | 1105 | 39 | 103 | 13 | 79 | 11 |
| 21F | 947 | 1673 | 190 | 757 | 206 | 45 | 272 | 44 | 275 | 1765 | 56 | 153 | 19 | 110 | 16 |
| 21J | 1641 | 3345 | 447 | 1899 | 397 | 84 | 324 | 41 | 231 | 1407 | 44 | 123 | 17 | 106 | 16 |
| 21J | 1620 | 3274 | 435 | 1864 | 391 | 83 | 316 | 41 | 222 | 1346 | 42 | 118 | 16 | 101 | 15 |
| 21J | 1596 | 3269 | 432 | 1846 | 391 | 81 | 318 | 40 | 220 | 1321 | 41 | 116 | 16 | 99 | 15 |
| 21K | 2098 | 3989 | 578 | 2600 | 567 | 116 | 435 | 54 | 294 | 1711 | 55 | 154 | 22 | 136 | 21 |
| 21K | 2044 | 3909 | 572 | 2550 | 563 | 115 | 437 | 54 | 290 | 1660 | 55 | 153 | 21 | 136 | 20 |
| 21K | 2031 | 3926 | 572 | 2556 | 560 | 115 | 429 | 52 | 288 | 1675 | 54 | 152 | 21 | 134 | 20 |
| 21L | 1016 | 1531 | 256 | 1165 | 266 | 60 | 234 | 31 | 177 | 1202 | 35 | 101 | 14 | 89 | 14 |
| 21L | 1158 | 1782 | 296 | 1331 | 293 | 65 | 248 | 32 | 181 | 1200 | 36 | 100 | 14 | 88 | 14 |
| 21L | 1164 | 1778 | 296 | 1337 | 298 | 66 | 250 | 32 | 179 | 1181 | 35 | 100 | 14 | 87 | 13 |
| 21M | 473 | 2260 | 150 | 712 | 272 | 83 | 478 | 88 | 555 | 2762 | 103 | 252 | 30 | 160 | 23 |
| 21M | 456 | 2157 | 143 | 682 | 256 | 78 | 443 | 82 | 514 | 2586 | 96 | 234 | 28 | 148 | 21 |
| 21M | 442 | 2110 | 140 | 660 | 251 | 77 | 441 | 81 | 513 | 2551 | 96 | 235 | 28 | 149 | 21 |
| 21N | 511 | 2462 | 142 | 587 | 174 | 45 | 218 | 36 | 208 | 915 | 37 | 86 | 10 | 56 | 8 |
| 21N | 526 | 2596 | 147 | 614 | 184 | 47 | 226 | 37 | 214 | 954 | 37 | 89 | 11 | 58 | 8 |
| 21N | 519 | 2502 | 145 | 606 | 180 | 47 | 228 | 38 | 216 | 959 | 38 | 90 | 11 | 59 | 9 |
| 22A | 578 | 1391 | 112 | 398 | 72 | 21 | 88 | 13 | 68 | 505 | 15 | 44 | 5 | 54 | 7 |
| 22A | 693 | 1634 | 129 | 439 | 73 | 20 | 95 | 14 | 69 | 537 | 15 | 45 | 5 | 50 | 7 |
| 22B | 1902 | 3691 | 500 | 2099 | 432 | 86 | 347 | 47 | 264 | 1598 | 51 | 146 | 21 | 132 | 21 |
| 22B | 1777 | 3524 | 473 | 1988 | 416 | 83 | 342 | 45 | 258 | 1594 | 51 | 145 | 20 | 131 | 21 |
| 22C | 559 | 3977 | 167 | 757 | 297 | 91 | 481 | 84 | 497 | 2344 | 91 | 223 | 27 | 153 | 23 |
| 22C | 558 | 4026 | 167 | 750 | 287 | 91 | 483 | 84 | 500 | 2344 | 91 | 224 | 27 | 153 | 23 |
| 22D | 3862 | 35847 | 915 | 3484 | 700 | 167 | 590 | 90 | 532 | 2610 | 106 | 305 | 44 | 284 | 42 |
| 22D | 3689 | 33995 | 879 | 3336 | 675 | 163 | 564 | 86 | 510 | 2457 | 102 | 292 | 42 | 272 | 40 |
| 22E | 1935 | 3149 | 373 | 1340 | 216 | 35 | 166 | 22 | 122 | 651 | 23 | 63 | 9 | 57 | 9 |
| 22E | 1741 | 2891 | 343 | 1229 | 201 | 33 | 154 | 20 | 115 | 623 | 22 | 61 | 9 | 56 | 9 |
| 22F | 919 | 1701 | 214 | 839 | 183 | 64 | 203 | 35 | 249 | 1606 | 57 | 180 | 28 | 190 | 31 |
| 22F | 879 | 1643 | 208 | 821 | 182 | 64 | 197 | 34 | 237 | 1489 | 54 | 169 | 26 | 180 | 29 |
| 22G | 1654 | 3031 | 359 | 1353 | 242 | 54 | 204 | 29 | 174 | 1021 | 35 | 100 | 14 | 94 | 14 |
| 22G | 1611 | 3009 | 359 | 1369 | 252 | 56 | 216 | 31 | 187 | 1096 | 38 | 109 | 16 | 102 | 18 |

*Correlation matrix for solution-based-ICP-MS trace element data for Kaisersberg (AUT)*

| *Kaisersberg (AUT)* | Mg | Al | V | Cr | Mn | Fe | Ni | Cu | Zn | Ga | Se | Rb | Sr | Mo | Ag | Cd | Ba | Tl | Pb | U |
|---|---|---|---|---|---|---|---|---|---|---|---|---|---|---|---|---|---|---|---|---|
| **Mg** | 1.00 | | | | | | | | | | | | | | | | | | | |
| **Al** | 0.94 | 1.00 | | | | | | | | | | | | | | | | | | |
| **V** | 0.91 | 0.99 | 1.00 | | | | | | | | | | | | | | | | | |
| **Cr** | 0.76 | 0.89 | 0.93 | 1.00 | | | | | | | | | | | | | | | | |
| **Mn** | 0.96 | 1.00 | 0.99 | 0.88 | 1.00 | | | | | | | | | | | | | | | |
| **Fe** | 0.97 | 0.93 | 0.93 | 0.86 | 0.95 | 1.00 | | | | | | | | | | | | | | |
| **Ni** | -0.85 | -0.97 | -0.95 | -0.83 | -0.95 | -0.81 | 1.00 | | | | | | | | | | | | | |
| **Cu** | -0.96 | -0.86 | -0.83 | -0.67 | -0.88 | -0.95 | 0.72 | 1.00 | | | | | | | | | | | | |
| **Zn** | -0.89 | -0.83 | -0.84 | -0.77 | -0.85 | -0.96 | 0.67 | 0.95 | 1.00 | | | | | | | | | | | |
| **Ga** | 0.93 | 1.00 | 0.99 | 0.89 | 1.00 | 0.93 | -0.97 | -0.85 | -0.83 | 1.00 | | | | | | | | | | |
| **Se** | 0.31 | 0.31 | 0.36 | 0.64 | 0.34 | 0.46 | -0.21 | -0.23 | -0.38 | 0.32 | 1.00 | | | | | | | | | |
| **Rb** | 0.92 | 1.00 | 1.00 | 0.90 | 0.99 | 0.92 | -0.97 | -0.83 | -0.82 | 1.00 | 0.32 | 1.00 | | | | | | | | |
| **Sr** | 0.93 | 1.00 | 0.99 | 0.87 | 1.00 | 0.92 | -0.97 | -0.85 | -0.82 | 1.00 | 0.29 | 1.00 | 1.00 | | | | | | | |
| **Mo** | 0.95 | 0.98 | 0.97 | 0.87 | 0.99 | 0.93 | -0.95 | -0.84 | -0.79 | 0.98 | 0.38 | 0.98 | 0.98 | 1.00 | | | | | | |
| **Ag** | -0.91 | -0.77 | -0.71 | -0.46 | -0.79 | -0.83 | 0.67 | 0.95 | 0.82 | -0.76 | 0.01 | -0.73 | -0.77 | -0.77 | 1.00 | | | | | |
| **Cd** | -0.92 | -0.86 | -0.86 | -0.79 | -0.88 | -0.98 | 0.70 | 0.96 | 1.00 | -0.85 | -0.41 | -0.84 | -0.85 | -0.83 | 0.83 | 1.00 | | | | |
| **Ba** | 0.93 | 1.00 | 1.00 | 0.89 | 0.99 | 0.93 | -0.95 | -0.86 | -0.85 | 1.00 | 0.30 | 1.00 | 0.99 | 0.97 | -0.76 | -0.87 | 1.00 | | | |
| **Tl** | 0.94 | 1.00 | 0.99 | 0.87 | 1.00 | 0.93 | -0.96 | -0.87 | -0.84 | 1.00 | 0.29 | 1.00 | 1.00 | 0.98 | -0.78 | -0.86 | 1.00 | 1.00 | | |
| **Pb** | 0.91 | 0.94 | 0.90 | 0.70 | 0.94 | 0.82 | -0.96 | -0.81 | -0.69 | 0.94 | 0.06 | 0.93 | 0.95 | 0.94 | -0.82 | -0.72 | 0.93 | 0.95 | 1.00 | |
| **U** | 0.96 | 1.00 | 0.99 | 0.88 | 1.00 | 0.95 | -0.95 | -0.88 | -0.85 | 1.00 | 0.34 | 0.99 | 1.00 | 0.99 | -0.79 | -0.88 | 0.99 | 1.00 | 0.94 | 1.00 |

*Correlation matrix for solution-based-ICP-MS trace element data for Minas Gerais* (BRA)*

| *Minas Gerais* (BRA)* | Mg | Al | V | Cr | Mn | Fe | Ni | Cu | Zn | Ga | Se | Rb | Sr | Mo | Ag | Cd | Ba | Tl | Pb | U |
|---|---|---|---|---|---|---|---|---|---|---|---|---|---|---|---|---|---|---|---|---|
| Mg | 1.00 | | | | | | | | | | | | | | | | | | | |
| Al | -0.76 | 1.00 | | | | | | | | | | | | | | | | | | |
| V | -0.78 | 0.84 | 1.00 | | | | | | | | | | | | | | | | | |
| Cr | -0.23 | 0.38 | 0.73 | 1.00 | | | | | | | | | | | | | | | | |
| Mn | -0.81 | 0.86 | 0.97 | 0.65 | 1.00 | | | | | | | | | | | | | | | |
| Fe | -0.82 | 0.85 | 0.99 | 0.69 | 0.96 | 1.00 | | | | | | | | | | | | | | |
| Ni | -0.66 | 0.77 | 0.89 | 0.68 | 0.81 | 0.91 | 1.00 | | | | | | | | | | | | | |
| Cu | 0.22 | -0.09 | 0.30 | 0.84 | 0.17 | 0.28 | 0.39 | 1.00 | | | | | | | | | | | | |
| Zn | -0.16 | -0.04 | -0.11 | -0.37 | -0.06 | -0.14 | -0.07 | -0.48 | 1.00 | | | | | | | | | | | |
| Ga | -0.73 | 0.98 | 0.80 | 0.34 | 0.79 | 0.82 | 0.80 | -0.07 | -0.07 | 1.00 | | | | | | | | | | |
| Se | 0.38 | -0.45 | -0.40 | -0.10 | -0.54 | -0.31 | -0.08 | 0.35 | -0.32 | -0.28 | 1.00 | | | | | | | | | |
| Rb | 0.05 | -0.04 | -0.29 | -0.44 | -0.38 | -0.17 | 0.06 | -0.19 | -0.08 | 0.14 | 0.73 | 1.00 | | | | | | | | |
| Sr | 0.17 | 0.11 | 0.26 | 0.45 | 0.22 | 0.23 | 0.20 | 0.47 | -0.61 | 0.08 | -0.07 | -0.23 | 1.00 | | | | | | | |
| Mo | -0.76 | 0.84 | 0.97 | 0.72 | 0.92 | 0.98 | 0.91 | 0.35 | -0.20 | 0.83 | -0.21 | -0.11 | 0.23 | 1.00 | | | | | | |
| Ag | 0.30 | -0.36 | -0.47 | -0.35 | -0.57 | -0.37 | -0.14 | 0.04 | -0.23 | -0.19 | 0.93 | 0.87 | -0.20 | -0.29 | 1.00 | | | | | |
| Cd | -0.63 | 0.82 | 0.93 | 0.80 | 0.90 | 0.92 | 0.82 | 0.42 | -0.31 | 0.79 | -0.29 | -0.27 | 0.24 | 0.94 | -0.37 | 1.00 | | | | |
| Ba | -0.81 | 0.82 | 0.96 | 0.65 | 1.00 | 0.96 | 0.81 | 0.19 | -0.03 | 0.75 | -0.52 | -0.38 | 0.21 | 0.91 | -0.56 | 0.87 | 1.00 | | | |
| Tl | -0.75 | 0.84 | 0.97 | 0.70 | 0.99 | 0.94 | 0.79 | 0.22 | -0.07 | 0.75 | -0.58 | -0.46 | 0.28 | 0.90 | -0.63 | 0.90 | 0.99 | 1.00 | | |
| Pb | -0.83 | 0.88 | 0.93 | 0.53 | 0.96 | 0.93 | 0.78 | 0.06 | -0.04 | 0.82 | -0.53 | -0.28 | 0.27 | 0.88 | -0.50 | 0.83 | 0.96 | 0.95 | 1.00 | |
| U | -0.79 | 0.85 | 1.00 | 0.72 | 0.99 | 0.98 | 0.86 | 0.27 | -0.11 | 0.79 | -0.45 | -0.34 | 0.25 | 0.95 | -0.52 | 0.93 | 0.98 | 0.98 | 0.95 | 1.00 |

*Correlation matrix for solution-based-ICP-MS trace element data for Hunan Lutang* (CHN)*

| *Hunan Lutang* (CHN)* | Mg | Al | V | Cr | Mn | Fe | Ni | Cu | Zn | Ga | Se | Rb | Sr | Mo | Ag | Cd | Ba | Tl | Pb | U |
|---|---|---|---|---|---|---|---|---|---|---|---|---|---|---|---|---|---|---|---|---|
| Mg | 1.00 | | | | | | | | | | | | | | | | | | | |
| Al | 0.56 | 1.00 | | | | | | | | | | | | | | | | | | |
| V | 0.94 | 0.23 | 1.00 | | | | | | | | | | | | | | | | | |
| Cr | 0.25 | 0.94 | -0.10 | 1.00 | | | | | | | | | | | | | | | | |
| Mn | 0.73 | -0.16 | 0.92 | -0.48 | 1.00 | | | | | | | | | | | | | | | |
| Fe | 0.93 | 0.22 | 1.00 | -0.11 | 0.93 | 1.00 | | | | | | | | | | | | | | |
| Ni | 0.11 | -0.76 | 0.45 | -0.93 | 0.76 | 0.46 | 1.00 | | | | | | | | | | | | | |
| Cu | 0.68 | -0.24 | 0.89 | -0.54 | 1.00 | 0.89 | 0.81 | 1.00 | | | | | | | | | | | | |
| Zn | -0.15 | 0.74 | -0.48 | 0.92 | -0.78 | -0.49 | -1.00 | -0.83 | 1.00 | | | | | | | | | | | |
| Ga | 0.57 | 1.00 | 0.25 | 0.94 | -0.15 | 0.23 | -0.76 | -0.22 | 0.73 | 1.00 | | | | | | | | | | |
| Se | -0.94 | -0.23 | -1.00 | 0.10 | -0.92 | -1.00 | -0.45 | -0.89 | 0.48 | -0.24 | 1.00 | | | | | | | | | |
| Rb | 0.54 | 1.00 | 0.21 | 0.95 | -0.18 | 0.20 | -0.78 | -0.26 | 0.75 | 1.00 | -0.21 | 1.00 | | | | | | | | |
| Sr | -0.94 | -0.81 | -0.76 | -0.57 | -0.45 | -0.75 | 0.24 | -0.38 | -0.20 | -0.82 | 0.76 | -0.80 | 1.00 | | | | | | | |
| Mo | -0.76 | 0.12 | -0.94 | 0.44 | -1.00 | -0.94 | -0.73 | -0.99 | 0.76 | 0.11 | 0.94 | 0.15 | 0.48 | 1.00 | | | | | | |
| Ag | 0.91 | 0.15 | 1.00 | -0.18 | 0.95 | 1.00 | 0.52 | 0.93 | -0.56 | 0.16 | -1.00 | 0.13 | -0.70 | -0.96 | 1.00 | | | | | |
| Cd | -0.67 | -0.99 | -0.37 | -0.89 | 0.02 | -0.36 | 0.66 | 0.09 | -0.63 | -0.99 | 0.37 | -0.99 | 0.89 | 0.02 | -0.29 | 1.00 | | | | |
| Ba | 0.85 | 0.91 | 0.62 | 0.72 | 0.26 | 0.61 | -0.43 | 0.19 | 0.39 | 0.91 | -0.62 | 0.90 | -0.98 | -0.30 | 0.55 | -0.96 | 1.00 | | | |
| Tl | 0.99 | 0.67 | 0.88 | 0.39 | 0.62 | 0.87 | -0.03 | 0.56 | -0.01 | 0.68 | -0.88 | 0.65 | -0.98 | -0.65 | 0.83 | -0.77 | 0.92 | 1.00 | | |
| Pb | -0.21 | -0.93 | 0.14 | -1.00 | 0.51 | 0.15 | 0.95 | 0.58 | -0.93 | -0.93 | -0.14 | -0.94 | 0.54 | -0.48 | 0.22 | 0.87 | -0.69 | -0.35 | 1.00 | |
| U | 0.44 | -0.51 | 0.72 | -0.76 | 0.93 | 0.73 | 0.94 | 0.96 | -0.96 | -0.50 | -0.72 | -0.53 | -0.10 | -0.92 | 0.78 | 0.38 | -0.10 | 0.30 | 0.79 | 1.00 |

*Correlation matrix for solution-based-ICP-MS trace element data for Inner Mongolia (CHN)*

| *Inner Mongolia* (CHN)* | Mg | Al | V | Cr | Mn | Fe | Ni | Cu | Zn | Ga | Se | Rb | Sr | Mo | Ag | Cd | Ba | Tl | Pb | U |
|---|---|---|---|---|---|---|---|---|---|---|---|---|---|---|---|---|---|---|---|---|
| **Mg** | 1.00 | | | | | | | | | | | | | | | | | | | |
| **Al** | 0.92 | 1.00 | | | | | | | | | | | | | | | | | | |
| **V** | 1.00 | 0.94 | 1.00 | | | | | | | | | | | | | | | | | |
| **Cr** | 0.99 | 0.86 | 0.98 | 1.00 | | | | | | | | | | | | | | | | |
| **Mn** | -0.81 | -0.97 | -0.84 | -0.72 | 1.00 | | | | | | | | | | | | | | | |
| **Fe** | -0.13 | 0.27 | -0.08 | -0.27 | -0.47 | 1.00 | | | | | | | | | | | | | | |
| **Ni** | 0.94 | 0.73 | 0.92 | 0.98 | -0.56 | -0.46 | 1.00 | | | | | | | | | | | | | |
| **Cu** | 0.97 | 0.81 | 0.96 | 1.00 | -0.66 | -0.35 | 0.99 | 1.00 | | | | | | | | | | | | |
| **Zn** | -0.21 | 0.19 | -0.16 | -0.35 | -0.40 | 1.00 | -0.54 | -0.43 | 1.00 | | | | | | | | | | | |
| **Ga** | -0.19 | 0.21 | -0.14 | -0.33 | -0.42 | 1.00 | -0.52 | -0.41 | 1.00 | 1.00 | | | | | | | | | | |
| **Se** | 0.88 | 0.63 | 0.86 | 0.94 | -0.44 | -0.58 | 0.99 | 0.97 | -0.64 | -0.63 | 1.00 | | | | | | | | | |
| **Rb** | 0.98 | 0.82 | 0.97 | 1.00 | -0.68 | -0.33 | 0.99 | 1.00 | -0.40 | -0.39 | 0.96 | 1.00 | | | | | | | | |
| **Sr** | 0.75 | 0.95 | 0.78 | 0.65 | -1.00 | 0.56 | 0.48 | 0.58 | 0.49 | 0.51 | 0.35 | 0.60 | 1.00 | | | | | | | |
| **Mo** | 0.98 | 0.83 | 0.97 | 1.00 | -0.69 | -0.32 | 0.99 | 1.00 | -0.39 | -0.37 | 0.96 | 1.00 | 0.61 | 1.00 | | | | | | |
| **Ag** | 0.85 | 0.99 | 0.88 | 0.77 | -1.00 | 0.41 | 0.62 | 0.71 | 0.33 | 0.35 | 0.51 | 0.73 | 0.99 | 0.74 | 1.00 | | | | | |
| **Cd** | 0.98 | 0.82 | 0.96 | 1.00 | -0.67 | -0.34 | 0.99 | 1.00 | -0.42 | -0.40 | 0.96 | 1.00 | 0.59 | 1.00 | 0.72 | 1.00 | | | | |
| **Ba** | 0.97 | 0.80 | 0.96 | 0.99 | -0.64 | -0.37 | 0.99 | 1.00 | -0.44 | -0.43 | 0.97 | 1.00 | 0.57 | 1.00 | 0.70 | 1.00 | 1.00 | | | |
| **Tl** | -0.82 | -0.98 | -0.85 | -0.73 | 1.00 | -0.46 | -0.57 | -0.67 | -0.39 | -0.41 | -0.46 | -0.69 | -0.99 | -0.70 | -1.00 | -0.68 | -0.65 | 1.00 | | |
| **Pb** | 0.49 | 0.11 | 0.44 | 0.61 | 0.11 | -0.93 | 0.76 | 0.67 | -0.96 | -0.95 | 0.84 | 0.65 | -0.21 | 0.65 | -0.04 | 0.66 | 0.69 | 0.10 | 1.00 | |
| **U** | 0.99 | 0.96 | 1.00 | 0.96 | -0.88 | 0.00 | 0.89 | 0.94 | -0.08 | -0.06 | 0.82 | 0.94 | 0.83 | 0.95 | 0.91 | 0.94 | 0.93 | -0.89 | 0.37 | 1.00 |

*Correlation matrix for solution-based-ICP-MS trace element data for Heilongjian (CHN)*

| *Heilongjian* (CHN)* | Mg | Al | V | Cr | Mn | Fe | Ni | Cu | Zn | Ga | Se | Rb | Sr | Mo | Ag | Cd | Ba | Tl | Pb | U |
|---|---|---|---|---|---|---|---|---|---|---|---|---|---|---|---|---|---|---|---|---|
| Mg | 1.00 | | | | | | | | | | | | | | | | | | | |
| Al | 0.76 | 1.00 | | | | | | | | | | | | | | | | | | |
| V | 0.94 | 0.50 | 1.00 | | | | | | | | | | | | | | | | | |
| Cr | 0.81 | 0.24 | 0.96 | 1.00 | | | | | | | | | | | | | | | | |
| Mn | 0.99 | 0.68 | 0.97 | 0.87 | 1.00 | | | | | | | | | | | | | | | |
| Fe | 1.00 | 0.80 | 0.92 | 0.78 | 0.99 | 1.00 | | | | | | | | | | | | | | |
| Ni | 0.96 | 0.56 | 1.00 | 0.94 | 0.99 | 0.95 | 1.00 | | | | | | | | | | | | | |
| Cu | 1.00 | 0.80 | 0.92 | 0.77 | 0.98 | 1.00 | 0.94 | 1.00 | | | | | | | | | | | | |
| Zn | 0.99 | 0.85 | 0.88 | 0.72 | 0.97 | 1.00 | 0.91 | 1.00 | 1.00 | | | | | | | | | | | |
| Ga | 0.54 | 0.96 | 0.23 | -0.05 | 0.45 | 0.59 | 0.30 | 0.60 | 0.66 | 1.00 | | | | | | | | | | |
| Se | -0.07 | 0.60 | -0.40 | -0.64 | -0.18 | -0.01 | -0.33 | 0.00 | 0.08 | 0.80 | 1.00 | | | | | | | | | |
| Rb | 0.56 | 0.96 | 0.24 | -0.03 | 0.46 | 0.61 | 0.31 | 0.61 | 0.68 | 1.00 | 0.79 | 1.00 | | | | | | | | |
| Sr | 0.94 | 0.93 | 0.77 | 0.57 | 0.90 | 0.96 | 0.82 | 0.96 | 0.98 | 0.79 | 0.27 | 0.80 | 1.00 | | | | | | | |
| Mo | 1.00 | 0.79 | 0.92 | 0.78 | 0.99 | 1.00 | 0.95 | 1.00 | 1.00 | 0.59 | -0.02 | 0.60 | 0.96 | 1.00 | | | | | | |
| Ag | 0.86 | 0.99 | 0.64 | 0.40 | 0.80 | 0.89 | 0.69 | 0.89 | 0.93 | 0.90 | 0.45 | 0.90 | 0.98 | 0.89 | 1.00 | | | | | |
| Cd | 0.89 | 0.97 | 0.68 | 0.46 | 0.83 | 0.92 | 0.73 | 0.92 | 0.95 | 0.87 | 0.40 | 0.88 | 0.99 | 0.91 | 1.00 | 1.00 | | | | |
| Ba | 0.60 | -0.06 | 0.84 | 0.95 | 0.69 | 0.55 | 0.79 | 0.55 | 0.48 | -0.34 | -0.84 | -0.33 | 0.30 | 0.56 | 0.11 | 0.17 | 1.00 | | | |
| Tl | -0.87 | -0.33 | -0.98 | -1.00 | -0.91 | -0.83 | -0.97 | -0.83 | -0.78 | -0.05 | 0.56 | -0.07 | -0.65 | -0.84 | -0.49 | -0.54 | -0.92 | 1.00 | | |
| Pb | 0.86 | 0.33 | 0.98 | 1.00 | 0.91 | 0.83 | 0.97 | 0.83 | 0.78 | 0.04 | -0.56 | 0.06 | 0.64 | 0.83 | 0.48 | 0.54 | 0.92 | -1.00 | 1.00 | |
| U | -0.99 | -0.82 | -0.90 | -0.75 | -0.98 | -1.00 | -0.93 | -1.00 | -1.00 | -0.63 | -0.04 | -0.64 | -0.97 | -1.00 | -0.91 | -0.93 | -0.52 | 0.81 | -0.80 | 1.00 |

*Correlation matrix for solution-based-ICP-MS trace element data for Kropfmühl (GER)*

| *Kropfmühl (GER)* | Mg | Al | V | Cr | Mn | Fe | Ni | Cu | Zn | Ga | Se | Rb | Sr | Mo | Ag | Cd | Ba | Tl | Pb | U |
|---|---|---|---|---|---|---|---|---|---|---|---|---|---|---|---|---|---|---|---|---|
| **Mg** | 1.00 | | | | | | | | | | | | | | | | | | | |
| **Al** | 0.82 | 1.00 | | | | | | | | | | | | | | | | | | |
| **V** | 0.67 | 0.12 | 1.00 | | | | | | | | | | | | | | | | | |
| **Cr** | 0.82 | 0.34 | 0.97 | 1.00 | | | | | | | | | | | | | | | | |
| **Mn** | 0.87 | 0.43 | 0.95 | 1.00 | 1.00 | | | | | | | | | | | | | | | |
| **Fe** | 0.96 | 0.64 | 0.84 | 0.94 | 0.97 | 1.00 | | | | | | | | | | | | | | |
| **Ni** | -0.80 | -1.00 | -0.09 | -0.31 | -0.40 | -0.61 | 1.00 | | | | | | | | | | | | | |
| **Cu** | 0.84 | 0.37 | 0.97 | 1.00 | 1.00 | 0.95 | -0.34 | 1.00 | | | | | | | | | | | | |
| **Zn** | -1.00 | -0.77 | -0.73 | -0.86 | -0.91 | -0.98 | 0.75 | -0.88 | 1.00 | | | | | | | | | | | |
| **Ga** | 0.20 | -0.40 | 0.86 | 0.72 | 0.65 | 0.45 | 0.44 | 0.70 | -0.27 | 1.00 | | | | | | | | | | |
| **Se** | -0.99 | -0.71 | -0.79 | -0.90 | -0.94 | -0.99 | 0.68 | -0.92 | 1.00 | -0.36 | 1.00 | | | | | | | | | |
| **Rb** | 0.95 | 0.95 | 0.41 | 0.61 | 0.68 | 0.84 | -0.94 | 0.63 | -0.93 | -0.11 | -0.89 | 1.00 | | | | | | | | |
| **Sr** | -0.35 | 0.25 | -0.93 | -0.83 | -0.77 | -0.59 | -0.28 | -0.81 | 0.43 | -0.99 | 0.51 | -0.05 | 1.00 | | | | | | | |
| **Mo** | -0.21 | -0.73 | 0.59 | 0.39 | 0.30 | 0.06 | 0.75 | 0.36 | 0.12 | 0.92 | 0.04 | -0.49 | -0.84 | 1.00 | | | | | | |
| **Ag** | -0.73 | -0.21 | -1.00 | -0.99 | -0.97 | -0.89 | 0.18 | -0.99 | 0.79 | -0.81 | 0.84 | -0.49 | 0.90 | -0.51 | 1.00 | | | | | |
| **Cd** | -0.46 | 0.13 | -0.97 | -0.89 | -0.84 | -0.69 | -0.16 | -0.87 | 0.54 | -0.96 | 0.61 | -0.18 | 0.99 | -0.77 | 0.94 | 1.00 | | | | |
| **Ba** | 0.25 | 0.76 | -0.55 | -0.35 | -0.26 | -0.02 | -0.78 | -0.32 | -0.17 | -0.90 | -0.08 | 0.53 | 0.82 | -1.00 | 0.47 | 0.74 | 1.00 | | | |
| **Tl** | 0.83 | 1.00 | 0.14 | 0.36 | 0.44 | 0.65 | -1.00 | 0.38 | -0.78 | -0.39 | -0.72 | 0.96 | 0.23 | -0.72 | -0.22 | 0.11 | 0.75 | 1.00 | | |
| **Pb** | -0.85 | -1.00 | -0.18 | -0.39 | -0.48 | -0.67 | 1.00 | -0.42 | 0.80 | 0.35 | 0.75 | -0.97 | -0.20 | 0.69 | 0.26 | -0.08 | -0.73 | -1.00 | 1.00 | |
| **U** | -0.66 | -0.97 | 0.12 | -0.11 | -0.20 | -0.43 | 0.98 | -0.14 | 0.59 | 0.61 | 0.52 | -0.85 | -0.47 | 0.87 | -0.03 | -0.36 | -0.89 | -0.97 | 0.96 | 1.00 |

*Correlation matrix for solution-based-ICP-MS trace element data for Balama (MOZ)*

| *Balama (MOZ)* | Mg | Al | V | Cr | Mn | Fe | Ni | Cu | Zn | Ga | Se | Rb | Sr | Mo | Ag | Cd | Ba | Tl | Pb | U |
|---|---|---|---|---|---|---|---|---|---|---|---|---|---|---|---|---|---|---|---|---|
| Mg | 1.00 | | | | | | | | | | | | | | | | | | | |
| Al | -0.79 | 1.00 | | | | | | | | | | | | | | | | | | |
| V | -0.78 | 0.84 | 1.00 | | | | | | | | | | | | | | | | | |
| Cr | -0.74 | 0.73 | 0.81 | 1.00 | | | | | | | | | | | | | | | | |
| Mn | -0.16 | -0.42 | -0.21 | -0.16 | 1.00 | | | | | | | | | | | | | | | |
| Fe | -0.74 | 0.31 | 0.36 | 0.34 | 0.71 | 1.00 | | | | | | | | | | | | | | |
| Ni | -0.78 | 0.96 | 0.87 | 0.78 | -0.42 | 0.24 | 1.00 | | | | | | | | | | | | | |
| Cu | -0.84 | 0.86 | 0.73 | 0.53 | -0.01 | 0.63 | 0.81 | 1.00 | | | | | | | | | | | | |
| Zn | 0.56 | -0.48 | -0.31 | -0.63 | 0.10 | -0.24 | -0.50 | -0.30 | 1.00 | | | | | | | | | | | |
| Ga | -0.65 | 0.84 | 0.92 | 0.64 | -0.36 | 0.27 | 0.79 | 0.72 | -0.15 | 1.00 | | | | | | | | | | |
| Se | -0.64 | 0.96 | 0.80 | 0.61 | -0.59 | 0.11 | 0.90 | 0.76 | -0.33 | 0.89 | 1.00 | | | | | | | | | |
| Rb | 0.71 | -0.80 | -0.42 | -0.49 | 0.27 | -0.32 | -0.76 | -0.74 | 0.61 | -0.38 | -0.69 | 1.00 | | | | | | | | |
| Sr | -0.50 | 0.62 | 0.74 | 0.57 | -0.15 | 0.38 | 0.52 | 0.57 | -0.02 | 0.88 | 0.66 | -0.14 | 1.00 | | | | | | | |
| Mo | -0.47 | 0.84 | 0.44 | 0.39 | -0.63 | -0.02 | 0.79 | 0.67 | -0.40 | 0.51 | 0.84 | -0.88 | 0.23 | 1.00 | | | | | | |
| Ag | 0.53 | 0.00 | -0.11 | -0.30 | -0.82 | -0.89 | 0.04 | -0.27 | 0.30 | 0.03 | 0.22 | 0.10 | -0.20 | 0.31 | 1.00 | | | | | |
| Cd | -0.34 | 0.71 | 0.57 | 0.27 | -0.56 | -0.11 | 0.70 | 0.56 | -0.07 | 0.61 | 0.76 | -0.52 | 0.26 | 0.73 | 0.47 | 1.00 | | | | |
| Ba | -0.59 | 0.68 | 0.83 | 0.64 | -0.18 | 0.36 | 0.60 | 0.58 | -0.13 | 0.94 | 0.72 | -0.18 | 0.97 | 0.26 | -0.16 | 0.32 | 1.00 | | | |
| Tl | 0.65 | -0.91 | -0.84 | -0.73 | 0.59 | -0.04 | -0.91 | -0.65 | 0.42 | -0.85 | -0.94 | 0.62 | -0.60 | -0.74 | -0.21 | -0.67 | -0.71 | 1.00 | | |
| Pb | 0.91 | -0.75 | -0.55 | -0.63 | -0.18 | -0.75 | -0.71 | -0.84 | 0.62 | -0.43 | -0.54 | 0.85 | -0.32 | -0.58 | 0.56 | -0.29 | -0.35 | 0.50 | 1.00 | |
| U | 0.93 | -0.83 | -0.64 | -0.64 | -0.09 | -0.72 | -0.77 | -0.90 | 0.53 | -0.58 | -0.66 | 0.85 | -0.46 | -0.64 | 0.49 | -0.39 | -0.49 | 0.61 | 0.97 | 1.00 |

*Correlation matrix for solution-based-ICP-MS trace element data for Skaland (NOR)*

| *Skaland (NOR)* | Mg | Al | V | Cr | Mn | Fe | Ni | Cu | Zn | Ga | Se | Rb | Sr | Mo | Ag | Cd | Ba | Tl | Pb | U |
|---|---|---|---|---|---|---|---|---|---|---|---|---|---|---|---|---|---|---|---|---|
| **Mg** | 1.00 | | | | | | | | | | | | | | | | | | | |
| **Al** | 0.83 | 1.00 | | | | | | | | | | | | | | | | | | |
| **V** | 0.55 | 0.91 | 1.00 | | | | | | | | | | | | | | | | | |
| **Cr** | 0.96 | 0.91 | 0.67 | 1.00 | | | | | | | | | | | | | | | | |
| **Mn** | 0.43 | 0.85 | 0.99 | 0.60 | 1.00 | | | | | | | | | | | | | | | |
| **Fe** | 0.91 | 0.96 | 0.80 | 0.90 | 0.70 | 1.00 | | | | | | | | | | | | | | |
| **Ni** | 0.87 | 0.98 | 0.86 | 0.89 | 0.76 | 0.99 | 1.00 | | | | | | | | | | | | | |
| **Cu** | 0.13 | -0.42 | -0.75 | -0.05 | -0.83 | -0.23 | -0.32 | 1.00 | | | | | | | | | | | | |
| **Zn** | 0.30 | 0.77 | 0.96 | 0.47 | 0.99 | 0.61 | 0.69 | -0.90 | 1.00 | | | | | | | | | | | |
| **Ga** | 0.99 | 0.88 | 0.61 | 0.97 | 0.50 | 0.93 | 0.90 | 0.06 | 0.37 | 1.00 | | | | | | | | | | |
| **Se** | 0.60 | 0.92 | 0.99 | 0.69 | 0.95 | 0.85 | 0.89 | -0.69 | 0.92 | 0.65 | 1.00 | | | | | | | | | |
| **Rb** | 0.95 | 0.92 | 0.69 | 1.00 | 0.61 | 0.91 | 0.90 | -0.08 | 0.50 | 0.97 | 0.71 | 1.00 | | | | | | | | |
| **Sr** | 0.61 | 0.92 | 0.98 | 0.74 | 0.97 | 0.81 | 0.86 | -0.69 | 0.92 | 0.67 | 0.96 | 0.75 | 1.00 | | | | | | | |
| **Mo** | 0.70 | 0.96 | 0.97 | 0.80 | 0.94 | 0.88 | 0.92 | -0.60 | 0.88 | 0.75 | 0.98 | 0.81 | 0.98 | 1.00 | | | | | | |
| **Ag** | 0.42 | 0.84 | 0.99 | 0.56 | 0.99 | 0.71 | 0.77 | -0.84 | 0.99 | 0.48 | 0.97 | 0.58 | 0.96 | 0.93 | 1.00 | | | | | |
| **Cd** | 0.50 | 0.88 | 1.00 | 0.64 | 0.99 | 0.76 | 0.82 | -0.79 | 0.98 | 0.56 | 0.98 | 0.65 | 0.98 | 0.96 | 0.99 | 1.00 | | | | |
| **Ba** | 0.92 | 0.73 | 0.40 | 0.93 | 0.32 | 0.76 | 0.73 | 0.24 | 0.19 | 0.92 | 0.41 | 0.93 | 0.48 | 0.55 | 0.26 | 0.36 | 1.00 | | | |
| **Tl** | 0.57 | 0.92 | 1.00 | 0.70 | 0.98 | 0.81 | 0.86 | -0.73 | 0.95 | 0.62 | 0.99 | 0.71 | 0.98 | 0.98 | 0.98 | 0.99 | 0.42 | 1.00 | | |
| **Pb** | 0.45 | 0.86 | 0.99 | 0.59 | 0.99 | 0.74 | 0.80 | -0.82 | 0.98 | 0.52 | 0.98 | 0.61 | 0.97 | 0.95 | 1.00 | 1.00 | 0.30 | 0.99 | 1.00 | |
| **U** | 0.61 | 0.93 | 0.99 | 0.71 | 0.96 | 0.85 | 0.89 | -0.69 | 0.93 | 0.67 | 1.00 | 0.73 | 0.98 | 0.98 | 0.97 | 0.98 | 0.44 | 0.99 | 0.98 | 1.00 |

*Correlation matrix for solution-based-ICP-MS trace element data for Tayginka (RUS)*

| *Tayginka (RUS)* | Mg | Al | V | Cr | Mn | Fe | Ni | Cu | Zn | Ga | Se | Rb | Sr | Mo | Ag | Cd | Ba | Tl | Pb | U |
|---|---|---|---|---|---|---|---|---|---|---|---|---|---|---|---|---|---|---|---|---|
| Mg | 1.00 | | | | | | | | | | | | | | | | | | | |
| Al | 0.55 | 1.00 | | | | | | | | | | | | | | | | | | |
| V | 0.96 | 0.52 | 1.00 | | | | | | | | | | | | | | | | | |
| Cr | -0.81 | -0.63 | -0.66 | 1.00 | | | | | | | | | | | | | | | | |
| Mn | 0.70 | -0.20 | 0.65 | -0.48 | 1.00 | | | | | | | | | | | | | | | |
| Fe | 0.69 | -0.22 | 0.65 | -0.44 | 1.00 | 1.00 | | | | | | | | | | | | | | |
| Ni | 0.87 | 0.76 | 0.76 | -0.94 | 0.42 | 0.40 | 1.00 | | | | | | | | | | | | | |
| Cu | 0.92 | 0.29 | 0.85 | -0.81 | 0.87 | 0.86 | 0.81 | 1.00 | | | | | | | | | | | | |
| Zn | 0.27 | 0.92 | 0.31 | -0.36 | -0.48 | -0.49 | 0.48 | -0.03 | 1.00 | | | | | | | | | | | |
| Ga | 0.83 | 0.92 | 0.80 | -0.81 | 0.21 | 0.19 | 0.92 | 0.64 | 0.73 | 1.00 | | | | | | | | | | |
| Se | 0.49 | 0.99 | 0.44 | -0.61 | -0.26 | -0.29 | 0.72 | 0.22 | 0.92 | 0.87 | 1.00 | | | | | | | | | |
| Rb | 0.59 | -0.35 | 0.57 | -0.32 | 0.98 | 0.99 | 0.26 | 0.77 | -0.59 | 0.06 | -0.41 | 1.00 | | | | | | | | |
| Sr | 0.40 | -0.54 | 0.37 | -0.17 | 0.93 | 0.94 | 0.08 | 0.63 | -0.74 | -0.16 | -0.59 | 0.97 | 1.00 | | | | | | | |
| Mo | 0.88 | 0.30 | 0.82 | -0.79 | 0.83 | 0.82 | 0.79 | 0.98 | -0.02 | 0.64 | 0.21 | 0.73 | 0.58 | 1.00 | | | | | | |
| Ag | -0.70 | 0.07 | -0.64 | 0.64 | -0.93 | -0.93 | -0.54 | -0.90 | 0.32 | -0.30 | 0.14 | -0.88 | -0.82 | -0.88 | 1.00 | | | | | |
| Cd | 0.18 | 0.91 | 0.19 | -0.38 | -0.52 | -0.53 | 0.51 | -0.03 | 0.93 | 0.69 | 0.90 | -0.65 | -0.78 | 0.01 | 0.33 | 1.00 | | | | |
| Ba | -0.40 | -0.97 | -0.34 | 0.61 | 0.32 | 0.35 | -0.70 | -0.18 | -0.90 | -0.83 | -0.98 | 0.48 | 0.64 | -0.20 | -0.17 | -0.94 | 1.00 | | | |
| Tl | 0.06 | -0.48 | 0.08 | 0.29 | 0.46 | 0.48 | -0.20 | 0.17 | -0.66 | -0.28 | -0.49 | 0.52 | 0.59 | 0.11 | -0.20 | -0.59 | 0.56 | 1.00 | | |
| Pb | 0.55 | 0.98 | 0.49 | -0.70 | -0.15 | -0.18 | 0.79 | 0.34 | 0.86 | 0.91 | 0.97 | -0.32 | -0.50 | 0.36 | 0.01 | 0.88 | -0.98 | -0.48 | 1.00 | |
| U | 0.46 | -0.15 | 0.30 | -0.55 | 0.78 | 0.74 | 0.43 | 0.72 | -0.49 | 0.15 | -0.19 | 0.70 | 0.69 | 0.74 | -0.76 | -0.33 | 0.14 | 0.43 | 0.00 | 1.00 |

*Correlation matrix for solution-based-ICP-MS trace element data for Ragedara (LKA)*

| *Ragedara (LKA)* | Mg | Al | V | Cr | Mn | Fe | Ni | Cu | Zn | Ga | Se | Rb | Sr | Mo | Ag | Cd | Ba | Tl | Pb | U |
|---|---|---|---|---|---|---|---|---|---|---|---|---|---|---|---|---|---|---|---|---|
| Mg | 1.00 | | | | | | | | | | | | | | | | | | | |
| Al | 0.76 | 1.00 | | | | | | | | | | | | | | | | | | |
| V | 0.93 | 0.57 | 1.00 | | | | | | | | | | | | | | | | | |
| Cr | 0.33 | 0.84 | 0.23 | 1.00 | | | | | | | | | | | | | | | | |
| Mn | -0.32 | -0.68 | -0.38 | -0.91 | 1.00 | | | | | | | | | | | | | | | |
| Fe | -0.21 | -0.40 | -0.41 | -0.68 | 0.92 | 1.00 | | | | | | | | | | | | | | |
| Ni | -0.58 | -0.81 | -0.60 | -0.88 | 0.96 | 0.86 | 1.00 | | | | | | | | | | | | | |
| Cu | -0.50 | -0.77 | -0.54 | -0.89 | 0.98 | 0.89 | 1.00 | 1.00 | | | | | | | | | | | | |
| Zn | -0.71 | -0.58 | -0.43 | -0.08 | -0.20 | -0.44 | 0.04 | -0.04 | 1.00 | | | | | | | | | | | |
| Ga | 0.22 | -0.07 | -0.02 | -0.52 | 0.78 | 0.91 | 0.61 | 0.67 | -0.75 | 1.00 | | | | | | | | | | |
| Se | -0.48 | -0.65 | -0.47 | -0.63 | 0.61 | 0.53 | 0.67 | 0.66 | 0.28 | 0.32 | 1.00 | | | | | | | | | |
| Rb | -0.35 | -0.22 | -0.04 | 0.23 | -0.57 | -0.80 | -0.39 | -0.46 | 0.89 | -0.95 | -0.09 | 1.00 | | | | | | | | |
| Sr | -0.08 | -0.59 | -0.10 | -0.93 | 0.96 | 0.84 | 0.85 | 0.89 | -0.29 | 0.80 | 0.56 | -0.58 | 1.00 | | | | | | | |
| Mo | -0.10 | -0.37 | 0.27 | -0.16 | -0.27 | -0.61 | -0.21 | -0.24 | 0.72 | -0.67 | 0.06 | 0.83 | -0.15 | 1.00 | | | | | | |
| Ag | -0.66 | -0.81 | -0.70 | -0.83 | 0.92 | 0.84 | 0.99 | 0.98 | 0.09 | 0.56 | 0.68 | -0.35 | 0.78 | -0.24 | 1.00 | | | | | |
| Cd | -0.61 | -0.66 | -0.27 | -0.26 | -0.09 | -0.42 | 0.09 | 0.03 | 0.96 | -0.69 | 0.25 | 0.87 | -0.13 | 0.85 | 0.12 | 1.00 | | | | |
| Ba | -0.69 | -0.78 | -0.37 | -0.39 | 0.08 | -0.25 | 0.27 | 0.20 | 0.92 | -0.56 | 0.29 | 0.77 | 0.02 | 0.77 | 0.29 | 0.98 | 1.00 | | | |
| Tl | -0.31 | -0.56 | -0.45 | -0.79 | 0.97 | 0.98 | 0.93 | 0.96 | -0.31 | 0.85 | 0.61 | -0.69 | 0.90 | -0.46 | 0.91 | -0.25 | -0.09 | 1.00 | | |
| Pb | -0.68 | -0.92 | -0.63 | -0.89 | 0.89 | 0.72 | 0.97 | 0.95 | 0.25 | 0.42 | 0.65 | -0.17 | 0.78 | -0.01 | 0.97 | 0.32 | 0.48 | 0.83 | 1.00 | |
| U | 0.53 | 0.31 | 0.66 | 0.21 | -0.45 | -0.53 | -0.56 | -0.53 | 0.10 | -0.30 | 0.12 | 0.33 | -0.24 | 0.54 | -0.60 | 0.14 | -0.03 | -0.51 | -0.53 | 1.00 |

*Correlation matrix for solution-based-ICP-MS trace element data for Zavallia (UKR)*

| *Zavallia (UKR)* | Mg | Al | V | Cr | Mn | Fe | Ni | Cu | Zn | Ga | Se | Rb | Sr | Mo | Ag | Cd | Ba | Tl | Pb | U |
|---|---|---|---|---|---|---|---|---|---|---|---|---|---|---|---|---|---|---|---|---|
| **Mg** | 1.00 | | | | | | | | | | | | | | | | | | | |
| **Al** | -0.96 | 1.00 | | | | | | | | | | | | | | | | | | |
| **V** | 1.00 | -0.95 | 1.00 | | | | | | | | | | | | | | | | | |
| **Cr** | 0.87 | -0.72 | 0.90 | 1.00 | | | | | | | | | | | | | | | | |
| **Mn** | 0.99 | -0.94 | 1.00 | 0.91 | 1.00 | | | | | | | | | | | | | | | |
| **Fe** | 1.00 | -0.96 | 1.00 | 0.87 | 0.99 | 1.00 | | | | | | | | | | | | | | |
| **Ni** | 1.00 | -0.97 | 1.00 | 0.86 | 0.99 | 1.00 | 1.00 | | | | | | | | | | | | | |
| **Cu** | 1.00 | -0.96 | 1.00 | 0.88 | 1.00 | 1.00 | 1.00 | 1.00 | | | | | | | | | | | | |
| **Zn** | 1.00 | -0.96 | 1.00 | 0.88 | 0.99 | 1.00 | 1.00 | 1.00 | 1.00 | | | | | | | | | | | |
| **Ga** | -0.75 | 0.90 | -0.71 | -0.34 | -0.70 | -0.75 | -0.76 | -0.75 | -0.73 | 1.00 | | | | | | | | | | |
| **Se** | 0.95 | -0.90 | 0.94 | 0.81 | 0.92 | 0.95 | 0.96 | 0.94 | 0.95 | -0.68 | 1.00 | | | | | | | | | |
| **Rb** | 1.00 | -0.96 | 1.00 | 0.88 | 1.00 | 1.00 | 1.00 | 1.00 | 1.00 | -0.74 | 0.95 | 1.00 | | | | | | | | |
| **Sr** | 0.97 | -0.99 | 0.95 | 0.74 | 0.94 | 0.97 | 0.98 | 0.97 | 0.97 | -0.86 | 0.94 | 0.97 | 1.00 | | | | | | | |
| **Mo** | 1.00 | -0.96 | 1.00 | 0.87 | 0.99 | 1.00 | 1.00 | 1.00 | 1.00 | -0.75 | 0.95 | 1.00 | 0.97 | 1.00 | | | | | | |
| **Ag** | -0.98 | 0.94 | -0.97 | -0.85 | -0.97 | -0.98 | -0.97 | -0.98 | -0.98 | 0.71 | -0.90 | -0.98 | -0.95 | -0.98 | 1.00 | | | | | |
| **Cd** | 1.00 | -0.96 | 1.00 | 0.89 | 1.00 | 1.00 | 1.00 | 1.00 | 1.00 | -0.73 | 0.94 | 1.00 | 0.97 | 1.00 | -0.98 | 1.00 | | | | |
| **Ba** | 1.00 | -0.96 | 1.00 | 0.88 | 1.00 | 1.00 | 1.00 | 1.00 | 1.00 | -0.74 | 0.94 | 1.00 | 0.97 | 1.00 | -0.98 | 1.00 | 1.00 | | | |
| **Tl** | 0.98 | -0.93 | 0.99 | 0.89 | 0.99 | 0.98 | 0.98 | 0.98 | 0.97 | -0.71 | 0.92 | 0.98 | 0.93 | 0.98 | -0.93 | 0.98 | 0.98 | 1.00 | | |
| **Pb** | 1.00 | -0.96 | 1.00 | 0.87 | 0.99 | 1.00 | 1.00 | 1.00 | 1.00 | -0.74 | 0.95 | 1.00 | 0.97 | 1.00 | -0.98 | 1.00 | 1.00 | 0.98 | 1.00 | |
| **U** | 0.98 | -0.99 | 0.97 | 0.78 | 0.96 | 0.98 | 0.99 | 0.98 | 0.98 | -0.84 | 0.94 | 0.98 | 1.00 | 0.98 | -0.97 | 0.98 | 0.98 | 0.95 | 0.98 | 1.00 |

## E. Sample List

| Sample ID | Mine/Province | Country | Continent | Note |
|---|---|---|---|---|
| 1A | Kaisersberg | Austria | Europe | |
| 2A | Kaisersberg | Austria | Europe | pellet not stable enough for LA-analyis |
| 4A | Hunan Lutang | China | Asia | |
| 1B | Balama | Mozambique | Africa | |
| 2B | Skaland | Norway | Europe | |
| 3B | Minas Gerais | Brazil | South America | |
| 4B | Zavallia | Ukraine | Europe | |
| 5B | Tayginka | Russia | Asia | |
| 6B | Inner Mongolia | China | Asia | |
| 7B | Heilongjian | China | Asia | |
| 10B | Ragedara | Sri Lanka | Asia | |
| 11B | Brickaville | Madagascar | Africa | |
| 13B | Passau | Germany | Europe | |
| 14B | Passau (raw ore) | Germany | Europe | Graphite particles too small for laser-ablation |
| 15B | Skaland | Norway | Europe | |
| 16B | Skaland (raw ore) | Norway | Europe | Graphite particles too small for laser-ablation |
| 21A | Shandong | China | Asia | |
| 21B | Balama | Mozambique | Africa | |
| 21C | Minas Gerais | Brazil | South America | |
| 21D | Brickaville | Madagascar | Africa | |
| 21E | Tayginka | Russia | Asia | |
| 21F | Ragedara | Sri Lanka | Asia | |
| 21G, H, I | Kaisersberg (raw ore) | Austria | Europe | |
| 21J, K, L | Balama | Mozambique | Africa | |
| 21M, N | Minas Gerais | Brazil | South America | |
| 22A | Shandong | China | Asia | |
| 22B | Balama | Mozambique | Africa | |
| 22C | Minas Gerais | Brazil | South America | |
| 22D | Brickaville | Madagascar | Africa | |
| 22E | Tayginka | Russia | Asia | |
| 22F | Zavallia | Ukraine | Europe | |
| 22G | Skaland | Norway | Europe | |
| 22H | Balama (raw ore) | Mozambique | Africa | |
| 22K-S | Zavallia | Ukraine | Europe | Graphite particles too small for laser-ablation |

## F. AI Declaration

| Subject | AI share in % | Tool/Version | Remarks | Prompting |
|---|---|---|---|---|
| Translation | 10 | DeepL (Free Version via Browser) | Translation from german to english, DeepL through browser | Online document |
| Translation | 10 | ChatGPT-3.5, -4 | Translation from german to english | Online document |
| Finding synonyms | 5 | ChatGPT-3.5, -4 | Improving readability | Online document |
| Suggestions for the structure of the work (table of content, outlook and recommendations) | 5 | ChatGPT-3.5, -4, | Improving linguistic readability and understanding for reader | Online document |
| Summarize own texts and suggest paraphrasing | 8 | ChatGPT-3.5, -4, | Improving linguistic readability and understanding | Online document |